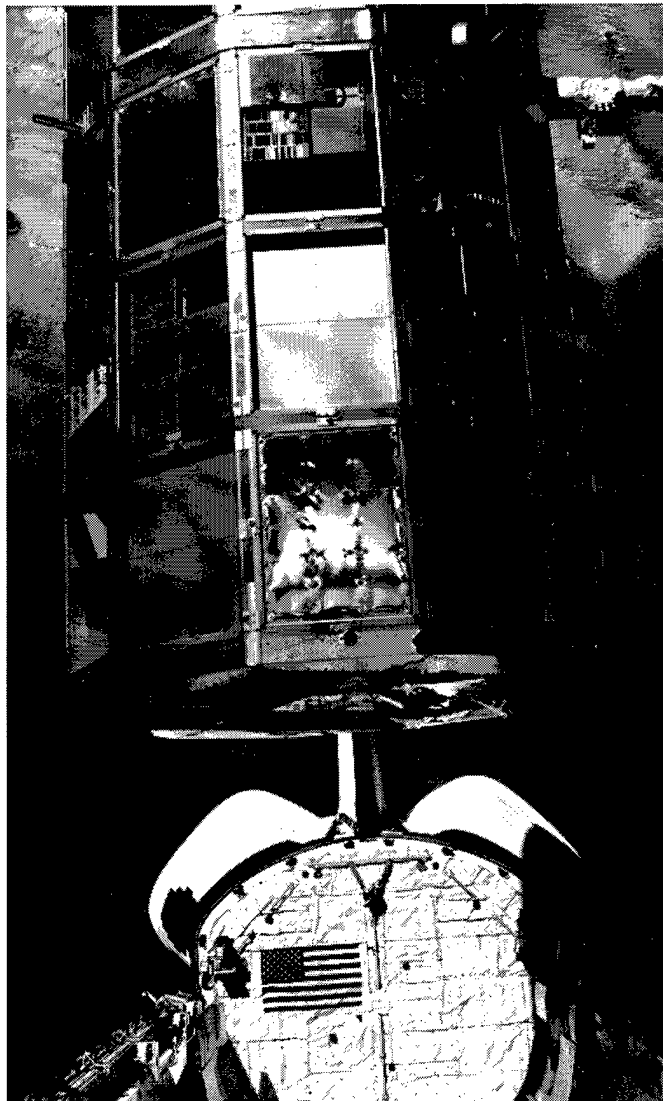


# LDEF — 69 Months in Space

*First  
Post-Retrieval  
Symposium*



*Proceedings of a symposium held in  
Kissimmee, Florida  
June 2-8, 1991*

**NASA**

**DISTRIBUTION STATEMENT A**

Approved for public release;  
Distribution Unlimited

**DTIC QUALITY INSPECTED**

PLEASE RETURN TO:

BMD TECHNICAL INFORMATION CENTER  
BALLISTIC MISSILE DEFENSE ORGANIZATION  
7100 DEFENSE PENTAGON  
WASHINGTON D.C. 20301-7100

19980309 222

43667

Accession Number: 3667

Publication Date: Jan 01, 1992

Title: LDEF - 69 Months in Space: First Post-Retrieval Symposium, Part 3

Personal Author: Levine, A.S. (Editor)

Corporate Author Or Publisher: NASA Langley Research Center, Hampton, VA 23665-5225 Report Number: L-17042

Report Prepared for: NASA, Washington, DC 20546-0001 Report Number Assigned by Contract Monitor: NASA CP-3134, Part 3

Comments on Document: This document is a compilation of papers presented at the First Long Duration Exposure Facility (LDEF) Post-Retrieval Symposium, June 2-8, 1991

Descriptors, Keywords: Space Experiment Data Analysis Material Coating Thermal System Power Propulsion Cosmic Ray Ion Micrometeoroid Electronics Optics Life Science

Pages: 00509

Cataloged Date: Aug 04, 1992

Document Type: HC

Number of Copies In Library: 000001

Record ID: 24432

# LDEF — 69 Months in Space

*First  
Post-Retrieval  
Symposium*

*Edited by  
Arlene S. Levine  
NASA Langley Research Center  
Hampton, Virginia*

*Proceedings of a symposium sponsored by the  
National Aeronautics and Space Administration,  
Washington, D.C., and held in  
Kissimmee, Florida  
June 2-8, 1991*



National Aeronautics and  
Space Administration  
Office of Management  
Scientific and Technical  
Information Program  
1991

## Foreword

On July 20, 1989, President George Bush charted a new course for human exploration of space:

“... a long-range continuing commitment. First, for the coming decade -- for the 1990's -- Space Station *Freedom*, our next critical step in all our space endeavors. And for the next century, back to the moon, back to the future, and this time, back to stay; then a journey into tomorrow, a journey to another planet -- a manned mission to Mars. Each mission should and will lay the groundwork for the next.”

The Long Duration Exposure Facility (LDEF) is providing critical technology for future spacecraft, including Space Station *Freedom*, and thus plays a major role in the President's vision of human exploration of space.

LDEF was carried into orbit in April 1984 by the Space Shuttle *Challenger*. The 11-ton satellite contained 57 experiments to assess the effects of the space environment, i.e., ionizing radiation, meteoroids, cosmic dust, and high altitude atomic oxygen on materials and mechanical, electronic, optical, and living systems. In January 1990, after 69 months in low Earth orbit, LDEF was retrieved by the Space Shuttle *Columbia* and returned to Earth. The retrieval occurred 57 months after it was originally planned, due in part to the *Challenger* tragedy. The 69 months in space provided experimenters the unique opportunity to sample and measure the space environment over a longer time period than originally planned.

The 57 LDEF experiments were returned to the Principal Investigators and their science teams for analyses and interpretation. In June 1991, over 400 LDEF researchers and data users met in Kissimmee, Florida for the First LDEF Post-Retrieval Symposium. The papers presented contained important new information about space environments and their impact on materials, systems, and biology. This publication contains the material presented at the symposium, categorized by subject:

- LDEF Mission and Induced Environments
- Space Environments - *Ionizing Radiation*
- Space Environments - *Meteoroid and Debris*
- Space Environmental Effects - *Materials*
- Space Environmental Effects - *Systems*
- Space Environmental Effects - *Biology*
- Space Environmental Effects - *Microgravity*
- The Future

During the symposium Sally A. Little, NASA Headquarters, chaired the **LDEF Mission and Induced Environments** session; William L. Quaide, NASA Headquarters,



chaired the **Space Environments - Meteoroid and Debris** session; Thomas W. Crooker, NASA Headquarters, and Bland A. Stein, NASA Langley Research Center, co-chaired the **Space Environmental Effects - Materials** session; Judith H. Ambrus, NASA Headquarters, and P. Rex Miller, W.J. Schaefer and Associates co-chaired the **Space Environmental Effects - Systems** session; and James L. Jones, NASA Langley Research Center chaired the session called **Others**.

Some presentations in these documents underwent a title change; others were combined with two or three presentations; two were not presented orally. However, all oral presentations are represented in written form. Where full-length papers were unavailable, the abstracts have been reprinted. All papers were reviewed for technical content as well as form.

We wish to thank the contributors, as well as the reviewers of these papers. We also wish to thank Dr. William H. Kinard, without whose vision and persistence, there would not be an LDEF project or the valuable data it has collected.

The LDEF Science Office plans to organize and conduct two additional symposia, one in San Diego in June 1992 and another in 1993. The proceedings from these two symposia will be published as NASA Conference Publications.

We believe that the LDEF data reported in this three-part document will make important contributions to charting the new course for the exploration of space.

*Use of manufacturers' trade names in this publication does not constitute an official endorsement of such products or manufacturers, either expressed or implied, by the National Aeronautics and Space Administration.*

Arlene S. Levine  
LDEF Science Office  
NASA Langley Research Center

# CONTENTS

FOREWORD .....	iii
----------------	-----

## \* PART 1

### LDEF MISSION AND INDUCED ENVIRONMENTS

LONG DURATION EXPOSURE FACILITY--A GENERAL OVERVIEW .....	3
Robert L. O'Neal and E. Burton Lightner	
LONG DURATION EXPOSURE FACILITY (LDEF) SPACE ENVIRONMENTS OVERVIEW .....	49
William H. Kinard and Glenna D. Martin	
PINHOLE CAMERAS AS SENSORS FOR ATOMIC OXYGEN IN ORBIT; APPLICATION TO ATTITUDE DETERMINATION OF THE LDEF .....	61
Palmer N. Peters and John C. Gregory	
USE OF THE LONG DURATION EXPOSURE FACILITY'S THERMAL MEASUREMENT SYSTEM FOR THE VERIFICATION OF THERMAL MODELS .....	69
William M. Berrios	
MEASURED SPACE ENVIRONMENTAL EFFECTS TO LDEF DURING RETRIEVAL .....	85
Carl R. Maag and W. Kelly Linder	
PARTICLE TYPES AND SOURCES ASSOCIATED WITH LDEF .....	101
E. R. Crutcher and W. W. Wascher	
MIGRATION AND GENERATION OF CONTAMINANTS FROM LAUNCH THROUGH RECOVERY: LDEF CASE HISTORY .....	121
E. R. Crutcher, L. S. Nishimura, K. J. Warner and W. W. Wascher	
QUANTIFICATION OF CONTAMINANTS ASSOCIATED WITH LDEF .....	141
E. R. Crutcher, L. S. Nishimura, K. J. Warner and W. W. Wascher	
MOLECULAR FILMS ASSOCIATED WITH LDEF .....	155
E. R. Crutcher and K. J. Warner	
ORGANIC CONTAMINATION OF LDEF .....	179
Gale A. Harvey	

### SPACE ENVIRONMENTS - IONIZING RADIATION

SUMMARY OF IONIZING RADIATION ANALYSIS ON THE LONG DURATION EXPOSURE FACILITY .....	199
T. A. Parnell	
PREDICTION OF LDEF IONIZING RADIATION ENVIRONMENT .....	213
John W. Watts, T. A. Parnell, James H. Derrickson, T. W. Armstrong and E. V. Benton,	
GAMMA RADIATION SURVEY OF THE LDEF SPACECRAFT .....	225
G. W. Phillips, S. E. King, R. A. August, J. C. Ritter, J. H. Cutchin, P. S. Haskins, J. E. McKisson, D. W. Ely, A. G. Weisenberger, R. B. Piercey and T. Dybler	

\* Part 1 is presented under separate cover.

THE INTERACTIONS OF ATMOSPHERIC COSMOGENIC RADIONUCLIDES WITH SPACECRAFT SURFACES .....	237
J. C. Gregory, G. J. Fishman, B. A. Harmon and T. A. Parnell	
SURFACE ACTIVATION OF CONCORDE BY $^7\text{Be}$ .....	249
P. R. Truscott, C. S. Dyer and J. C. Flatman	
CHARGED PARTICLE ACTIVATION STUDIES ON THE SURFACE OF LDEF SPACECRAFT .....	255
Ilhan Olmez, Forrest Burns and Paul L. Sagalyn	
RADIOACTIVITIES OF LONG DURATION EXPOSURE FACILITY (LDEF) MATERIALS: BAGGAGE AND BONANZAS .....	257
Alan R. Smith and Donna L. Hurley	
MEASUREMENTS OF INDUCED RADIOACTIVITY IN SOME LDEF SAMPLES .....	271
C. E. Moss and R. C. Reedy	
GAMMA-RAY SPECTROMETRY OF LDEF SAMPLES AT SRL .....	287
Willard G. Winn	
INDUCED RADIOACTIVITY IN LDEF COMPONENTS .....	301
B. A. Harmon, G. J. Fishman, T. A. Parnell and C. E. Laird	
THERMOLUMINESCENT DOSIMETRY FOR LDEF EXPERIMENT M0006 .....	313
J. Y. Chang, D. Giangano, T. Kantorcik, M. Stauber, and L. Snead	
RADIATION EXPOSURE OF LDEF: INITIAL RESULTS .....	325
E. V. Benton, A. L. Frank, E. R. Benton, I. Csige, T. A. Parnell and J. W. Watts, Jr.	
CHARGED PARTICLE LET-SPECTRA MEASUREMENTS ABOARD LDEF .....	339
I. Csige, E. V. Benton, A. L. Frank, L. A. Frigo, E. R. Benton, T. A. Parnell and J. W. Watts, Jr.	
IONIZING RADIATION CALCULATIONS AND COMPARISONS WITH LDEF DATA .....	347
T. W. Armstrong, B. L. Colborn and J. W. Watts, Jr.	
LDEF GEOMETRY/MASS MODEL FOR RADIATION ANALYSES .....	361
B. L. Colborn and T. W. Armstrong	
THE LDEF ULTRA HEAVY COSMIC RAY EXPERIMENT .....	367
D. O'Sullivan, A. Thompson, J. Bosch, R. Keegan, K.-P. Wenzel, A. Smit and C. Domingo	
PRELIMINARY RESULTS FROM THE HEAVY IONS IN SPACE EXPERIMENT .....	377
James H. Adams, Jr., Lorraine P. Beahm and Allan J. Tylka	
HEAVY ION MEASUREMENT ON LDEF .....	393
R. Beaujean, D. Jonathal and W. Enge	
 <b>SPACE ENVIRONMENTS - METEOROID AND DEBRIS</b>	
LARGE CRATERS ON THE METEOROID AND SPACE DEBRIS IMPACT EXPERIMENT .....	399
Donald H. Humes	

STUDY OF COSMIC DUST PARTICLES ON BOARD LDEF: THE FRECOPA EXPERIMENTS AO138-1 AND AO138-2 .....	419
J. C. Mandeville and Janet Borg	
METEOROID/SPACE DEBRIS IMPACTS ON MSFC LDEF EXPERIMENTS .....	435
Miria Finckenor	
HYPERVELOCITY IMPACT MICROFOIL PERFORATIONS IN THE LEO SPACE ENVIRONMENT (LDEF, MAP AO023 EXPERIMENT) .....	443
J. A. M. McDonnell and T. J. Stevenson	
METEOROID AND DEBRIS SPECIAL INVESTIGATION GROUP DATA ACQUISITION PROCEDURES .....	459
Thomas H. See, Martha K. Allbrooks, Dale R. Atkinson, Clyde A. Sapp, Charles G. Simon, and Mike E. Zolensky	
METEOROID AND DEBRIS SPECIAL INVESTIGATION GROUP PRELIMINARY RESULTS: SIZE-FREQUENCY DISTRIBUTION AND SPATIAL DENSITY OF LARGE IMPACT FEATURES ON LDEF .....	477
Thomas H. See, Friedrich Hörz, Michael E. Zolensky, Martha K. Allbrooks, Dale R. Atkinson and Charles G. Simon	
PRELIMINARY ANALYSIS OF LDEF INSTRUMENT AO187-1 "CHEMISTRY OF MICROMETEOROIDS EXPERIMENT" .....	487
Friedrich Hörz, Ronald P. Bernhard, Jack Warren, Thomas H. See, Donald E. Brownlee, Mark R. Lurance, Scott Messenger and Robert B. Peterson	
SIMS CHEMICAL ANALYSIS OF EXTENDED IMPACT FEATURES FROM THE TRAILING EDGE PORTION OF EXPERIMENT AO187-2 .....	503
Sachiko Amari, John Foote, Charles Simon, Pat Swan, Robert M. Walker, Ernst Zinner, Elmar K. Jessberger, Gundolf Lange and Frank Stadermann	
IDE SPATIO-TEMPORAL IMPACT FLUXES AND HIGH TIME-RESOLUTION STUDIES OF MULTI-IMPACT EVENTS AND LONG-LIVED DEBRIS CLOUDS .....	517
J. Derral Mulholland, S. Fred Singer, John P. Oliver, Jerry L. Weinberg, William J. Cooke, Nancy L. Montague, Jim J. Wortman, Philip C. Kassel and William H. Kinard	
ION MICROPROBE ELEMENTAL ANALYSES OF IMPACT FEATURES ON INTERPLANETARY DUST EXPERIMENT SENSOR SURFACES .....	529
Charles G. Simon, Jerry L. Hunter, Jim J. Wortman and Dieter P. Griffis	
LDEF IMPACT CRATERS FORMED BY CARBON-RICH IMPACTORS: A PRELIMINARY REPORT .....	549
T. E. Bunch, F. Radicati di Brozolo, Ronald H. Fleming, David W. Harris, Don Brownlee and Terrence W. Reilly	
DYNAMIC (COMPUTER) MODELLING OF THE PARTICULATE ENVIRONMENT: TRANSFORMATIONS FROM THE LDEF REFERENCE FRAME TO DECODE GEOCENTRIC AND INTERPLANETARY POPULATIONS .....	565
J. A. M. McDonnell and K. Sullivan	
LDEF DATA CORRELATION TO EXISTING NASA DEBRIS ENVIRONMENT MODELS .....	567
Dale R. Atkinson, Martha K. Allbrooks and Alan J. Watts	
DERIVING THE VELOCITY DISTRIBUTION OF METEOROIDS FROM THE MEASURED METEOROID IMPACT DIRECTIONALITY ON THE VARIOUS LDEF SURFACES .....	569
Herbert A. Zook	

M AND D SIG PROGRESS REPORT: LABORATORY SIMULATIONS OF LDEF IMPACT FEATURES .....	581
Friedrich Hörz, R. P. Bernhard, T. H. See, D. Atkinson and M. Allbrooks	
PRELIMINARY MICROMETEOROID AND DEBRIS EFFECTS ON LDEF THERMAL CONTROL SURFACES .....	583
Martha K. Allbrooks, Dale R. Atkinson, Thomas See and Fred Hörz	
THE INTERSTELLAR GAS EXPERIMENT .....	585
D. L. Lind, J. Geiss, F. Bühler and O. Eugster	
COLOR PHOTOGRAPHS .....	595
AUTHOR INDEX .....	605

## \* PART 2

### SPACE ENVIRONMENTAL EFFECTS - MATERIALS

PRELIMINARY FINDINGS OF THE LDEF MATERIALS SPECIAL INVESTIGATION GROUP .....	617
Bland A. Stein and H. Gary Pippin	
ATOMIC OXYGEN AND ULTRAVIOLET RADIATION MISSION TOTAL EXPOSURES FOR LDEF EXPERIMENTS .....	643
R. J. Bourassa, J. R. Gillis and K. W. Rousslang	
EFFECTS OF SPACE ENVIRONMENT ON STRUCTURAL MATERIALS .....	663
C. Miglionico, C. Stein, R. Roybal, R. Robertson, L.E. Murr, S. Quinones, J. Rivas, B. Marquez, A.H. Advani, W.W. Fisher and R. Arrowood	
MEASUREMENT OF THE $O^{18}$ TO $O^{16}$ ISOTOPE RATIO FOR CHARACTERIZING OXIDE SURFACE LAYERS ON LDEF SAMPLES .....	679
Paul L. Sagalyn	
CHEMICAL CHARACTERIZATION OF SELECTED LDEF POLYMERIC MATERIALS .....	687
Philip R. Young and Wayne S. Slemp	
CHARACTERIZATION OF POLYMER FILMS RETRIEVED FROM LDEF .....	705
Alan Letton, Neil I. Rock, Kevin D. Williams, Thomas W. Strganac and Allan Farrow	
MEASUREMENTS OF EROSION CHARACTERISTICS FOR METAL AND POLYMER SURFACES USING PROFILOMETRY .....	723
Ligia C. Christl, John C. Gregory and Palmer N. Peters	
LONG DURATION EXPOSURE FACILITY (LDEF) PRELIMINARY FINDINGS: LEO SPACE EFFECTS ON THE SPACE PLASMA - VOLTAGE DRAINAGE EXPERIMENT .....	737
Brian K. Blakkolb, James Y. Yaung, Kelly A. Henderson, William W. Taylor and Lorraine E. Ryan	
INTERACTIONS OF ATOMIC OXYGEN WITH MATERIAL SURFACES IN LOW EARTH ORBIT: PRELIMINARY RESULTS FROM EXPERIMENT AO114 .....	753
J. C. Gregory, L. Christl, G. N. Raikar, J. J. Weimer, R. Wiser and P. N. Peters	
EFFECTS ON LDEF EXPOSED COPPER FILM AND BULK .....	755
Palmer N. Peters, John C. Gregory, Ligia C. Christl and Ganesh N. Raikar	

\* Part 2 is presented under separate cover.

LDEF EXPERIMENT AO034: ATOMIC OXYGEN STIMULATED OUTGASSING .....	763
Roger C. Linton, Rachel R. Kamenetzky, John M. Reynolds and Charles L. Burris	
ATOMIC OXYGEN UNDERCUTTING OF LDEF ALUMINIZED-KAPTON MULTILAYER INSULATION .....	781
Kim K. deGroh and Bruce A. Banks	
PRELIMINARY RESULTS FOR LDEF/HEPP THERMAL CONTROL SAMPLES .....	797
Lonny Kauder	
ATOMIC OXYGEN INTERACTIONS WITH FEP TEFLON AND SILICONES ON LDEF .....	801
Bruce A. Banks, Joyce A. Dever, Linda Gebauer and Carol M. Hill	
VACUUM ULTRAVIOLET (VUV) RADIATION - INDUCED DEGRADATION OF FLUORINATED ETHYLENE PROPYLENE (FEP) TEFLON ABOARD THE LONG DURATION EXPOSURE FACILITY (LDEF) .....	817
David E. Brinza, A. E. Stiegman, Paul R. Staszak, Eric G. Laue and Ranty H. Liang	
SPACE ENVIRONMENTAL EFFECTS ON SILVERED TEFLON THERMAL CONTROL SURFACES .....	831
C. S. Hemminger, W. K. Stuckey and J. C. Uht	
RESULTS OF EXAMINATION OF SILVERED TEFLON FROM THE LONG DURATION EXPOSURE FACILITY .....	847
Ken Rousslang, Russ Crutcher and Gary Pippin	
SILVER TEFLON BLANKET: LDEF TRAY C-08 .....	861
E. R. Crutcher, L. S. Nishimura, K. J. Warner and W. W. Wascher	
PRELIMINARY INVESTIGATIONS INTO UHCRE THERMAL CONTROL MATERIALS .....	875
François Levadou, Mike Froggatt, Martin Rott and Eberhard Schneider	
INITIAL MATERIALS EVALUATION OF THE THERMAL CONTROL SURFACES EXPERIMENT (S0069) .....	899
Donald R. Wilkes, M. John Brown, Leigh L. Hummer and James M. Zwiener	
UNUSUAL MATERIALS EFFECTS OBSERVED ON THE THERMAL CONTROL SURFACES EXPERIMENT (S0069) .....	919
James M. Zwiener, Kenneth A. Herren, Donald R. Wilkes, Leigh Hummer and Edgar R. Miller	
EFFECTS OF LOW EARTH ORBIT ENVIRONMENT ON THE LONG DURATION EXPOSURE FACILITY THERMAL CONTROL COATINGS .....	935
Thomas R. Sampair and William M. Berrios	
SPACECRAFT THERMAL CONTROL COATINGS .....	945
Jean-Claude Guillaumon and Alain Paillous	
LONG DURATION EXPOSURE FACILITY EXPERIMENT M0003-5 THERMAL CONTROL MATERIALS .....	961
Charles J. Hurley	
RESULTS OF EXAMINATION OF THE A276 WHITE AND Z306 BLACK THERMAL CONTROL PAINT DISKS FLOWN ON LDEF .....	975
Johnny L. Golden	
ION BEAM TEXTURED AND COATED SURFACES EXPERIMENT (IBEX) .....	989
Michael J. Mirtich, Sharon K. Rutledge, Nicholas Stevens, Raymond Olle and James Merrow	

ELLIPSOMETRIC STUDY OF OXIDE FILMS FORMED ON LDEF METAL SAMPLES .....	1005
W. Franzen, J. S. Brodtkin, L. C. Sengupta and P. L. Sagalyn	
SPACE ENVIRONMENTAL EFFECTS ON THE INTEGRITY OF CHROMIC ACID ANODIZED COATINGS .....	1023
Walter L. Plagemann	
M0003-10: LDEF ADVANCED COMPOSITES EXPERIMENT .....	1041
Gary L. Steckel and Tuyen D. Le	
LDEF - SPACE ENVIRONMENTAL EFFECTS ON MATERIALS: COMPOSITES AND SILICONE COATINGS .....	1055
Brian C. Petrie	
PRELIMINARY RESULTS FROM THE LDEF/UTIAS COMPOSITE MATERIALS EXPERIMENT .....	1057
R. C. Tennyson, G. E. Mabson, W. D. Morison and J. Kleiman	
LONG DURATION EXPOSURE FACILITY EXPERIMENT M0003 DEINTEGRATION/ FINDINGS AND IMPACTS .....	1073
M. J. Meshishnek, S. R. Gyetvay, and C. H. Jagers	
SURVEY OF RESULTS FROM THE BOEING MODULES ON THE M0003 EXPERIMENT ON LDEF .....	1109
H. G. Pippin, Owen Mulkey, Juris Verzemnieks, Emmett Miller, Sylvester Hill and Harry Dursch	
RESULTS FROM ANALYSIS OF BOEING COMPOSITE SPECIMENS FLOWN ON LDEF EXPERIMENT M0003 .....	1115
Pete E. George and Sylvester G. Hill	
HIGH-TOUGHNESS GRAPHITE/EPOXY COMPOSITE MATERIAL EXPERIMENT .....	1143
David K. Felbeck	
EFFECTS OF LDEF FLIGHT EXPOSURE ON SELECTED POLYMER MATRIX RESIN COMPOSITE MATERIALS .....	1149
Wayne S. Slemple, Philip R. Young, William G. Witte, Jr. and James Y. Shen	
EFFECT OF SPACE ENVIRONMENT ON COMPOSITE MATERIALS AND THERMAL COATINGS (AO138-9) .....	1163
Michel Parcelier and Jean Pierre Assié	
EFFECT OF SPACE EXPOSURE OF SOME EPOXY MATRIX COMPOSITES ON THEIR THERMAL EXPANSION AND MECHANICAL PROPERTIES (AO138-8) .....	1175
Heinrich Jabs	
MECHANICAL PROPERTIES OF SILICATE GLASSES EXPOSED TO A LOW-EARTH ORBIT .....	1187
David E. Wiedlocher, Dennis S. Tucker, Ron Nichols and Donald L. Kinser	
PATTERNS OF DISCOLORATION AND OXIDATION BY DIRECT AND SCATTERED FLUXES ON LDEF, INCLUDING OXYGEN ON SILICON .....	1189
A. R. Frederickson, R. C. Filz, F. J. Rich and P. Sagalyn	
COLOR PHOTOGRAPHS .....	1201
AUTHOR INDEX .....	1205

### PART 3

#### SPACE ENVIRONMENTAL EFFECTS - SYSTEMS

SYSTEMS SPECIAL INVESTIGATION GROUP OVERVIEW .....	1217
James B. Mason, Harry Dursch and Joel Edelman	
SPACE AGING OF SOLID ROCKET MATERIALS .....	1225
Dean M. Lester, Leon L. Jones, R. B. Smalley, Jr. and R. Neil Ord	
EFFECTS OF THE SPACE ENVIRONMENT ON SPACE-BASED RADAR PHASED-ARRAY ANTENNA; STATUS AND PRELIMINARY OBSERVATIONS (LDEF EXPERIMENT AO133) .....	1227
J. B. Whiteside, D. Giangano, R. L. Heuer, E. Kamykowski, M. Kesselman, W. D. Rooney, R. Schulte and M. Stauber	
AN OVERVIEW OF THE FIRST RESULTS ON THE SOLAR ARRAY MATERIALS PASSIVE LDEF EXPERIMENT (SAMPLE), AO171 .....	1241
Ann F. Whitaker and Leighton E. Young	
EXPERIMENT M0003-4 ADVANCED SOLAR CELL AND COVERGLASS ANALYSIS, AN OVERVIEW .....	1255
Terry M. Trumble	
PRELIMINARY ANALYSES OF WL EXPERIMENT # 701, SPACE ENVIRONMENT EFFECTS ON OPERATING FIBER OPTIC SYSTEMS .....	1257
E. W. Taylor, J. N. Berry, A. D. Sanchez, R. J. Padden and S. P. Chapman	
LDEF FIBER OPTIC EXPOSURE EXPERIMENT NO. S-0109 .....	1283
A. R. Johnston, L. A. Bergman and R. Hartmayer	
OPTICAL PERFORMANCE OF EXPOSED SOLAR CELL COVERS .....	1299
Thomas H. Allen, Bryant P. Hichwa, Steven R. Selee, Jerry Dodds and Greg S. Long	
RULED AND HOLOGRAPHIC DIFFRACTION GRATINGS EXPERIMENT (AO138-5) .....	1301
Francis Bonnemason	
POST-FLIGHT CHARACTERIZATION OF OPTICAL SYSTEM SAMPLES, THERMAL CONTROL SAMPLES, AND DETECTORS FROM LDEF EXPERIMENT M0003, SUB-EXPERIMENTS 6 AND 13 .....	1315
Randall R. Hodgson, James N. Holsen and Robert A. Drerup, Jr.	
LDEF ACTIVE OPTICAL SYSTEM COMPONENTS EXPERIMENT .....	1317
M. D. Blue	
EFFECTS OF LONG-DURATION EXPOSURE ON OPTICAL SYSTEM COMPONENTS .....	1327
Gale A. Harvey	
EFFECTS OF LONG TERM EXPOSURE ON OPTICAL SUBSTRATES AND COATINGS (S0050-2) .....	1341
John Vallimont and Keith Havey	
VACUUM DEPOSITED OPTICAL COATINGS EXPERIMENT .....	1343
Jean Charlier	
SPACE ENVIRONMENTAL EFFECTS ON COATED OPTICS .....	1361
T. M. Donovan, J. M. Bennett, R. Z. Dalbey, D. K. Burge and S. Gyetvay	



CONTAMINATION OF OPTICAL SURFACES IN EARTH ORBIT .....	1377
Donald L. Kinser, Robert A. Weller, M. H. Mendenhall, D. E. Wiedlocher, R. Nichols, D. Tucker and A. Whitaker	
DURABILITY EVALUATION OF PHOTOVOLTAIC BLANKET MATERIALS EXPOSED ON LDEF TRAY (S1003) .....	1379
Sharon K. Rutledge and Raymond M. Olle	
ADVANCED PHOTOVOLTAIC EXPERIMENT, S0014: PRELIMINARY FLIGHT RESULTS AND POST-FLIGHT FINDINGS .....	1395
David J. Brinker, John R. Hickey and David A. Scheiman	
EVALUATION OF LDEF EXPERIMENT S1002 .....	1405
L. Preuss	
LDEF SP-HVDE (SPACE PLASMA-HIGH VOLTAGE DRAINAGE EXPERIMENT) POST- FLIGHT RESULTS: LEAKAGE CURRENT AND DISCHARGE .....	1419
J. Y. Yaung, W. C. Wong, B. K. Blakkolb, L. E. Ryan, J. E. Chedotte and W. W. L. Taylor	
LONG DURATION EXPOSURE FACILITY (LDEF) LOW TEMPERATURE HEAT PIPE EXPERIMENT PACKAGE (HEPP) FLIGHT RESULTS .....	1431
Roy McIntosh, Craig McCreight and Patrick J. Brennan	
LONG DURATION EXPOSURE FACILITY LOW-TEMPERATURE HEAT PIPE EXPERIMENT PACKAGE POWER SYSTEM RESULTS .....	1441
Smith E. Tiller and David Sullivan	
RESULTS FROM THE LDEF/AO076 CASCADED VARIABLE CONDUCTANCE HEATPIPE EXPERIMENT .....	1455
Michael G. Grote	
TRANSVERSE FLAT PLATE HEAT PIPE EXPERIMENT .....	1467
David Shular	
EXPOSURE TO SPACE RADIATION OF HIGH-PERFORMANCE INFRARED MULTILAYER FILTERS AND MATERIALS TECHNOLOGY EXPERIMENT (AO056) .....	1477
Gary J. Hawkins, John S. Seeley and Roger Hunneman	
PASSIVE EXPOSURE OF EARTH RADIATION BUDGET EXPERIMENT COMPONENTS LDEF EXPERIMENT AO147: POST-FLIGHT EXAMINATIONS AND TESTS .....	1493
John R. Hickey	
TRANSMITTANCE MEASUREMENTS OF ULTRAVIOLET AND VISIBLE WAVELENGTH FILTERS FLOWN ABOARD LDEF .....	1511
Thomas A. Mooney and Ali Smajkiewicz	
RADIATION SENSITIVITY OF QUARTZ CRYSTAL OSCILLATORS EXPERIMENT FOR THE LONG DURATION EXPOSURE FACILITY (LDEF) .....	1523
J. S. Ahearn and J. D. Venables	
LDEF ELECTRONIC SYSTEMS: SUCCESSES, FAILURES AND LESSONS .....	1533
E. A. Miller, L. K. Brooks, C. J. Johnson, J. L. Levorsen, O. R. Mulkey, D. C. Porter and D. W. Smith	
EFFECT OF SPACE EXPOSURE ON PYROELECTRIC INFRARED DETECTORS .....	1547
James B. Robertson	
LDEF MECHANICAL SYSTEMS .....	1549
W. Steve Spear and Harry W. Dursch	

ON-ORBIT COLDWELDING FACT OR FRICTION? .....	1565
Harry Dursch and Steve Spear	
THERMAL CONTROL SURFACES EXPERIMENT - FLIGHT SYSTEMS PERFORMANCE .....	1577
Donald R. Wilkes, Leigh L. Hummer and James M. Zwiener	
FRENCH COOPERATIVE PASSIVE PAYLOAD (FRECOPA) SYSTEM RESULTS .....	1593
Christian Durin	
EFFECTS OF ULTRA-VACUUM AND SPACE ENVIRONMENT ON CONTACT OHMIC RESISTANCE LDEF EXPERIMENT AO138-11 .....	1607
Jean-Pierre Assié and Alfred Perotto	
MICROWELDING (OR COLD-WELDING) OF VARIOUS METALLIC MATERIALS UNDER THE ULTRA-VACUUM LDEF EXPERIMENT AO138-10 .....	1613
Jean Pierre Assié and Eric Condé	
 <b>SPACE ENVIRONMENTAL EFFECTS - BIOLOGY</b>	
SEEDS IN SPACE EXPERIMENT .....	1625
Jim A. Alston	
SPACE EXPOSED EXPERIMENT DEVELOPED FOR STUDENTS (SEEDS) (P0004-2) .....	1635
Doris K. Grigsby and Nelson J. Ehrlich	
SURVIVAL OF EPIPHYTIC BACTERIA FROM SEED STORED ON THE LONG DURATION EXPOSURE FACILITY (LDEF) .....	1637
Andrew C. Schuerger, Bret L. Norman and Joseph A. Angelo, Jr.	
FIRST BIOLOGICAL AND DOSIMETRIC RESULTS OF THE FREE FLYER BIOSTACK EXPERIMENT AO015 ON LDEF .....	1639
G. Reitz, H. Bucker, R. Facius, G. Horneck, M. Schäfer, J. U. Schott, J. Bayonove, R. Beaujean, E. V. Benton, M. Delpoux, C. Heilmann, W. Heinrich, A. R. Kranz, H. Planel, Y. Gasset, G. Gaubin, G. Portal, E. H. Gaul, W. Rüther, E. Schopper, C. A. Tobias and T. C. Yang	
PRELIMINARY TOTAL DOSE MEASUREMENTS ON LDEF .....	1643
G. Reitz	
TOTAL DOSE EFFECTS (TDE) OF HEAVY IONIZING RADIATION IN FUNGUS SPORES AND PLANT SEEDS - PRELIMINARY INVESTIGATIONS - .....	1651
A. R. Kranz, M. W. Zimmermann, R. Stadler, K. E. Gartenbach and M. Pickert	
PRELIMINARY RESULTS OF THE ARTEMIA SALINA EXPERIMENTS IN BIOSTACK ON LDEF .....	1661
E. H. Gaul, W. Rüther and C. O. Hiendl	
LONG-TERM EXPOSURE OF BACTERIAL SPORES TO SPACE .....	1667
G. Horneck, H. Bucker and G. Reitz	

## **SPACE ENVIRONMENTAL EFFECTS - MICROGRAVITY**

<b>RESULTS OF THE TTF-TCNQ AND THE CALCIUM CARBONATE CRYSTALLIZATION ON THE LONG DURATION EXPOSURE FACILITY .....</b>	<b>1675</b>
Kjeld Flemming Nielsen and M. David Lind	

## **THE FUTURE**

<b>THE ROLE OF THE LONG DURATION EXPOSURE FACILITY IN THE DEVELOPMENT OF SPACE SYSTEMS .....</b>	<b>1687</b>
Sally A. Little	

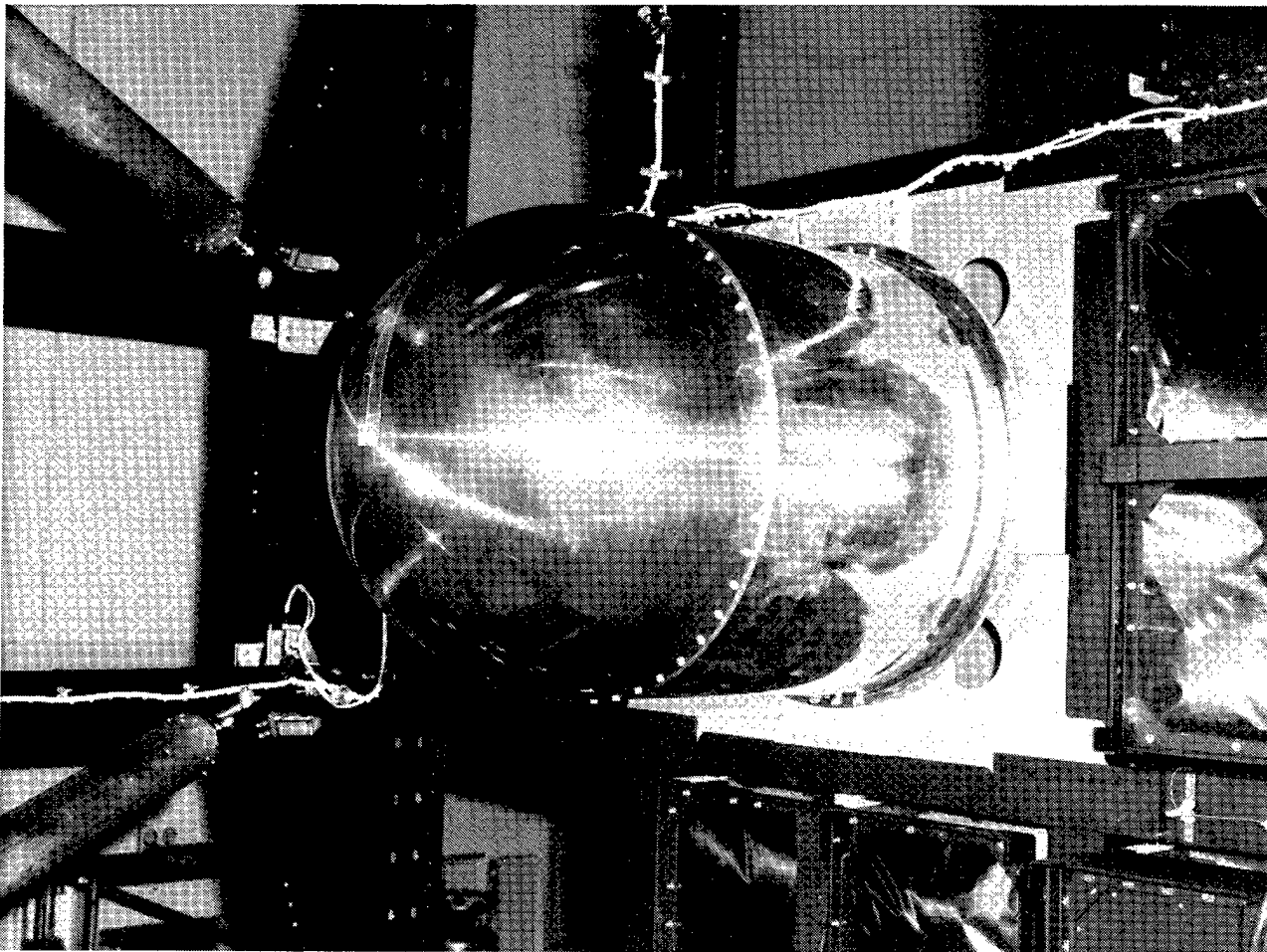
<b>RETRIEVABLE PAYLOAD CARRIER--NEXT GENERATION LONG DURATION EXPOSURE FACILITY .....</b>	<b>1691</b>
Arthur T. Perry	

<b>COLOR PHOTOGRAPHS .....</b>	<b>1701</b>
--------------------------------	-------------

<b>AUTHOR INDEX .....</b>	<b>1703</b>
---------------------------	-------------

## **PART 3**

### **SPACE ENVIRONMENTAL EFFECTS *SYSTEMS***



## SYSTEMS SPECIAL INVESTIGATION GROUP OVERVIEW

James B. Mason  
NASA Goddard Space Flight Center  
Greenbelt, MD 20771  
Phone: 301/286-6555, Fax: 301/286-4653

Harry Dursch  
Boeing Aerospace and Electronics  
Seattle, WA 98124  
Phone: 206/773-0527, Fax: 206/773-4946

Joel Edelman  
LDEF Newsletter  
Silver Spring, MD 20914  
Phone: 301/236-9311, Fax: 301/286-4653

### SUMMARY

The Systems Special Investigation Group (SIG) has undertaken investigations in the four major engineering disciplines represented by LDEF hardware: electrical, mechanical, thermal and optical systems. Testing was planned for the highest possible level of assembly, and top level system tests for nearly all systems have been performed at this time.

Testing to date has been performed on a mix of LDEF and individual experimenter systems. No electrical or mechanical system level failures attributed to the spaceflight environment have yet been detected by the Systems SIG. Some low cost electrical components were used successfully, although relays were a continuing problem. Extensive mechanical galling has been observed, but no evidence of coldwelding has yet been identified. A working index of observed systems anomalies has been created and will be used to support the tracking and resolution of these effects.

LDEF hardware currently available to the Systems SIG includes most of the LDEF facility systems hardware, and some significant experimenter hardware as well. A series of work packages has been developed for each of several subsystem types where further testing is of critical interest.

The Systems SIG is distributing a regular newsletter to the greater LDEF community in order to maintain coherence in an investigation which is widely scattered both in subject matter and in geography. Circulation of this informal document has quadrupled in its first year.

### INTRODUCTION

The Systems SIG was chartered to investigate the effects on systems of the nearly six years of exposure in the low earth orbit spaceflight environment on the Long Duration Exposure Facility (LDEF). The Systems SIG was also given the responsibility of coordinating the data from the analysis of both the LDEF systems and experiment systems into a single LDEF Systems Data Base.

The Systems SIG is chaired by Dr. James B. Mason at NASA Goddard Space Flight Center, and the SIG Committee includes members from eight NASA field centers, the Department of Defense, the European Space Agency, and the domestic commercial sector. The Systems SIG Committee has provided essential review and guidance for this investigation, and the role of the Committee will include review and assessment of the Systems SIG final report.

## BACKGROUND

Historically the Systems SIG has faced a particularly complex investigation, from the standpoint of diversity of hardware types to be evaluated in combination with several possible alternatives for the acquisition and test of specific hardware items. For logistical purposes the LDEF systems hardware was divided into three categories: LDEF Standalone, LDEF Shared, and Experimenter. The Standalone systems include that hardware which was provided by the LDEF Project and functioned in support of the LDEF as an integrated vehicle. The LDEF Shared systems include that hardware which was also provided by the LDEF project but which was distributed to individual experimenters and functioned independently in support of individual experiments. Experimenter systems included unique hardware support items developed independently by the individual experimenters for use only within the confines of their own experiments.

LDEF Standalone systems hardware included the LDEF structure, a viscous magnetic damper, Shuttle interface trunnions and grapple fixtures, and the Experiment Initiate System (EIS). LDEF Shared systems hardware included an Environment Exposure Control Canister (EECC) and a standard Experiment Power and Data System (EPDS) which was comprised of a Data Processor Control Assembly (DPCA), a Magnetic Tape Memory unit (MTM) and a lithium disulphide battery power source. Finally, Experimenter systems hardware encompassed a wide variety of systems, including optical calibrators, heat pipes, fiber optics, detectors, radiators, batteries, high voltage power supplies, exposure control mechanisms, charged surfaces, and more.

Each of the three groups of systems is of interest for a unique reason. The LDEF Standalone hardware represents the highest level of assembly and the broadest span of function of all of the systems on the LDEF mission. The LDEF Shared hardware is of particular interest because it was the only group of systems in which there were multiple examples of identical hardware, exposed to different aspects of the space flight environment or different operational histories. The Experimenter systems are of interest because of the tremendous diversity of hardware and system types.

## THE INVESTIGATION PROCESS

The initial effort for the Systems SIG was the identification of systems hardware on the LDEF and among the experiments that was pertinent to the Systems Investigation. The largest and easiest part of the process was hardware associated with the so-called "active" experiments, which were those with battery power and systems which were designed to perform some functions during the mission. These hardware items were generally more available to the Systems SIG as they were not originally an integral part of the experimental design, from a science standpoint. The harder part has been the identification of isolated passive components of systems interest, often included in an experiment package as experiment specimens or ancillary items.

Experimenter systems hardware included an enormous diversity of equipment. The management of this hardware was facilitated by the division of the Systems SIG scope into four

major disciplines: mechanical, electrical, thermal, and optical systems (fig. 1). This division has been carried through the program, from the development of test plans to the development of data analysis teams and the documentation of results.

In order to unify the investigation process, the Systems SIG developed a set of standardized test plans for each of these four major discipline areas represented in LDEF systems hardware. These plans included broad investigative guidelines for systems in their highest level of assembly, and specific test requirements for subsystems and components of particular interest.

The approach to the test program by the Systems SIG has always emphasized the testing of each system at its highest practicable level of assembly (fig. 2). The results of testing at this level provide pointers for further testing, in the form of anomalies, failures, deviations, or even nominal behavior. Anomalies, in conjunction with educated concerns about specific environmental effects that should be sought, provide a clear set of directions for subsequent testing of subsystems and failure or degradation analysis.

The process of developing systems data from the identified hardware of interest has, because of the diverse origins of the hardware, necessarily involved a diverse array of investigators, including experimenters, other SIGs, the LDEF Data Groups, and Systems SIG contractors. Thus test data and results of three types have been obtained by the Systems SIG; these types are distinguished by the distinct route through which they were obtained (fig. 3). The primary type has been from Boeing Aerospace and Electronics, the Systems SIG contractor for hardware testing; their test activities have been the most expedient because of the combination of direct access to hardware and direct funding of support personnel. A second type of data is labeled "Systems SIG inspired" test data and is comprised of results obtained by experimenters who have performed evaluations recommended by the Systems SIG. The final type of data which has become available to the Systems SIG is systems-related data developed by experimenters and other independent investigative groups in the course of their own investigations.

The culmination of the data gathering process is the dissemination of the results in meaningful form to those who need the information. To accomplish this, the Systems SIG has a three point plan. The first component is the documentation of the results in a comprehensive report. An interim report of this type has already been issued, and a final report is planned for December of 1991. A second component is an index to identify specific hardware items or types and which will provide pointers to help locate specific test results, relevant publications, available untested components, and cognizant investigators for further reference.

The third component in the Systems SIG data dissemination plan has been the distribution of a regular newsletter to the LDEF community at large. The purpose of this activity has been to provide the earliest possible updates on current activities and to attempt to retain some cohesiveness in an investigation which is widely scattered in terms of both geography and technological disciplines. The distribution of this newsletter has increased nearly four-fold (fig. 4), and the steady growth in its popularity has included every facet of the LDEF community - NASA employees, private contractors, university researchers, Department of Defense researchers, and international partners. Because of its impact on the community at large, the LDEF Science Office has assumed responsibility for the continuation of this activity.

## SYSTEMS SIG STATUS

At this time the Systems SIG has performed or supported high level system functional tests on all available systems; included are functional testing and inspection of the EIS and exercising of two of the EPDS units at the NASA Kennedy Space Center during the deintegration of the LDEF,

and numerous system functional tests on experimenter hardware conducted subsequently at experimenter facilities. Data on systems tests performed outside the auspices of the Systems SIG is currently being acquired.

The Systems SIG has acquired an extensive base of LDEF hardware in most of the systems categories defined above. A number of specific items have been extensively tested, including fasteners, wire harnessing, the end support beam, and a failed electronics package. The remaining hardware is in controlled storage and available for further evaluation.

A number of anomalies have been observed, one or more in virtually every system tested. It is noteworthy that at this time the great majority of these systems anomalies have been attributed to non-environmental causes, such as hardware selection processes, fabrication or assembly procedures, or preflight test inadequacies.

Systems SIG publications include the standardized Test Plan, the Interim Report, and numerous issues of the LDEF Spaceflight Environmental Effects Newsletter.

### SYSTEMS SIG FINDINGS

The Systems SIG findings at this point in time are based primarily on tests conducted on systems at the highest possible level of assembly. These tests have been conducted by the Systems SIG, by experimenters, and by other investigation groups.

No electrical or mechanical system failures have yet been detected which can be attributed to the low earth orbit spaceflight environment. Most of the tested systems worked well, and relatively few failures were noted. This is regarded as a successful demonstration of practical, low-cost space flight systems. The low earth orbit conditions will permit high-reliability long term use of such systems if properly designed, manufactured, integrated, tested, and shielded.

A variety of low cost electrical and electronic components were used successfully. The implication is that it may be possible to relax some requirements under benign conditions, providing proper testing, shielding, and redundancy are assured. This assertion is preliminary, pending further study, but this issue is critical in spaceflight design and should be addressed thoroughly.

Neither preliminary nor surprising is the conclusion that electromechanical relays are a continuing problem area in electronics design.

No evidence of coldwelding has been found, despite numerous reports of unexpected mechanical adhesion or interference. Difficulties in removing fasteners in a number of locations has been clearly determined to be a result of galling during preflight assembly. This galling was primarily the result of improper lubrication schemes. Other contributing causes were installation procedures, build-up of tolerances between a series of fasteners and the hardware being assembled, and preflight cleaning practices.

A separate concurrent study of the history of coldwelding in the spaceflight environment has reinforced the conclusion that coldwelding was not a factor in any of the LDEF mechanical anomalies.

The thermal systems aboard the LDEF, including several experiments, performed well by and large, with a few exceptions which are still under investigation at this time; these exceptions are believed to be unrelated to the spaceflight environment. The degradation of thermal surfaces



appears to be moderate at worst and largely a result of the infamous silicone-based contamination that characterizes the LDEF mission..

Although the contamination investigation is not a part of the Systems SIG charter, there are many systems issues that are directly related to contamination evidence. These include

- degradation of optical surfaces;
- drop in electrical potential of charged surfaces, speculated to be from periodic development of an ionized contamination cloud;
- drifting of conductive materials, including residual vapor deposited metallics from eroded polymer films, and minute particles from mechanical galling;
- decreased performance of thermal control surfaces;
- degraded solar cell performance due to contamination induced loss of transmittance through cover glasses;
- introduction of particles on mechanical surfaces which may initiate subsequent galling.

### PLANS AND RECOMMENDATIONS

The Systems SIG is essentially funded only through the end of Calendar 1991, and current plans are to emphasize the gathering and collating of externally generated data. The expectation is to publish a Final Report in December, 1991. At that time the Systems Index should also be completed and available to interested parties through the LDEF Science Office.

The Systems SIG will be unable to complete the investigation plan originally envisioned. Specifically, a large portion of the available systems hardware will not be tested. In order to develop and preserve the maximum possible amount of systems data from the LDEF mission, the Systems SIG has divided the remaining systems hardware into specific subsystem "work packages". These packages include the identification of specific hardware components of a given type available for test, and a list of recommended functional tests of particular interest to the Systems SIG. These work package descriptions are being distributed to all possible interested organizations in the hopes of identifying organizations with vested interest in the results of each of these potential sub-investigations.

Subsystems in which work packages have been developed include

- Mechanisms
- Lubricants
- Fasteners
- Electronic components and assemblies
- Motors
- Seals
- High voltage supplies

EXPER ID NO.	OTHR BATT	EPDS DPCA		MTM	EECC	ELEC	OPT	MECH	THER	COMMENTS
A 0038						•		•		PYRO CABLE CUTTER, FLIP UP MECH
A 0054						•				HIGH VOLTAGE EQUIP, COULOMBMETER
A 0076						•		•	•	VARIABLE CONDUCTANCE HT PIPES
A 0133						•		•		RADAR ANTENNA, SOLID STATE MEMORY
A 0138-8						•		•		FRECOPA
A 0139-A						•		•	•	SEALED CRYSTAL DEWERS
A 0180						•		•		SEALED CASSETTE RECORDER
A 0187-1						•		•		CLAM SHELL AND ELECTROMECHANISMS
A 0201		•	•			•				SUN SENSOR
M 0003		• •	• •	• •		•	•	•	•	ALL SYSTEMS TYPES
M 0004		•	•			•	•		•	FIBER OPTICS ELECTRONICS
M 0006					•		•			OPTICAL SURFACES
P 0003						•			•	THERMOCOUPLES, EXTENSIVE HARNESS
S 0010					•					EECC ACCESSIBLE AT LaRC
S 0014		•	•			•	•			PV CELLS, SUN SENSOR, RADIOMETER
S 0069	LiCF		•			•	•	•	•	CAROUSEL, OPT SYSTEM, THERMAL SYS
S 1001	NiCd	•	•			•	•		•	SOLAR ARRAY, POWER SYSTEM, HT PIPES
S 1002				•		•				SOLAR CELLS, QCM
S 1005	LiCF	•	•			•			•	HEAT PIPES
7 PASSIVE										MANUAL VALVES, SEALS

Figure 1. LDEF Experiment Systems

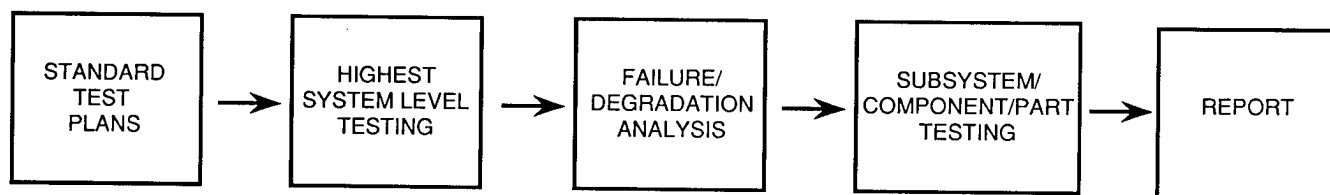


Figure 2. Systems SIG Investigation Approach

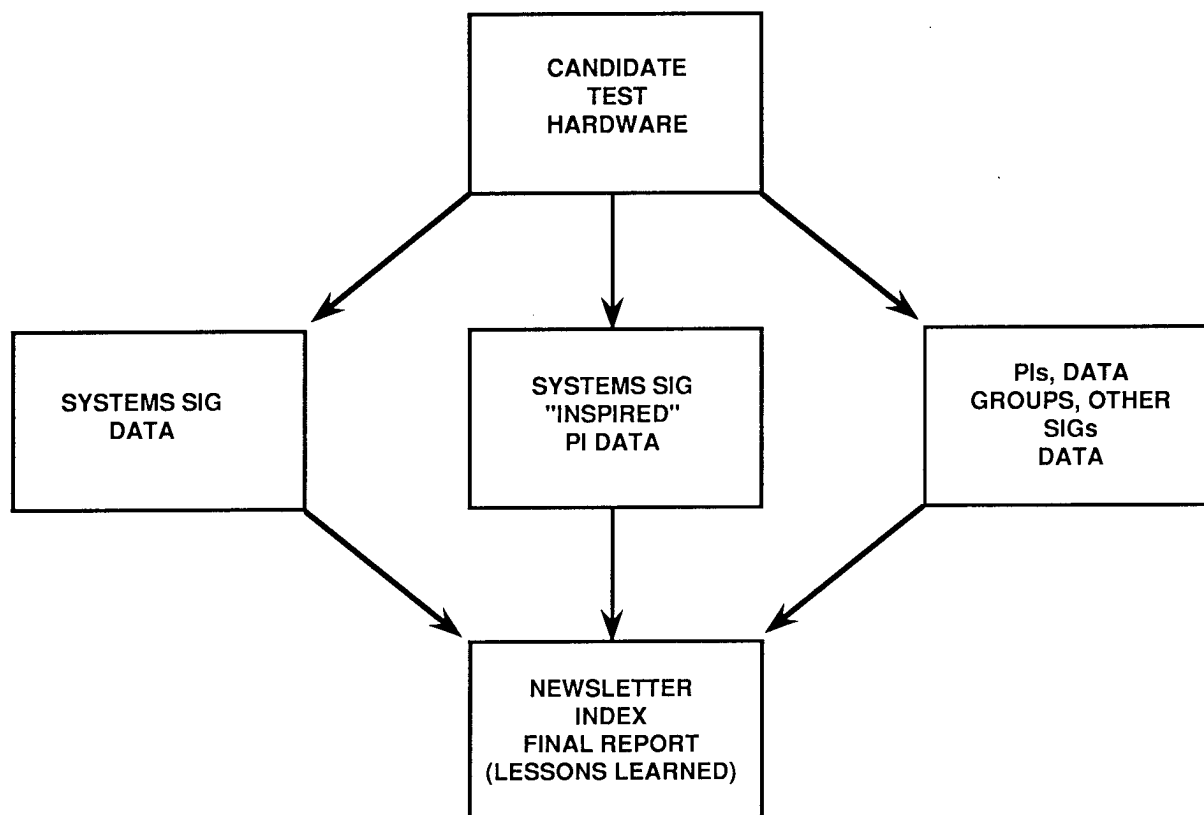


Figure 3. The Development of Systems Data

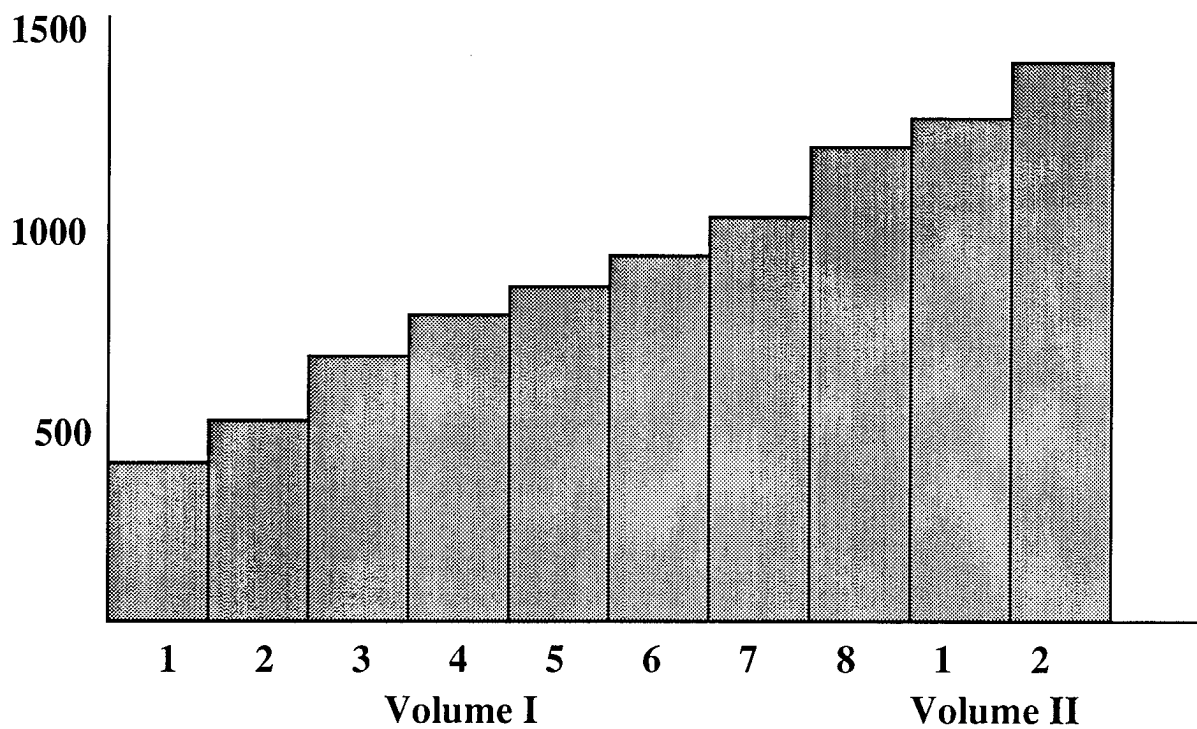


Figure 4. LDEF Newsletter Distribution History

## SPACE AGING OF SOLID ROCKET MATERIALS

Dean M. Lester, Leon L. Jones, R. B. Smalley, Jr.,

R. Neil Ord

Thiokol Corporation

Brigham City, Utah 84302-0707

### ABSTRACT

Solid rocket propellant and rocket motor components were aged in a vented container on the interior of the LDEF. This paper will present the results of aging IPSM-II/PAM-DII space motor components. Ballistic and mechanical properties of the space aged main propellant, igniter propellant, and ignition system were compared with similar data from preflight and ground aged samples. Mechanical properties of the composite materials and bonded joints used in the motor case, insulation, liner, nozzle, exit cone, and skirt were similarly evaluated. The space aging results will be compared to data collected in a ground based vacuum aging program on similar components. The operation of the vacuum actuated venting valve and pressure actuated resealing of the container will also be addressed.

The materials tested showed no significant changes due to space aging. These results indicate that properly designed solid rocket motors can be expected to perform reliably after extended periods of exposure to a space environment.

EFFECTS OF THE SPACE ENVIRONMENT ON  
SPACE-BASED RADAR PHASED-ARRAY ANTENNA;  
STATUS AND PRELIMINARY OBSERVATIONS  
(LDEF Experiment A0133)

J.B. Whiteside, D. Giangano, R.L. Heuer, E. Kamykowski,  
M. Kesselman, W.D. Rooney, R. Schulte, and M. Stauber

Grumman Corporate Research Center  
Bethpage, New York 11714  
Phone: (516) 575-2354; Fax: (516) 575-7716

### SUMMARY

The overall objective of Experiment A0133 was to evaluate the effect of the space environment on components considered for the Grumman Space-Based Radar (SBR) Phased-Array Antenna. Of primary interest was a study of the degradation of the polyimide film Kapton (DuPont trademark), the material considered for use in the antenna plane. The most striking result of the experiment was the overall good condition of the Kapton antenna planes and Kapton tensile specimens, despite nearly six years of exposure to the space environment. This was largely attributable to the orientation of the Kapton (parallel and flush on the space end) and the stability of the Long Duration Exposure Facility (LDEF) in orbit. However, weathering of exposed Kapton surfaces was not insignificant. Results on elongation and mechanical properties of the plain and the fiberglass-reinforced Kapton are presented. Stress-dependent permanent deformation and some reductions in strain to failure were observed. Reduction in strain to failure of flight-exposed Kapton is attributed to surface defects of these specimens. Physical property testing of the materials to date reveals no significant difference between flight-exposed and control material. The second objective was to investigate the interaction between high-voltage electrodes and typical spacecraft contaminants in simulation of discharge triggering across differentially charged dielectric surfaces (spacecraft charging conditions). Electronic data acquisition and memory systems appeared to operate correctly, but very few discharges were recorded. Induced radioactivity, contamination, impacts, and orientation features of atomic oxygen erosion were observed.

### INTRODUCTION

Large space structures of low areal density are being developed for applications such as phased-array antennae for SBR and the Earth Observation System (EOS). The practical implementation of these structures depends largely on identifying low-cost, low-density, high-strength-to-weight materials that are not degraded by the geosynchronous Earth orbit (GEO) or the LEO environments. Polymeric materials satisfy many of these requirements; however, the long-term stability of these materials exposed to the space environment is a major concern. This is because chemical bonds within polymers are susceptible to some degree of degradation from either ultraviolet or charged-particle (particularly high-energy electron) components of the space environment. Atomic oxygen erosion is not a major concern in the SBR application environment, but it certainly becomes an issue at the lower altitudes flown by LDEF.

The primary objective of Experiment A0133 was to determine the nature and the extent of degradation that materials chosen for Grumman's SBR suffered during prolonged exposure to the LEO space environment. The principal material studied in this report is DuPont's Kapton H polyimide, poly(N,N'-(p,p'-oxidiphenylene) pyromellitimide), which was selected as a baseline material to be used in

the phased-array antenna plane. The tray housing this experiment was located at the space end of the LDEF satellite (bay H, row 7). A photograph of the experiment tray, taken prior to its integration into the LDEF satellite, is shown in figure 1. Roughly one-half of the area was occupied by tension assemblies containing panels of Kapton and glass/Kapton maintained at one of four stress levels. It was of interest to determine the mechanical integrity, dimensional stability, and extent of physical property degradation these panels suffered from long-duration exposure to the space environment. The remainder of the tray contained a portion of the SBR antenna plane and active electronic components. The electronic components included a high-voltage power supply, timing control circuitry, and a memory system. This part of the experiment was designed to investigate discharge triggering across high-voltage electrodes, and determine the effects of the subsequent high-voltage discharge events on the Kapton of the antenna plane.

## MATERIALS AND METHODS

Polyimide sheets were obtained from DuPont (Kapton, DuPont Co., Wilmington, DE). 75- $\mu\text{m}$ -thick material was used to construct a polyimide/glass scrim/polyimide reinforced structure. The glass scrim was bonded to the polyimide film using a thermoplastic polyester adhesive (T100, Sheldahl). Since the proposed antennae are large, e.g., 20 m x 60 m, and the Kapton is provided in 1-m-wide rolls, the antenna plane must be fabricated with splices. Accordingly, each specimen contained a central splice region approximately 2 cm long. Sheets of plain Kapton (127  $\mu\text{m}$  thick) and glass/Kapton (196  $\mu\text{m}$  thick) were cut into panels with widths of either 2.54 or 1.27 cm and lengths of about 50 cm. The tension module (shown in figure 1) contained eight 2.54-cm-wide specimens and sixteen 1.27-cm-wide specimens exposed directly to the space environment and a like number of "shadowed," or flight control, specimens. The shadowed specimens experienced limited thermal excursions, were exposed to a minimum of solar and charged particle radiation, and were protected from direct atomic oxygen and micrometeoroid and debris impact. Four stress levels, 0.31, 1.03, 2.07, and 3.10 MPa (45, 150, 300, and 450 psi), were selected, based on anticipated SBR antenna plane average sustained and peak local stresses. The maximum stress was selected to accelerate the extent of creep. Stress levels were maintained by springs of known force constant. The Kapton and glass/Kapton sheets from which these panels were cut were stored under ambient conditions. This material was used as the source of ground-based control specimens.

*Tensile Tests.* Selected panels of plain and reinforced Kapton, with representatives from each stress level, were removed from the flight tension assembly. Two 8.64-cm-long sections were cut from either side of the splice from these panels. A cutting fixture and a single-edge razor were used to produce uniform 0.50-cm-wide strips. The edges cut in this manner were free of defects that could lead to premature failure during mechanical testing. The leading and the trailing edges were trimmed from the 1.27-cm-wide panels, and none of the strips cut from these panels contained an original edge. From the 2.54-cm-wide flight panels strips were cut that contained the original leading or trailing edge. These strips were retained for mechanical testing and carried the designations LE and TE for leading edge and trailing edge, respectively. The remaining material from the 2.54-cm-wide panel was sufficient for an additional six strips, all of which had freshly cut edges. Thus, each 1.27-cm-wide panel provided four strips for mechanical testing, and each 2.54 cm-wide panel provided ten strips. The laboratory temperature ranged from 22 to 25°C and the relative humidity ranged from 31 to 47% during the period of testing.

The tensile tests were conducted using an Instron Model TT-B Universal Test Machine. Test specimens were secured using pneumatically actuated grips with smooth jaws operating at a pressure of  $6.4 \times 10^5$  Pa (90 psi). Grip jaws were cleaned periodically with a fine grit abrasive cloth to prevent specimen slippage. The initial distance between grips was 4.06 cm, and this value was used as the gage length. A crosshead speed of 0.254 cm/minute was used for all tests. Analog and digital data were collected simultaneously. Data were stored on an IBM PC-AT for subsequent analysis. The crosshead displacement was used to estimate strain. Average values of specimen dimensions were used for property calculations.

*Creep Tests.* In order to provide a discrete reference for elongation measurements, three 0.5-mm-diameter holes were precisely located along each specimen centerline, the first two holes being 2.54 cm apart with the splice region between them. The third hole was located 8.26 cm away from one hole and 10.80 cm from the other. After the specimens were loaded in the tension module (see figure 1), contact photographs were made on glass plates to provide a record of the hole spacing before flight. The original intent was to make a similar set of post-flight contact plates that was to be compared with the pre-flight set to determine the permanent elongation under load. Instead, post-flight measurements were made, using a non-contacting precision traveling microscope. This method was preferred since it would better preserve surface erosion features.

*High-Voltage Discharges.* Electrodes were formed from knife-edge cuts in copper dipole elements bonded to the glass/Kapton antenna plane. Discharge events at the four electrodes (two each at either 1.5 or 3.0 kV) were counted during 20-minute blocks of time and then transferred sequentially to a non-volatile memory location. A timer-sequencer was designed to delay the application of high voltage until day 32 (to allow for satellite outgassing), to power up the memory system every 20 minutes for 0.6 second, and to shut the high voltage down on day 243 (or upon retrieval, in case retrieval took place first).

*Energy Dispersive Spectroscopy.* Energy dispersive spectroscopy (EDS) was used to identify contaminants on the surface of flight specimens and surrounding areas. The 20-kV electron beam of an Amray Model 1810 scanning electron microscope (SEM) was used to excite fluorescence of surface elements. Fluorescence was collected using a SiLi detector interfaced to a Tracor-Northern spectrometer. This spectrometer could not detect elements with atomic numbers less than that of fluorine ( $Z=9$ ). Spectra were processed using a semi-quantitative subroutine supplied by Tracor-Northern.

*Induced Radioactivity Measurements.* An unshielded, high-purity germanium (HPGe) detector with active volume of  $64\text{ cm}^3$  and relative efficiency of 14% (1.33 MeV) was used to acquire 4096 channel gamma spectra. Energy calibration data were obtained using  $^{137}\text{Cs}$  (662 keV) and  $^{60}\text{Co}$  (1322 KeV) isotopic sources and from the annihilation (511 keV) and  $^{40}\text{K}$  (1460 keV) background gamma ray lines in the measured spectra. In order to isolate a specific section of the package, the detector was positioned 1.27 cm directly in front of a vertical array of tension assembly rollers that provided support for the tension panels. Each roller was a cylinder made from 6160 alloy (97.9% aluminum) with a radius of 2.45 cm. The rollers were oriented in such a way that the detector viewed the sides of the cylinders. A measurement was made for 16 hours and was followed immediately by a background run of similar duration.

*Infrared Spectroscopy.* Transmission spectra were obtained from 125- $\mu\text{m}$ -thick films, using a Mattson Fourier transform infrared (FTIR) spectrometer. The FTIR spectra were acquired at a resolution of  $4\text{ cm}^{-1}$  over the energy range of 400 to  $4000\text{ cm}^{-1}$ . The spectra were acquired after flushing the sample chamber with dry air for at least twenty minutes. Infrared spectra of the background atmosphere were collected under identical conditions and have been subtracted from all spectra. Transmission FTIR spectra also were obtained from the brown residue found on the ram-facing surface of the trailing side of the aluminum tray downstream of the tensile panels. This residue was removed from the aluminum surface with a single edge razor and mounted on an IR fixture with double-sided tape.

*Mass Loss.* The mass and the overall dimensions of sections selected for mechanical tests were accurately determined prior to the final cutting. Mass was normalized for dimensions of length and width, and a comparison was made between the flight-exposed and the flight control specimens. The mass deficits of the space-exposed sections were used to estimate surface erosion.

*Profilometry.* Surface roughness was determined using a Tencor Instruments profilometer. The polyimide film was secured to the surface of a polished (to 1  $\mu\text{m}$  diamond) aluminum plate using low viscosity adhesive (Loctite 430). The polyimide surface was scanned over a distance of 200  $\mu\text{m}$  with a stylus mass of 9 mg. Reported surface roughness values represent the average of five measurements.

*Scanning Electron Microscopy*. An Amray Model 1810 SEM, operating at 10 kV, was used to determine surface morphology of flight specimens. All polyimide films examined in the SEM were first sputtered with gold to a thickness of about 100 Å.

## RESULTS

Measurement of the induced activity of the materials of the experimental package was initiated on 4 April 1990. Preliminary survey measurements of short duration (30 minutes) at various points along the facing plane of the experimental package gave little indication of discernible gamma emissions above background levels. A spectrum obtained from the tension assembly roller contains a gamma ray line at 1274 keV, which does not appear in the background spectrum. Gammas of this energy are from the decay of  $^{22}\text{Na}$ , which are produced by activation of  $^{27}\text{Al}$ . No other significant features were noted in the gamma spectrum that spanned the energy range from 100 keV to 3 MeV.

The Meteoroid & Debris Special Investigation Group reported 206 visible features on the experiment tray and experiment surfaces, (ref. 1). Figure 2 illustrates an impact feature in a 1.27-cm-wide glass/Kapton strip. Delamination damage extends several diameters around the penetration site, typical of impact events in a bonded structure. For comparison, a reference hole machined in the strip before flight also is visible in figure 2. Figure 3 illustrates an impact site that removed a ligament between holes in the perforated aluminum ground plane. What appears to be collateral damage also is visible in figure 3 on the adjacent bonded aluminum foil doubler that supports one of the ceramic electronics modules.

Two striking manifestations of contamination appeared throughout visual inspection of the experiment tray: fine shiny particles clinging to the Kapton and brownish staining of many light-colored surfaces. The particles were probably metal from degraded thermal insulation systems elsewhere on LDEF, but so far we have done no analysis to confirm this. Such particles were clearly present as airborne debris during deintegration of the experiment tray from LDEF.

Brown stains were seen on unpainted aluminum surfaces of the tray, typically in locations that were exposed to direct sunlight and ram plasma. Distinct shadowing patterns could be observed where adjacent upstream parts interfered with the ram and/or the sunlight. The EDS spectrum (not shown) indicates the presence of only silicon; however, elements lighter than fluorine cannot be detected with our spectrometer. The infrared spectrum of the brown contaminant is presented in figure 4. A mottled pattern of brown staining was observed on the white-painted ceramic electronics modules of the antenna ground plane (see figure 3). Here, the complicated geometry of the antenna plane and dipole drop lines above the ground plane may have contributed to a complex, less distinct pattern of staining. Several surface particles noticed on flight Kapton specimens during SEM examinations also were determined to be predominantly silicon.

The upper surfaces of the space-exposed Kapton panels suffered significant weathering, as is evident by the diffuse appearance of these surfaces. This is in contrast to the flight control Kapton specimens that had a specular appearance (see figure 5). Regions of space-exposed Kapton that were situated behind an object that obstructed the ram flow retained their original specular appearance. Kapton surfaces in regions located directly behind the lip of tension assembly rollers retained a specular appearance very similar to control panels, as can be seen in figure 5. The diffuse appearance of space-exposed Kapton is likely the result of surface erosion by the atomic/molecular fluence. The SEM photomicrograph of figure 6a shows a region of the leading edge of a space-exposed reinforced Kapton panel that was shielded from the atomic and molecular ram flow. The sandwich structure of the glass/Kapton and the reasonably good condition of this surface are clearly evident in the photograph. Figure 6b shows an SEM photomicrograph obtained from a region just a few centimeters removed from the region of figure 6a; the only difference is that this region experienced direct normal exposure to the ram flow. This region shows significant surface erosion and cratering, as compared to shielded regions. Figures 6c and 6d show oblique views (photographs obtained with a 20 degree stage tilt) of the leading edge for shielded and direct ram exposure,



respectively. The SEM photomicrograph displayed in figure 6f shows the typical triangular erosion pattern observed for Kapton exposed to low-angle-of-incidence ram flow (ref. 2). The triangular erosion patterns point in the direction of the satellite's velocity vector. A photomicrograph of a shielded region on the same panel and obtained under the same conditions as the photograph in figure 6f shows no such erosion; this is evident from casual inspection of figure 6e.

The surface roughness of the flight-space-exposed specimen was significantly greater than for either flight or ground control specimens. The values (average  $\pm$  standard deviation;  $n=5$ ) obtained from profilometry were  $287 \pm 35$  nm,  $72 \pm 32$  nm, and  $62 \pm 15$  nm for flight space, flight control, and ground control specimens, respectively. The surface erosion suffered by the polyimide exposed to the space environment is estimated to be  $8.0 \pm 1.4$   $\mu$ m (average  $\pm$  standard deviation,  $n=6$ ) from mass loss data. Unfortunately, neither SEM nor profilometry has been able to provide reasonable estimates of surface erosion for the the samples we have examined to date. The near parallel grazing incidence of the atomic/molecular flux appears to have eliminated surface contaminant features that might have been used to estimate erosion depth using SEM.

Figure 7 shows the creep elongation measured in the plain Kapton and the glass/Kapton. The creep strains for the plain Kapton are slightly higher and somewhat more stress dependent than the glass/Kapton. There was little or no significant difference in creep between the flight space specimens and the flight controls. Results from the splice sections have not yet been evaluated.

Representative stress-strain curves for the Kapton and the reinforced Kapton strips are shown in figure 8. The reinforced Kapton shows a yield point after which stress increases slowly with strain. This is in contrast to the plain Kapton strips which do not show yield points. The ultimate strength and elongation at break of the polyimide films as determined from tensile tests are presented in figure 9. The error bars indicate standard deviations.

The infrared spectra, x-ray diffraction (XRD) patterns, and differential scanning calorimetry (DSC) thermal traces of flight space exposed, flight control, and ground control specimens showed no significant differences and are not shown.

Very few discharge events were recorded during the active experiment time. The numbers and times of events are included in table I. One event was recorded for gap-A of the 3-kV experiment, and none for gap-B of the 3-kV experiment. Five events were recorded for gap-A of the 1.5-kV experiment, and six events for gap-B of the 1.5-kV experiment (two at each of three sample times). Although sparse, counts appear for three out of the four gaps. These data indicate low counts, which are consistent with data in other cells of zero counts. Thus, a single-event upset in these few cells, although possible, is unlikely.

## DISCUSSION

The most striking difference between flight-exposed and control Kapton surfaces is the severe weathered appearance evident on exposed surfaces. This weathering has previously been observed on short-duration exposures of organic films during Shuttle flights (ref. 3), and has been attributed to the impact of atmospheric constituents of high relative velocity in the fixed reference frame of the satellite (ref. 3 and ref. 4). The primary constituent of the atmosphere at altitudes between 200 and 600 km is atomic oxygen (ref. 5). The kinetic energy of the 8 km/sec atomic oxygen fluence is approximately 5 eV, and is sufficient to rupture chemical bonds within the molecular structure of the polyimide film. Continued bombardment by atomic oxygen can lead to significant erosion of organic surfaces. We estimate that the surface erosion of the flight exposed Kapton during the 2106 days in orbit is  $8.0 \pm 1.4$   $\mu$ m. The erosion yield for Kapton in the 8 km/sec fluence has been reported to be  $3.0 \times 10^{-24}$  cm<sup>3</sup>/atom (ref. 5). From these values, we estimate the fluence to be  $3.0 \pm 0.5 \times 10^{20}$  atoms/cm<sup>2</sup>, which is in reasonable agreement with the reported fluence at the space end of the LDEF satellite of  $3.64 \times 10^{20}$  atoms/cm<sup>2</sup> (ref. 6). Interpolating

the reported fluence of ref. 6 to account for the  $1.1 \pm 0.4$  degrees forward pitch (ref. 7) indicates a fluence of  $4.5 \pm 0.3 \times 10^{20}$  atoms/cm<sup>2</sup> on the space-facing surfaces. Although the surface erosion estimates seem reasonable, the limitations associated with the comparative mass loss technique do not escape us, and we are working to establish more quantitative measurements.

Creep deformations experienced by the Kapton were slightly above those estimated from time extrapolation of short-term, room temperature, and ground tests. The space environment appeared to have little or no detrimental effect on the creep behavior of the Kapton or glass/Kapton.

The mechanical properties of the flight Kapton were, in general, no different from those of ground-based controls. Space-exposed specimens typically showed reductions in ultimate stress and elongation compared to controls; however, in most cases differences were not significant. The reductions are thought to be the result of a higher incidence of surface defects associated with the exposed specimens, although these differences could also be explained by increased exposure to a high-radiation environment (ref. 8 and ref. 9). However, a large percentage of the space exposed specimens failed quite early during mechanical tests. Thus, although the average values of mechanical properties of the space exposed specimens are less than those of the controls, the associated standard deviations are large, and in most instances no statistical significance could be established. Specimens that contained an original leading edge showed a reduction in mechanical integrity, with an ultimate elongation that was about 30% of control values. These specimens were eroded not only on the upper surface, but also at the leading edge. In contrast, the properties determined for space-exposed specimens containing the trailing edge were quite similar to specimens taken from the middle regions. The fact that many space-exposed specimens displayed a mechanical integrity equal to that of the control specimens supports the argument that surface defects cause these reductions.

No significant differences between flight-space-exposed, flight control, and ground control have been detected using DSC, transmission FTIR, or XRD. This is perhaps not surprising since these techniques measure bulk properties, and it is likely that the greatest change in material properties will be localized to the surface regions of space-exposed specimens. Although these surface regions were exposed to the space environment for nearly six years, the erosion process continually refreshed the surface, which maintains a steady state composition, and gross changes in chemical properties due to the atomic/molecular fluence are likely to be small. In fact, even ESCA studies (ref. 10) of Kapton film exposed to LEO showed very little difference from control specimens. This is in contrast to Kapton etched in an Earth-based oxygen reactor, which did show significant differences (ref. 10).

The EDS spectrum of the brown residue indicates silicon as the primary elemental constituent. Elements lighter than fluorine could not be detected with our energy-dispersive spectrometer. However, EDS spectra of a similar brown residue recovered from other locations on the LDEF satellite shows that carbon and oxygen also are present (ref. 11). The peaks in the FTIR spectrum at  $2900\text{--}3000\text{ cm}^{-1}$  (perhaps a C-H stretch) suggest the presence of aliphatic groups within this residue. This residue is thought to result from the condensation of outgassed silicon and organic products on cold surfaces followed by ultraviolet catalyzed polymerization (ref. 11).

The experiment timer-sequencer apparently functioned perfectly. It powered up the experiment on day 32 and powered it down on day 243. This is corroborated by the block of ones in the appropriate memory cells. There is no evidence of any single-event upsets in these cells. There was no charring of the Kapton or other damage visible at the gaps, but close examination awaits disassembly of the antenna plane, following performance testing of the antenna, which is still in progress.

The high-voltage experiment was designed specifically to record discharges initiated across spark gaps by environmental interactions, e.g., contaminant transport and/or coupling to the space plasma. Specific analyses of the four spark gaps formed (by severing of dipole elements) on the antenna section will be performed after completion of radiometric tests. These analyses will include studies of the quantitative conditions under which discharges are triggered and of the extent to which these conditions were realized in the LDEF environment. Measurements in progress of LDEF-environment-exposed, flight control, and

ground control Kapton surfaces\* suggest that the surface conductivity increase, resulting from exposure to a space plasma accelerated by high voltage, was not sufficient to produce significant leakage current between the electrodes and thus did not affect the discharge triggering.

## CONCLUSIONS

The most important environmental factor was the atomic oxygen erosion experienced at low altitudes. The survivability of the Kapton is largely attributable to the stability of LDEF and the orientation, close to one degree grazing incidence. This extreme orientation produced surface and leading-edge erosion and some interesting surface features. The surface recession was estimated to be 8  $\mu\text{m}$ .

The mechanical properties of the Kapton and the glass/Kapton experienced only slight degradation except for specimens taken from areas containing eroded edges. The eroded edges had significant effects on tensile strength and strain to failure.

The active circuitry to control the high-voltage discharge experiment and record the number and time of electrostatic discharges apparently functioned as intended, although full systems functional tests have not been accomplished. The memory locations reserved for diagnostics were unchanged. Few discharges, one at 3 kV and 11 at 1.5 kV, were recorded.

The experiment demonstrated the functionality and the durability of the Kapton antenna plane materials and other materials and systems on board A0133.

## ACKNOWLEDGMENTS

Dr. Richard DeIasi directed the design and integration of experiment A0133. Mechanical tests were performed by Robert Schwarz. The late Martin Rossi designed the high-voltage discharge experiment. Dr. Philip Young of NASA Langley Research Center performed independent tests and provided many useful discussions. Dr. Bruce Banks of NASA Lewis Research Center inspected the experiment and provided his insight. Dr. Stephen Walters and Dr. Michael Duck of UKAEA/Harwell provided in-progress results on surface conductivity. This project was supported by the Grumman Corporate Research Center Independent Research & Development Program.

## REFERENCES

1. See, T.; Allbrooks, M.; Atkinson, D.; Simon, C.; and Zolensky, M.: Meteoroid and Debris Impact Features Documented on the Long Duration Exposure Facility; A Preliminary Report. NASA Johnson Space Center Report 24608-84, Aug. 1990.
2. Tennyson, R.C.; Mabson, G.E.; Morison, W.D.; and Kleiman, J.: LDEF Mission Update: Composites in Space. Advanced Materials and Processes. May 1991, pp. 33-36.
3. Smith, K.A.: Evaluation of Oxygen Interaction with Materials: STS-8 Atomic Oxygens Effects. AIAA #85-7021, 1985, pp. 190-197.

---

\*Walters, W. S.; and Duck, M. J.: AEA Technology/Reactor Chemistry Dept., Harwell Laboratory, Oxfordshire, OX11 0RA, U. K., (Private Communication), 1991.

4. Leger, L.J.; and Visentine, J.T.: Protecting Spacecraft from Atomic Oxygen. Aerospace America, July, 1986, pp. 32-35.
5. Banks, B.A.; Rutledge, S.K.; Auer, B.M.; and DiFilippo, F.: Atomic Oxygen Undercutting of Defects on SiO<sub>2</sub> Protected Polyimide Solar Array Blankets. Materials Degradation in LEO, Eds V. Srinivan and B.A. Banks, The Minerals, Metals, and Materials Society, Warrendale PA, 1990, pp. 15-34.
6. Bourassa, R.J.; and Gillis, J.R.: LDEF Atomic Oxygen Flux and Fluence Calculations; LDEF Materials Data Analysis. NAS1-18224 Task 12, Boeing, January 18, 1991.
7. Gregory, J. C.; and Peters, P. N.: LDEF Attitude Measurement Using a Pinhole Camera with a Silver/Oxygen Atom Detector. First LDEF Post-Retrieval Symposium, NASA CP-3134, 1992.
8. Sasuga, T.; Hayakawa, N.; Yoshida, K.; and Hagiwara, M.: Degradation in Tensile Properties of Aromatic Polymers by Electron Beam Irradiation. Polymer, vol. 26, 1985, pp. 1039-1045.
9. Funk, J.G.; and Sykes, G.F.: Space Radiation Effects on Poly[Aryl-Ether-Ketone] Thin Films and Composites. SAMPE Quarterly, vol. 19, 1988, pp. 19-36.
10. Golub, M.A.; Wydeven, T.; and Cormia, R.D.: ESCA Study of Kapton Exposed to Atomic Oxygen in Low Earth Orbit or Downstream from a Radio-Frequency Oxygen Plasma. Polymer Communications, vol. 29, 1988, pp. 285-288.
11. Stein, B.A.: Preliminary Report on LDEF Related Contaminants. LDEF Materials Special Investigation Group, August 1990.

TABLE I.- HIGH-VOLTAGE DISCHARGE EVENTS RECORDED IN EXPERIMENT MEMORY

<u>HOUR</u>	<u>COMMENT</u>	<u>3 kV COUNTS</u>		<u>1.5 kV COUNTS</u>	
		<u>GAP-B</u>	<u>GAP-A</u>	<u>GAP-B</u>	<u>GAP-A</u>
768.0	Exp. On				
1642.0		0	1	0	0
2069.6		0	0	0	1
2076.0		0	0	0	1
2114.0		0	0	2	0
2138.6		0	0	2	0
2143.0		0	0	2	0
2155.0		0	0	0	1
2161.3		0	0	0	1
3330.3		0	0	0	1
5832.0					
	Exp. Off				

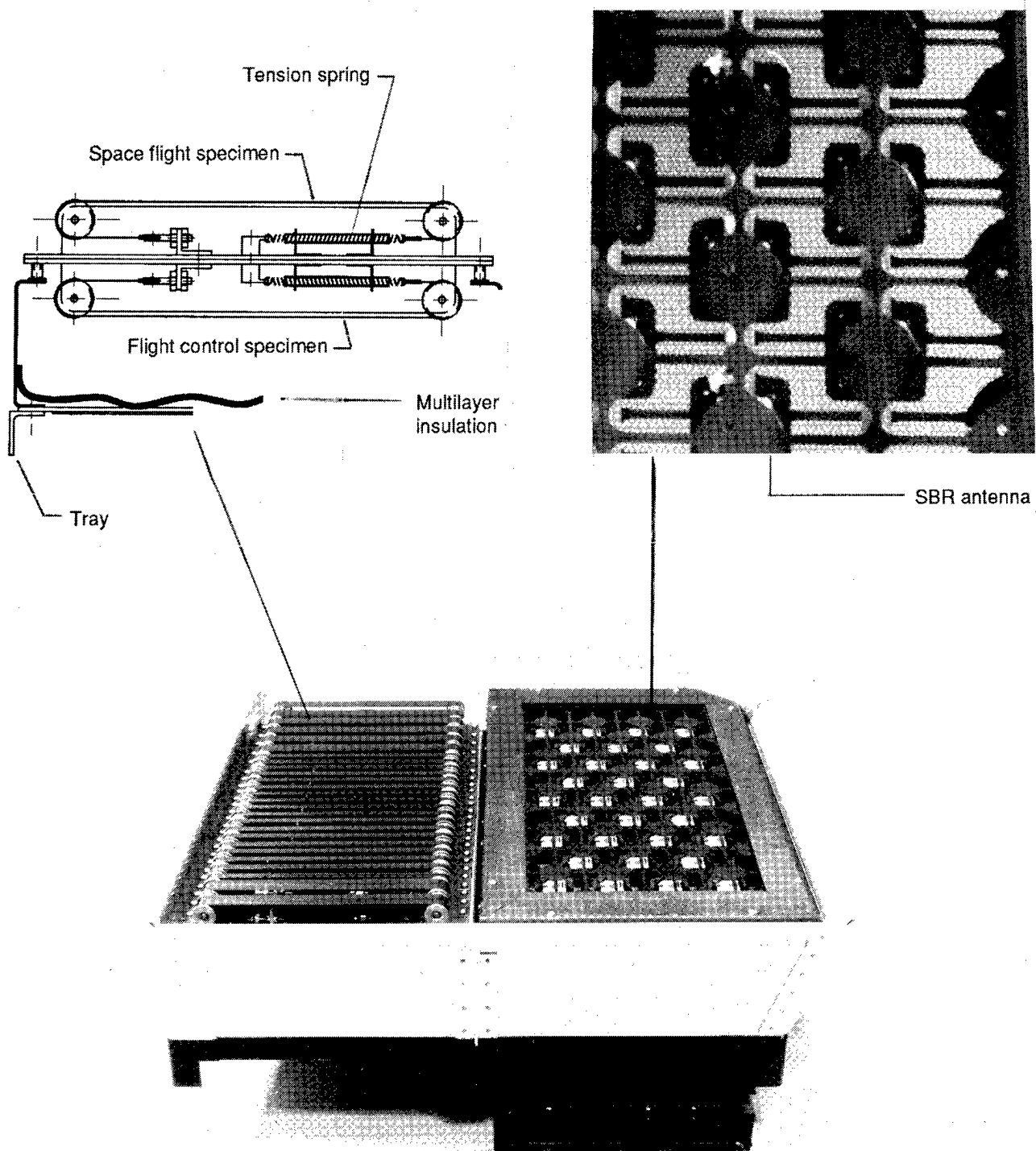


Figure 1. Space-based radar phased-array antenna experiment.

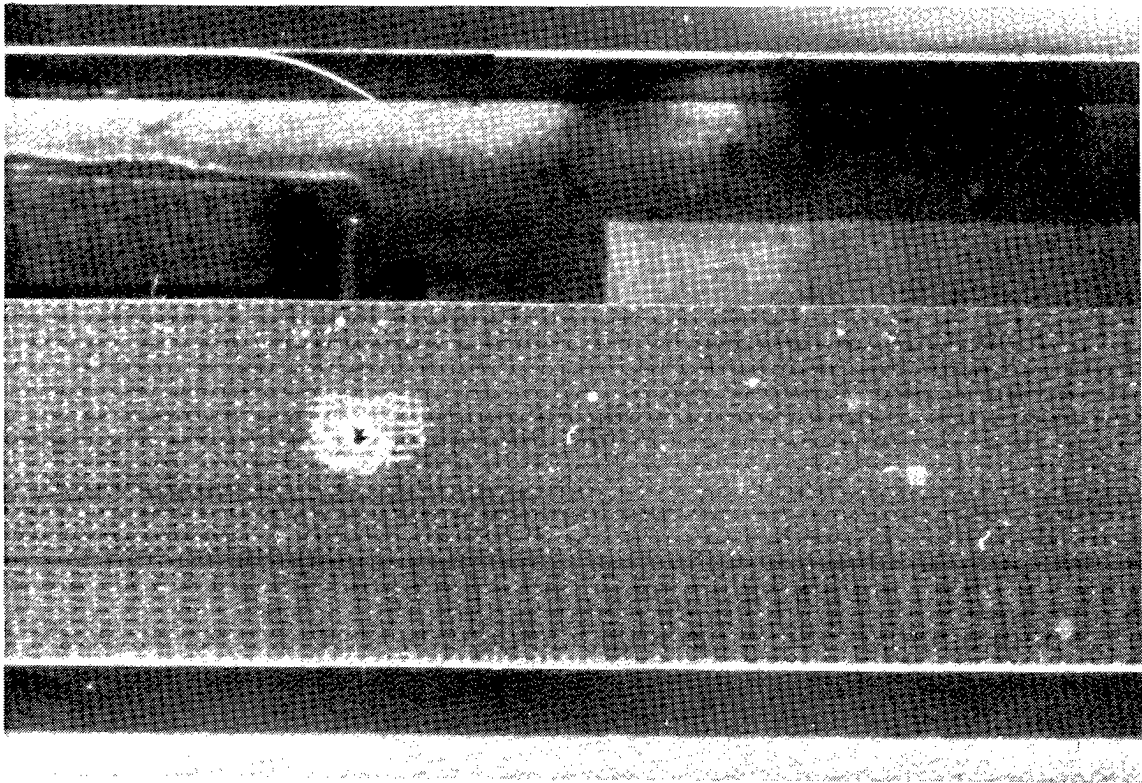


Figure 2. Impact site in glass/Kapton specimen.

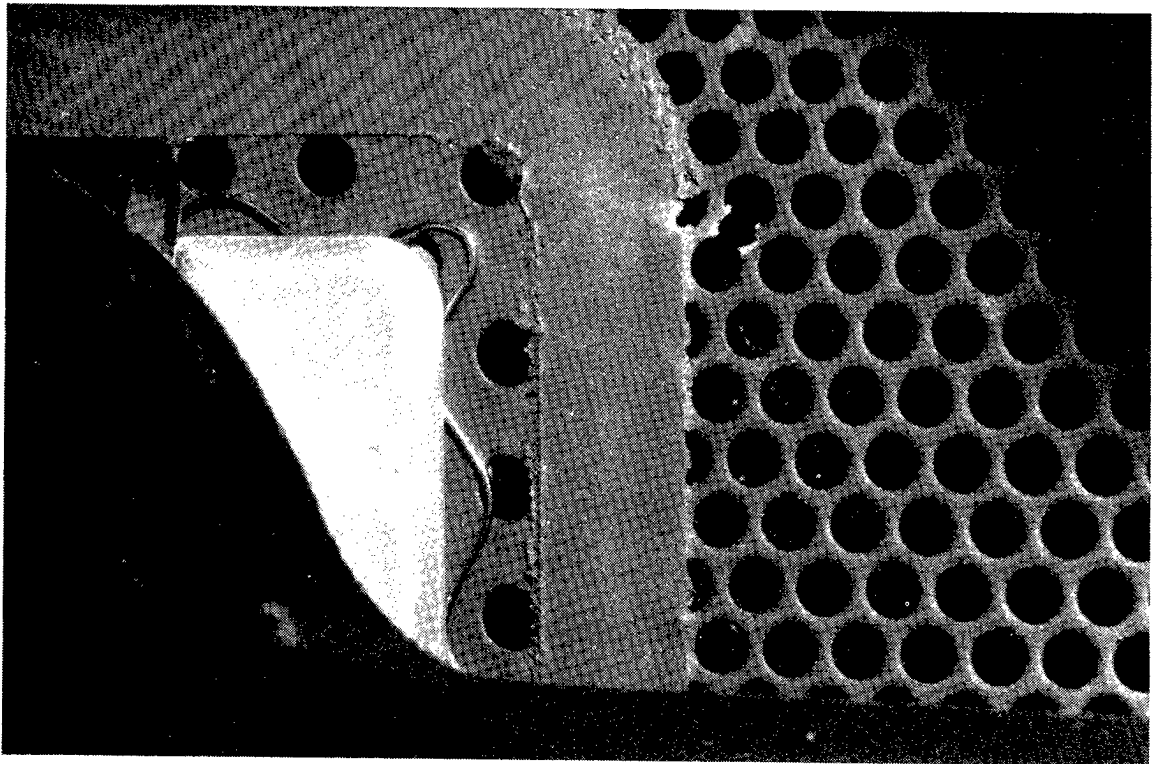


Figure 3. Impact site in perforated aluminum ground plane.

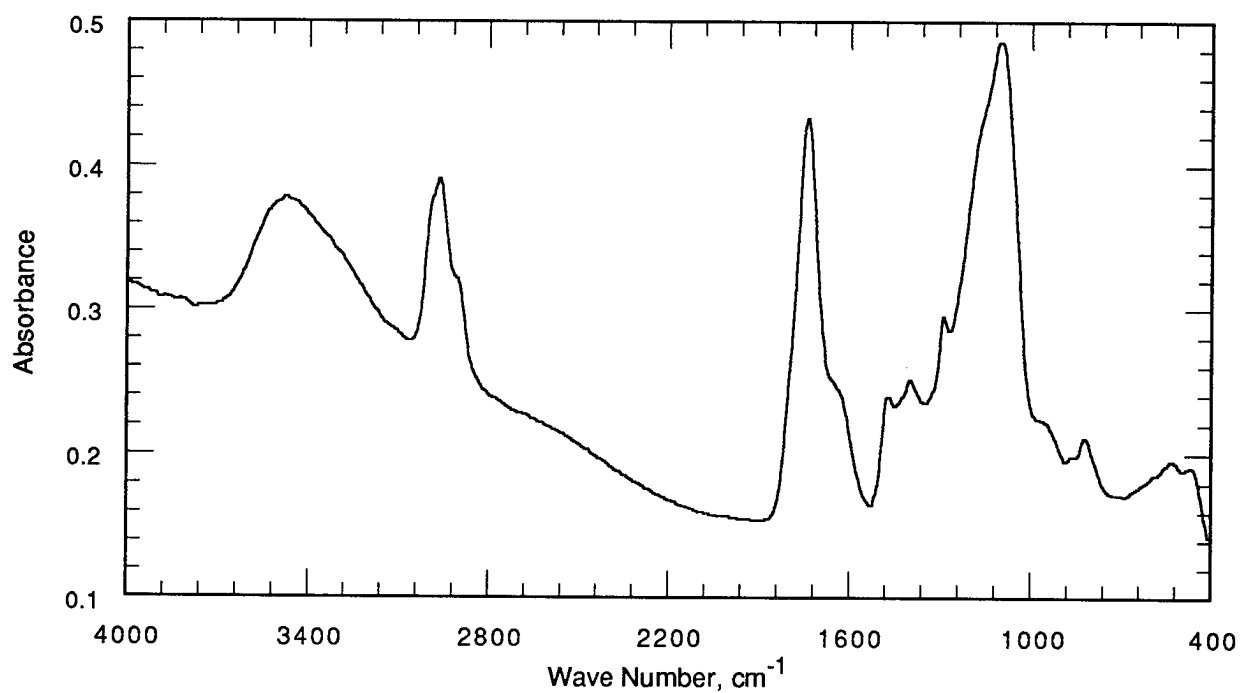


Figure 4. Transmission FTIR of brown contaminant from tray

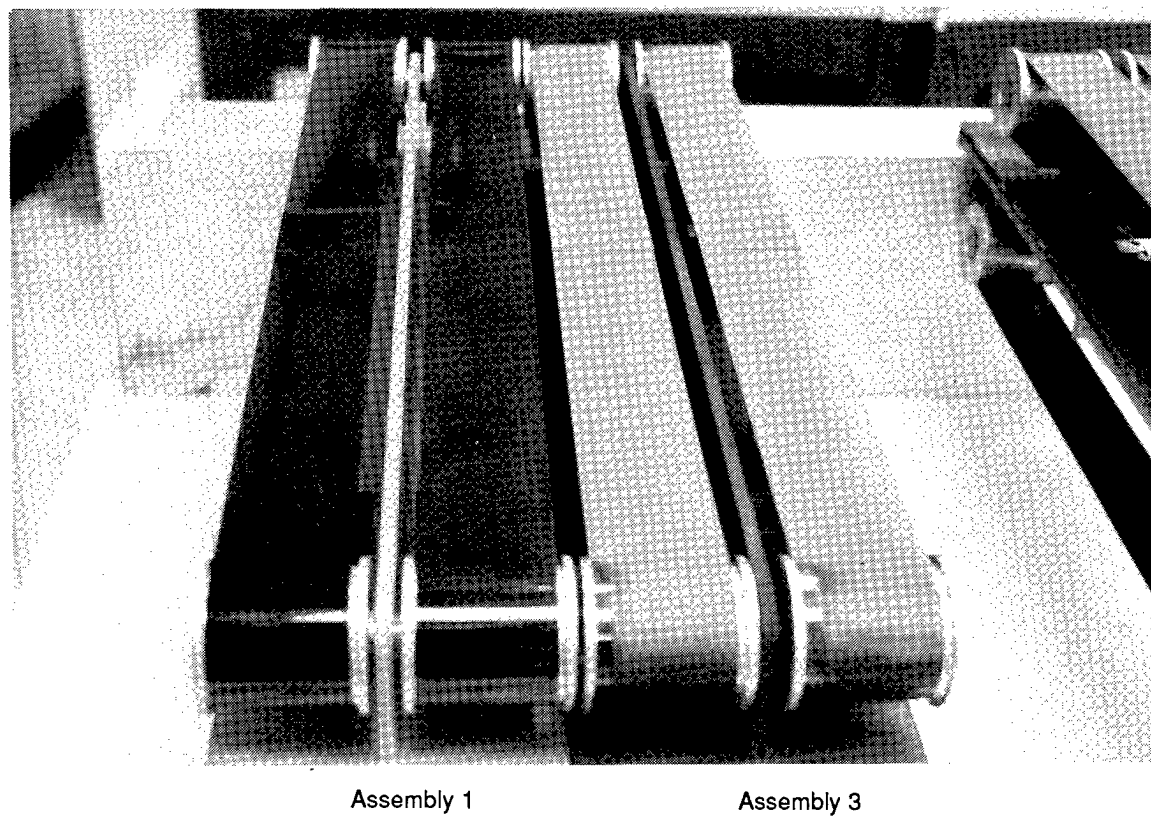


Figure 5. Kapton specimens showing specular appearance of flight controls in assembly no.1 and diffuse appearance of flight space specimens in assembly no. 3.



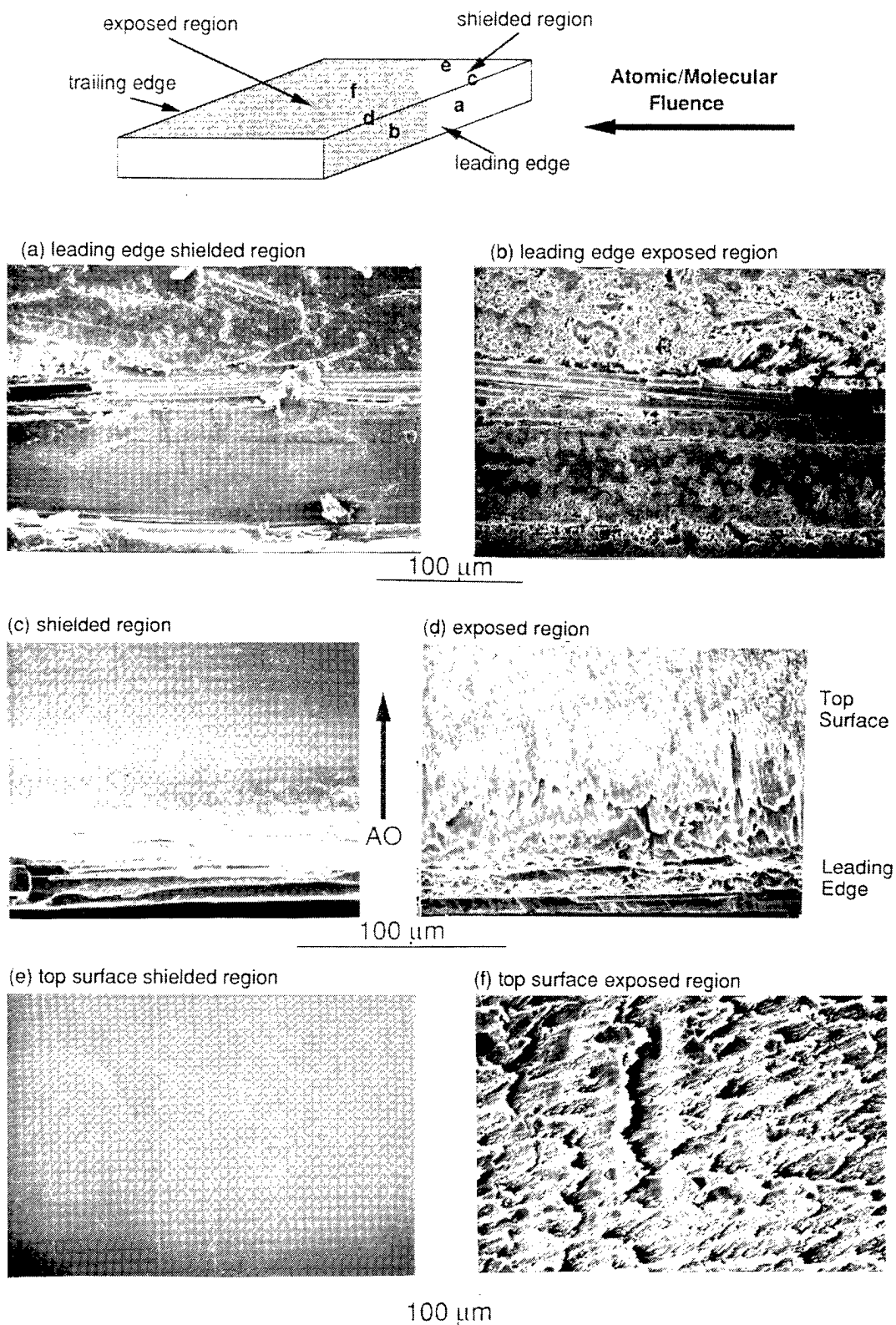


Figure 6. SEM photomicrographs of flight space glass/Kapton.



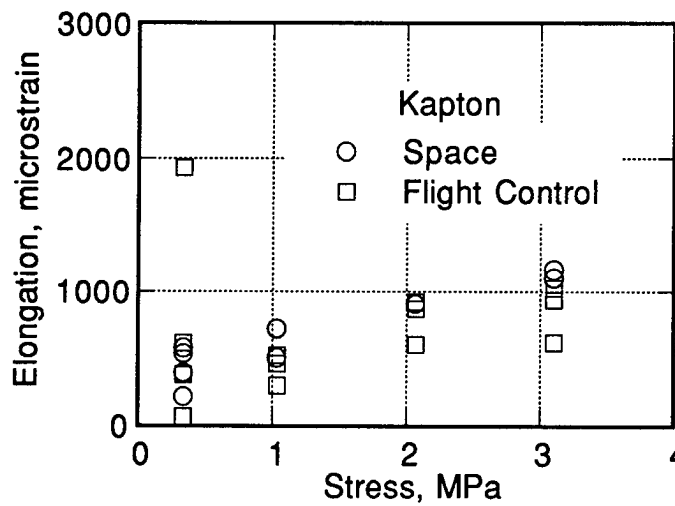


Figure 7a. Creep strain of Kapton

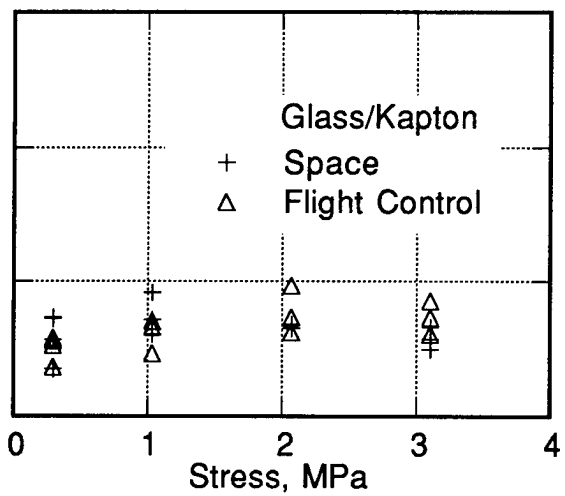


Figure 7b. Creep strain of glass/Kapton

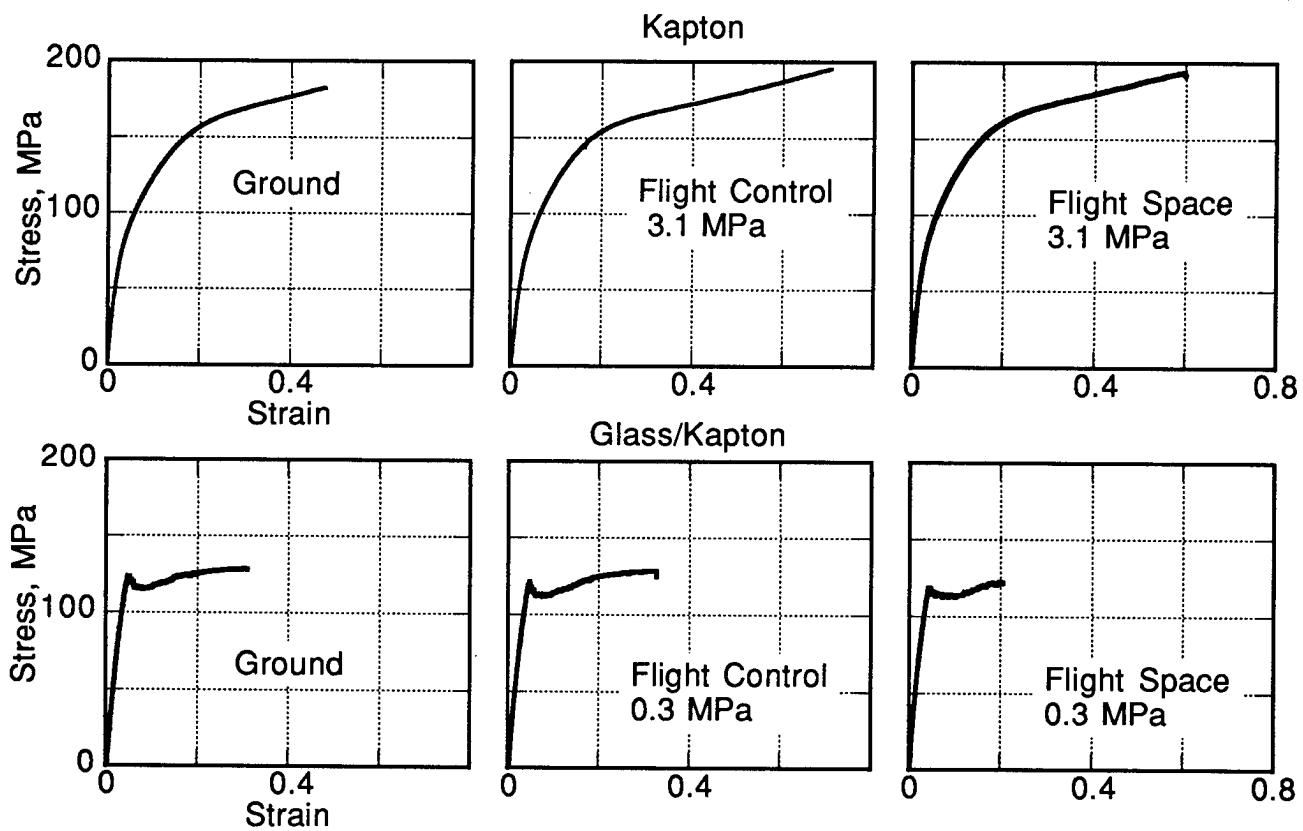


Figure 8. Representative tensile stress-strain curves

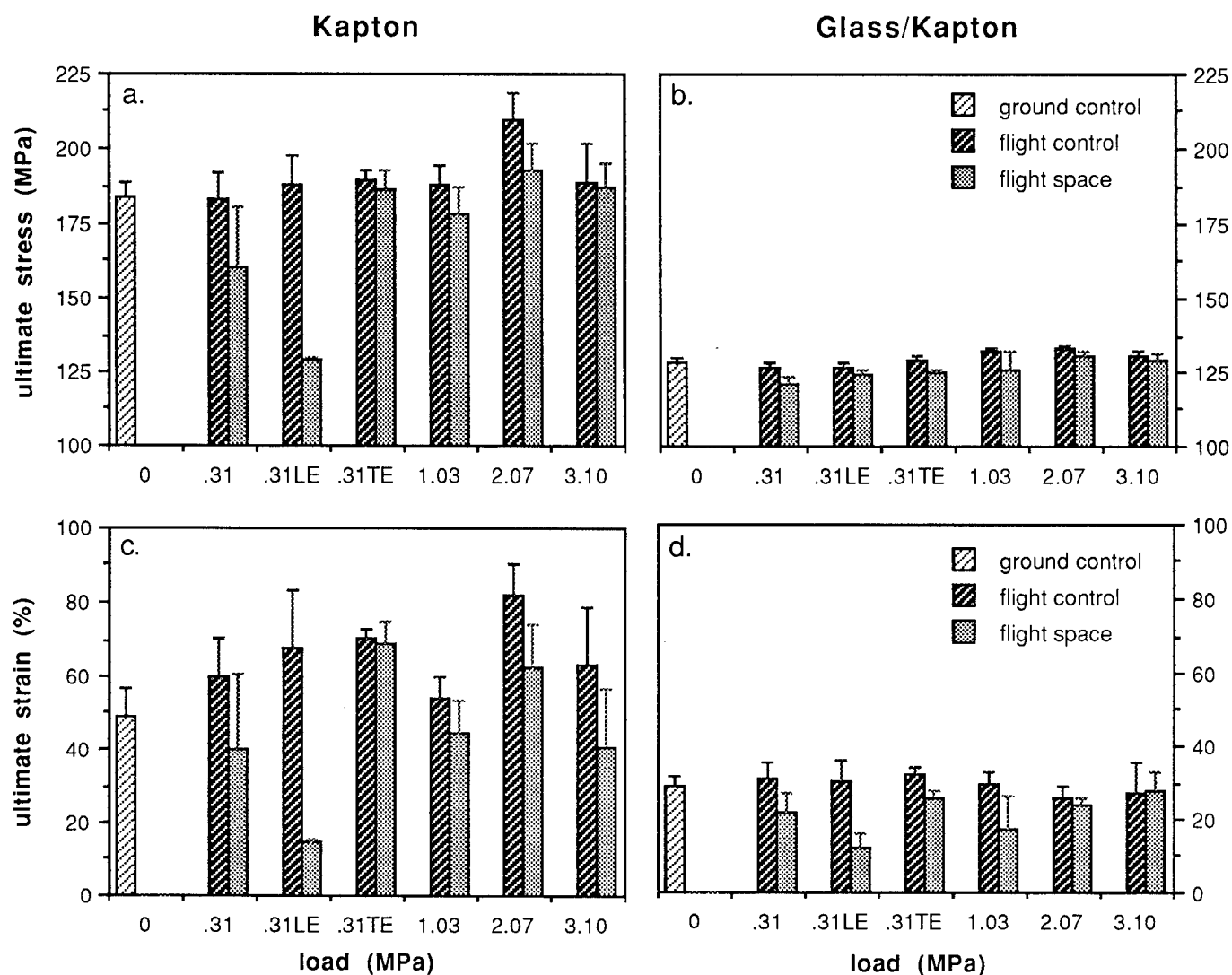


Figure 9. (a) Ultimate tensile stress of Kapton.. (b) Ultimate tensile stress of glass/Kapton. (c) Ultimate tensile strain of Kapton. (d) Ultimate tensile strain of glass/Kapton.

# AN OVERVIEW OF THE FIRST RESULTS ON THE SOLAR ARRAY MATERIALS PASSIVE LDEF EXPERIMENT (SAMPLE), AO171

Ann F. Whitaker and Leighton E. Young  
NASA Marshall Space Flight Center  
MSFC, AL 35812  
Phone: 205/544-2510, Fax: 205/544-0212

## SUMMARY

Power degradation in experiment solar cells was consistent with the exposure environment and appears to be produced principally by the radiation and atomic oxygen environments. Atomic oxygen erosion was generally as expected; atomic oxygen effects dominated for the most part in materials that were both atomic oxygen and ultraviolet vulnerable. Silicone coatings appear to protect Kapton, and adhesive systems contained under photon opaque materials were surprisingly environmentally resistant. A high density of small micro-meteoroid/space debris impacts were observed on mirrors, protective coatings, paints and composites. New synergistic effects of the space environment were noted in the interaction of atomic oxygen and copious amounts of contamination and in the induced luminescence of many materials.

## INTRODUCTION

This paper describes some of the key results of AO171 materials evaluations performed to date. This passive experiment contains about 100 materials and material processes which address primarily solar array materials although other materials of interest to the aerospace industry were included in the experiment complement. Figure 1 shows the experiment after space exposure. The experiment objective was to determine the electrical, mechanical and optical property changes induced by the combined space environments. The space environments in which this experiment were exposed as a result of its location on LDEF row 8 are described in Table I.

Although this experiment was configured for 18 months of exposure, the longer than anticipated exposure of about 70 months generally enhanced the experiment even though most of the thin film polymeric materials were eroded away as a result of atomic oxygen exposure. From an analyses standpoint it is important to consider that well heat sunk, thermally conductive materials on row 8 probably saw no temperature greater than 100°F and that isolated materials of low thermal conductivity, mass and emittance saw wide temperature cycling. Outgassing of materials would have occurred early in the mission, and the atomic oxygen environment was most severe during the last 6 months of the mission.

## RESULTS

### General Observations

From a molecular contamination standpoint, the experiment was generally considered to be very clean with the exception of one localized area where the materials outgassed as a result of insufficient thermal vacuum bakeout prior to flight. Particulate contamination was wide spread over the experiment presumed, primarily, from disintegrated silicone coatings and metallized films which were transferred during the post retrieval process. Dark deposits were found on the interior sides of the experiment tray at vents to the external environment consistent with the angle of atomic oxygen impingement but not consistent with sun angle. This phenomena suggests a new synergistic effect between atomic oxygen and copious contamination. The chemistry of the deposits has not been fully identified but the unbaked polyurethane paint and primer system on the interior of the LDEF surface are suspected to be the principal contributors of materials exposed to the incoming atomic oxygen at these vent locations. Many phenomena were observed on this experiment that have never been reported on in materials exposure experiments either from flight or in ground based simulations. Some of these phenomena are listed as follows and are described as they apply to various categories of materials evaluations.

1. Organic materials such as polyimides, silicones, and polyurethanes were found to luminesce after flight upon exposure to far UV irradiation.
2. Fibrous "ash" material was observed on carbon fiber based composite materials.
3. Silicone adhesives were found to function surprisingly well after 5.8 years in space.
4. A high density of small ( $< 1\text{mm}$ ) micrometeoroid and space debris impacts was obvious on all materials.
5. New synergistic effects were noted where atomic oxygen and copious amount of contamination were interactive.

## Solar Cells

Seven separate MSFC photovoltaic (solar cell) test articles were flown on this experiment. They were fabricated for MSFC by Lockheed Missiles and Space Company (LMSC) who also supplied the pre-flight electrical performance test data.

As a result of the longer than planned duration of the flight, all test articles underwent substantial atomic oxygen erosion of their polyimide (Kapton) substrate structures with the result that one module was lost prior to Orbiter rendezvous with LDEF, one came loose and drifted away when LDEF was grappled, and one (M3) was attached at only one corner when LDEF was retrieved. The latter was found on the floor of the cargo bay when LDEF was removed. A description of the solar cell test articles on hand post-flight is found in Table II.

Atomic oxygen degradation was obvious from visual examination of the polyimide substrates of the cells. Solar cell to solar cell interconnect bonds withstood the effects of thermal cycling well with no debonding found at the parallel-gap weld of the copper interconnect to the cell contact pads. Thermal analyses have not as yet been performed, but since the solar cell modules were thermally isolated from the LDEF structure by polyurethane foam padding, temperature excursions are expected to be reasonably broad over the orbit. The module that was retrieved from the cargo bay had 5 (of 12) cells that contained cracks in either the solar cell or cell cover. Micrometeoroids/space debris impacts were evident on all the test articles. These ranged from small surface nicks to solar cell coverslide breakage and rather deep penetrations within the cells. At this time no correlation between cell/module electrical performance and impacts has been established.

During post flight electrical performance testing of module M3, it was discovered that an apparent voltage calibration error was made on this module as evidenced by post-flight open circuit voltage higher than that measured pre-flight. For this reason, pre-flight performance for M3 was fabricated by using the pre-flight performance of the single cell C8 and expanding it to the configuration of M3 (4 cells in series by 3 cells in parallel). Cell C8 performance was selected because its short circuit current, when multiplied by 3, was the closest match to the actual M3 module performance. Additionally, there were no other indicators to suggest a current calibration error of any significance. After the overall electrical performance of M3 was established through testing, the module was cut apart to determine individual cell performance.

Solar cell and solar cell module maximum power point (Pmp) degradation ranged from 4.3% to 80% with 76% of the single cells tested having less than 10% degradation, Figure 2. There were 4 cells out of 17 that had Pmp degradation greater than 20%. Three of these were from the module which was retrieved from the cargo bay. The other was the cell (C6) which was flown without a coverslide. Discounting these cells, the average cell Pmp degradation was 6.5% with a standard deviation of 1.75%. The thin cell module (M4), which was retrieved intact but with severe damage to its Kapton substrate degraded 5.2% in Pmp. Four cells had discernible degradation in open circuit voltage (Voc) which is typical of a decrease in cell shunt

resistance. Three of these cells were from the module retrieved from the cargo bay with the other being the cell flown without a coverslide. Two of the cells with Voc degradation were from the four which degraded more than 20%. Three cells showed evidence of severe series resistance increases. All three of these were from the cargo bay module. Two are from the four having discernible degradation in Voc. Figure 3 illustrates the differences in current/voltage (IV) characteristics between three poor performance cells and cell C1 that underwent the lowest degradation.

In summary the electrical performance of the cells is consistent with the expected performance for the environment experienced. To date no partition of cell degradation to specific environmental effect has been made. Loss of Kapton substrate from atomic oxygen attack was not a surprise since the materials were in space much longer than planned with no protective coatings. Some portions of the Kapton substrate containing adhesives are still intact and require more evaluation to determine the reasons for their survival in the atomic oxygen environment.

### Composites

The carbon fiber and glass fiber composites contained in this experiment are described, along with a summary of their data generated to date, in Table III. The most obvious visible effect noted on these composites is the increased optical diffuseness of the surfaces which is commonly observed in materials exposed to orbital atomic oxygen. All of the carbon fiber composites have a charred appearance and show the fiber direction as a result of preferential atomic oxygen erosion of the matrix material. A porous ash structure formed on the exposed carbon fiber composite surfaces with the greatest concentration being on the polysulfone materials. Micrometeoroid/space debris impacts less than 1 millimeter in diameter were present on all composites. Concentration of these impacts ranged from 2 to 7 impacts per 25 in<sup>2</sup>. Non-penetrating splattered contaminants, probably from spacecraft fluid dumps, were also noted on the composites.

Mass loss was consistent with thickness loss with the carbon fiber based composites losing approximately 1 ply. Atomic oxygen reactivity numbers are not inconsistent with those generated for carbon composites but no short term data is available currently for comparison of short and long term reactivity numbers for these specific composites. Another factor to consider is that short term exposure data probably would not be correlatable to the long term exposure data since the composite surfaces are matrix material rich. Aluminized tape was effective in protecting the composites from atomic oxygen erosion although penetrations of the protective aluminized tape were made by small impacts. The silicone adhesives on these tapes were well preserved and as effective as the controls. Further evaluations of the tapes are planned.

## Thin Films

A cursory assessment of metallized and thin polymeric films is provided in Table IV which is a summary of post-flight visual observations of the films. No analyses other than a SEM examination of the white Tedlar have been made to date. Visually, the white Tedlar appears intact but the inert particles in the material are basically the only remaining component of the material. The intact Kapton protected by the silicone coatings provide some promise that silicones can furnish long term protection for Kapton against atomic oxygen attack. However, the extent of the effectiveness of their protection remains to be quantified. Thin films of Kapton, Mylar and Teflon which were aluminized with the aluminum surface exposed appear to have been protected from atomic oxygen erosion.

## Paints

During the post-flight examination of this experiment under black light illumination, it was discovered that various types of materials were luminescing (fluorescing). Among these fluorescing materials were the polyurethane and silicone based paints. The intensity and wavelength dependence of this fluorescence varies with material and are the subject of a separate report.

Upon exposure, specular paints became diffuse and diffuse paints became more diffuse - a phenomena which is known from short term exposures and results principally from atomic oxygen induced surface texturing and also from preferential atomic oxygen attack of diffuse paint constituents. Inert particles in the paint accumulate on the paint surface as it erodes thereby providing more shielding of the underlying surface with increased exposure. Atomic oxygen erosion is, as observed from these results and those from the STS flight, non-linear in time in those paints subject to this preferential attack so their mass loss cannot be used to predict erosion rates. Optical properties and mass loss of these paints, Table V, are compared to data from control paints prepared at about the same time as the flight samples. As noted by the data, exposure of pigments in white and yellow diffuse paints tend to decrease absorptivity. S13GLO silicone paint which resists atomic oxygen attack showed darkening, presumably from ultraviolet/particulate irradiation. One of the more interesting effects noted in the paints is that atomic oxygen effects dominate in those paints which are both ultraviolet and atomic oxygen vulnerable. Without evaluating this phenomena in great detail, it would appear that any synergism, if it exists, between atomic oxygen and irradiation effects under these exposure conditions for these paints is minimal.

## Metals

Metals flown on this experiment include aluminum, titanium, silver (disk and cold rolled ribbon), niobium, magnesium, copper (disk and cold rolled ribbon), molybdenum, tantalum, and Tophet-30, HOS-875 and Ni-Cr alloys in the as received condition and preoxidized. Several other combination of metals and coatings were also flown but are not part of this report. All of these metals gained weight from interaction with atomic oxygen except the preoxidized alloys which showed a slight mass loss. Macroscopic atomic oxygen effects were observed on silver and copper. Of all the metals silver was the most affected, as expected, and tantalum was the least affected. Accommodation of atomic oxygen in silver ranged from one atom per 1000 incident atoms in disk samples which were well heat sunk to 7 atoms per 1000 incident atoms in cold rolled stressed ribbon samples which were thermally isolated from the base structure. Mass increase in these materials, total incident fluence of atomic oxygen and the assumption that the highest oxidation state of the oxide was achieved, were used to generate these accommodation numbers.

## Other Polymers

Materials including RTV-511, Halar and the PEEK resin, configured into tensile, shear and miscellaneous rectangular samples, and TFE Teflon washers comprised the majority of structural polymers on the experiment. The RTV-511 materials received an insufficient thermal vacuum bakeout (for contamination control) prior to flight resulting in outgassing with deposition on the near adjacent experiment area.

Considerable darkening of all elastomers occurred as a result of exposure and a 10% increase in Shore A hardness was noted in RTV 511. Halar, which is both ultraviolet and atomic oxygen susceptible, appears to be dominated by irradiation effects but further evaluations are required to identify and quantify these effects. Mass loss in these materials ranged up to 7% of their initial weight. Thirty six TFE washers were examined for atomic oxygen erosion and an atomic oxygen reactivity number of  $(1.9 \pm .4) \times 10^{-25} \text{ cm}^3/\text{atom}$  generated for this material.

## ACKNOWLEDGEMENTS

The authors gratefully acknowledge the contribution of Messrs. Doug Willowby in the solar cell characterization and Ed White for profilometry measurements, Ms. Whitney Hubbs for coordination of the major portions of the evaluations and Ms. Freda Summers for typing the text.



TABLE I. - EXPERIMENT AO171 EXPOSURE CONDITIONS

• High Vacuum	-	$10^{-5} - 10^{-7}$ Torr (estimated)
• UV Radiation	-	10,041 ESH
• Proton Fluence	-	$10^9 \text{p}^+/\text{cm}^2$ (.05 - 200 MeV)
• Electron Fluence	-	$(10^{12} - 10^8) \text{e}^-/\text{cm}^2$ (.05 - 3.0 MeV)
• Atomic Oxygen	-	* $7.68 \times 10^{21}$ atoms/ $\text{cm}^2$
• Micrometeoroid/ Space Debris	-	2 to 7 impacts per composite, < 1mm
• Thermal Cycles	-	$\simeq 32,000$ cycles (temp TBD)

\*This number was derived for Row 8 from the JSC provided number of  $9.75 \times 10^{21}$  atoms/ $\text{cm}^2$  for total atomic oxygen fluence on the RAM surface. All reactivity and accommodation numbers provided in this paper are based on this number.

TABLE II. - SOLAR CELL TEST ARTICLES

M3 ASEC 12 Cell Module

- Applied Solar Energy Corp. (ASEC) 200 micron, 2 cm x 4 cm silicon N on P, 2 ohm-cm, back-surface reflector cells
- Chemically Vapor Deposited (CVD) dielectric, wrap-around contacts
- 150 micron microsheet coverslides with UV filters and AR coatings
- Rear surface of module facing space

M4 ASEC 6 Cell Module

- ASEC 50 micron, 2 cm x 4 cm silicon N on P, 10 ohm-cm back-surface field cells
- Wrap-around contacts with wrap-around junction
- 2 each 50 micron, 4.7 cm x 6.7 cm coverslides
- Cells mounted facing space

Cells C6 through C10 - ASEC cells same as M3 but with coverslides as follows:

- C6 - None
- C7 - 150 micron microsheet with AR coating
- C8 - 150 micron microsheet with UV filter and AR coating
- C9 - 150 micron frosted fused silica with UV filter and AR coating
- C10 - 150 micron fused silica with UV filter and AR coating

Note: Each test article has a copper interconnect system laminated between 2 sheets of Kapton that comprise the structural substrate for the solar cells.

TABLE III. - ATOMIC OXYGEN EFFECTS IN AO171 COMPOSITE SAMPLES

Composite Materials (No. of Specimens)	Average Thickness Loss (Mils)	Atomic Oxygen Reactivity $10^{-24}$ cm/Atom	General Observations
HMF 322/P1700/ $\pm 45^\circ$ (5)	4.7 to 11.5*	(1.6 - 3.8)	Materials (1-5) "black", i.e., more diffuse. "S" glass- epoxy much darker - probably from UV effects.
HMS 934/0° (5)	2.5**	0.8	
HMS 934/90° (6)	2.7	0.9	
P75S/934/90° (6)	2.7	0.9	Fibers evident in materials (1-6). Closer observations show micrometeoroid/ space debris hits on all specimens.
P75S/934/0° (5)	2.8	0.9	
"S" Glass-epoxy (3)	0.36***	0.11	
Thermal Control Aluminized Taped "S" Glass-epoxy (3)	Indeterminate	--	Material (7) shows unexplained corrugated features on aluminum tape.

\* Matrix erosion much greater than fiber

\*\* Average of rates from 2 ends of sample; contamination likely on forward end

\*\*\* Fibers uneroded and become protective after initial matrix mass loss

TABLE IV  
POST FLIGHT ASSESSMENT OF  
METALLIZED AND POLYMERIC FILMS

<u>Materials/Configuration</u> (Exposed $\Rightarrow$ inner material)	<u>Post Flight Condition</u>
1. DC-2577 Coated Kapton	Intact
2. RTV-670 Coated Kapton	Intact
3. 1.0 mil Kapton H	Eroded away
4. Sandwich configuration of 1/2 mil Kapton, 1 mil Black Kapton/2 mil Kapton	Eroded away
5. Aluminized Mylar	Intact
6. 5 mil Kapton H	Eroded away
7. Aluminized Teflon	Intact
8. Kapton F	Eroded away
9. 1/2 mil Teflon	Eroded away
10. 1.0 mil White Tedlar	Still white but matrix eroded away
11. Aluminized Kapton	Intact
12. Aluminized tape on composite	Intact, surface fatigue, adhesive good

TABLE V. - PROPERTY DATA ON PAINTS ON AO171 EXPERIMENT

<u>PAINT</u>	<u>MASS LOSS (MG/cm<sup>2</sup>)</u>	<u>SOLAR ABSORPTIVITY</u>	
		<u>Unexposed</u>	<u>Exposed</u>
A-276 (White diffuse)	1.00	.284	.237
401-C10 (Black diffuse)	1.13	.990	.995
Z-853 (Yellow diffuse)	0.94	.491	.428
Z-306 (Black diffuse)	1.60	.978	.973
Z-302 (Black specular)	4.06	.973	.974
S13GLO (White)	Negligible	.186	.319

\*Inert pigments in diffuse paints tend to retard atomic oxygen produced erosion.  
Specular Z-302 was eroded to the metal substrate

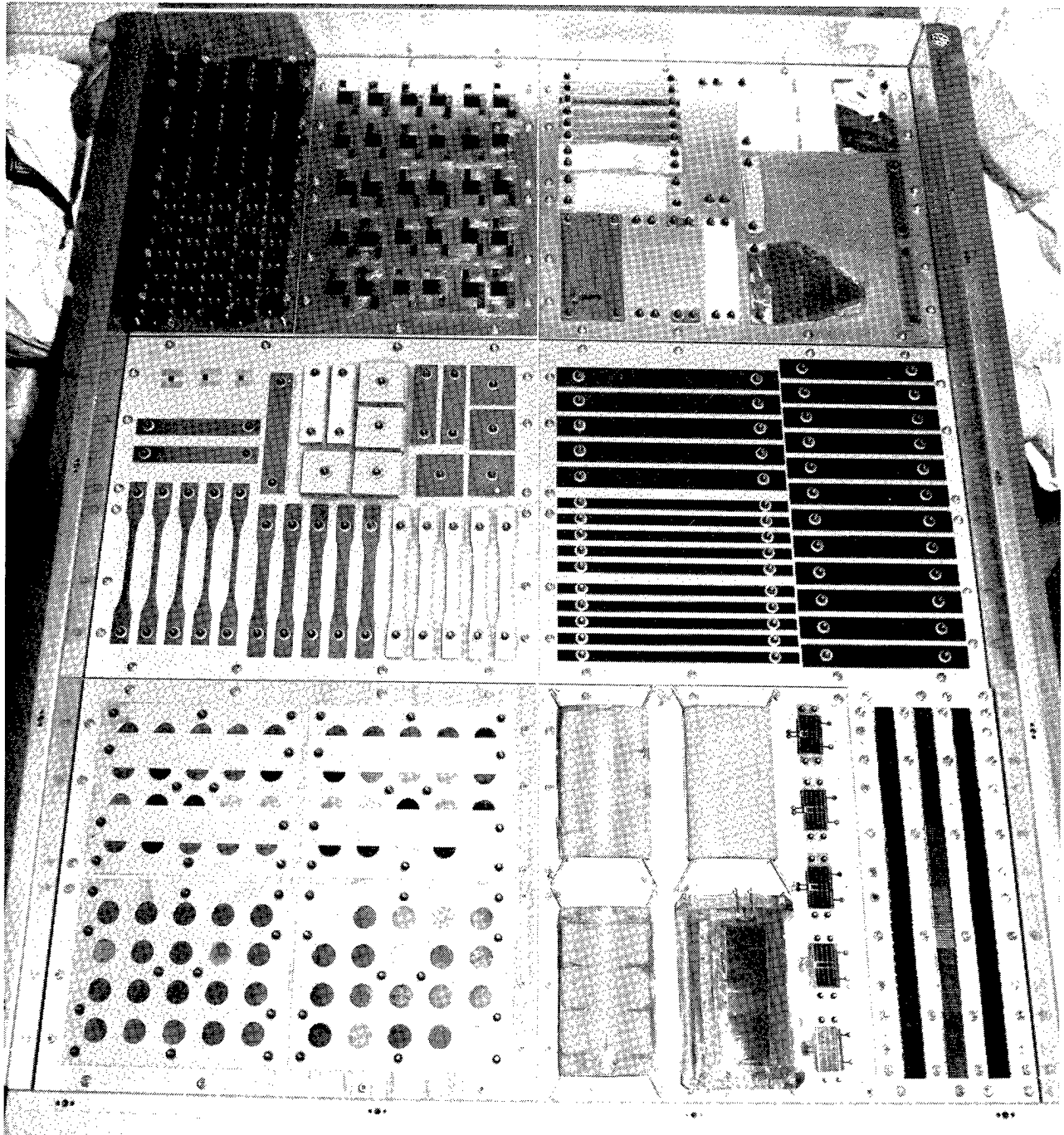


Figure 1. AO171 Experiment After 5.8 Years Exposure in LEO

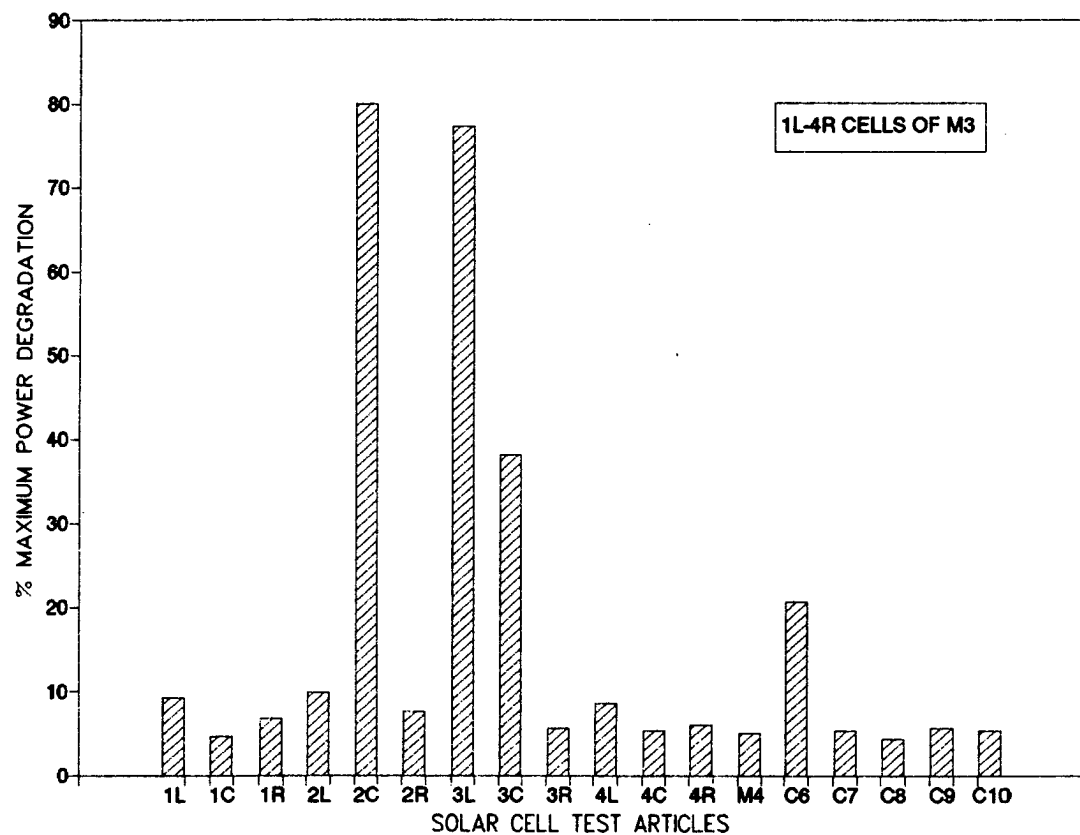


Figure 2. Percent Degradation in Solar Cell Test Article Maximum Power Output

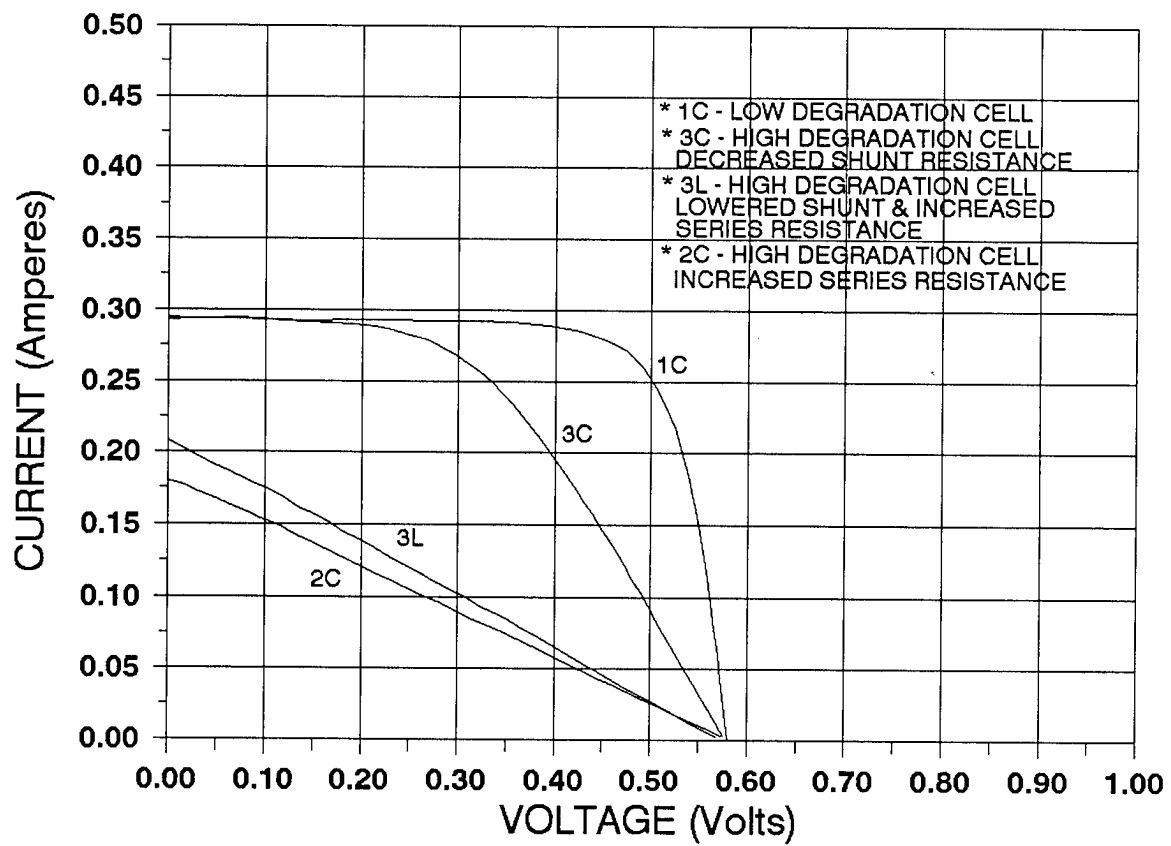


Figure 3. Variations in Current/Voltage Characteristics of Poor Performance Cells and Best Performing Cell C1



EXPERIMENT M0003-4  
ADVANCED SOLAR CELL AND COVERGLASS ANALYSIS, AN OVERVIEW

Terry M. Trumble  
Principal Investigator M0003-4  
Aerospace Power Division  
Aero Propulsion and Power Directorate  
Wright Patterson AFB, OH 45433-6563

SUMMARY

The experiment consists of 51 coverglass samples and 12 solar cell strings. Sixteen (16) of the coverglass samples were on the leading edge and 16 on the trailing edge. An additional 16 samples were used as control samples and were not flown. The scenario for analysis was established for the coverglasses as follows. A photographic and Nomarski survey were taken. Selected sites were then analyzed in their "dirty" condition for optical transmission, reflectance and absorbance. The coverglass samples have yet to be cleaned and resulting residue analyzed. The next stage of the analysis of the filters will be by probing through their layers to evaluate the multilayers used in their design. The solar cells have been visually inspected and photographed. Tape recorder data is being analyzed and selected cell strings are being evaluated for their electrical properties. The first phase of the optical studies has been completed.

OPTICAL PROPERTIES

The first phase of the coverglass samples analysis has been completed. The full results of the transmission, reflection and absorption are being analyzed and will be presented in a publication within a few months, however a brief summary is presented. There are more pronounced changes in the optical properties on the trailing edge than on the leading edge. The existing surface contamination did not interfere with the optical properties measurements made on the coverglass samples. The short wavelength cutoff of the optical samples has moved noticeably toward the longer wavelengths. Changes noted otherwise have been primarily in absorbance.

SURFACE ANALYSIS

The initial results from the surface stoichiometry analysis of the  $\text{MgF}_2$ ,  $\text{ThF}_4$  and  $\text{SiO}_2$  fluorine are as follows. The leading edge analysis of the  $\text{MgF}_2$  indicates the presence of fluoridated organic contaminants. It also appears that oxygen has replaced some of the fluorine in the material. There is no thick layer of oxide as was observed for the  $\text{ThF}_4$  samples, however. Analysis of the  $\text{ThF}_4$  sample indicates that almost all of the fluorine has been removed from the leading edge  $\text{ThF}_4$  sample.  $\text{SiO}_2$  appears to be unchanged.

All of the trailing edge samples have experienced a layer of greater than 100 Angstroms of contamination. There are also high levels of Si, C and O with about half of the samples showing trace amounts of N, F and Sn. There is contamination of this type on the leading edge, but to a lesser degree. There is evidence on the trailing edge of silicone based material contamination. The fluorine contamination found on the LDEF is likely to be an organic derived from Teflon.

## PHOTOGRAPHIC SURVEY

A second level Nomarski and conventional microscope survey of the coverglass samples and the solar cell samples has been completed. The purpose of the survey is to identify and isolate specific areas, describe what is found, and then proceed with a detailed analysis of the area. Considerable loose surface contamination has been found. The Tedlar mounting rings for the coverglass samples, for example, account for a portion of the contamination. This material was not a space qualified material.

Two additional photographic surveys were conducted after the initial survey conducted by the Aerospace Corporation in Los Angeles. The Materials Directorate and the Aeropropulsion and Power Directorate each conducted a survey. The results confirmed earlier information showing micrometeoroid damage, thermal cycling stresses and considerable amounts of loose surface contamination.

## SOLAR CELL ANALYSIS

The analysis of the six different solar cells began with a photographic survey. A visual comparison of cell strings indicated that the fabrication process used for the metalization of each of the cell strings had a large effect on the lifetime of the cells themselves. Metal migration and contamination between the coverglass and the cell proper were two of the main concerns. Loss of silver, or considerable oxidation for unprotected silver appears to be a problem. Contamination, discoloration, shows up mainly on the cell contacts and interconnects. Electrical properties have not yet been measured.

## CONCLUSIONS

The initial investigation is nearing completion for the optical samples. There is concern that  $\text{ThF}_4$  and  $\text{MgF}_2$  will require a passivating coating to survive in Low Earth Orbit (LEO). We are just now beginning to correlate the information from our studies. We now know better ways to design and test optical coatings and solar cells for use in LEO. Future reporting will cover each analysis area in detail.

## ACKNOWLEDGEMENTS

The analysis work performed under this study has been accomplished by the following individuals: Dr. Walter Haas and Lt. Allen Day of the Materials Directorate of Wright Laboratory; Dr. Peter John of the University of Dayton; Tom Allen of the Optical Coatings Laboratory in Santa Rosa, California; Jim Malone and John Leonard of the Aero Propulsion and Power Directorate of Wright Laboratory.

PRELIMINARY ANALYSES OF WL EXPERIMENT #701, SPACE  
ENVIRONMENT EFFECTS ON OPERATING FIBER OPTIC SYSTEMS

E W Taylor, J N Berry, A D Sanchez, R J Padden, S P Chapman,  
Air Force Systems Command Phillips Laboratory  
Directorate of Space and Missiles Technology  
Optoelectronics Section, PL/STET  
Kirtland AFB, NM, 87117-6008  
Phone: (505) 846-4741, FAX (505) 846-1724

22 March 1991

ABSTRACT

A brief overview of the analyses performed to date on WL Experiment #701 is presented, highlighting the successful operation of the first known active fiber optic links orbited in space. Four active digital fiber optic links were directly exposed to the space environment for a period of 2114 days. The links were situated aboard the Long Duration Exposure Facility (LDEF) with the cabled, single fiber windings atop an experimental tray containing instrumentation for exercising the experiment while in orbit. Despite the unplanned and prolonged exposure to trapped and galactic radiation, wide temperature extremes, atomic oxygen interactions, and micro-meteorite and debris impacts, in most instances the optical data links performed well within the experimental limits. Analysis of the recorded orbital data clearly indicates that fiber optic applications in space will meet with success. Ongoing tests and analysis of the experiment at the Phillips Laboratory's Optoelectronics Laboratory will expand this premise, and establish the first known and extensive database of active fiber optic link performance during prolonged space exposure. WL Exp #701 was designed as a feasibility demonstration for fiber optic technology in space applications, and to study the performance of operating fiber systems exposed to space environmental factors such as galactic radiation, and wide temperature cycling. WL Exp #701 is widely acknowledged as a benchmark accomplishment that clearly demonstrates, for the first time, that fiber optic technology can be successfully used in a variety of space applications.

## I. INTRODUCTION AND BACKGROUND

The space-exposed fiber optic experiment was first conceived at the Air Force Weapons Laboratory by E. W. Taylor, the Principal Investigator (PI), and was approved for spaceflight on the first LDEF mission by the Director of Space, HQ USAF on 3 Mar 1978 as STP Flight S80-1. The selection of the radiation tested optical fibers for the experiment and the cabling for each individual data link were predicated on the various radiation effects studies [1-5] conducted to ascertain the then State-of-the-Art for optical data link performance under severe radiation and temperature conditions. Based on this empirical data, an experiment was formulated that was eventually developed under an Air Force Weapons Laboratory independent laboratory research effort (ILIR 7802). The experimental apparatus was developed [6,7] by the Jet Propulsion Laboratories, La Canada, CA, with direct interaction and overall direction provided by the WL PI.

The original and prime objectives [7] of the experiment were to study the space environment parameters of temperature cycling and radiation effects on the data transmission performance of four digital optical data links. Parameters to determine link signal-to-noise ratios (SNR), bit error rates (BER) and other system criteria were measured in orbit and stored on magnetic recording tape. Eight temperature measurements were also performed in separate tray locations. An active analog link was later incorporated which was located within the tray volume and was intended to measure temperature. The analysis of this link is on-going and will not be discussed within this report.

These were the prime experiment objectives formulated at the time of the experiment conception that drove the development of the experiment. Secondary objectives for analysis evolved after launch due to the delayed retrieval of LDEF, since other space effects which could impact the experiment performance became evident. It was always recognized that the optical fiber cabling materials would be somewhat deteriorated by the space ultraviolet radiation. There also existed a finite probability that meteorites of sufficient size and kinetic energy could damage the experiment. However, these effects were not considered significant at the time, since the orbital duration was expected to be optimally one year. No provisions were made for studying the effects of atomic oxygen, nor were any concerns addressed to this end. Thus, no separate instrumentation for measurement of these effects was included in the original experiment design.

However, because of the retrieval delays incurred, recognition of these other space environment effects became of increasing concern as the LDEF 1990 retrieval date approached. These concerns were validated with the early (Fig. 1) photography provided by the *Columbia* crew, indicating numerous micro-meteorite and debris impacts experienced on LDEF surfaces. Fig. 1c clearly shows the effects of ultraviolet degradation of the optical cabling materials used to protect each of the four single optical fiber data links. Atomic oxygen effects, in combination

with ultraviolet radiation and possible thermal effects, will be discussed in separate documents<sup>†</sup>.

An early analysis was performed to assess a portion of the space environment effects arising from the unplanned and extended time in orbit. A technical paper [8] titled, *Space Debris and Micrometeorite Events Experienced by WL Experiment #701 in Prolonged Low Earth Orbit*, communicated this early data to the general scientific community. Portions of the data found in the publication are also discussed later in this paper.

For the most part, this paper is focused on presenting the preliminary analysis of the orbital flight data recorded aboard WL Exp #701 for the first year in orbit.

## II. IN SITU ANALYSIS PERFORMED AT THE KENNEDY SPACE CENTER

The decision to exercise the experiment at KSC was primarily based on the reasoning that any damage incurred during the transit of the experiment from KSC to the WL would irrevocably influence the test results.

A second reason for exercising the links at KSC was based on the documented [3,4] ability of certain fibers, selected for the experiment, to incur doses in excess of the LDEF environment with little or no permanent damage. Thus, the combined effects of the expected low exposure dose and the experiment fibers' ability to quickly recover from radiation exposure, especially under elevated temperatures (both in orbit and during re-entry within the shuttle cargo bay) necessitated the KSC investigations performed by the WL team.

There were also concerns<sup>†††</sup> that by functionally operating the links at KSC, optical signal photobleaching might occur, which would remove the long-term effects of any accumulated radiation damage incurred by the glass/glass and plastic coated silica optical fiber links. However, while the photobleaching concerns were valid, previous fiber optic radiations effects research data [9-15] tended to lessen these concerns.

The early visual analysis of the experiment at KSC involved two aspects. Prior to our reactivating the experiment to ascertain the functionality of the links, both the M/D Special Investigation Group and the Phillips Laboratory photography team photographed the experiment surface. Subtle changes to the optical fiber cabling were observed. Two cables (see Fig. 1b, 1c) began to slightly return to their original color states, as indicated in Table 1. The cabling

---

<sup>†</sup> Unpublished Phillips Laboratory Draft Reports.

<sup>††</sup> Conversations with Space Station Freedom Project Office, 1989-1990.

<sup>†††</sup> Conversations with Alan H. Johnston (PI for LDEF Experiment S0109), Jet Propulsion Laboratories, 1990-1991.

materials and other parameters describing the optical fiber characteristics are also discussed in Table 1.

The most important visual data recorded by the WL Recovery/Deintegration team during the period of analysis at KSC was that the cabled optical fiber windings were nearly intact on the tray surface and had sustained numerous micro-meteorite and/or debris impacts. *However, none of these cabled single fiber links was observed to be "varied in their degree of damage from simple breakage and splintering, to various degrees of melting,"* as reported erroneously in a preliminary report compiled by the LDEF Meteoroid and Debris SIG [16].

On the contrary, all four of the M/D impacted cabled fiber links were activated within hours of deintegration and three links were found to be fully operational. The fourth data link (Link #4), consisting of a cabled, single fiber, could not be operated at KSC. While there was circumstantial evidence to suggest that an M/D impactor might have contributed to the malfunction of the link, attempts to optically detect energy emissions from the impactor site did not substantiate any severing of the cabled single fiber link. There was no photographic or visually enhanced evidence [16] at any time of the analysis performed to validate the claims. (Note: it is important to mention that all of the fiber optic data links aboard WL Experiment #701 were composed of cabled, single fiber links, *not "hardened fiber-optics bundles,"* as reported elsewhere [16].

Other investigations, such as the measurement of the experiments' surface absorption/emissivity, contaminant collection, and thermal blanket material sample collection were performed by various SIGs and the results will be discussed in more comprehensive reports, currently in preparation<sup>†</sup>.

### III. PRELIMINARY MEASUREMENTS AND ANALYSES OF WL EXP #701 (M0004) PERFORMED AT THE AFSC WEAPONS LABORATORY AND AFSC PHILLIPS LABORATORY

#### *Optical Data Transmission Measurements*

Following orbital deployment by the *Shuttle Challenger*, the experiment was activated and performed the first of its scheduled 76 optical data transmission measurements [6] for the planned year in orbit. Thirty measurements were performed in the first six months at intervals of six days, while the remaining 46 measurements were performed at four day intervals over the second half of the year. Shown in Fig. 2 is a block diagram of the measurement circuitry. Fig. 3 illustrates a portion of the electronic/optoelectronic layout.

---

<sup>†</sup>Unpublished Phillips Laboratory Draft Reports.

Two basic tests were conducted on each space-exposed fiber optic link by the circuitry as represented in Fig. 2. The first of these tests was designed to measure the signal strength (and hence Signal-to-Noise Ratio) of each digital fiber optic link. This test is referred to as the "SNR measurements". The second test was designed to record any "burst" or dependent errors that may be affecting the transmission of the digital data through the fiber optic link. This test is referred to as the "Burst Error Runs." A 10-bit pseudo-random generator is used to generate a digital stream of "data" for the measurements. The receivers are AC coupled and the data is in a bipolar, Non-Return to Zero (NRZ) format. The experiment uses a model developed by Gilbert [17] to examine the bit stream for errors.

In the SNR measurements, the voltage from the optical receivers is compared to a "threshold voltage." A high-speed comparator uses this threshold voltage to decide if the signal from the optical receivers is a logical "1" or a logical "0". Initially, the error counters are cleared, the threshold is set to zero volts, and a "packet" of 130,944 bits is passed through the fiber optic link. The data stream from the optical receivers is compared to a reference signal from the pseudo-random generator. If there are less than 128 independent (Type I in the Gilbert model) errors in the data that was passed through the fiber optic link, the experiment increments the threshold voltage by 1.25 mV, the error counters are reset to zero, and another packet of 130,944 bits is passed through the link. This process continues until at least 128 independent errors are detected in a packet of 130,944 bits. At this point, the experiment records into RAM the values of the error counters and the number of times the threshold voltage was incremented. The experiment then conducts an SNR measurement on the next link in the sequence until all four links have been examined.

After each link has been interrogated concerning its SNR, the experiment begins the Burst Error Runs. In this mode, the threshold voltage at the comparator is held constant at zero volts. Since the receivers are AC coupled, zero volts is the optimal threshold for the system. That is, for any given signal strength, zero volts as a threshold will result in the least possible errors in the data stream. The error counters are reset to zero at the beginning of the Burst Error Run for each fiber optic link but they are not cleared between successive packets of 130,944 bits. With zero volts as the threshold, a packet of 130,944 bits is passed through the link. If less than 128 independent errors have accumulated, the experiment passes another packet of 130,944 bits through the fiber optic link. The process continues until either 128 (or more) independent errors accumulate or a total of  $10^9$  bits have been passed through the link. When either of these conditions has been met, the experiment records into RAM the values of the error counters and the number of bit packets that have been passed through the link. A Burst Error Run is then conducted on the next space-exposed link in the sequence until all four links are tested.

After completion of the Burst Errors Runs the experiment transfers the data stored in its RAM to the Experiment Power and Data System (EPDS). The EPDS gives the data a "time stamp" and records the data to magnetic tape. Both the Data Processor Control Assembly (DPCA) and the Magnetic Tape Memory (MTM) units of the EPDS functioned properly during the entire mission and continue to work in post-flight testing.

## *In-Orbit Temperature Cycling Measurements*

Prior to performing the SNR and burst error runs, the experiment controller directed the measurement of temperatures at eight thermistor locations within the experiment tray volume (see Fig. 3b). These temperatures were valuable in studying the optical fiber performance. However, it must be realized that the temperature measurements were made at the very beginning of the four fiber optic link performance runs. Therefore, as much as 30 minutes could have elapsed between the temperature measurements and the measurement of the last Burst Error data.

The time stamp assigned to each experiment reflected the end of that data taking period. By examining the performance of each link, it was possible to determine the total time elapsed for completing the entire experiment run. If a link was greatly degraded in performance for a particular run, then the time required to evaluate the link was significantly reduced. The experiment controller would then proceed to examine the next link.

Therefore, under this scenario, the maximum time required to fully sequence each of the four links would be less than 31 minutes, bringing the temperature measurements in time proximity with the link performance measurements. Thus, the temperature gradient, or change, was minimized for the special case where a link was highly degraded in performance and the data run was truncated.

Discerning the orbital beta-angle [18] during the periods of experiment operation is very important, since temperature variations can be accounted for and correlated to the on-board WL Exp #701 thermistor readings. Since the LDEF orbital period was approximately 94 minutes, the actual tray temperature may have changed significantly during many of the data runs. For example, the experiment could have passed from the daytime space exposure condition to the daytime sun exposure condition, or vice-versa, or other variations, in the interval of 30 minutes, changing the conditions under which the link measurements were performed.

Because of these possible transient conditions, an accounting and correlation between LDEF Therm Data [18,19] and the WL Exp #701 thermistor measured data is underway. Fig. 4 illustrates a partial analysis of this situation, while tables 2a and 2b illustrate the thermistor locations and typical temperatures recorded for the inner tray volume.

### *Brief Analysis of In-Orbit Recorded Optical Fiber Transmission Data*

Shown in Figs 5a-5d are the performance data for the four optical fiber links described in Table 2. The data indicate that Link #3 and #4 experienced approximately 1.0 dB and 0.2 dB deviation, respectively in SNR during the first year in orbit. Currently, the reduction of SNR data in links #1 and #2 is still under analysis. Until calibration of all optical sources, receivers, and optical fibers is complete, no conclusions can be reached regarding the temperature dependence



exhibited by these links. However, the preliminary results indicate that using updated fibers and cabling in space will result in excellent fiber optic link performance.

An example of possible cabling influence on the ability of optical fibers to perform in space can be seen in Figs 5b and 5c. Here, two identical plastic coated silica fibers were cabled using different technologies available at the time that the experiment was designed. Fiber link #2 used a loose tube configuration which theoretically allowed a fiber encased by the loose tube to experience a greater degree of freedom than that of a tightly wrapped fiber, such as link #3. The intent in the loose configuration was to lessen micro- and macro-bending losses induced by cabling restrictions or flexing.

However, as our preliminary data indicates the conformal wrapped fiber performance far exceeded that of the loose tube configuration. These results however, will not be conclusive until other studies of link parameters such as post-flight connector integrity and temperature effects are performed.

Other factors including electronic malfunctions, fiber optic connector instabilities, cabling differences, and the effects of radiation must first be analyzed before any direct malfunction on the part of these two links can be ascertained. Thus, a rigorous and sequential protocol, investigating each and every factor, is currently underway, with an estimated completion date within this calendar year.

#### *Brief Analysis of In-Orbit Radiation Dosimeter Measurements*

Another objective of WL Exp #701 involved the study of the trapped and galactic radiation effects on the space exposed fiber optic link performances. Several studies have thus far been conducted on LDEF received doses<sup>†</sup> [20-21]. The selection of optical fibers for inclusion in the experiment over the period 1978-1982 was based upon the best known technology at the time of the experiment fabrication, and on the results of radiation sensitivity experiments that were performed [1-5] on a variety of candidate fibers. Table I contains a listing of the space exposed fibers and a short description of their characteristics.

In order to measure the accumulated dose and spectrum of the space radiation environment, both thermo-luminescent dosimeters (TLDs) and plastic nuclear-track detectors (PNTDs) were located within the experimental tray volume. This inclusion of the detectors on WL Exp #701 constituted a cooperative arrangement between the University of San Francisco and the WL Exp #701 project office.

---

<sup>†</sup>E. V. Benton, *Analysis of Dosimeters Aboard LDEF Exp M0004*, 26 Jun 90 and 29 Aug 90 (Unpublished Reports).

The TLDs and PNTDs were enclosed in a sealed container, and co-located within the EPDS shielded volume (Fig. 6). Each was mounted on a separate 45° wedge, with their inclined surfaces facing 90° with respect to each other. This orientation was chosen to optimize the varying shielding directions experienced within, and exterior to, the tray volume. A complete description of the composition of the TLD and PNTD materials may be found elsewhere<sup>†</sup>.

The results of an interim analysis<sup>†</sup> based on a 1-D shielding model indicated that the space exposed optical fibers experienced a total dose varying from 238 rad(Si), to 25 Krad(Si), depending on shielding provided by the fiber cabling materials and hold down clamps. The analysis accounts for boundary conditions of lightly shielded fibers (typically 0.01 to 0.05 g/cm<sup>2</sup>) to substantial shielded portions of the fiber, particularly those portions under the hold down clamps (1.06 g/cm<sup>2</sup>, see Fig. 1b). The fiber doses resulted primarily from geo-magnetically trapped electrons, since the galactic cosmic ray contribution was estimated to constitute [20] approximately 1% to 3% of the trapped proton dose at typical shieldings (greater than 1 g/cm<sup>2</sup>). Therefore, for a shielding of less than 1.0 g/cm<sup>2</sup>, trapped electrons dominate the surface-absorbed dose [20]. Shown in Table 3 is an analysis<sup>†</sup> performed for predicting ranges of doses experienced by the fiber optic links.

While the optical fiber links were calculated to have received a substantial dose over the 2114 days in orbit, no direct evidence of permanent induced radiation damage has been observed to date. As may be seen in Fig. 4, the external tray temperature - extrapolated from the internal measurements and calibrations - ranged from approximately +57° C to -29° C. The fibers orbited in this experiment were known to possess good radiation annealing properties, enhanced by elevated temperatures. Optical power levels present in the fiber links during the first year in orbit (typically 30 μW) would have significantly contributed to any photo-induced annealing (photo-bleaching). The one notable exception to this early prediction involves Fiber Link #1. However, while radiation induced damage is not ruled out, more probable causes for the observed losses include micro and macro bending effects, fiber pistoning, and/or connector caused misalignments. All of these effects can be explained by temperature dependence and are currently under investigation.

Thus, as a result of this early analysis, it is concluded that no permanent effects due to space induced radiation occurred to the external fiber optic links. The same rationale may be used to predict any expected radiation damage for the passive fibers within the tray volume, and also the light emitting diode sources and the pin photodiode detectors (all currently under investigation). The doses received by these components are currently being correlated to the TLD and PNTD calibrations. For example, an interim analysis<sup>†</sup> determined that the experiment tray shielding (minimum of 2.4 g/cm<sup>2</sup>) resulted in a high LET data of 0.88 mrad(Si)/day (total dose of 1.86 rad(Si), with measured integral flux of  $3.6 \times 10^{-4} \text{ cm}^{-2} \text{ s}^{-1} \text{ sr}^{-1}$  (for LET<sup>∞</sup> Si ≥ 50 MeV cm<sup>2</sup> g<sup>-1</sup>). The TLD doses varied from 100 times to 125 times the LET dose, or 186 - 233 rad(Si). The FO components used in the experiment would not have been expected to be affected at these levels.

---

<sup>†</sup>E. V. Benton, *Analysis of Dosimeters Aboard LDEF Exp M0004*, 26 Jun 90 and 29 Aug 90 (Unpublished Reports).

Following de-integration of the experiment, the individual components will be radiation tested to substantiate this prediction.

### *Brief Analysis of In-Orbit Micro-Meteorite and Debris Impacts*

Shown in Fig. 7a is a photograph of one section of the experiments' surface. This surface (which provided shielding for the EPDS) measured 0.41 m x 0.91 m and was composed of a 1 mm thick aluminum alloy (6061-T6) and was painted with Chemglaze (A276). This coated protective sheet (PS) and a thermal fiberglass cover coated with aluminized mylar provided additional protection to the shielded EPDS, MTM, DPCA and dosimeters immediately below. As may be seen in Fig. 7b, the impactors on the PS [9] were tallied and compared to impactors experienced by the Solar Max satellite during its four year stay in orbit. While both satellites were in low-inclination orbits, they experienced different periods of solar activity (Solar Max: 1980-1985; LDEF: 1984-1990). This may account for the differences in flux values. A tally of the number of large craters ( $>300\text{ }\mu\text{m}$ ) and small craters ( $>100\text{ }\mu\text{m}$ ) yielded 29 large, and 264 small. A more detailed accounting of analyses performed on impactor chemical composition, directionality of impacts, and other related effects can be found in recently published data [6].

Figs 8a and 8b illustrate some typical impactor sites experienced by the space exposed optical fiber cables and surrounding materials. Evident in Fig. 9 is a classic impactor region on a fiber link face plate. As may be observed, there is no evidence from these photographs to show that the single optical fibers contained within the individual cables are severed or melted, as was previously reported [16]. Protective materials between the exterior cabling and the single element optical fiber can be seen protruding from the outer-most cabling in Fig. 8a. However, this optical fiber still continues to function correctly.

Fig. 10 is a photographic close-up of the impactor site on Link #4. Notice there is no evidence of any optical fiber damage although the cabling and protective jacketing materials are damaged. Our recent analysis and testing of this particular link has revealed that the single fiber within the cabling was indeed broken by an impactor. In order to detect the breakage, two investigative methods were used, since normal microscopy and IR detection methods employed at KSC did not ascertain any breakage.

The first method consisted of passing continuous visible laser light ( $\lambda = 6328\text{ }\text{\AA}$ ) through the transmitter end of the fiber. This allowed a very small amount of scattered light to penetrate or scatter through the Kevlar strength members and Hytrel jacketing and be observed. Under normal link operating conditions, light of a wavelength of 830 nm is present for approximately 26 ms, making detection of any low-level short-duration scattered light difficult.

The second investigative scheme involved an optical time-domain reflectometer (OTDR) measurement. Fig. 11 illustrates that the impactor caused breakage at a distance of 18.9 m from the optical transmitter end, or 27.4 m from the receiver end. The sum of these distances measured to the impactor site resulted in correlating within OTDR error to the link length, 48 m.

It is estimated that this breakage occurred between day 365 and day 2114 in orbit. Prior to the 365th day, this particular link performed in an excellent manner, as recorded in the orbital data tape, testifying to the applicability of fiber optics in space.

#### IV. CONCLUSIONS

The Preliminary results presented within this paper confirm and solidly demonstrate that fiber optics systems are mature and suitable for applications in the space environment.

Analyses to date confirm that the four space exposed fiber optic links orbited performed within their expected performance profile under temperature cycling extremes and direct space exposure to galactic and trapped radiations, atomic oxygen, and ultraviolet radiation.

Activation of the experiment at KSC some 2185 days following its April 1984 deployment into low-earth orbit resulted in excellent performance by three of the four space-exposed links. The links continue to operate, thus providing a benchmark and invaluable data base for on-going and future space photonics programs and for fiber optics space survivability and reliability studies.

Despite numerous micro-meteorite and debris impacts experienced by the cabled fibers and experiment surfaces, only a single optical fiber was observed to be severed over the 2115 days in orbit. This event occurred after the data acquisition portion of the mission was completed. Thus, the experiment operation and demonstration of technology concept were both fully successful.

Perhaps the most profound conclusion that may be drawn from the preliminary data presented is that this experiment demonstrated that 1978-1980 era fiber optic technology can and did operate excellently in space for a prolonged time period. One need only apply the much improved technology and advances in fiber optic or photonic technologies during the past decade to fully realize fiber optic applications in space.

This experiment demonstrated for the first time, under severe and deliberate space exposure conditions, that fiber optic systems can survive in a prolonged space orbit.

#### V. ACKNOWLEDGEMENTS:

The authors wish to acknowledge former Jet Propulsion Laboratory staff members who were responsible for developing the experiment during various periods of its seven year pre-launch evolution. They included: Messrs Fred Chamberlin, George Lagomarcini, and Don Hultberg. Special thanks and recognition to Drs Alan H. Johnston and Larry Bergman of JPL, for their excellent design and development and fabrication of the experimental apparatus, and their many important contributions leading to the success of the mission.

Special recognition is also directed to former Weapons Laboratory personnel, including Major Jonathan Emmes and Mr Jeffery D. Wiltse for their technical assistance during development and efforts prior to launch; and to Major Glen Kuller and Lt Col Marion F. Schneider, for their encouragement to the PI in pursuing this mission, and their helpful coordination. Mr Arthur Goodman deserves special recognition for his outstanding photographic skills during the retrieval and deintegration activities at the Kennedy Space Center.

The PI wishes to acknowledge the contributions of the entire Phillips Laboratory Optoelectronic Section, and in particular, Messrs Stephen DeWalt, Mark F. Mitcham, and Delphino Antonio for assisting in the preparation of this preliminary report on short notice.

Finally, profound thanks to the NASA LDEF team that provided excellent support during the entire mission. The excellent efforts of Messrs Lenwood G. Clark, William Kinard, Jim Jones, Bob O'Neil, Carol Kaiser and Mrs Glenna Martin contributed directly to the success of our mission.

## REFERENCES

- [1] E. W. Taylor, "FIBER OPTICS SPACE EFFECTS," (presented at FOC 78, Chicago, IL) Proceedings of Fiber Optics and Communication, Sep 78, pp 245-7.
- [2] E. W. Taylor, "SOME RECENT FIBER OPTICS RESEARCH, DEVELOPMENT AND APPLICATIONS CONDUCTED BY THE AIR FORCE", Proc. Fiber Optics in the Nuclear Environment, Vol 1 - Applications, DNA 5308P-1, pp 209-221, 30 May 80.
- [3] E. W. Taylor, J. M. Emmes, C. E. Barnes, and J. Wiczer "BEHAVIOR OF IRRADIATED PLASTIC CLAD SILICA FIBERS AT LOW TEMPERATURES," Photon 80 Conf. Proc. Comptes-Rendu, Paris, FR, Oct 80, pp 110-117.
- [4] E. W. Taylor, J. M. Emmes, W. R. Ayres, J. D. Wiltse, and J. K. Merritt, "RESPONSE OF IRRADIATED OPTICAL WAVEGUIDES AT LOW TEMPERATURES," SPIE Vol 296, Aug 82, pp 40-50.
- [5] E. W. Taylor, L. J. Myatt, and J. D. Wiltse, "LOW TEMPERATURE GAMMA IRRADIATION RESPONSE OF POLYMER COATED OPTICAL WAVEGUIDES," Photon 83, SPIE Vol 404, Paris, FR, May 1983, pp 55-59.
- [6] A. R. Johnston, L. A. Bergman, E. W. Taylor, "FIBER OPTIC EXPERIMENT FOR THE SHUTTLE LONG DURATION EXPOSURE FACILITY," SPIE Vol 296, Aug 82, pp 40-50.
- [7] E. W. Taylor, "SPACE EFFECTS ON FIBER OPTICS SYSTEMS," NASA SP-73, The Long Duration Exposure Facility, Mission 1 Experiments, edited by L. G. Clark et al., Washington, DC, 1984, pp 182-184.
- [8] D. S. McKnight, R. E. Dueber, and E. W. Taylor, SPACE DEBRIS AND MICROMETEORITE EVENTS EXPERIENCED BY WL EXP #701 IN PROLONGED LOW-EARTH ORBIT, J. Geophysical Research Space Physics, Vol 96, No A6, June 1, 1991, pp 9829-9833.
- [9] E. W. Taylor, AN EXPERIMENT FOR STUDYING MONOLITHIC INTEGRATED OPTICS PERFORMANCE IN THE SPACE ENVIRONMENT, SPIE Cambridge Symposium on Optical and Electro-optical Engineering, Integrated Optical Circuit Engineering II, Vol 548, 17-19 Sep 85, pp 46-50.

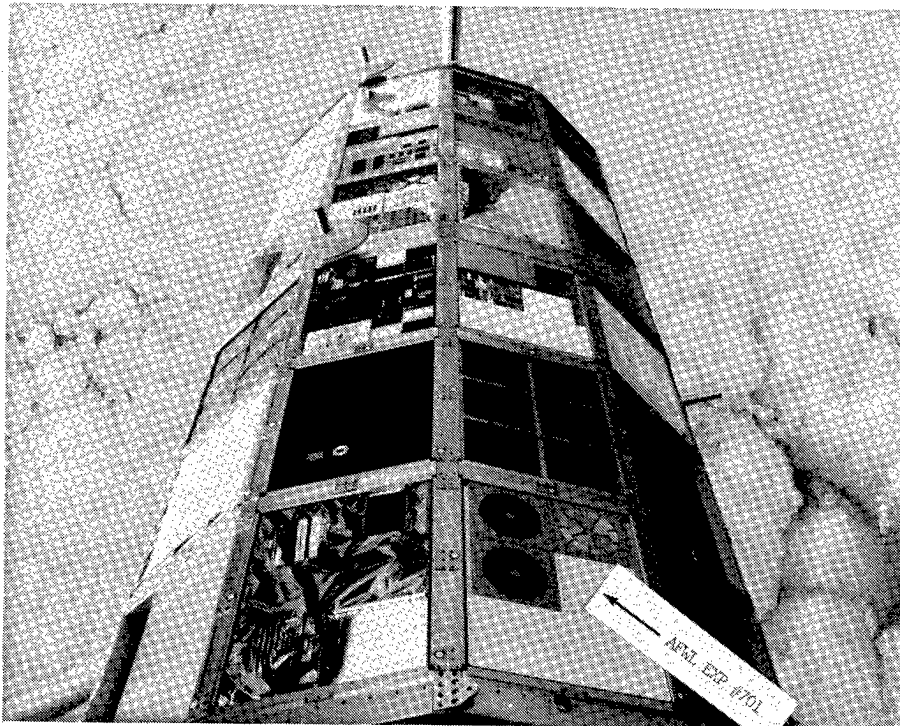
- [10] E. W. Taylor, V. R. Wilson, J. D. Wiltse, J. H. Yeatts, and T. E. Suppan, GAMMA RAY IRRADIATION OF OPTICAL FIBER WAVEGUIDES USING OPTIMIZED EXPOSURE AND LAUNCH PARAMETERS Paper presented at OPTO 86 6th European Symposium on Optoelectronics, Paris FR, 13-15 May 86, ESI Pub., pp 477-485.
- [11] E. W. Taylor, OVERVIEW OF AIR FORCE RADIATION EFFECTS PROGRAMS IN FIBER OPTICS, First International Military and Government Fiber Optics and Communication Expositions, March 1987, and Int. J. of Optical Sensors, Vol 2, No. 3, Jun 87, pp 201-209.
- [12] E. W. Taylor, A. D. Sanchez, V. R. Wilson, et al., A COMPARISON OF INTEGRATED AND FIBER OPTIC RESPONSES IN THE PRESENCE OF NUCLEAR FIELDS, Presented SPIE OE-Laser 88 Symposium on Fiber and Integrated Optics, Optoelectronic Materials and Devices, 10-15 Jan 88 Los Angeles, CA., Proc. SPIE, Vol 898, 1988, pp 42-45.
- [13] E. J. Friebele, E. W. Taylor, G. Turquet de Beauregard, J. Wall, and C. E. Barnes, INTERLABORATORY COMPARISON OF RADIATION INDUCED ATTENUATION IN OPTICAL FIBERS, I. STEADY STATE EXPOSURES, IEEE/OSA, J. of Lightwave Technology, Vol 6, No. 2, Feb 1988, pp 165-171.
- [14] E. W. Taylor, and E. J. Friebele et al; IBID, Part II, IEEE/OSA J. of Lightwave Technology, Vol 8, No 6, June 1990, pp 967-976
- [15] E. W. Taylor, E. J. Friebele, and P. B. Lyons STANDARDIZED MEASUREMENTS FOR DETERMINING THE RADIATION INDUCED RESPONSES IN OPTICAL FIBERS, Presented at the Symposium on Optical Fiber Measurements, Boulder, CO, 11-12 Sep 90, NIST Technical Digest, SP 792, pp 159-162.
- [16] METEOROID AND DEBRIS IMPACT FEATURES DOCUMENTED ON THE LONG DURATION EXPOSURE FACILITY: A PRELIMINARY REPORT, NASA Pub. #84, JSC #24608, August 1990, pp 351-358
- [17] E. N. Gilbert, CAPACITY OF A BURST-NOISE CHANNEL, Bell System Technical Journal, Vol 39, 1960, pp 1253.
- [18] W. M. Berrios and T. R. Sampir, LONG DURATION EXPOSURE FACILITY POST-FLIGHT THERMAL ANALYSIS, CALCULATED FLIGHT TEMPERATURE DATA PACKAGE, PRELIMINARY, NASA CP-3134, 1992.

- [19] W. M. Berrios and T. R. Sampir, LONG DURATION EXPOSURE FACILITY, SOLAR ILLUMINATION DATA PACKAGE, NASA CP-3134, 1992. NASA/LDEF Project Office.
- [20] E. V. Benton and W. Heinrich, IONIZING RADIATION EXPOSURE OF LDEF, USF-TR-77, August 1990.
- [21] T. W. Armstrong and B. L. Colborn, SCOPING ESTIMATES OF THE LDEF SATELLITE INDUCED RADIOACTIVITY, SAIC-90/1462, Sept. 1990.



**Table 1***Some Characteristics of Space-Exposed Active Optical Fibers Prior To Launch*

Variable	Link #1	Link #2	Link #3	Link #4
<b>Original Cable Color:</b>	Purple	Yellow	Biege	Blue
<b>Cable Type:</b>	Loose Tube	Loose tube	Conformal	Conformal
<b>Cable Material:</b>	Polyurethane	Tefzel	TBD	Hytrel
<b>Fiber Type:</b>	Glass/Glass Semi-Graded	PCS Step Index	PCS Step Index	PCS Step Index
<b>Core/Clad um/um:</b>	100/140	207/327	207/327	198/358
<b>Numerical Aperature:</b>	0.30	0.22	0.22	0.33
<b>Bandwidth (3db) (MHz - km):</b>	20	25	25	25
<b>Attenuation (db/Km):</b>	6.0 @ 850nm	5.0 @ 850nm	5.0 @ 850nm	9.2 @ 850nm
<b>Wavelength (nm):</b>	1300	830	830	830
<b>Link Length (m):</b>	45.0	19.7	20.5	48.0

**Figure 1a. WL EXP #701 aboard LDEF**

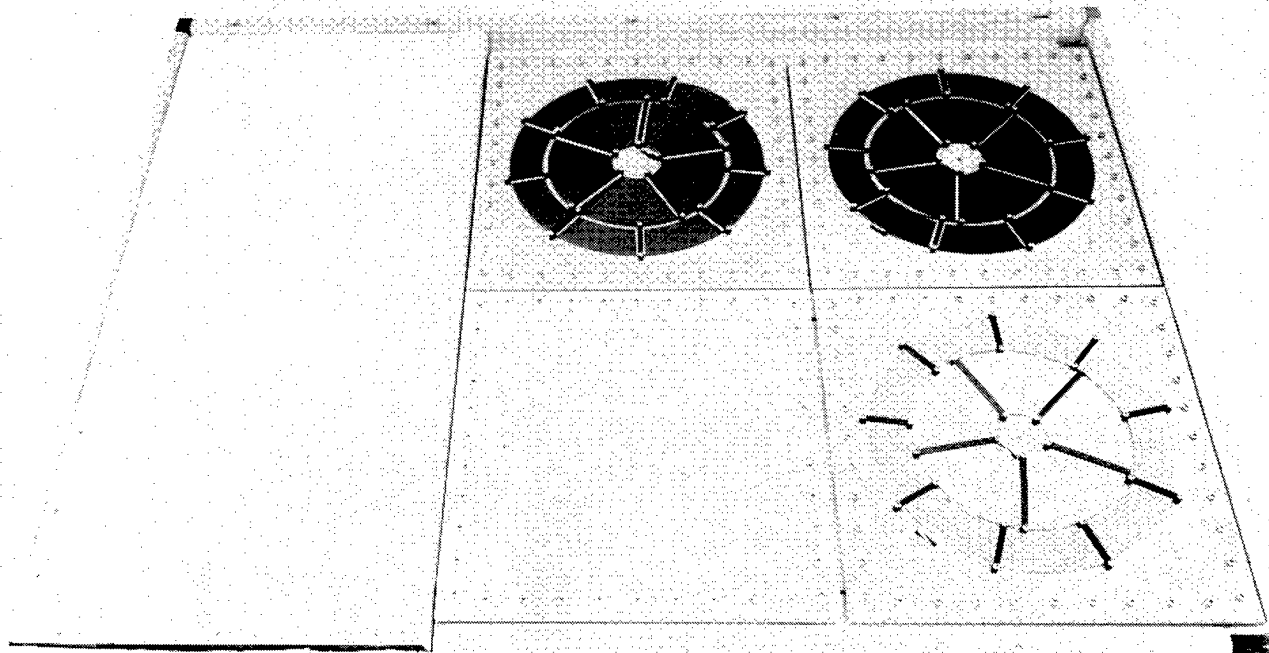


**Figure 1b. Pristine condition of WL EXP #701 prior to launch**

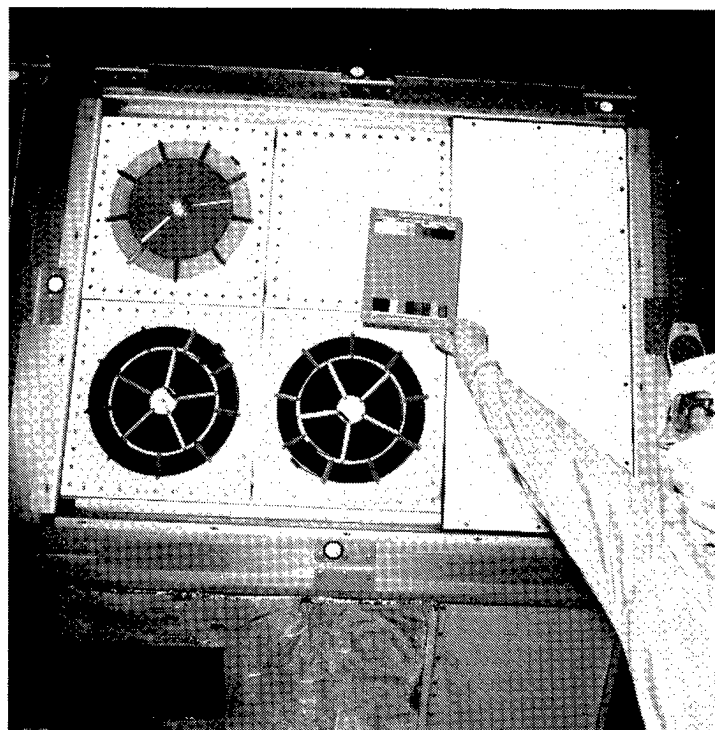
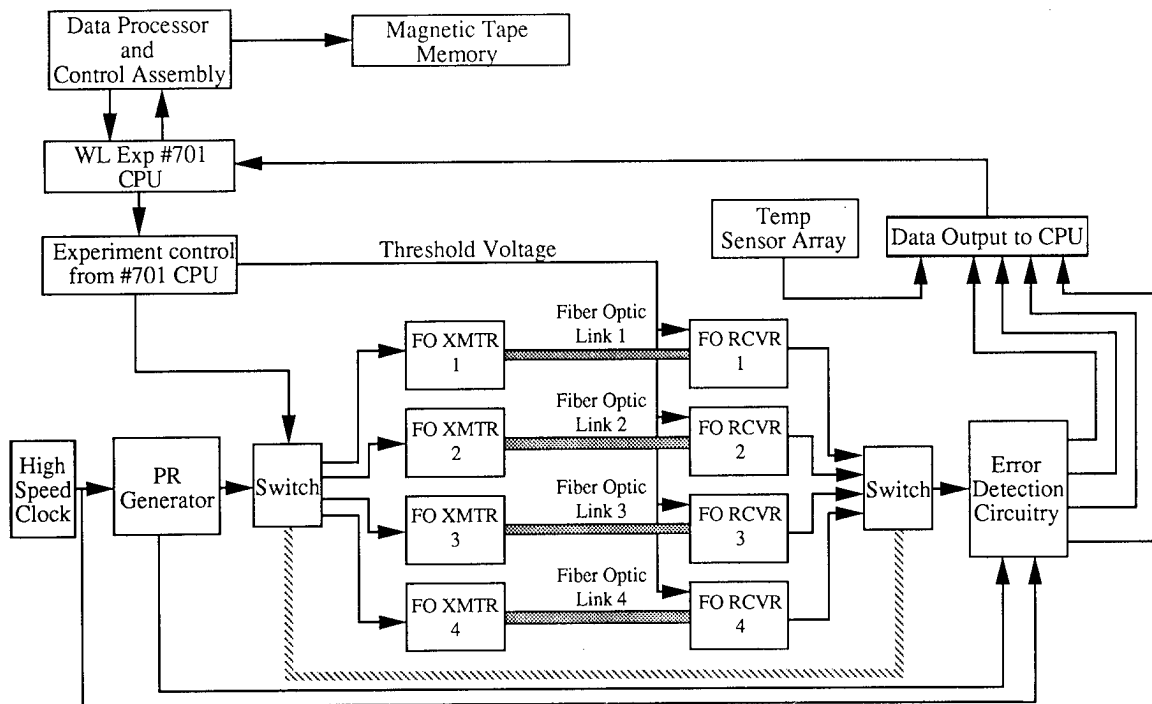


**Figure 1c. Observation of cabling color changes shortly after LDEF recovery**



Configuration of experiment hardware used to measure the performance of the four active digital optic links contained in WL Experiment #701 (M0004). The experiment measured the temperature at various locations within the tray volume and the performance of the fiber optic links by measuring the Signal-to-Noise Ratio and Bit-Error Rate of each link.

Figure 2.

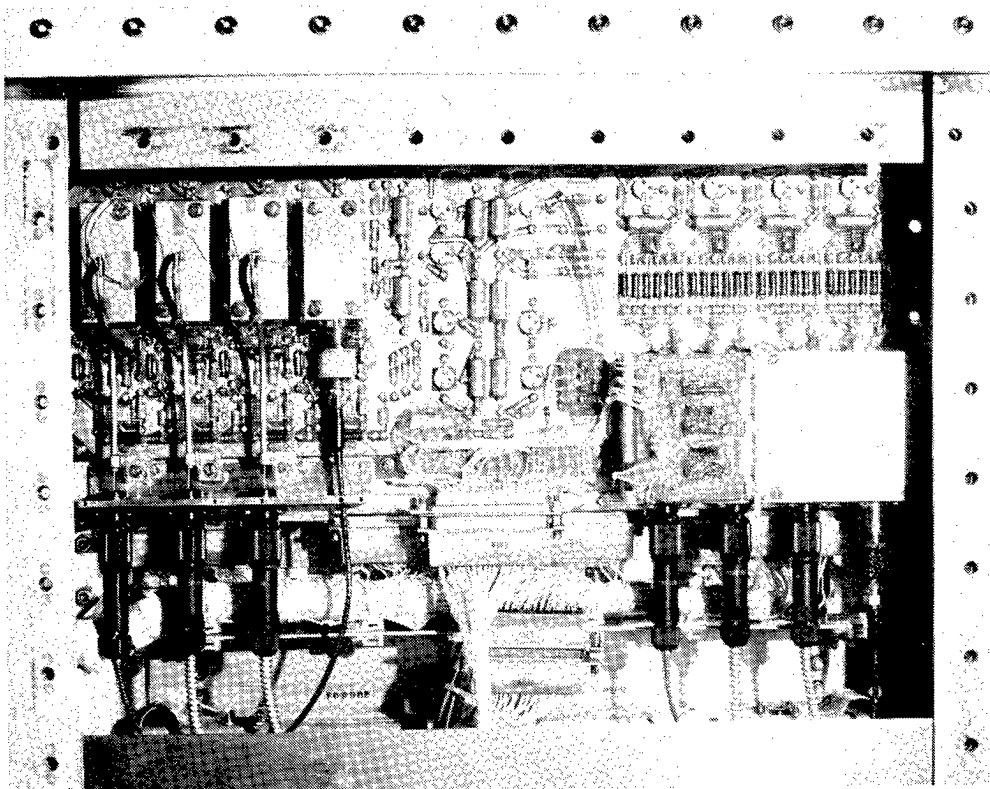


Figure 3a. View of Experimental Measurement System

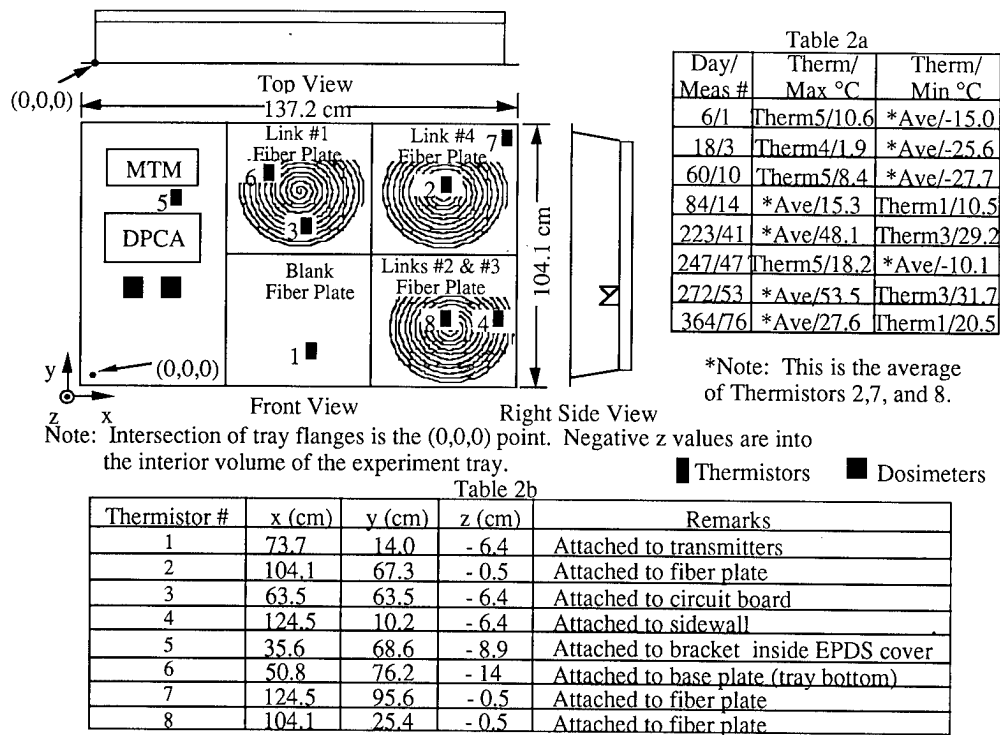


Figure 3b. Thermistor, optical fiber, and dosimeter locations

TABLE 3

Interim Analysis of Radiation Doses Experienced by WL Experiment #701

Shielding Depth (g/cm )	Trapped Electrons (rad)	Trapped Protons (rad)	GCR <sup>δ</sup> , other (rad)	Total Dose (rad)
0.01	24,500	515	33	25,000
0.02	12,100	471	33	12,600
0.03	7,320	444	33	7,800
0.04	4,980	425	33	5,440
0.05	3,540	410	33	3,980
0.86	11.9	218	33	263
1.06	3.3	202	33	238
1.25	2.6	193.5	28.4*	224.5 ± 6.0**
2.48	0.1	149.5	37.0*	186.5 ± 5.8**

δ - Values determined from comparison of measurement and calculation.

\* - Difference between measured and calculated doses.

\*\* - Measured TLD Values.

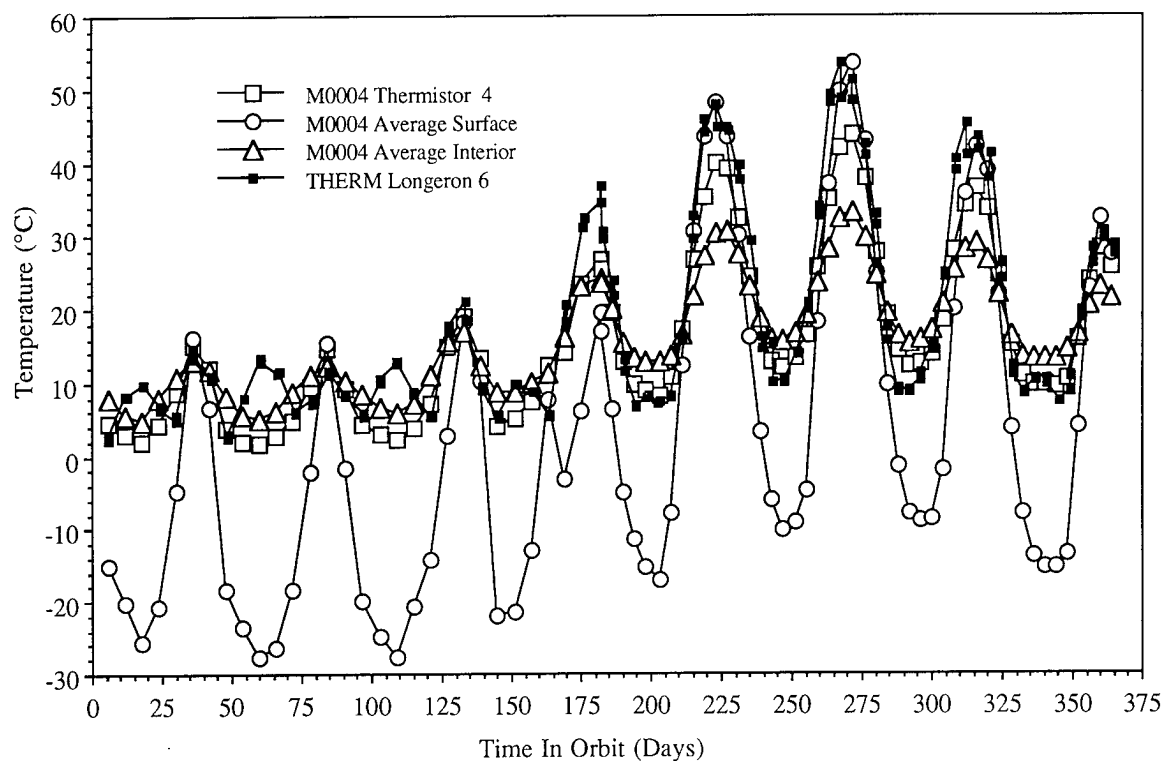


**Figure 4. Comparison of M0004 and selected THERM experiment temperature data**

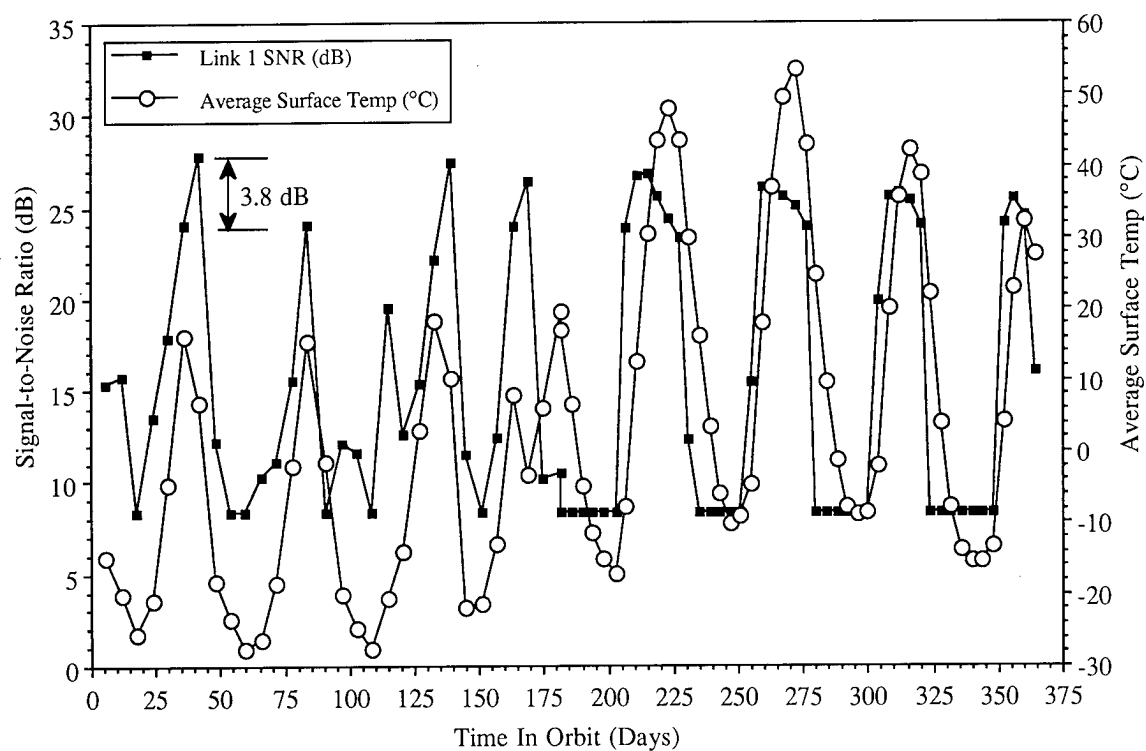


**Figure 5a. M0004 in-flight performance of Link #1**

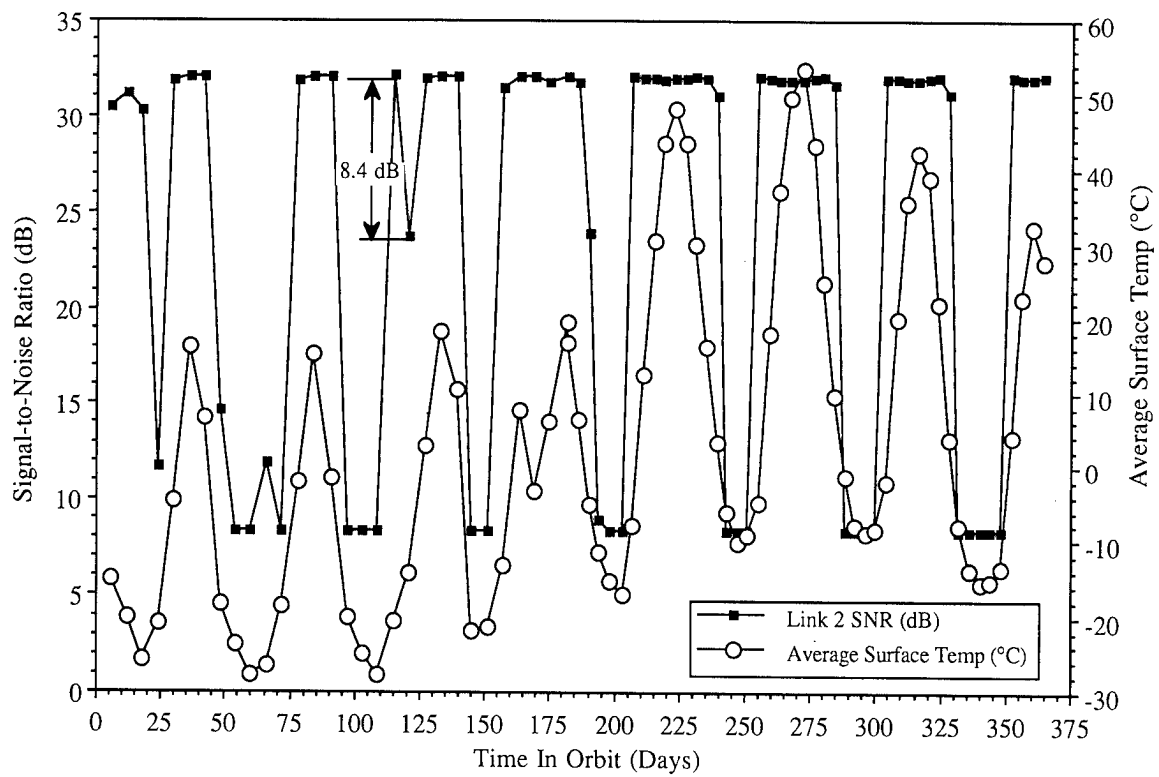


**Figure 5b. M0004 in-flight performance of Link #2**

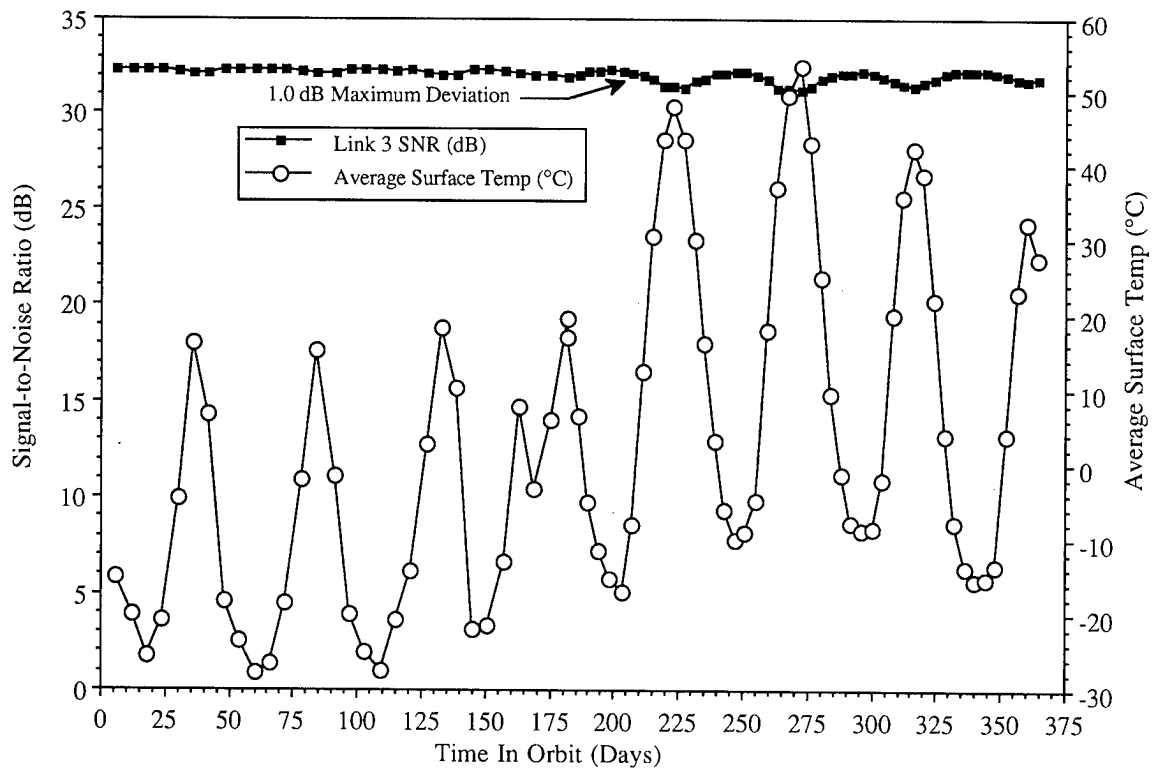


**Figure 5c. M0004 in-flight performance of Link #3**

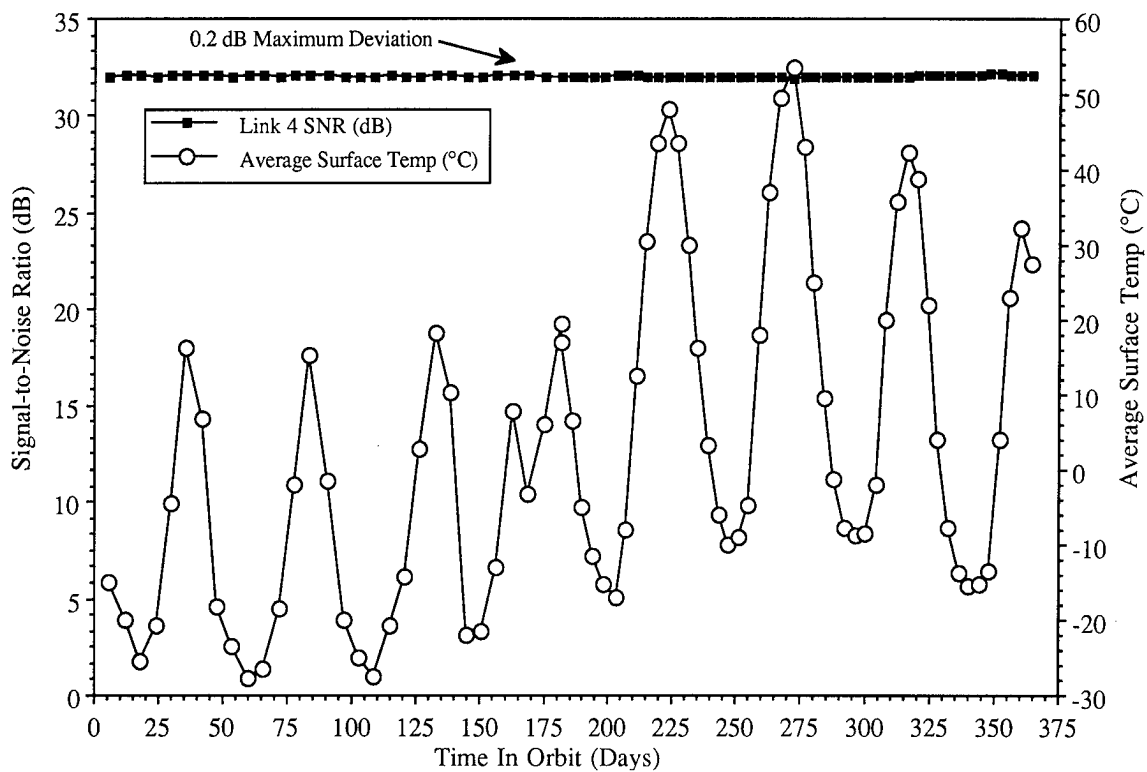


**Figure 5d. M0004 in-flight performance of Link #4**

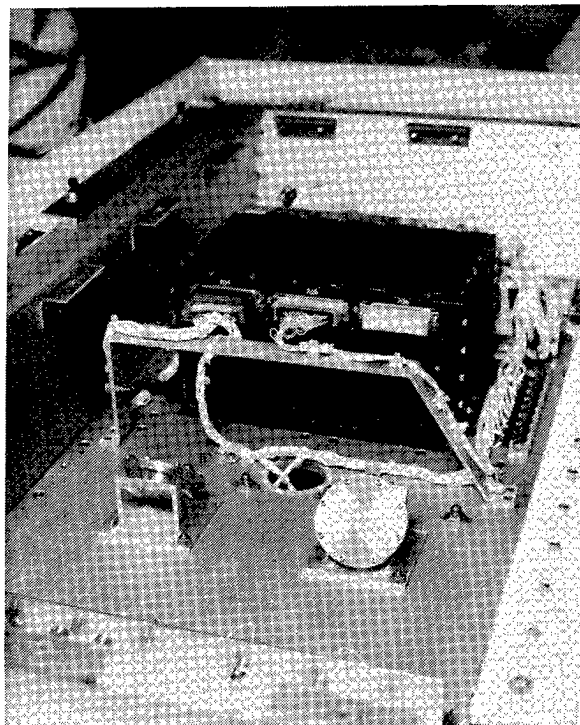


**Figure 6. Location and orientation of dosimeters**

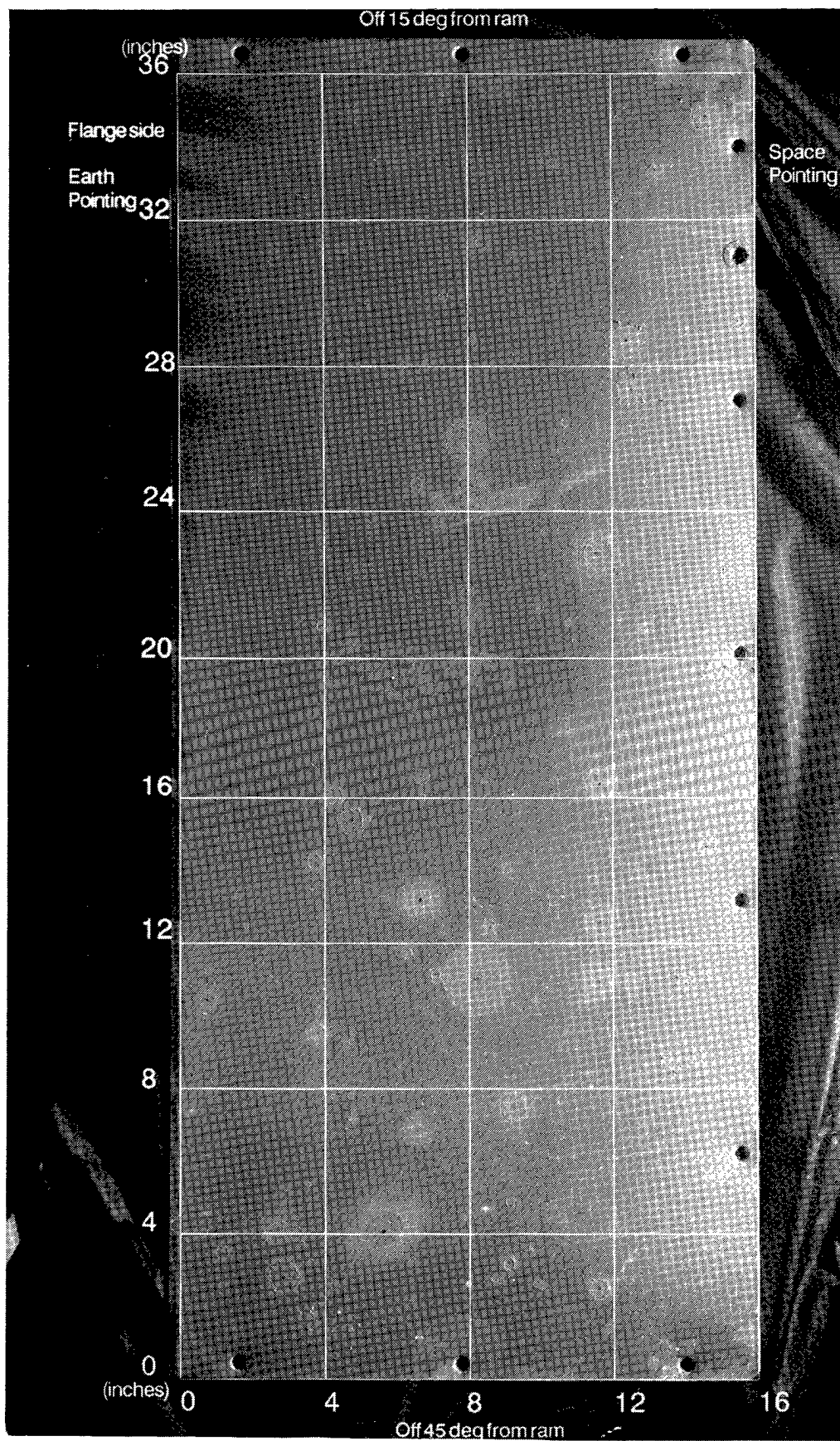


Figure 7a. Shadowed photograph [9] illustrating impactors on WL EXP 701



# FLUX CALCULATION COMPARISON

## LDEF VS SOLAR MAX

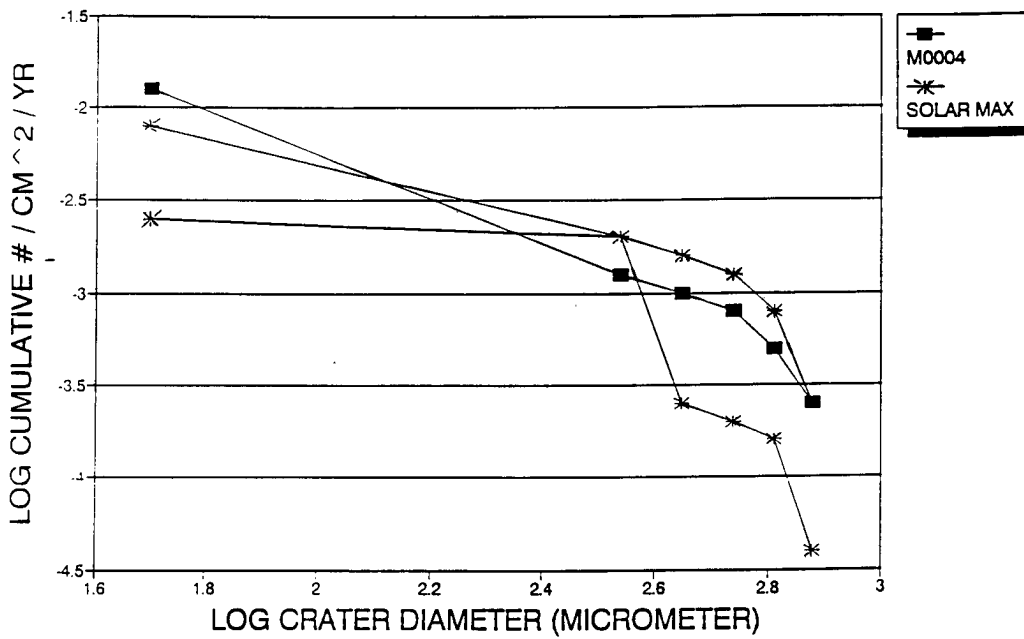


Figure 7b. Comparison [9] of WL EXP and Solar Max Satellite impactor flux data

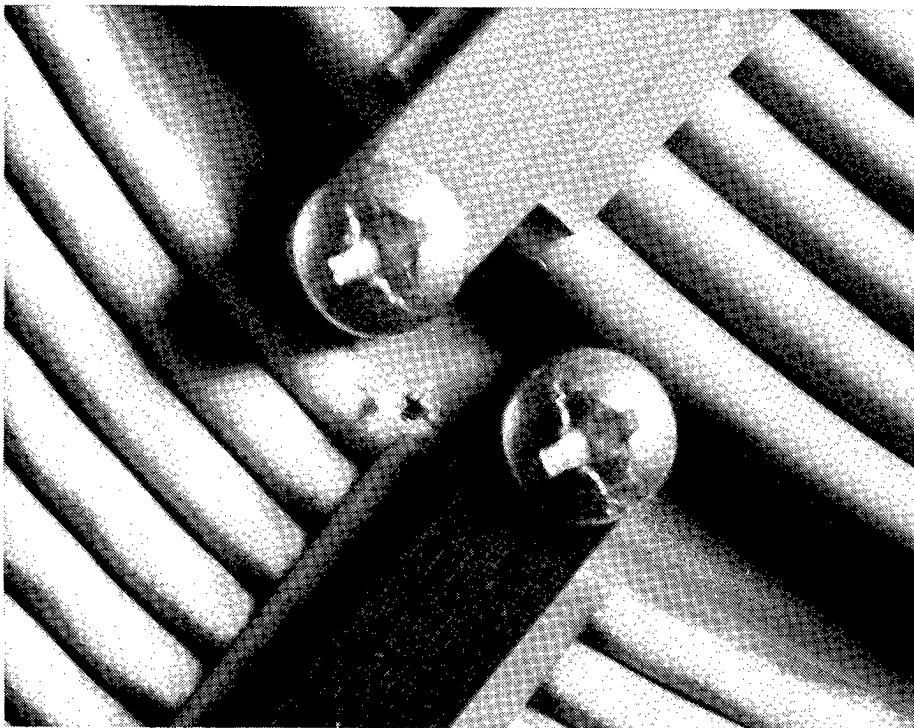
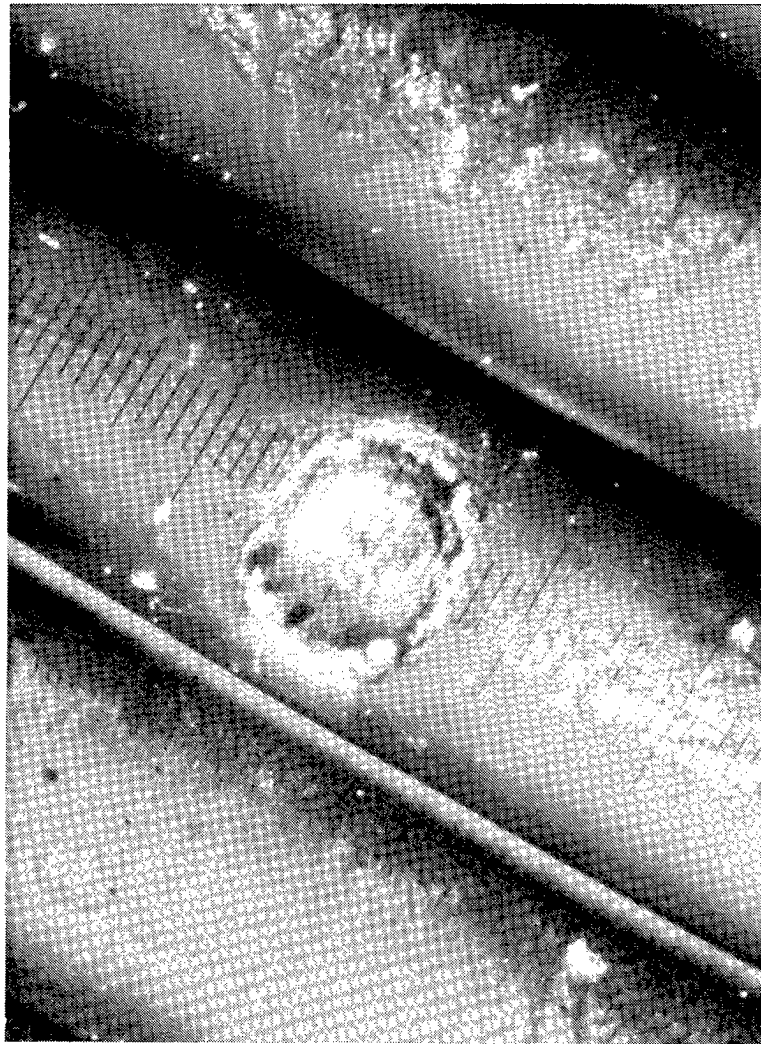
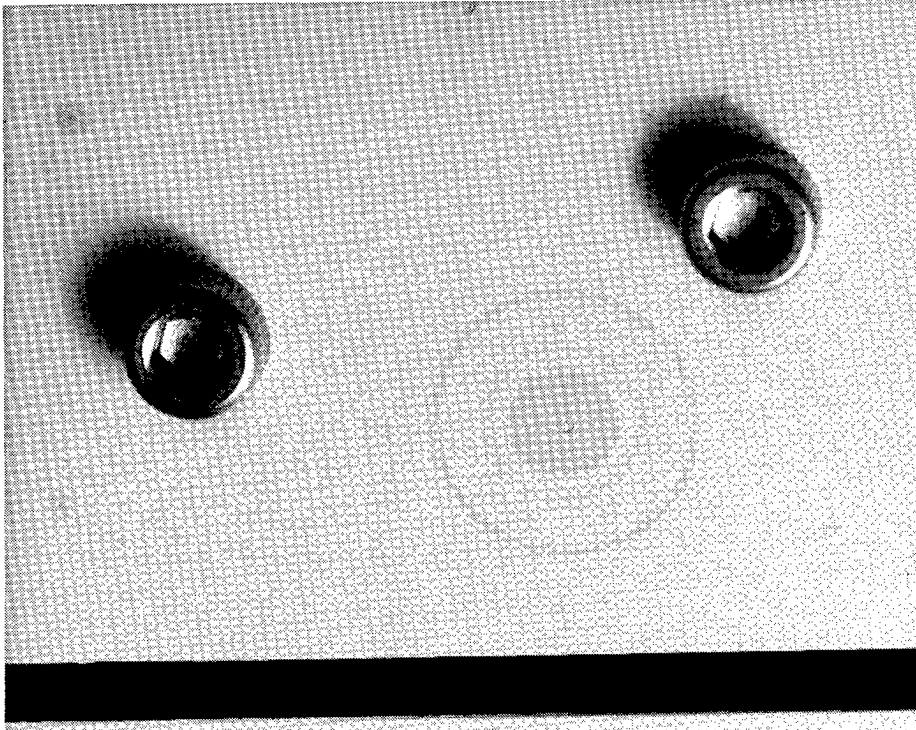


Figure 8a. Example of impactor site on WL EXP fiber optic Link #2



**Figure 8b. Example of impactor site on WL EXP fiber optic Link #4**



**Figure 9. Close-up of WL EXP 701 Link #4 impactor region**

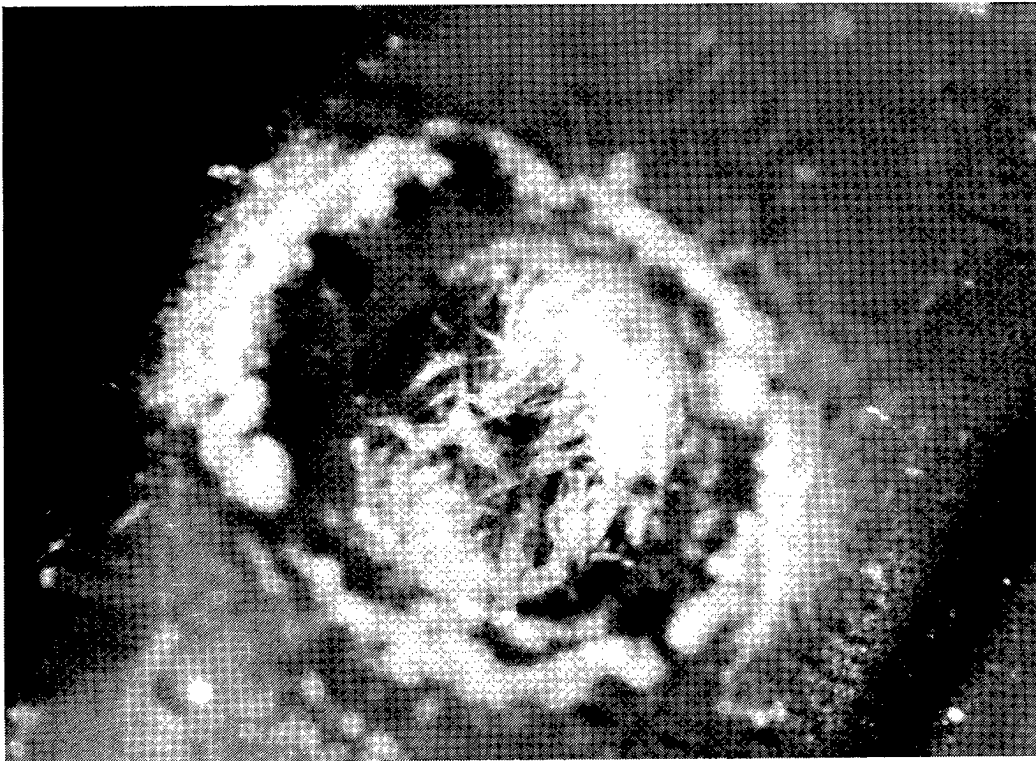
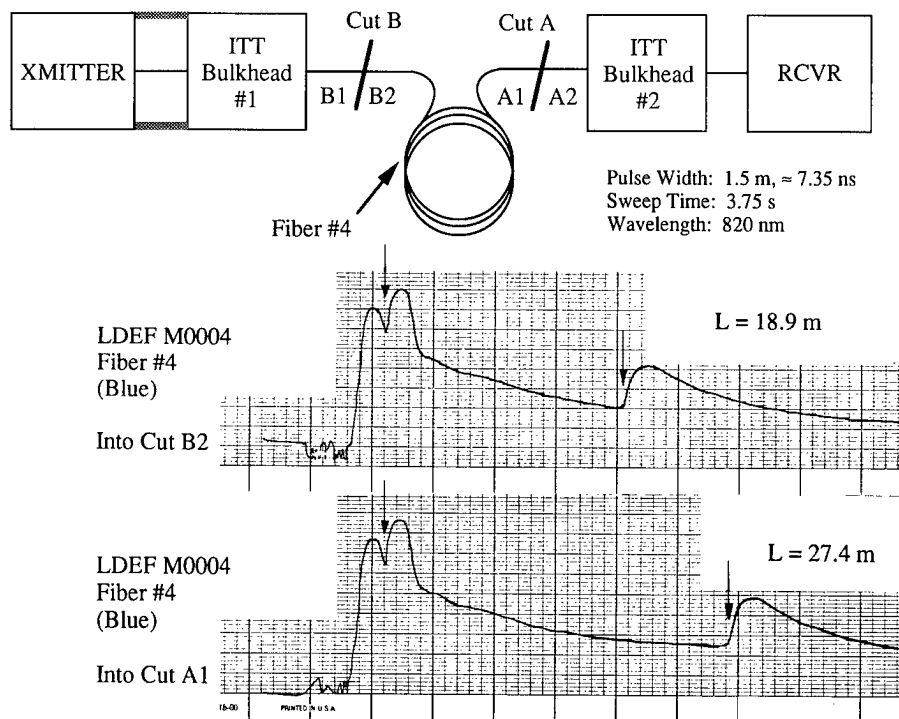


**Figure 10. Close-up of impactor region on WL EXP 701 fiber optic Link #4**



Optical time domain reflectometry analysis of impactor location on WL EXP 701 fiber optic Link #4

Figure 11.

## LDEF FIBER OPTIC EXPOSURE EXPERIMENT NO. S-0109

A. R. Johnston,  
818/354-4054

L. A. Bergman  
818/354-4689

R. Hartmayer  
818/354-1925

Jet Propulsion Laboratory  
California Institute of Technology  
Pasadena, California 91109  
Fax: 818/393-4820

### SUMMARY

Ten fiber optic cable samples of different types were exposed in low earth orbit for over 5 1/2 years on the Long-Duration Exposure Facility (LDEF). Four of the samples were mounted externally, and the remaining six were internal, under approximately  $1/2 \text{ g cm}^{-2}$  of aluminum. The experiment was recovered in January of 1990, and laboratory evaluation of the effects of the exposure has continued since. An increase in fiber loss, presumed to be from radiation darkening, aging effects on polymer materials used in cabling, unique contamination effects on connector terminations, and micrometeoroid impacts were observed. In addition, the sample loss was measured for each sample as a function of temperature before and after the flight. All cable samples were functional, and the best exhibited no measurable change in performance, indicating that conventional fiber optic cables can perform satisfactorily in spacecraft. Experimental results obtained to date are presented and discussed.

### INTRODUCTION

The purpose of the fiber optic exposure experiment to be described in this paper was to study the effects of the low earth-orbit space environment on optical fiber cable and connector samples. The effects of ionizing radiation, periodic temperature cycling, polymer aging, mechanical deterioration of the packaging, contamination of connectors, and micrometeoroid impacts on the fiber cables are all of great importance for future system designs. The resulting data will, therefore, provide an increased level of confidence in the use of optical fiber technology in future NASA spacecraft and military satellites.

The JPL fiber optic exposure experiment was initiated in 1975, with the selection of fiber cable samples taking place in 1982. The experiment tray was delivered to the LDEF project in 1983, and launched on board the space shuttle in April, 1984. It was recovered 68 months later, in January of 1990, with the post-flight analysis commencing in April, 1990.

In this paper we will describe the initial results of the experiment tray post-flight analysis, performed over the last 12 months. We first describe the configuration of the experiment tray, and the fiber optic cables and connectors used. The next section discusses the post-flight observations of the components and the tray itself, followed by a section presenting the experimental data obtained to date. The paper concludes with a discussion of the results obtained, and finally summarizes their significance for future system design.

## EXPERIMENT CONFIGURATION

The experiment tray was mounted in row 12, bay 'C' of the LDEF structure, which was located 90° from the leading edge (row 9) and slightly off-center, towards the earth end (the third bay of six). The aluminum experiment tray measured approximately 120 cm by 100 cm and 15 cm deep. The front surface of the tray was divided into six approximately square areas. Four of these areas carried fiber optic cable samples mounted on 4.8 mm thick aluminum plates, while the remaining two areas were covered by a single aluminum plate, about 2.3 mm thick, acting only as a protective cover. An additional six fiber cable samples were placed inside the tray, one underneath each of the six square areas. Figure 1 is a photograph taken from the shuttle during the recovery showing the experiment tray mounted in the LDEF. The aluminum sample plates and the protective cover were coated with an off-white thermal control paint. The four surface-mounted sample plates or modules were thermally isolated from the rest of the experiment tray by means of fiberglass spacers under the aluminum plate and an aluminized kapton thermal shield mounted under each sample plate. The thermal isolation was provided in order to increase the magnitude of the temperature swings experienced by the surface mounted samples during the orbital cycle.

Each of the ten fiber optic cable samples was of a different type. The cables chosen were felt to be types which might be considered for spacecraft application. All were off-the-shelf products, available in the early 1980's, except the single-mode fiber, which was a developmental item, cabled in an off-the-shelf cable type. All the major fiber types, plastic-clad, large-core, graded index and single-mode, were represented. For each flight sample, an identical control fiber cable sample was kept at JPL for post-flight comparisons.

The expected temperature range, determined from pre-flight thermal modeling, was estimated to be between 0° and 90°F inside the tray; for the surface mounted samples it was expected to be between -85° and 185°F. The total expected radiation dose seen by the fiber cables while in space was estimated from published information [Ref. 1] at around 300 rads for the internal samples, and 7500 rads for the external samples.

The six internally mounted fiber cable sample coils were mounted on the bottom of the tray by means of cable ties as shown in Figure 2. An aluminum bracket in the center of the coil, carried two connector bushings, and the two connectors terminating each sample were mounted in these bushings, to physically support the cable ends, but were not used as optical connectors. For each sample, the terminations were prepared following the procedure recommended by the connector manufacturer. The connector termination also could be inspected, cleaned, if appropriate, and used for coupling light in and out of each sample for characterization. Three types of SMA connectors were used.

Each of the four external cable samples was mounted in the form of a planar, helical coil on its supporting plate, and was held down by black-anodized aluminum clamps, as shown in Figure 3. Silicone-rubber spacers were used as cushions between the fiber and the clamps, but the clamps were dimensioned so they could be tightened securely without applying any pressure to the sample cable. Both fiber ends were led through slots to the rear side of the plate, and were connectorized as the internal samples were.

Table 1 presents data about the cable construction and materials for each sample as well as some nominal performance parameters. The sample length was approximately 26 meters for the external samples and 50 meters for the internal ones, except for samples P-3 and C-4, which were 30 and 68 meters in length, respectively. External fiber cable samples are identified by the letter 'P', while the internal samples are identified by the letter 'C' in the sample designation. All fibers were intended for operation at 830 nm.

## POST-FLIGHT OBSERVATIONS

Generally, there were no changes in the components mounted inside of the experiment tray that could be seen by comparing before and after photographs. However, two external samples exhibited an obvious color change, and there were slight stains near the clamps that appeared to be due to outgassing of the silicone hold-down pads, as well as brown stains on areas around openings to the interior, which were observed throughout the LDEF. The color of the P-1 cable jacket turned from a bright orange into a dark brown, while the light-blue P-3 cable faded to a grey blue. The P-2 and P-4 cables retained their black color, but lost their gloss. We believe these changes are probably due to the extended exposure of the polymer jackets to sunlight, and are not relevant to the performance of the fiber-optic cables.

On the other hand, in some places, the external samples developed a slight unevenness in the winding of the helical coil, and buckled slightly upward from the surface of the mounting plate. These small residual displacements are probably a result of the rather severe thermal cycling of the external samples, indicating there was some slight mechanical distortion of the polymer cable structures during the flight. The LDEF was exposed to approximately  $3 \times 10^4$  thermal cycles during the course of the mission. These mechanical movements in the cable structure do not directly involve the fiber, especially when it is isolated in a loose tube cable structure. However, they could conceivably cause microbending effects. Another observation was that the jacket of one of the internal samples, C-6, pulled back on one end, out of the short piece of heat shrink tubing used to seal the connector backshell, leaving a short length of the kevlar strength member exposed.

A closer examination, during the dismantling of the tray at JPL, revealed many micro-meteoroid impacts on the surface of the tray, the sample plates, and on the fiber cables. There were three impact craters approximately 0.5 mm in diameter on different cable samples. One of these is illustrated in Figure 4. The average number of impacts larger than 0.01 mm, was: 33 on a sample plate, 21 on the fiber cable sample coil, and 2 on each of the fiber mounting clamps. None of the micrometeoroid impacts caused any detectable damage to the optical fiber.

A study of microphotographs of each connector termination made after the flight showed that the twenty fiber-optic connectors typically appear clean with no visible change from pre-flight microphotographs. However, four of the twenty show evidence of contamination on the polished end surface of the termination. The unknown contaminant appears visually to have been extruded through micro-cracks in the epoxy used to secure the fiber in the connector ferrule. Essentially none of the contamination could be seen visually in the small but optically important core area of the fiber on any of the four. The core diameter of the ten samples varied from 50 to 200  $\mu\text{m}$ , compared to the typical 3 mm (3,000  $\mu\text{m}$ ) diameter of the polished ferrule end. One of the contaminated connector ends is illustrated in Figure 5 as an example. The microphotograph covers about half of the area of the polished ferrule end. The four prominent circular objects are the ends of precision-ground steel pins used to mechanically center the fiber. The voids are filled with epoxy. It should be noted that polishing scratches were seen on all of the terminations. These are not visible in transmitted light in the fiber core area, but contribute to connector loss through scattering on all samples - flight, control and reference.

Finally, we noted a qualitative difference in handling of certain of the flight samples in comparison to their control counterparts when these samples were reterminated later in the analysis work. One cable, P-3, was noticeably stiffer, possibly due to the hardening of the cabling material. Even though no visible difference can be seen, the fiber buffer coatings typically were slightly more difficult to strip, and possibly were more easily broken during a termination process.

## EXPERIMENTAL DATA

In this section we present the results of the post-flight measurements performed to date. The parameters or phenomena investigated so far were photobleaching, direct attenuation, OTDR (optical time-domain reflectometry), spectral loss, and temperature-induced loss.

A non-contact technique was developed to make the first two measurements without demounting the flight sample connectors from their position inside the connector bushings, in order to avoid any possible consequences of moving or manipulating the sample ends. The apparatus used to perform the measurements was built around an LED light source, and graded-index (GRIN) lenses used for lens coupling into and out of the sample fiber core. A 50  $\mu\text{m}$  core fiber was used to deliver light to the input GRIN lens, and a stop controlled the numerical aperture (NA) of the beam focussed on the sample core. The lens slightly underfilled a 50  $\mu\text{m}$  core sample fiber both in area and NA, and more severely underfilled the larger core fibers. A longer GRIN lens was used to couple the light out from the other end of the sample into an optical power meter. Only comparison measurements were made, between a flight sample and the identical control and between each of these and a short reference fiber. A diagram of the set-up is shown in Figure 6. Both source and detector lens assemblies were attached to a five-degree of freedom angular and translational positioning device. This allowed the insertion of the GRIN rod lens inside the connector bushing, and the alignment of the light focal spot with the fiber core without physical contact. The alignment was then optimized by maximizing the output reading of the optical power meter. The repeatability of the comparison measurement, involving mainly errors in positioning the lens assemblies was  $\pm 0.02$  dB. As will be seen later, the overall accuracy of the loss measurements proved to be roughly 0.1 dB.

### Photobleaching

Before performing any other measurements, each flight sample was directly compared to the corresponding control sample using the setup just described, with a low power, ( $< 1 \mu\text{W}$ ) 1300 nm LED light source. These measurements were then repeated after the flight samples were saturated with a high power (30mW) laser diode light source at 830 nm for at least one hour. A few samples were exposed to the high power level for a longer time (16 hrs). The attenuation change observed at 1300 nm in six samples was averaged, the result being  $-0.027 \pm .05$  dB. The change in attenuation was not measured in four of the samples because two were lossy at 1300 nm, the single mode fiber could not be measured accurately enough, and the remaining sample was not measured because preliminary indications were that there was no attenuation increase during the flight.

The results indicate that there was no measurable photobleaching, and that the precision of the sample to control comparison was about 0.05 dB or 1%.

### Attenuation

Immediately following the photobleaching tests, direct attenuation measurements were performed at both 830 nm and 1300 nm, using the set-up described above. These measurements were obtained by comparing the flight sample or control with a short ( $\sim 1$  m) reference of the same type of fiber, and were repeated a number of times. These comparisons were also done without contact to the flight sample terminations and without disturbing the cable and connector mountings.

Because of concern that cladding modes would introduce error, especially in view of the short reference fiber length, careful visual and instrumental checks were made for cladding light. No significant amount was found. Note that the launch conditions somewhat underfilled both



the core area and NA. The comparison with OTDR measurements, described below also served as a cross-check.

The results of the direct attenuation measurements at 830 nm are given for the control samples in Table 2 and for the flight samples in Table 3.

Separate attenuation measurements were performed using an Optical Time Domain Reflectometer (OTDR), in order to provide an independent attenuation value, and also in order to determine whether the observed attenuation increase was distributed, or localized due to fiber defects or connector loss. The OTDR measurements were made with a multimode instrument at 830 nm.\* A long feeder fiber was used between the OTDR and the sample. An example of an OTDR signal from one of the fibers is given in Figure 7. The samples are rather short for accurate OTDR measurements. Index matching gel was used at the input connection to minimize the back reflection, but even so, the back scattered signal was obscured in roughly the first half of the sample, as seen in Figure 9. Measurements were made from both ends of each sample in order to examine its entire length. The results of the OTDR loss measurements are also shown in Tables 2 and 3, for comparison with the direct loss measurements. The two values for each end of a sample were averaged to obtain the value shown in the tables. No defects or localized loss were observed in any of the samples.

We feel that this comparison provides the best estimate of the overall accuracy of the loss data because the measurement techniques used are quite different. For the control samples, the difference between direct and OTDR attenuation values, averaged over all samples (except the single mode fiber) was  $0.07 \pm 0.08$  dB, leading to our conclusion that the overall accuracy is approximately  $\pm 0.1$  dB. The stated deviations are  $1\sigma$  values for one measurement, throughout this paper. For the flight samples, the same difference is  $0.15 \pm 0.11$  dB, omitting (perhaps somewhat arbitrarily) samples P-3, P-4 and C-6 because of an anomalously high difference. In the absence of other errors, a difference between the direct loss and the OTDR loss can be attributed to the optical fiber terminations. We feel that, on average, the flight samples incurred a small (between 0.1 and 0.2 dB) increase in loss, and that the larger difference for the three samples noted is from anomalously high connector loss. Our experience with sample P-3, which was a plastic clad fiber which we reterminated a number of times, indicated some difficulty with our terminating technique for that type of fiber.

Since lens coupling was unreliable and no single-mode OTDR instrument operating at 830  $\mu\text{m}$  was available to us, the single-mode fiber attenuation measurement was performed using the cut-back method. The pigtail of a temperature controlled single-mode 1300 nm laser diode source was fusion spliced to a 50 meter long single-mode fiber jumper. The flight fiber sample was then fusion spliced to the jumper and an optical power measurement was taken. The measurement was repeated, after the fiber sample was cleaved at a point immediately following the fusion splice. This procedure was repeated twice, for the flight sample as well as for the control sample. The values shown in Tables 2 and 3 are the average of the two determinations. The difference between the two was 0.06 dB and 0.01 dB for the control and flight sample, respectively. It should be noted that the single mode sample was designed for the 0.8  $\mu\text{m}$  window, and was more lossy at 1.3  $\mu\text{m}$ . The OTDR measurements were done with the same 830 nm multimode OTDR that was used for the other samples, and as a result are less reliable.

The loss increment that occurred during the flight is shown in Table 3. The data were obtained at 830 nm, and were determined from a series of direct comparisons of sample to control after the flight. OTDR measurements were not considered in deriving these numbers, and, as already mentioned, yield a somewhat smaller loss increase overall. The loss increment values shown in Table 3 differ slightly from the arithmetical difference of the corresponding values of the flight sample direct attenuation as shown in Table 3 and the control direct attenuation column in Table 2. The reason is that a different combination of the measurements was used, not involving comparisons to a short reference. The difference is another expression of experimental error.

\* Laser Precision, Model No. TD-2000 with TD-260 multimode plugin.

To summarize the loss data at 830 nm, four of the six internally mounted samples showed no increase in loss, within our estimated measurement accuracy. The remaining two had a small increase, on the order of 0.5 dB. Three of the four external samples exhibited a larger increase, 2 to 4 dB. The fourth external sample showed no loss increase.

### Spectral Loss

Preliminary measurements of spectral loss have been obtained on three samples and these measurements are continuing. The purpose of these tests was twofold, first to help confirm that the observed loss increases during the mission were due to radiation, and second to serve as additional information for characterization. A white light source and a fiber-optic spectrum analyzer were used to obtain loss versus wavelength data. A short, 1/2 m fiber of the same type as the sample was used as a reference. The samples tested to date show a broad absorption near 600 nm, which is typical for radiation damaged fibers. This data may also be helpful in estimating radiation effects in the fibers which were not darkened enough to measure accurately at 830 nm. The much larger attenuation change, at say 650 nm, may be useful for estimating the damage at longer wavelengths, which was not possible to measure with our short samples.

### Loss vs Temperature

Although the experiment was passive, with no measurement data obtained during the flight, we believe that temperature dependent loss will be an important design consideration for future systems. Accordingly, the sample attenuation was measured in our laboratory as a function of temperature over a range representing typical spacecraft environments. The measurements were made both before the LDEF launch and after recovery, but the post-flight measurement apparatus was better controlled, and post flight data are presented here. The preflight data are in agreement. Both the flight and control samples were tested. They were inserted in a computer controlled temperature chamber, and the temperature was varied at a fixed rate, starting at room temperature, up to 70°C, down to -40°C and back up to room temperature, over a twelve hour period. Both ends of the sample were left outside of the temperature chamber, and were connected to an LED source and to an optical power meter. A direct input from the LED to a second channel of the optical power meter allowed for compensation of changes in LED output. The computer monitored the temperature of the fiber sample and of the plate to which the sample was mounted, the temperature in the vicinity of the LED source, and the room temperature. The measured attenuation change as a function of temperature is shown in Figure 8 for sample P-1. This was the sample least affected by temperature, showing an overall change of about 0.1 dB or 4 dB/km. Figure 9 shows a more typical temperature performance, where a variation of about 0.5 dB was observed. An increase in loss with decreasing temperature, becoming much steeper near the lower end of our temperature range, is observed in most (but not all) fiber cables. The largest change was seen in the C-6 sample, which had an attenuation increase of about 3.5 dB at the low temperature extreme. This behavior is due to the specific cable structure (rather than the fiber), and would preclude its use in a severe space environment. The typical attenuation versus temperature data exhibited a hysteresis type behavior because of the large rate of change of temperature during the test cycle.

## DISCUSSION

### Radiation Effects

It is well known that ionizing radiation induces added attenuation in optical fibers. The initial damage anneals out due to thermal effects or to light, but a small fraction remains

indefinitely and constitutes the damage observed over a long-term exposure such as in the LDEF or other similar missions. The presence of phosphorus in the fiber inhibits the annealing and thus makes fibers containing it more sensitive to radiation [Refs. 2,3,4]. Analysis to date of our data appears to be consistent with earlier laboratory results, and does appear to correlate with phosphorous content. However, our correlations are not yet complete, and more information will become available in the coming months.

The LDEF experiment extends the duration of long-term radiation darkening measurements to nearly 6 years. In addition, the LDEF has subjected the samples to a real space environment with a combination of effects. The bulk of the existing laboratory data, with some exceptions [Ref. 3], extends to 1 day or less after exposure. Preliminary indications are that annealing data to  $10^5$  sec (1 day) can be useful for predicting the effect of much longer exposures, but more work is needed on this point.

We did not detect any photobleaching effects, but we did not expect to because our samples did not remain cold throughout the mission. Our results are consistent with published data [Refs. 5,6,7]. Photobleaching may be important, however, in special applications where the fiber remains cold, is also kept dark, and no signal is transmitted for an extended time. If instant operation is required after turn-on, as might be the case for a signalling link, or possibly in an optical instrument application, typical long-term low-dose data may underestimate the radiation damage. In fact, providing means for intentional photobleaching in flight systems could be useful under these conditions.

Turning to the attenuation increase accumulated during the flight, and presumed to be primarily due to radiation, we found that one of the external samples, P-1, performed very well after the 5 1/2 year exposure, as did all of the internal samples. Our samples were standard products, now nearly 10 years old, not present day rad-hard products. Even so, the best samples would have performed very satisfactorily in spacecraft systems involving distances of the order of 100 m. The best available present-day rad hard fibers are considerably better than ours were so it appears reasonable to expect much longer runs to be possible in the future, even for missions that may have an order of magnitude or more larger total radiation dose.

Converting the attenuation data presented earlier to dB/km and combining it with our rough preflight estimate of dose, we obtain for P-1 a loss increment of approximately  $10^{-3}$  dB/km-rad, and for C-1 approximately  $2.5 \times 10^{-2}$  dB/km-rad. Sample P-1 was a germanium-doped core fiber with a small amount of phosphorous along the axis of the core. The core of sample C-1 was doped with germanium and phosphorous throughout. The other three external samples suffered loss increases between 1 and  $3 \times 10^{-2}$  dB/km-rad, consistent with expectations for a Ge-P doped fiber [Ref. 4], but we do not yet know their composition.

We plan to obtain analyses of the remaining fibers and make laboratory radiation damage measurements on our own control samples in the near future. Results from these tests will be an important part of our effort to understand radiation damage in our LDEF samples and to correlate it accurately with the existing data.

### Temperature Effects

Temperature, especially colder temperatures, can affect cable performance in two ways. In plastic clad silica (PCS) cables, the polymer acting as the optical cladding may have a refractive index vs wavelength characteristic that reduces the NA of the fiber with decreasing temperature, ultimately cutting off transmission [Ref. 8]. In glass-clad fiber cables, mechanical changes in the polymers in the cable, particularly in the buffer, can also increase the loss by inducing microbending at low temperature. The magnitude of the low temperature attenuation increase is dependent on cable design, and can be eliminated or greatly reduced, as seen by the data for sample P-1.

However, most fiber optic cables have a significant low-temperature loss increase, and, in an extreme space environment, its magnitude may actually be larger than that related to radiation damage. Our best cable, P-1, exhibited less than 0.1 dB of temperature dependent loss (4dB/km), but the average was closer to 0.5 dB. Again, none of the cables were specially developed for the space environment; they were standard commercial products. For future systems, careful attention must be given to improving the temperature stability of cable structures, and to qualification testing to verify their performance.

### Connector Contamination

Our connectors were not mated or covered. They were mounted in a compatible bulkhead bushing, which held the termination about 3 diameters deep in a hole matching the ferrule diameter. The connector assembly was exposed to the interior volume of the tray.

There is no positive indication from direct measurements of the flight connectors after they were cut off from the cable sample that significant loss can be attributed to the contamination. There is only the suggestion, from comparing OTDR and direct loss measurements, of a slight increase in loss on average, for all terminations. The average added loss is similar in magnitude but perhaps slightly larger than our estimated measurement accuracy.

In a visual inspection, at most only a very small percentage,  $< 1\%$ , of the core area of the contaminated connectors was covered by foreign particles; generally, the core areas were clean. An exception was one end of sample C-6, which appeared in an interference microscope to have a film over it several fringes thick. However, this was a special case because the cable jacket material for sample C-6 outgassed, and would not be used in a spacecraft. The film was transparent, and we did not observe anomalous loss for that particular connector in separate measurements. The opposite end of sample C-6 was clean.

We feel that any contamination effects would have been inhibited or decreased if the connectors had been mated, whether the source of the foreign material were external or internal to the cable sample. An independent source of information about connector performance comes from LDEF experiment No. M0003-8, which carried a multipin connector through which one fiber channel had been looped.<sup>†</sup> No significant change in connector loss was observed in that experiment.

Nevertheless, it is important to understand the possible sources and mechanisms for the observed contamination in order to eliminate the possibility of degradation in performance. It is probably related to the volatile organic materials used in cable construction, such as plasticizers, or it may involve the epoxy materials used in the connector termination. The only information we have to date comes from optical microphotographs. Further analysis of the contaminated connectors is planned. It may also be desirable to conduct laboratory tests to attempt to reproduce the observed effects.

### Polymer aging

The materials in fiber cables, the fiber buffer, the cladding in PCS fibers, and the cements used in making up a connector termination may all undergo changes in optical or mechanical properties which would affect performance. The LDEF flight samples may be holding important information on this subject, and additional tests to bring it out can be done. To date, however, we have only qualitative information. Our observations to date do not provide definitive answers, but they do suggest areas where further investigation would be useful.

<sup>†</sup>Mulke, Owen and Dursch, H.; "Final report on the LDEF M0003-8 Fiber Optics Experiment," Unpublished Report, Boeing Corp., Jan. (1991)

## CONCLUSIONS

In summary, our conclusions to date are as follows:

- 1) All samples were functional; with the proper optical power design margin, all of them would have performed well in a system function for the duration of the mission.
- 2) Tentatively, damage from ionizing radiation appears consistent with laboratory experiments. Measurements producing an annealing curve extending to  $10^5$  sec or more in duration appear useful to predict damage over missions as long as LDEF.
- 3) The choice of the most radiation resistant fibers available now, by extrapolation, will enable missions with significantly higher dose and longer runs to be achievable.
- 4) Internally located connectors performed well. However, contamination thought to be volatiles derived from the cable materials was observed. Additional thermal-vac tests aimed at understanding this phenomenon are desirable.
- 5) Three micrometeoroid pits about 0.5 mm in diameter were observed on our four external cables, but the fibers were not damaged. An exposed 1 km fiber cable would have seen the order of 10 such impacts per year, with unknown risk to the fiber.
- 6) No photobleaching (or conversely no incomplete annealing of radiation damage) was observed.
- 7) A better understanding of the long-term effects of the space environment (vacuum and heat) on polymer material (both mechanical and optical materials) is needed.

## ACKNOWLEDGMENTS

The authors would like to acknowledge the contributions of project team members Shannon Jackson and John Morookian. We also owe a special thanks to Mike Clawson at JPL, who was extremely helpful with the OTDR measurements, and generous with special tools and techniques for making terminations. We also thank Joan Brandt for preparing the manuscript for publication.

The research described in this paper was carried out at the Jet Propulsion Laboratory, California Institute of Technology, and was sponsored by the National Aeronautics and Space Administration. Reference herein to any specific commercial product, process, or service by trade name, trademark, manufacturer, or otherwise, does not constitute or imply its endorsement by the United States Government, NASA, or the Jet Propulsion Laboratory, California Institute of Technology.

## REFERENCES

- [1] Stassinopoulos, E. G. and Raymond, J. P.: "The space radiation environment for electronics," *Proc. IEEE*, 76, 1423 (1988)
- [2] Friebele, E. J.; Schultz, P.C.; and Gingerich, M. E.: Compositional effects on the radiation response of ge-doped silica core optical fiber waveguides, *Appl. Opt.* 19, 2910 (1980)
- [3] Friebele, E. J.; Askins, C. G.; and Gingerich, M. E.: "Effect of low dose-rate irradiation on doped silica core optical fibers," *Appl. Opt.*, 23, 4202 d(1984)
- [4] Friebele, E. J.; Long, K.J.; Askins, C. G.; Gingerich, M.E.; Marrone, M. J.; and D. L. Griscom: "Overview of radiation effects in fiber optics," *SPIE Proc.*, v. 541, 70 (1985)

- [5] Friebele, E. J. and Gingerich, m. E.: "Photobleaching effects in optical fiber waveguides," Appl. Opt. 20, 3448 (1981)
- [6] Barnes, C. E.: "Laser-diode induced photobleaching at low temperatures in co-60 irradiated fibers," IEEE Trans, Nucl. Sci., NS-29, 1479 (1982)
- [7] Gilbert, R.M.: "Photobleaching of radiation-induced color centers in a germania-doped glass fiber," IEEE Trans. Nucl. Sci., NS-29, 1484 (1982)
- [8] Yeung, W. F. and Johnston, A. R.: "Effect of temperature on optical fiber transmission," Appl. Opt., 23, 3703 (1978)

**TABLE 1. - LDEF FIBER SAMPLE DATA**

CABLE No.	CORE/CLAD/ CABLE DIA.	CORE/CLADDING MATERIAL	BUFFER MATERIAL	TUBE MATERIAL	STRENGTH MEMBER/ CABLE JACKET	FIBER NA	NOMNL ATTEN.	BAND WIDTH
-	$\mu\text{m}/\mu\text{m}/\text{mm}$	-	-	-	-	-	dB/km	MHz-km
P-1	100/140/3.0	GERMANIUM DOPED SILICA/ PURE SILICA	ACRYLATE COATING	HYTREL TIGHT	KEVLAR/ POLYURETHANE	0.29	7	100
P-2	100/140/3.0	GLASS/GLASS	POLYMER COAT/ UV CURED OUTER COAT	HYTREL TIGHT	KEVLAR/ POLYURETHANE	0.24- 0.30	8	20
P-3	200/230/2.5	PURE SILICA/ PROPRIETARY	ACRYLATE SOFT COATING	ACRYLATE HARD COAT	---/ URETHANE	0.38	8	-
P-4	50/125/3.0	PURE SILICA/ BOROSILICATE	ACRYLATE COATING	-	KEVLAR/ POLYURETHANE	0.21	6	200
C-1	50/125/3.0	GERMANIUM DOPED SILICA/ PURE SILICA	ACRYLATE COATING	HYTREL TIGHT	KEVLAR/ POLYURETHANE	0.20	7	400
C-2	50/125/2.5	PURE SILICA/ BOROSILICATE	SILICONE	HYTREL TIGHT	KEVLAR/ POLYURETHANE	0.22	6	150
C-3	10/125/3.5	BOROSILICATE/ BOROSILICATE	HALAR 300	POLYESTER LOOSE	FIBERGLASS/ POLYURETHANE	-	-	-
C-4	100/140/3.0	PURE SILICA/ BOROSILICATE	ACRYLATE COATING	-	KEVLAR/ POLYURETHANE	0.30	7	20
C-5	200/375/2.3	PURE SILICA/ RTV SILICONE	RTV SILICONE	TEFZEL TIGHT	KEVLAR/ HYTREL	0.33	12	11
C-6	50/125/5.1	PURE QUARTZ/ QUARTZ	POLY- ACRYLATE	NYLON LOOSE	KEVLAR/ PVC	0.20	4	200

TABLE 2. - DATA FROM LOSS MEASUREMENTS AT 0.83 mm IN THE CONTROL SAMPLES.

<u>SAMPLE</u>	<u>LENGTH</u> m	<u>NOMINAL</u> <u>LOSS</u> dB	<u>DIRECT</u> <u>ATTEN</u> dB	<u>OTDR</u> <u>ATTEN</u> dB	<u>DIR-</u> <u>OTDR</u> dB	—
P-1	18	0.13	0.31	0.12	0.19	
P-2	26	0.21	0.34	0.33	0.01	
P-3	26	0.21	0.22	0.21	0.01	
P-4	26	0.21	0.32	0.23	0.09	
C-1	50	0.35	0.21	0.21	0.0	
C-2	50	0.30	0.14	0.19	-0.05	
C-3	50	a)	1.05 <sup>b</sup>	0.51	--	
C-4	44	0.44	0.36	0.30	0.06	
C-5	50	0.60	1.08	0.91	0.17	
C-6	47	0.19	0.28	0.14	0.14	

a) Not available.

b) Determined by cutback method at 1.3  $\mu$ m.

TABLE 3. - DATA FROM LOSS MEASUREMENTS FOR THE FLIGHT SAMPLES AT 830 NM.

<u>SAMPLE</u>	<u>LENGTH</u> m	<u>NOMINAL</u> <u>LOSS</u> dB	<u>DIRECT</u> <u>ATTEN</u> dB	<u>OTDR</u> <u>ATTEN</u> dB	<u>DIR-</u> <u>OTDR</u> dB	<u>LOSS</u> <u>INCREMENT</u> dB
P-1	26	0.18	0.38	0.19	0.19	0.07
P-2	26	0.21	2.07	1.98	-0.03	1.68
P-3	30	0.24	4.72	3.56	1.16	4.45
P-4	26	0.21	2.83	2.02	0.81	2.46
C-1	50	0.35	0.77	0.58	0.19	0.56
C-2	50	0.30	0.30	0.19	0.11	0.19
C-3	50	--	-1.02 <sup>a</sup>	0.46	--	-0.03 <sup>a</sup>
C-4	68	0.68	0.42	0.32	0.10	0.07
C-5	50	0.60	1.07	0.75	0.32	-0.01
C-6	50	0.20	0.70	0.29	0.41	0.37

a) Measured by the cutback method at 1.3  $\mu$ m.

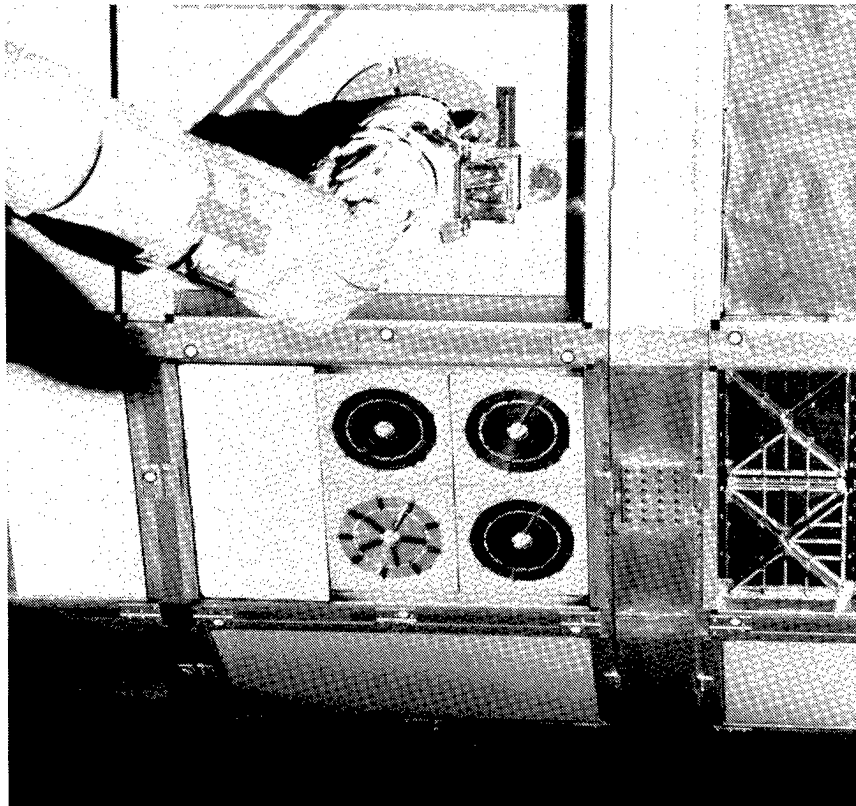


Figure 1. A photograph of the complete tray mounted on LDEF, taken during the retrieval by STS-32 in January 1990 (Courtesy of LDEF Project Office).

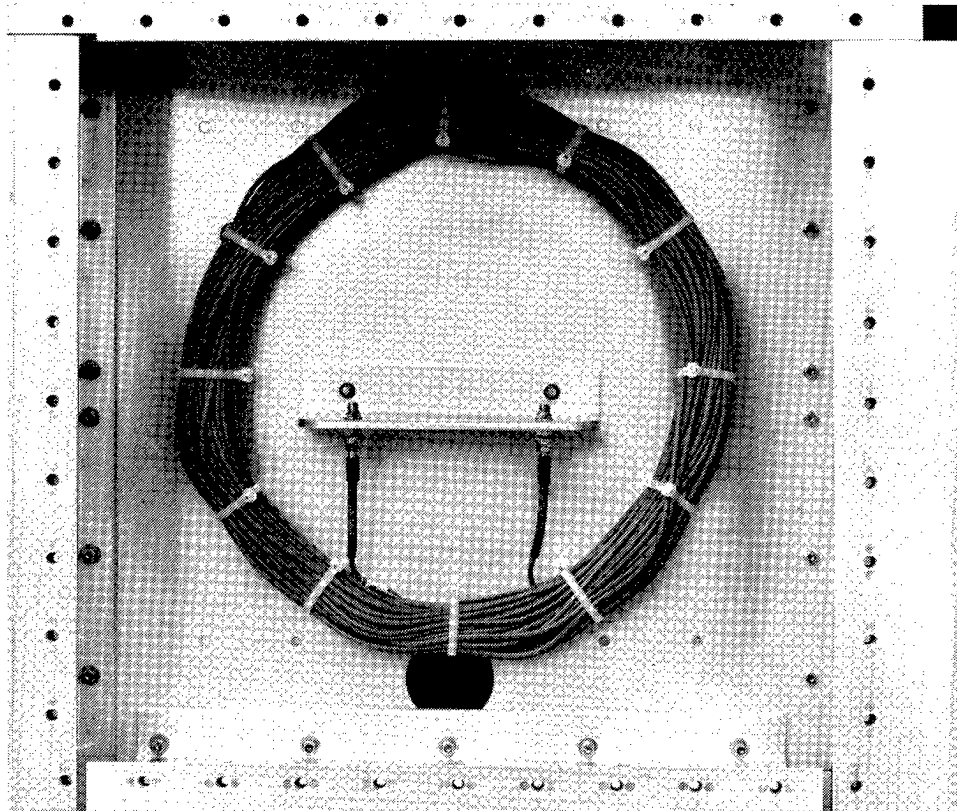


Figure 2. A photograph of an internally mounted fiber cable sample.



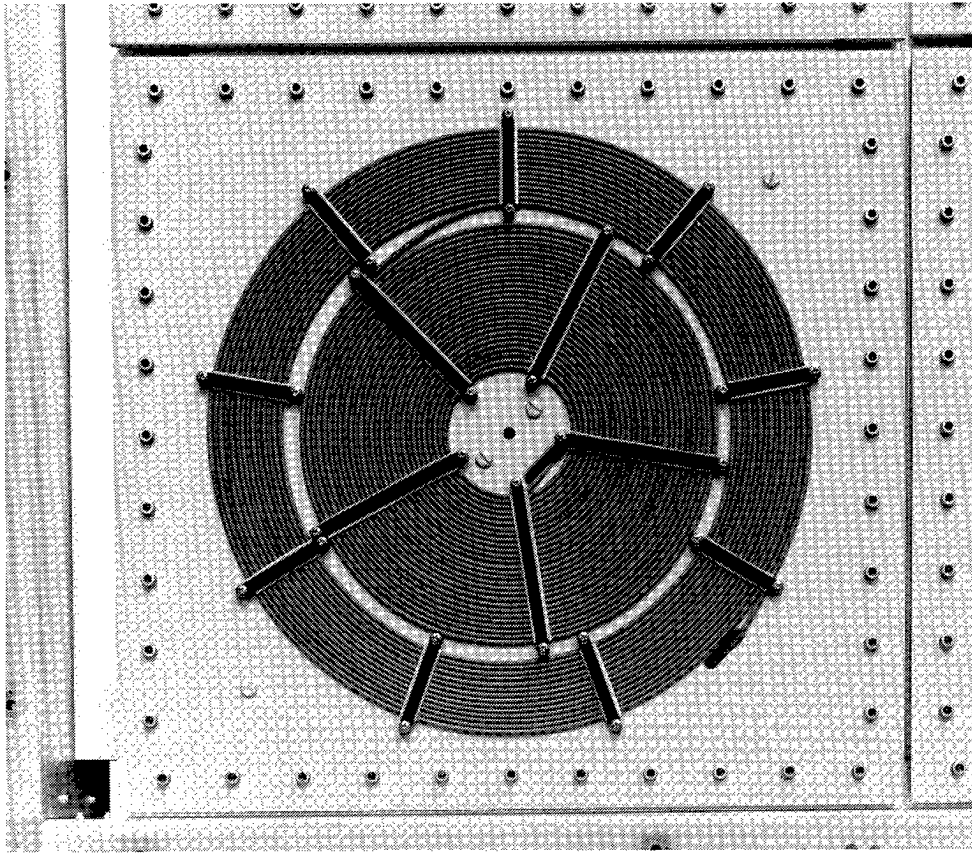


Figure 3. A photograph of an externally mounted fiber cable sample.

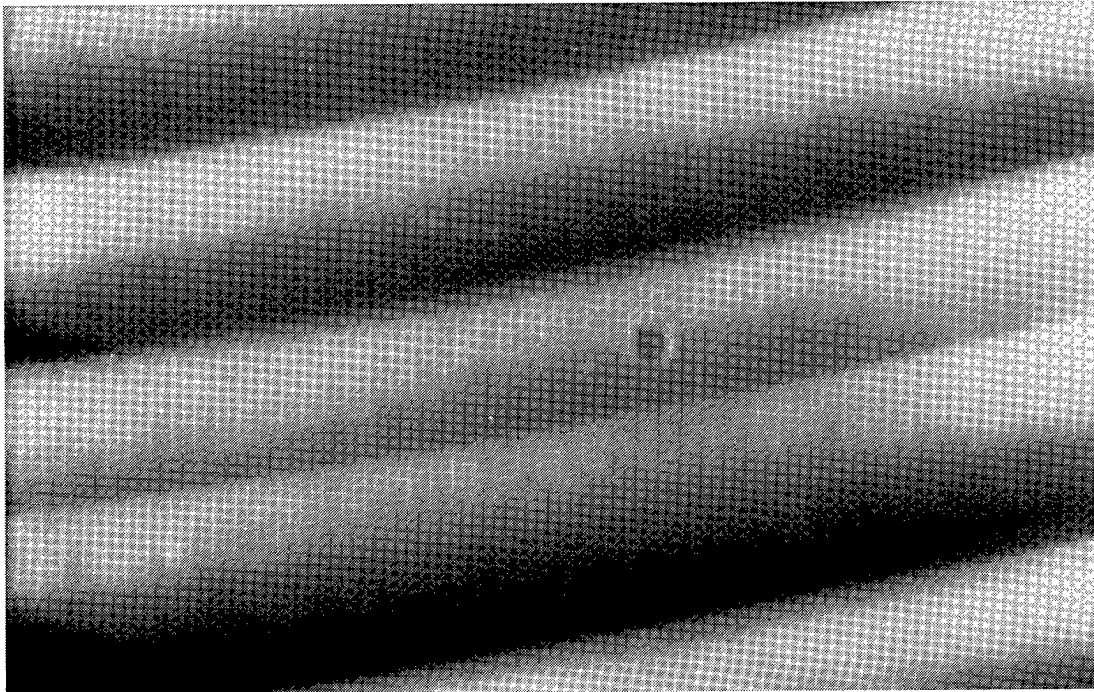


Figure 4. A micrometeoroid impact crater on one of the fiber cables. The crater is approximately 1/2 mm in diameter, but did not affect the fiber itself.

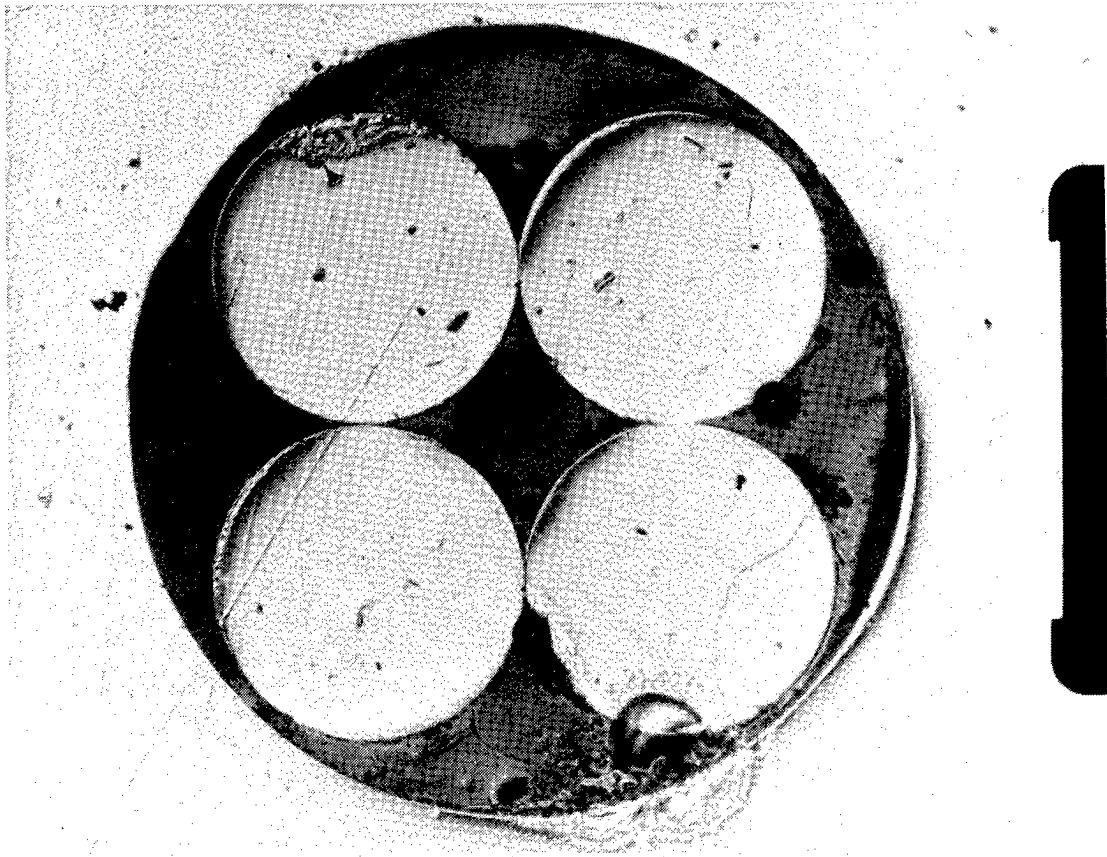


Figure 5. A microphotograph of a contaminated connector termination.

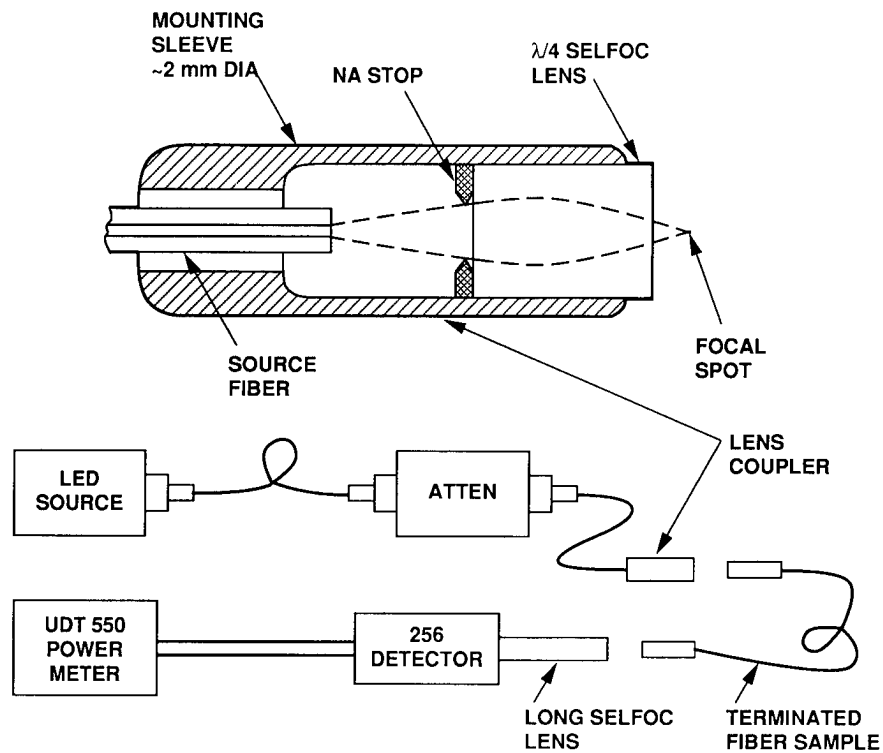


Figure 6. A sketch showing the microlens-coupled technique using GRIN microlenses for direct attenuation measurements.

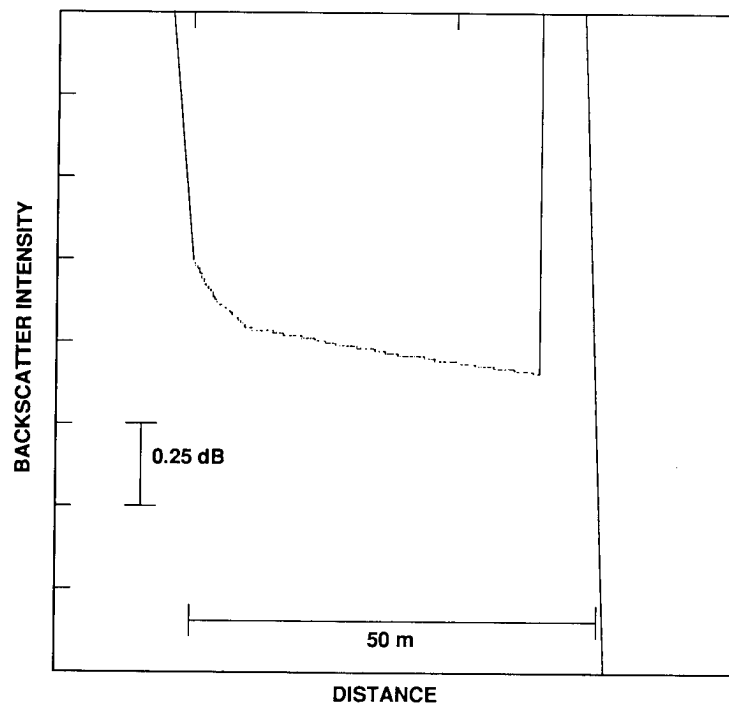


Figure 7. An example of an OTDR signal, from sample No. C-2.

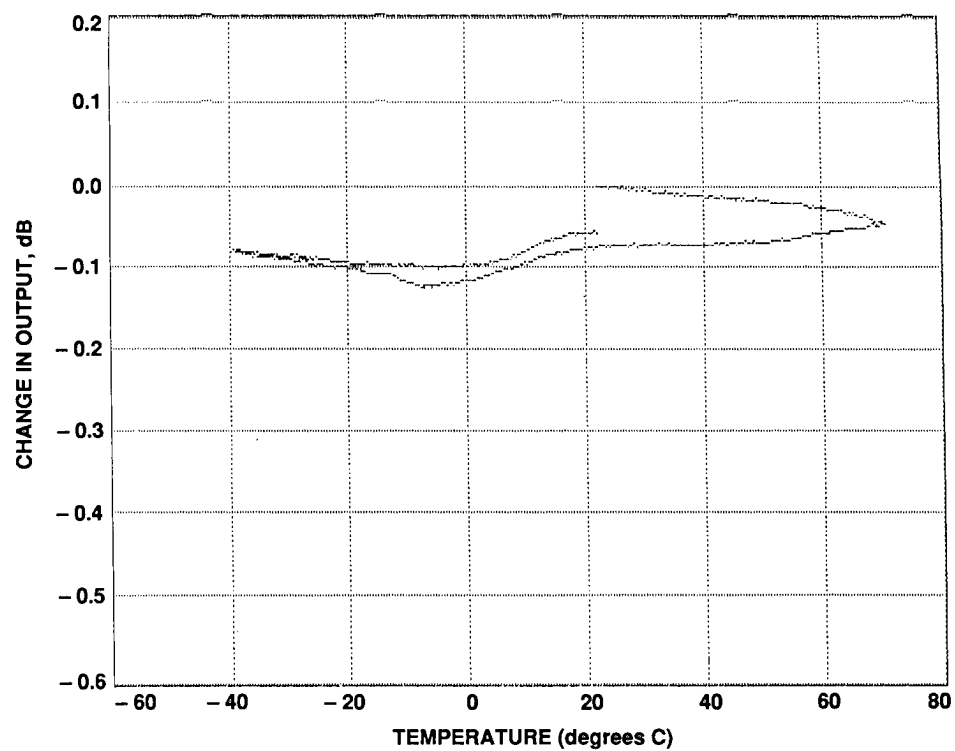


Figure 8. Attenuation change as a function of temperature for sample P-1.

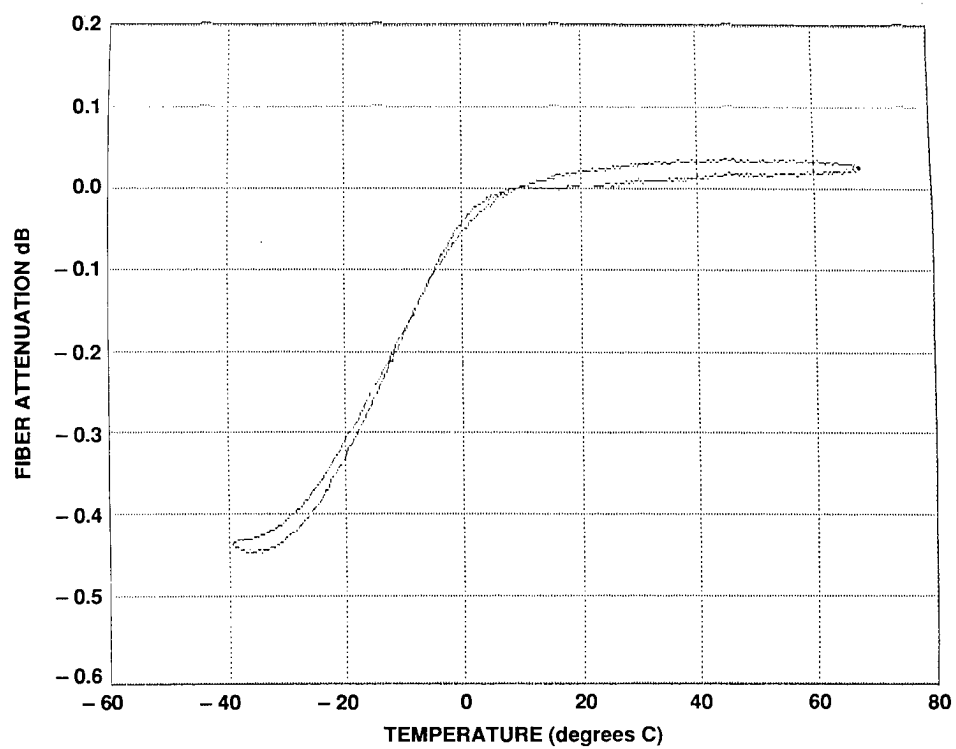


Figure 9. Attenuation change versus temperature for sample C-1.

## OPTICAL PERFORMANCE OF EXPOSED SOLAR CELL COVERS

Thomas H. Allen

Bryant P. Hichwa, Steven R. Selee, Jerry Dodds, Greg S. Long

OCLI--Optical Coating Laboratory, Inc.  
2789 Northpoint Parkway  
Santa Rosa, CA 95407-7397

### ABSTRACT

This paper discusses the characterization results of samples flown on the Long Duration Exposure Facility (LDEF). These samples included both coated and uncoated fused silica and ceria glass substrates used in the manufacture of solar cell covers. The coatings comprised a single-layer magnesium fluoride antireflection coating and an all-dielectric high-reflector multilayer coating centered at 350 nm. Samples were mounted on both the leading and trailing surfaces of the LDEF for exposure to the environment of space. The optical properties of the coatings will be compared to control samples which were stored on the ground during the LDEF Mission. Results of Auger Electron Spectroscopy and Rutherford Backscatter Spectroscopy measurements made on several of the coatings will be presented to explain the effects of space on the chemical composition of the coatings.

**RULED AND HOLOGRAPHIC DIFFRACTION GRATINGS EXPERIMENT  
( AO 138-5 )**

**Francis BONNEMASON**  
**INSTRUMENTS SA Jobin Yvon Division**  
**16-18 rue du Canal, BP 118 91163 LONGJUMEAU (France)**  
**Phone: 33/64 54 13 00, Fax: 33/69 09 93 19**

**SUMMARY**

Ruled and Holographic Gratings (originals and replicas) proposed for use on loaded spectroscopic experiments; optical performances were tested in space vacuum and environment exposure. Correlation with identical components, stored on ground under Air-Nitrogen pressure during all the experiment duration was made; the operated tests are Wavefront Planeity, Light Efficiency and Stray Light level.

**INTRODUCTION**

The experiment aimed to study the optical behaviour of diffraction gratings with various coatings depending on space vacuum and environment long exposure. To separate these environmental parameters influence from senescence on ground, three sets of samples were manufactured.

The selected materials and manufacturing processes were representative of standard grating production for loaded spectroscopic applications: one set stored on ground, one loaded space environment and sun illumination shaded, one loaded space environment and sun illuminated during a pre-defined duration (10 months).

Witness Mirrors were joined to the experiment to distinguish coatings behaviour.

Because non exposed configuration is the most representative of classically loaded grating on spectroscopic systems, the very extended (10 to 69 months) flight duration gives a major interest to loaded and shaded sets of samples.

Optical performances were tested before and after the flight and operated with the same instrumentation. By test results comparison and analysis we can appreciate the behaviour of each type of gratings and coatings.

## SYMBOLS

Values are given in SI customary units.

Al aluminum coating

Pt platinum coating

g/mm groove density per mm

## SPECIMEN DETAIL

Gratings and control mirrors were selected in the way to be representative to some materials and manufacturing processes used for standard production.

Each set of samples is composed of three gratings and one double-coated mirror :

- replica from a ruled grating (type G)

Glass blank + epoxy resin + coating  
1200 g/mm, blazed at 250 nm  
dimension 40x40x5 (mm<sup>3</sup>), Aluminum coated

- original holographic grating (type H)

Glass blank + sensitive photoresist + coating  
3600 g/mm, 50 – 150 nm spectral range  
dimension 40x40x5 (mm<sup>3</sup>), Platinum coated

- original ion-etched holographic grating (type HU)

Glass blank + coating  
1200 g/mm, blazed at 250 nm  
dimension 40x40x5 (mm<sup>3</sup>), Aluminum coated

- control mirror (type W)

Glass blank + coating  
Aluminum and Platinum coated by half area

## EXPERIMENT PRESENTATION AND FLIGHT ENVIRONMENT

The loaded samples were set in a cannister included on the FRECOPA (FRench COoperative passive PAYload). This cannister was opened in space during ten months.

The FRECOPA plate was located on the B3 trailing edge of LDEF, the Atomic oxygen fluence was evaluated to  $3.71\text{E}+03$  atoms/cm<sup>3</sup>. However the solar irradiation has been very important with solar flux quite perpendicular to the experiment once an orbit, the cumulative equivalent sun hours was evaluated to 1600. Micrometeroids and debris impacts were quantified to 90 impacts/m<sup>2</sup> ( $> 50 \mu\text{m}$ ).

Two sets of four components, one of each type (G, H, HU, W) were mounted on a dedicated plate, one set (exposed model) with optical area samples looking at space and the second one (shaded model) turned back.

The sample plate is shown in figure 1.

A third set of spare samples (reference model) was stored on ground in a same box, under Air-Nitrogen during all the experiment duration.

## EXPERIMENT PRINCIPLE

The experiment goal is the optical behaviour study of Ruled and Holographic gratings with various coatings subjected to space vacuum long exposure (69 months, about 34000 orbits, thermal cycle/orbit from  $-30$  to  $+70$  °C) and space environment (cosmic dust and sun irradiation) during ten months, according to the critical triple point of view : wave front quality, light efficiency and stray light level.

The gratings are masters and replica representative to the main grating manufacturing processes.

Specific objectives include examining the coating damage, the senescence on ground parameter and differentiating between the influences of space vacuum and solar irradiation.

The instrumentation used for pre and post-flight tests is strictly identical. Stray light tester optics have been re-coated.

The Wavefront Planeity test is operated with a Fizeau interferometer at 632.8 nm on the 0 and 1 order when accessible, the Efficiency test for Aluminium coated gratings with a photogoniometer on the (220-600)nm spectral range, the Efficiency test for Platinum coated gratings with a photogoniometer working under vacuum at three wavelengths (58.4, 74.4, 121.6 nm). The integrated level of stray light is operated, for Aluminum coated gratings, with a spectro-photometer at three wavelengths (200, 205 and 210 nm) according to short cut-off filter method.

By tests results comparison and combination on the three sets of samples a complete investigation is accessible.



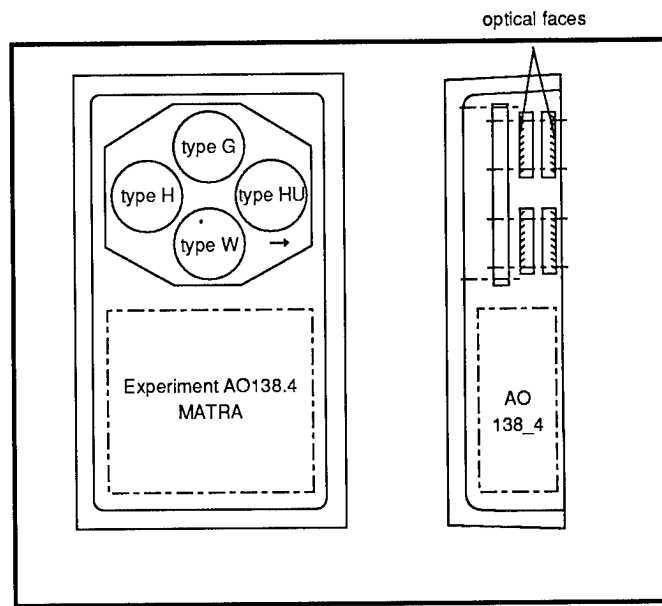


figure 1

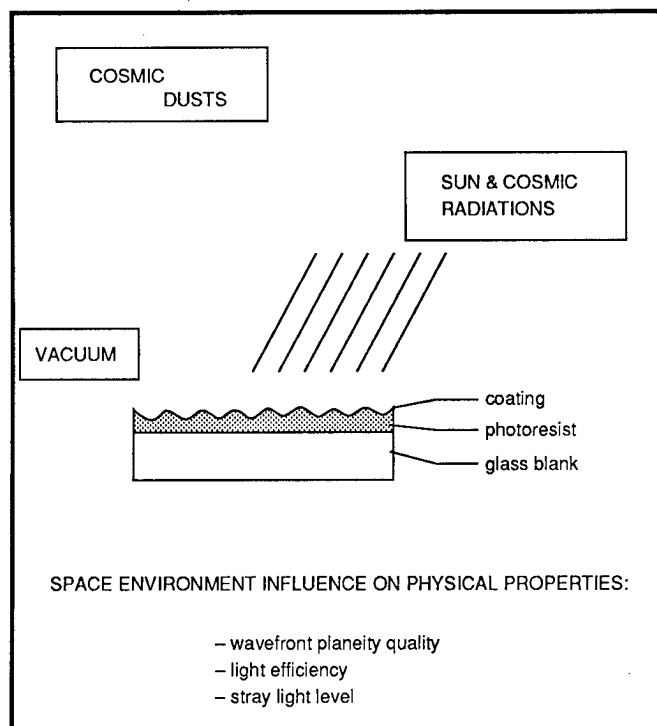


figure 2

## DATA ANALYSIS PLAN

A synoptic diagram is proposed in figure 3.

Reference Unit (spare samples) post and pre flight test results comparison determine the optical performance degradations with time. (69 months stored under Air-Nitrogen pressure). Gratings, control mirrors and by combination coatings senescence is evaluated.

Flight Unit shaded samples post and pre flight test results comparison, in relation with senescence on ground effect determine the long duration space vacuum exposure (69 months, thermal cycle per orbit  $-30$  to  $+70$  °C, 34000 orbits) influence on each type of gratings and coated control mirror optical performances.

By combination, coatings behaviour with space vacuum is separated.

Flight Unit exposed samples, post and pre flight test results comparison, related to senescence on ground and long duration space vacuum determine the space environment (cosmic dust) and sun illumination (solar flux quite perpendicular to experiment once an orbit, cumulative equivalent sun hours : 1600) influence on each type of gratings and coated control mirrors optical performances.

By combination, coatings behaviour with space environment is separated.

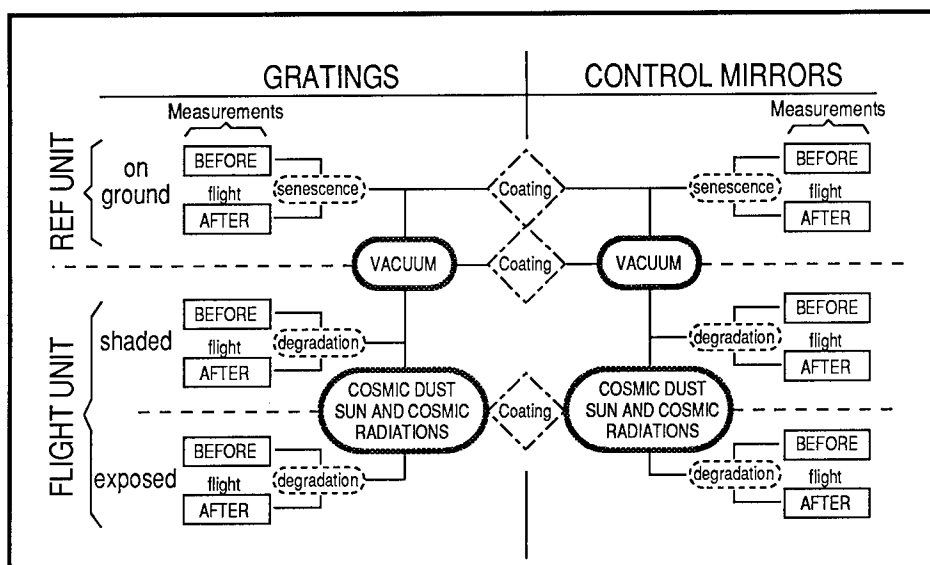


figure 3

## DATA RESULTS

### SENESCENCE ON GROUND

Reference Unit components were stored on earth in an identical cannister than the one used for the loaded set of samples, under Air-Nitrogen pressure during all the experiment duration : **69 months**

#### I COATINGS REFLECTANCE – CONTROL MIRRORS (TYPE W3)

Pre and Post flight reflectance test comparison shows no degradations for both experimented coatings, Al and Pt.

#### II WAVEFRONT PLANEITY

Pre and Post flight wavefront planeity test comparison shows no degradation for all the experimented gratings.

#### III. ABSOLUTE EFFICIENCY

Efficiency curves and data are presented in figure 4 : continuous line shows pre-flight measurement result and non-continuous line post-flight measurement result.

. TYPE G3 (Replica from a ruled grating)

We note an efficiency decrease on the (220–300) nm spectral range, up to 10% at 220 nm.

. TYPE HU3 (Original ion-etched holographic grating)

Very slight decrease and shift of the efficiency curve on the whole spectral range.

. TYPE H3 (Original holographic grating)

No significant change in conservation and distribution of energy among orders –1, 0 and +1.

#### IV. STRAY LIGHT LEVEL

Stray light data are presented in figure 4a

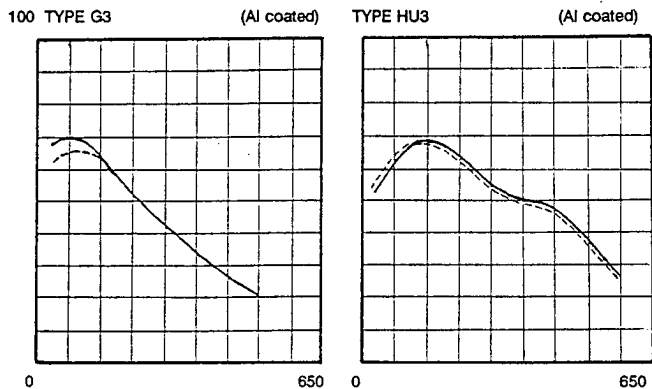
. TYPE G3 (Replica from a ruled grating)

Degradation from 15 to 25 % depending to the wavelength-test.

. TYPE HU3 (Original ion-etched grating)

Degradation from 15 to 25 % depending on the wavelength-test.

#### SENESCENCE ON GROUND EFFICIENCY CURVES AND DATA

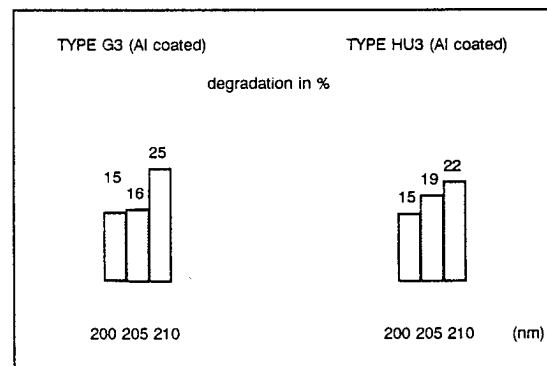


TYPE H3		(Pt coated)			
wavelength (nm)		58.4	74.4	121.6	
O -1		0.6	2.2	6.1	Pre-flight
		0.6	2.0	5.0	Post-flight
R		6.5	1.1	4.2	
D %	0	5.0	0.3	4.0	
E		1.5	3.0	6.7	
R +1		2.0	3.0	5.0	
% $\Sigma$		8.6	6.3	17.0	
		7.6	5.3	15.0	

figure 4

#### SENESCENCE ON GROUND STRAY LIGHT DATA

#### STRAY LIGHT VARIATIONS



4 a

Loaded and shaded components were subjected to an extended space vacuum long duration – 69 months, about 34000 orbits, thermal cycle per orbit from – 30 °C to + 70 °C – the cannister was opened to space during 10 months but the shaded samples were not submitted to direct solar irradiation.

#### I COATINGS REFLECTANCE – CONTROL MIRRORS (type W 1.2)

Al and Pt coatings were experimented :

- . Al coating : loss of reflectivity less than 10% on the whole spectral range
- . Pt coating : loss of reflectivity around 10% at the three wavelengths.

(Data results are presented in figures 5 & 6).

#### II WAVEFRONT PLANEITY

Wavefront Planeity test comparison shows no degradation for all the Gratings.

#### III ABSOLUTE EFFICIENCY

Efficiency curves and data are presented : continuous line shows pre-flight measurement result and non-continuous line post-flight measurement result.

- . TYPE G 1.2 (Replica from a ruled grating)

Efficiency decrease less than 10% on the whole spectral range.

- . TYPE HU 1.2 (Original ion-etched holographic grating)

Slight Efficiency decrease up to 10% at 220 nm.

- . TYPE H 1.2 (Original holographic grating)

Data results are presented on figure 6

#### IV. STRAY LIGHT LEVEL

Stray light data are presented in figure 6 a

- . TYPE G1.2 (Replica from a ruled grating)

Degradation around 90% for all the wavelength-test.

- . TYPE HU1.2 (Original ion-etched holographic grating)

Degradation from 15 to 25% depending to the wavelength-test.

VACUUM INFLUENCE  
Al COATED COMPONENTS EFFICIENCY CURVES

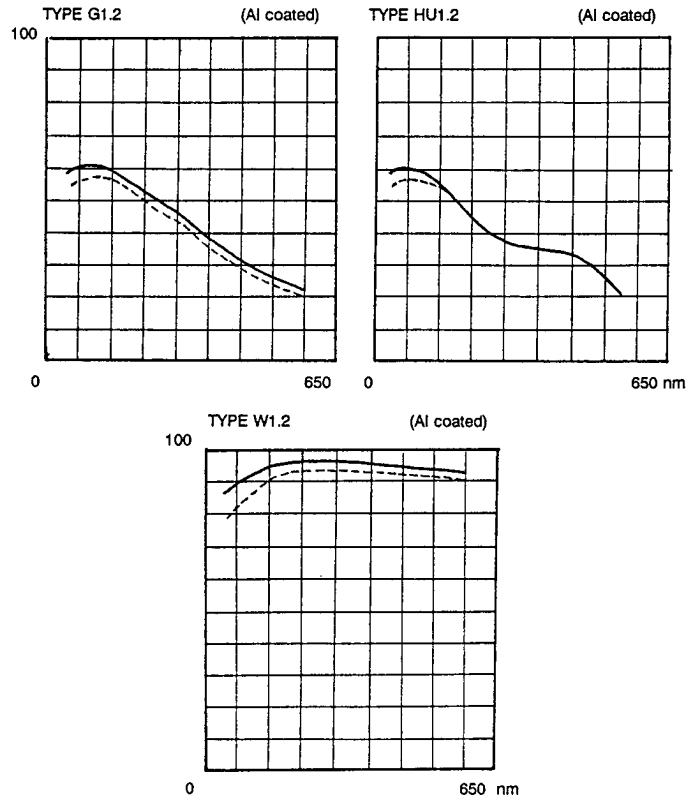


figure 5

VACUUM INFLUENCE  
Pt COATED COMPONENTS EFFICIENCY DATA

TYPE H1.2 & W1.2 (Pt coated)

wavelength (nm) 58.4 74.4 121.6

reflectivity %		20.0	13.0	20.0	Pre-flight
		18.0	12.0	18.0	Post-flight

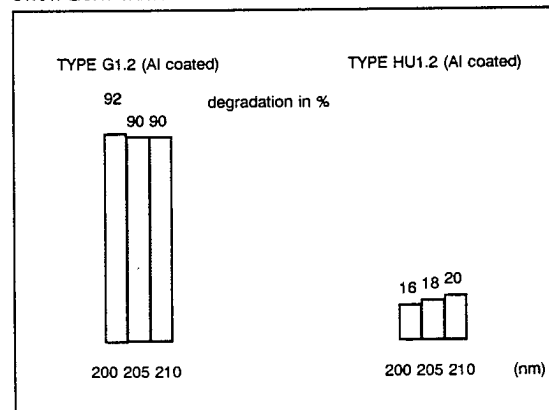
  

O	-1	0.4	2.7	7.7	Pre-flight
		0.8	2.6	4.9	Post-flight
R	0	8.7	2.1	3.9	
		5.8	0.8	4.1	
E	+1	0.9	3.2	8.6	
		1.8	3.4	5.7	
% $\Sigma$		10.0	8.0	20.0	
		8.0	7.0	15.0	

figure 6

VACUUM INFLUENCE  
STRAY LIGHT DATA

STRAY LIGHT VARIATIONS



6 a

## SPATIAL ENVIRONMENT INFLUENCE

Loaded and non shaded components were subjected to an extended space vacuum long duration exposure - 69 months, about 34000 orbits, thermal cycle per orbit from - 30 °C to + 70°C - to direct solar irradiation - cumulative equivalent sun hours 1600 - and to space environment - Atomic oxygen fluence 3.71E+03 atoms by cm3, micrometeoroids and debris 90 impacts by m2 (50µm) - .

### I. COATINGS REFLECTANCE - CONTROL MIRRORS (type W 1.1)

Al and Pt coatings were experimented :

- . Al coating : loss of Reflectivity up to 30% at 220 nm.
- . Pt coating : loss of Reflectivity around 35% at 121.6 nm.

(Data results are presented in figures 7 & 8).

### II. WAVEFRONT PLANEITY

Wavefront Planenity test comparison shows no degradation for all the Gratings.

### III. ABSOLUTE EFFICIENCY

Efficiency curves and data are presented : continous line shows pre-flight measurement result and non-continous line post-flight measurement result.

- . TYPE G 1.1 (Replica from a ruled grating)

Efficiency decrease up to 35% at 220 nm, lower than 10% on the (300-600) nm spectral range.

- . TYPE HU 1.1 (Original ion-etched holographic grating)

Efficiency decrease up to 35% at 220 nm, lower than 20% on the (300-600) nm spectral range.

- . TYPE H 1.1 (Original holographic grating)

Data results are presented in figure 8.

### IV STRAY LIGHT LEVEL

Stray light data are presented in figure 9.

- . TYPE G1.1 (Replica from a ruled grating)

Degradation around 90% for all the wavelenght-test.

- . TYPE HU1.1 (Original ion-etched holographic grating)

Degradation from 15 to 20% depending to the wavelenght-test.

SPATIAL ENVIRONMENT INFLUENCE  
Al COATED COMPONENTS EFFICIENCY CURVES

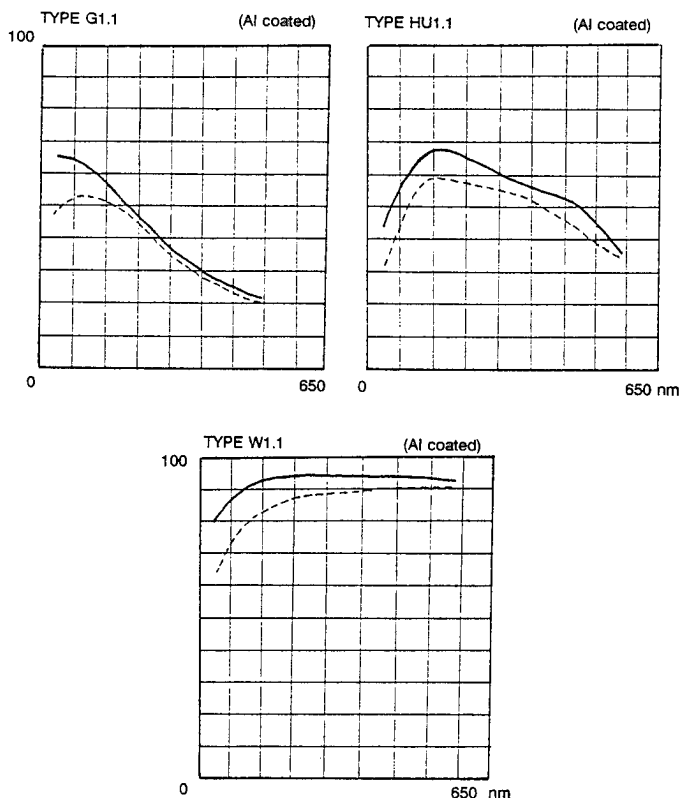


figure 7

SPATIAL ENVIRONMENT ENFLUENCE  
Pt COATED COMPONENTS EFFICIENCY DATA

TYPE H1.1 & W1.1

(Pt coated)

wavelength (nm)	58.4	74.4	121.6
--------------------	------	------	-------

reflectivity %	22.0	14.0	20.0	Pre-flight
	20.0	14.0	13.0	Post-flight

O	-1	1.2	3.2	4.6	Pre-flight
		4.0	4.0	2.0	Post-flight
R	0	7.6	1.9	7.7	
		1.0	1.0	6.0	
E	+1	1.5	3.7	8.1	
		6.0	5.0	3.0	
% $\Sigma$		10.3	8.8	20.4	
		11.0	10.0	11.0	

figure 8



## SPATIAL ENVIRONMENT ENFLUENCE

### STRAY LIGHT DATA

#### STRAY LIGHT VARIATIONS

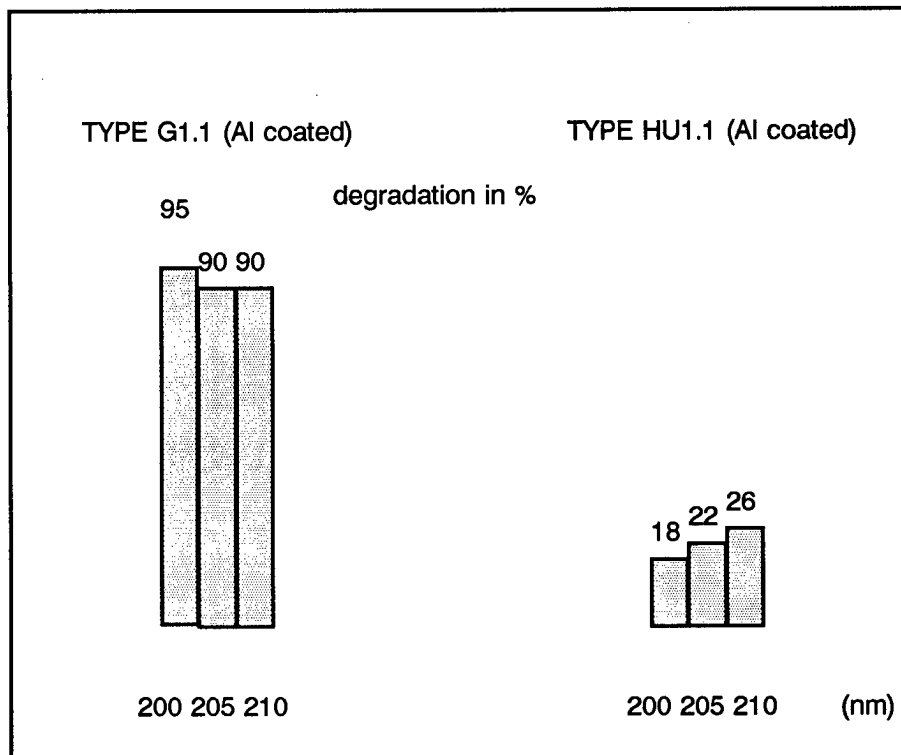


figure 9

## TESTS RESULTS DISCUSSION

Wavefront Planeity, Absolute Efficiency and Stray Light tests have been operated with the same instrumentation than the one used for pre-flight samples characterisation, on the reference (stored on ground under, Air-Nitrogen pressure) and loaded (space environment shaded and exposed) sets of components.

The components selected for being submitted to the experiment were Ruled and Holographic, Original and Replica Gratings, and double coated control mirrors.

These components were representative to the main grating manufacturing processes.

**WAVEFRONT QUALITY :** We have noted no degradation for all the gratings. That clearly shows the correct thermal behaviour of the different materials used : no glass blank distorsion, no groove line deformation depending on sensitive photoresist or epoxy resin.

**SENESCENCE ON GROUND :** A set of samples have been stored on ground during all the experiment duration. The senescence test has revealed a slight efficiency alteration, less than 10% with the ruled grating replica.

Both Holographic and ion-etched holographic masters show a lower efficiency decrease.

Stray Light level studie reveale a degradation between 15 to 25 % depending on the wavelenght-test, this result is in agreement with our previous experiments.

**SPACE VACUUM LONG EXPOSURE :** The extended long space vacuum exposure duration (69 months, about 34,000 orbits, thermal cycling by orbit from - 30 °C to + 70 °C) has induced a slight decrease of Aluminum and Platinum coatings reflectivity up to 10% in the U.V. region.

Al coated gratings have been affected in a same proportion.

Pt coated gratings : The sum of the diffracted energy in -1 , 0 and +1 orders at each wavelenght has decreased sensibly as the coating reflectivity (10 to 20%). Changes in repartition of energy depending on wavelenght and orders can be explained by a slight decrease of modulation of the grating (3 to 4 nm) in correlation with the great number of vacuum thermal cycling.

A Stray light level degradation (90%) has been measured with the ruled grating replica, this degradation has to be appreciated relatively to the very low initial level.

For the original ion-etched holographic grating the degradation (15 to 25% depending on the wavelenght-test) is in a same order than for samples stored on earth.

**SOLAR IRRADIATION :** One set of components have been subjected to direct solar irradiation during 10 months (cumulative equivalent sun hours 1600) and to space environment (Atomic oxygen fluence  $3.71\text{E}+03$  atoms by  $\text{cm}^3$ , Micrometeoroids and debris, 90 impacts by  $\text{m}^2$ ). This particularly critical test has damage the optical properties of coatings up to 35% reflectivity loss . Aluminum coated gratings have been affected in a same proportion .

Pt coated gratings : The sum of the diffracted energy in -1 , 0 and +1 orders at each wavelenght has decreased sensibly as the coating reflectivity (35 to 40%). Changes in repartition of energy depending on wavelenght and orders can be explained by a slight decrease of modulation of the grating (8 to 9 nm) in correlation with the great number of vacuum thermal cycling.

About stray light level parameter, we note the same phenomena than for the non-exposed samples

## CONCLUSIONS

The extended space vacuum long duration experiment – 69 months, about 34000 orbits, thermal cycling per orbit from  $-30^{\circ}\text{C}$  to  $+70^{\circ}\text{C}$  – has shown the rather satisfying behaviour of Aluminum and Platinum coatings and of Ruled and Holographic – masters and replica – gratings depending to wavefront planeity quality and absolute efficiency.

This is also true for original ion-etched holographic grating according to the Stray light level parameter and also for the ruled grating replica despite an higher relative increase.

Samples subjected to direct space environment and direct solar irradiation (which are not usual conditions for space experiment using gratings) present no additionnal deterioration according to wavefront planeity quality and stray light level.

A loss of coating reflectivity and absolute efficiency is detected in the Ultra-Violet region for all the samples, for these extreme conditions.

POST-FLIGHT CHARACTERIZATION OF OPTICAL SYSTEM SAMPLES,  
THERMAL CONTROL SAMPLES, AND DETECTORS FROM  
LDEF EXPERIMENT M0003, SUB-EXPERIMENTS 6 AND 13

Randall R. Hodgson, James N. Holsen  
McDonnell Douglas Electronic Systems Company  
St. Louis, MO 63166

Robert A. Drerup Jr.  
USAF Wright Laboratory - Materials Directorate  
Wright Patterson AFB, OH 45433-6533

ABSTRACT

Flight samples and control samples of optical and thermal control coatings have been measured for hemispheric reflectance and transmission. Data was recorded for wavelengths from .25 microns to 18 microns. The samples were exposed directly to the orbital environment, but were on the trailing edge of the LDEF satellite. Preliminary analysis shows no significant change in the reflectance or transmission values of most of the samples.

Post-flight tests of avalanche photodiodes have yielded results. The tests consist of measuring the following detector parameters: breakdown voltage for set values of reverse current, responsivity vs. bias voltage, noise equivalent power, and uniformity of photoresponse. The avalanche photodiodes were mounted on the leading edge of the LDEF satellite, but were shielded from the outside by a silver-coated teflon foil cover. Small puncture holes are present in the foil, probably caused by impact of particles in orbit. For most of the detectors, there has been no significant change in noise or response.

## LDEF ACTIVE OPTICAL SYSTEM COMPONENTS EXPERIMENT

M. D. Blue

Georgia Tech Research Institute  
Atlanta, Georgia 30332  
Phone 404/894-3646, Fax 404/894-5073

### SUMMARY

A preliminary report on the Active Optical System Components Experiment is presented. This experiment contained 136 components in a six inch deep tray including lasers, infrared detectors and arrays, ultraviolet light detectors, light-emitting diodes, a light modulator, flash lamps, optical filters, glasses, and samples of surface finishes. Thermal, mechanical, and structural considerations leading to the design of the tray hardware are discussed. In general, changes in the retested component characteristics appear as much related to the passage of time as to the effects of the space environment, but organic materials, multilayer optical interference filters, and extreme-infrared reflectivity of black paints show unexpected changes.

### I. INTRODUCTION

Components exposed to the space environment aboard the LDEF experiment Effects of Long-Duration Exposure on Active Optical System Components are now being remeasured. This report details the experiment and summarizes the status at this time.

The objective of the experiment is to determine quantitatively the effects of long-duration space exposure on the relevant performance parameters of lasers, radiation detectors, and selected optical components, to evaluate the results and implications of the measurements indicating real or suspected degradation mechanisms, and to establish guidelines, based on these results, for selection and use of components for space-based electro-optical systems. A total of 136 components were mounted on the 6-inch deep tray provided for this experiment. The experiment was unpowered. No bias or temperature control were provided. All components experienced ambient temperature conditions. Future experiments on the effects of exposure at normal operating conditions (cryogenic for example) can be combined with the ambient temperature data to separate degradation effects that are specifically related to operating temperature. As discussed in Section III, typically components were mounted so

as to simulate the expected mounting conditions and minimum environmental protection in a working space-based system. Exceptions were made to satisfy our curiosity as to the effect of direct exposure in some cases. Many components were mounted under aluminum covers to protect them against direct exposure to the space environment. Infrared detectors were usually mounted inverted in most cases with the chip carrier or detector package exposed to space and the detector looking toward the base plate.

The experiment tray was mounted in row five, column E, which put it on the starboard side of the LDEF in the four o'clock position relative to a twelve o'clock direction of motion. In this position, the components experienced reduced exposure to atomic oxygen and micrometeoroid impacts compared to the leading edge, but craters were nonetheless observed. The position of the tray on the LDEF is shown in Figure 1. As this figure indicates, the tray was divided into six subtrays, five of which were covered with a sunscreen. The total atomic oxygen fluence at this location was about  $10^{13}$  atoms/cm<sup>2</sup> (ref. 1).

The thermal, structural, and mechanical design aspects of the experiment are summarized in Sections II and III. Component characteristics are discussed in Section IV where our initial results for lasers, modulators, detectors, filters, and black paints are reviewed briefly. Some components on the tray were supplied by other investigators and will be reported separately.

## II. THERMAL DESIGN CONSIDERATIONS

Ambient temperature limitations vary substantially among the components included in the experiment. A maximum temperature of 85°C applies for the ADP (NH<sub>2</sub>PO<sub>4</sub>) used in the light modulator. Above this temperature, limits for infrared detectors range from 100°C for HgCdTe detectors to 145°C, the softening point of the indium-alloy solder used for lead attachment. Minimum temperatures were not considered to be a problem. Maximum temperatures were controlled through the use of surface coatings of defined emissivity and absorptivity. Maximum temperatures were not a strong function of the percentage transmission of the sunscreens.

The basic method used to analyze the thermal control techniques for the LDEF tray was the manipulation of surface coating properties to produce the desired temperature values. Thus, it was important to accurately model the radiation heat transfer to and from the tray and its contents.

The LDEF 6-inch regular tray is constructed of 6061-T6 aluminum sheet. The six subtray base plates are also of this material. Components were typically captured between fiberglass-epoxy panels and attached to 6061-T6 aluminum sheets 0.06-inch thick, formed to a hat-shaped cross-section, and bolted to the LDEF base plates. Figure 2 shows how the base plate, hat sections, aluminum angles, and sunscreen go together to form a subtray assembly. All four sides of the tray were assumed to have an anodized coating with values of solar absorptivity/IR emissivity of (0.30/0.30). The bottom of all tray frames and all experiment surfaces facing the interior of the vehicle were assumed to be painted with Chemglaze Z306 (Houghson Chem. Co.) black polyurethane paint with a solar absorptivity/IR emissivity ratio of (0.92/0.90).

The sunscreen design had a transmission of 0.56 over the central region. The calculated maximum temperatures for the various cases considered were found to be weakly dependent upon the transmission of this screen.

Analysis showed that heat conduction between the base plate and the hot sections upon which the components were mounted played a predominant role in the heat transfer mechanism. Our model assumed that the hat section and the plate had the same temperature. Analysis indicated that the tray would cycle toward a high temperature extreme of 82°C. However, thermal inertia would prevent this temperature from being attained. Post-recovery analysis (ref.1) indicates a calculated maximum temperature of 66°C for this tray position with an uncertainty of 10°C in reasonable agreement with our estimates.

### III. STRUCTURAL CONSIDERATIONS

The 16.25" x 16" tray subpanel was made from 1/4" aluminum plate. The resonant frequency of the bare plate was estimated to be 173 Hz. The addition of the hat-shaped sections for mounting components increases the rigidity of the plate, and raises the natural frequency. The sunscreens were expected to have a lower vibrational frequency, less than 100 Hz. The sunscreens also provided protection against inadvertent damage to the mounted components.

During vibration tests using one subpanel, a weak resonance occurred at 94 Hz for motion normal to the tray surface. This frequency occurs outside the critical range for both the Qualification and Flight Assurance requirements. Other weak resonant vibrations were observed at 270 and 330 Hz, and were not large enough to be of concern.

Vibrational analysis and testing of this subpanel indicated that the design produced no unusual or unexpected vibrational resonances, and all vibrational amplitudes were within LDEF test specifications.

Calculated stress levels on the structure were near 50 psi; a safe value. Weight of the experiment was not a major consideration, and therefore considerable design freedom was possible. The final experiment weight was 125.08 pounds, with an unbalance of 5.4 foot-pounds. Maximum allowed weight for the tray was 175 pounds.

Thermal expansion of the screen relative to the support structure could be accommodated by making the holes for the mounting screws 0.032 inches larger than the screw diameter. The sun screen was sandwiched between two 1/8-inch thick silicone rubber gaskets. The compressibility of the silicone rubber allowed the sunscreen to expand or contract without direct metal-to-metal contact at the mounting surfaces, thus preventing structural stresses on the subtray panel itself.

Post-recovery examination of the tray and contents indicated that all components were intact with no mechanical damage.

## IV. COMPONENT CHARACTERISTICS

Table I lists the components contained in the experiment. A summary of the results obtained in the post-recovery measurements for the first year is presented in the following.

### Lasers

HeNe and CO<sub>2</sub> laser tubes were retested in May, 1990. No laser action could be obtained from the tubes. The characteristics of the tubes suggested that the mixture of fill gas had changed during the period between initial and post-flight tests. While the extended period in orbit was unplanned, the experimental result is consistent with changes expected from gas diffusion through the glass envelope. Gas lasers for long-term space applications must not be sealed systems. The tubes were in good physical condition, and survived the launch and recovery phases without apparent degradation.

The GaAlAs semiconductor diode lasers in this experiment were the single-heterostructure close-confinement type as manufactured in the middle 1970's. The diodes were tested with a circuit containing a silicon controlled rectifier which provided low-voltage high-current pulses at a rate controlled by an external pulse generator. Diode radiation output was monitored by a silicon photodiode. Remeasurement indicated greater light output from all devices, a result believed caused by the better collection efficiency of a new experimental arrangement rather than improved diode properties. The performance of the devices relative to one another has not changed significantly. Our conclusion is that, for the laser diodes, space exposure and the years in storage did not degrade device performance.

We also tested a GaAsP light-emitting diode that was on the tray, and compared it to a companion diode that was stored over the time period of the experiment. The characteristics of these devices were unchanged over the course of the experiment, although the plastic dome of the unit exposed to space did show some indentations that are assumed to be the result of micrometeoroid impacts.

YAG laser rods aboard the LDEF remain to be tested.

### Modulators

A light modulator based on ADP supplied by Coherent Associates was on the component tray, and an identical modulator was stored in our laboratory. The modulator parameters measured were optical transmission, half-wave voltage, and roll-off frequency. The modulator on the tray was mounted with a fixture covering the apertures, and the stored unit had plastic caps covering the apertures. No measurable changes in optical transmission were found. The



half-wave voltage and roll-off frequency were unchanged within experimental error for both units.

### Detectors

Detector measurements have just been started. Most of these are to be performed by the manufacturers. The early results are the following.

First measurements of a HgCdTe detector indicate that it performs better than indicated by the previous measurements. We believe that we have again a situation where the improved test setup is responsible for the difference in performance rather than a situation where the device improves with age.

Measurements of an InGaAsP photodiode also indicate good performance. This detector is a swap-out (replacing another type before launch) and we do not have the original data. The pair of on-board devices and the pair stored in our laboratory have similar characteristics, and the low junction leakage current for the devices indicates good temporal stability. The leads to the diode contact pads eventually came off on all devices before shipment to the manufacturer for post-recovery measurements. These were experimental devices and the technique for lead attachment had not been optimized. No space-related degradation effects were found.

Several large-area silicon photodiodes and PIN diodes were remeasured. The original current-voltage and capacitance-voltage characteristics of these devices were reproduced. Active areas of these devices were directly exposed to the space environment, and show the effects of micrometeoroid impacts. An example of such an impact is shown in Figure 3. This crater is visible to the eye.

For other detectors where the gold-plated back of the chip carrier was exposed to the space environment, the craters resulting from dust impacts were noted and photographed.

Measurements of the set of pyroelectric detectors were reported by Dr. James Robertson. Results indicate that space-related degradation is not observed for pyroelectric detectors. The remainder of the detectors and arrays await remeasurement.

Results of the detector measurements are in accord with our findings in related areas. The space environment as experienced by the LDEF does not degrade active components such as detectors, laser diodes, and modulators at ambient temperature.

### Optical Filters

Eight optical filters were included in the component set. Three filter types were represented: narrow band, broad band, and neutral density. One representative of each filter type was placed under an aluminum cover while the remainder were directly exposed to the

space environment. The most notable effect for the optical filters was a reduction in transmission for all but the neutral density filters. Narrow-band filters experienced a small shift in center wavelength. Changes in bandwidth were small but not consistent among the five narrow-band filters. Figure 4 shows the pre-launch and post-recovery transmission characteristic for one of the narrow-band filters. While the band shift is small, it is significant.

The reduction in transmission for some of the filters is believed related to degradation of the cement used in their construction. In the case of the neutral density filters, the covered filter was unchanged while the exposed filter showed slightly increased transmission. These results are consistent with slight erosion of the metal film used in the construction of the neutral density filters. The brown stain or organic film residue noted throughout the LDEF structure did not produce measurable absorption in these filters in the visible wavelength region.

### Paints

Some of the most unexpected changes observed in this set of components are found in the extreme-infrared reflectivity of the set of six black paint samples with aluminum substrates. Figure 5 shows before and after normal incidence spectral reflectivity at room temperature in the 40 to 600 micrometer region for one of the better known optical baffle coating materials, Chemglaze Z306 (Houghson Chem. Co.). The post-recovery data show the striking reduction in normal reflectivity. Data at cryogenic temperatures indicate somewhat increased reflectivity (compared to room temperature performance) for all samples both before and after space exposure.

The results shown in Figure 5 are typical for all six paint samples on the tray. The post-recovery data indicate reduced reflectivity and, more importantly, low reflectivity at extreme infrared wavelengths. This result, both surprising and pleasing, indicates that black paints for sensor baffle coatings will not only survive in the space environment, but will provide enhanced performance with aging. Preliminary analysis indicates that an increase in the extinction coefficient (imaginary component of the index of refraction) is required to reproduce the reflectivity characteristics, but that additional changes such as wavelength dependence for the refractive index may also be necessary. Degradation of pigment and binder is the suspected cause of these changes.

## VI. ACKNOWLEDGMENTS

Many colleagues and students contributed to this program over its decade-long existence. Prominent among this group were R. G. Shackleford, J. J. Gallagher, D. O. Gallentine, Marie Fair, Kevin Bottler, David W. Roberts, C. W. Gorton, Sid Perkowitz, Charles Ueng, and

Azmitava Roy. Component suppliers included Lockheed, Rockwell, New England Research Center, Santa Barbara Research Center, Corion, RCA, Galileo Electro-Optics, Coherent Associates, Quantrad, Coherent Radiation, and the US Army Night Vision and Electro- Optic Laboratories. The assistance of these and many other contributors is acknowledged and appreciated.

## VII. REFERENCES

1. Roger J. Bourassa and James J. Gills, "Data Summary: Atomic Oxygen Flux and Fluence Calculation for Long Duration Exposure Facility (LDEF)," LDEF MSIG, NASA Contract NAS1-18225, Jan. 18, 1991.
2. William M. Berrios and Thomas R. Sampair, "Long Duration Exposure Facility, Post-Flight Analysis, Calculated Flight Temperature Data Package, Preliminary," Lockheed Engineering & Sciences Co.

TABLE I.  
LIST OF ELECTRO-OPTICAL COMPONENTS

PASSIVE COMPONENTS	ACTIVE COMPONENTS	DETECTORS
Black Paint Samples	ADP Modulator	Silicon PIN
Neutral Density Filters	Channeltron Array	Silicon PV
Narrow-Band Filters	GaAlAs Laser Diodes	Silicon Gamma-Ray
Laser Mirrors	GaAsP LED	InGaAsP PV
Hot-Mirror Filter	Nd:YAG Rods	InSb PV
Lyman-Alpha Filter	CO <sub>2</sub> Waveguide Laser	PbS
UV Filter 1600 Å	HeNe Laser	PbSe
LiF Window	Holographic Crystals	HgCdTe PV
AlMgF <sub>2</sub> Mirror	Laser Flash Lamps	HgCdTe PC
Optical Glasses		PdSi Arrays
MgF <sub>2</sub> Window		Pyroelectrics
Al <sub>2</sub> O <sub>3</sub> Window		UV PMT
SiO <sub>2</sub> Window		UV Silicon
35-mm UV Film		
Various Optical Glasses		
Black Polyethylene		

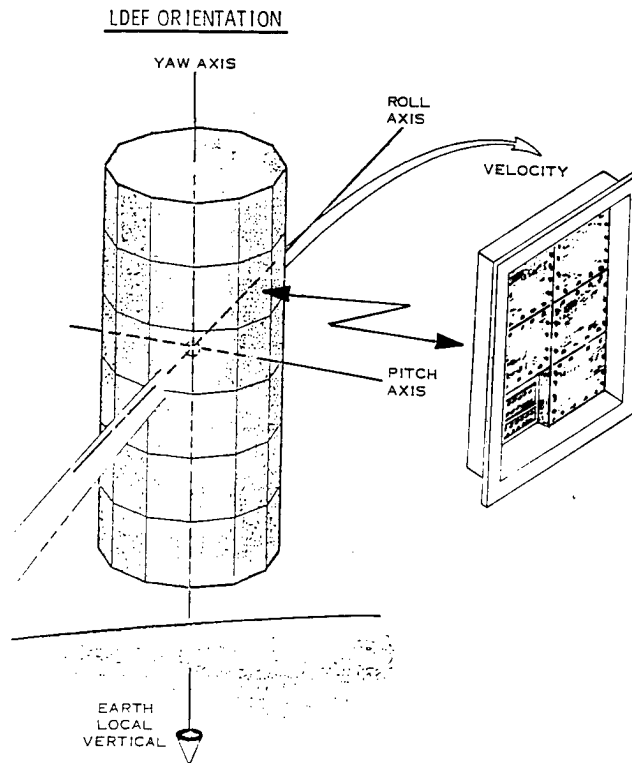


Figure 1. Location Of The Active Optical System Components Experiment On The LDEF. In this location, expected effects from atomic oxygen and particle impacts are reduced from leading-edge locations.

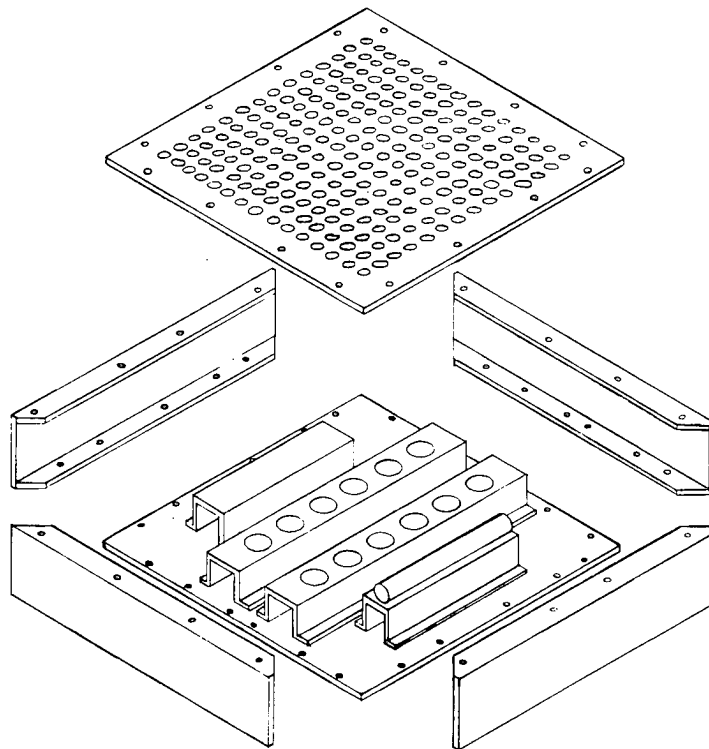


Figure 2. Typical Subtray Panel Showing Hat Sections Which Bolt To A Base Plate And Sun Screen Which Attaches To Aluminum Channels. The Central Portion Of The Sun Screens Transmit 56% Of The Incident Solar Radiation.

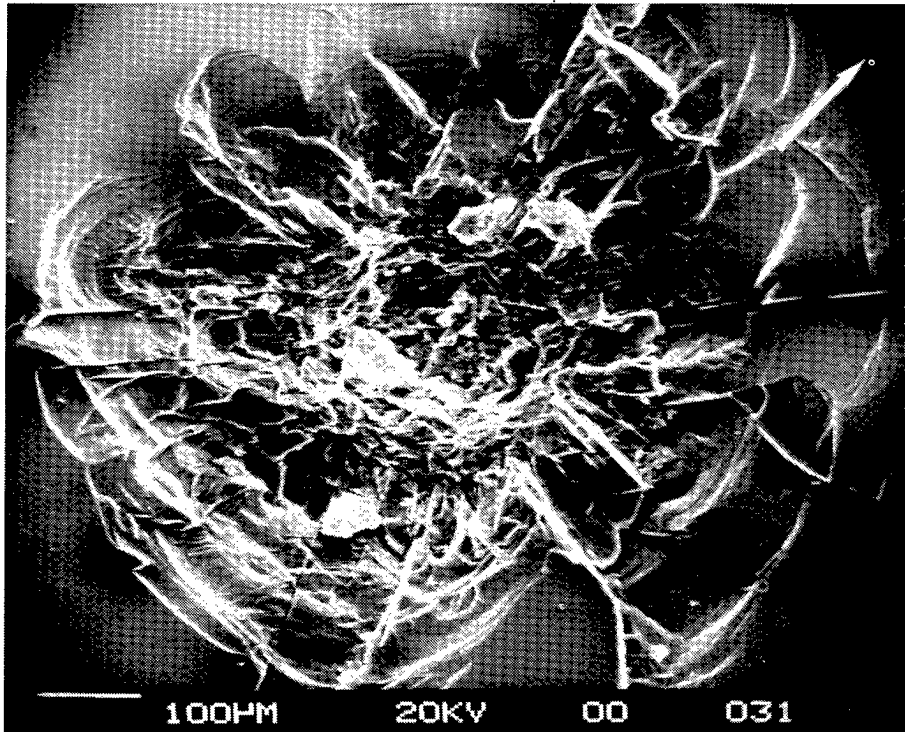


Figure 3. Scanning Electron Microscope Photograph Of The Impact Crater From A Micrometeoroid Collision With A Large-Area Silicon Infrared Detector. The Arrow Indicates Flight Direction. No Measurable Changes In Junction Leakage Or Capacitance Were Found In These Devices (Photo by Dr. John Sparrow).

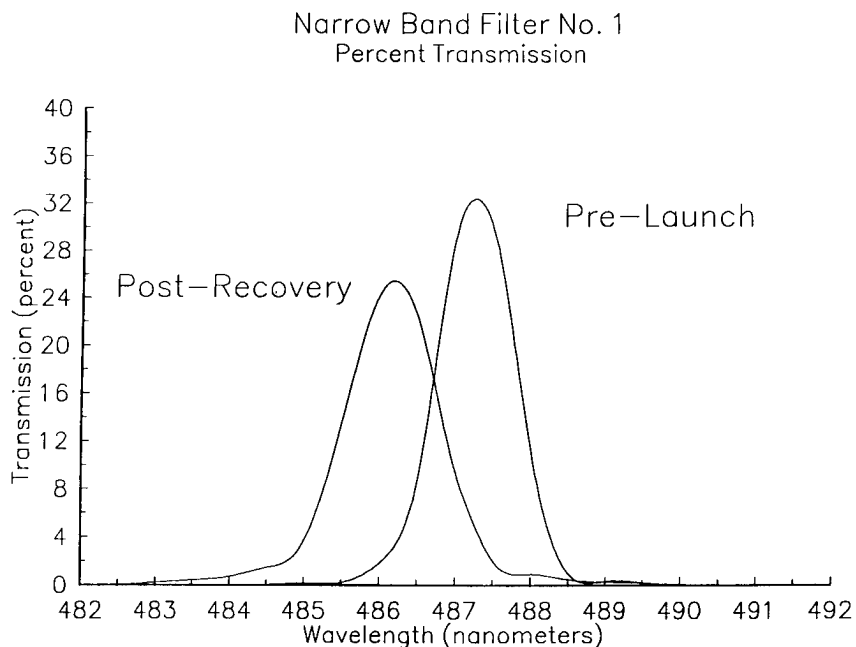


Figure 4. Transmission Characteristics Of A Narrow-Band Optical Filter Before And After Space Exposure. A Reduction In Transmission Was A Typical Result For All Filters On The Tray. The Shift In Center Wavelength Is Small But Significant.

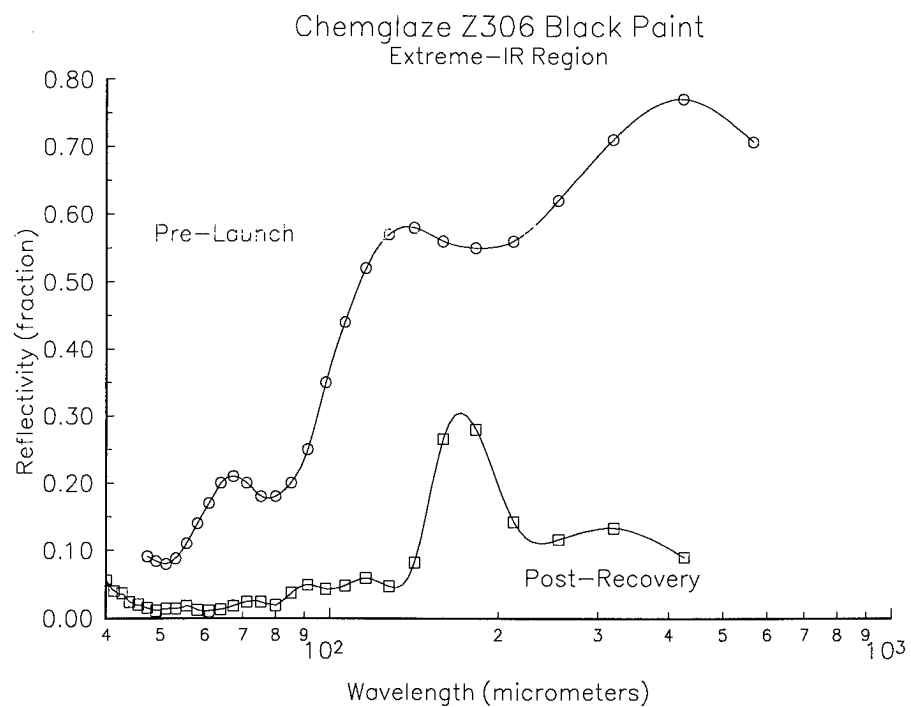


Figure 5. Reflectance Spectra In The Extreme Infrared For Chemglaze Z306 At Room Temperature. Paint Thickness Is 53 Micrometers With An Aluminum Substrate. The Reduction In Reflectivity Shown In The Post-Recovery Measurements Is Typical For All Six Paint Samples.

# EFFECTS OF LONG-DURATION EXPOSURE ON OPTICAL SYSTEM COMPONENTS

Gale A. Harvey  
NASA Langley Research Center  
Hampton, VA 23665-5225  
Phone: 804-864-4672, Fax: 804-864-7790

## SUMMARY

The optical materials and UV detectors experiment (SOO50-1) was a set of 15 optical windows, filters, and ultraviolet detectors. The optical specimens were all retrieved in excellent condition. No discoloration of the bulk optical window materials occurred, but the optical windows did experience several types of contamination. The most notable degradation of the optics were the deposition of an organic film on both surfaces. The films' absorptions were measured using a Fourier Transform Infrared spectrometer and UV spectrometers. The UV absorptions were almost 100 percent at 200 nm and about 50 percent at 380 nm.

## INTRODUCTION

Experiment SOO50-1 (ref. 1) consisted of 15 ultraviolet optical windows, filters, mirrors, and detectors. These optical components were selected as representative of optical components which would be used in Earth-looking ultraviolet spectroscopy from low Earth-orbit. The region of the spectrum 100 nm to 300 nm was the principal region of interest and defines ultraviolet (UV) as used in this report. This experiment occupied 1/6 of Tray E5 (figs. 1 and 2) on the LDEF. The SOO50-1 tray section had a 50 percent transmitting sun screen of 1/8-inch sheet aluminum. Sunlight passed through 3/8-inch diameter holes to the interior of the tray section. The back side of the sun screen was painted with Chemglaz Z306 black paint for thermal control. One-inch diameter fluoride, synthetic sapphire, and fused silica optical windows were mounted on a raised platform (fig. 3) within the tray section. This paper reports measurements and observations of these windows.

## VISUAL INSPECTIONS

All six of the optical windows were retrieved and delivered to a spectroscopy lab at LaRC in excellent condition. That is, none of the windows were cracked or chipped. Therefore, the mounting platform performed its primary function of protecting the optical windows from physical damage. A light brown stain is readily apparent on all of the windows when they are placed on a white background and viewed by doubly transmitted light.

The windows were examined microscopically at 40x and 1000x. Several types of deposits are present on both sides of the windows. A thin uniform surface layer covers both sides of the windows. Circular deposits up to 1 millimeter in diameter are present on the space exposed side of the windows. Aggregates of approximately 10 micron diameter particles are also present. The center portion of the back surface layer on the MgF<sub>2</sub> window adhered to the Cohrlastic R-500 silicon rubber used as gasket material behind the optical windows.

Figure 4 is a photograph of a back surface region of the MgF<sub>2</sub> window with adhering film and without adhering film at 40x. Figure 5 is a photograph of the same region at 1000x, and figure 6 is a photograph of the ground control window at 1000x. The sharp edges of the adhering film indicate that the film is brittle. Flakes of film debris in adjacent areas also indicate that the film is brittle. However, patterns in the film indicate the film may have once been of low viscosity.

Figure 7 is a photograph of the front surface of the flight LiF window at 40x. Figure 8 is a similar photograph of a surface of the ground control LiF window at 40x. The flight window has a "sprayed" texture compared to the control window. No discoloration of the bulk optical material was noticed on any of the optical windows.

## OPTICAL TRANSMISSION MEASUREMENTS

The HALOE program at LaRC has used 3.4  $\mu$  spectroscopy to measure thin organic films (ref. 2 and 3). The transmission of an optical window is measured with an FTIR spectrometer optimized for the 3.4  $\mu$  spectral region. Strong, narrow methyl (CH<sub>3</sub>) and methylene (CH<sub>2</sub>) absorption bands are in this spectral region.

The 3.4  $\mu$  spectrum of the flight CaF<sub>2</sub> window ratioed to the ground control window is presented in figure 9. The 3.4  $\mu$  absorptions result from the films on both surfaces of the flight window.

Figure 10 shows similar 3.4  $\mu$  absorption through the films on both surfaces of the MgF<sub>2</sub> window. The absorptions in figures 9 and 10 are typical of many hydrocarbons. The spectrum in figure 11 was obtained from the center area of the MgF<sub>2</sub> window where the rear surface film adhered to the Cohrlastic R-500 silicon rubber gasket material behind the window. Therefore, the absorption in figure 11 is from only the front surface film. The two spectra shown in figure 11 indicate the measurement repeatability. The 3.4  $\mu$  absorption on the front surface is similar to outgassing deposits from Chemglaz polyurethane paints (ref. 4). The 3.4  $\mu$  spectrum of the LiF window is presented in figure 12 and is similar to that of both surfaces of the CaF<sub>2</sub> and MgF<sub>2</sub> windows. The 3.4  $\mu$  spectra of both surfaces of the synthetic sapphire (Al<sub>2</sub>O<sub>3</sub>) window are shown in figure 13 and 14. The methyl absorption, 2960 cm<sup>-1</sup>, is stronger relative to the methylene absorption, 2930 cm<sup>-1</sup>, on the Al<sub>2</sub>O<sub>3</sub> window than on the fluoride windows. The broad absorptions on either side of the 3.4  $\mu$  methyl and methylene absorptions indicate non-hydrocarbon organic contamination. Two fused silica windows were flown. The 3.4  $\mu$  absorption [both surfaces] of one of the fused silica (SiO<sub>2</sub>) windows is presented in figure 15. The flight window spectrum was ratioed to the ground control window spectrum and shows a very small increase in transmission in the methylene bands of the flight window. The absence of 3.4  $\mu$  absorptions on the SiO<sub>2</sub> window indicates a substrate selectivity effect. A similar result was reported in reference 5.

The ultraviolet transmission of the CaF<sub>2</sub> window (ratioed to the transmission of a ground control window) is presented in figure 16. The transmission is monotonically increasing from almost zero at 200 nm to more than 50 percent at 380 nm. The unratioed ultraviolet transmissions of the MgF<sub>2</sub> and LiF windows over this spectral region are presented in figures 17 and 18. The transmissions of the ground control windows are also presented in figures 17 and 18. The higher transmission of the MgF<sub>2</sub> window relative to the CaF<sub>2</sub> and LiF windows are probably because the back film is missing from the MgF<sub>2</sub> window.



The vacuum ultraviolet transmission of the MgF<sub>2</sub> and LiF windows are presented in figure 19 and 20 over the spectral interval 100 nm to 200 nm. There is no measurable transmission through the LiF window in this spectral region. The low transmission through the MgF<sub>2</sub> window is probably because the back contaminant film is missing from the flight window. The optical window measurements are summarized in Table 1.

### CONCLUDING REMARKS

Surface contamination is the only deterioration seen on Experiment SOO50-1 optical windows in Tray E5 on LDEF. A faint brown visual stain is present on the front surface of all six windows. A brittle film is also present on the back surface of the three UV transmitting fluoride windows. The change in vacuum ultraviolet transmission of the fluoride windows is catastrophic. The absence of 3.4  $\mu$  absorptions on the SiO<sub>2</sub> window indicates the film depositions were dependent on the substrates.

### REFERENCES

1. Clark, L. G., Kinard, W. H., Carter, D. J. Jr., and Jones, J. L. Jr., "The Long Duration Exposure Facility Mission 1 Experiments," NASA SP-473, 1984.
2. Harvey, G. A., Raper, J. L., and Messier, R. N., "Microcontamination of IR Spacecraft Optics," in Proceedings of Microcontamination Conference and Exposition, Anaheim, CA, pp. 237-259, October 1989.
3. Harvey, G. A. and Raper, J. L., "Halogen Occultation Experiment (HALOE) Optical Witness-Plate Program," NASA TM 4081, February 1989.
4. Harvey, G. A., "Organic Contamination of LDEF," First LDEF Conference Publication. NASA CP-3134, 1992.
5. Stewart, T. B., Arnold, G. S., Hall, D. F., and Marten, H. D., "Absolute Rates of Vacuum-Ultraviolet Photochemical Deposition of Organic Films," J. Phys. Chem., **93**, pp. 2393-2400, March 1989.

TABLE 1. S0050-1 OPTICAL WINDOW MEASUREMENTS

<u>Window</u>	<u>3.4 <math>\mu\text{m}</math> Absorption Results</u>	<u>UV Transmission Results</u>
CaF <sub>2</sub>	Organic films present on both sides	Transmission increasing from almost zero at 200 nm to more than 50% at 380 nm. Catastrophic loss in UV transmission.
MgF <sub>2</sub>	Organic film present on front side.	Higher transmission of MgF <sub>2</sub> window relative to CaF <sub>2</sub> and LiF because back film is missing on the MgF <sub>2</sub> . Catastrophic loss in UV transmission.
LiF	Organic films present on both sides.	Similar transmission to CaF <sub>2</sub> . Catastrophic loss in UV transmission.
Al <sub>2</sub> O <sub>3</sub>	Methyl absorption stronger than on CaF <sub>2</sub> , MgF <sub>2</sub> , and LiF; also shows presence of a non-hydrocarbon organic contaminant.	Substrate does not transmit below 150 nm. Near UV not measured.
SiO <sub>2</sub>	Absence of 3.4 $\mu\text{m}$ absorptions, suggesting a substrate selectivity ( film deposition dependent on substrate.)	Substrate does not transmit below 150 nm. Near UV not measured.

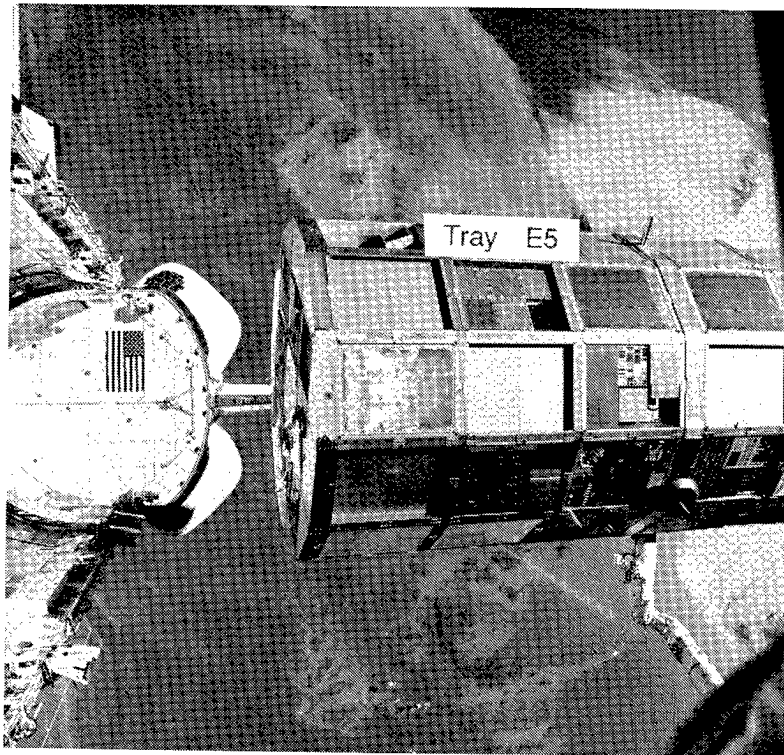


Figure 1. Tray E5 during retrieval.

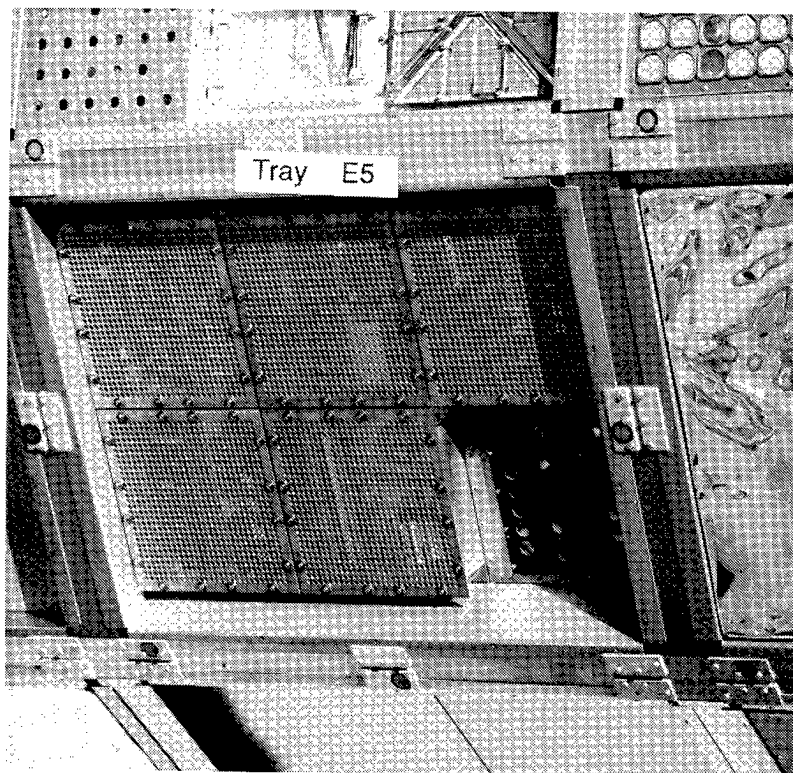


Figure 2. Tray E5 at Kennedy Space Center.

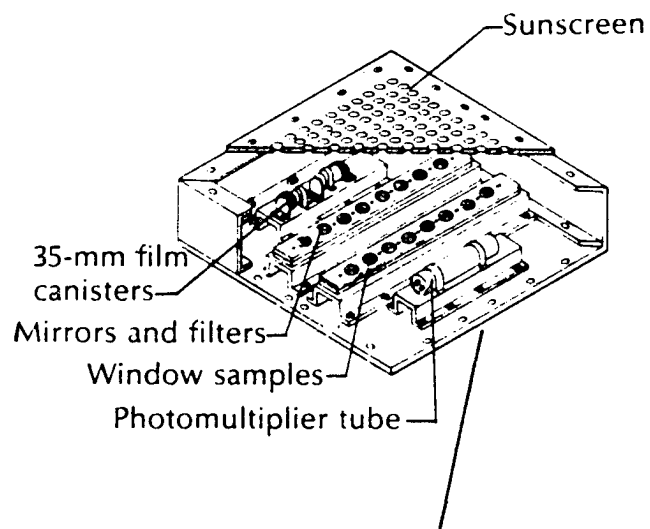


Figure 3. Drawing of Experiment S0050-1.

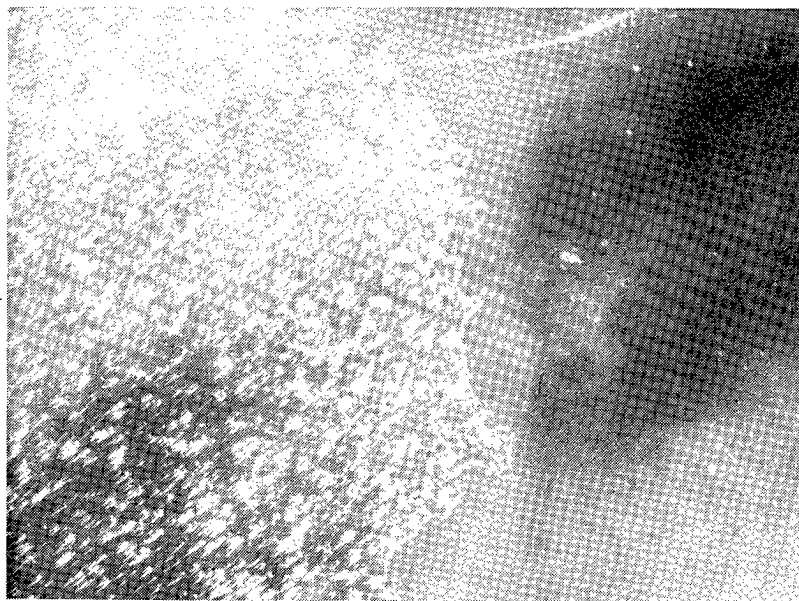


Figure 4. Photograph of  $\text{MgF}_2$  window, back surface, 40X.

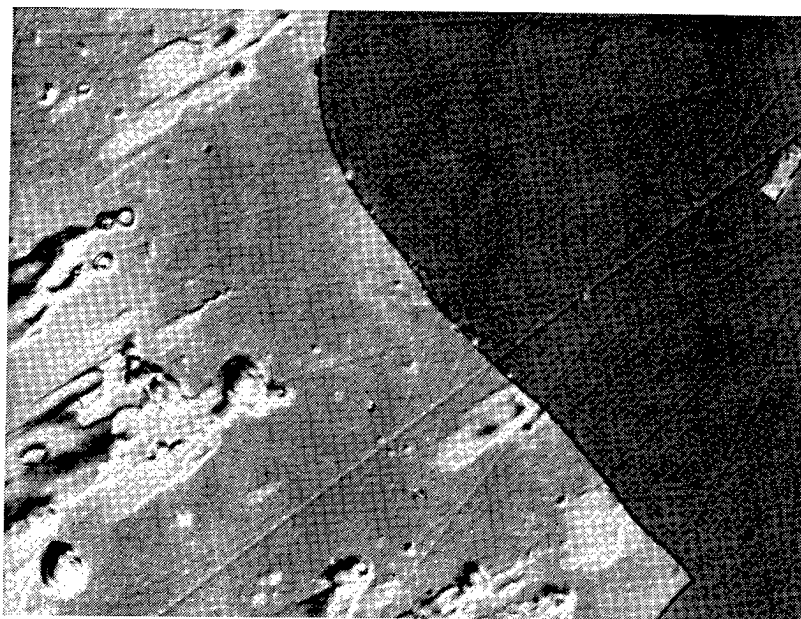


Figure 5. Photograph of MgF<sub>2</sub> window, back surface, 1000X.

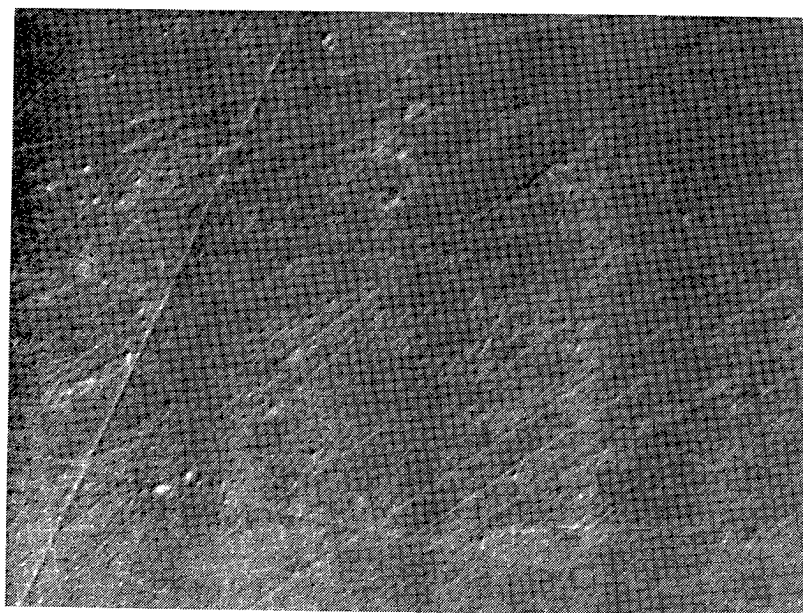


Figure 6. Photograph of MgF<sub>2</sub> ground control window, 1000X.

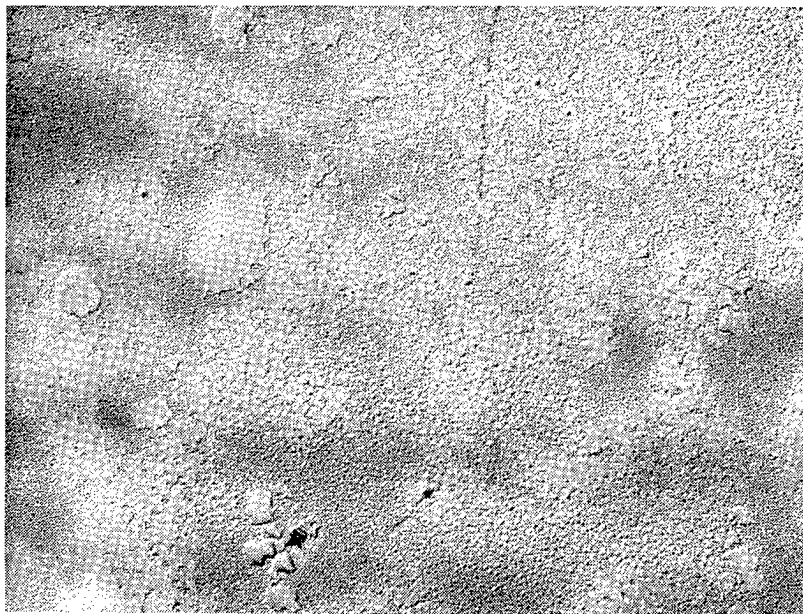


Figure 7. Photograph of LiF window, front surface, 40X.



Figure 8. Photograph of LiF ground control window, 40X.

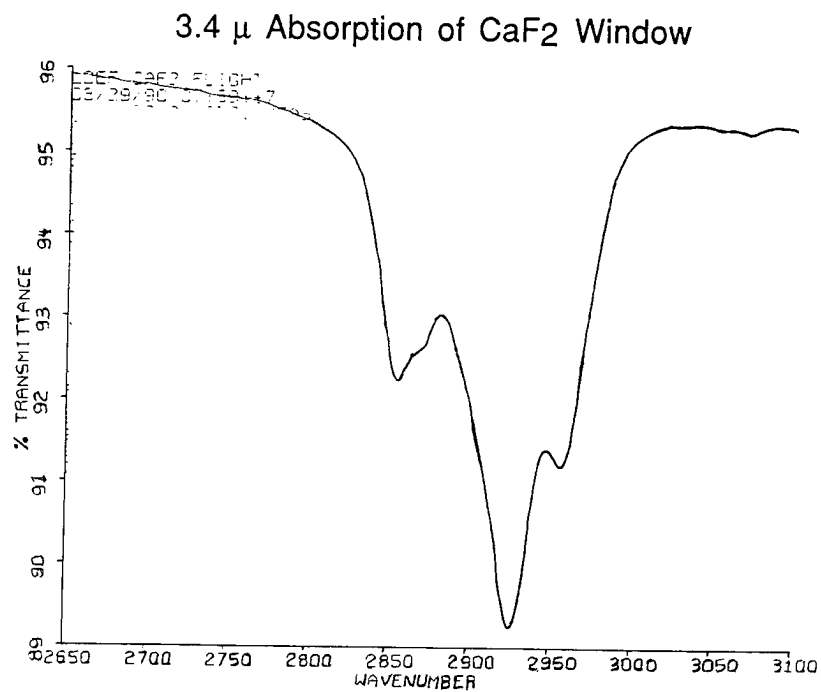


Figure 9. 3.4  $\mu$  spectrum of CaF<sub>2</sub> window.

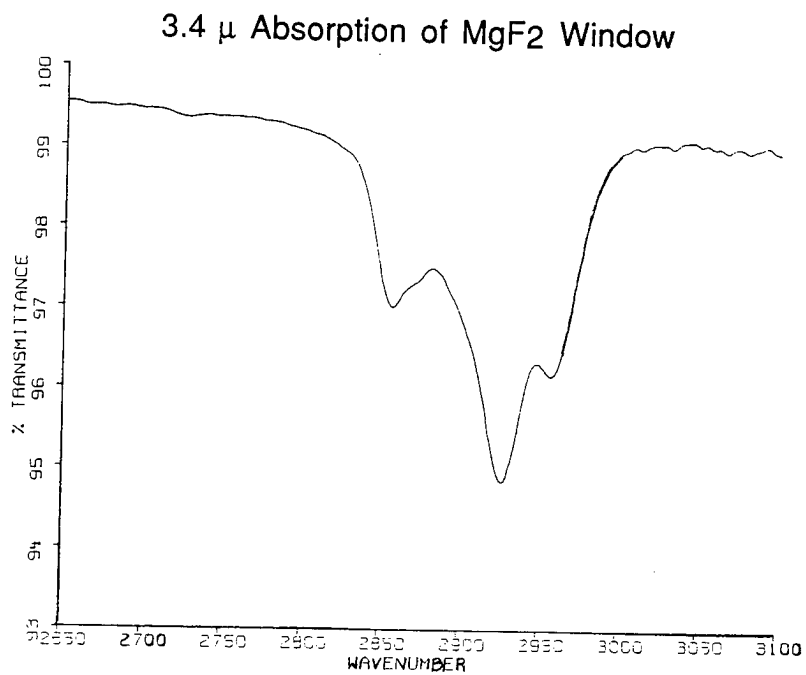


Figure 10. 3.4  $\mu$  spectrum of both surfaces of MgF<sub>2</sub> window.

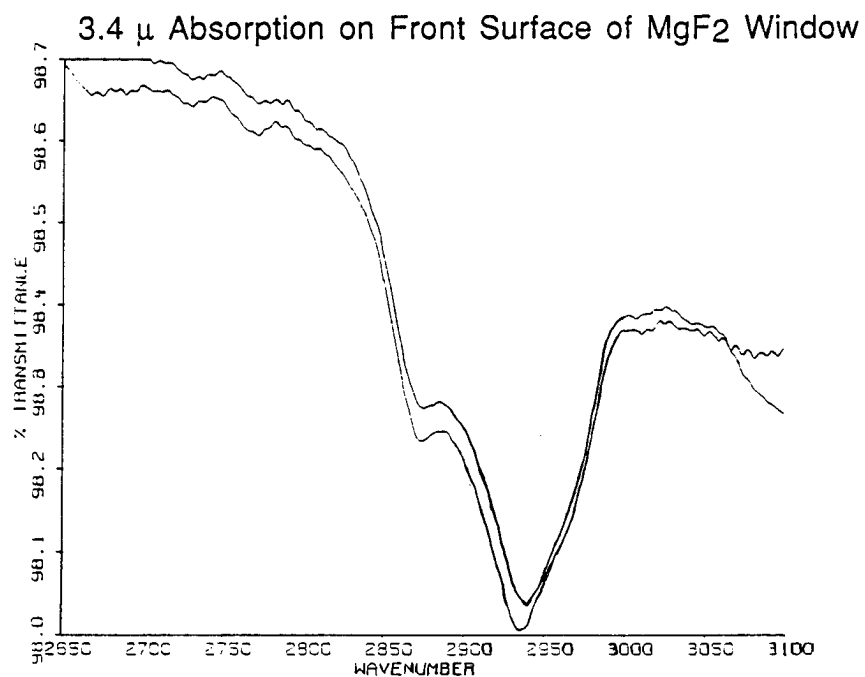


Figure 11. 3.4  $\mu$  spectra of front surface of MgF<sub>2</sub> window.

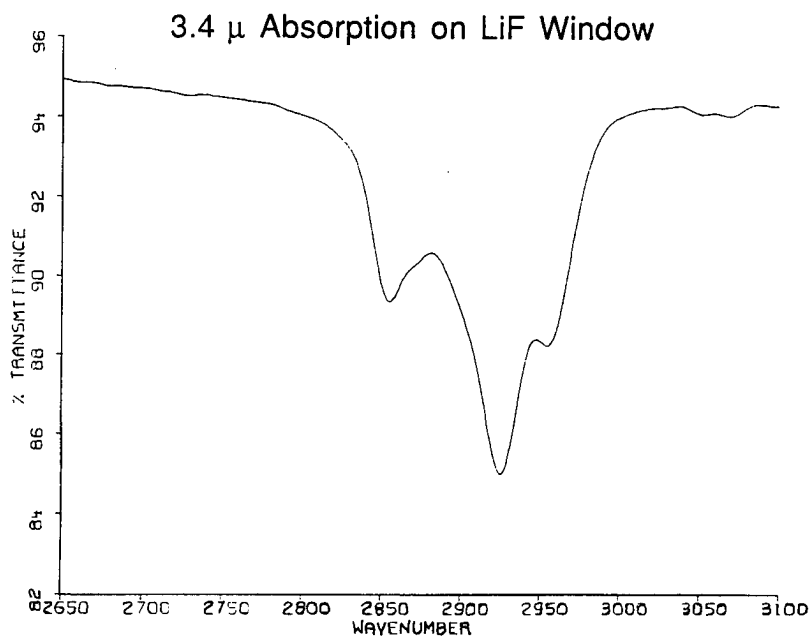


Figure 12. 3.4  $\mu$  spectrum of both surfaces of LiF window.



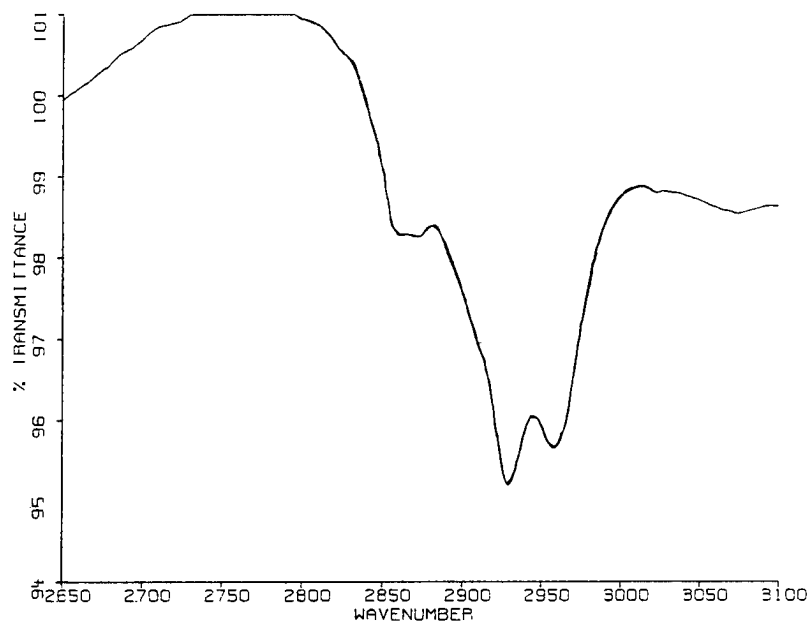


Figure 13. 3.4  $\mu$  spectrum of both surfaces of Al<sub>2</sub>O<sub>3</sub> window.

#### 3.4 $\mu$ Absorption on Al<sub>2</sub>O<sub>3</sub> Window

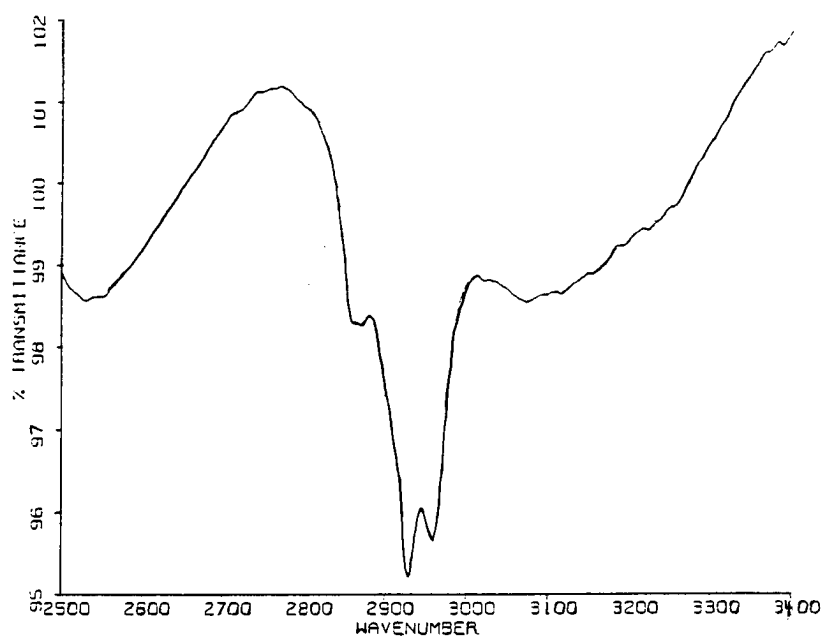


Figure 14. Wide 3.4  $\mu$  spectrum of both surfaces of Al<sub>2</sub>O<sub>3</sub> window.

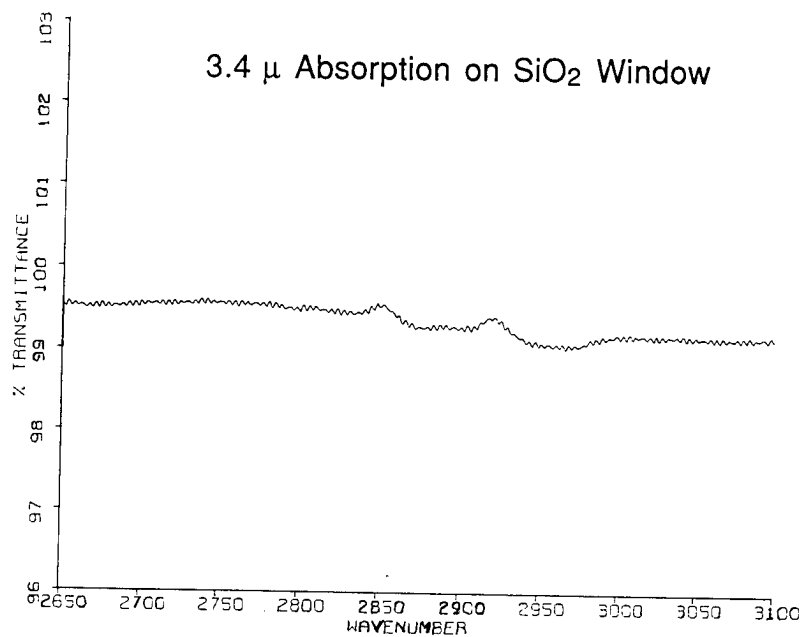


Figure 15. 3.4  $\mu$  spectrum of both surfaces of SiO<sub>2</sub> window.

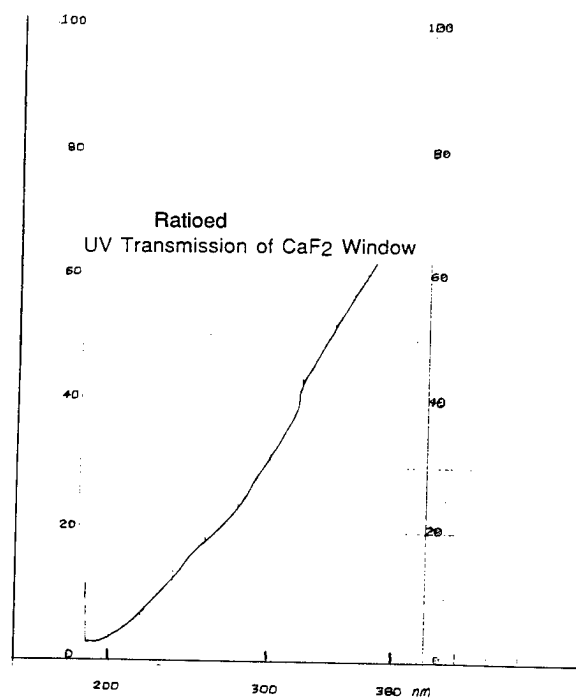


Figure 16. Ultraviolet transmission of CaF<sub>2</sub> window (both surfaces).

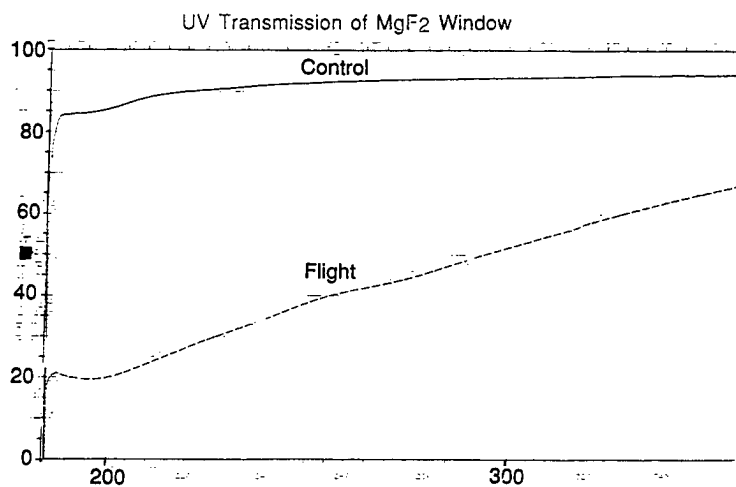


Figure 17. Ultraviolet transmission of center (front surface) of MgF<sub>2</sub> window.

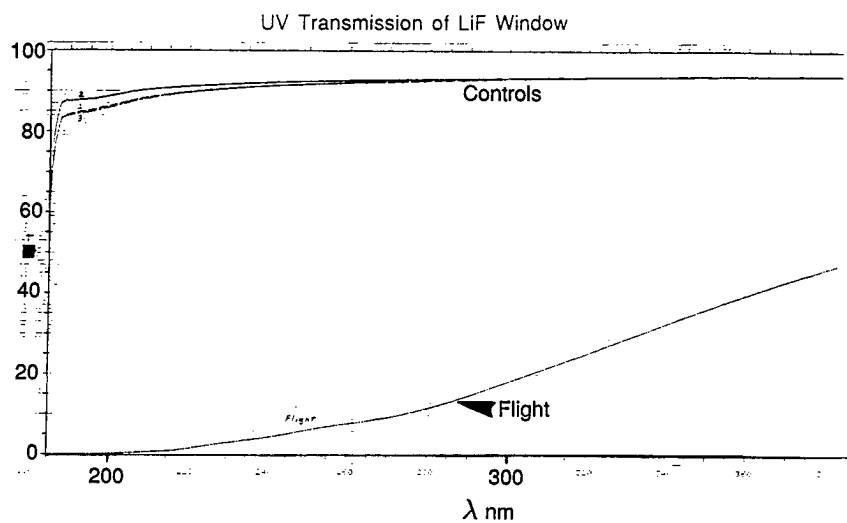


Figure 18. Ultraviolet transmission of LiF window (both surfaces).

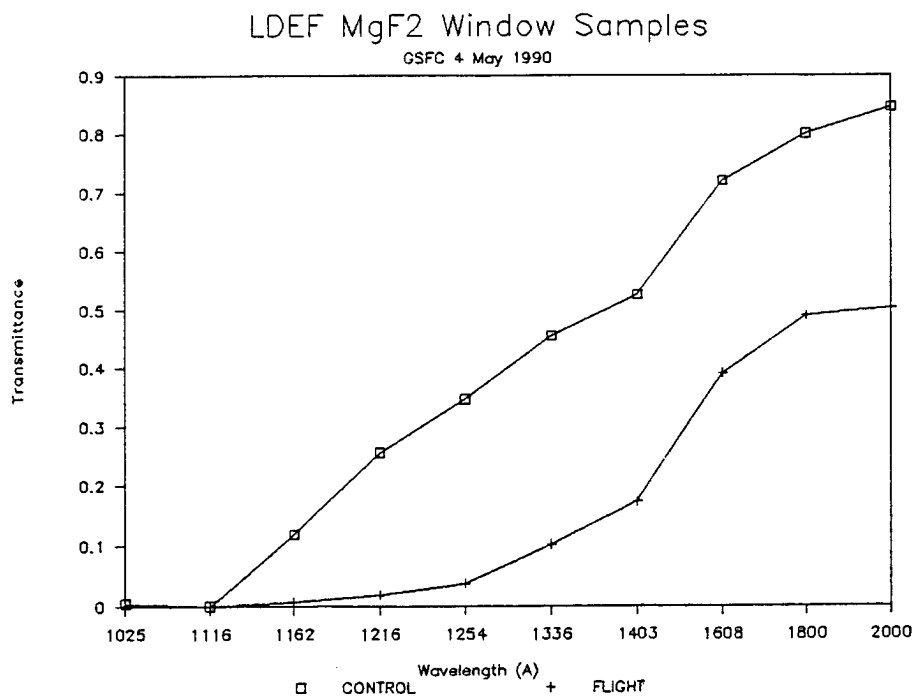


Figure 19. Vacuum ultraviolet transmission of center (front surface) of MgF<sub>2</sub> window.

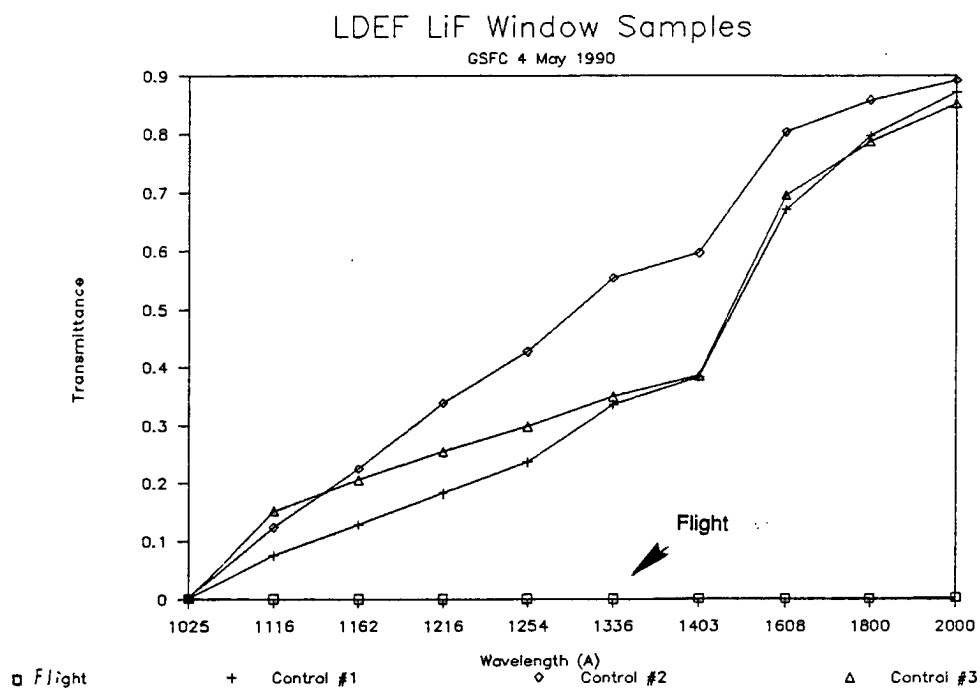


Figure 20. Vacuum ultraviolet transmission of LiF window (both surfaces).

**EFFECTS OF LONG TERM EXPOSURE  
ON OPTICAL SUBSTRATES AND COATINGS  
(S0050-2)**

John Vallimont and Keith Havey  
Eastman Kodak Company, Rochester N.Y.

Kodak included 12 substrate and coating samples on the LDEF structure. There were 3 Fused Silica and 3 Ultra Low Expansion (ULE(tm)) uncoated glass samples, 2 ULE(tm) samples with a high reflectance silver coating, 2 Fused Silica samples with an antireflectance coating, and 2 Fused silica samples with a solar rejection coating. The sample dimensions were 32 mm diameter by 1 mm thick. A set of duplicate control samples was also manufactured and stored in a controlled environment for comparison purposes.

A preliminary evaluation of the flight samples for effects from the 5 year mission showed that a contaminant was deposited on the samples, a micrometeoroid impact occurred on one of the samples, and the radiation darkening which was expected for the glass did not occur. The results are listed below in more detail.

**CONTAMINANT ANALYSIS**

The contaminant on the samples was analyzed using X-ray Photoelectron Spectroscopy (XPS), which showed the substrates and coatings to be covered with a thin layer of polymer which contained silicon. On the uncoated ULE(tm) substrate and the Antireflection coating the contaminant appeared similar in structure to the silicon of the rubber gasket which was used to mount the optics. However, neither the relative atomic percentages or the relative sizes of the silicon and oxygen peaks from the XPS conclusively prove that the contaminant is a residue from the mounting rubber gasket. Other silicon sources must be considered as well. On the remainder of the samples the contaminant was visibly lighter and was silica-like in nature.

**MICROMETEOROID IMPACT**

A micrometeoroid impact site was found on one of the samples. The impact crater measured .3mm in diameter by .03 mm deep. Multiple fractures occurred in the glass at the impact site and are shown in figure 1.

**RADIATION DARKENING**

Some radiation darkening could be expected of the Ultra Low Expansion (ULE(tm)) glass which is not a radiation tolerant glass. No darkening of either the ULE(tm) or the Fused Silica glass was evident. See figures 2 & 3.

## SUMMARY

The 5+ year exposure of the samples to the space environment resulted in a contaminant being deposited on the samples. One sample received a micrometeroid impact. Cleaning of the uncoated glass samples showed that no degradation occurred to the optical transmission of either the Fused Silica or ULE(tm) glasses (see figures 2 & 3). The cleaning of the coated samples is in process, the results of which will be presented in a more comprehensive final report.



**MICROMETEROID IMPACT CRATER**  
**FIGURE 1**

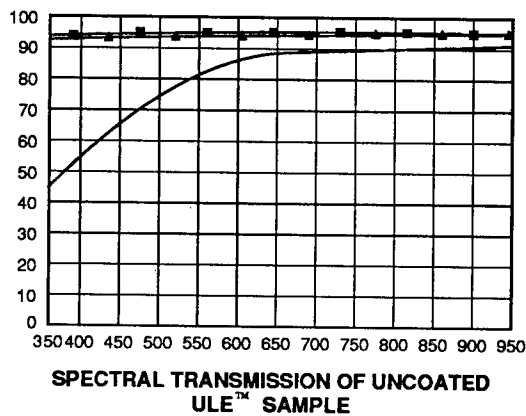


**FIGURE 2**

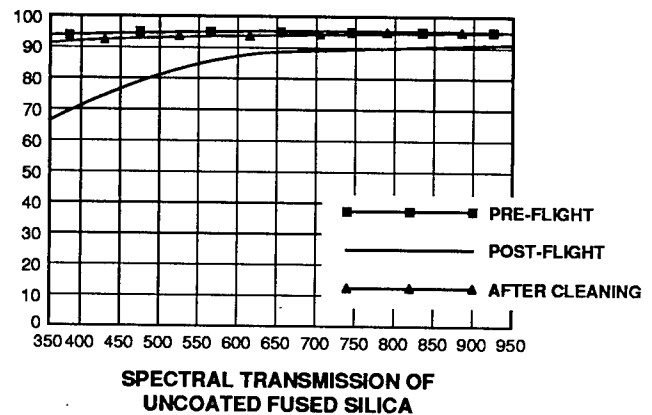


**FIGURE 3**

# VACUUM DEPOSITED OPTICAL COATINGS EXPERIMENT

Jean CHARLIER

MATRA DEFENSE

DET/DTO

17, rue Paul Dautier

78140 VELIZY VILLACOUBLAY

FRANCE

Phone : (33-1) 39.46.97.86 - FAX : (33-1) 39.46.64.87

## SUMMARY

The 138-4 Frecopa experiment consisted of 20 sorts of optical components and coatings subjected to space exposure. They covered a large range of use from UV to IR spectrum : filters, mirrors, dichroïcs, beam splitters and anti-reflection coatings made of several different materials as layers and substrates. By comparing pre and post flight spectral performances it was possible to put into evidence the alterations due to space exposure.

## 1 - INTRODUCTION

All layers were deposited by evaporation under vacuum. Five samples of each component or coating were manufactured. Two flight samples were mounted in the canister, one directly exposed to space, the other looking backwards. In a same arrangement 2 spare samples were stored on ground and kept under vacuum during the LDEF flight. Endly one set of reference samples was stored in a sealed canister under dry nitrogen atmosphere.

Description of the components was as follows :

- 3 UV filters
- 1 NIR cemented filter
- 5 metallic mirrors including 2 for specific UV use
- 5 dielectric mirrors including 2 for specific UV use
- 1 visible beam splitter
- 1 visible-IR dichroïc beam-splitter
- 1 IR dichroïc beam-splitter
- 3 antireflection coating including - 2 for IR use

The flight samples were located on the trailing edge.

## 2 - UV COMPONENTS

### 2.1 - BAND PASS FILTERS

The 3 double halfwave filters are respectively centered at 1216, 1270 and 2430 Å. The Al-MgF<sub>2</sub> layers are deposited on MgF<sub>2</sub> substrates for the 1216 and 1270 filters and quartz for the last one. The transmittance results are as follows (\* = exposed) :

		MgF <sub>2</sub>				QUARTZ	
		1216		1270		2430	
		PRE	POST	PRE	POST	PRE	POST
<b>MAX TRANSMIT. (%)</b>	FLIGHT	12.2* 11.4	6* 7.9	12* 12.6	8.4* 8.4	22.1* 22.7	19.8* 20.8
	SPARE	10.6	9.3	11	9.4	22.1	20.9
	REFERENCE	11.3	8.8	8.5	7.4	22.8	21
<b>RELATIVE TRANSMIT. LOSS (%)</b>	FLIGHT		51* 31		30* 33		10* 8
	SPARE		12		14		5
	REFERENCE		22		13		8

See figures 1 ⇔ 6



## 2.2 - METALLIC MIRRORS

The 2  $MgF_2$  protected Al mirrors are respectively deposited on B1664 glass and kanigened aluminium. In the following table the reflectance averages are calculated over 1200-2000 Å spectral range.

		GLASS		KANIGEN	
		PRE	POST	PRE	POST
REFLECTANCE AVERAGE (%)	FLIGHT	80.5* 80.3	67.7* 73.7	74.9* 76.9	57.9* 72.7
	SPARE	83.2	80.7	75.2	76.3
	REFERENCE	81.7	80	76.3	75.8
RELATIVE REFLECTANCE LOSS (%)	FLIGHT		16 8.2		23 6
	SPARE		3		-
	REFERENCE		2		1

See figures 7 ⇔ 10

## 2.3- DIELECTRIC MIRRORS

Two kinds of coatings were manufactured :

- MgO/MgF<sub>2</sub> mirror on B1664 glass substrate centered at 250 nm
- LaF<sub>3</sub>/chiolite/MgF<sub>2</sub> mirror on B1664 glass substrate centered at 170 nm. This last one did not survive because of highly stressed layers. All samples (flight spare and reference) failed with cracks and blisters.  
(hr measurements made)

MgO / MgF <sub>2</sub> MIRROR		PRE	POST
<b>SPECTRAL WIDTH (R &gt; 0.9) (%)</b>	FLIGHT	11.2* 12	6.9* 9.6
	SPARE	11.1	10.9
	REFERENCE	12.2	10.9
<b>RELATIVE WIDTH CHANGE (%)</b>	FLIGHT		38* 20
	SPARE		2
	REFERENCE		10

See figures 11 ⇔ 12

### 3 - 820 nm BANDPASS FILTER

This double half-wave filter was made of ZnS-chiolite layers deposited on BK7G18 and RG780 cemented glasses.

		PRE	POST
<b>CENTER nm</b>	FLIGHT	820.5* 819.7	819.5 818.7
	SPARE	820.7	820.3
	REFERENCE	818.2	818.5
<b>MAX TRANSMITTANCE (%)</b>	FLIGHT	73.6 75.8	69.7 73.2
	SPARE	75.4	73.9
	REFERENCE	77.8	74.6
<b>RELATIVE TRANSMITTANCE LOSS (%)</b>	FLIGHT		5* 3
	SPARE		2
	REFERENCE		4

See figures 13 ⇔ 14

#### 4 - VISIBLE + INFRARED METALLIC MIRRORS

Three types of coating were tested :

- gold mirror on B1664 glass
- $\text{Al}_2\text{O}_3$  protected Ag mirror on kanigened aluminium substrate
- $\text{ThF}_4$  protected Ag mirror on B1664 glass

In its useful spectral range ( $> 700 \text{ nm}$ ) the gold mirror does not show particular change due to space exposure.

Some results concerning the Ag mirrors follow :

		$\text{Al}_2\text{O}_3$ PROTECTED		$\text{ThF}_4$ PROTECTED	
		PRE	POST	PRE	POST
<b>REFLECTANCE AVERAGE (%)</b>	FLIGHT	96.1* 96.8	94.9* 95.7	97.6* 97.6	97.4* 97.6
	SPARE	96.6	95.8	97.5	97.6
	REFERENCE	96.7	96.3	97.3	97.6
<b>RELATIVE REFLECTANCE LOSS (%)</b>	FLIGHT		1.2 1.1		
	SPARE		0.8		
	REFERENCE		0.4		

The average is calculated over 400-1200 nm spectral range

See figures 15  $\Leftrightarrow$  18

## 5 - ANTIREFLECTION COATINGS

Three types of coating were tested :

- (450-1100nm) wide band AR coating on B1664 glass substrate using  $\text{Al}_2\text{O}_3.\text{MgF}_2$  MERK11611 layers materials
- 15 microns AR coating on Germanium (single ZnS layer)
- (8-12) microns AR coating on Germanium using Ge-ZnS-ThF<sub>4</sub> LAYERS

There is no significant difference between pre and post flight optical performances for the two last coatings.

For the first one we obtained :

AR COATING/ B1664		PRE	POST
<b>TRANSMITTANCE AVERAGE (%)</b>	FLIGHT	98.3* 98.3	97.9* 98
	SPARE	98.3	98.3
	REFERENCE	98.3	98.3
<b>RELATIVE TRANSMITTANCE LOSS (%)</b>	FLIGHT		0.4* 0.3
	SPARE		0
	REFERENCE		0

The average is calculated over 400-1100 nm spectral range

See figures 19 ⇔ 20

## **6 - VISIBLE AND IR DIELECTRIC MIRRORS**

Three types of coating were tested :

- Visible + 1060 nm mirror on B1664 glass with  $\text{TiO}_2\text{-SiO}_2$  layers materials
- 1060 nm mirror in the same materials configuration as above
- 10.6 microns mirror on B1664 glass with  $\text{Ge-ZnS-ThF}_4$  layers materials

The first one shows thin cracks in the coating for flight and spare samples but still remains optically efficient with reflectance comparable to the reference one.

For the second one flight and spare samples are degraded by peeling of the coating. These coatings are highly stressed and withstand with difficulty vacuum or thermal cycling.

The last case shows no significant change after space exposure

## **7 - BEAM-SPLITTERS**

Three types of coating were tested :

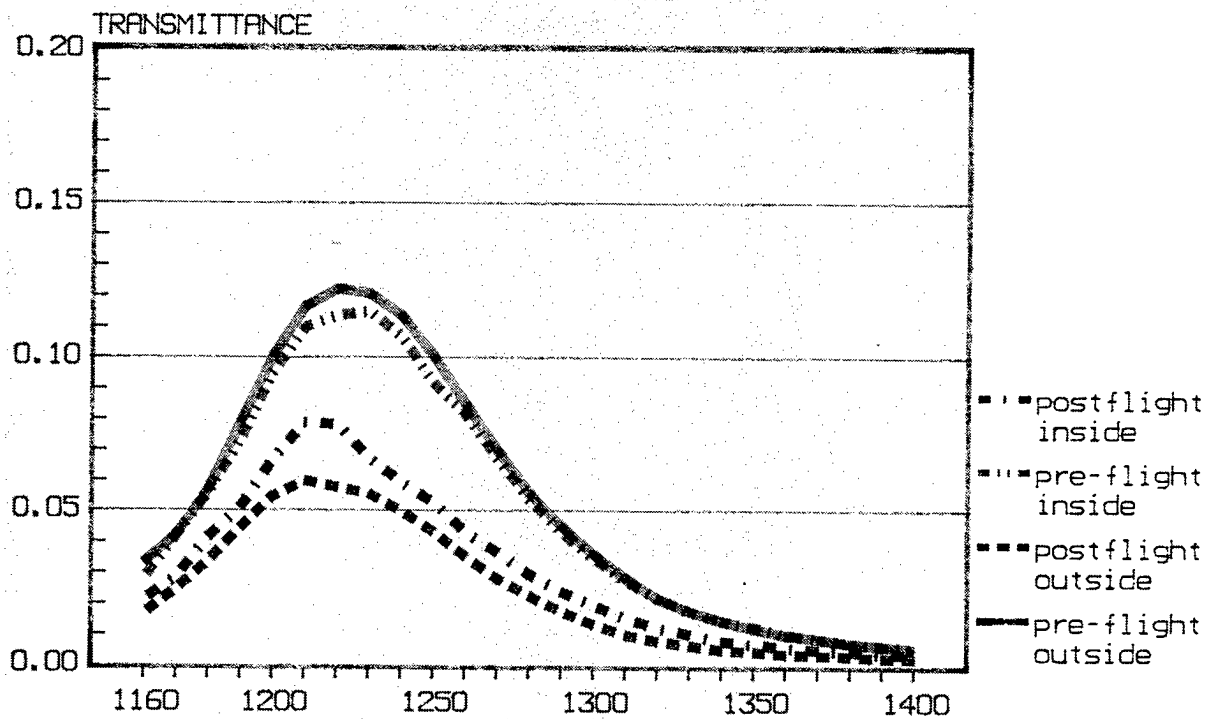
- Visible beam-splitter ( $R=T$ ) with  $\text{TiO}_2\text{-ZrO}_2\text{-SiO}_2$  layers materials deposited on B1664 glass substrate
- Visible reflective/IR transmittive (8-12) microns dichroic beam-splitter on ZnSe substrate and with  $\text{ZnSe-ZnS-ThF}_4$  layers materials

In all cases any significant difference in spectral performances after the flight was not found

## **8 - CONCLUDING REMARKS**

- UV filters and mirrors are usually space exposure-sensitive. Probably  $\text{MgF}_2$  material is the main factor of weakness
- Components and coatings for visible and infrared applications have been little or not affected in their optical performances by space exposure
- Coatings including many high-stressed layers (oxides and fluorides) show an evident risk of mechanical degradation (vacuum cycling)

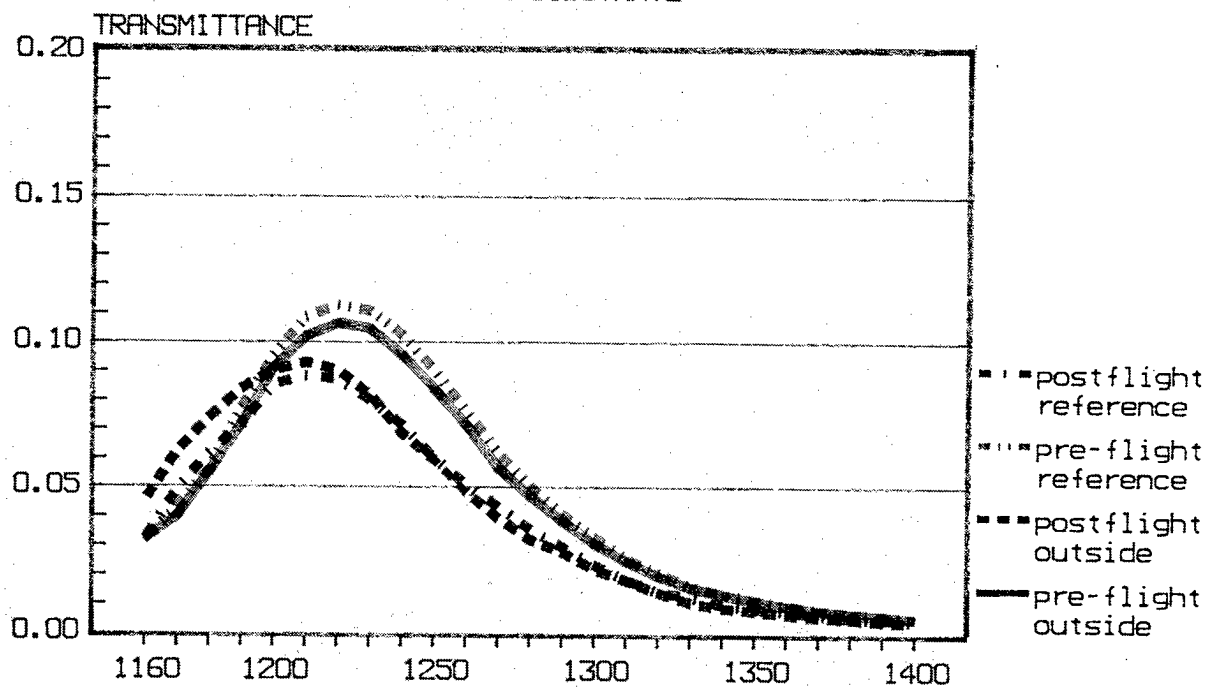
UV 1216 FILTER FLIGHT SAMPLES  
ON MGF2 SUBSTRATE



WAVELENGTH (ANGSTROM)

FIGURE 1

UV 1216 FILTER  
SPARE AND REFERENCE SAMPLES  
ON MGF2 SUBSTRATE



WAVELENGTH (ANGSTROM)

FIGURE 2

UV 1270 FILTER FLIGHT SAMPLES  
ON MGF2 SUBSTRATE

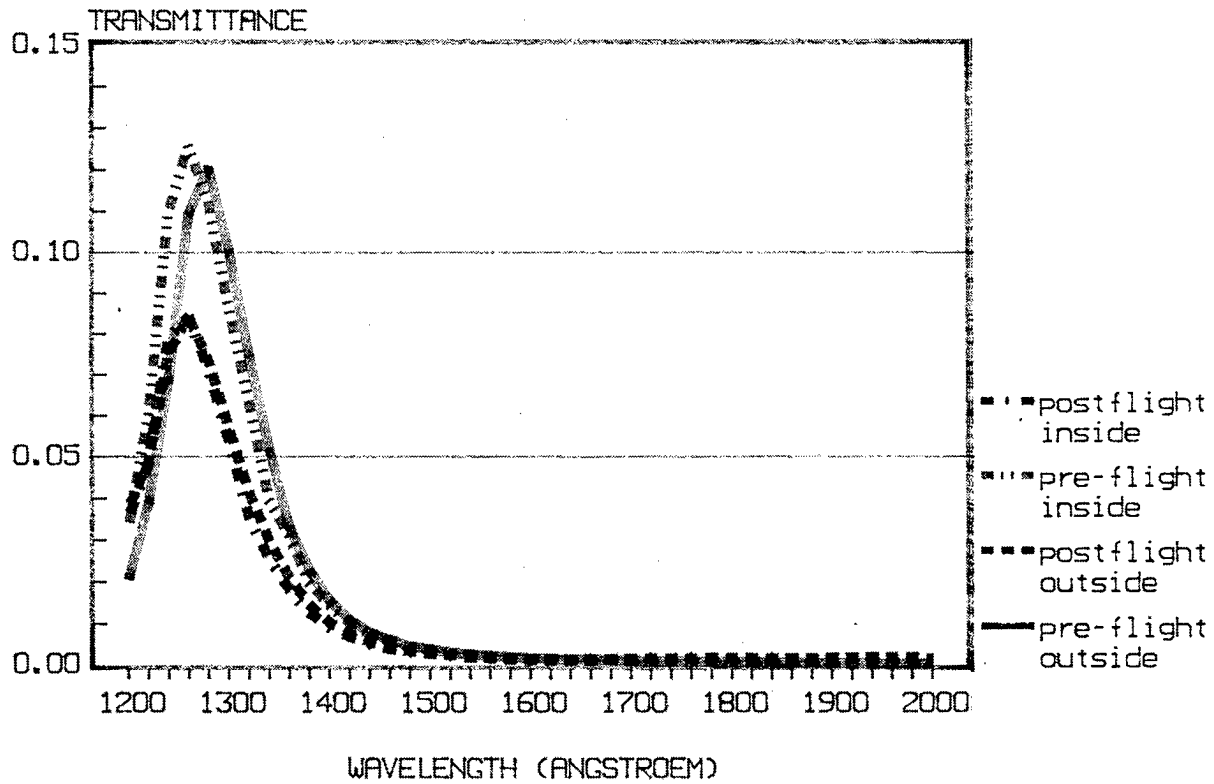


FIGURE 3

UV 1270 FILTER SPARE AND REFERENCE  
SAMPLES  
ON MGF2 SUBSTRATE

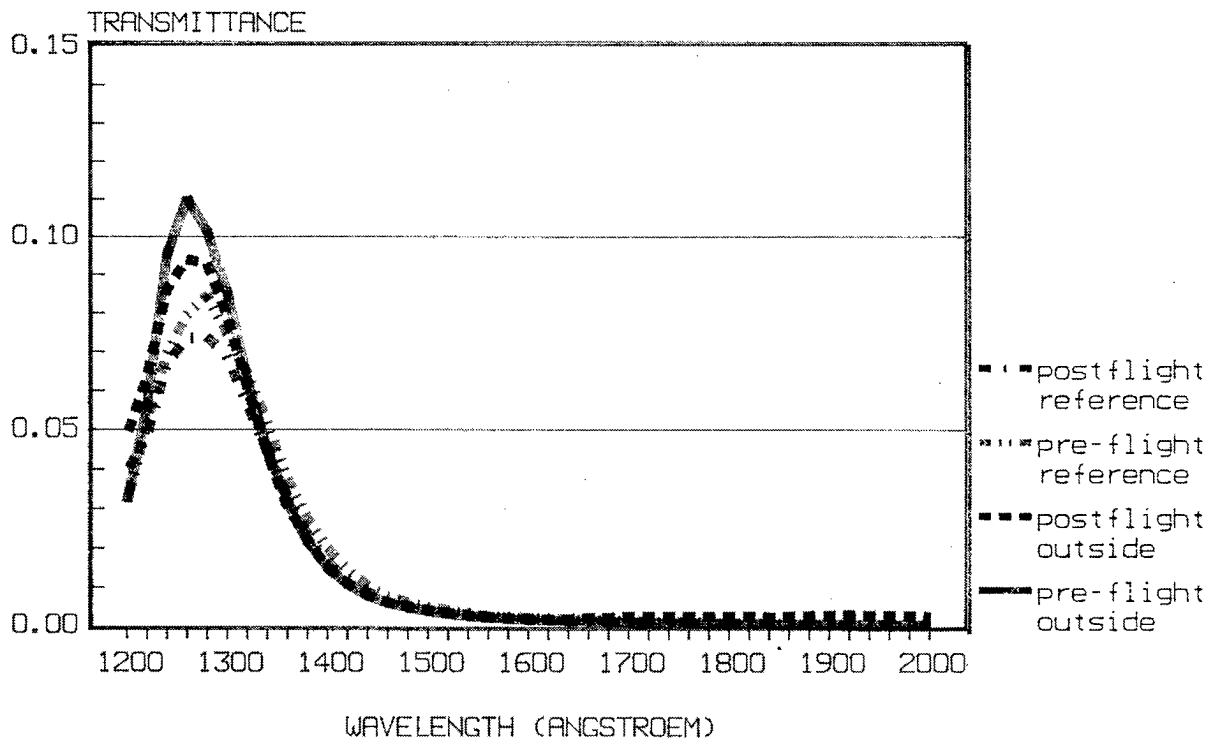


FIGURE 4



2430 UV FILTER  
ON SiO<sub>2</sub> SUBSTRATE  
FLIGHT SAMPLES

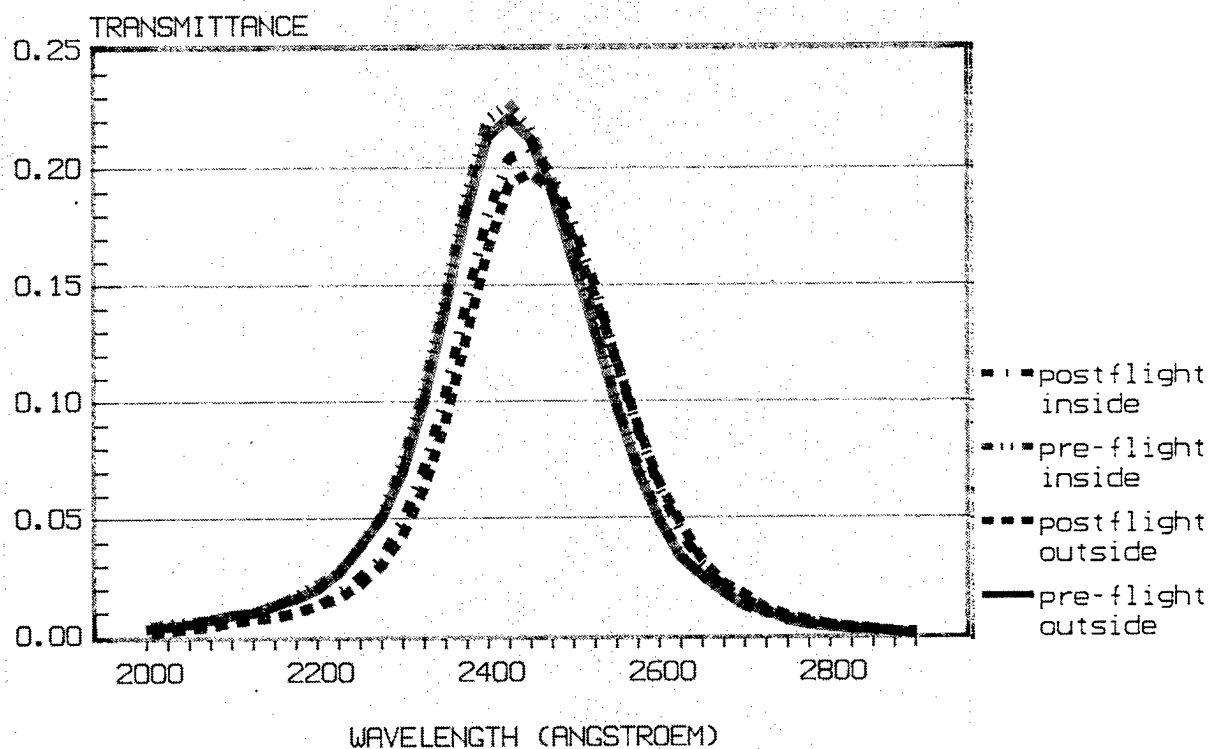


FIGURE 5  
2430 UV FILTER  
ON SiO<sub>2</sub> SUBSTRATE  
SPARE AND REFERENCE SAMPLES

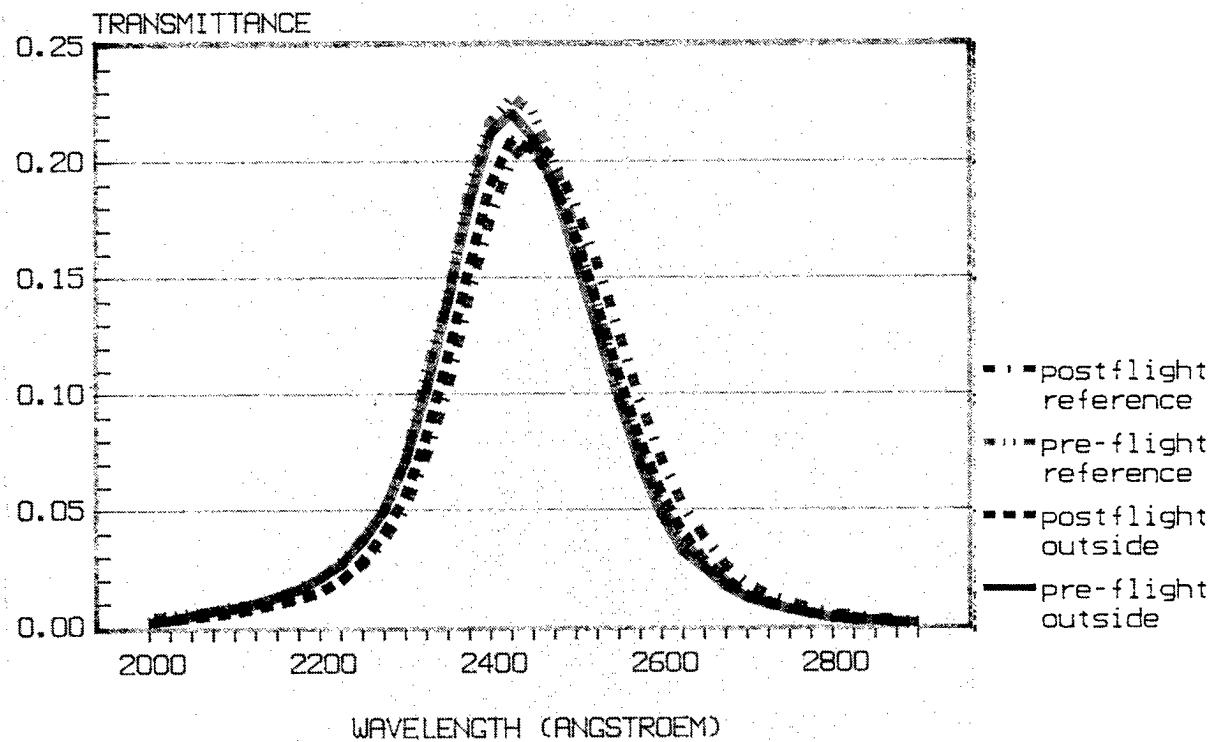
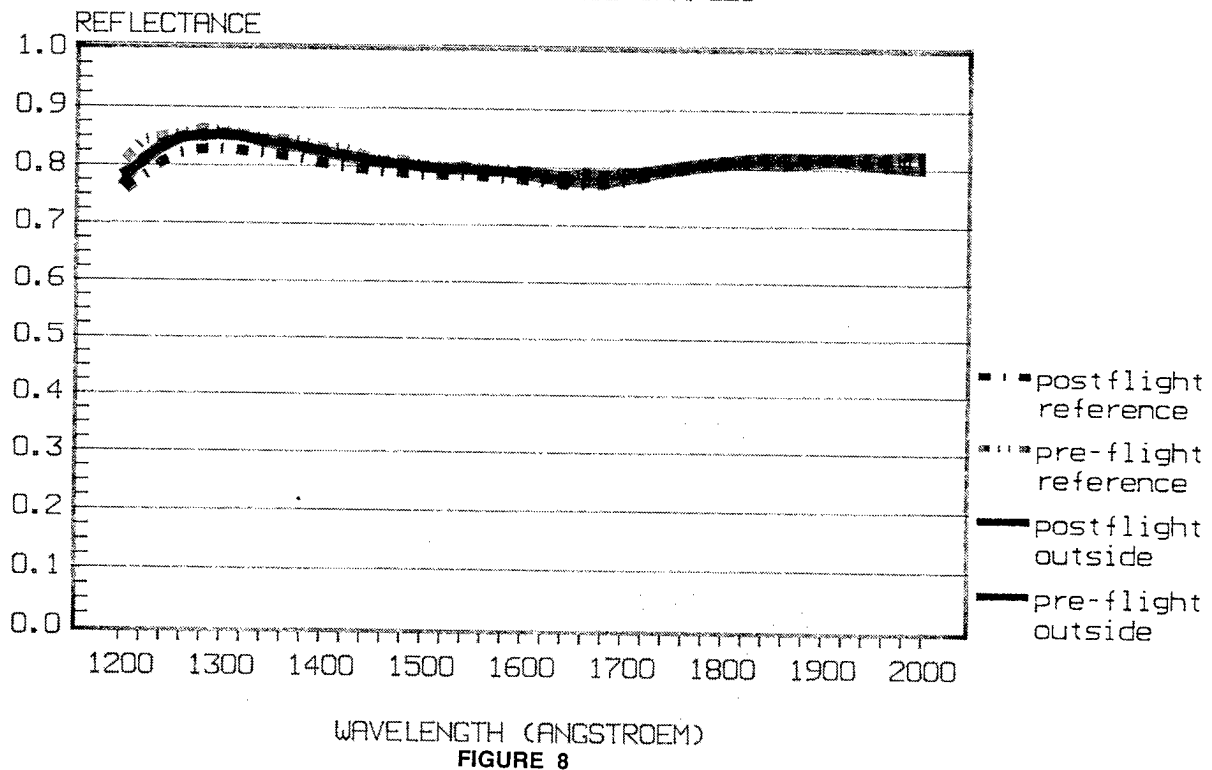
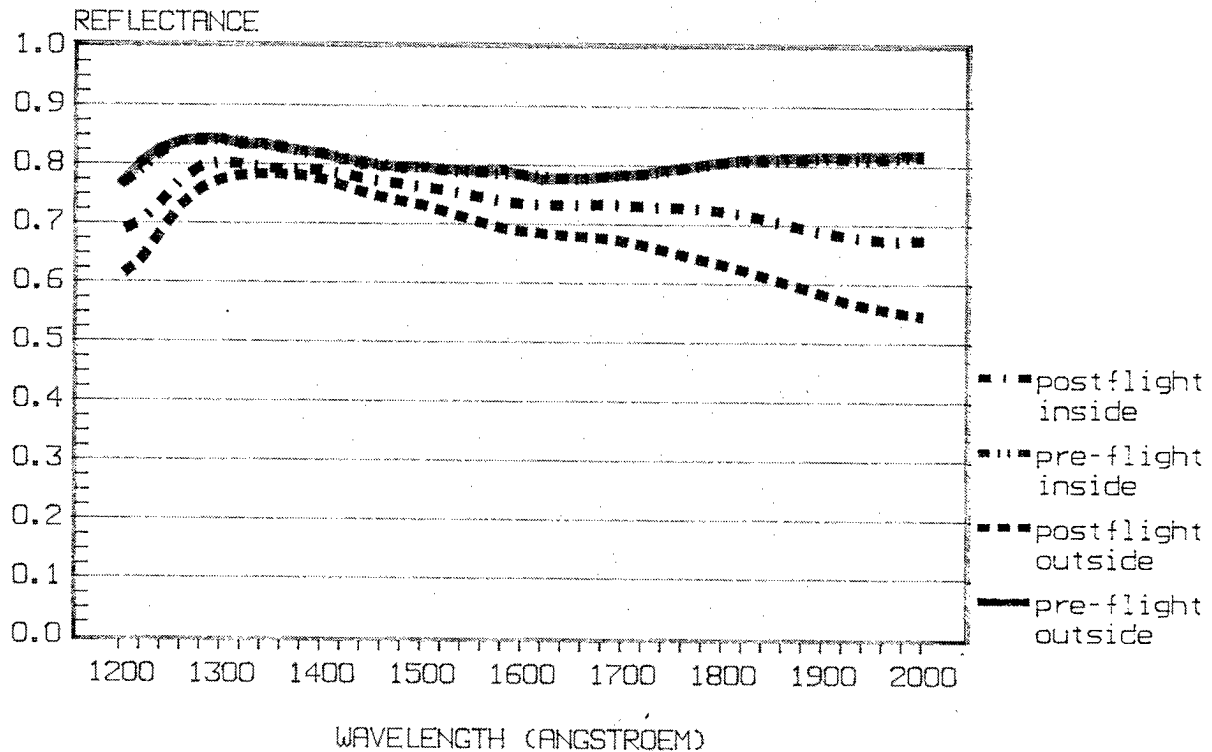


FIGURE 6

1216 AL-MGF2 MIRROR  
ON B1664 GLASS SUBSTRATE  
FLIGHT SAMPLES



1216 UV AL-MGF2 MIRROR  
ON KANIGEN SUBSTRATE  
FLIGHT SAMPLES

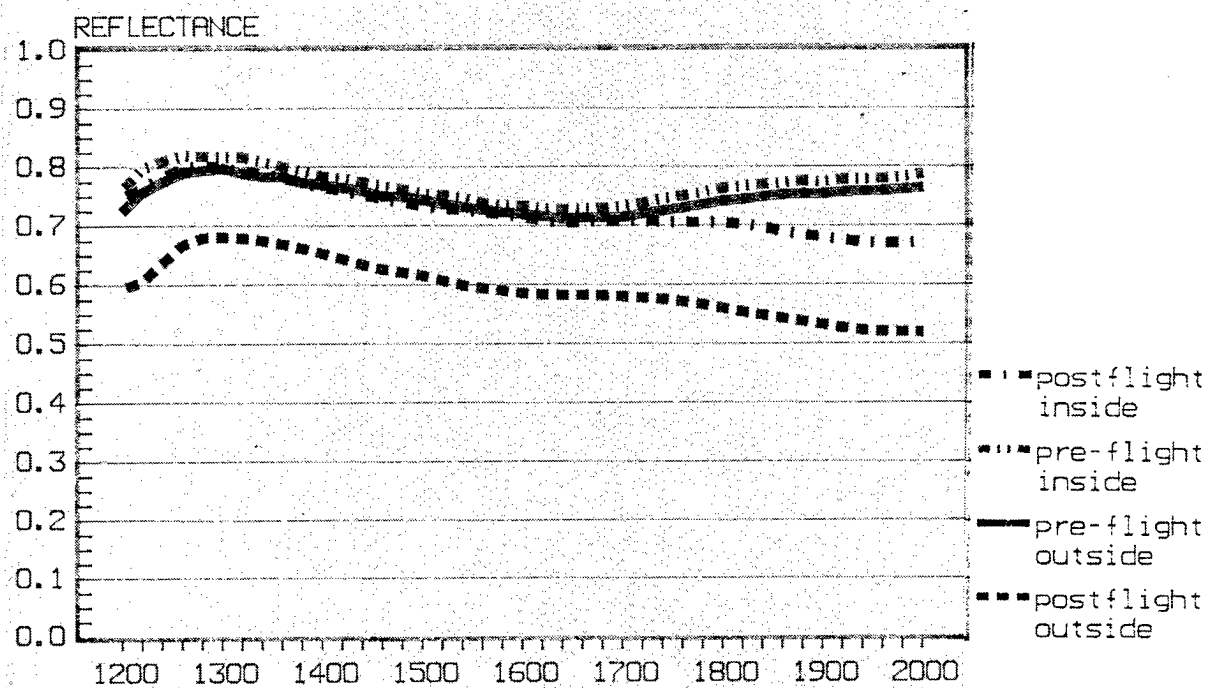


FIGURE 9  
1216 UV AL-MGF2 MIRROR  
ON KANIGEN SUBSTRATE  
SPARE AND REFERENCE SAMPLES

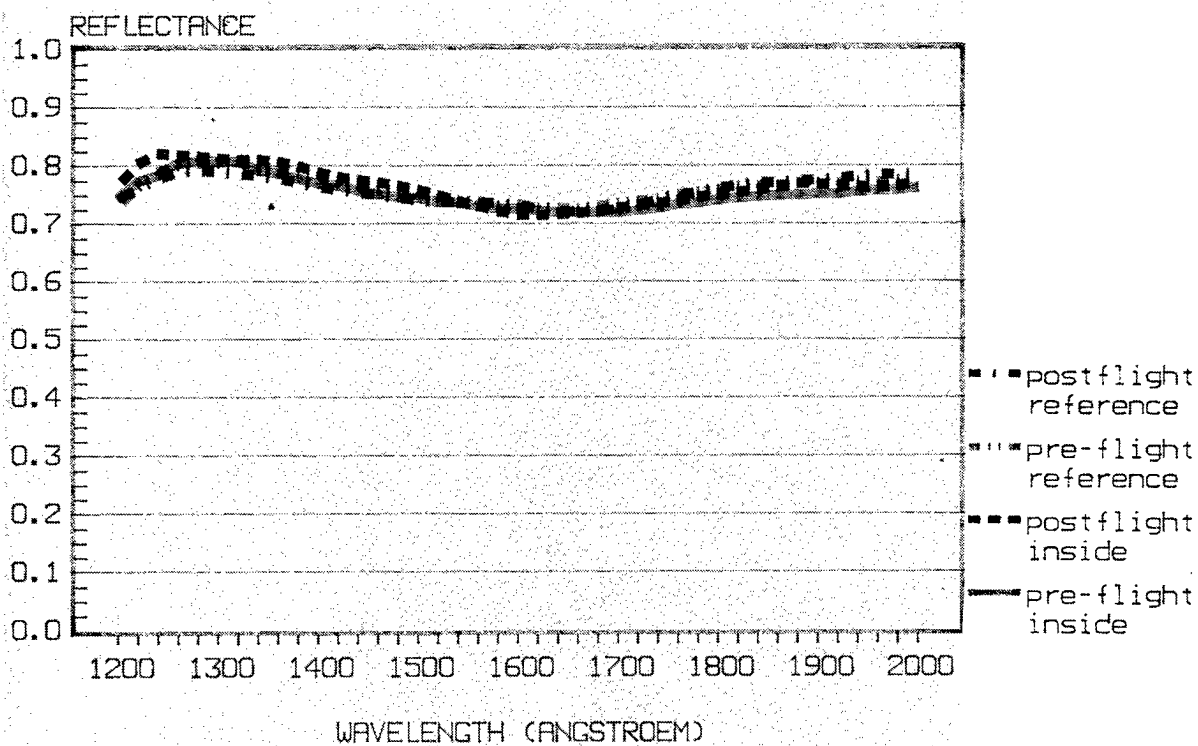


FIGURE 10

250 NM DIELECTRIC UV MIRROR  
ON B1664 GLASS SUBSTRATE  
FLIGHT SAMPLES

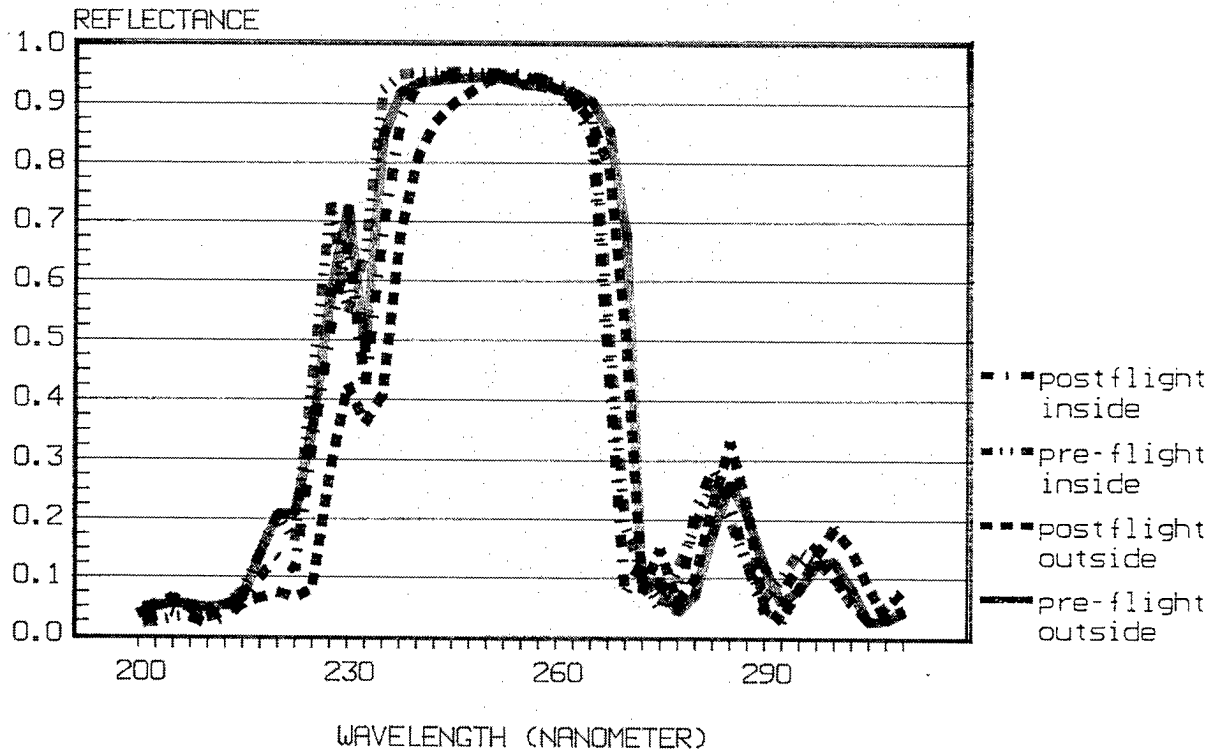


FIGURE 11

250 NM DIELECTRIC UV MIRROR  
ON B1664 GLASS SUBSTRATE  
SPARE AND REFERENCE SAMPLES

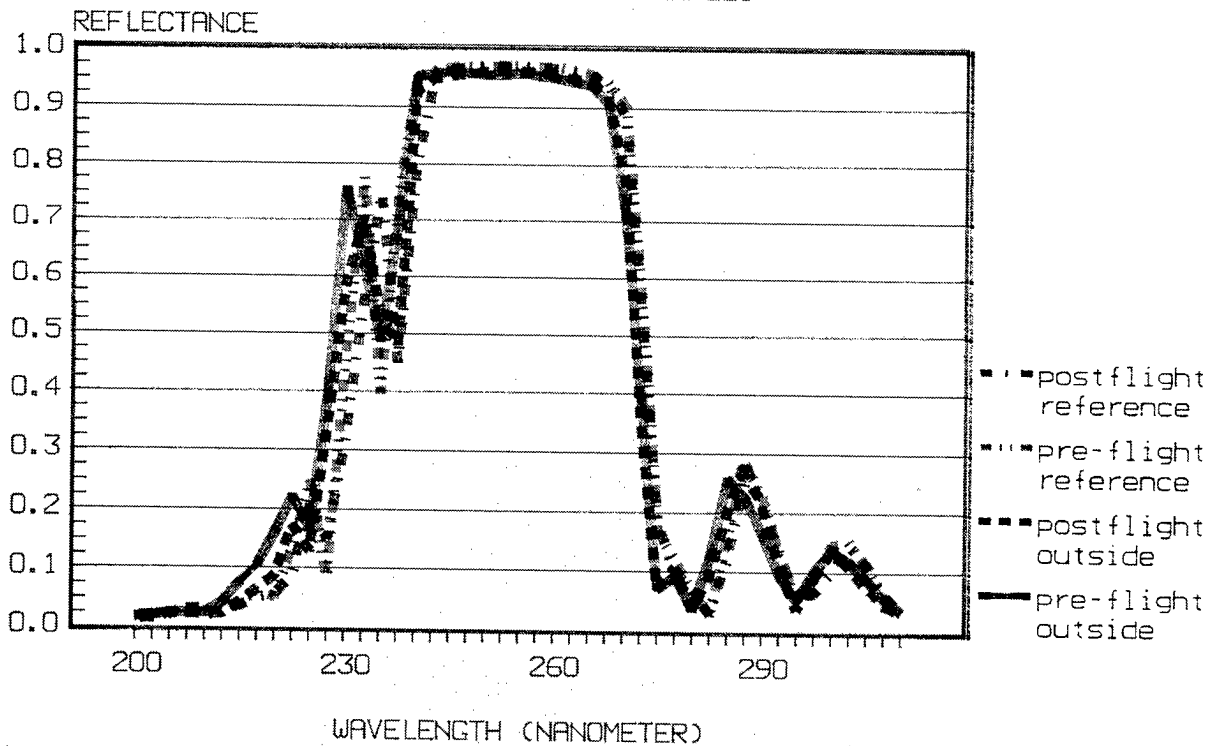


FIGURE 12

820 NM INTERFERENCE FILTER  
ON GLASS SUBSTRATES (cemented)  
FLIGHT SAMPLES

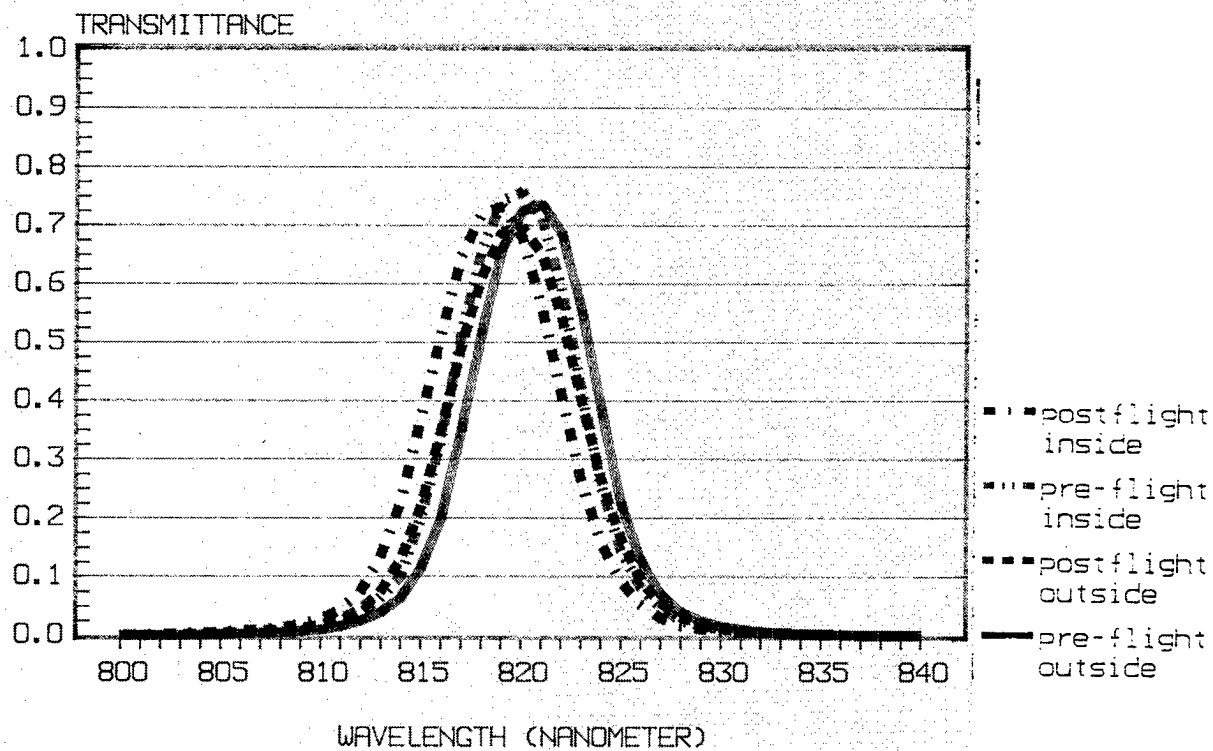


FIGURE 13

820 NM INTERFERENCE FILTER  
ON GLASS SUBSTRATES (cemented)  
SPARE AND REFERENCE SAMPLES

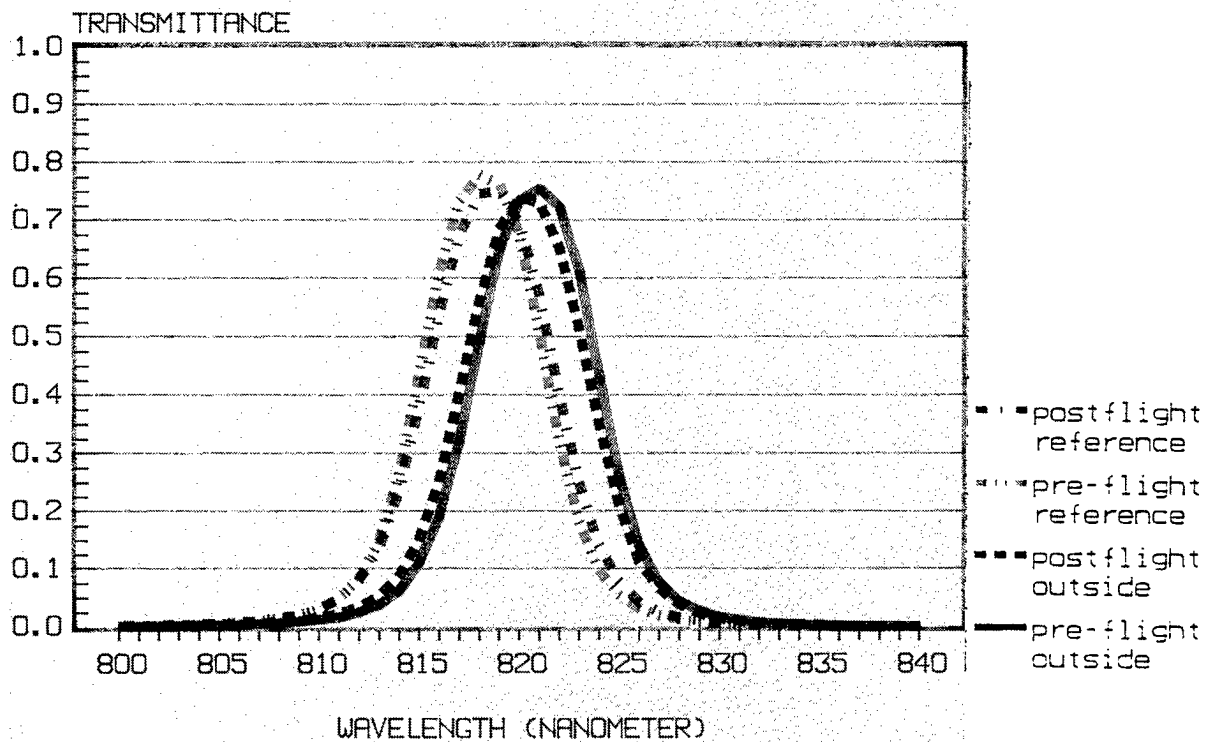


FIGURE 14

AL2O3 PROTECTED AG MIRROR  
ON KANIGEN SUBSTRATE  
FLIGHT SAMPLES

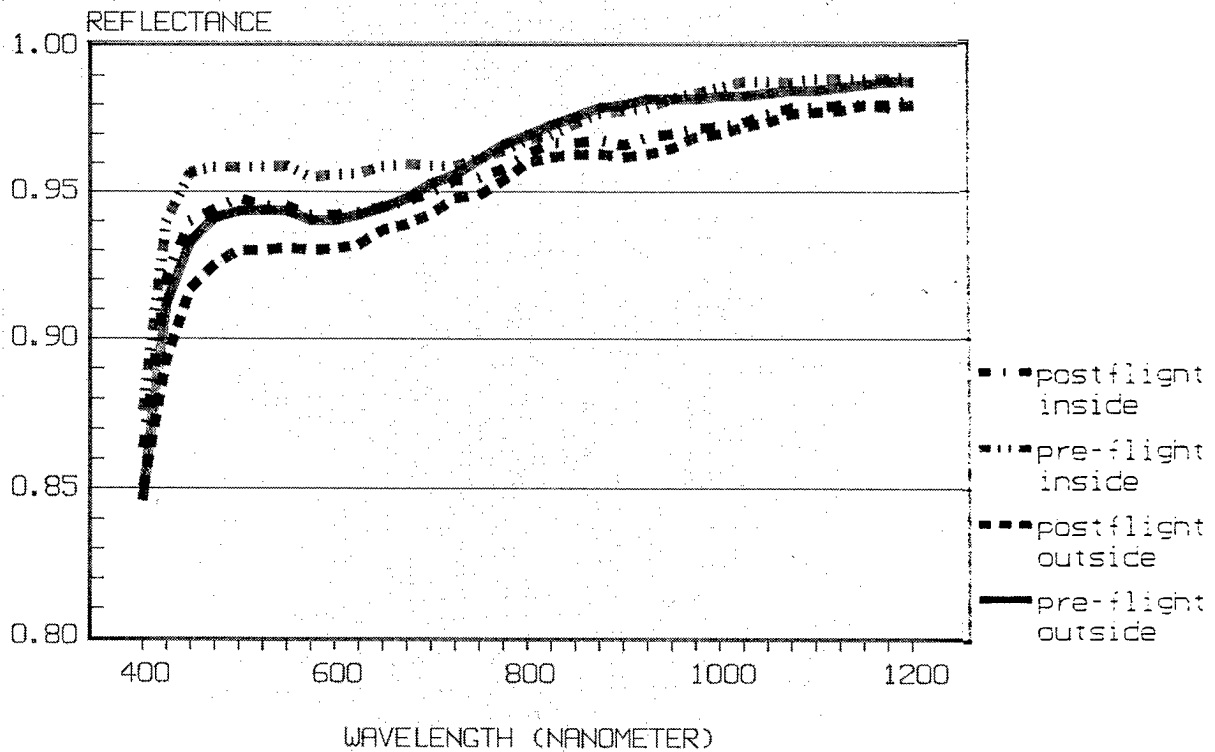


FIGURE 15

AL2O3 PROTECTED AG MIRROR  
ON KANIGEN SUBSTRATE  
SPARE AND REFERENCE SAMPLES

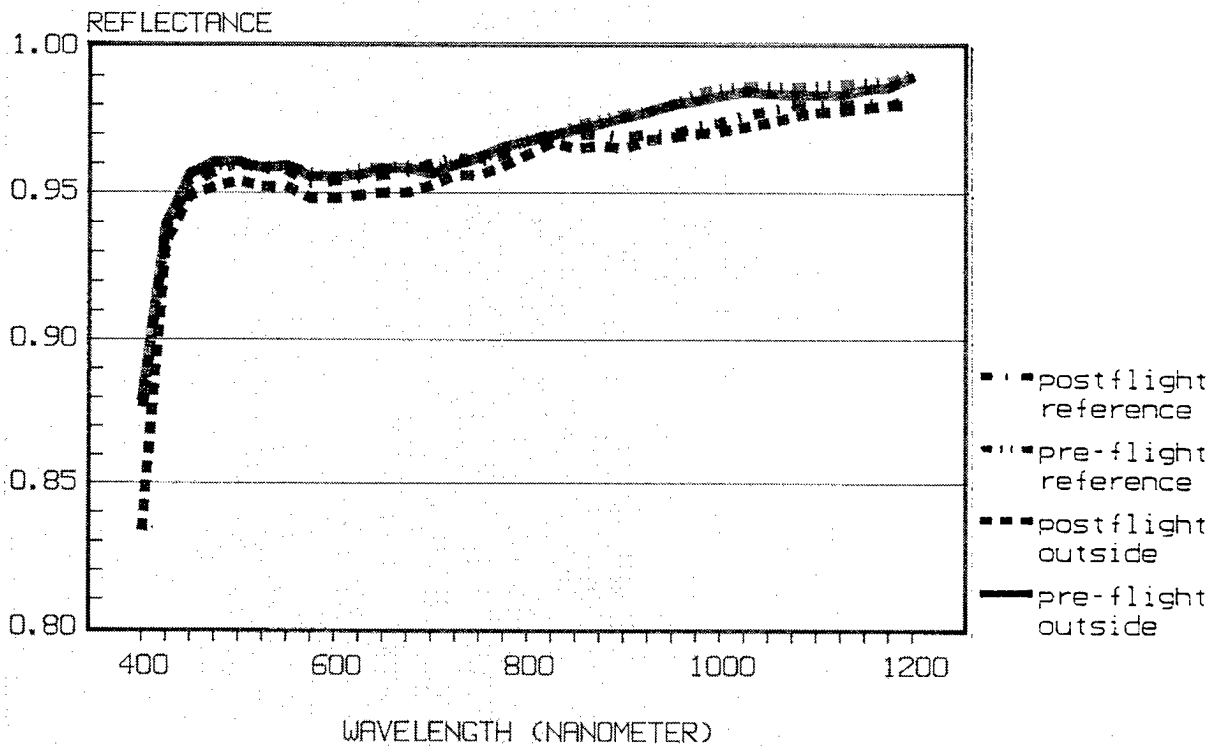


FIGURE 16

THF4 PROTECTED AG MIRROR  
ON B1664 GLASS SUBSTRATE  
FLIGHT SAMPLES

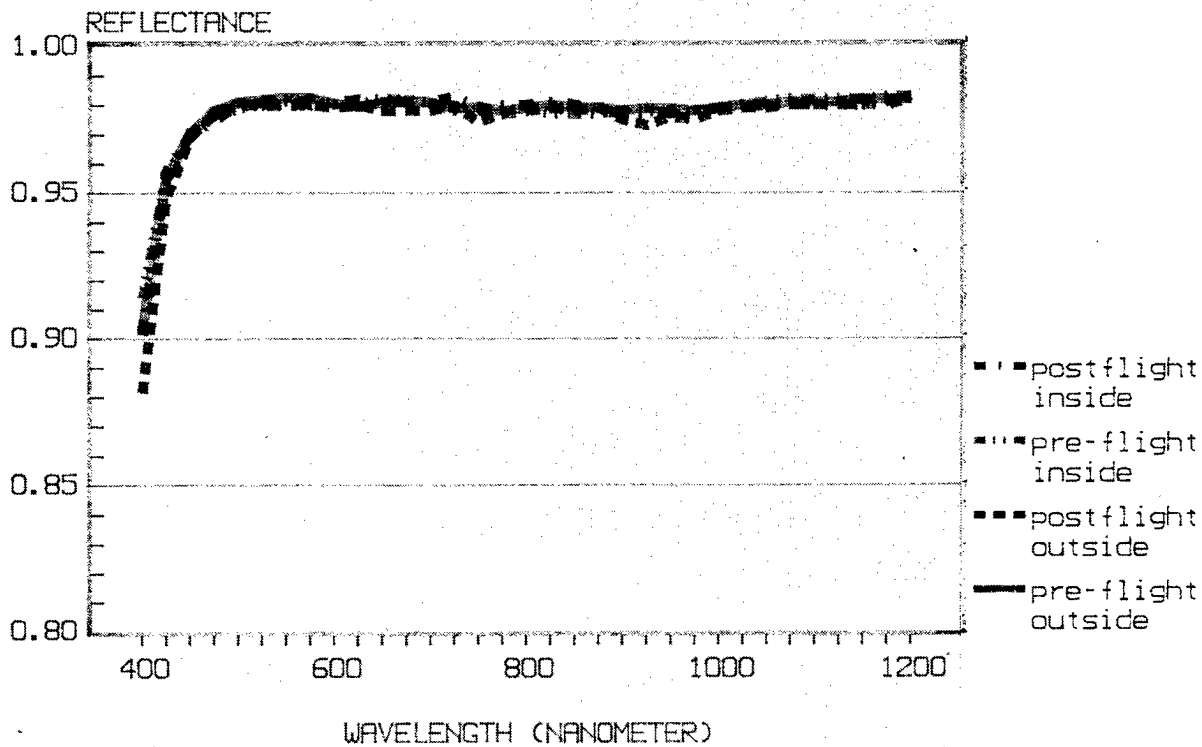


FIGURE 17

THF4 PROTECTED AG MIRROR  
ON B1664 GLASS SUBSTRATE  
SPARE AND REFERENCE SAMPLES

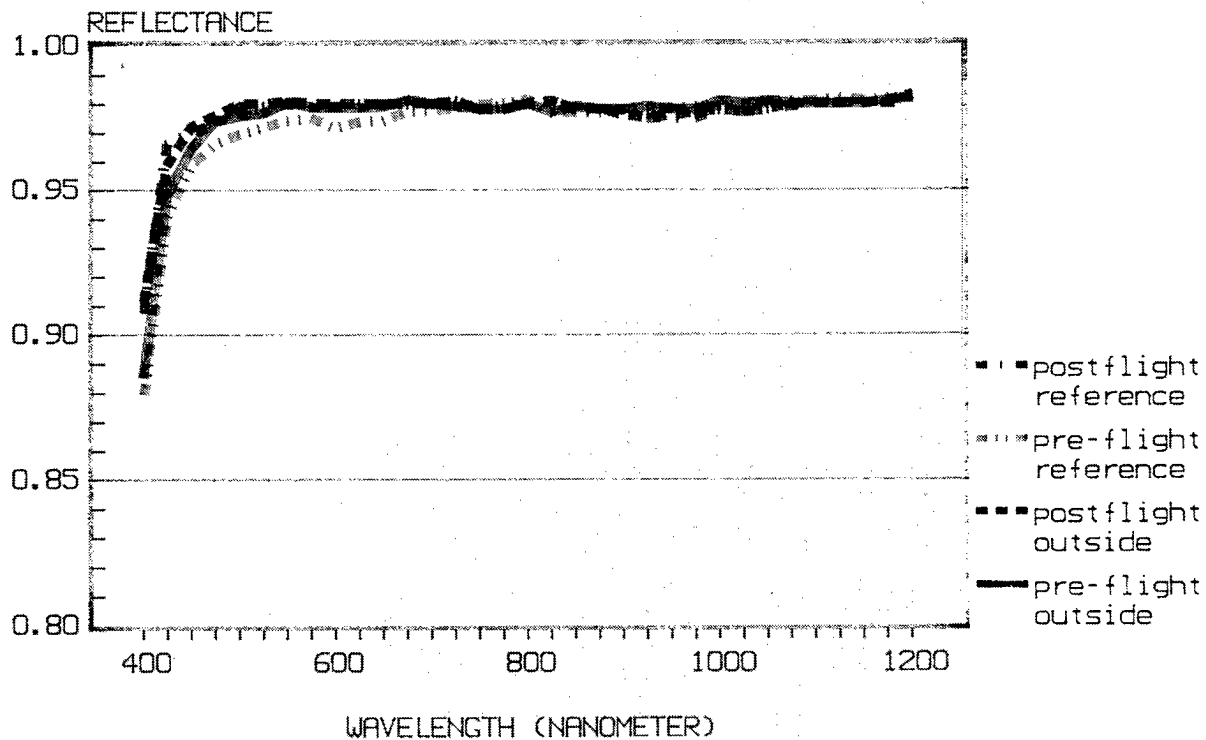
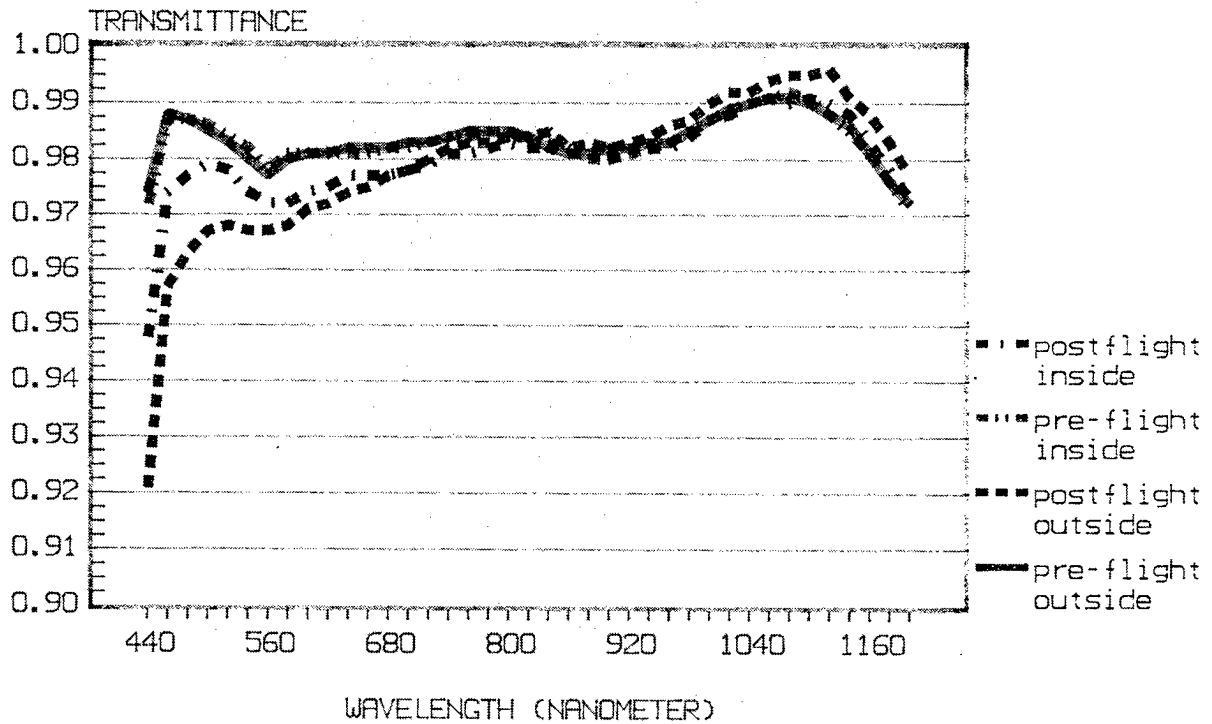
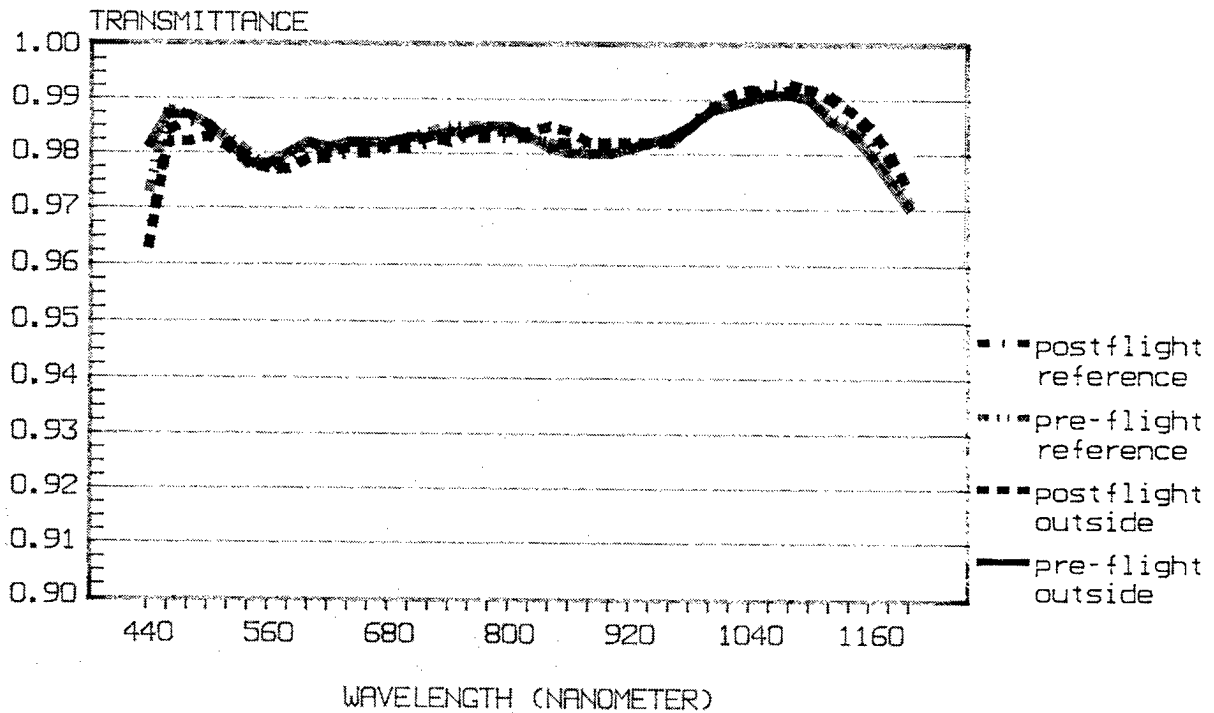


FIGURE 18

ANTIREFLECTING COATING ON GLASS  
SUBSTRATE (B1664)  
2 faces coated  
FLIGHT SAMPLES



ANTIREFLECTING COATING ON GLASS  
SUBSTRATE (B1664)  
2 faces coated  
SPARE AND REFERENCE SAMPLES





## SPACE ENVIRONMENTAL EFFECTS ON COATED OPTICS\*

T. M. Donovan, J. M. Bennett, R. Z. Dalbey and D. K. Burge  
Naval Weapons Center, China Lake, CA 93555  
Phone: 619/939-1401, Fax: 619/939-1409

S. Gyetvay  
Aerospace Corporation, Los Angeles, CA 90245  
Phone: 213/336-7313, Fax: 213/336-6983

### SUMMARY

Several high reflectance mirrors and an output window were selected for LDEF by pre-flight screening using laboratory simulation of natural space radiation. One mirror, a silicon/aluminum oxide design, showed expected excellent stability in orbit and a long shelf life. An aluminum oxide coated calcium fluoride window also showed good stability. Less stable but more interesting behavior was observed in the zinc sulfide based mirrors that showed contamination effects and related dendrite formation. These samples, which were located on both leading and trailing edges, also had interesting impact sites.

### INTRODUCTION

This paper presents preliminary post-flight results on high reflectance mirrors and a coated calcium fluoride window. The samples included three multilayer enhanced silver high reflector designs deposited on either molybdenum or silicon substrates and an aluminum oxide coated calcium fluoride window.

Optical performance requirements included high mirror reflectivity, low optical absorption, low scatter, environmental durability, and radiation hardness. The individual designs were selected in screening tests using combined electron, proton, and simulated solar UV radiation (ref. 1). Also, an optical study of zinc sulfide-coated germanium UV mirrors irradiated in high vacuum by Hass *et al.* (ref. 2), is relevant to the present work.

The purpose of the flight-test was to validate the above screening results and to further determine the added effects of atomic oxygen, thermal cycling, meteoroids and debris, and spacecraft contamination on optical performance.

\*Pre-Flight work sponsored under DARPA Order No. 3154  
NASA Experiment No. M0003-7

## TEST PLAN

Three high-reflectance mirror designs, including an industrial mid-IR standard were selected for the flight test. One sample of each design was located in a vacuum cassette on the leading edge of LDEF (D8). Two designs including the standard were also located on the trailing edge (D4) in a second vacuum cassette. The single aluminum oxide coated calcium fluoride window was located in a tray on the trailing edge (D3).

Pre-flight laboratory simulations using solar UV and charged particles were conducted in an ion pumped ultra high vacuum system on representative samples at the Boeing Radiation Effects Laboratory (ref. 1). The energy of the electrons and protons was selected so the energy would be deposited in the coatings and not in the substrates.

Single layer coatings deposited on fused silica substrates were used as witness samples; duplicates were located on the leading (D9) and trailing edges (D3). The witness samples and the calcium fluoride window were exposed for the 70 month duration of the flight. The mirrors located in the vacuum cassettes had timed exposures that were based on the original nine month to one year flight plan.

Pre-flight the mirror absorption at the design wavelength ( $2.8\text{ }\mu\text{m}$ ) was measured calorimetrically. Also, the total integrated scatter at  $3.39\text{ }\mu\text{m}$  was determined. A value for the reflectance was inferred from  $R = 1 - A - S$ . In addition, detailed environmental durability data, including adhesion, humidity, thermal cycling, abrasion resistance and absorption as a function of temperature from room temperature to  $200^{\circ}\text{C}$  were obtained on the silicon/aluminum oxide coating design.

Post-flight the mirrors, calcium fluoride window, and witness pieces were examined microscopically. The roughness of the optics has been measured using a Talystep surface profiler. Total integrated scatter measurements are planned. The spectral dependence of the reflectance of the mirrors has been measured from  $2.7\text{ }\mu\text{m}$  to approximately  $5\text{ }\mu\text{m}$  using a precision reflectometer. Similar measurements have been made on laboratory controls.

Finally, detailed surface measurements are in progress to determine contamination, changes in surface composition, and details of surface features as well as impact crater residues. These measurements include scanning electron and Auger microscopies (SEM and AES), profiling Auger and x-ray photoemission spectroscopy (XPS).

## MIRROR RESULTS

The three mirror designs used in the test are shown in Table 1 along with position on LDEF and duration of exposure. In the notation used, the dielectric materials in parentheses and Ag are reflectance enhancing coating layers and Mo and Si are substrate materials.

Figure 1 shows the results of pre-flight simulations. The industry standard zinc sulfide/thorium fluoride design showed increases in absorptance with dose (ref. 1). This increase in absorptance was presumably caused by the reaction of zinc sulfide with water impurity in the coating under the influence of ionizing radiation. Attempts to reduce water impurity resulted in increased stability (ref. 1) as shown, e.g., by the zinc sulfide/aluminum oxide results in figure 1. Clearly, one of the most stable designs tested was the silicon/aluminum oxide design shown in figure 1. Similar stable performance

was also found with Si/SiO<sub>x</sub> multilayers (ref. 1). As mentioned above, the silicon/aluminum oxide multilayer also showed excellent environmental durability.

Figure 2 shows the post-flight reflectance of the silicon/aluminum oxide-coated mirror that occupied a leading edge position (sample #1) compared with a laboratory control. The reflectance at the design wavelength (2.8 μm) has decreased to only slightly less than R = 0.998. The shelf life or aging effect (the samples were fabricated in 1979) is on the order of a 0.1% reflectance loss judging by the reflectance of the control. The reflectance loss of the test sample at longer wavelengths is somewhat greater and possibly relates to absorption caused by surface oxidation. Surface measurements and modeling are planned to determine if reaction with atomic oxygen could explain the above observation.

Figure 3 shows the post-flight reflectance of the zinc sulfide/aluminum oxide coating (sample #3) compared with a laboratory control. The reflectance decrease at the design wavelength of about 0.7% is a significant loss for a laser mirror. The apparent shift of the high reflectance band to shorter wavelengths is also significant, and could result from a reduction in optical thickness of the outer coating layer(s). The maximum in reflectance at 3.5 microns is presumed to be a wavelength-shifted long wavelength sideband to the first order reflectance maximum.

Profiling Auger data taken on this sample at Stanford University show the presence of an oxide layer approximately 200-300 Å thick. Data for the outer two layers of sample #3 are shown in figure 4. The data are taken intermittently after slow sputter etches to avoid problems of charging. Figure 5 is an enlargement of the surface region of figure 4. Note in this figure that the C contamination layer is gone after 5 minutes of sputter etching and that the O persists for 15 to 20 minutes. Note also that Si appears as a second contamination layer.

A complete sputter profile of the zinc sulfide/thorium fluoride coating (sample #4) is shown in figure 6. This profile was taken at NWC at a relatively high rate of sputtering by balancing the incident current with the secondary electron yield to reduce the charging effect. The data show an apparent reduction in thickness of the outer zinc sulfide layer by about 50%. Both effects, refractive index reduction with oxide formation and thickness reduction, could contribute to the apparent shift of the spectral curve to shorter wavelengths. Further surface analysis and model calculations will be required to verify this tentative conclusion.

A second feature of interest in the sputter profile data in figure 6 is the presence of a copper contamination layer, possibly coming from two nearby copper mirrors in the vacuum cassette. This contamination layer, which is on the surface of both zinc sulfide coatings that were located in the vacuum cassette at D8, appears to be related to a second common phenomenon, dendrite formation.

Figure 7 shows one of a large number of dendrites found on sample #3. Similar dendrites were found on sample #4, as shown in the SEM image in figure 8; also shown are Auger profiles in the dendrite area (point #1) and background area (point #2). It is seen in figure 8 and in the detailed depth profiles (figures 9 and 10) that the copper concentration is higher in the darker background area. It appears from the features of the dendrites that they are thermally produced, i.e., melt is observed. We have, however, produced similar features in the SEM by the sputter ion beam, so that it may be a combination of both thermal and radiation effects that have produced them in space. It is clear that the copper contamination also played a role in the formation of the dendrites.

Figure 11 shows a second area of dendritic material on sample #4 along with Auger data. Here again the light area is the dendrite and the background is dark. Figure 12 shows copper and zinc maps of the same area. It is interesting that the gradient in copper concentration provides the contrast for successfully imaging the dendrites in the SEM. When the copper is removed by sputter etching, the contrast is lost. In areas of copper contamination, i.e., dendrite formation, there is apparently no oxide growth.

### CALCIUM FLUORIDE WINDOW

Post-flight examination of the calcium fluoride sample showed very little damage. An FTIR transmission plot showed little or no change from the pre-flight condition. The one or two surface features observed could relate to impact phenomena or could simply be handling features or scratches.

### IMPACT CRATERS

All samples were examined for the presence of impact craters. No features that could be associated with space could be found on either sample #1 or sample #2. Impact sites were found on samples #3-5. Figure 13 shows two small impact sites found on sample #3. In both cases the multilayer structure of the coating design is revealed. The individual particle sizes appear to be a few microns to about 10  $\mu\text{m}$ . Definite signs of melt appear in the crater on the left. A third impact site is shown in figure 14; this site is on sample #5 which was on the trailing edge (D4). The character of this site is different in that the multilayer structure is not revealed and debris is splattered around the site. Several other sites of this nature but smaller were observed on this sample. Detailed analysis to identify the origin of these sites is planned.

### CONCLUSIONS AND FURTHER WORK

The high reflectance silicon/aluminum oxide coated mirror #1 exposed for three months on the leading edge of LDEF performed as expected with minimal reduction in reflectance at the design wavelength, 2.8  $\mu\text{m}$ , but with an indication of surface oxidation and reduction in reflectance at longer wavelengths, i.e., 3-4  $\mu\text{m}$ . Surface analysis measurements are in progress to assess the degree of oxidation during the early orbits. No impact sites were observed on either the leading or trailing edge on samples of this design.

Both zinc sulfide-based coating designs, samples #3-5, showed significant reductions in reflectance at the design wavelength, apparent large spectral shifts of the reflectance maxima, and dendrite formation. The dendrite formation was related to a thin copper contamination layer and was found only on samples in the vacuum cassette on the leading edge. Concentration gradients of copper between dendrite and dendrite-free regions provided excellent contrast in the SEM. No oxidation was found in the contaminated area but was found as expected in contamination free regions. A combination of thermal cycling and irradiation effects probably provided energy for the dendrite formation process.

Interesting small impact sites were found on both leading and trailing edge zinc sulfide samples and the craters and surrounding areas are being studied in more detail for clues to the nature of the impacting particles.

Finally, the aluminum oxide coated calcium fluoride window, sample #6, remained essentially unchanged after 70 months exposure on the trailing edge.

#### REFERENCES

1. Natural and Induced Space Radiation Effects on Optical Coatings and Materials, Final Report on Contracts N00123-78-C-0989 and N60530-79-C-0263 to the Naval Weapons Center by L.B. Fogdall, *et al.* of the Boeing Radiation Effects Laboratory, April 1981.
2. Hass, G.; Heaney, J. B.; Hunter, W. R.; and Angel, D. W.: Effect of UV Radiation on Evaporated ZnS Films. *Appl. Opt.*, vol. 19, 1980, pp. 2480-2481.

TABLE 1. FLIGHT SAMPLES, DESIGN, POSITION ON LDEF, AND LENGTH OF EXPOSURE

Sample #	Design	Position	Exposure (months)
1	(Si/Al <sub>2</sub> O <sub>3</sub> ) <sup>3</sup> /Ag/Si	(D8)	3
2	(Si/Al <sub>2</sub> O <sub>3</sub> ) <sup>2</sup> /Ag/Mo	(D4)	3
3	(ZnS/Al <sub>2</sub> O <sub>3</sub> ) <sup>4</sup> /Ag/Mo	(D8)	9
4	(ZnS/ThF <sub>4</sub> ) <sup>5</sup> /Ag/Mo	(D8)	6
5	(ZnS/ThF <sub>4</sub> ) <sup>5</sup> /Ag/Mo	(D4)	9
6	(Al <sub>2</sub> O <sub>3</sub> )/CaF <sub>2</sub> λ/2 @ 2.8μm	(D3)	70

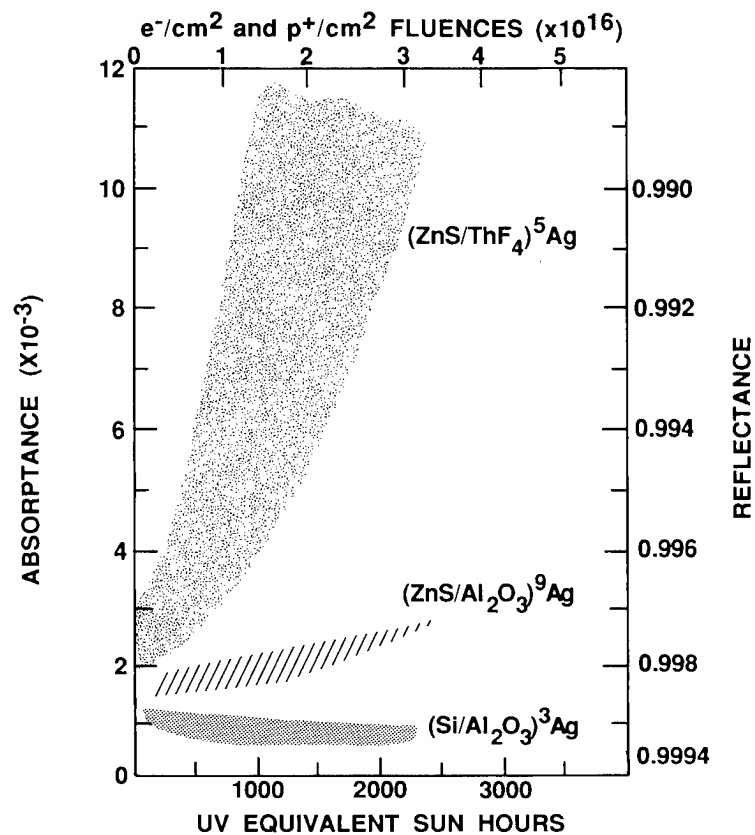


FIGURE 1. Laboratory simulation of natural space radiation effects on flight mirror designs. Note zinc sulfide/thorium fluoride results are sensitive to water contamination.

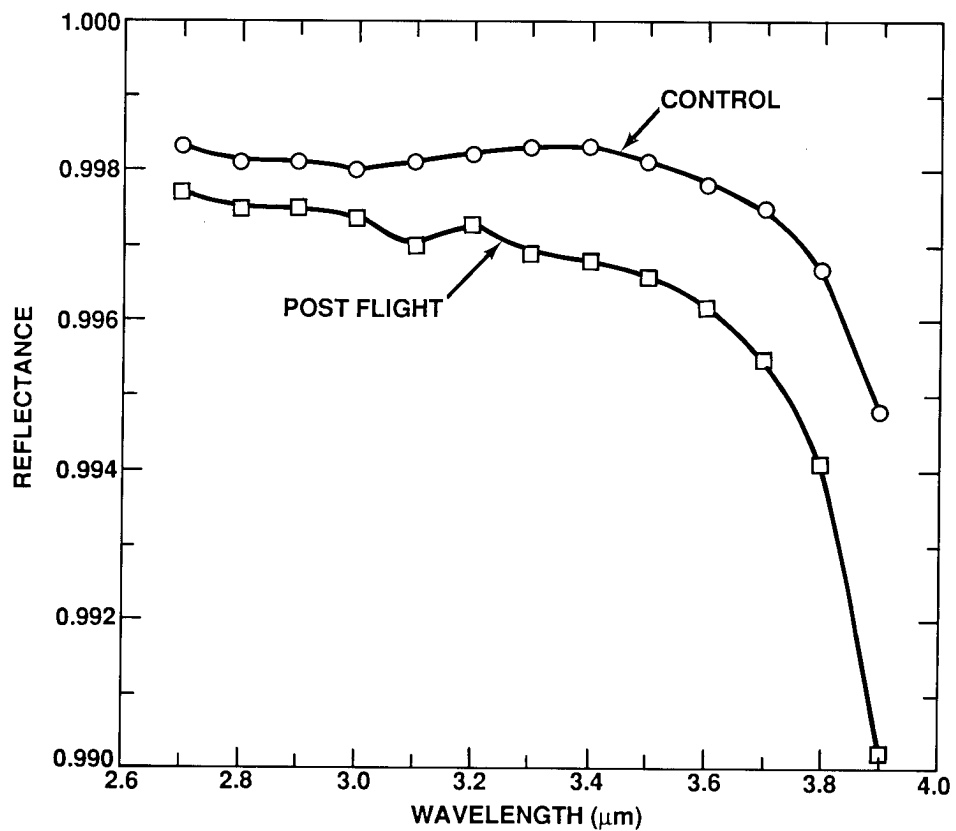


FIGURE 2. Post-flight reflectance of the silicon/aluminum oxide design (sample #1) compared to a laboratory control. Increased reflectance loss at longer wavelengths is possibly due to oxide formation.

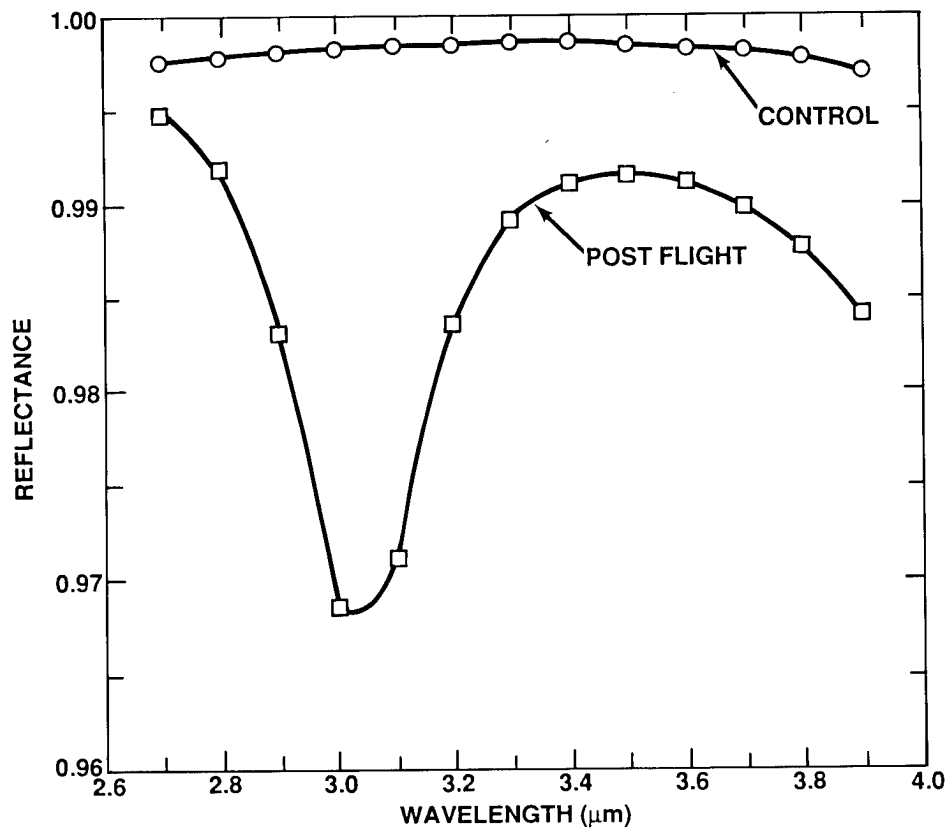


FIGURE 3. Post-flight reflectance of the zinc sulfide/aluminum oxide design (sample #3) compared to a laboratory control. Note the reflectance loss and apparent spectral shift of the high reflectance band.



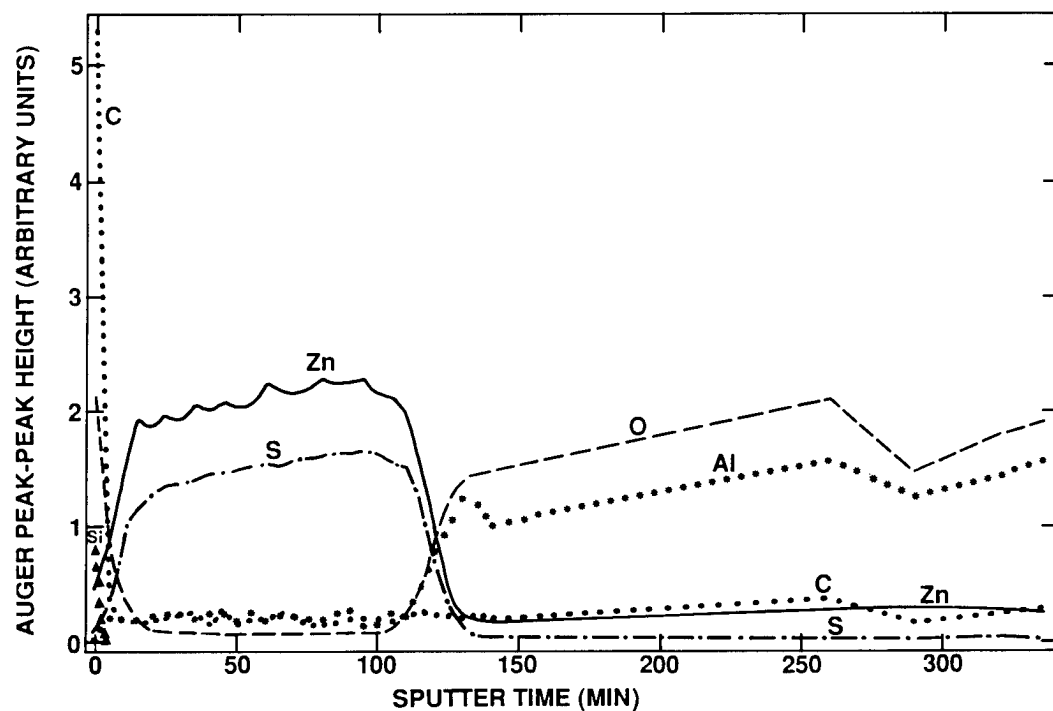


FIGURE 4. Auger profile of outer zinc sulfide/aluminum oxide layers (sample #3). Material sensitivity factors were used in the reduction of these data.\*

\* (Data by G. Scott, T. Beerling, and C. R. Helms, Electrical Engineering Department, Stanford University.)

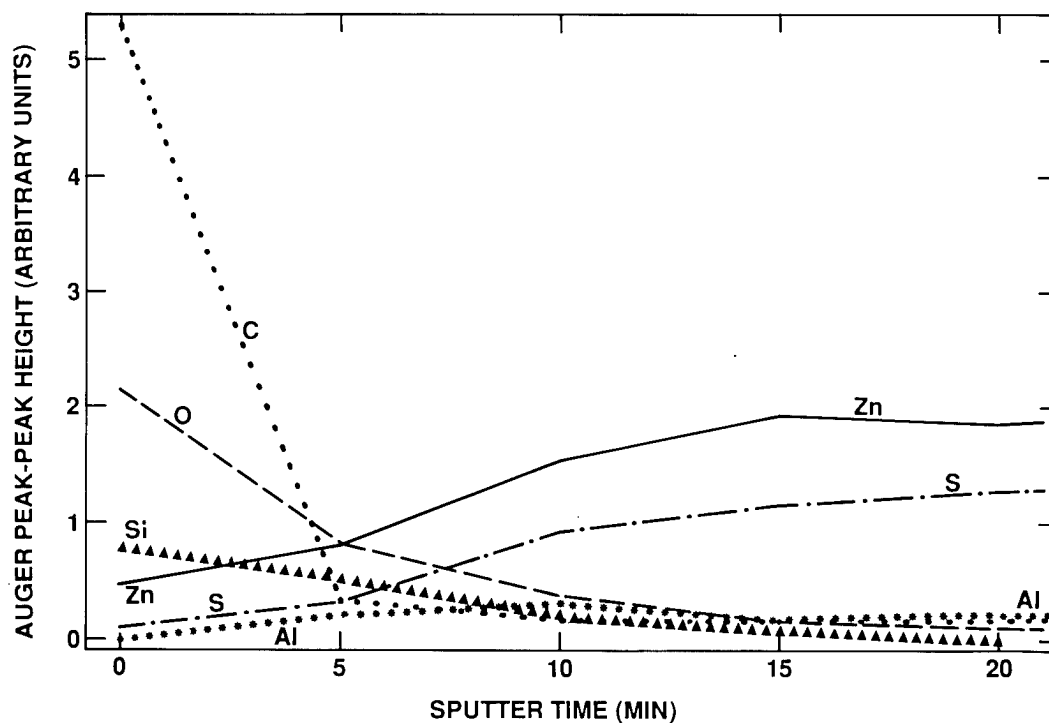


FIGURE 5. Enlargement of the surface region of data from figure 4 showing possible 200-300Å oxide layer.

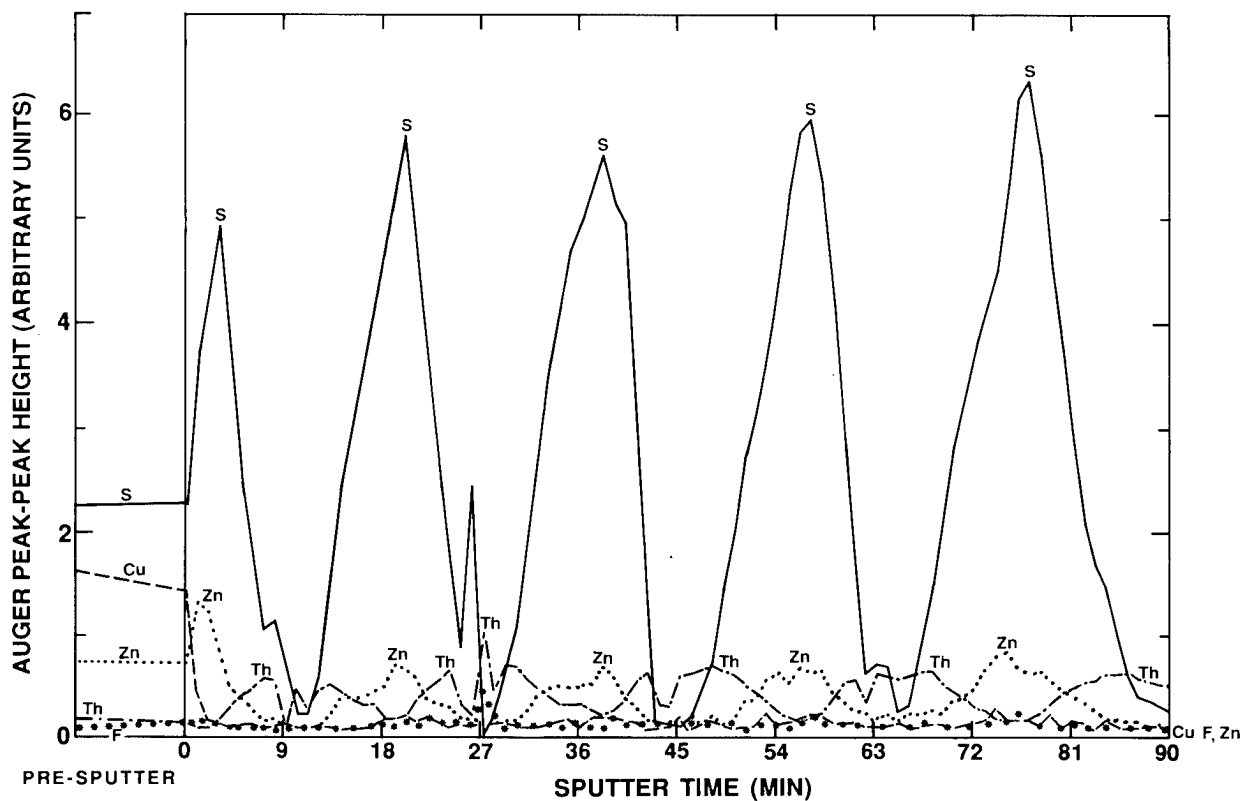


FIGURE 6. Auger profile of zinc sulfide/thorium fluoride design (sample #4) showing (1) apparent reduced thickness of surface zinc sulfide layer and (2) copper contamination. Note the absence of oxide.



FIGURE 7. Optical micrograph showing a dendrite on zinc sulfide/aluminum oxide design (sample #3).

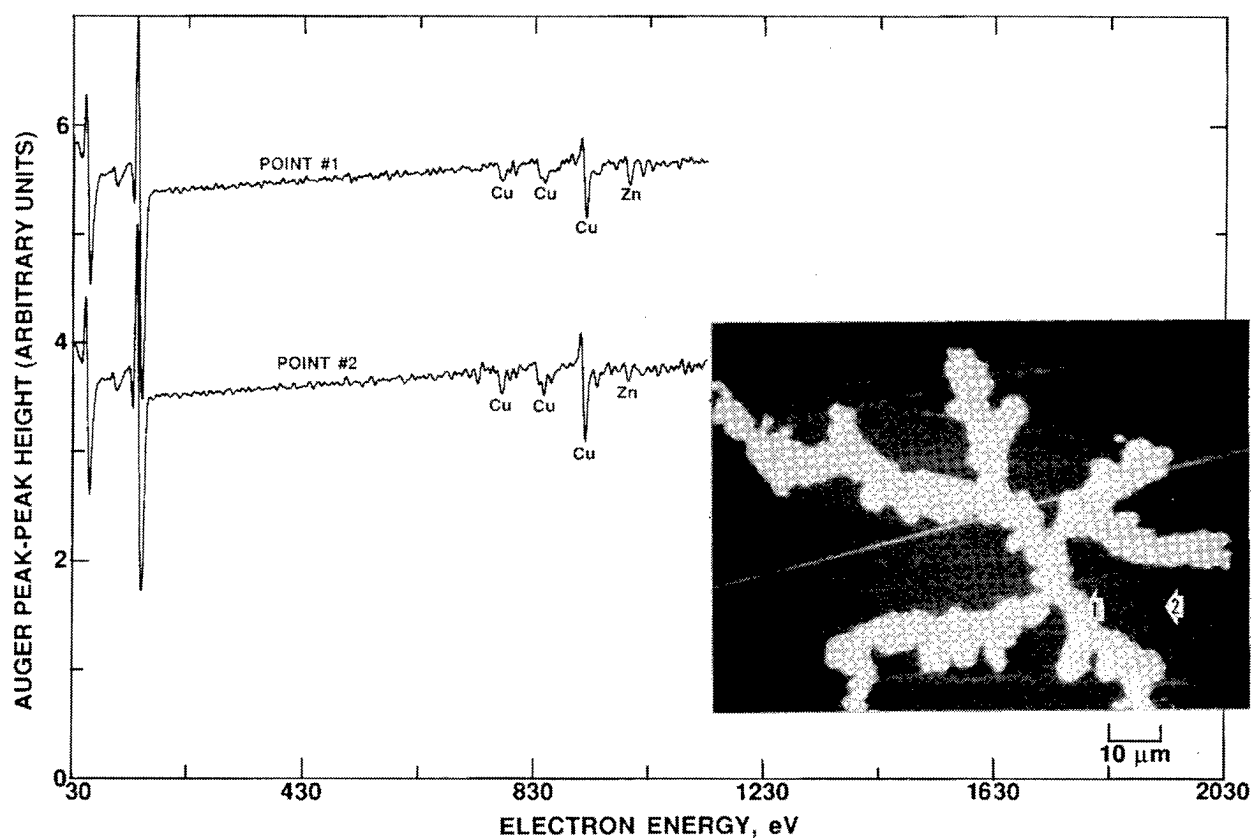


FIGURE 8. SEM image of dendrite on zinc sulfide/thorium fluoride design (sample #4). Auger data show Cu contamination levels are different in dendrite and background areas.

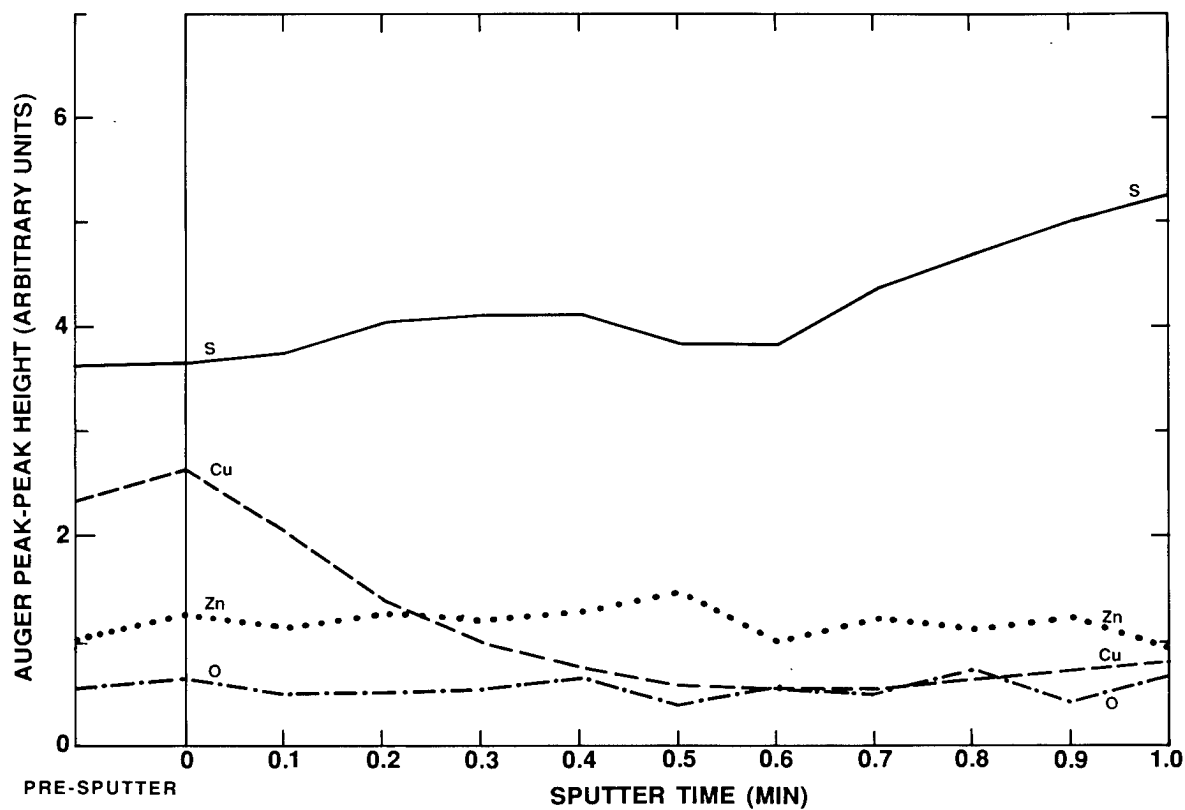


FIGURE 9. Auger profile showing copper on dendrite on sample #4 above.

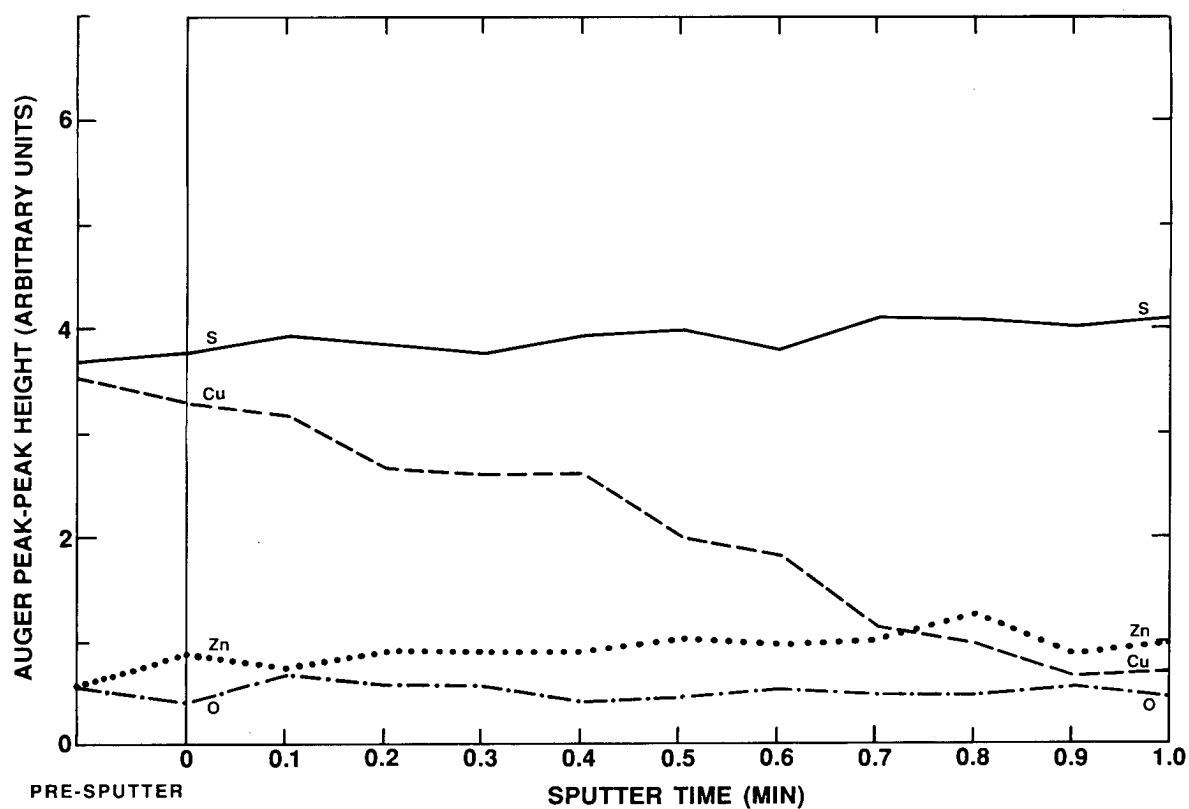


Figure 10. Auger profile in background region of sample #4 showing higher copper concentration and penetration into zinc sulfide in this area. When copper was removed, SEM image contrast was lost.

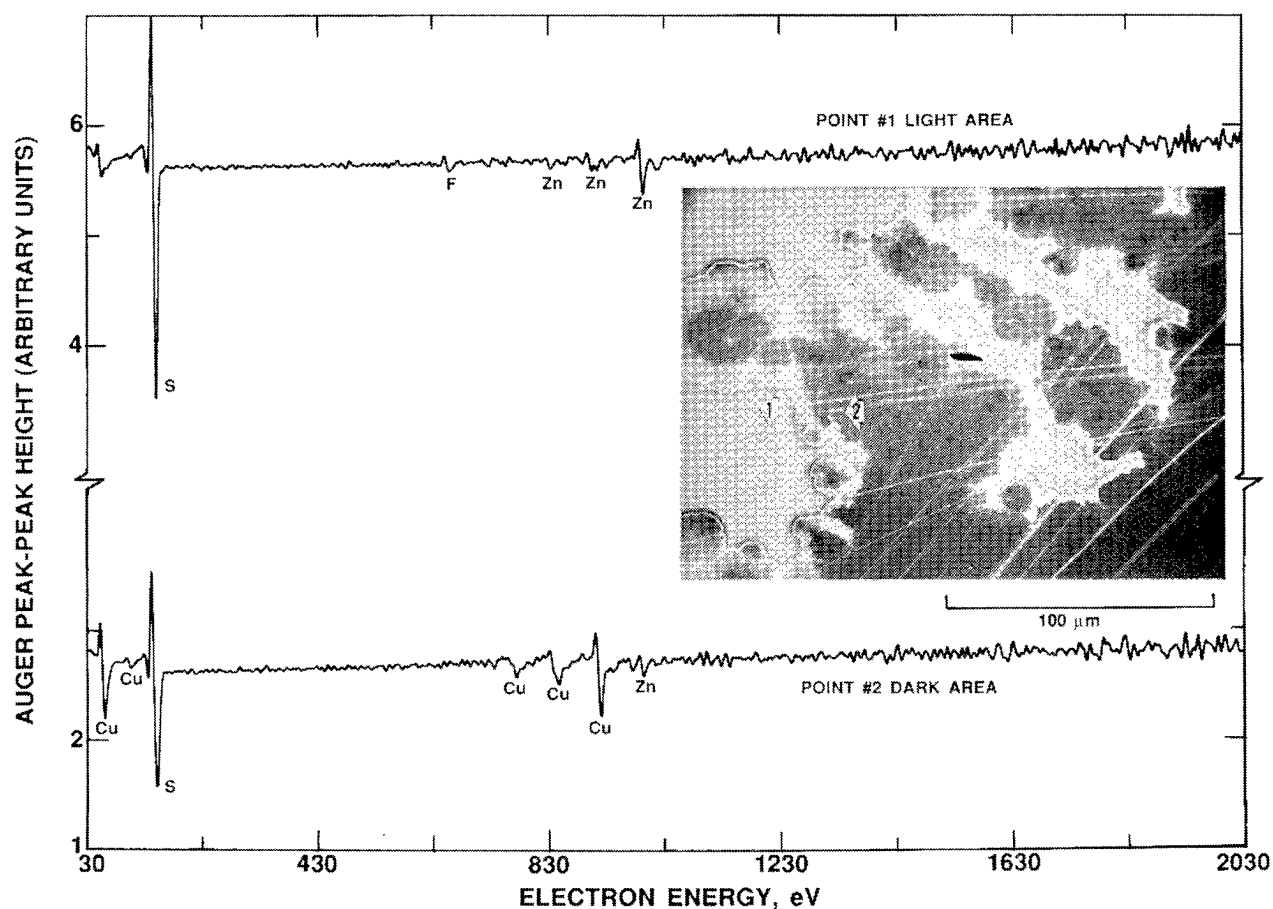
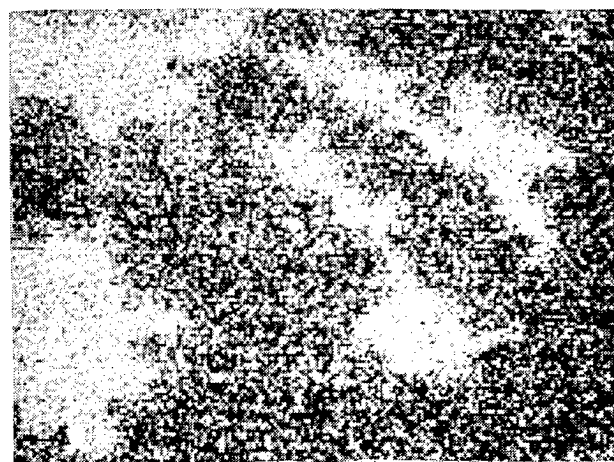
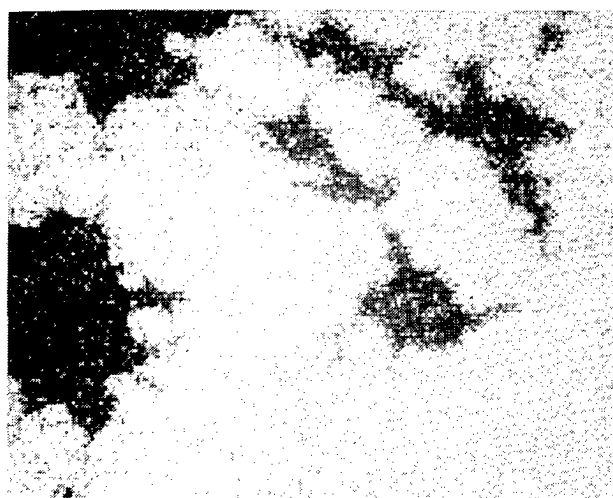


FIGURE 11. Dendrite region on sample #4 with Auger data in both dendrite and background areas. Note there is no copper in the dendrite region.

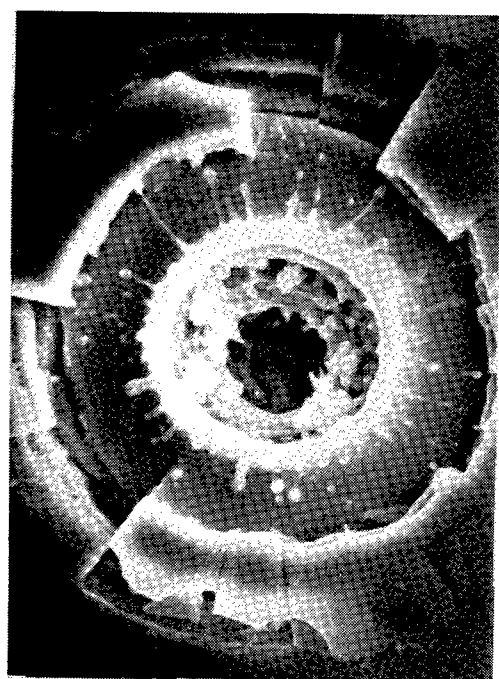
COPPER

ZINC

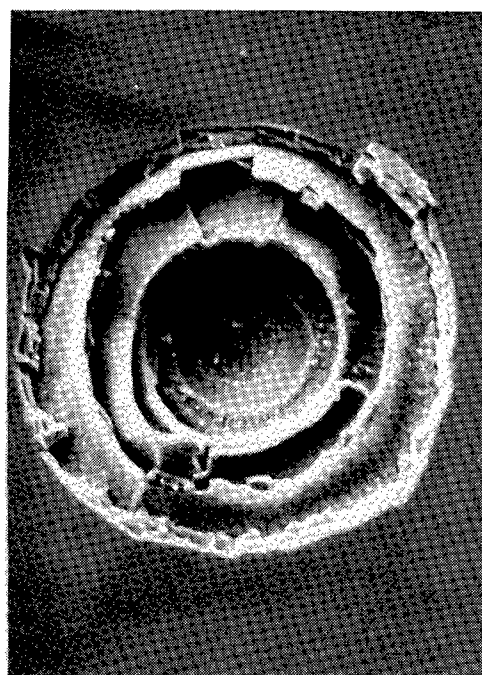


100 μm

FIGURE 12. Copper and zinc maps of the region shown in figure 11.

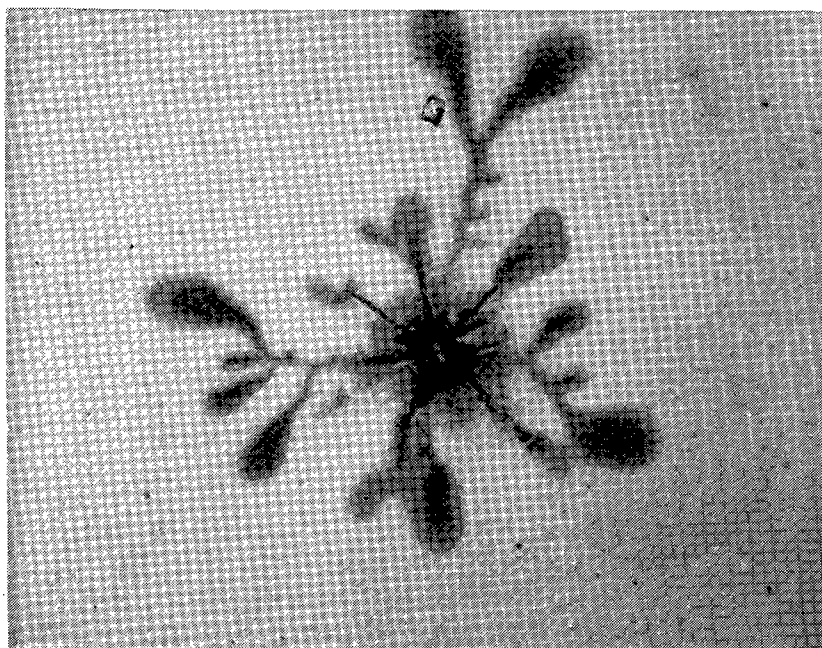


10  $\mu\text{m}$



10  $\mu\text{m}$

FIGURE 13. Impact craters from sample #3 revealing details of the multilayer structure of the coating. Note the melted areas in the smaller crater on the left.



50  $\mu\text{m}$

FIGURE 14. Impact crater from sample #5 from the trailing edge. The coating structure is not revealed and a large amount of debris surrounds the crater.

## CONTAMINATION OF OPTICAL SURFACES IN EARTH ORBIT

Donald L. Kinser, Robert A. Weller, M. H. Mendenhall, D. E. Wiedlocher  
Vanderbilt University, Nashville, TN 37235

R. Nichols, D. Tucker and A. Whitaker  
Marshall Space Flight Center, MSFC, AK 35812

### EXTENDED ABSTRACT

Glass and glass ceramic samples exposed to the low earth orbit environment for approximately 5 ½ years on LDEF were found to display limited degradation in optical transmission. Commercial optical quality fused silica samples display decreases in transmission in the 200 to 400 nm wavelength region, and this degradation appears to be a consequence of surface contamination. The contamination, found only on internal surfaces of samples, was measured by medium energy backscattering spectrometry and found to be primarily carbon. Additional thin film contamination by a species with atomic mass near 64, which was present at the level of about  $8 \times 10^{14} \text{ cm}^{-2}$ , has not been identified.

These observations are consistent with the interpretation that organic binders used in the black absorbing paint (Chem Glaze Z-306) inside the sample holding tray were concentrated in the vicinity of the samples and photolytically cracked by solar UV radiation. The resulting decomposition products were deposited on the interior sample surface and gave rise to the optical transmission loss.

No detectable contamination was observed on the external or space exposed surfaces of the samples. No measurable damage was detected which could be attributed to the direct action of gamma or UV radiation on the glass samples.

These results emphasize the need for special precautions in the preparation of spacecraft carrying precision optical components on long duration missions.



DURABILITY EVALUATION OF PHOTOVOLTAIC BLANKET MATERIALS  
EXPOSED ON LDEF TRAY S1003

Sharon K. Rutledge  
NASA Lewis Research Center  
Cleveland, Ohio 44135  
Phone: 216/433-2219, Fax: 216/433-6106

Raymond M. Olle  
Cleveland State University  
Cleveland, Ohio 44115

SUMMARY

Several candidate protective coatings on Kapton and uncoated Kapton were exposed to the low Earth orbital (LEO) environment on the Long Duration Exposure Facility (LDEF) to determine if the coatings could be used to protect polymeric substrates from degradation in the LEO environment. The coatings that were evaluated were 700 Å of aluminum oxide, 650 Å of silicon dioxide, and 650 Å of a 4% polytetrafluoroethylene-96% silicon dioxide mixed coating. All of the coatings evaluated were ion beam sputter deposited. These materials were exposed to a very low atomic oxygen fluence ( $4.8 \times 10^{19}$  atoms/cm<sup>2</sup>) as a result of the experiment tray being located 98° from the ram direction. As a result of the low atomic oxygen fluence, determination of a change in mass was not possible for any of the samples including the uncoated Kapton. There was no evidence of spalling of any of the coatings after the approximately 33,600 thermal cycles recorded for LDEF. The surface of the uncoated Kapton, however, did show evidence of grazing incidence texturing. There was a 7-8% increase in solar absorptance for the silicon dioxide and aluminum oxide coated Kapton and only a 4% increase for the mixed coating. It appears that the addition of a small amount of fluoropolymer may reduce the magnitude of absorptance increase due to environmental exposure. Thermal emittance did not change significantly for any of the exposed samples. Scanning electron microscopy revealed few micrometeoroid or debris impacts, but the impact sites found indicated that the extent of damage or cracking of the coating around the defect site did not extend beyond a factor of three of the impact crater diameter. This limiting of impact damage is of great significance for the durability of thin film coatings used for protection against the LEO environment.

## INTRODUCTION

The effect of the low Earth orbital (LEO) environment on materials for orbiting satellites and other space structures has been under study since the early 1980's (ref. 1-4). Most of the studies have been performed in ground-based space simulation facilities due to the high expense and lengthy qualification needed for flight tests. Several very short Space Shuttle flight experiments such as those on STS-5 and STS-8 allowed information to be gathered on materials exposed to LEO. This data became a basis of comparison for the ground test data (ref. 5-6). The limited exposures obtained during these flights were informative but longer exposures were needed for many materials in order to obtain measurable material degradation information. In April of 1984, a cylindrical free flyer called the Long Duration Exposure Facility (LDEF) was launched from the bay of the Space Shuttle using the shuttle's remote manipulator arm. The satellite, which is roughly the size of a school bus, contained 82 trays of active and passive experiments many of which were materials oriented. The LDEF was to be retrieved 12 months later by the Space Shuttle; however due to the explosion of the Space Shuttle Challenger and a heavy schedule, the retrieval was delayed until January of 1990. The results of the nearly 6 year LEO exposure will provide an important new data base from which ground tests can be compared and to enable a more informed selection of materials for satellites, orbiting platforms, and Space Station Freedom. Polyimide (Kapton), the baseline material for the flexible solar array panel on Space Station Freedom and on the Hubble Space Telescope, is known to be susceptible to attack by atomic oxygen in LEO. Considerable research has been performed to identify coatings for Kapton which are durable and protect it against atomic oxygen attack (ref. 3-4). When LDEF was launched, two metal oxide coatings and a metal oxide-fluoropolymer mix coating were being investigated for protection of Kapton. Pairs of these materials were placed on LDEF to determine the effect of atomic oxygen on coated Kapton material loss, the effect of ultraviolet radiation from the sun on the optical properties of the coatings, and the effect of micrometeoroid impacts on the coating durability and integrity. The results of the post flight testing to date are presented in this paper.

## FLIGHT EXPOSURE AND EXPERIMENTAL PROCEDURE

Two samples each of unprotected Kapton, 700 Å of ion beam sputter deposited  $\text{Al}_2\text{O}_3$  on Kapton, 650 Å of ion beam sputter deposited  $\text{SiO}_2$  on Kapton, and 650 Å of ion beam co-sputter deposited 4% polytetrafluoroethylene-96% silicon dioxide on Kapton were exposed on the Ion Beam Textured and Coated Surfaces Experiment tray on LDEF (S1003). The leading edge of the LDEF was originally oriented to allow direct or ram impact of its surface with the atmosphere that co-rotates with the earth. The atmosphere present in LEO is composed predominantly of atomic oxygen. Figure 1 contains a drawing showing the relation of the experiment tray to the LDEF satellite and the Earth. Upon launch, tray S1003 was to be oriented 90° from the ram direction near the space end of the satellite so as to receive a grazing incidence arrival of atomic oxygen. During the flight, however, the satellite was misoriented at approximately 8° from the ram direction so that tray S1003 was approximately 98° from the ram direction (ref. 7). After the

launch of LDEF, undercutting of Kapton at defect sites in protective coatings was found to occur and was investigated in ground test facilities (ref. 8). It was hoped that grazing incidence undercutting information would be obtained to compare to ground laboratory tests and models. However, the misorientation resulted in a flux of atomic oxygen too low for such measurements. Micrometeoroid or debris impacts and UV radiation effects could still be determined at the new position.

Prior to flight, mass measurements were taken on all of the samples with a Fisher Microgram Balance to assess material loss due to oxidation upon exposure in LEO. Unfortunately, at the time LDEF was launched, little was known about the proper mass measuring techniques for Kapton. Kapton is very hygroscopic causing its mass to be sensitive to changes in humidity. Currently, mass measurements are made after dehydrating the samples for 48 hours and quickly weighing before moisture can be reabsorbed. The LDEF samples were not dehydrated prior to the pre-flight mass measurement, and the humidity of the room they were weighed in was not monitored. Errors of as much as 2% can be caused by changes in the amount of moisture the Kapton absorbs (ref. 9). Since there were no backup samples that were weighed and not flown, a correction for humidity could not be made. Therefore, only large changes in mass could be measured accurately. Post flight mass measurements were made on a Sartorius microbalance.

Sheets of the original coated material were saved in order to compare the solar absorptance and thermal emittance of the samples flown on LDEF with those kept on the ground for the same duration. Solar absorptance was measured with a Perkin Elmer Lambda-9 Spectrophotometer with an integrating sphere attachment. Thermal emittance was measured with a Gier Dunkle model DB-100 Reflectance measurement system. Surface morphology and post flight appearance were obtained with a Cambridge 200 Stereoscan Scanning Electron Microscope (SEM) and a JOEL 840 Scanning Electron Microscope (SEM). Surface chemistry was determined with Energy Dispersive X-Ray Spectroscopy (EDS) using a Kevex system with a windowless detector.

## RESULTS AND DISCUSSION

A photograph of the post flight S1003 tray is shown in figure 2 with an arrow indicating the expected ram direction for the coated and uncoated Kapton samples. Overall, the visual appearance of the Kapton is very similar to that of unexposed Kapton. The same is true for the coated Kapton samples except for the presence of a few micrometeoroid or debris impacts which will be discussed later in this text. Closer examination by an electron microscope revealed that the surface of the exposed Kapton was not smooth and had a surface texture to it indicative of grazing incidence arrival (figure 3). A definite difference is seen between the exposed surface and that covered by the edge of the sample holder during flight. The texture points in the direction of the leading edge. A scanning electron photomicrograph of a particle indicates the directional arrival of the atomic oxygen by a shadow region on the side shielded from atomic oxygen arrival (figure 4). Only the lip of the ridge that is sticking up was textured. Similar texturing occurs along ridges parallel to the ram direction with the texture always pointing back to the leading edge. Since this tray was 98° from the ram direction, one might expect that there should have been no arrival to these samples at

all. The texture can be explained by a thermal component to the velocity vector arriving on S1003. Atomic oxygen arrival based on thermal atomic oxygen was determined to be  $4.8 \times 10^{19}$  atoms/cm<sup>2</sup> for this tray (ref. 7). Based on the directed nature of the pattern on the samples, it appears that the atomic oxygen flux as a function of angle significantly declines between 90 and 180° from the ram direction. This would make the texture appear to be caused by grazing incidence attack because the majority of the flux is arriving at grazing incidence. Micrometeoroid or debris impact sites found in the Kapton also showed evidence of texturing only on the lip facing the leading edge (figure 5). The texturing is similar to that observed on STS-8 (ref. 3). EDS scans taken of the Kapton surface indicate traces of silicon, which is believed to be due to contamination from silicones from other samples and trays on LDEF (figure 6a) (Gold peaks are from the conductive coating applied post flight to prevent charging during SEM examination). Similar contamination was seen on the aluminum oxide coated sample. The scans on the silicon dioxide containing coatings were inconclusive since they contain Si. The amount of contaminant must be very small to have allowed texturing of the Kapton to occur. An EDS spectra of unexposed Kapton does not have a silicon peak (figure 6b). (Aluminum peak is caused by the aluminum sample holder that was used to mount the Kapton for viewing.)

The mass loss from all of the samples was very low due to the low fluence of atomic oxygen that arrived at the surface. The worst case mass loss was for Kapton (0.2% of the original mass). This is much smaller than the possible error due to the presence of absorbed water. Due to the lack of extensive texturing, lack of any undercutting and the low fluence, it was concluded that the mass loss was negligible for all of the exposed samples tested.

Solar absorptance, total reflectance, total transmittance and thermal emittance measurements for these samples are contained in table I. Both uncoated Kapton samples exhibited minimal changes in optical properties compared with the Kapton, from the same batch, that remained on Earth. There was a slight increase in total transmittance which resulted in a slight decrease in solar absorptance. The uncoated and coated Kapton samples exhibited no significant change in thermal emittance when compared with their unexposed counterparts. The aluminum oxide coated samples did not change significantly in total reflectance after exposure; however, the two coatings containing silicon dioxide exhibited a decrease in reflectance on the average of 7%. Total transmittance decreased for all of the coated samples (Al<sub>2</sub>O<sub>3</sub>/Kapton: 4%, SiO<sub>2</sub>/Kapton: 3%, and 4% PTFE-96% SiO<sub>2</sub>/Kapton: 1%). This resulted in solar absorptance increases of 8% for Al<sub>2</sub>O<sub>3</sub>, 7% for SiO<sub>2</sub>, and 4% for 4% PTFE-96% SiO<sub>2</sub> coatings on Kapton. Since the solar absorptance of the uncoated Kapton samples located on the same tray did not increase upon exposure, it is unlikely that the increase in absorptance of the coated samples is due to contamination, because evidence of contamination was observed on the Kapton samples as well. Darkening is believed to be the result of UV or other radiation attack on the coatings. The UV level seen by LDEF is approximately 7% that which will be experienced in 15 years on the solar facing side of Space Station Freedom's solar arrays. It is interesting to note that the addition of a small amount of fluoropolymer appeared to result in almost a factor of two improvement in the solar absorptance. It is unknown at this time why the fluoropolymer addition made a significant difference. Although the solar absorptance changes seen on these samples are not detrimental to array performance, it is unclear whether further exposure would further increase the absorptance and what function the increase would follow. In addition, more recently manufactured metal oxide coatings being tested for SS Freedom solar arrays exhibited negligible changes in solar absorptance after greater levels of UV exposure. It is possible that impurities may be present in these coatings from the deposition process which

may play a large role in their response to UV exposure. Further chemical analysis by Electron Spectroscopy for Chemical Analysis (ESCA) is needed to help determine why this occurs.

The LDEF underwent approximately 33,600 thermal cycles during its nearly 6 year mission. Post flight examination of the thin film coated Kapton samples by electron microscopy revealed no spalling of the coating from the Kapton surface.

Figures 7a-7e contain SEM photomicrographs of micrometeoroid or debris impact sites observed on the coated Kapton samples. There were very few impacts that actually penetrated the coatings. The largest observed was on the 4% PTFE-96% SiO<sub>2</sub> sample (#7) (figure 7a). This appeared to be an impact by either a collection of particles or one large loosely distributed or extended particle. Another impact on the same sample (figure 7b and 7c) is of a much smaller impact diameter. It appears that the type of damage is very dependent on particle size and possibly particle velocity. Large impact areas appear to produce delamination, while smaller areas result in a region around the impact which is similar to the splash which is generated by a raindrop in a puddle (figure 7c). There is cracking around the splash region. Similar types of impacts were observed on the silicon dioxide and aluminum oxide coated Kapton samples (figures 7d and 7e). It appears that the impact site morphology is not dependent on the coating composition for these materials since an area of delamination at an impact site on an aluminum oxide coated Kapton sample flown on STS-8 looks similar to that on the 4% PTFE-96% SiO<sub>2</sub> coated Kapton in this experiment (figure 8). It appears that the area of crack damage or delamination is limited in extent for the impact crater sizes observed. In all cases the damage was contained within a diameter less than three times the impact crater diameter. This is very encouraging for the use of protective coatings in LEO since the damage that will result from an impact is not as extensive as originally believed. EDS scans at the impact crater sites were not conclusive. Any impacting particle material that remained in the crater was small in comparison to the coating material. There were a few locations where a particle was embedded in the surface and did not penetrate the coating. An EDS scan from one of these particles indicated the presence of silicon, aluminum, calcium, and potassium in addition to carbon and oxygen (figure 9). There were other particles on the surfaces (figure 10), but EDS scans showed the presence of mostly sodium and chlorine which is believed to be salt spray obtained prior to launch or after landing (figure 11).

## CONCLUSIONS

The atomic oxygen durability of the samples of Kapton protected with thin film coatings exposed on LDEF was not possible to assess because of the low fluence and lack of initial dehydrated sample mass data. By observing the atomic oxygen arrival at the Kapton surface and at the impact sites, the significance of thermal atomic oxygen arrival was verified since this tray was exposed 98° from the ram direction. The effect of UV radiation and micrometeoroid or debris impacts on these coatings was determined from the LDEF flight exposure. Silicon dioxide and aluminum oxide ion beam sputter deposited thin film coatings appeared to increase in solar absorptance between 7-8% upon exposure to LEO. Solar absorptance of the coating of silicon dioxide with a small amount of fluoropolymer increased only 4%. It appears that the addition of

fluoropolymer has a positive effect on the optical property durability of metal oxide coatings. Absorptance changes observed on LDEF are not at levels which would be detrimental to solar array performance, however it is unclear at this time whether further increases would occur with longer exposure or if coating impurities would play a role. Thermal emittance changes were insignificant for the coated Kapton. No evidence of spalling of the thin film coatings on Kapton was observed post flight after receiving approximately 33,600 thermal cycles. Micrometeoroid or debris impacts do not appear to cause a serious threat to the coatings because the damage area is limited to a small region less than a factor of three times the impact crater diameter. Overall, the protective coatings remained intact and exhibited no major detrimental changes which would hinder their performance for protecting solar array surfaces in LEO.

## REFERENCES

1. Banks, B.A.; Rutledge, S.K.; Paulsen, P.E.; and Stueber, T.J.: Simulation of the Low-Earth-Orbital Atomic Oxygen Interaction with Materials by Means of an Oxygen Ion Beam. NASA TM 101971, 1989.
2. Whitaker, A.F.; et. al.: Protective Coatings for Atomic Oxygen Susceptible Spacecraft Materials-STS-41G Results. AIAA-85-7017-CP, 1985.
3. Banks, B.A.; Mirtich, M.J.; Rutledge, S.K.; and Swec, D.M.: Sputtered Coatings for Protection of Spacecraft Polymers. NASA TM-83706, 1984.
4. Banks, B.A.; Mirtich, M.J.; Rutledge, S.K.; and Nahra, H.K.: Protection of Solar Array Blankets from Attack by Low Earth Orbital Atomic Oxygen. Proceedings of the 18th IEEE Photovoltaic Specialists Conference, Las Vegas, Nevada, Oct. 21-25, 1985.
5. Slemp, W.S.; Santos-Mason, B.; Sykes Jr., G.F.; and Witte Jr., W.G.: Atomic Oxygen Effects Measurements for Shuttle Missions STS-8 and 41-G. Vol. 1, 1988, NASA TM-100459, 1988, pp. 5-1 to 5-15.
6. Zimcik, D.G. and Maag, C.R.; Atomic Oxygen Effects Measurements for Shuttle Missions STS-8 and 41-G. Vol. 1, 1988, NASA TM-100459, 1988, pp. 10-1 to 10-10.
7. Bourassa, R.J.; Gillis, J.R.; and Rousslang, K.W.: Atomic Oxygen and Ultraviolet Radiation Mission Total Exposures for LDEF Experiments, First LDEF Post-Retrieval Symposium, NASA CP- 3134, 1992.
8. Banks, Bruce A.; Auer, Bruce M.; Rutledge, S.K. and Hill, C.M.: Atomic Oxygen Interaction with Solar Array Blankets at Protective Coating Defect Sites, 4th Annual Workshop on Space Operations Applications and Research (SOAR), NASA CP-3103, Vol. II, 1990.
9. Rutledge, S.K. et. al.: An Evaluation of Candidate Oxidation Resistant Materials for Space Applications in LEO. NASA TM-100122, 1986.

Table I. Optical properties of coated and uncoated Kapton exposed on LDEF tray S1003

MATERIAL AND SAMPLE DESIGNATION	TOTAL REFLECT- ANCE	TOTAL TRANSM- ITTANCE	SOLAR ABSORP- TANCE	THERMAL EMIT- TANCE
UNCOATED KAPTON (NOT FLOWN)	0.135	0.576	0.289	0.70
UNCOATED KAPTON (LDEF #6)	0.136	0.580	0.285	0.72
UNCOATED KAPTON (LDEF #34)	0.130	0.583	0.286	0.71
SiO <sub>2</sub> ON KAPTON (NOT FLOWN)	0.116	0.573	0.311	0.72
SiO <sub>2</sub> ON KAPTON (LDEF #9)	0.105	0.561	0.334	0.72
SiO <sub>2</sub> ON KAPTON (LDEF #16) *	---	---	---	---
4% PTFE-96% SiO <sub>2</sub> ON KAPTON (NOT FLOWN)	0.109	0.584	0.307	0.72
4% PTFE-96% SiO <sub>2</sub> ON KAPTON (LDEF #7)	0.103	0.578	0.319	0.72
4% PTFE-96% SiO <sub>2</sub> ON KAPTON (LDEF #14)	0.103	0.576	0.321	0.71
Al <sub>2</sub> O <sub>3</sub> ON KAPTON (NOT FLOWN)	0.120	0.571	0.309	0.72
Al <sub>2</sub> O <sub>3</sub> ON KAPTON (LDEF #12)	0.118	0.545	0.337	0.71
Al <sub>2</sub> O <sub>3</sub> ON KAPTON (LDEF #26)	0.119	0.551	0.330	0.72

\* Sample sectioned for analysis prior to optical measurements



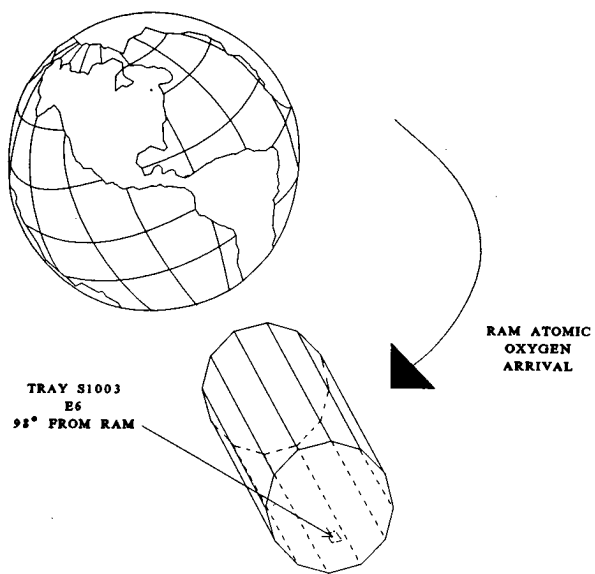


Figure 1. Location of LDEF tray in relation to the directed ram atomic oxygen arrival direction.

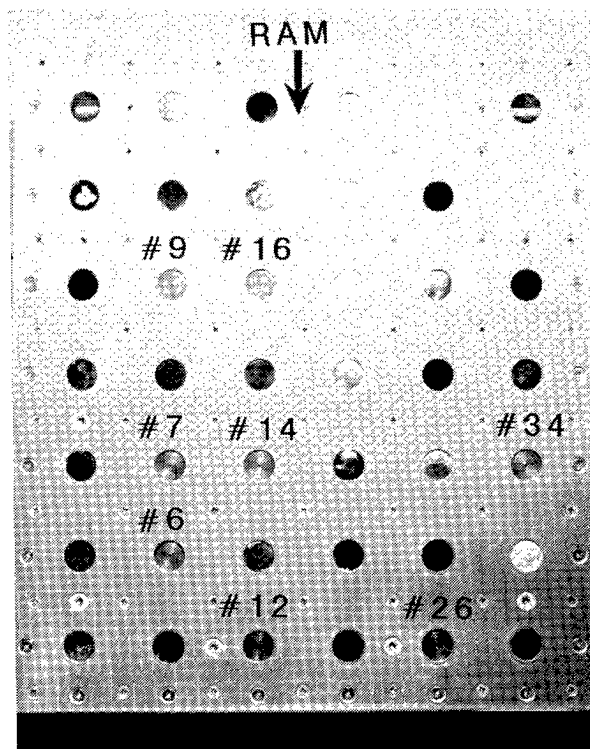


Figure 2. Photograph of LDEF sample tray with ram direction and sample numbers labeled.

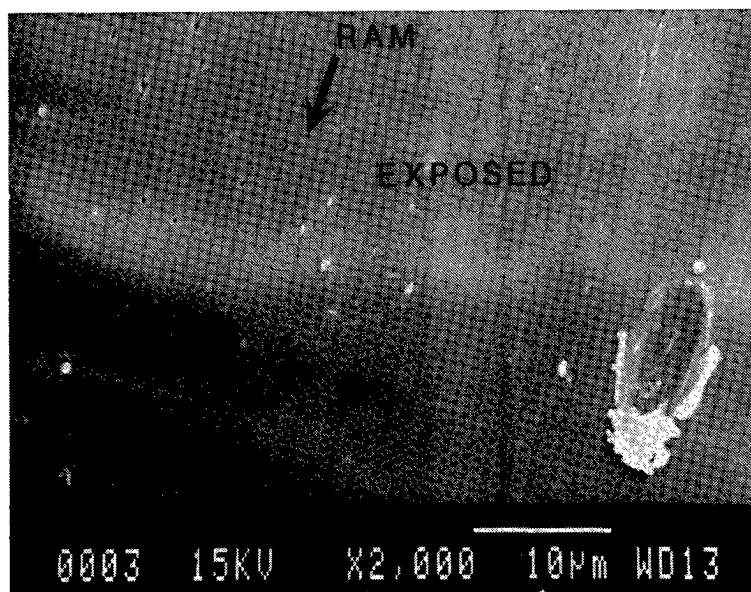


Figure 3. Scanning electron photomicrograph showing uncoated Kapton with the top half exposed on LDEF and the bottom half covered by the sample tray.



Figure 4. Uncoated Kapton flown on LDEF showing shadowing of the surface behind a particle.

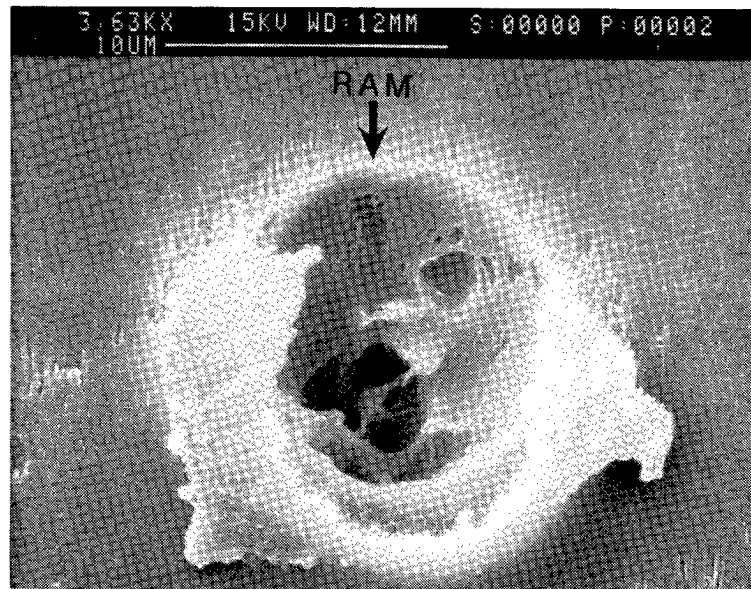
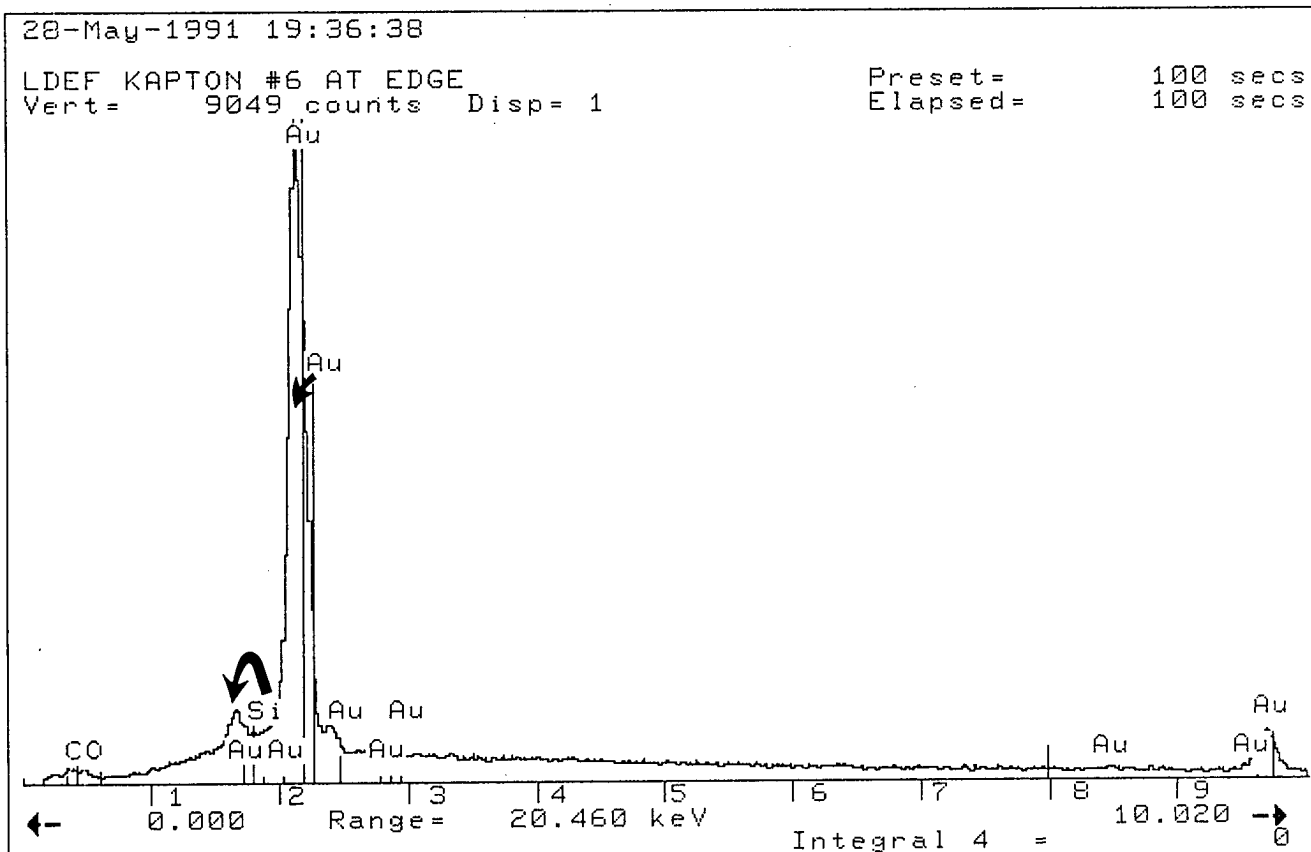


Figure 5. Micrometeoroid or debris impact on LDEF uncoated Kapton showing texturing of the crater lip facing the ram direction.

(a)



(b)

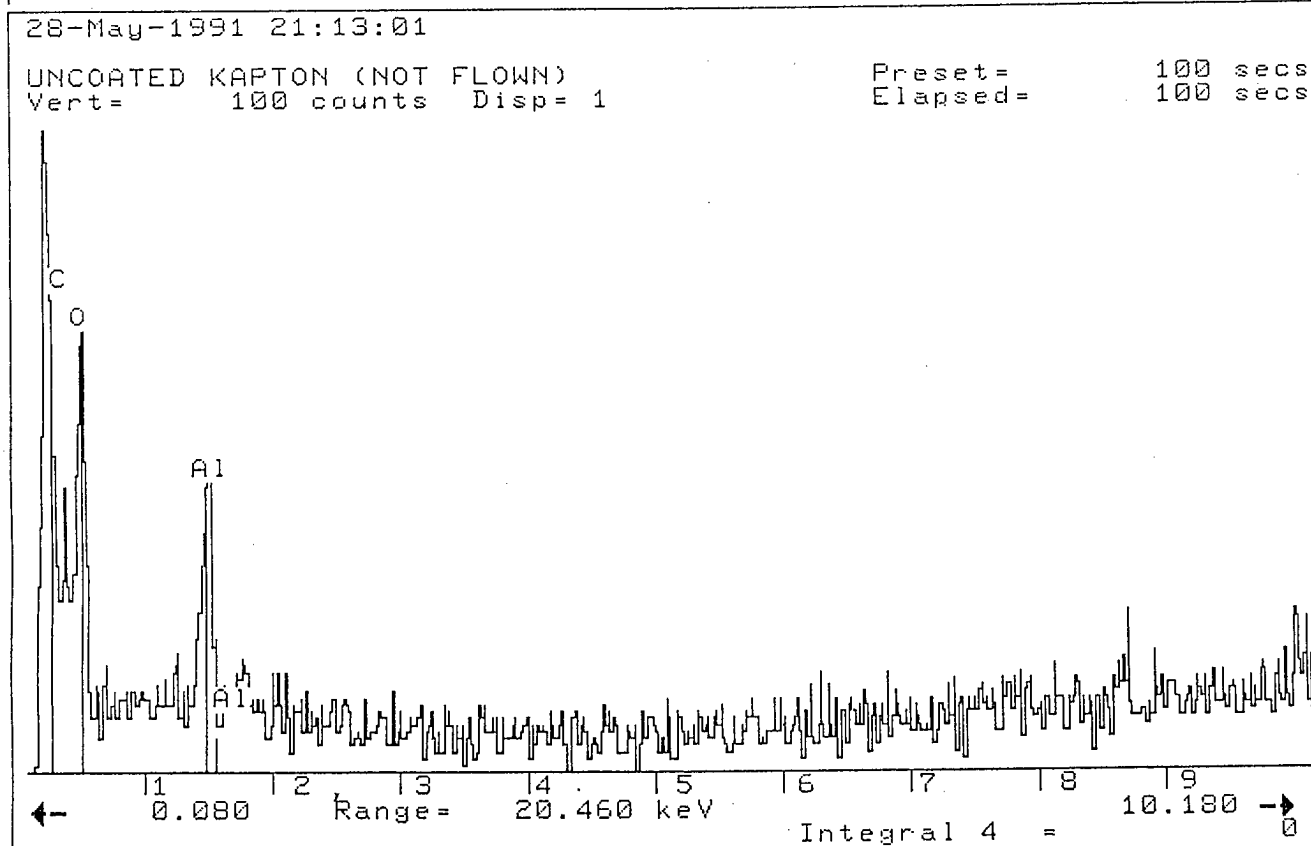
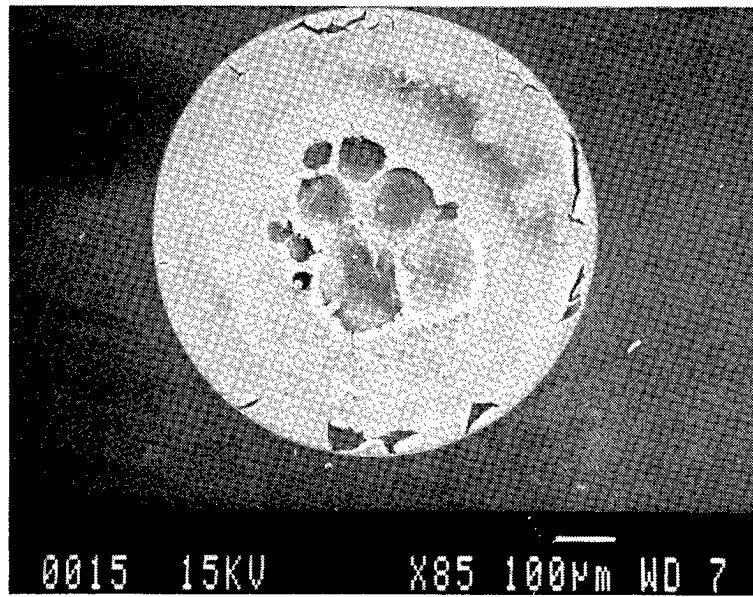
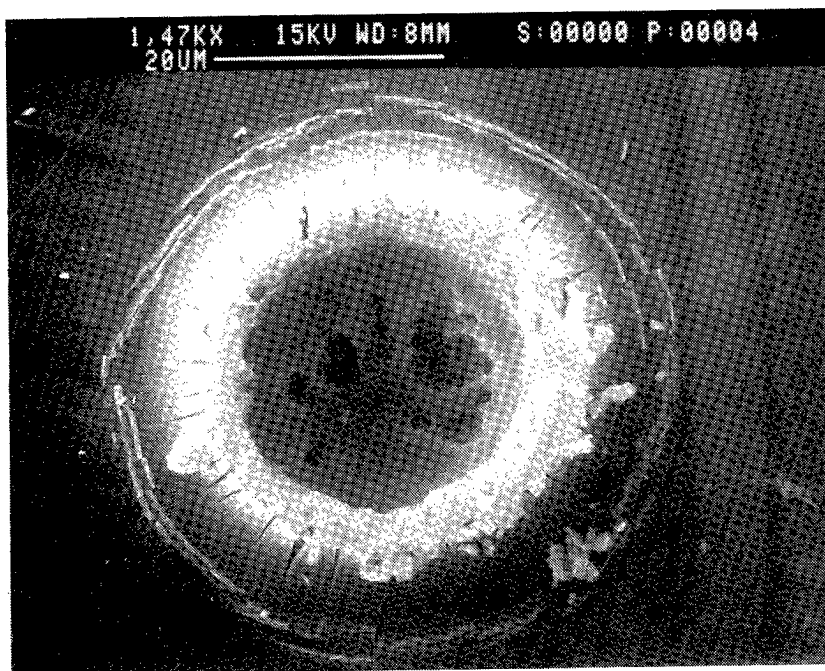


Figure 6. Energy dispersive X-ray analysis of a) uncoated Kapton exposed on LDEF and b) unexposed Kapton that remained on the ground.

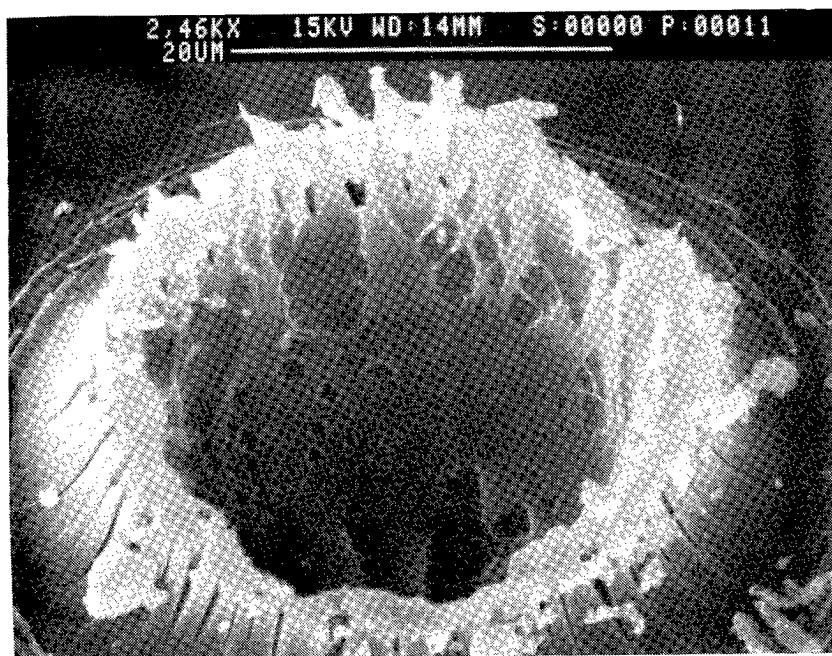


(a)

Figure 7. Scanning electron photomicrographs of a). conglomerate micrometeoroid or debris impact on 4% PTFE-96%  $\text{SiO}_2$  coated Kapton, b-c). micrometeoroid or debris impact on 4% PTFE-96%  $\text{SiO}_2$  coated Kapton, d). micrometeoroid or debris impact on silicon dioxide coated Kapton, and e). micrometeoroid or debris impact on aluminum oxide coated Kapton.

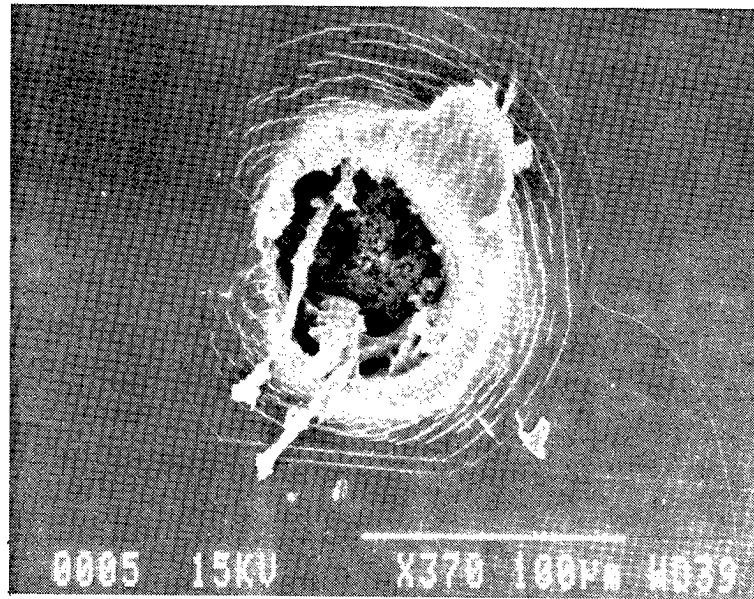


(b)

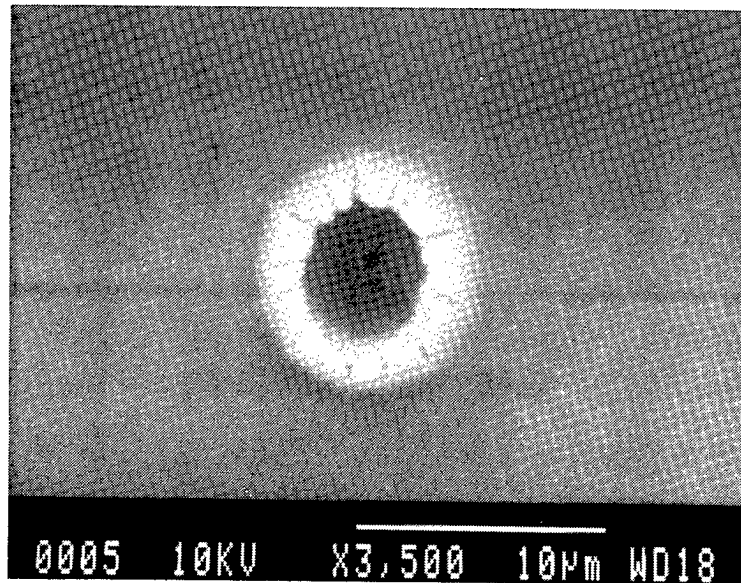


(c)

Figure 7. Continued



(d)



(e)

Figure 7. Concluded.



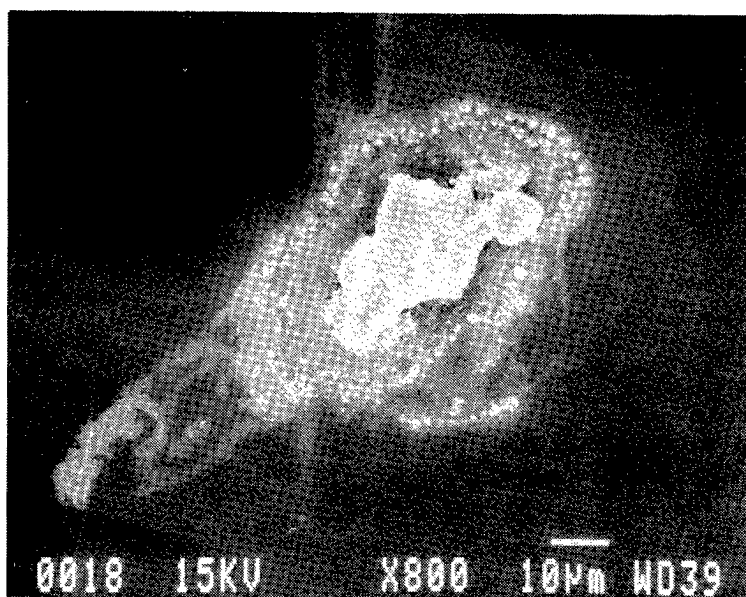


Figure 10. Photograph of salt spray found on uncoated Kapton

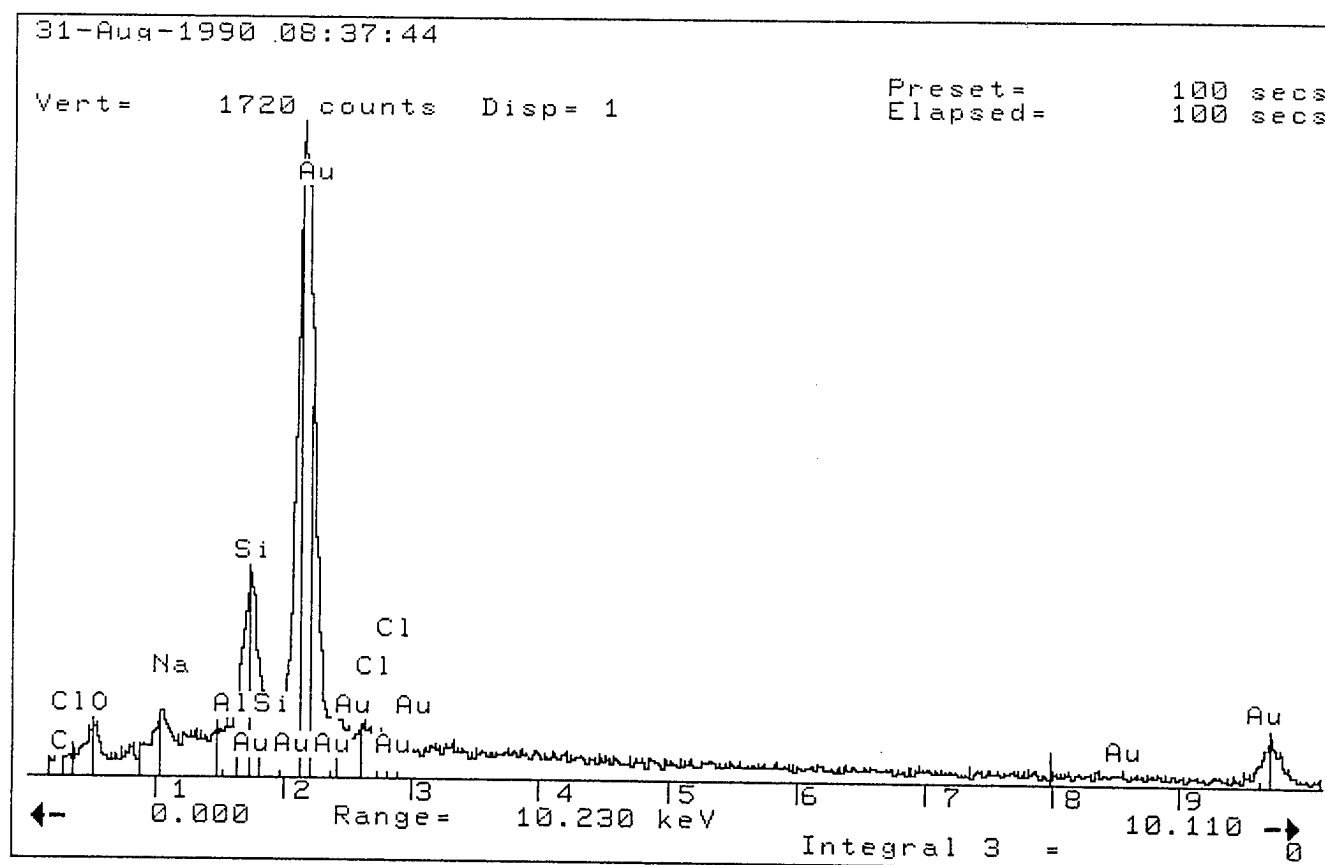


Figure 11. Energy dispersive X-ray analysis of salt spray region found on uncoated Kapton.



ADVANCED PHOTOVOLTAIC EXPERIMENT, S0014:  
PRELIMINARY FLIGHT RESULTS AND POST-FLIGHT FINDINGS

David J. Brinker, John R. Hickey\* and David A. Scheiman  
NASA Lewis Research Center  
Cleveland, OH 44135  
Phone: 216/433-2236, Fax: 216/433-6106

\*The Eppley Laboratory, Inc.  
Newport, RI 02840  
Phone: 401/847-1020, Fax: 401/847-1031

## SUMMARY

The Advanced Photovoltaic Experiment is an LDEF experiment originally designed to provide reference solar cell standards for laboratory measurements as well as to investigate the solar spectrum and the effects of long term exposure of space solar cells to the LEO environment. The experiment functioned on-orbit as designed, successfully measuring and recording cell performance and solar insolation data over the first 325 days. The objectives and design of the experiment are presented here, as well as the preliminary flight results and post-flight findings.

## INTRODUCTION

The Advanced Photovoltaic Experiment (APEX) is a space flight test designed to provide reference cell standards for laboratory photovoltaic performance measurements as well as to investigate the solar spectrum and the effect of long term exposure of solar cells to the space environment. Toward this end, 155 solar cells of the widest available variety of design and material were incorporated into the experiment along with sensors to measure total solar irradiance and sun angle. Experiment control and data storage were accomplished using a custom electronic unit and the Langley provided Electronic Power and Data System (EPDS). The experiment was designed around the original flight time of about one year, with battery capacity the principal lifetime limiting factor. Preliminary examination of recorded flight data indicates that the experiment performed as designed, recording 325 days of useful solar cell performance data and sensor data. However, the unplanned sixfold increase in flight time due to the delay in retrieval of LDEF has resulted in the inability to meet some of the original mission objectives, but will yield valuable data concerning the survivability of solar cells in low earth orbit.

In this paper we present the preliminary flight results and the post-flight findings of APEX. The original objectives of the experiment, details of the design and the sensors and solar cell complement will also be discussed.

## BACKGROUND AND OBJECTIVES

In response to an announcement of opportunity released by Langley in 1976, a project plan was written by Henry W. Brandhorst, Jr. and Americo F. Forestieri of the Lewis Research Center. After

acceptance of the project plan, a contract was awarded to The Eppley Laboratory, Inc. of Newport, Rhode Island in September, 1977 for definition and fabrication of APEX. Russell E. Hart, Jr. became principal investigator during the middle stages of experiment fabrication and remained so until early 1989. APEX, designated experiment S0014, occupied position E9, the second experimental tray from the space end of LDEF on the leading edge.

The experiment was designed to implement three specific objectives concerning the performance of space solar cells in the extraterrestrial solar environment and the distribution of energy in the solar spectrum. The first objective was to determine the performance and endurance of advanced solar cell designs under low earth orbit conditions. This was to be accomplished by the daily measurement and recording of the short-circuit current ( $I_{sc}$ ) of 120 cells whenever the sun angle was optimum. The current-voltage characteristic of 16 cells was determined at the same time by measuring the open-circuit voltage and the cell current and voltage as defined by six different load resistors.

The second objective was to calibrate reference solar cells for use as intensity standards in laboratory solar simulators. The daily determination of short-circuit current and the concomitant solar intensity and sun angle data of the 120  $I_{sc}$  cells throughout the duration of the flight would satisfy the requirements of this objective.

The measurement of the energy distribution in the extraterrestrial solar spectrum was the final objective. Three instruments were included in APEX for this purpose. An absolute cavity radiometer measured the total solar irradiance when solar cell illuminated performance was being recorded. The measure of the broad band solar spectrum was obtained using a 45° dichroic mirror to divide the spectrum into two roughly equal parts. Silicon cells were used as sensors. Sixteen bandpass filters coupled with silicon solar cell detectors were used to measure the solar spectrum over a wavelength span of 0.3 to 1.1 micrometers. These filters could then be used for the calibration of a laboratory spectral response system.

The unplanned sixfold increase in time on orbit has had significant consequences on these objectives. The first objective, to measure the endurance of solar cells in LEO has been greatly enhanced, while the cavity radiometer and sun angle sensor are now of increased value for endurance studies. In fact, the entire experiment is of interest for material science investigations. The second objective, the calibration of standard cells can not be met because of the five year period on orbit without performance data. The measurement of the spectral content of the sun was successfully completed with the recovery of the flight data, although several of the filters show delamination of the interference coatings, thus compromising their utility in the laboratory.

## EXPERIMENTAL DESIGN

The Advanced Photovoltaic Experiment was required to be completely self-contained in terms of control, data acquisition and storage, and power. To attain maximum accuracy in cell calibration, it was necessary to minimize the amount of Earth reflected radiation reaching the cells. Since relative solar azimuth changes with time in orbit and the minimum relative solar elevation occurs at the terminator crossing, a slat-slot approach was used for the cell field-of-view (FOV) design. The cell's FOV is therefore small in the elevation axis and large in the cross-axis. The twelve inch deep, full size (50 x 34 inches) tray was divided into three bays. The smaller cells, typically two centimeters square or two by four centimeters and requiring less depth than larger cells to attain the proper FOV, are mounted in bays 1 and 3. The larger area cells, requiring a greater depth, are mounted in the central bay 2.

The shallowness of bays 1 and 2 provides room for the electronic systems. The four batteries needed for power were mounted on the rear of the tray. Baffles located between the rows of cells further minimize reflection. The baffles and the underside and upper surfaces of the FOV plates were painted with Chemglaze Z-306 matte black paint. The lower half of the outside of the tray was similarly painted for

thermal control purposes. A photograph of APEX after retrieval is seen in Figure 1.

The Eppley Type HF cavity radiometer can be seen in Figure 1 as the round object in the upper part of the tray. Next to it is the Digital Solar Angle Sensor (built by Adcole Corporation) which measures sun angle on two orthogonal axes and enables optimal conditions to be selected for performance measurement. To the right of the DSAS is the dichroic mirror assembly with its two silicon cell sensors. In the row below these instruments are the Barr Associates bandpass filters which are mechanically clamped over the silicon cell sensors. Also included in the experiment are two ultraviolet exposure monitors. They are disks of fused silica which degrade in short wavelength transmittance as they are exposed to the ultraviolet rich AMO insolation.

The solar cells were permanently mounted on removable aluminum plates, either singly or in pairs of smaller cells, using RTV 511 adhesive and primer. For the 120 Isc samples, a precision 0.1 ohm resistor was wired across the cell and mounted on the rear of the plate using insulated feedthroughs. Short-circuit current was easily determined by measuring the analog voltage across the resistor. The short-circuit current of the sensors cells in the dichroic mirror instrument and under the bandpass filters was determined in the same manner. The sixteen I-V cells had a six point current-voltage characteristic measured by the switching of a number of predetermined load resistors across each cell.

The temperature of many of the cells as well as several locations on the tray were measured and recorded by 128 sensors. Yellow Springs Instruments type 16429 thermistors (for space applications) were utilized. The thermistors were mounted in a slot machined in the aluminum cell mounting plate, directly beneath the cell and bonded into place with Eccobond 555 adhesive.

The experiment was designed to acquire performance data from the cell samples and associated instruments once per day while they were illuminated by the sun, on those days when the orbital conditions allowed such a measurement. Two distinct electronics systems provided this capability. One, the Langley provided Electronics Power and Data System (EPDS), provided timing signals, data storage, power to the experiment and an interface to LDEF for deployment initiation purposes. The other, the APEX Data Acquisition System performed the primary control and data acquisition functions. This system was designed and built by Gulton Industries under subcontract to Eppley Labs. The most optimum sun angle conditions for each data scan were insured by the DSAS. Figure 2 shows the schematic diagram of the APEX data acquisition system.

After data acquisition was completed the data was transferred to the flight recorder, the Magnetic Tape Memory (MTM), through the EPDS. The data words were handled in a twelve bit format. Because the capacity of the EPDS was 4096 words per interrogation and that of the APEX electronics was 8000 words, the data was transferred in two scans, 12 hours apart. Upon receipt of the data, the EPDS wrote the data to the tape three times for redundancy. Every eight days a night scan was conducted, which enabled calibration of various instruments and a measure of the dark currents of the solar cells. This data was also recorded.

After fabrication and functional testing of APEX was completed at Eppley Labs, the experiment was shipped to Lewis for thermal-vacuum and vibration qualification testing. Final verification of system operation was performed at the Kennedy Space Center in November, 1983, prior to integration with LDEF. APEX, as was LDEF, was designed and constructed for multiple flights. This is no longer the case, as the entire experiment, not just the solar cells, is of considerable scientific and engineering interest.

### SOLAR CELL COMPLEMENT

The solar cells on APEX were provided by a number of industrial and governmental institutions for calibration and return for use as reference standards (Table 1). The cell complement represents the state-

of-the-art in space solar cells as of mid-1982 as well as production cells and examples indicative of solar cells used on a number of satellites. Standards which had been previously calibrated using aircraft, rocket flights and high-altitude balloons were also included, as were radiation damaged cells. The majority of the cells are silicon, although a number of gallium arsenide cells were included. Table 2 summarizes the cell types flown. Space limitations prevents listing all the permutations of cells, coverglasses and adhesives.

## POST-RETRIEVAL OBSERVATIONS

A number of physical changes in APEX after nearly six years in LEO are readily apparent. Much of the black paint has been removed from the upper surface of the field-of-view plates. The Chemglaze primer, reddish-brown in color, is visible. The differences from plate to plate in the amount of paint remaining is possibly a function of the initial paint thickness, as the plate covering bay 2 was painted at a different time than the other FOV plates. However, the black paint coating the rear of the tray was not changed in appearance, neither was the paint on the baffles and the underside of the FOV plates. The top plate of the DSAS, an aluminum alloy with a clear anodize, is now golden in color.

A contaminating film is found over much of the front surfaces of APEX, as well as LDEF itself. The yellow-gold film is particularly evident on cells and mounting plates in the two rows nearest the space end of the tray. Discoloration is also seen on the baffle plates and the underside of the field-of-view plates. Fairly heavy deposits of the same colored material were discovered inside the APEX tray, aligned with access openings for hold-down bolts. The location of the deposits agrees with preliminary reports that LDEF was rotated along its axis toward Row 10. Preliminary analysis of the the contaminating films on the front surfaces of APEX indicates that it has as major constituents silicon, oxygen and carbon. Our early results, obtained using Rutherford Backscattering and Auger Electron Spectroscopy are in agreement with those obtained by the LDEF Materials Special Investigation Group (Ref.1).

APEX sustained a large number of impacts from meteoroids and debris, due to its position on the leading edge. A survey of APEX conducted in SAEF-2 at the Kennedy Space Center at the time of deintegration (Ref. 2) yielded a count of 632 impacts, 569 of which were 0.5 millimeter in diameter or

Table 1 -APEX SOLAR CELL INVESTIGATORS

ASEC	A. F. WRIGHT AERONAUTICAL LAB
COMSAT	EUROPEAN SPACE AGENCY
SOLAREX	JET PROPULSION LABORATORY
SPECTROLAB	LEWIS RESEARCH CENTER
	MARSHALL SPACE FLIGHT CENTER

Table 2 - SUMMARY OF APEX SOLAR CELL TYPES

SILICON:	BSR/BSF	STANDARDS:	BALLOON
	VIOLET		ROCKET
	VERTICAL JNCTN		AIRPLANE
	TEXTURED		RADIATION DAMAGED
	5.9 x 5.9 cm PEP		
	2 MIL THICK	COVERGLASS:	FUSED SILICA
			V- & U-GROOVED
GALLIUM ARSENIDE: LPE			CERIA DOPED MICROSHEET

smaller. The remainder were greater in diameter than 0.5 millimeter, with the largest crater 1.8 millimeters in diameter. Among the impacted surfaces are one of the glass reticles of the DSAS, one of the bandpass filters and a number of solar cells. Damage to the cells includes cratered and cracked coverglasses, craters extending into the cell itself, and in one case, a small portion of a silicon cell and coverglass was removed as the particle continued into the aluminum substrate.

## PRELIMINARY POST-RETRIEVAL TEST RESULTS

### APEX Data Acquisition System

Preliminary analysis of the flight data began with transcription of the MTM data records onto computer discs by Lockheed personnel. A summary of the Data Acquisition System performance is given in Table 3. The Gulton system, providing solar cell and sensor control and signal conditioning, presumably ceased operation when its batteries discharged to below a threshold level, as the two 28 volt batteries powering the Gulton system were totally discharged when they were removed. The 358 day operational lifetime falls between the span of 233 to 467 days calculated prior to flight. Values of cell currents, voltage calibration data, the cavity radiometer heater current and thermopile signal are all within nominal, expected values for the first 325 days, after which the Gulton calibration voltages fall below their normal values. The EPDS continued to function for 2017 days, nearly the entire orbital duration. It appears that the only data stored on the tape after day 358 were timing, synchronization and calibration words. The battery powering the EPDS was also completely discharged, accounting for the termination of data records on the MTM. The battery powering the MTM retained some charge. Detailed analysis of the data from the nearly 300 discrete signal channels has begun and is expected to continue into the foreseeable future.

### Absolute Cavity Radiometer

The Eppley absolute cavity radiometer was included to provide a measure of the total solar irradiance concurrent with the cell performance data. It is similar to an instrument that is presently in orbit on Nimbus 7 and has returned over 12 years of data. The APEX radiometer is unique in that it is the only

Table 3 - APEX DATA SYSTEM PERFORMANCE

DAYS 1-325	SOLAR CELLS AND SENSOR DATA ACQUIRED AND WRITTEN TO MTM. GULTON ELECTRONIC UNIT CALIBRATION VOLTAGES AT DESIGN SPECIFICATION VALUES.
DAYS 326-358	GULTON CONTINUES TO FUNCTION; HOWEVER CALIBRATION VOLTAGES BELOW SPECIFICATION VALUES. CELL AND SENSOR DATA ERRATIC AND DEEMED UNRELIABLE.
DAY 358	GULTON ELECTRONIC UNIT CEASES TO FUNCTION.
DAYS 358-2017	EPDS AND MTM CONTINUE TO FUNCTION. EPDS TIME AND SYNC WORDS WRITTEN TO MTM EVERY SIX DAYS.
DAY 2017 (66 MONTHS)	LAST DATA WRITTEN TO MTM.

such sensor ever returned after a significant exposure to the space environment. A detailed post-retrieval analysis was performed both at Eppley Laboratory in Newport, Rhode Island and at the Seventh International Pyrheliometric Comparison (IPC VII) at the World Radiation Center in Davos, Switzerland in October, 1990. Comparison of preflight calibrations to similar post-flight tests shows that the radiometer performance is unchanged within present ability to measure it. A detailed discussion of the cavity radiometer results is presented elsewhere in this proceeding in a paper concerning Experiment AO-147 (Ref. 3).

### Digital Sun Angle Sensor

The Digital Sun Angle Sensor (DSAS) is an Adcole Corporation Model 22500 two axis sensor with a field of view of  $\pm 32^\circ$  by  $\pm 32^\circ$  and a resolution in each axis of  $0.5^\circ$ . The front surface, aluminum with a clear anodize (Mil-A-8625, Type II) had changed to a golden color. The quartz window of reticle B was cratered. After de-integration from APEX the sensor and its amplifier were returned to Adcole for testing. This post-flight calibration indicated that the unit did not change in performance or resolution. However, the impact crater on reticle B did cause shadowing at extreme angles...Preliminary analysis of the flight data agrees with other techniques that indicate that LDEF was rotated toward Row 10 about  $8-10^\circ$ .

### Solar Cells

Extensive testing of the solar cells flown on APEX was conducted prior to their integration with the experiment. This testing was performed to ensure the survivability of the cells throughout the flight and to provide baseline data for flight and post-flight comparisons. Cell illuminated performance has been remeasured using laboratory solar simulators after removal from APEX. The solar cells did not show any significant signs of physical change due to the flight. Although the contaminating film found over much of LDEF has coated many of the cells to varying degrees, no loss or changes in coverglasses or antireflection coatings was observed. Some discoloration of the RTV used to fasten cell wiring is seen. A number of cells have sustained cratering from micrometeoroid and/or debris, the severity of the crater varying from a tiny chip in the coverglass to penetration of the coverglass, cell and aluminum substrate. Figure 3 shows the illuminated current-voltage characteristics taken in a laboratory simulator of cell M-3. This cell is a 5.9 cm. by 5.9 cm. silicon cell with a wrap-around front contact on the four corners. The development of this cell was undertaken to provide power for the Shuttle on extended missions (PEP Program) and is similar to the wrap-through technology used in for Space Station Freedom. This cell sustained a small crater in the coverglass which did not penetrate to the silicon cell itself. From Figure 3 it can be seen that little change in performance resulted.

The current-voltage characteristic of another large area, wrap-around silicon cell (M-9) is shown in Figure 4. In this case, however, the micrometeoroid/debris damage extended into the cell itself, cracking both the coverglass and the silicon cell. The crack in the solar cell extend about 90% of the way across the cell while the coverglass crack extends from side to side, although on a different path than the cell crack. The wrap-around feature of cell front contact provides sufficient redundancy to maintain electrical continuity. The loss in fill factor evident in Figure 4 is due to this cell crack, but the short-circuit current and open-circuit voltage are unchanged.

The silicon solar cell designated NA-9 has largest diameter (1.8 millimeter) crater on APEX. The crater extends into the silicon cell through the coverglass, although neither the cell nor cover are cracked. Figure 5 is the pre- and post-flight simulator data. The approximately 100 mV drop in open-circuit voltage is due to shunting of the cell pn junction at the sight of the crater. The 5% drop in current is due to area loss associated with the crater and a contaminating layer evident on the cell.

## CONCLUSION

Post-flight analysis of the Advanced Photovoltaic Experiment indicates that it successfully completed its mission and returned 325 days of valid solar cell and solar intensity and spectrum data. A number of physical changes are readily apparent, including micrometeoroid and debris impact craters, loss of black paint from the surface of the experiment and a contaminating film similar in nature to that found over most of LDEF. Detailed post-flight analysis and calibration of many of the sensors and components of APEX has been conducted. The cavity radiometer is unchanged with regards to sensitivity, reflectance and overall condition. The Digital Sun Angle Sensor has not changed in either resolution or sensitivity. The post-flight performance of the solar cells analyzed thus far has revealed no unexpected behavior.

The analysis of APEX is continuing, with emphasis placed on the interpretation and understanding of the flight data, post-flight inspection of the numerous solar cells and components and investigation of the materials science issues now of interest. As the investigation moves forward, we are finding many fascinating phenomena, which we will report in future papers.

## ACKNOWLEDGEMENTS

The authors would like to thank Donald Brasted of the Lewis Computer Services Division for his unflagging efforts in reduction and analysis of the APEX flight data; particularly difficult after a hiatus of nearly six years. We also wish to thank Richard Hoffman of the Photovoltaic Branch for his invaluable assistance in post-flight processing. Materials analysis was performed at Case Western Reserve University by Richard W. Hoffman, Abbas Lamouri, Christian Zorman and Liangyu Chen.

## REFERENCES

1. Preliminary Report on LDEF-Related Contaminants, Materials Special Investigation Group, LDEF Project Office, Langley Research Center, August 1990.
2. Meteoroid and Debris Impact Features on the Long Duration Exposure Facility, A Preliminary Report, Meteoroid and Debris Special Investigation Group, Johnson Space Center, August 1990.
3. J. R. Hickey, Passive Exposure of Earth Radiation Budget Experiment Components, LDEF Experiment AO-147: Post-Flight Examinations and Tests, NASA CP-3134, 1992.

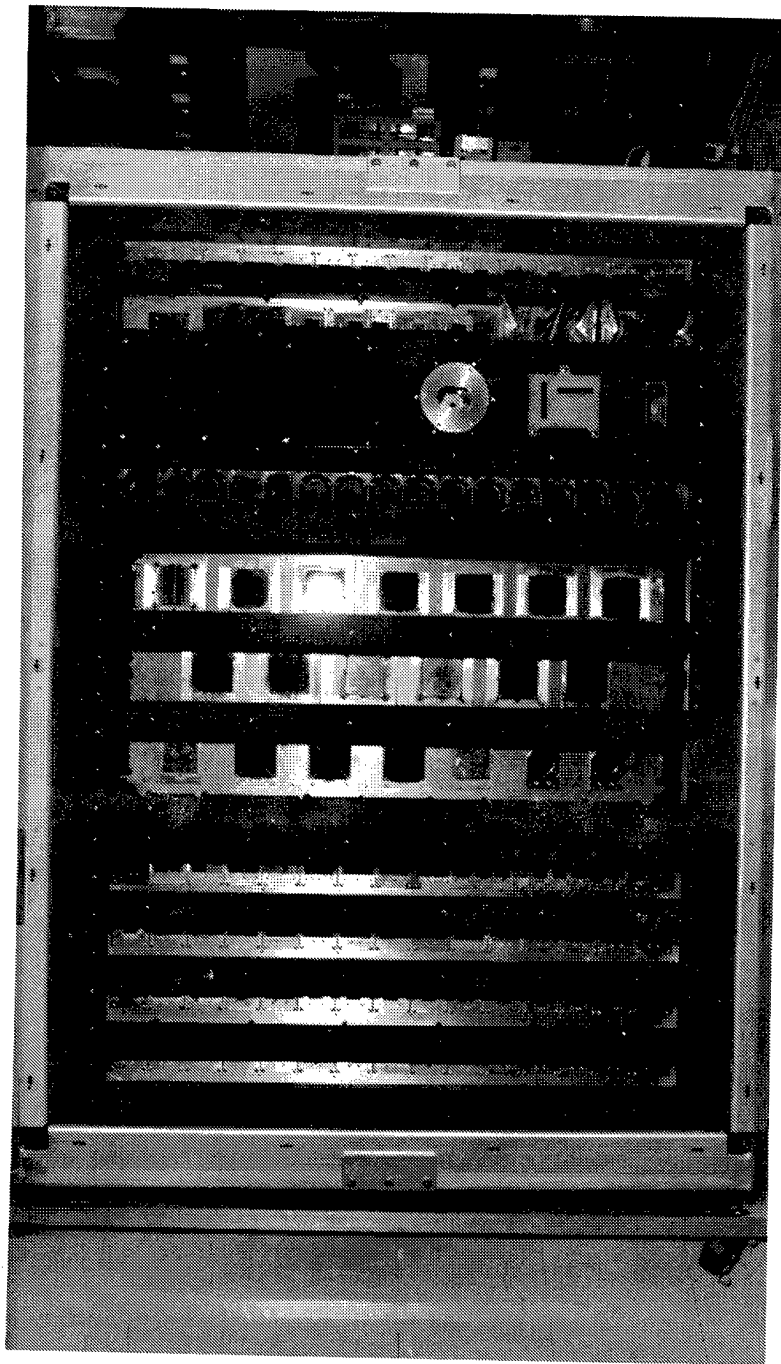


Figure 1 - POST-RETRIEVAL PHOTOGRAPH OF APEX



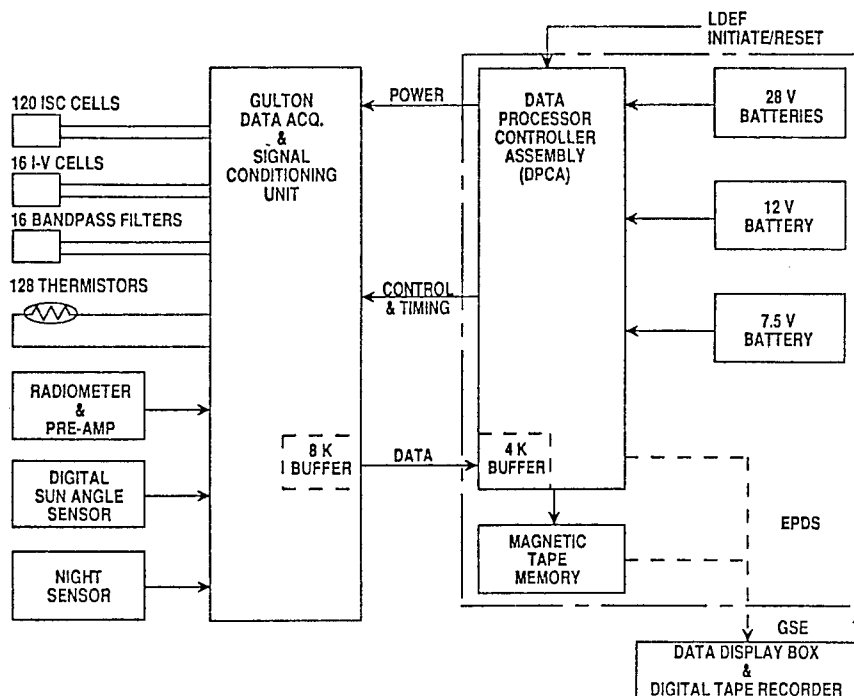


Figure 2 - SCHEMATIC DIAGRAM OF THE APEX DATA ACQUISITION SYSTEM

Cell: ISC #93 M-3	Pre-Flight	Post-Flight
Area: 34.7 cm <sup>2</sup>	Is <sub>c</sub> = 1.37850	Is <sub>c</sub> = -1.36833
Temp: 25 deg C	Voc = .569	Voc = -.570
Air Mass 0	F.F. = 69.591	F.F. = 68.280

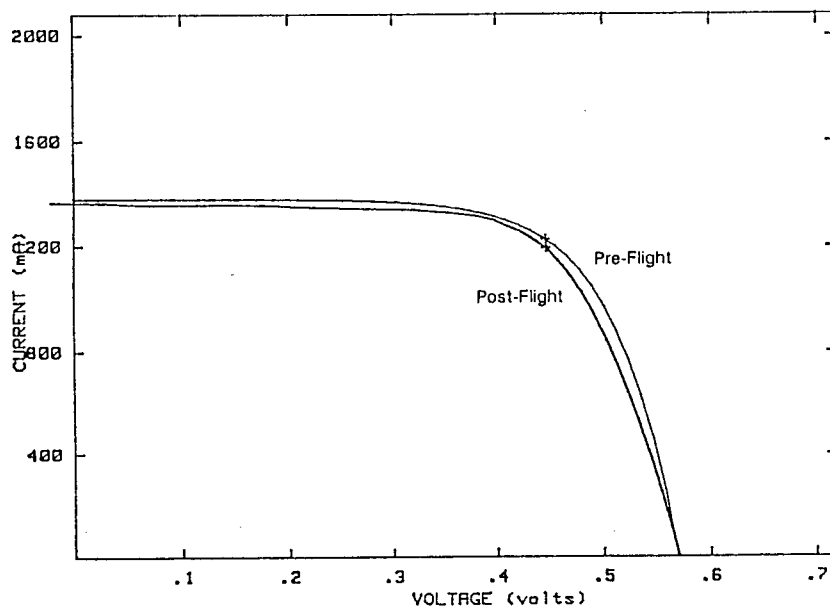


Figure 3 - ILLUMINATED PERFORMANCE OF CELL M-3

Cell: ISC #100 M-9	Pre-Flight	Post-Flight
Area: 34.3 cm <sup>2</sup>	Is <sub>c</sub> = 1.22340	Is <sub>c</sub> = -1.22030
Temp: 25 deg C	Voc = .577	Voc = -.580
Air Mass 0	F.F. = 73.415	F.F. = 58.340

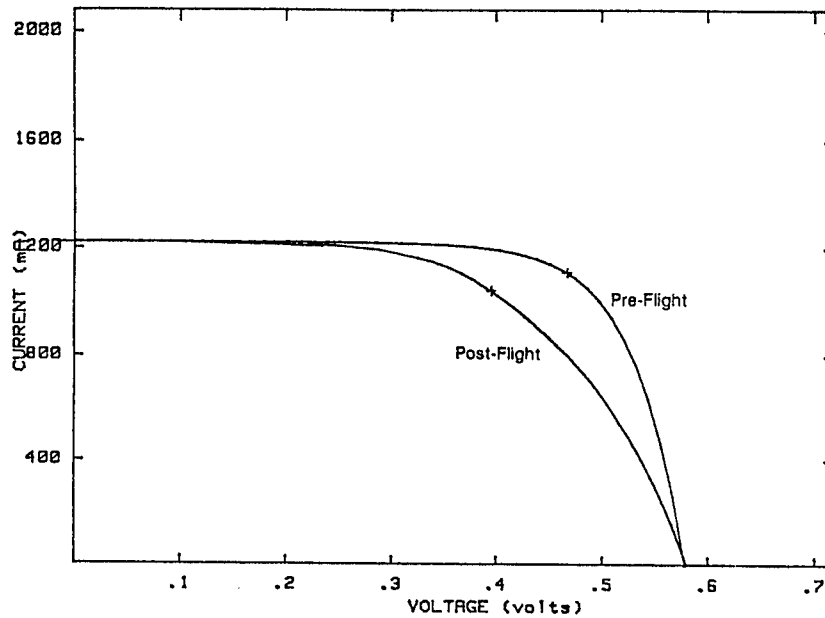


Figure 4 - ILLUMINATED PERFORMANCE OF CELL M-9

Cell: ISC #64 NA-9	Pre-Flight	Post-Flight
Area: 4 cm <sup>2</sup>	Is <sub>c</sub> = .13600	Is <sub>c</sub> = -.12949
Temp: 25 deg C	Voc = .589	Voc = -.503
Air Mass 0	F.F. = 75.124	F.F. = 70.050

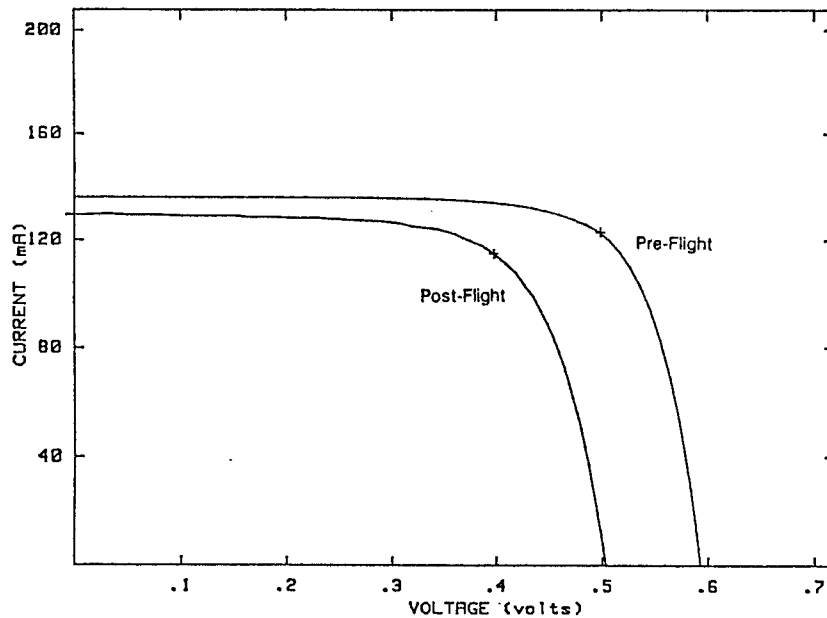


Figure 5 - ILLUMINATED PERFORMANCE OF CELL NA-9

# EVALUATION OF LDEF EXPERIMENT S 1002

L. Preuss

Deutsche Aerospace AG - MBB

Munich, Germany

Phone: 089/60727297, Fax: 089/60727252

## SUMMARY

Thermal control coatings, solar cells and micrometeoroid capture cells developed under government contract have been flown on the experiment to investigate both the behavior of these components under space conditions and to collect micrometeoroids and debris.

The visual inspections, electrical and thermooptical measurements as well as chemical and metallurgical investigations conducted on the complete experiment as well as on individual components are described, analysed and discussed.

The postflight results of the thermal control coatings proved to be in good accordance with laboratory results.

## 1. INTRODUCTION

Thermal control coatings, solar cells and micrometeoroid capture cells developed under government contract were flown on LDEF - Experiment S1002 to investigate the behavior of these components under space conditions and to collect micrometeoroids and debris. After a over 5 1/2 years mission in a low earth orbit (LEO) the experiment was back on earth in January 1990 for data acquisition and - analysis and for investigation of components.

## 2. DESCRIPTION OF EXPERIMENT

On LDEF the experiment was located on the trailing edge, position E3.

The complete experiment consisted of

- the coatings/solar cells experiment, integrated in the Experiment Exposure Control Canister (EECC) and shown on the left side of Figures 1 and 2.
- the measuring electronic box belonging to the coatings/solar cells experiment as well as the micrometeoroid experiment comprising 77 capture cells on the honeycomb plate and shown on the right side of Figures 1 and 2.

In Figure 3 the experiment is presented with honeycomb plate removed and with EECC - drawer open, where the coatings/solar cells experiment (Figure 4) is located.

### 3. EVALUATION OF EXPERIMENT

The evaluation of the experiment consisted of the following activities:

- activities on the complete experiment such as data acquisition and - analysis as well as visual and thermooptical investigations of components,
- investigation of individual components such as visual inspections, electrical and thermooptical measurements as well as chemical and metallurgical analyses.

#### 3.1 Investigated Components

##### 3.1.1 Micrometeoroid Capture Cells

9 capture cells from the honeycomb plate and 2 capture cells from the coatings/solar cells experiment were deintegrated and delivered to the Technical University of Munich for further investigations.

##### 3.1.2 Complete Experiment

Visual inspections and thermooptical measurements have been conducted on

- Tray
- Honeycomb plate
- EECC cover
- EECC harness

##### 3.1.3 Individual Components

The coatings/solar cells experiment was deintegrated into individual components. Investigations conducted on individual components are summarized in Table 1. The cross sections of the individual components are shown in Figures 5 to 14.

#### 3.2 Results

The results are based on the following environmental conditions:

- The complete experiment was exposed to a LEO for over 5 1/2 years and was irradiated by about 11000 equivalent sun hours.
- The coatings/solar cells experiment was exposed to a LEO for about 9 months and was irradiated by about 1440 equivalent sun hours and about  $7 \times 10^{11}$  equivalent 1 MeV electrons for solar cells.

##### 3.2.1 Visual Inspection

###### 3.2.1.1 Complete Experiment

The anodized surfaces exposed to space turned to yellow colour. This is caused by contamination of the surfaces by contaminants from the space environment. This is highlighted by the particularly intensive yellow colouring of areas, where residues of adhesive from glueing activities were not removed totally. (Figures 15 and 16). Yellow colouring occurred also on transparent harness components by formation of colour centers and by contaminants.

After a over 5 1/2 years mission in a LEO only a few micrometeoroids/debris impacts could be detected, but the experiment contained the largest impact that occurred on LDEF (Figures 17 to 20).

#### 3.2.1.2 Individual Components

Coatings, solar cells, QCM - calorimeter and QCMs did not show significant changes except the SSM/IF/LS coating where unregularly distributed brown areas were visible (Figures 21 and 22). This is due to the complex and not yet fully harmonized composition of this coating. The space exposed surfaces of the anodized calorimeter support turned to yellow colour, which is caused by contaminants from space environment.

On each of the GEOS solar cell modules 3 of the 4 interconnectors were cracked, but an electrical contact was still available. One of the 3 interconnector fingers on a GEOS solar cell had a crack. All silver interconnectors turned to dark colour (Silversulfide)

### 3.2.2 Electrical Measurements

#### 3.2.2.1 Electrical Resistance

The  $\text{In}_2\text{O}_3$  - layers on the SSM/IF/LS and on the GEOS solar cells show good electrical behaviour. The square resistance is in the  $\text{k}\Omega$  range.

The increase of the electrical resistance in air is maximum 40% for the GEOS solar cells and maximum 400% for the SSM/IF/LS. The reason for this difference may be the fact that the SSM/IF/LS has a flexible substrate causing cracks in the  $\text{In}_2\text{O}_3$  - layer during alternating loads which increases the electrical resistance by itself and by formation of conduction restraining bulk defects. The results are presented in Table 2.

#### 3.2.2.2 Frequencies of QCMs

The QCM frequencies increased during the mission. The frequency of the QCM ( $\text{ZnS}$ ) increased relatively strong by 225 Hz and of the QCM ( $\text{In}_2\text{O}_3$ ) by 33 Hz only (column 3 of Table 3). Assuming a diameter of 3 Å for organic radicals and a density of 1,2  $\text{g}/\text{cm}^3$  and taking into account a change of 8 Hz per monolayer of the QCM frequency the contamination on the QCM ( $\text{ZnS}$ ) is about 28 monolayers (about 8nm) and on the QCM ( $\text{In}_2\text{O}_3$ ) about 4 monolayers (about 1nm). The thickness of the contamination is in the same order as found on the coating SSM/IF/LS and on the calorimeter support by XPS - analysis in chapter 3.2.4. It must be assumed, that a contamination of this range is deposited on all coatings and solar cells.

#### 3.2.2.3 Solar Cell Characteristics

A degradation of short circuit current  $I_{\text{sc}}$  respectively open circuit voltage  $V_{\text{oc}}$  by 3% respectively 1,5% for the OTS solar cell module and by 5% respectively 1% for the GEOS solar cell modules was not expected due to the low space environmental loads.

The reason for this behaviour is the type of solar cells used. The OTS solar cells as well as the GEOS solar cells are  $1\Omega\text{cm}$  cells and were produced by floating molten zone recrystallization method. Solar cells of this type are sensible to space radiation. The IV-characteristics of the solar cell modules are shown in Figures 23 and 24.

### 3.2.3 Thermo-optical Measurements

#### 3.2.3.1 Complete Experiment

The yellow colouring of the anodized surfaces did not cause a change of the  $\epsilon_{\text{H}}$  - values within the error of measurement, while the  $\alpha_{\text{s}}$  - values increased by up to 25%. This increase is caused by contamination.

The results of the thermo-optical measurements on the complete experiment are presented in Table 4.

### 3.2.3.2 Individual Components

The results of the thermo-optical measurements on individual components are shown in Table 5.

Though a contamination layer of 1 to 8 nm is expected on the single components the effect on the  $\epsilon_H$  - values is negligible and very low on the  $\alpha_s$  - values. The increase of the  $\alpha_s$  - values after the mission is within the error of measurement except the dark yellow areas on the calorimeter support.

- The SSM/IF does not show any changes in the  $\alpha_s$  -value and is thermo-optically very stable
- The  $\alpha_s$  - value of the SSM/IF/LS is 0,03 higher compared to the SSM/IF, due to the  $\text{In}_2\text{O}_3$  -layer. During mission the increase of the  $\alpha_s$  - value turned out as the highest of all coatings. The reason for this behaviour are the unregularly distributed brown areas on the surface with a shift of the interference filter reflection maximum to longer wave lengths, which is caused by a not yet identified disharmonic behaviour of the interference filter. By this fact the amount of reflection of the interference filter in the solar maximum is decreasing and as a consequence the PMMA intermediate layer, the FEP foil and the silver reflector cannot be protected sufficiently anymore. Thus induced degradation leads to increased absorption.
- On the yellow coloured sulfuric acid anodized surface of the calorimeter support the  $\alpha_s$  - values increased up to 5%. This is caused by the above mentioned contamination layer which creates a higher effect due to the porosity of the surface material.
- The OTS - and GEOS solar cells did not show any change in the  $\alpha_s$  - values, though this can be expected due to the degradation of the  $I_{sc}$  - values. This fact is confirming the assumption that the  $I_{sc}$  degradation is caused by the type of solar cells itself.
- The reference coatings SSM, ORS and Chemglaze Z 306 show very low changes in the  $\alpha_s$  - values.

### 3.2.4 Chemical Investigations

The EDX - and XPS - analyses indicate contamination layers on coatings, solar cells, QCMs and calorimeter support, containing mainly Si and C. From this it can be supposed that the contamination is composed of silicones. The XPS - analyses indicate a contamination layer of < 1nm on the SSM/IF/LS and of < 3 nm to > 3nm for the yellow coloured surfaces of the calorimeter support depending on the intensity of the yellow colour. The intensity of yellow colour is increasing with layer thickness.

IR - analyses on SSM/IF/LS indicate no chemical change of PMMA - and FEP - layer during the mission, which can be deduced from the nearly identical spectrum of control and flight samples. It seems, that the unregularly distributed brown areas are formed in the interface between the  $\text{In}_2\text{O}_3$  - and ZnS - layer, which leads finally to a shift of the interference filter reflection maximum to longer wave lengths.

In the micrometeoroid craters on the smaller EECC cover no foreign material from space could be detected.

### 3.2.5 Metallurgical Investigations

Microfractographical investigations were conducted on a broken loop interconnector of a GEOS solar cell module using a raster electron microscope. On the fracture a series of fine, parallel grooves can be detected, the so called oscillatory bands, which indicate the step by step advance of the delamination front under an oscillatory load and which characterize the microfractographical criterion of a fatigue fracture.

The solar cells were bonded to an aluminum structure and not to a carbon fiber sheet on a honeycomb structure usually used for solar panels. Thus thermal cycles caused a larger gap variation and thus imposed a higher mechanical load on the loop interconnectors. Therefore the fractional behavior of the loop interconnector is not fully representative for practice.

#### 4. CONCLUSIONS

The conclusions from the results of the LDEF experiment evaluation are:

- Complete experiment

The complete experiment was exposed to a LEO environment for over 5 1/2 years. All space exposed anodized surfaces turned to yellow colour with a respective increase of solar absorptivity  $\alpha_s$  ( $\Delta \alpha_s < 0.07$ ). A particularly intensive yellow colouring can be detected on areas, where residues of adhesive have not been removed totally ( $\Delta \alpha_s < 0.12$ ). The  $\epsilon_H$  - values did not change within the error of measurement. On the one hand the increase of  $\alpha_s$  of anodized surfaces has to be considered in thermal analysis; on the other hand attention must be paid to the fact that residues of adhesives have to be removed totally. Anodized surfaces are very sensitive to contamination. A low number of micrometeoroid impacts could be detected. The diameters of the impacts are mostly between 0.1 to 0.5 mm. Only one large impact of 1x3 mm in dimension could be detected and was probably caused by a piece of debris. No atomic oxygen degradation could be detected. This was due to the experiment being located on the trailing edge of LDEF.

- Individual components

The individual components of the coatings/solar cells experiment were exposed to space in a LEO for about 9 months.

QCM measurements and physical surface analyses indicate a contamination layer between 1 and 8 nm on all space exposed surfaces.

The contamination does not influence the thermal emissivity  $\epsilon_H$ , while the solar absorptivity  $\alpha_s$  is increased for most components by a small amount. An influence of the contamination on the electrical conductivity of the  $\text{In}_2\text{O}_3$  layer could not be detected.

- Developed Coatings

SSM/IF and SSM/IF/LS were developed under government contract and are designed to be space qualified.

- SSM / IF

This coating shows excellent behavior. Laboratory results (Ref 1) are confirmed.

$$\alpha_s = 0.11; \Delta \alpha_s = 0$$

$$\epsilon_H = 0.77; \Delta \epsilon_H = 0$$

- SSM / IF / LS

This coating shows good behavior, as far as thermooptical characteristics and electrical conductivity are concerned. Laboratory results (Ref 1) are confirmed.

$$\alpha_s = 0.14; \Delta \alpha_s = 0.02$$

$$\epsilon_H = 0.75; \Delta \epsilon_H = 0$$

$$R(\text{In}_2\text{O}_3) \approx 6 \text{ k}\Omega$$

- SSM, ORS and Chemglaze Z 306

The coatings SSM and ORS served as reference coatings for SSM/IF and SSM/IF/LS. SSM and ORS show very good behavior.

The same holds for Chemglaze Z 306 which served as a relative sun sensor.

- SSM:

$$\alpha_s = 0.10; \Delta \alpha_s = 0.01$$

$$\epsilon_H = 0.77; \Delta \epsilon_H = 0.01$$

- OSR:
  - $\alpha_s = 0.08; \Delta \alpha_s = 0.01$
  - $\epsilon_H = 0.78; \Delta \epsilon_H = 0.01$
- Chemglaze Z 306:
  - $\alpha_s = 0.96; \Delta \alpha_s = -0.02$
  - $\epsilon_H = 0.90; \Delta \epsilon_H = 0.01$
- Anodized surfaces
 

The space exposed sulfuric acid anodized surfaces of the calorimeter support show yellow colouring and increased absorptivity  $\alpha_s$  ( $\Delta \alpha_s < 0.02$ ). This increase has to be considered in thermal analysis.
- Solar Cells
 

The GEOS solar cells were also developed under government contract. The electrically conductive layer on the solar cells and the pertaining interconnections are designed to be space qualified.

  - GEOS solar cells
 

The electrically conductive layer on the cover glasses shows excellent behavior. Concerning the power the solar cell proved to be fairly stable only.

$R(\text{In}_2\text{O}_3) \approx 4 \text{ k } \Omega$

$\Delta I_{sc} = -5\%; \Delta V_{oc} = -1\%$
  - OTS solar cells
 

This solar cell served as a reference for the GEOS solar cell. Concerning the power the solar cell proved to be fairly stable only.

$\Delta I_{sc} = -3\%; \Delta V_{oc} = -1,5\%$
- General remarks
 

In general the results of the LDEF-Experiment S 1002 are interesting and important but not spectacular. The coatings and solar cells investigated exhibited good behavior under space conditions in a LEO.

Considering both laboratory results (Ref 1) and results of the LDEF mission it can be concluded that the components investigated are space qualified.

## 5. REFERENCES

- (Ref 1) L. Preuss et. al., Qualifikation flexibler SSM hoher Laufzeitstabilität,  
 MBB-Bericht Nr. UR-436/80  
 DFVLR / BPT-Vertrag Nr. 01 TB 067B-AK / RT - WRT 2076



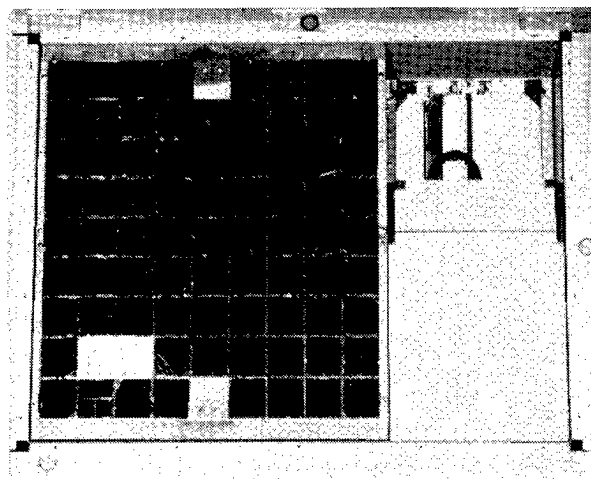


Figure 1: Experiment after mission

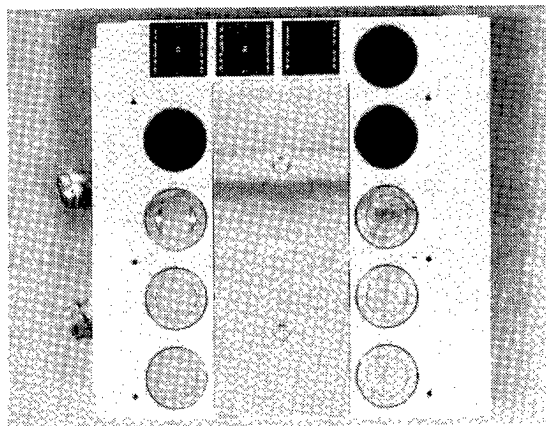


Figure 4: Coatings/solar cells experiment

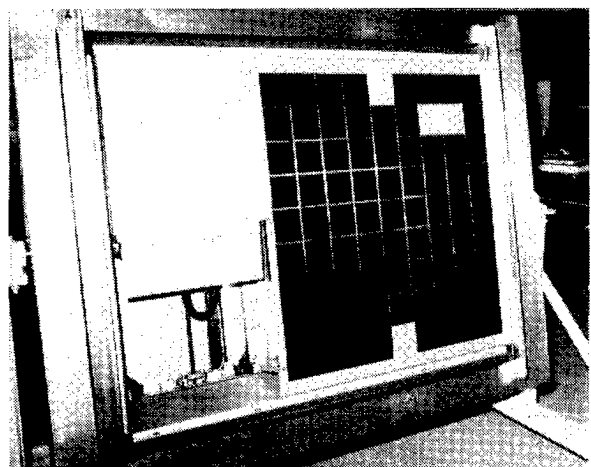


Figure 2: Experiment before mission

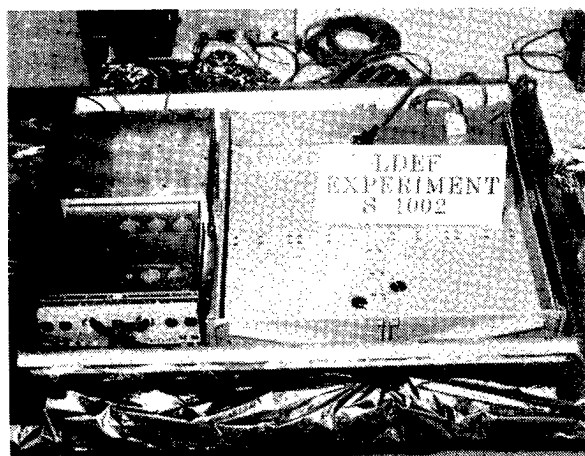


Figure 3: Experiment with honeycomb plate removed and EECC - drawer open

	ZnS	$\lambda/4$
	$\text{Al}_2\text{O}_3$	$\lambda/4$
	ZnS	$\lambda/4$
	$\text{Al}_2\text{O}_3$	$\lambda/4$
	ZnS	$\lambda/4$
	$\text{Al}_2\text{O}_3$	$\lambda/4$
	ZnS	$\lambda/4$
	Al	20 Å
	Teflon	127 $\mu\text{m}$
	Al	20 Å
	Ag	1700 Å
	Inconel	200 Å
	DC 93500	20 $\mu\text{m}$
	Al	

Figure 5: Configuration SSM/IF

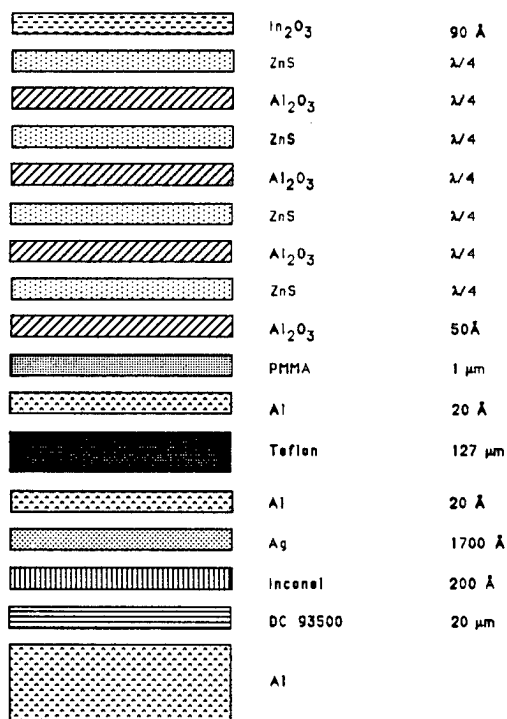


Figure 6: Configuration SSM/IF/LS

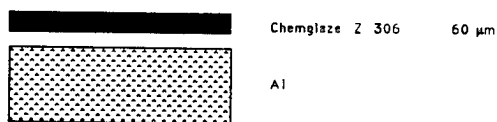


Figure 9: Configuration Chemglaze Z 306

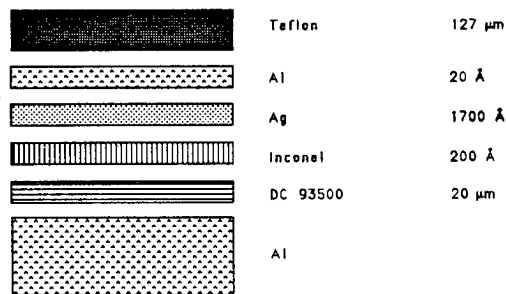


Figure 7: Configuration SSM

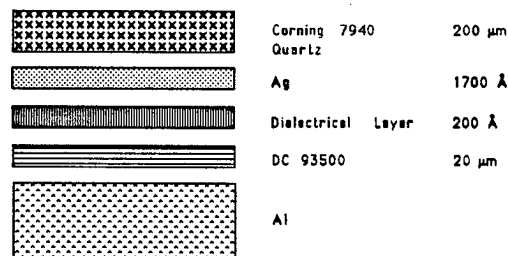


Figure 8: Configuration OSR

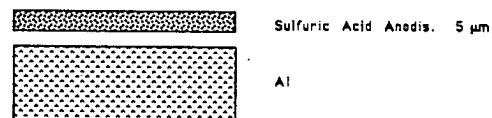


Figure 10: Configuration Calorimeter Support

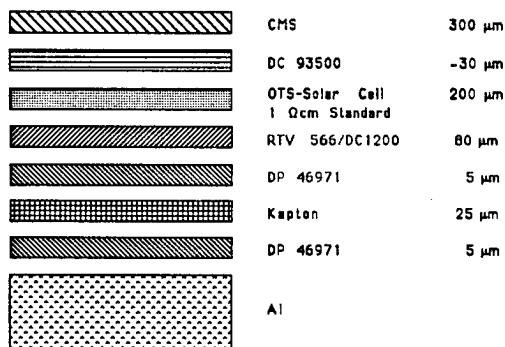


Figure 11: Configuration OTS solar cell module

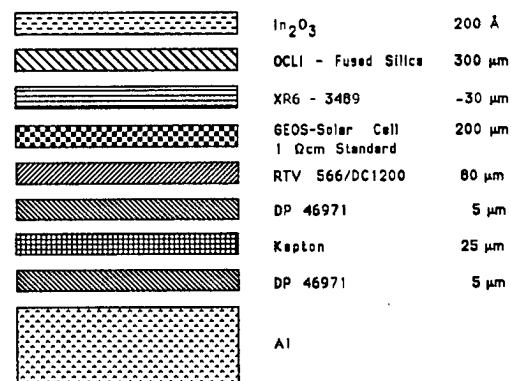


Figure 12: Configuration GEOS solar cell module

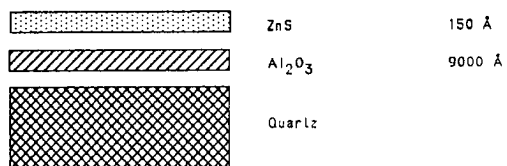


Figure 13: Configuration QCM(ZnS)

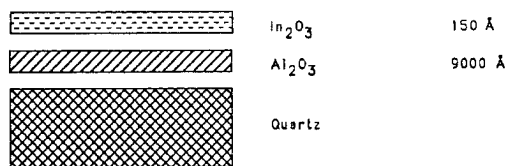


Figure 14: Configuration QCM(In<sub>2</sub>O<sub>3</sub>)

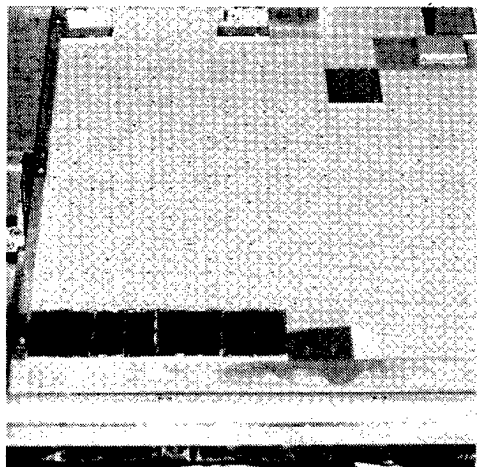


Figure 15: Yellow colouring on tray and honeycomb plate

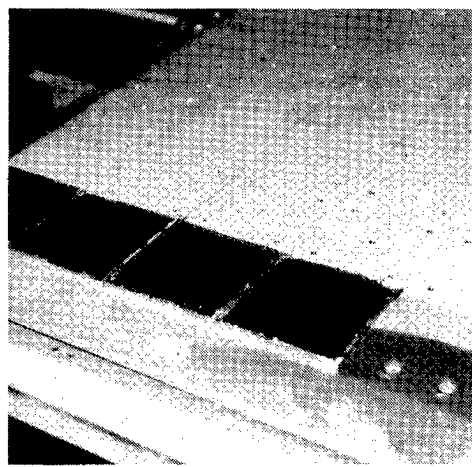


Figure 16: Yellow colouring on tray and honeycomb plate in detail

(See color photographs, p. 1702.)



Figure 17: Impact 1 x 3 mm on honeycomb plate



Figure 18: Impact 1 x 3 mm on honeycomb plate in detail

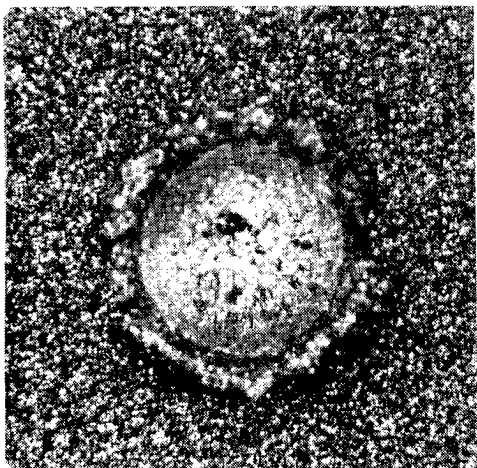


Figure 19: Impact 0,5 mm on EECC cover

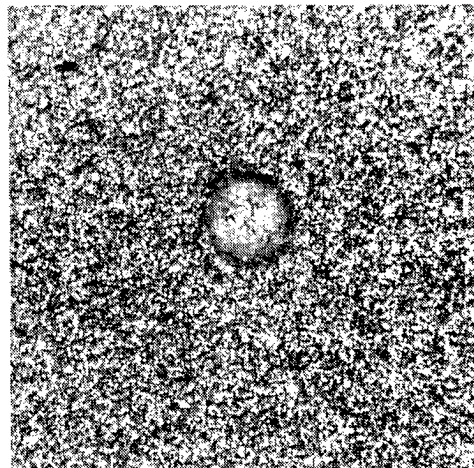


Figure 20: Impact 0,2 mm on EECC cover

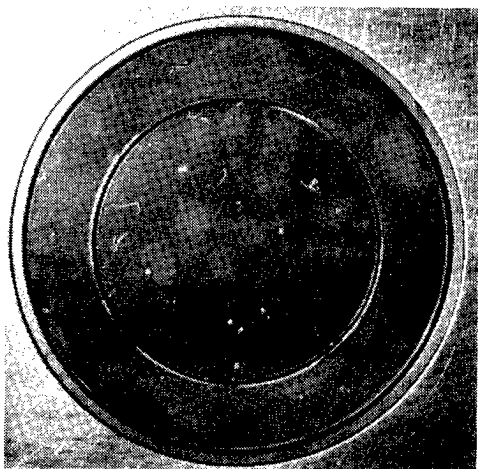


Figure 21: SSM/IF/LS



Figure 22: SSM/IF/LS in detail

(See color photographs, p. 1702.)

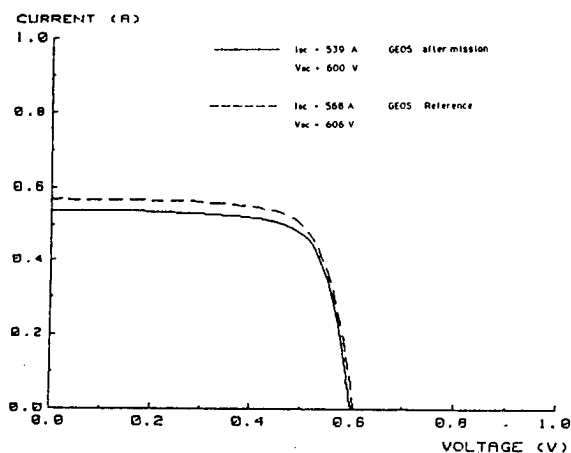


Figure 23: IV - Characteristic GEOS solar cell module

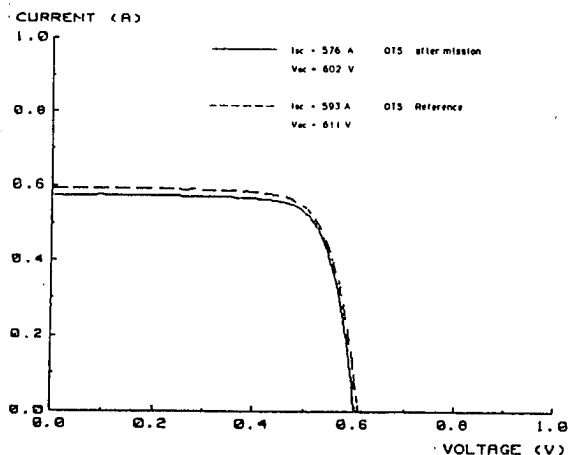


Figure 23: IV - Characteristic OTS solar cell module

Table 1: Single Components and Investigations

Components	Figure Nr.	Visual Inspection	Electrical Measurements	Thermoopt. Measurements	Chem. Investigations	Metallurg. Investigations
SSM/IF	5	x		x	x	
SSM/IF/LS	6	x	x	x	x	
SSM	7	x		x	x	
OSR	8	x		x	x	
Chemglaze Z306	9	x		x	x	
Calorimeter Support	10	x		x	x	
GEOS-Sol.Cell Module	11	x	x	x	x	x
OTS-Sol.Cell Module	12	x	x	x	x	
QCM (ZnS)	13	x	x		x	
QCM (In <sub>2</sub> O <sub>3</sub> )	14	x	x		x	

**Legend:**

SSM	Second Surface Mirror	Chemglaze Z306	Black Coating
IF	Interference Filter	QCM	Quartz Crystal
LS	Conductive Layer (In <sub>2</sub> O <sub>3</sub> )		Microbalance
OSR	Optical Solar Reflector	GEOS, OTS	Satellites

Table 2: Electrical Resistance of  $\text{In}_2\text{O}_3$  - Layers

Date	23.03.79	29.11.83	12.03.90	18.05.90	22.05.90	30.05.90
Conditions	under Atmosphere	EECC closed under Atmosphere	EECC closed under Vacuum	EECC closed under Atmosphere	EECC open under Atmosphere	
Sample	Electrical Resistance R ( kΩ )					
Flight - SSM/IF/LS	6,2	8,4	3,6	4,6	7,6	21,8
Control - SSM/IF/LS	0,85	-	-	-	-	0,9
Flight - GEOS - Solar cell module11	4,2	-	-	-	4,2	4,4
Flight - GEOS - Solar cell module 12	4,8	5,0	4,6	5,2	5,5	6,9
Control - GEOS - Solar cell module 10	3,9	-	-	-	-	4,6
Control - GEOS - Solar cell module 1	4,7	-	-	-	-	5,2

Table 3: Frequencies of QCMs

Column	1	2	3	4	5	6
Date	23.03.79	29.11.83	12.03.90	18.05.90	22.05.90	30.05.90
Conditions	under Atmosphere	EECC closed under Atmosphere	EECC closed under Vacuum	EECC closed under Atmosphere	EECC open under Atmosphere	
Sample	Beat - Frequency ( Hz )					
QCM (ZnS)	1120	1027	1252	1252	1326	1339
QCM (In <sub>2</sub> O <sub>3</sub> )	2444	2322	2355	2377	2452	2473

Table 4: Thermo-optical Characteristics of Complete Experiment Components

Component	$\alpha_s$	$\Delta\alpha_s$ (%)	$\epsilon_H$	$\Delta\epsilon_H$ (%)
Tray - Rim				
- space exposed area	$0,38 \pm 0,03$	15	$0,22 \pm 0,02$	0
- area covered by bracket	$0,33 \pm 0,03$	0	$0,22 \pm 0,02$	0
Honeycomb Plate				
- space exposed contaminated dark-yellow area	$0,60 \pm 0,03$	25	$0,65 \pm 0,04$	3
- space exposed middle-yellow area	$0,53 \pm 0,03$	10	$0,64 \pm 0,04$	2
- space exposed light-yellow area	$0,49 \pm 0,03$	2	$0,63 \pm 0,04$	0
- area covered by micrometeoroid capture cells	$0,48 \pm 0,03$	2	$0,63 \pm 0,04$	0
EECC - Cover large				
- space exposed area	$0,36 \pm 0,03$	24	$0,19 \pm 0,02$	-5
- values before flight	$0,29 \pm 0,03$	0	$0,20 \pm 0,02$	0
EECC - Cover small				
- space exposed area	$0,36 \pm 0,03$	24	$0,20 \pm 0,02$	5
- values before flight	$0,29 \pm 0,03$	0	$0,19 \pm 0,02$	0

Table 5: Thermo-optical Characteristics of Single Components

Component	$\alpha_s$	$\Delta\alpha_s$ (%)	$\epsilon_H$	$\Delta\epsilon_H$ (%)
Flight - SSM/IF 1	$0,11 - 0,02$	0	$0,77 \pm 0,04$	0
Flight - SSM/IF 2	$0,11 - 0,02$	0	$0,77 \pm 0,04$	0
Control - SSM/IF 1 and 2 mean value	$0,11 - 0,02$	0	$0,77 \pm 0,04$	0
Flight - SSM/IF/LS 3	$0,16 - 0,02$	14	$0,75 \pm 0,04$	0
Flight - SSM/IF/LS 4	$0,16 - 0,02$	14	$0,75 \pm 0,04$	0
Control - SSM/IF/LS 5 and 6 mean val.	$0,14 - 0,02$	0	$0,75 \pm 0,04$	0
Flight - SSM 5	$0,11 - 0,02$	10	$0,78 \pm 0,04$	1
Control - SSM 9	$0,10 - 0,02$	0	$0,77 \pm 0,04$	0
Flight - OSR 6	$0,09 - 0,02$	13	$0,79 \pm 0,04$	1
Control - OSR 10	$0,08 - 0,02$	0	$0,78 \pm 0,04$	0
Flight - Chemglaze 7	$0,94 \pm 0,01$	2	$0,89 \pm 0,05$	1
Control - Chemglaze 12	$0,96 \pm 0,01$	0	$0,90 \pm 0,05$	0
Calorimeter support				
- space exposed dark-yellow area	$0,40 \pm 0,01$	5	$0,76 \pm 0,04$	0
- space exposed middle-yellow area	$0,39 \pm 0,01$	3	$0,76 \pm 0,04$	0
- Control area protected from space	$0,38 \pm 0,01$	0	$0,76 \pm 0,04$	0
- Flight - OTS - Solar cell module 13	$0,83 \pm 0,01$	1	$0,79 \pm 0,04$	0
- Control - OTS - Solar cell module 5	$0,82 \pm 0,01$	0	$0,79 \pm 0,04$	0
- Flight - GEOS - Solar cell module 12	$0,81 \pm 0,01$	0	$0,77 \pm 0,04$	0
- Flight - GEOS - Solar cell module 11	$0,81 \pm 0,01$	0	$0,77 \pm 0,04$	0
- Contr. - GEOS - Solar cell module 10	$0,81 \pm 0,01$	0	$0,77 \pm 0,04$	0
- Contr. - GEOS - Solar cell module 1	$0,81 \pm 0,01$	0	$0,77 \pm 0,04$	0

LDEF SP-HVDE(SPACE PLASMA-HIGH VOLTAGE DRAINAGE EXPERIMENT) POST-  
FLIGHT RESULTS : LEAKAGE CURRENT AND DISCHARGE

J.Y. YAUNG, W.C. Wong, B.K. Blakkolb  
L.E. Ryan, J.E. Chedotte & W.W.L. Taylor  
TRW, Space & Technology Group  
One Space Park  
Redondo Reach, CA 90278  
Phone: 213/812-7176, Fax: 213/812-1277

SUMMARY

TRW designed and fabricated two identical SP-HVDE trays which were flown in the NASA LDEF(Long Duration Exposure Facility) for five and three-fourth years in the LEO(Low Earth Orbit) environment. One tray was placed near the leading edge and one near the trailing edge, and investigations have been performed to compare the environmental interactions on the dielectric samples of the two trays. Each tray consisted of six assemblies with Kapton dielectric samples of varying thicknesses (i.e., 2 mils, 3 mils, and 5 mils) biased under  $\pm 300$  V,  $\pm 500$  V, and  $\pm 1000$  V. The original objective has been successfully achieved by measuring the first in-flight average leakage current through the samples. Less than 5% of the post-flight coulometers behaved anomalously. The data should be valuable to the design and evaluation of spacecraft with high voltage systems. M/D (Micrometeoroid and Debris) impacts over the dielectric samples were examined using a SEM(Scanning Electron Microscope) and an EDS(Energy Dispersive X-ray Spectrometer). These impact sites were sprayed by silver which were most likely caused either by the impact or a "local ESD" (Electrostatic Discharge).

INTRODUCTION

TRW's SP-HVDE on LDEF provides the first in-flight investigation of current through biased dielectric films.

The LEO environment is characterized by cosmic rays, ultraviolet light, high energy positive ions and electrons, micrometeoroids and debris(M/D), atomic oxygen, and molecules. The



leading-edge surface of the SP HVDE saw micrometeoroids and debris as well as energetic atomic oxygen, whereas the trailing-edge tray saw no energetic atomic oxygen and only a small flux of space debris, relative to the leading-edge tray. Both trays were exposed to UV, cosmic rays, and ionizing radiation (less at the trailing-edge).

The LDEF trapped proton and electron environment is available in reference 1, where the plasma environment was calculated through the following codes: AP8MIN and AP8MAX (ref. 2) and AE8MIN and AE8MAX (refs. 3 & 4). The plasma environment contributes the major source of the leakage currents. The cosmic rays cause much less impact to the experiment since they tend to penetrate the samples. The electromagnetic radiation environment is also of minor interest, for it will induce insignificant leakage current through photoabsorption process in our experimental samples.

The M/D and atomic oxygen combined play an important role in degrading the characteristics of the key materials which subsequently affect the average leakage current data. For example, the M/D impacts will degrade the dielectric material which would cause more leakage current. Also, possible local ESDs will cause additional power loss to high voltage systems deployed in the LEO space environment. Atomic oxygen can erode surface material as demonstrated in the samples of the leading-edge tray. Since the TRW SP-HVD Experiment was performed during the first 233 days of the mission, dielectric material thickness reduction caused by atomic oxygen during that time should be less than a quarter mil which would not make any significant impact.

#### EXPERIMENT HARDWARE DESCRIPTION

LDEF consisted of 57 experiments. TRW designed and fabricated two experiment trays which were flown with other experiments for the unexpected five and three-fourth years in the LEO environment. By placing the two identical trays with one near the leading edge (D-10) and the other near the trailing edge (B-4) (fig. 1), average leakage currents were obtained for two different exposure geometries. The experiment was designed to investigate the long term leakage of dielectric materials under high voltage bias. Other benefits such as material degradations caused by the LEO environment and functional degradation of high voltage systems can be investigated. The material investigation related to the two experiment trays was reported in another paper (ref. 5).

Each tray is a combination of three thicknesses of kapton dielectric samples (2 mils, 3 mils, and 5 mils) coated on one side

with Vapor Deposited Aluminum(VDA). The VDA side of these samples were bonded to the glass/epoxy substrate with Eccobond 57C, which is a 60 wt% silver loaded epoxy (figure 2). Figure 3 shows the electrical configuration. The long-term average leakage currents are determined by using coulombmeters via a matrix of dielectric samples of different thicknesses and biases comprising 21 dielectric samples per tray. The average leakage currents (figs. 4-5) show significant contrasts between the leading-edge and trailing-edge trays.

Figure 3 depicts the SP-HVDE coulombmeter current and voltage integration configuration. These Plessey coulometers had been rated to 10,000 mA \* sec by the manufacturer. They can record currents flowing in either direction by either deplating or plating the electrode. The coulombmeter was used as either a leakage current time integrator or a bias voltage time integrator. Of the 152 coulombmeters, six showed anomalies during data retrieval, indicating a failure percentage less than 5%. The anomalies among the six coulometers are : 1) Three of them were "open circuit" such that our readout equipment would not deplete the coulombmeter. 2) The other three were "short circuit" and showed no sign of completion of deplating.

A detailed analysis of a dielectric sample was performed using a Cambridge S-360 SEM(Scanning Electron Microscope) System configuration with a Kevex EDS (see figures 6 & 7). The surface morphology of a large pit and a small pit shows light color deposits scattered around the vicinity. The elemental composition of the light color deposits determined by EDS is mainly silver which may be from the Eccobond adhesive.

#### POST-FLIGHT RESULTS AND DISCUSSION

From these coulombmeter data, the average leakage currents were obtained for various samples on the two trays. The data (see figs. 4-5) show significant contrasts between the leading-edge and trailing-edge trays. Two mil thick samples seem to have the smallest average leakage current.

For positively biased samples(fig. 4), the leakage currents collected during ground tests increase with biasing voltage. One group of data follows the trend of ground test data(refs. 6-7), i.e., currents collected at the 3-mil trailing-edge sample and at the 2-mil leading-edge sample. The other group of data (i.e., the data with other thicknesses) shows an unexpected decreasing trend for data biased at 500 V and 1000 V.

For the samples with negative biases(fig. 5), the data show strong dispersion at -300 V (especially those of the trailing-edge tray) and reach a plateau at -1000 V for both trays. The results showing leakage current limitation at -1000 V and overall lower leakage currents compared to those collected at the positively biased samples is consistent with ground test data. Discharges were observed in the ground tests(refs. 6-9) and may be used to explain the limiting of leakage currents collected at the samples with high voltage biases.

#### SEM/EDS CHARACTERIZATION

A dielectric sample (6" x 7" size) from the top left corner of the leading-edge (D10) tray (i.e., the sample with 1000 V bias) was characterized using SEM/EDS. The sample was removed from the tray by cutting through the glass/epoxy support structure using a CO<sub>2</sub> laser. Examination of charred edges showed no apparent heat effect on the adjacent dielectric material, which consisted of a 2 to 5 mil thick Kapton layer on top of 0.1 micron thick Vapor-Deposited-Aluminum (VDA) film. This dielectric material was bonded to the glass/epoxy substrate with Eccobond 57C, which is a 60 wt% silver loaded epoxy.

Visual examination of the surface of the dielectric layer (after almost six years in LEO) revealed that nearly all of the Kapton layer was lost for the leading edge tray samples due to atomic oxygen erosion, leaving partially etched VDA film exposed directly to the environment. There were three large pits about 10 mil in diameter and several small pits of about 1 mil in diameter on the outer surface of VDA film.

A detailed analysis of the sample was performed using a Cambridge S-360 SEM and a Kevex EDS system. The surface morphology and feature of a large pit and a small pit are shown in figures 6 and 7, respectively. They are typical of pits that have been analyzed. The feature in figure 6 consists of a central pit with light color deposits in the vicinity. The elemental composition of the light color deposits determined by EDS is mainly silver(Ag). The most likely source of Ag is from the Eccobond adhesive. Foreign matter of cosmic sources was not detected inside or in the vicinity of the pit. The silver deposits were most likely caused by either a hypervelocity impact by micrometeoroid/debris or possibly by a local ESD. The continuous glass fibers of the support structure are clearly visible inside the pit. The coverage of VDA film is discontinuous with dark patches distributed randomly throughout the surface. The EDS spectrum for the dark patches is comprised of carbon(C), oxygen(O), chlorine(Cl), aluminum(Al) and

silver(Ag) which may be Eccobond adhesive. Figure 7 shows the unusual morphology of a small pit. The sponge-like structure of deposits is most likely caused by the selective erosion of organic components of the Eccobond adhesive by atomic oxygen at inclined angles.

## CONCLUSIONS & RECOMMENDATIONS

1. The leakage current data were retrieved from more than 95% of the coulometers. The failed coulometers are candidates for functional failure testing and analysis.
2. The average leakage current through 2-5 mil Kapton films when biased between 300 V and 1000 V was about  $52-70 \mu\text{A}/\text{m}^2$ . The average leakage current through 2-5 mil Kapton films when biased between -300 V and -1000 V was about  $9-18 \mu\text{A}/\text{m}^2$ .
3. The data derived from the two trays needs further analysis. End-to-end analysis associated with computer modeling and simulation should be performed to investigate the generation and collection of leakage current for high voltage systems in the LEO environment.
4. The differences and similarities between the first long-term flight data and ground test data should trigger further studies for better understanding the environmental interactions under combined space environment.
5. Combined energetic atomic oxygen, micrometeoroid and debris exposure has the potential of degrading spacecraft surface materials. Even in the absence of atomic oxygen effects, surfaces may be adversely affected by hypervelocity particulate impacts. Molecular contamination can even complicate the surface physical properties. System impacts of M/D with or without atomic oxygen and contamination on high voltage systems should be studied.
6. The hypervelocity particulate impact phenomenology should be studied. Through a controlled ground experiment and computer simulation, one can better understand the mechanism of the silver spreading phenomenon and further investigate possible existence of local ESDs through M/D sites for high voltage systems in the LEO environment.

## ACKNOWLEDGMENTS

We acknowledge the financial support of the NASA LDEF project through Langley Research Center. The guideline and encouragement from W. Kinard and J. Jones of LaRC have been very helpful. Discussions with N. J. Stevens and S. L. Moses of TRW have made the investigations more profound. We would like to thank the support from the following TRW managers: S. K. Young, D. Arnush, A. J. Masley, G. T. Rosiak, H. M. Rosner, M. J. Santy, L. A. Rosales, and I. B. Gordon. Without their support the investigations would be impossible.

## REFERENCES

1. Edited by E.V. Benton and W. Heinrich, "Ionizing Radiation Exposure of LDEF", August 1990, USF-TR-77.
2. Sawyer, D.M. and J.I. Vette, "AP8 Trapped Proton Environment for Solar Maximum and Solar Minimum", National Space Science Data Center, Goddard Space Flight Center, NSSDC/WDC-A-R&S 76-06 June (1976). Also see NASA TM-X-72605
3. Teague, M.J. and J.I. Vette, "A Model of the Trapped Electron Population for Solar Minimum", National Science Data Center, Goddard Space Flight Center, NSSDC 74-03(1974).
4. Teague, M.J. et. al., "AE6: A Model Environment of the Trapped Electrons for Solar Maximum", National Science Data Center, Goddard Space Flight Center, NSSDC/WDC-A-R&S 76-04 (1976).
5. B.K. Blakkolb, J.Y. Yaung, W.W.L. Taylor, and L.E. Ryan, "LEO Space Environmental Effects on Materials : TRW LDEF Experimental Trays", NASA LDEF 1st Conference, June 2-8, 1991.
6. N.J. Stevens, et al., "Investigation of high Voltage Spacecraft System Interactions with Plasma Environments", NASA TM-78831, 1978.
7. Cole, R. K., Ogawa, H.S., & Sellen, J.M., "Operation of Solar Cell Arrays in Dilute Streaming Plasmas", AIAA paper No. 69-262, 1969.
8. Nahra, H. K., Felder M. C., Sater B. L. and Staskus J. V., "The Space Station Photovoltaic Panels Plasma Interaction Test Program : Test Plan and Results", NASA TM-102474, 1990.
9. Kuninaka, H. et.al., "High Voltage Solar Array Interacting with Ionospheric Plasma", Space Power, Vol.8 Nos. 1/2, 1989.

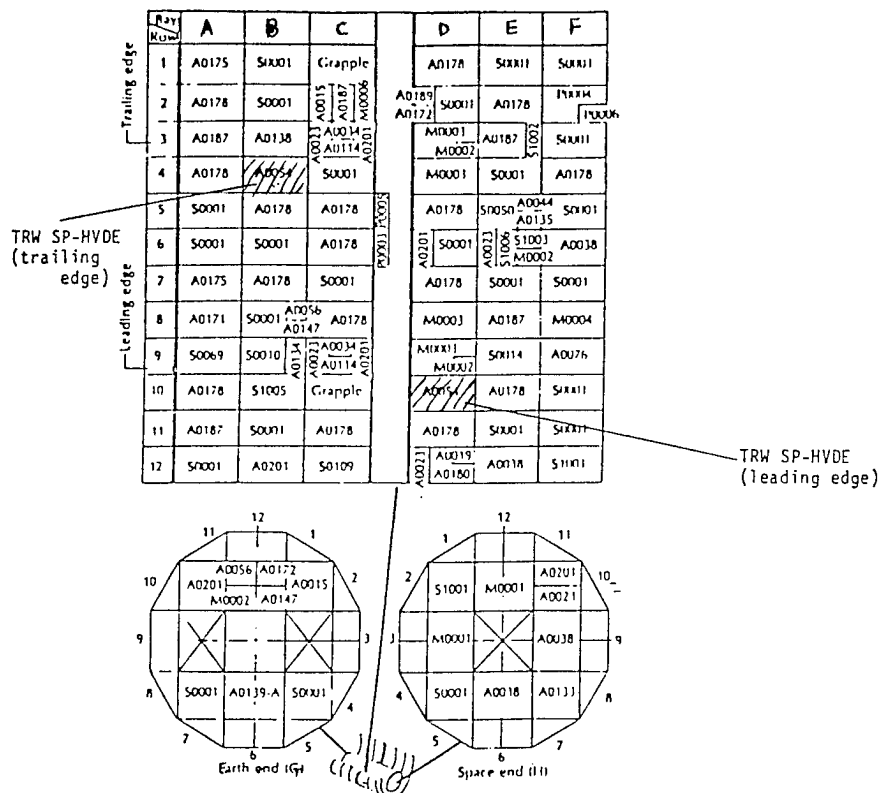


Figure 1.

Layout of Experiment Trays on the LDEF  
(TRW Trays Located at B-4 & D-10).

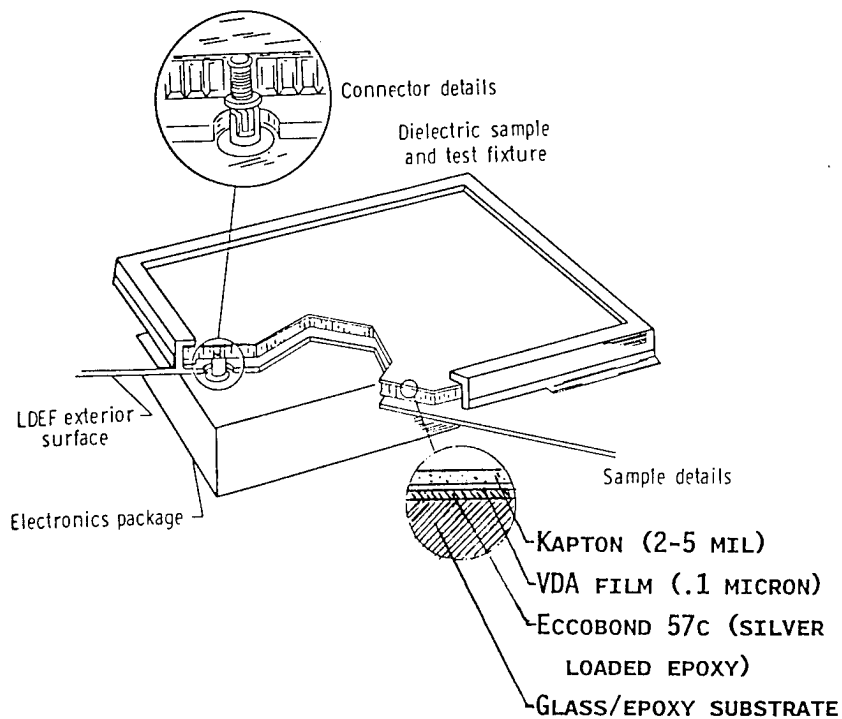


Figure 2.

Laboratory Model Dielectric Sample Construction.

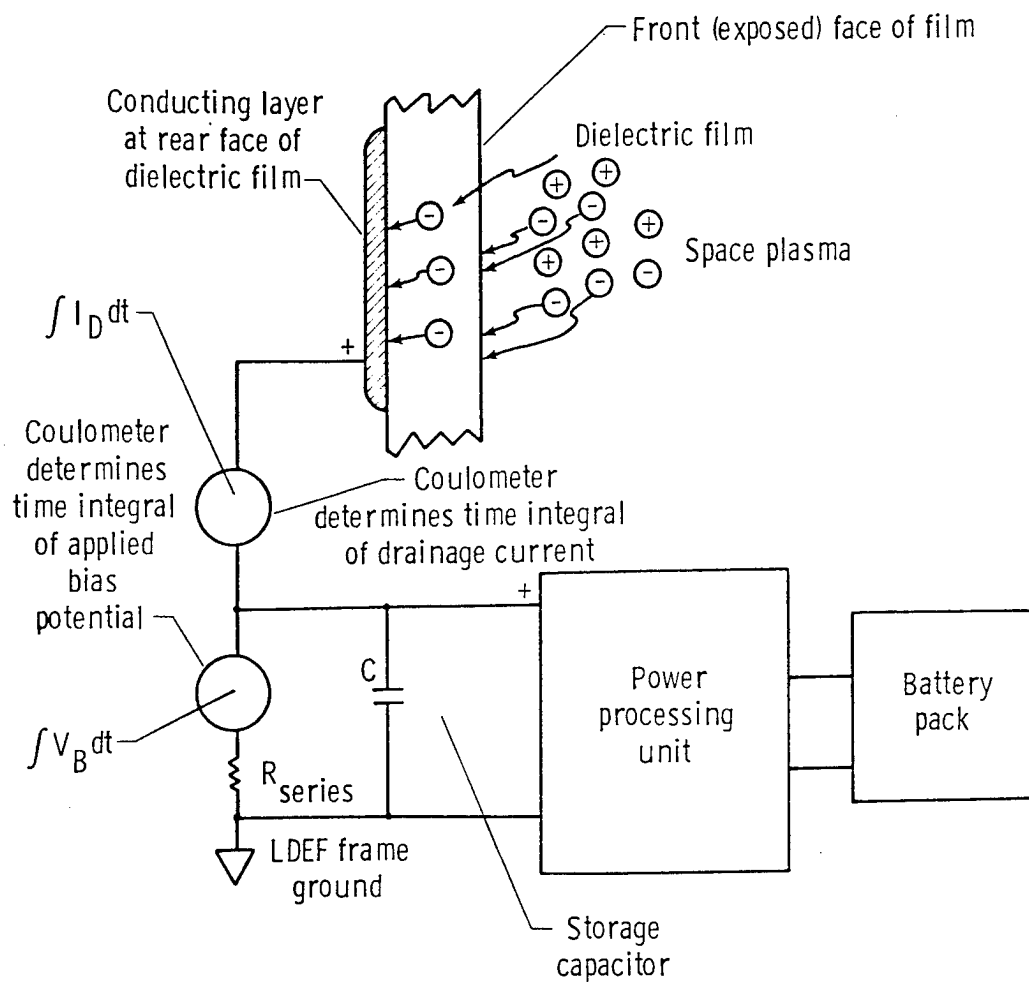


Figure 3.

High Voltage Drainage Experiment Configuration.

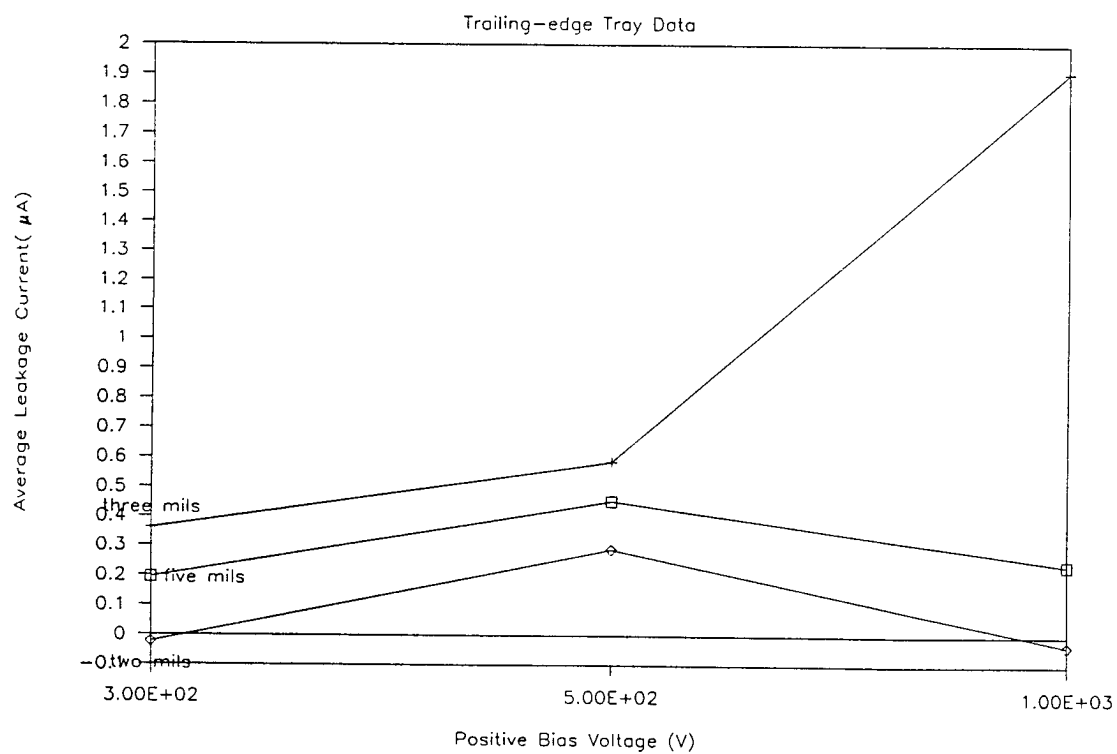
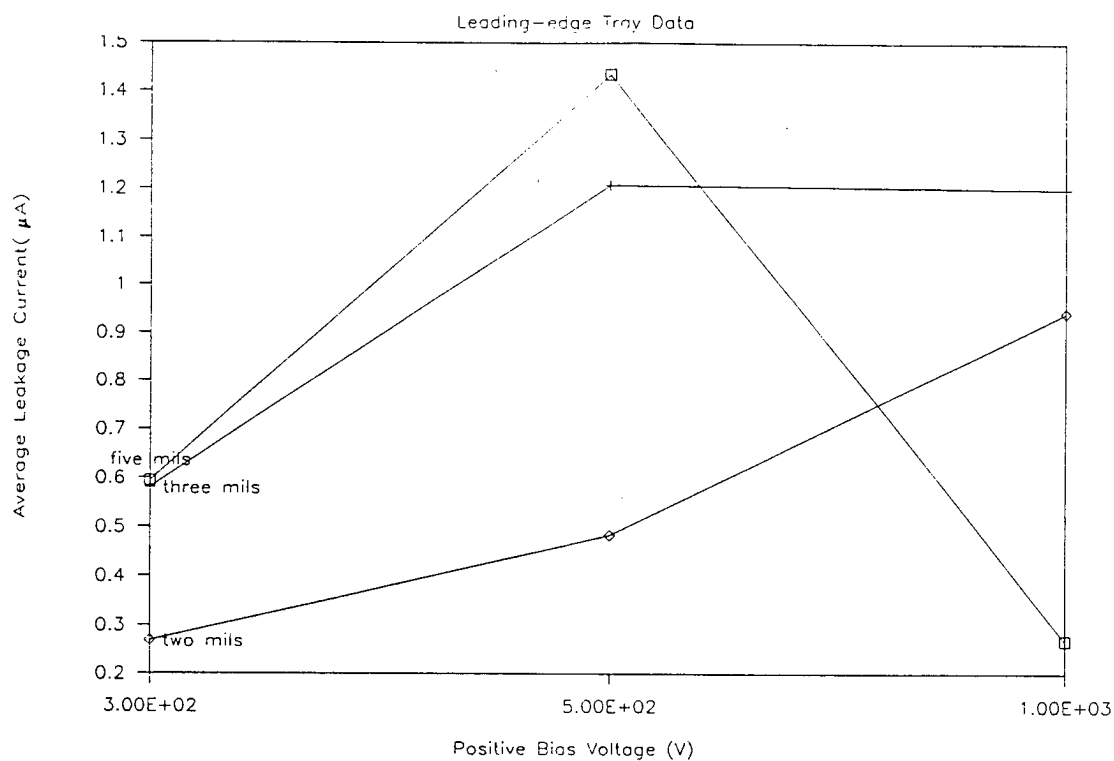


Figure 4.

LDEF Average Leakage Currents Collected at the Positively Biased Samples for Both TRW Trays.



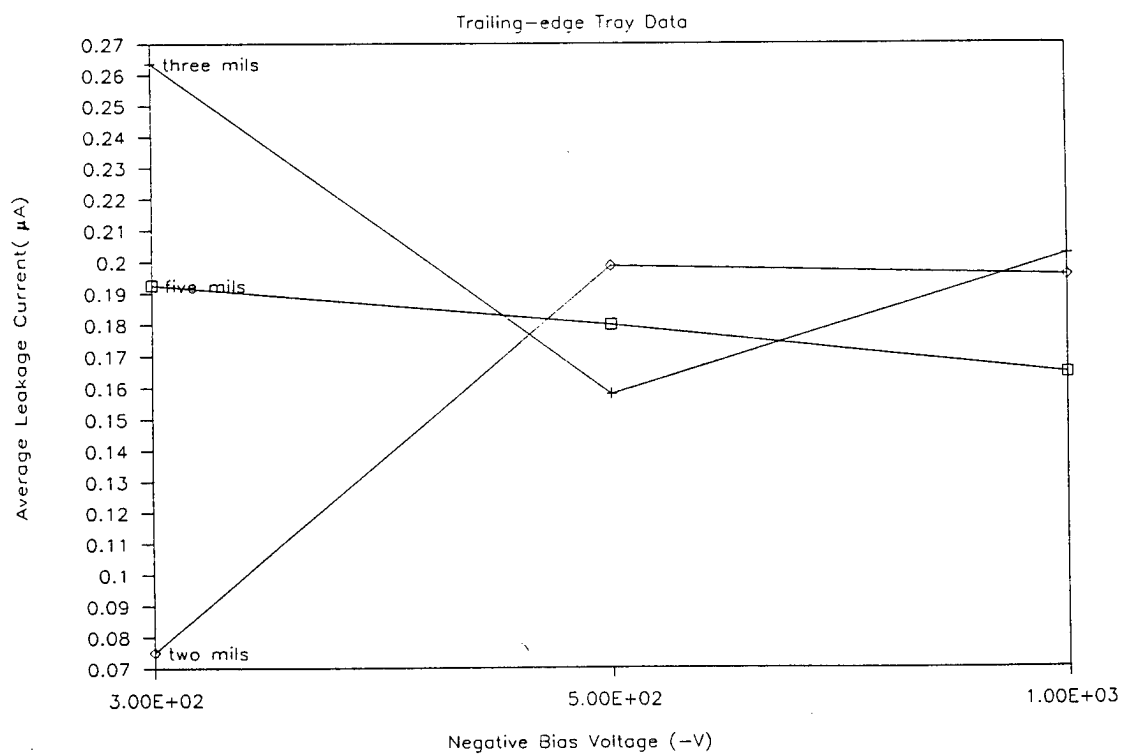
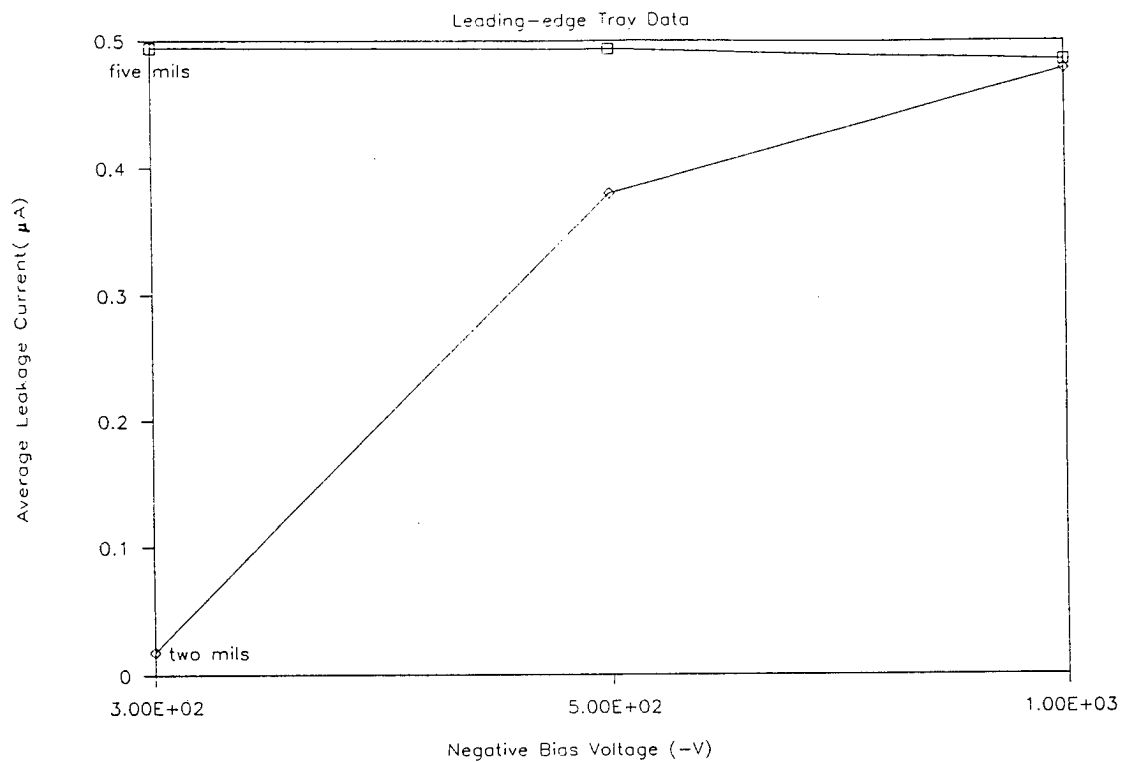
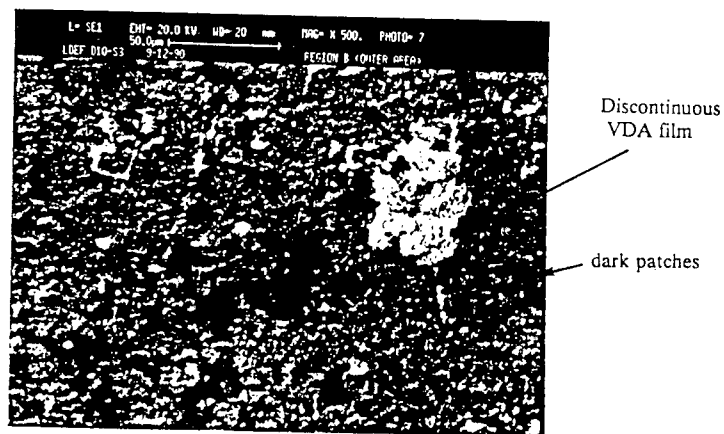


Figure 5.

LDEF Average Leakage Currents Collected at the Negatively Biased Samples for Both TRW Trays.



(a) Magnification at 50X



(b) Magnification at 500X

Figure 6.

Photomicrographs of a Typical Large Pit on the Dielectric Surface

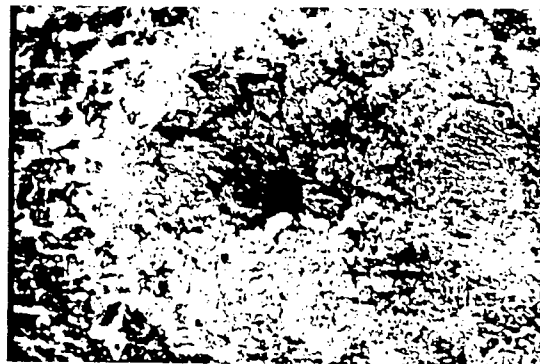


Figure 7.

Photomicrograph of a Typical Small Pit on the Dielectric Surface at 1KX.

Original photos not available.

LONG DURATION EXPOSURE FACILITY (LDEF)  
LOW TEMPERATURE HEAT PIPE EXPERIMENT PACKAGE (HEPP)  
FLIGHT RESULTS

Roy McIntosh  
NASA Goddard Space Flight Center  
Greenbelt, MD 20770  
Phone: 301/286-3478, Fax: 301/286-6237

Craig McCreight  
NASA Ames Research Center  
Moffett Field, CA

Patrick J. Brennan  
OAO Corporation  
Greenbelt, MD 20770  
Phone: 301/345-0750, Fax: 301/286-6237

### SUMMARY

The Low Temperature Heat Pipe Flight Experiment (HEPP) is a fairly complicated thermal control experiment that was designed to evaluate the performance of two different low temperature ethane heat pipes. A total of 388 days of continuous operation with an axially grooved aluminum transporter heat pipe and an axially grooved stainless steel heat pipe diode was demonstrated before the EPDS batteries lost power. Preliminary post flight tests showed that the heat pipes are still functioning. This paper presents a summary of the flight data analysis for the heat pipes and the related support systems.

### INTRODUCTION

A schematic of the HEPP is presented in Figure 1. This system contains an axially grooved aluminum constant conductance transporter heat pipe (THP) and a stainless steel axially grooved liquid trap diode heat pipe. Both heat pipes use ethane as the working fluid for operation in the range of 150 to 250°K. The condenser of each heat pipe is thermally coupled to a radiant cooler system. A phase change material (PCM) canister is integrated with the radiator to provide temperature stability at its 182°K melting point. The PCM is n-heptane and it is used to provide a 27 watt-hr latent heat capacity for constant temperature operation during transport tests.

A schematic of the total HEPP Experiment System is presented in Figure 2. The HEPP assembly also includes a stainless tubular structure, an electronics module for signal conditioning and power sequencing, multi-layer insulation (MLI) blankets, and kapton foil heaters, platinum resistance temperature sensors (PRTs) for low temperature data and thermistors for ambient temperature measurements. The HEPP and its EPDS which is used for data acquisition and data recording were flown in Tray F12. The HEPP EPDS also recorded temperature data from six thermocouples and two thermistors from the THERM (P0003) and 6 thermistors from the CVCHPE (A0076) experiments. HEPP subsystems and components are summarized in Table 1. Heat pipe designs are listed in Table 2 and the PCM design is presented in Table 3.

Power to the HEPP's electronics module was provided by a Direct Energy Transfer (DET) Power System which included a 12-ampere-hour, 28 VDC Nickel Cadmium battery, four solar array panels and power system electronics. The DET was installed into Tray H1 and connected by power cables to the HEPP in Tray F12. Analysis of the flight data shows that the power system provided nominal operation without any anomalies over the 388 days of recorded data. Nominal DET operation was also demonstrated prior to deintegration from LDEF at KSC. A detailed discussion of this system is presented in Reference 1.

Finally 5 sets of 65 thermal control coatings samples were attached to trays F12, H1 and F9 for evaluation with the HEPP. Flight results for these samples are presented in Reference 2.

The LDEF and its extended mission provided a unique opportunity for the long term evaluation not only of the ethane use in heat pipes but also the various space flight subsystems that were needed to support the HEPP. This paper summarizes results obtained to date for the heat pipes, electronics module and instrumentation, and the EPDS.

### Flight Results

Operation of the HEPP commenced upon deployment of the LDEF when the HEPP radiator system began to cool down. Also, upon execution of the LDEF initiate, power from the DET is transferred to the HEPP electronics module which was preprogrammed to apply 1.2 watts and 1.0 watts to the evaporator heaters of the THP and diode heat pipes, respectively. This power level is consistent and in fact exceeds heat loads that would be experienced with detectors that are currently proposed for operation from 200°K down to cryogenic temperatures as low as 60°K. In future applications, the heat pipe could be used to transport these heat loads and the local thermal heat leaks to a remote radiator or active cooler system.

Figures 3 and 4 show the transient cycling of the evaporator section of the THP and diode heat pipe, respectively. The temperature cycling is due to changes in the external environment that affect the net cooling capacity and correspondingly the heat rejection temperature of the HEPP radiator. The temperature drops across each heat pipe are shown in Figures 5 and 6.

These results show that both heat pipes are operating continuously over the range of 192°K to 260°K throughout the 390 days of recorded data. In flight, the diode average temperature drop is 2.5°C whereas ground tests show more than a 15°C temperature drop at the diode's evaporator when it is "dried-out" and not operating at an adverse tilt. A 10°C drop was observed in the THP when it was "dried-out" versus the average 0.6°C drop recorded in flight.

Post flight ambient tests show that both heat pipes are still operating. Thermal vacuum tests will be conducted before year end to evaluate any degradation to their performance.

In addition to demonstrating successful heat pipe operation, the HEPP demonstrated successful performance of the electronics module, and associated instrumentation. The HEPP's EPDS and its MTM and lithium batteries also performed without any difficulty. The HEPP's battery power supply also performed as designed. Each of these subsystems showed nominal post flight performance.

The one problem that the HEPP experienced was its failure to cool below 190°K. This prevented the freezing and subsequent melting of the n-heptane PCM canister. Also, since the HEPP electronics had a preprogrammed test sequence that was set for activation when the PCM cooled below 180°K, transport tests with the THP and diode could not be conducted and the diode reverse mode shutdown could not be demonstrated.

The reason for the inability to cool below 180°K in flight should be resolved when thermal vacuum tests are conducted. At that time various possibilities will be simulated to establish why the HEPP experienced a lower than expected heat rejection capability. Also, transport tests and freeze/thaw cycles will be performed to establish the effects of long term space exposure. These results will be reported as they become available.

#### REFERENCES

1. Smith E. Tiller and David Sullivan, "Long Duration Exposure Facility (LDEF), Low Temperature Heat Pipe Experiment Package (HEPP) Power System Results." NASA CP-3134, 1992.
2. Lonny Kauder, "Preliminary Results for LDEF/HEPP Thermal Control Samples." NASA CP-3134, 1992.

Table 1  
**HEPP SUBSYSTEMS/COMPONENT SUMMARY**

---

**THERMAL**

1. ETHANE/ALUMINUM AXIALLY GROOVED HEAT PIPE
2. ETHANE/STAINLESS STEEL AXIALLY GROOVED/LIQUID TRAP DIODE HEAT PIPE
3. n-HEPTANE/ALUMINUM PHASE CHANGE MATERIAL CANISTER
4. LOW TEMPERATURE RADIATOR/SHIELD SYSTEM INCLUDING SILVER TEFLON OPTICAL SURFACES
5. PLATINUM TRANSDUCERS (33 PRTs)
6. KAPTON/FOIL RESISTANCE HEATERS
7. MLI BLANKETS, VELCRO FASTENERS, PHENOLIC SNAPS AND FASTENERS
8. BONDING COMPOUND FOR PRTs AND TAPE FOR BLANKETS
9. THERMAL ISOLATORS
10. ATOMIC OXYGEN EXPOSURE THERMAL CONTROL SAMPLES

Table 1  
**HEPP SUBSYSTEMS/COMPONENT SUMMARY  
(CONT'D)**

---

**ELECTRICAL**

1. ELECTRONICS MODULE INCLUDING SIGNAL CONDITIONING AND POWER SEQUENCING, COMMAND LOGIC
2. EPDS INCLUDING LITHIUM BATTERY, DATA ACQUISITION, POWER CONDITIONING AND TAPE RECORDER
3. HEPP POWER SUPPLY
  - NICKEL CADMIUM BATTERY
  - SOLAR ARRAY (4 PANELS)
  - POWER CONVERSION & CONDITIONING
4. CURRENT AND VOLTAGE SENSORS
5. CONNECTORS AND HARNESSSES

**MECHANICAL**

1. HONEYCOMB BASEPLATE AND BOND MATERIALS

## Table 2

### TRANSPORTER HEAT PIPE (TPHP) DESIGN SUMMARY

Wick configuration	ATS extruded axial groove	
Working fluid	Ethane	
Material	6063 aluminum	
Geometry	in.	cm
O.D.	5/8	1.59
Lengths		
Overall	50.8	129.0
Evaporator	6.0	15.2
Adiabatic	26.8	68.1
Condenser	18.0	45.7
Effective	38.8	98.6
Internal pressure @ 27°C	630 psia	
Burst safety factor @ 27°C	7.1	
Transport capacity	33 W-m @ 180°K (0-g)	
Conductance	5.0 W/°C	

### LIQUID TRAP DIODE HEAT PIPE DESIGN SUMMARY

Wick Configuration		
Heat pipe	Axially grooved 20 grooves 30 mesh cylindral slab, 100 mesh bridges, circumferentially grooved wall	
Liquid trap reservoir		
Material	Stainless Steel	
Working Fluid	Ethane - 9.0g	
Operating temperature	180°K	
Geometry	in.	cm
Heat pipe O.D.	.413	1.05
Heat pipe lengths		
Overall	46.85	119.0
Evaporator	4.0	10.16
Adiabatic	24.45	62.10
Condenser	18.40	46.74
Effective	35.65	90.55
Reservoir O.D.	1.00	2.54
Reservoir length	4.00	10.16
Internal pressure	630 psia	
Burst safety factor @ 70°C	12.3	

### Table 3

## PCM CANISTER DESIGN SUMMARY

Envelope	TIG welded 6061-T6 aluminum assembly
Core	3/16-in. cell by 0.002-in. thick 5052 aluminum honeycomb
PCM	753-g of n-heptane
Heat storage capacity	27 W-hr
Minimum thermal conductance	8 W/°C

## HEAT PIPE EXPERIMENT PACKAGE (HEPP)

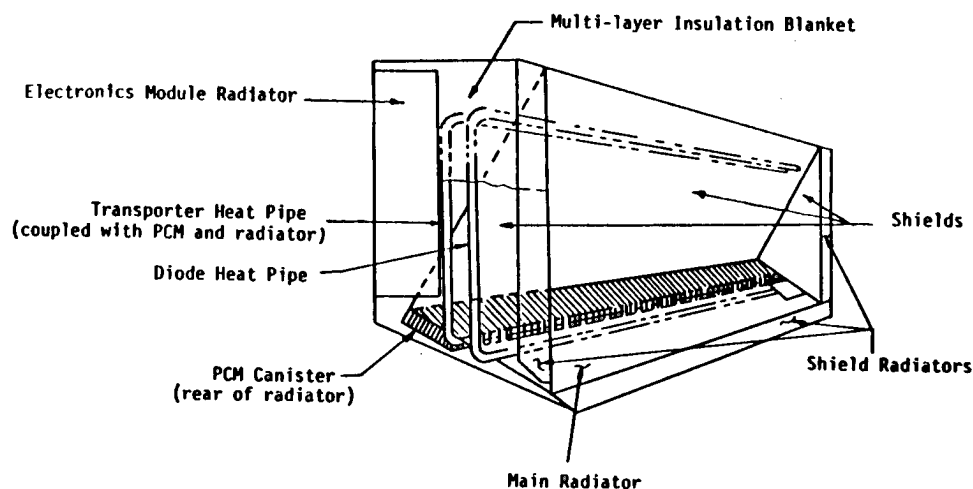


Figure 1



## HEPP SYSTEM DESCRIPTION

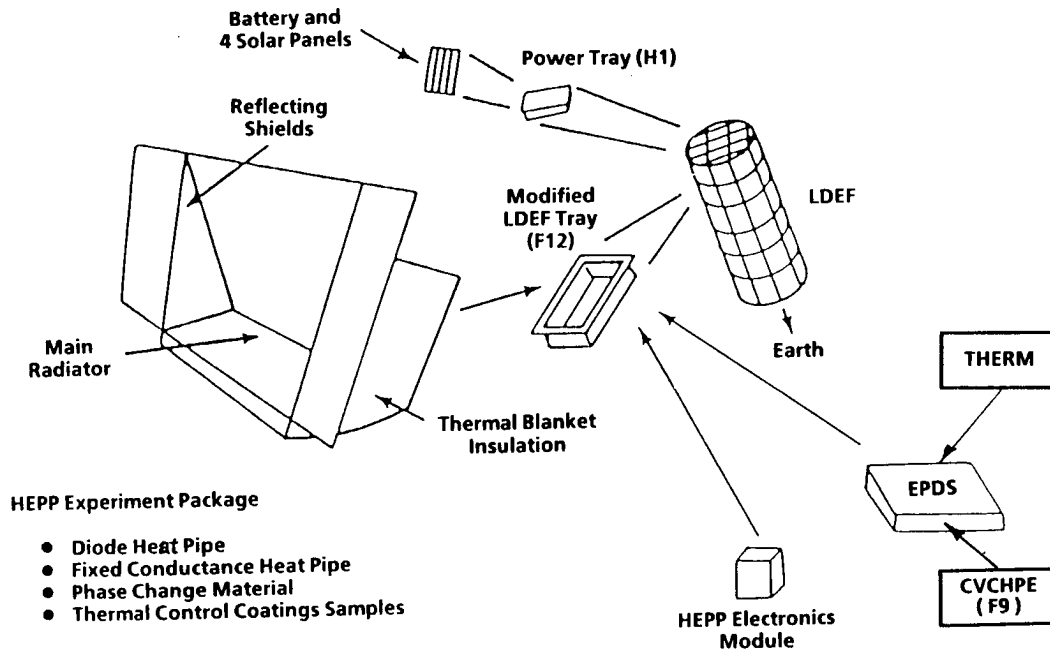


Figure 2

## LDEF/HEPP FLIGHT DATA

TRANSPORTER EVAPORATOR - LOCATION A

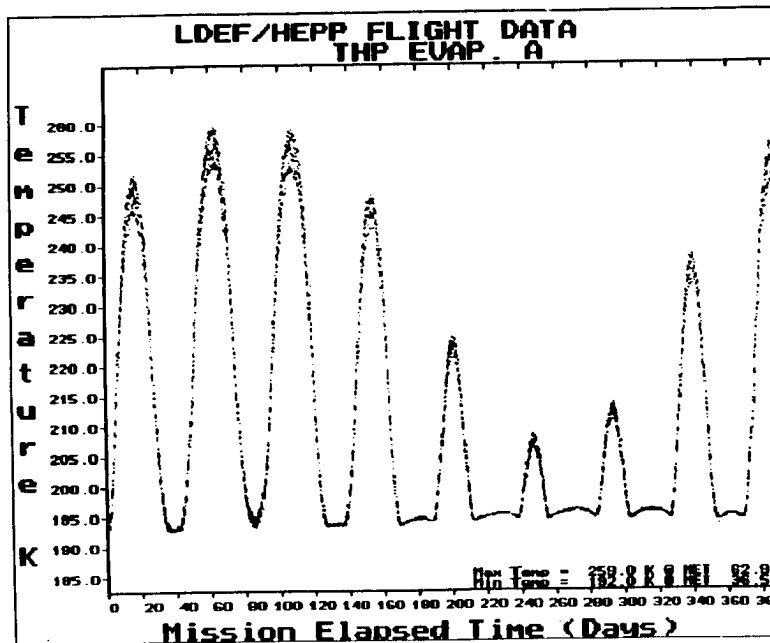


Figure 3

# LDEF/HEPP FLIGHT DATA

DIODE EVAPORATOR - LOCATION A

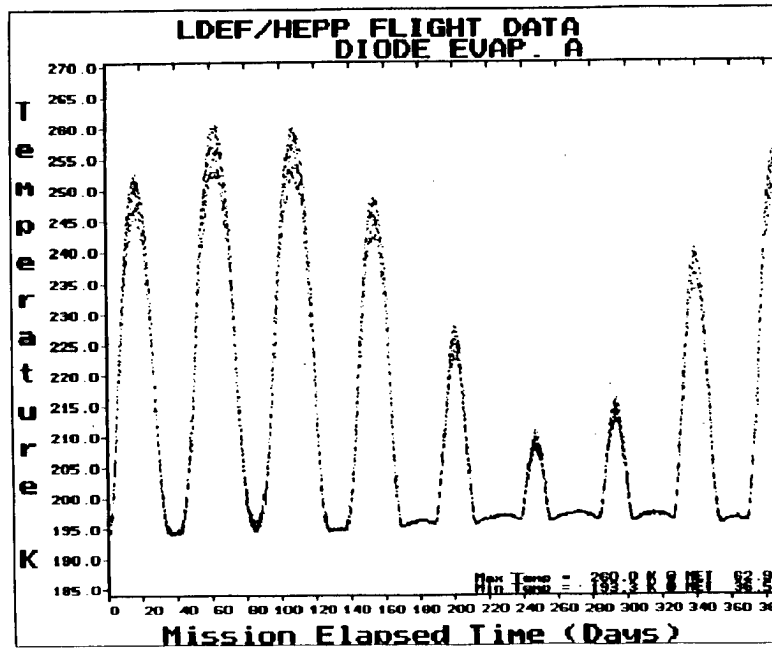


Figure 4

## THP TEMPERATURE DROP VERSUS MISSION ELAPSED TIME

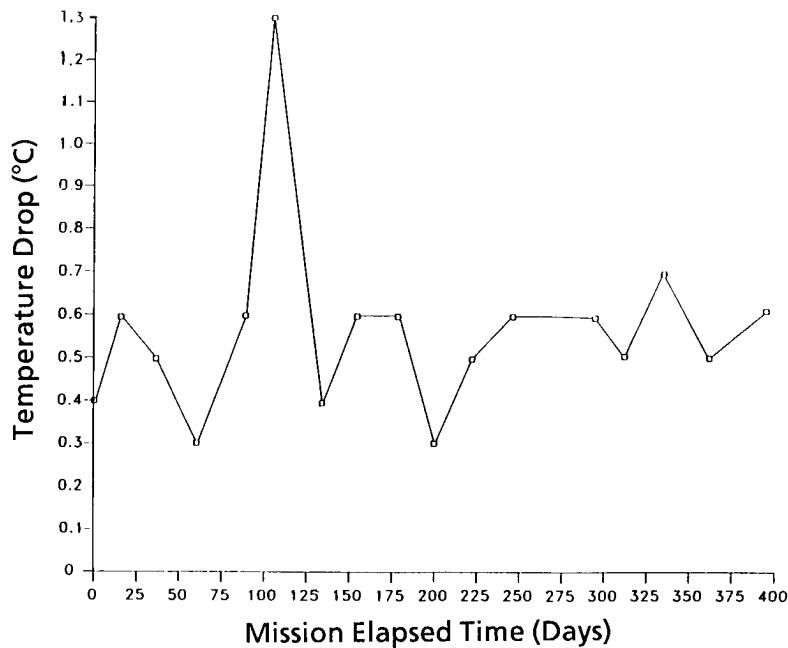


Figure 5

## DIODE TEMPERATURE DROPS VERSUS MISSION ELAPSED TIME

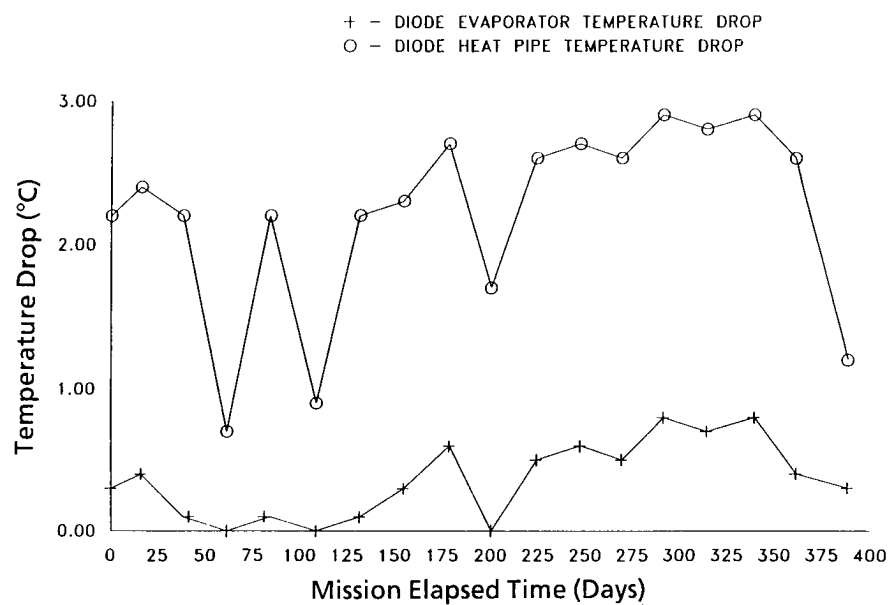


Figure 6

LONG DURATION EXPOSURE FACILITY  
LOW-TEMPERATURE HEAT PIPE EXPERIMENT PACKAGE  
POWER SYSTEM RESULTS

Smith E. Tiller and David Sullivan  
Space Power Applications Branch  
NASA Goddard Space Flight Center  
Greenbelt, Maryland 20771  
Phone: (301) 286-6489, Fax (301) 286-2717

SUMMARY

This paper presents an overview of a self-contained Direct Energy Transfer Power System which was developed to provide power to the Long Duration Exposure Facility Low-Temperature Heat Pipe Experiment Package. The power system operated successfully for the entire mission. Data recorded by the on-board recorder shows that the system operated within design specifications. Other than unanticipated overcharging of the battery, the power system operated as expected for nearly 32,000 Low Earth Orbit cycles, and was still operational when tested after the LDEF recovery. Some physical damage was sustained by the solar array panels due to micrometeoroid hits, but there were no electrical failures. Future papers will present results from post-flight characterization and Destructive Physical Analyses (DPAs) performed to evaluate the internal physical properties of the power system components.

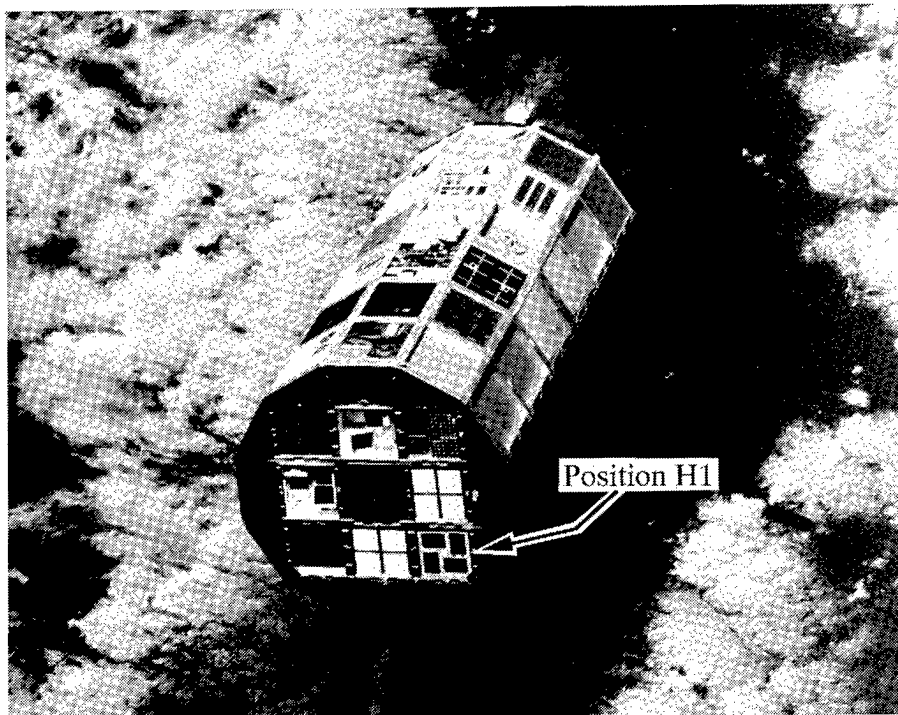


Figure 1: Location of power system tray on space end of LDEF

## INTRODUCTION

The Long Duration Exposure Facility (LDEF) Low-Temperature Heat Pipe Experiment Package (HEPP) Power System was developed to autonomously provide the power required by the HEPP experiment (designated S1001) during the LDEF mission. The power system tray was located separately from the HEPP experiment tray, and can be seen in Figure 1 on the space end of the LDEF structure in position H1. The system was designed as a self contained Direct-Energy-Transfer power system, in which the solar arrays are directly connected to the battery and main power bus. The power system tray is shown in Figure 2 with the solar array protective covers installed. The system consisted of four solar array panels, one 18-cell, 12 ampere-hour, nickel-cadmium (NiCd) battery, and a Power System Electronics (PSE) unit. Figure 3 shows an inside view of the power system tray, as well as the protective thermal blankets lining the inside of the tray and the aluminum baseplate (30 in.x 30 in.x 3/4 in. / 76.2cm x 76.2cm x 1.91cm) to which the tray was mounted for mechanical stability and thermal control.

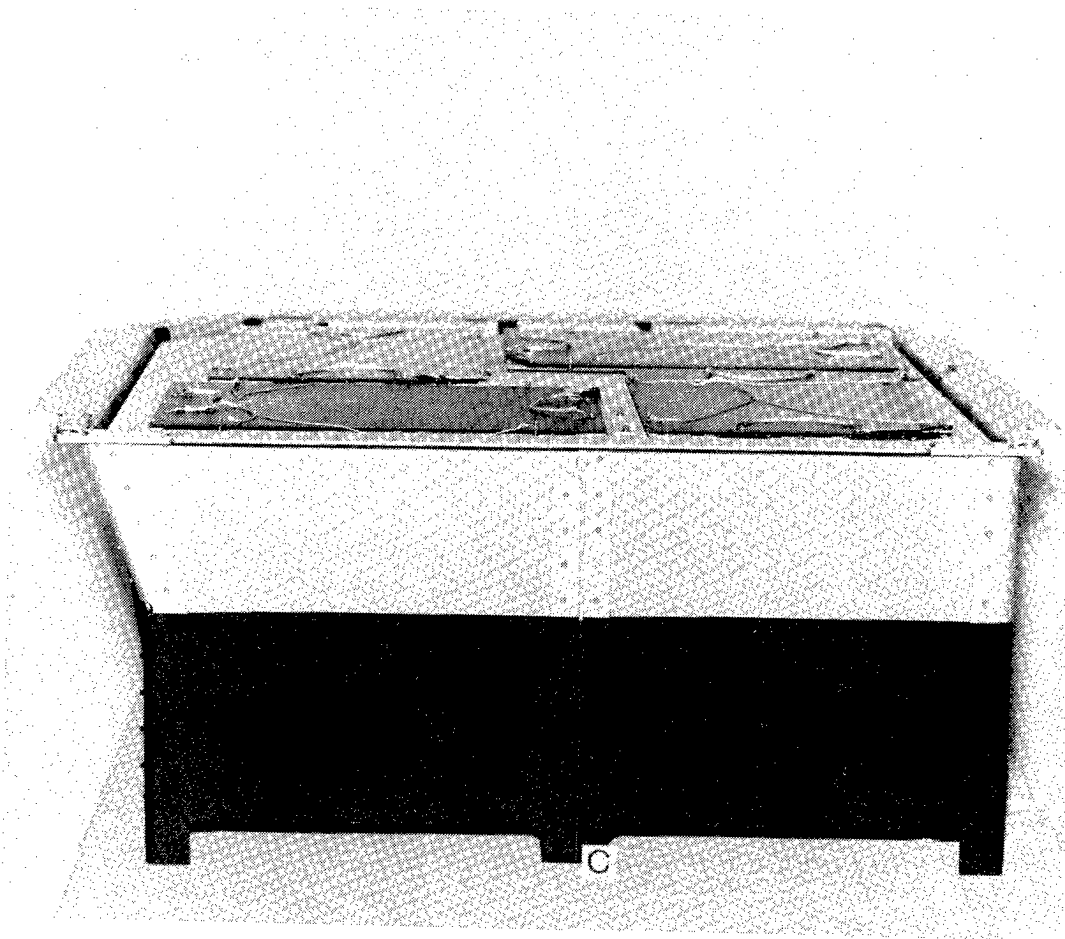


Figure 2: Power system tray with solar panel protective covers

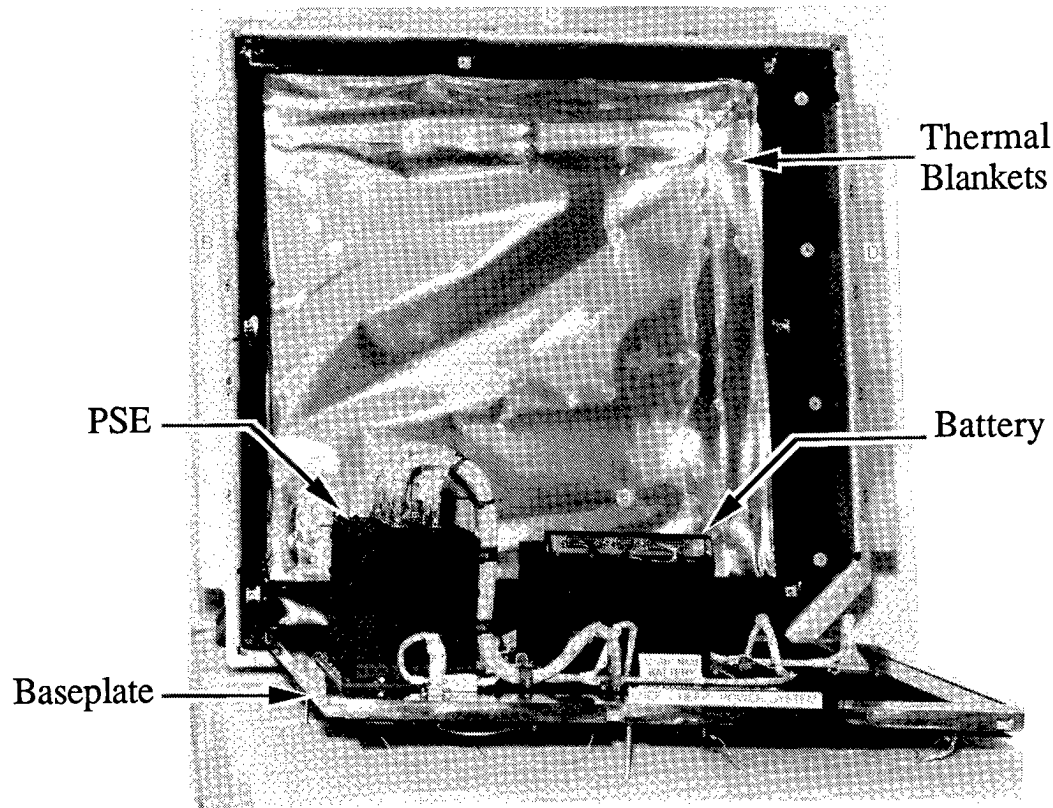


Figure 3: Interior of power system tray

## POWER SYSTEM DESIGN

The power system was designed to utilize the available sun's energy to charge the battery, provide power to the HEPP as required, and recharge the battery when depleted, repeating the cycle indefinitely. A simplified block diagram of the power system is shown in Figure 4. During the mission the power system performed two main functions, the first of which was to provide power to the HEPP experiment whenever the battery was fully charged. The battery contained two cells manufactured with an additional electrode ("third-electrode") that provided an output voltage proportional to the generation of oxygen when the cell approached a full state of charge. The PSE automatically switched on the main power bus to the HEPP experiment whenever either of the third-electrode voltages reached 250mV. During cold temperatures ( $-30^{\circ}\text{C}$  to  $+10^{\circ}\text{C}$ ), the rate of the third electrode reaction slows down and may fail to respond adequately. A second detector was incorporated in the PSE to sense battery full state of charge during these cold temperature periods. This detector was designed to switch on the main power bus when the battery voltage reached 27V and began shunting excess solar array current. The second function of the power system was to remove power from the HEPP experiment if either of two conditions occurred: the battery voltage dropped below 18V (indicating the battery was fully discharged), or a delta of 0.5V or greater was measured between the top and bottom halves, or 9 cell groups, of the battery (indicating unbalanced cell voltages).

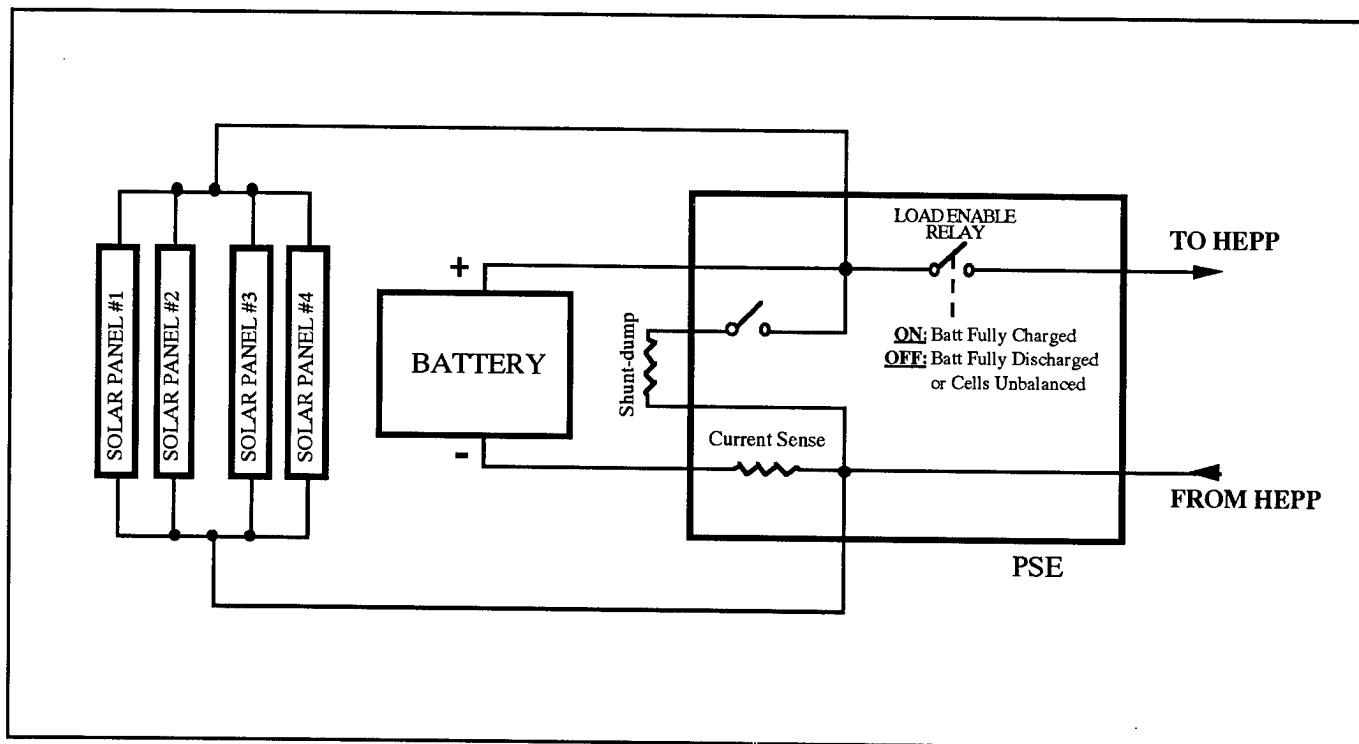


Figure 4: Block diagram of power system

## PRE FLIGHT PERFORMANCE

Prior to launch the power system components were tested at the NASA Goddard Space Flight Center (GSFC) and Kennedy Space Center (KSC). The solar panels were tested in the Solar Array Test Facility at GSFC, and it was determined that each panel had the capability to produce 0.4A peak power at 25V, which was more than sufficient to provide the power necessary to maintain battery charge. The battery was tested in the GSFC Battery Laboratory using a profile similar to that predicted for the LDEF mission, i.e. LEO cycling, and was also tested for battery capacity. Results of these tests indicated that the battery capacity ranged from 9.1 to 16.5 ampere-hours at temperatures  $-30^{\circ}\text{C}$  to  $+20^{\circ}\text{C}$ , sufficient to power the HEPP experiment with the predicted load profile. The Power System Electronics unit (PSE) was tested extensively in accordance with "LDEF/HEPP Power System Long Form test procedure, LDEF-GSFC-347." The complete power system was tested with the HEPP experiment at GSFC and KSC to verify compatibility between the systems prior to launch. These tests verified that all systems were acceptable for flight.

## FLIGHT DATA ANALYSIS

Data recovered from the on-board tape recorder indicates that the system operated within the design limits during the first 388 days of the mission. The LDEF was not expected to remain in orbit longer than this, and so data was not recorded for the remainder of the 69 month mission. We assume, however, that the power system operations followed the same trends throughout the mission. The battery voltage and current data is shown in Figures 5 and 6. The voltage ranged between a minimum of 23.98V and a maximum of 26.72V, with an average of 25.83V. The current ranged between a minimum of -0.14A and a

maximum of 1.29A, with an average of 0.126A. The positive current values indicate that the battery was charging, and the negative current reflects the discharge current used by the HEPP Heater and the power system electronics during eclipse periods of the orbits. The current profiles shown in Figure 6 and the temperature profiles shown in Figure 7 closely correlate with the LDEF solar illumination profile. The battery temperature was passively controlled within the allowable limits of  $-30^{\circ}\text{C}$  to  $+35^{\circ}\text{C}$  by using a 67 lb (30.39 kg) aluminum baseplate, thermal blankets and thermal control paint. The battery temperature data is shown superimposed on the baseplate temperature data in Figure 7. The battery temperature ranged between  $-29.5^{\circ}\text{C}$  and  $+14.2^{\circ}\text{C}$ , with an average of  $-0.08^{\circ}\text{C}$ , while the baseplate temperature ranged between  $-32.9^{\circ}\text{C}$  and  $+16.1^{\circ}\text{C}$ , with an average of  $-4.3^{\circ}\text{C}$ . These voltage, current and temperature values fall within the ranges predicted prior to launch.

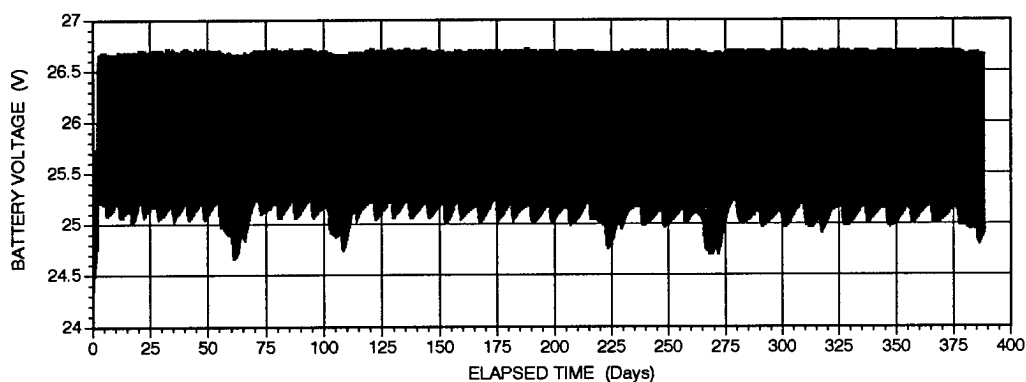


Figure 5: Battery voltage for first 388 days

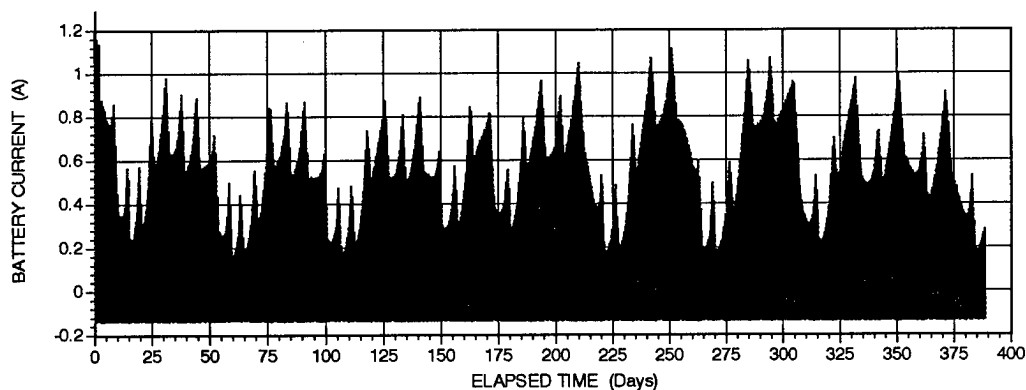


Figure 6: Battery current for first 388 days

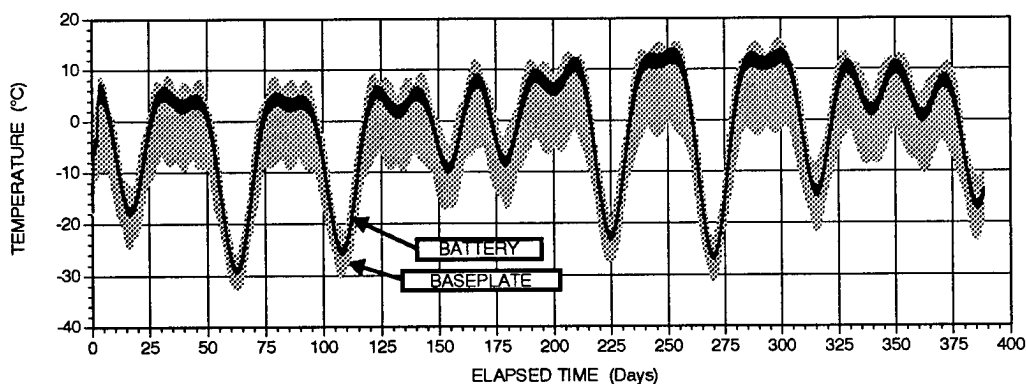


Figure 7: Battery and baseplate temperature for first 388 days



For safety reasons the battery was launched in a completely discharged condition, with the HEPP experiment switched off-line. The flight data, however, indicates that the battery was supplying load current when the data acquisition was initiated. This indicates that the battery had reached a full state of charge and that the PSE had switched on the main power bus to the HEPP experiment prior to deployment of the LDEF from the shuttle payload bay. Since the solar array panels were directly connected to the battery, the battery started charging as soon as the LDEF space end achieved sun acquisition. After reviewing the mission log, it was confirmed that the LDEF space end had indeed been exposed to the sun in the shuttle bay for an extended period of time before deployment. Although this was not expected, charging of the battery had no adverse effect on subsequent power system operations.

The power system was designed to provide 2 to 3 amps of load current to the HEPP experiment, but from the flight data it was found that this load did not materialize due to the reduced flight activities of the HEPP experiment. Because of the reduced power demand, and because the power system did not contain an active charge controller, the battery's recharge ratio remained high, causing the battery to be constantly overcharged during the entire mission. The overcharge eventually used up the battery's chemically built-in overcharge protection, causing generation of gas and an excessive build up of pressure in the cells, which resulted in cell bulging and physical damage to the battery structure. This was found upon visual inspection of the battery when the tray was disassembled.

## **POST FLIGHT VISUAL INSPECTION**

### **Power System Tray**

A post-flight visual inspection of the LDEF HEPP power system tray external components (baseplate, solar panels and connectors) was initiated on March 23, 1990, approximately 3 months after the LDEF recovery. There were no signs of major physical damage noted, such as warping, cracks or fatigue of any of the power system components that were exposed to the space environment. The bottom edge of the tray exterior contained a shiny gloss or oily appearance. Samples were taken by the LDEF inspectors, and the evaluation is currently in progress. With the exception of micrometeoroid strikes on the exposed surfaces, and the areas of discoloration, all components appeared to be in the same physical condition as that observed during final inspection of the system prior to launch.

The power system baseplate had small traces of Apiezon H (thermal conducting compound manufactured by Apiezon Products Limited), used during final assembly of the power system that apparently bled into the baseplate's paint. Counter-bored bolt holes in the external surface of the baseplate had a dark coating on the trailing edge (during flight) of each hole. This may also have been caused by thermal grease bleed off and exposure to the space environment. Other physical damage noted were pin holes in the top plate's painted surface that were apparently caused by micrometeoroid hits.

### **Solar Panels**

During an in-depth visual inspection of the four solar array panels, 99 hits were recorded of which 29 hits apparently caused cover glass cracks. Fifteen additional cover glass cracks were found that could not be directly attributed to micrometeoroid hits. One of the cell interconnects was slightly damaged by a micrometeoroid hit. Other visual findings were a small bubble in the structure surface, a small spot of burned residue on panel #223, a small area of debris on panel #200, and adhesive spread on the edges of all of the panels. Chips and pits on the solar cells can be observed in Figure 8. The solar array panels also had

small traces of Apiezon H that apparently bled into the edges of the panels. The Solithane compound, manufactured by Morton Thiokol, used to protect the wiring and diode terminations on the solar panels had turned darker after being exposed to the space environment (see Figure 9). However, it should be noted that the solar panels were manufactured during 1971 and 1972, and were already showing some effects of aging prior to launch.

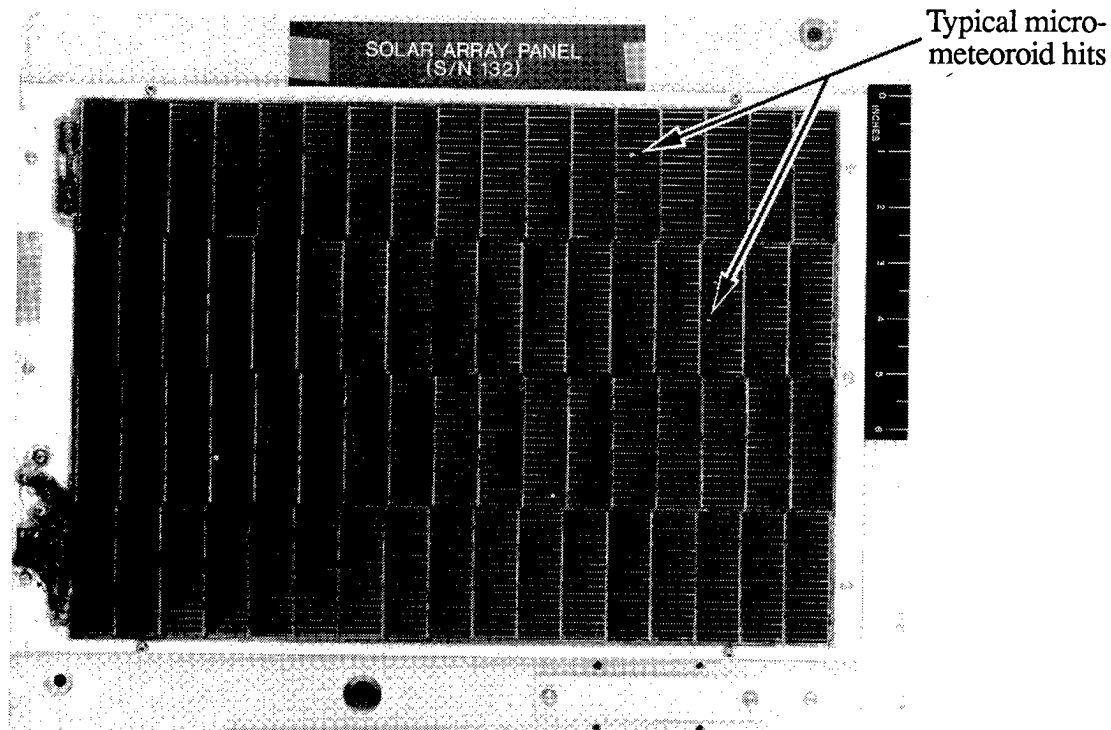


Figure 8: Micrometeoroid damage on one of the solar panels

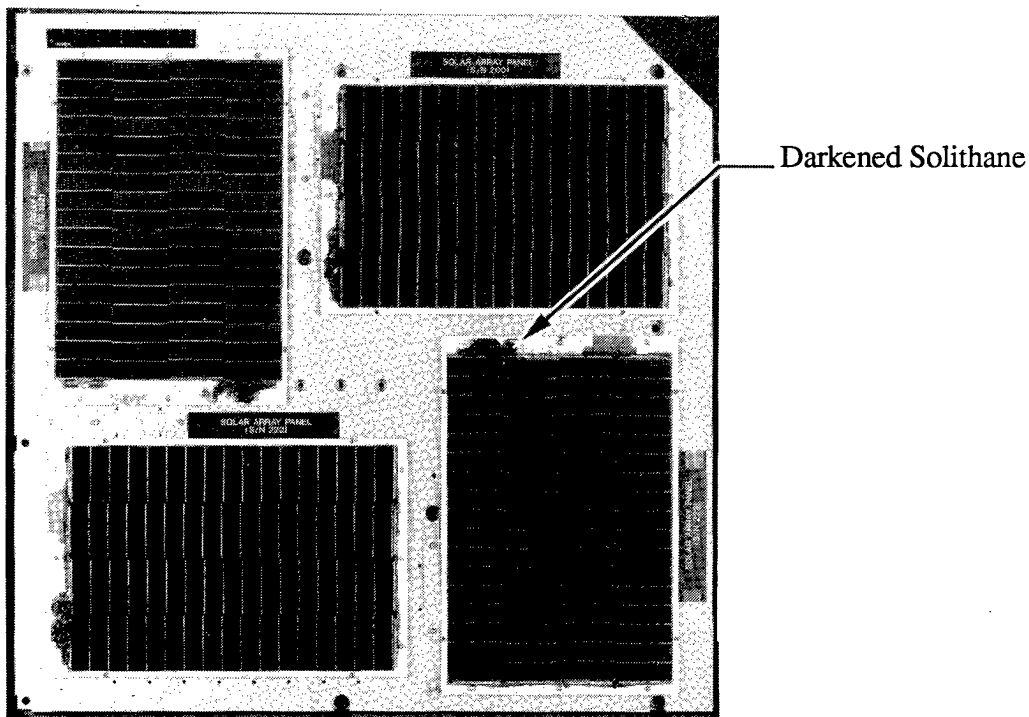


Figure 9: Darkening of the solithane on the solar panels

## Battery

Upon visual inspection of the power system battery, it was immediately apparent that several of the cells had bulged and deformed the battery structure in several places. The most severe bulge is shown in Figure 10. This cell bulging confirms the fact that the battery was overcharged during the mission. When the battery was disassembled and the individual cells examined, it was found that all 18 cells were affected, although the four adjacent to the end plates showed the most bulge. These end cells measured 0.200 to 0.336 inches (0.508cm to 0.853cm) above manufacturer's specification thickness, with edge measurements ranging from 0.010 to 0.048 inches (0.025cm to 0.122cm) above specifications. The sides of the remaining 14 cells measured an average of 0.130 inches (0.330cm) above manufacturer's specifications, whereas the edge measurements were flat and did not show signs of bulging. The Cho-Therm thermal transfer sheet, manufactured by Chomerics, Inc., under the battery was found to be in good condition except for the areas under the mounting tabs which showed signs of cold flow.

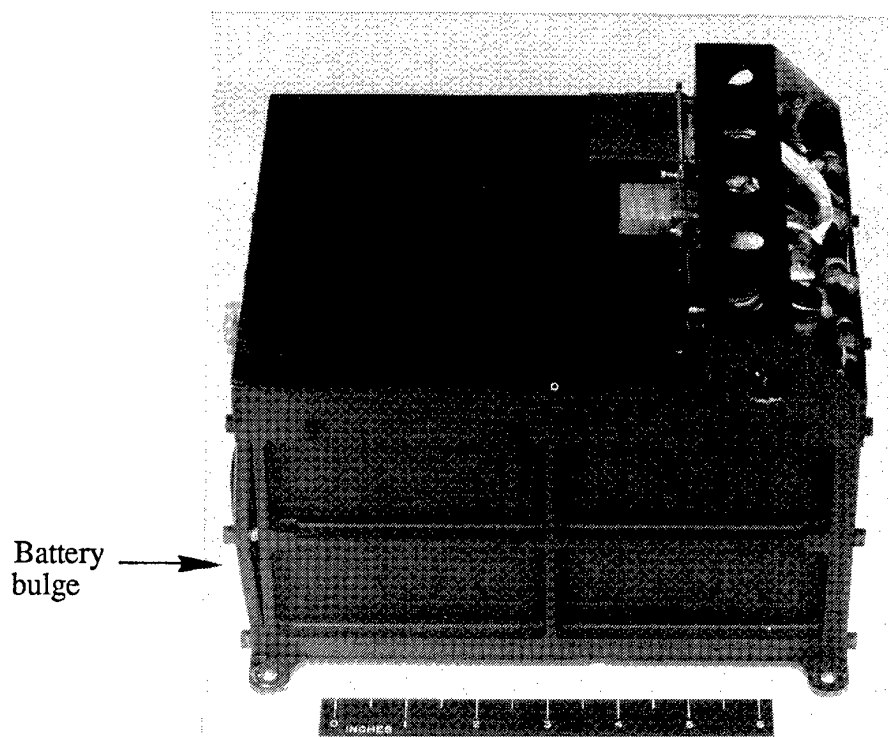


Figure 10: Bulging of the battery case

## Power System Electronics (PSE)

The connectors on the PSE also looked comparable to the pre-flight conditions, especially the uralane protective coatings. Figure 11 is a good illustration of the clear coating on the PSE connectors after flight. All of the connectors were located inside the power system tray and not directly exposed to the space environment. Visual inspection of the interior will be performed during the DPA of the PSE.

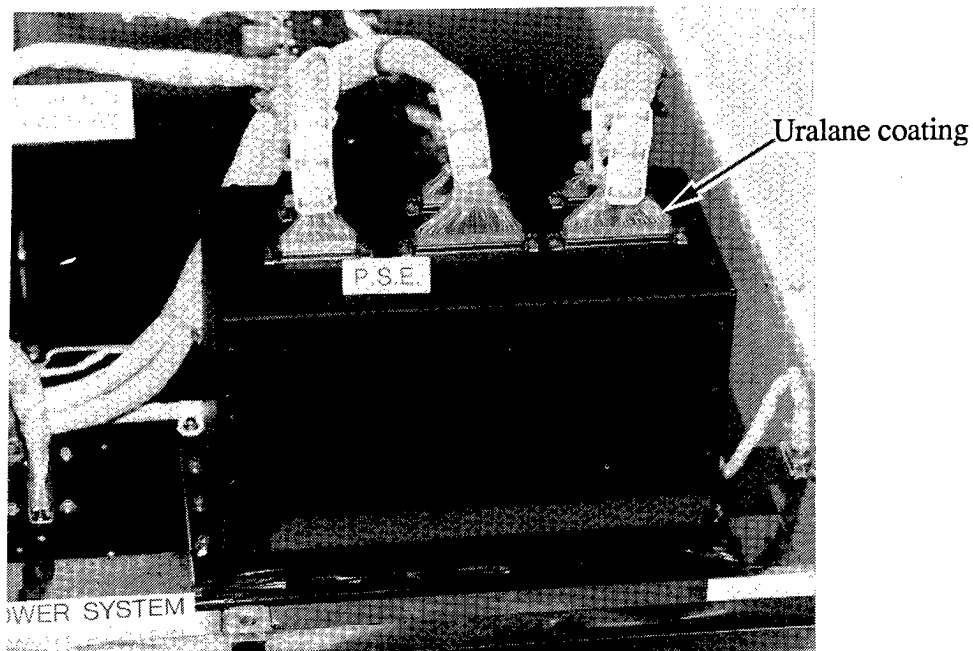


Figure 11: Clear uralane coating on PSE connectors

### Thermal Blankets

The thermal blankets, shown in Figure 12, exhibit the excellent condition characteristic of blankets that were protected from the space environment, located inside the power system tray. The Kapton tape, manufactured by CHR Industries, Inc., used to hold the blankets in place was also in good condition.

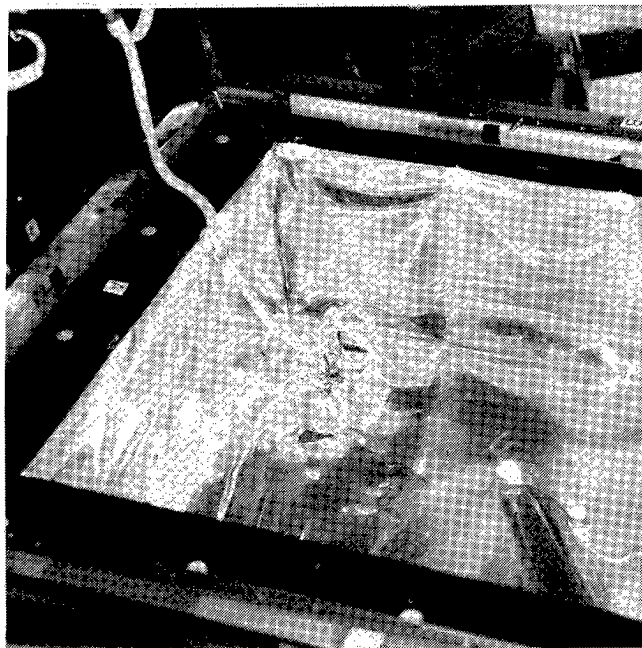


Figure 12: Thermal blankets inside the power system tray

## POST FLIGHT TEST AND EVALUATION

Operation of the power system before removal from the LDEF structure at KSC after recovery indicated that the power system was completely operational and performed as expected with the HEPP experiment. Except for the solar array current, which was simulated by Ground Support Equipment, the power system and experiment were tested together in flight configuration. After tray removal, tests were performed separately on the power system components at GSFC.

The power system was found to be in an excellent mechanical condition. Most screw and bolt torque values were found to be higher after flight than values measured prior to launch. This condition was expected due to the fact that all screw and bolt threads were coated with solithane prior to final insertion and torque. The measured re-torque values of 150 screws (#4-40, 6-32, 8-32, and 10-32) were found to be 24 percent higher than the values measured prior to launch. Measured values of eight 1/4-20 size bolts were found to be 20 percent higher. The exception to the rule was the value of screws torqued against plastic inserts such as the ones used to anchor the thermal blankets. These values were found to be 60 percent lower than the initial values. Epoxy added to screw and bolt heads in preparation for pre-launch vibration tests was found to be intact during the post-flight visual inspection. This was also true where uralane was used to provide additional bonding to the connector clamp screws.

### Solar Array Panels

The solar array panels were tested at GSFC to measure the current versus voltage (I/V) output degradation of the four solar array panels. These tests were conducted during May, 1990, approximately five months after the LDEF retrieval. The data indicates that the solar array panels' current and voltage output capabilities had degraded an average of 1.5% and 3.3% respectively, compared to pre-launch data. Data acquired during the testing of solar array panel #132 before and after space flight is shown in Figure 13. Since the data shown represents typical data acquired from all four panels, only the data from one panel will be included in this paper. It can be seen that the panel's output capability has degraded only a small amount since the testing in 1985 before launch of the LDEF. Testing of a fifth panel (S/N 100), identical to the power system panels, but which had been stored in a closed container at GSFC since the LDEF launch, indicated that the panel's output current and voltage capabilities had degraded only 0.27% and 0.6%, respectively.

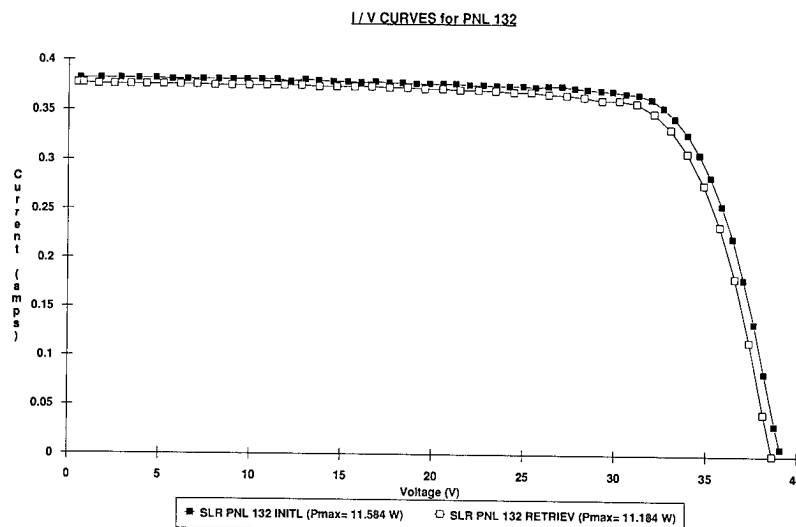


Figure 13: Pre- and post-flight I/V curves for solar array panel #132

It is believed that most of the flight degradation of the solar array panels was due to charged particle radiation, darkening of the cover adhesive, and micrometeoroid damage, while little degradation can be attributed to degradation of the solar cells due to thermal cycling.

### Battery

At KSC, and later at GSFC, the battery was tested to determine its electrical characteristics. At GSFC the battery was charged at a C/10 (1.2A) constant current rate following a complete discharge, and a comparison of the pre- and post-flight data curves is shown in Figures 14 and 15 respectively. As evident in Figure 15, the cell voltages failed to "roll over" after the complete charge, and instead climbed until cell #10 reached the maximum allowable limit of 1.52V, and the test was terminated. It is concluded that at least some of the cells have lost their overcharge protection. We assume loss of cell overcharge protection when cell voltages diverge as the cells reach full charge and continue to increase in voltage. Continued charging under these conditions causes excess gas to be generated in the cell and consequently the pressure to increase within the cell. Cells containing sufficient overcharge protection can be overcharged, at low rates, for extended periods without causing detrimental cell voltage divergence or pressure build up.

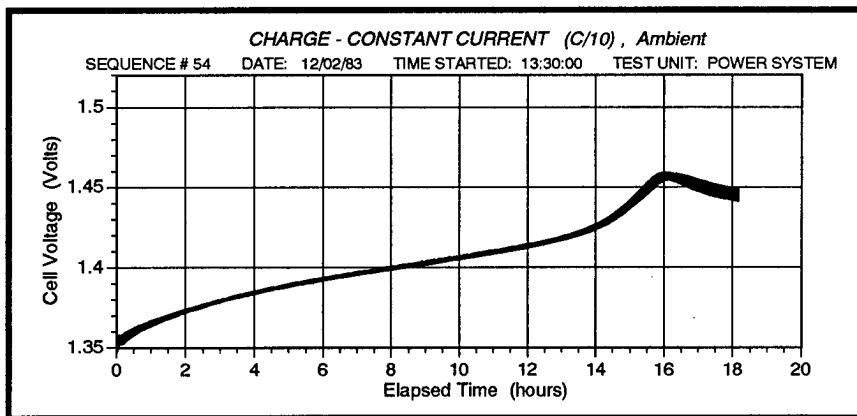


Figure 14: Pre-flight Capacity Charge

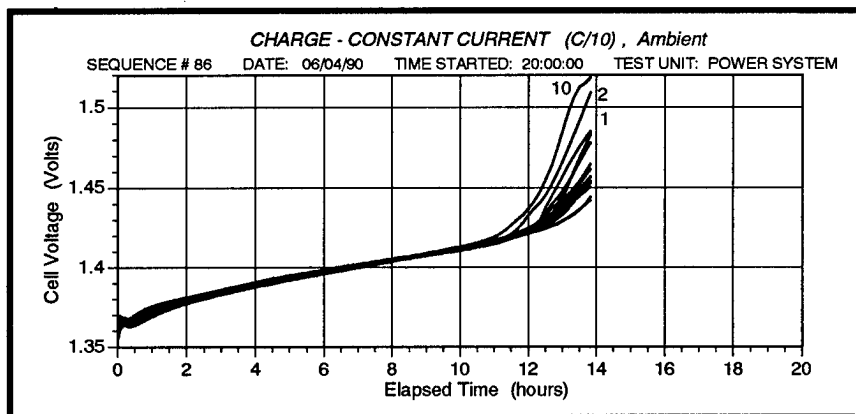


Figure 15: Post-flight Capacity Charge showing loss of overcharge protection

To determine the post-flight capacity, the battery was then discharged at a C/4.8 (2.5A) constant current rate until the test was terminated when the first cell dropped below 1.0V. The resulting discharge profile closely matches the pre-flight profile shown in Figure 16, when the battery capacity was 16.46 ampere-hours. Figure 17 shows the post-flight discharge profile, and the battery capacity was found to be 14.5 ampere-hours. Following the discharge each battery cell was let-down with a one ohm resistor for 16 hours. The resistive let-down was followed by an open circuit recovery test (Figure 18) where all cells except cell #10 recovered within a 24 hour period to a value above the acceptance level of 1.17V. Cell #10 is the cell that was bulged most during the mission; this is also the cell that terminated the charge due to high voltage and the first cell to fall below 1.0V during the discharge. Note that the battery was evaluated several times at KSC and in the battery lab at GSFC. The data shown in Figures 14 through 18 are representative samples.

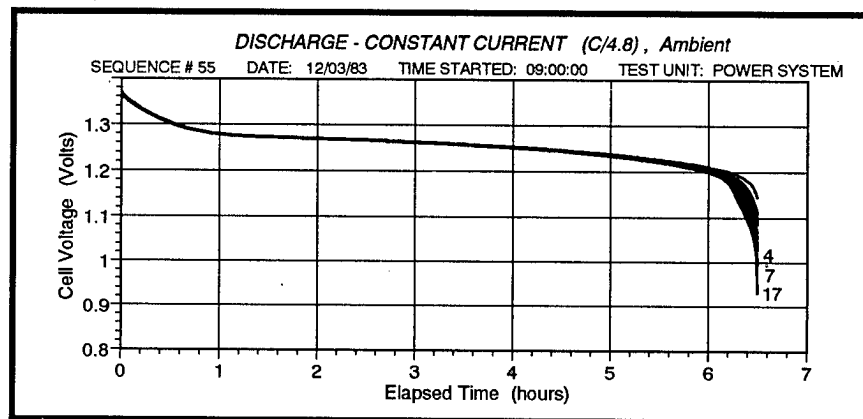


Figure 16: Pre-flight Capacity Discharge

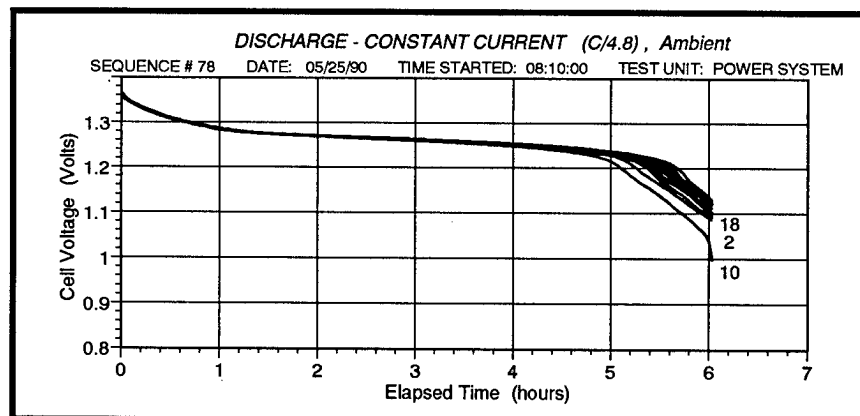


Figure 17: Post-flight Capacity Discharge

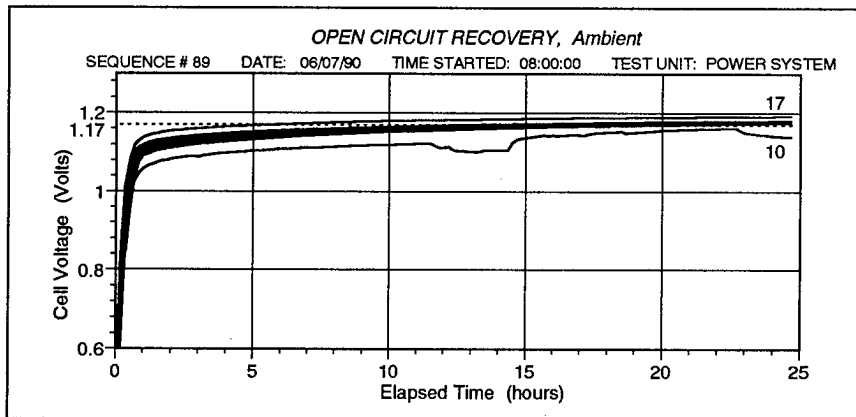


Figure 18: Post-flight Open Circuit Recovery Test

Despite the obvious bulging of some cells, loss of overcharge protection, and the failure by cell #10 of the open circuit recovery test, the battery still has the capability to provide output current in excess of the cell manufacturer's rated capacity of 12.0 ampere-hours. Having been exposed to over 32,000 LEO orbits, this is a major accomplishment even with today's battery technology. The only apparent difficulty is the inability to charge the cells under a normal charge regime. Since the loss of overcharge protection is apparent, a modified charge profile is now required to prevent excessive overcharge and associated build up of pressure.

#### Power System Electronics

The PSE was tested using the same long-form procedure as that called out previously for the pre-flight tests. During the post-flight tests all circuits worked correctly when input signals were simulated, i.e. third electrodes, battery voltage and shunt-dump current. All functions performed as recorded during pre-flight testing with no differences noted.

### CONCLUSIONS AND FUTURE PLANS

The power system automatically operated electrically to design specifications. Temperatures of the battery, solar arrays, PSE, and structural baseplate were maintained within limits established by computer modeling during design of the system. Post-flight inspections indicated that the power system withstood the rigors of launch, over 32,000 LEO cycles, and recovery by the space shuttle without showing any flight electrical anomalies. However, the battery case did show damage, caused by excessive cell pressure build up. Comprehensive Destructive Physical Analysis (DPA) of selected battery cells is needed to confirm loss of overcharge protection and to determine the extent of cell degradation. Micrometeoroid impacts and some minor discolorations were noted around the solar panels and baseplate, apparently caused by creep of thermal compounds. Analyses of these materials are in progress.

The power system design proved successful and could be flown again as-is, but minor changes could enhance operations and improve performance. One suggested change would be to incorporate a minimum



load, such as a shunt-dump panel, to support an adequate battery charge/discharge profile (i.e. 10% depth-of-discharge) to help minimize the possibility of battery overcharge.

The planned future tests are as follows: (1) characterization testing of battery cell packs at the GSFC Battery Lab and life cycle testing at NWSC Crane, (2) DPA of battery cells at NWSC and COMSAT, and (3) DPA of the PSE electronic components, solar panels and cells by GSFC Quality Assurance. Results of these tests will be presented in future papers.

## **ACKNOWLEDGEMENTS**

### **LDEF/HEPP Power System Team:**

Roy McIntosh (Code 732.2) - HEPP Experiment Principal Investigator

Smith E. Tiller (Code 711.5) - Power System Manager

John Paulkovich (Code 711.3) - Electronics Designer

Nicolas V. Mejia (Code 711.4) - Solar Array Manager

David Sullivan (Code 711.5) - GSE Software and Test Engineer

Richard H. Hoffman (Code 732.0) - Thermal Engineer

Grace M. Miller (Code 732.5) - Thermal Coatings

Michael C. Shai (code 732.5) - Thermal Coatings

Carol H. Clatterbuck (313.2) - Polymers

Mega Analytical Research, Services Inc. - Power System Structure Design and Analysis

# RESULTS FROM THE LDEF/A0076 CASCADED VARIABLE CONDUCTANCE HEATPIPE EXPERIMENT

Michael G. Grote  
McDonnell-Douglas Electronics Systems Co.  
Laser And Electronics Systems Division  
Mail Code 1067307  
St. Louis, Missouri 63166  
Phone: 314-234-8452, Fax 314-232-3393

## SUMMARY

The A0076 Variable Conductance Heatpipe Experiment (CVCHPE) on the Long Duration Exposure Facility (LDEF) demonstrated temperature control better than  $\pm 0.3^{\circ}\text{C}$  during fifty days of on-orbit data collection in a widely varying external environment. The experiment used two series connected, dry reservoir variable conductance heatpipes which require no electrical power for operation. The heatpipes used a central artery design with ammonia working fluid and nitrogen control gas. The LDEF was in orbit for almost six years rather than the planned one year mission. Although no additional data were taken during this extended period, post-test data indicated that the set point drifted upward less than  $1^{\circ}\text{C}$  per year. There were significant changes to the appearance of all external thermal control surfaces primarily due to atomic oxygen degradation, and one small anomaly in the electronics. These changes, though, had little effect of the CVCHPE performance.

## INTRODUCTION

Precision temperature control which requires no electrical power for operation can be beneficial in a number of spacecraft applications for controlling temperature sensitive components. Reference 1 describes the development and testing of a cascaded Variable Conductance Heatpipe (VCHP) that fulfilled the needs for such a system. This concept used two series connected dry reservoir VCHPs to maintain temperatures within a  $\pm 0.3^{\circ}\text{C}$  control band in a simulated thermal vacuum environment. The heatpipes used ammonia as the working fluid and nitrogen as the control gas. (Reference 2 and 3 present a more detailed description of the theory of operation of VCHPs.) In a dry reservoir, as shown in Figure 1, the control gas in the reservoir is isolated from ammonia in the heatpipe. The gas reservoir is thermally tied to the evaporator to maintain the noncondensable gas above the evaporator temperature and to maintain the reservoir at a constant temperature. In initial analysis, a single VCHP could not maintain a precise temperature control in the widely ranging heat loads and environments, but could easily maintain a control of  $\pm 3.0^{\circ}\text{C}$ . A second, series connected (i.e. cascaded) VCHP was added to provide precise temperature control. Using the  $\pm 3.0^{\circ}\text{C}$  control of the "coarse" control VCHP as the sink temperature, the "fine" control VCHP could provide  $\pm 0.3^{\circ}\text{C}$  control without requiring an excessive reservoir size.

The key to the success of the dry reservoir concept is to keep the ammonia vapor out of the noncondensable gas reservoir. If ammonia enters the reservoir, the temperature set point will rise. The unique feature of the CVCHPE concept was the inclusion of a long capillary tube between the heatpipe and the reservoir to prevent diffusion of ammonia into the reservoir. Reference 1 showed that the concept worked over the short time period of a thermal vacuum test, but a long term space test was still required to determine the long term drift in setpoint due to diffusion.

NASA Langley Research Center's (LaRC) Long Duration Exposure Facility (LDEF), Reference 4, provided an ideal means of economically testing the system. McDonnell-Douglas provided the design and fabrication of the CVCHPE which is described in Reference 5. The LDEF program provided the experiment tray, the flight batteries, and the mission support functions. Goddard Space Flight Center agreed to record the CVCHPE data using a data system on their Low Temperature Heat Pipe Experiment, Reference 6.

## CVCHPE DESCRIPTION

Figure 2 shows a schematic of the CVCHPE, and Reference 5 presents a complete description of the CVCHPE. The VCHP does not require electrical power to operate, but does require a heat throughput (e.g. equipment waste heat). On the LDEF, we used a black chrome solar collector to provide heat input and a silver/Teflon radiator for heat rejection. Although the solar collector was used to simulate an equipment heat load, it also illustrates how this system could be used to precisely control a totally quiescent system as long as there was a limited amount of solar exposure. The CVCHPE was located on the leading edge of the gravity gradient stabilized LDEF, thus providing some solar exposure on each orbit, but also providing a highly varied external environment that ranges from full solar to full shade. Analysis predicted that the solar collector would provide from 3 to 30 watts of heat, and the effective space temperature of the radiator would range from 0°C down to -100°C. The CVCHPE was designed to control to a nominal setpoint of  $14.0 \pm 3.0^\circ\text{C}$  on the coarse VCHP and  $23.0 \pm 0.3^\circ\text{C}$  on the fine VCHP. The coarse control VCHP condenser end was attached to the radiator and the evaporator end is in the coarse-to-fine heat exchanger block. The fine control VCHP evaporator end is attached to a plate which radiates to the solar collector. The reservoirs were conductively tied to their respective evaporator sections. Apiezon-H grease was used in all thermal interface joints. The experiment was isolated from the experiment tray and LDEF by mounting it on fiberglass standoffs and using internal insulation blankets. The outside of the CVCHPE was covered with a multilayer insulation (MLI) blanket except for the collector and radiator areas. The outside layer of the MLI was .076 mm thick Kapton. Figure 3 shows the assembled CVCHPE. The two patches on the external blanket were atomic oxygen experiment samples that were added by NASA/GSFC.

Figure 4 shows the CVCHPE fluid system. Each VCHP has a heatpipe, a manual fill valve, a solenoid valve, a 12 meter (40 ft.) long capillary tube and a gas reservoir. The heatpipes were central artery type with screen wall wicks. The solenoid valves were required to isolate the ammonia from the gas reservoir prior to the start of on-orbit operations. The opening of the valves was controlled by electronics onboard the CVCHPE. When the coarse control VCHP cools to  $-6^\circ\text{C}$ , the coarse control solenoid valve was designed to open and start a timer. Twenty-five hours later, the fine control solenoid valve was designed to open. Both solenoid valves were "borrowed" from the gas system on the old SKYLAB vehicle on display at the Smithsonian Air and Space museum. The 2.4 mm diameter capillary tube was wound around a spool to fit into a compact size. The reservoirs were commercial sample cylinders. The coarse control reservoir had a volume of 490 cc (30 cubic inches), and the fine control reservoir was 980 cc (60 cubic inches). Figure 5 shows the assembled fluid system prior to installation in the experiment tray.

Figure 6 presents a schematic of the electrical / data system. The flight data consists of six thermistors on the CVCHPE. The electronics box contains the circuits for the thermistors and the

control logic for opening the solenoid valves. The actual thermistor data that comes out of the electronics box is recorded in the data system of an adjacent experiment. There was one thermistor on each of the coarse and fine control reservoirs, one on the coarse control heatpipe, two on the fine control heatpipe and one on the backside of the solar collector.

Although the VCHPs do not require power, both the thermistor circuits and the solenoid valves require electrical power for operation. Two Lithium batteries were supplied by the LDEF program office for the CVCHPE. The 28 VDC battery was used to power the solenoid valves, and the 7.5 VDC battery was used to power the thermistor circuits.

The LDEF was launched on the space shuttle and deployed from the cargo bay in April, 1984. Figure 7 shows the on-orbit pictures taken just before the LDEF was released from the manipulator arm. All external surfaces on the CVCHPE were in excellent shape.

## FLIGHT RESULTS

The LDEF mission was to be in earth orbit for about one year before it was to be retrieved by the space shuttle. Thus, most active experiments were designed to collect data over this time period. Due to delays in shuttle operations and the suspension of shuttle activities after the Challenger accident, the LDEF was not retrieved until January, 1990. The flight data for the CVCHPE experiment were successfully recovered from the tape recorder on the Reference 6 experiment. The CVCHPE data were reduced and printed in engineering units by NASA GSFC based on pre-flight thermistor calibration data. The extended mission, though, did provide very valuable data on the long term effects of the space environment on the external surfaces of the CVCHPE which were on the leading edge (i.e. ram direction) of the LDEF.

Figure 8 shows the data from the initial start-up sequence. The coarse control VCHP temperature initially cooled down until it reached about  $-6^{\circ}\text{C}$ . When the solenoid valve opened, the coarse control started operating in the VCHP mode. The temperature gradually rose for about four hours until it reached its set point, and then controlled at this set point for the remainder of the mission. The fine control heatpipe continued to operate as an ordinary heatpipe until its solenoid valve opened (25 hours after the coarse control), and in about two hours it was controlling within its control band. Within a day and a half after LDEF initiation, both VCHPs were controlling in the VCHP mode.

Figure 9 shows data plotted for an initial period where the LDEF was in a low Beta angle orbit to show the orbital fluctuations. Data were taken approximately every two hours. Thus, there was only one data point per orbit, but since the data period was slightly longer than the 94 min. orbit period, the data plotted over a few days provided a good indication of the orbital variations. The solar collector went through orbital swings as the surface was exposed to varying degrees of solar exposure from full sun to full shade. In spite of this widely varying environment, both VCHPs maintained almost constant temperature, although one can see very slight variation in the fine control temperature in response to the varying solar collector input.

Figure 10 presents the LDEF orbit angle (i.e. "Beta" angle) and the calculated incident flux on the CVCHPE (tray F9). This information was provided by the LDEF program office based on the actual on-orbit data. Figure 11 shows the corresponding variation in the solar collector temperatures. For clarity, only the maximum and minimum solar collector temperatures per day were plotted, and thus represents typical orbital variations in that time period. Between day 10 and 20, the temperatures reach minimum values corresponding to the decreased incident flux, and the orbital variations are slightly smaller (corresponding to the longer periods in the sunlight at the higher Beta angles). The greatest orbital variations correspond to the low Beta angles. During this period, the leading edge CVCHPE experiment

saw conditions from full sunlight to full deep space exposure. Post-flight analysis indicated that the solar collector should have provided from two to 15 watts of orbit averaged heat into the fine control VCHP during the 45 days of data collection.

Figure 12 shows the data for the coarse control VCHP. The VCHP temperature was nearly constant, with its minimum value between day 10 and 20 which corresponds to the minimum environmental conditions. The reservoir temperature was closely coupled to the heatpipe, and had very little temperature change throughout the mission. Maintaining the reservoir at a nearly constant temperature just above the setpoint temperature is key to maintaining temperature control in a dry reservoir VCHP. The flight data showed that this "bootstrap" type of design worked extremely well in the real orbital operating conditions.

Figure 13 shows the data for the fine control VCHP. The fine control heatpipe had a thermistor on the back end of the evaporator (T1) and one on the heatpipe between the evaporator and condenser sections (T2). T2 is the best data for the actual heatpipe (i.e. vapor) temperature. Even in preflight tests, T1 was always about 2°C higher than T2 due to its closer thermal tie to the warmer mounting plate. The reservoir temperature was at about the same level as T1, and was very constant throughout the mission. The reservoir temperature may be more typical of the temperature control that could be provided to a hardware component in a real operating system. The reservoir was controlled within a  $\pm 1^\circ\text{C}$  control band.

Figure 14 shows that the coarse control VCHP remained with a  $\pm 0.25^\circ\text{C}$  control band and the fine control VCHP remained within a  $\pm 0.3^\circ\text{C}$  control band. The fine control band was almost identical to the preflight calculations, but the coarse control was significantly better than predicted. The smaller on-orbit heat load would have some effect, but it was still exposed to the wide variations in the on-orbit environments used in the pre-flight calculations. The flight data would indicate that for small loads, fine temperature control can be obtained with only a single dry reservoir VCHP.

One of the key goals of the flight experiment was to determine if there would be a long term upward temperature drift due to diffusion of ammonia into the reservoir, but the data indicated no major temperature changes. Both VCHPs reached their minimum temperatures between day 10 and 20 and then rose slightly through day 45, but it was impossible to determine if this very slight increase was due to a very small amount of diffusion or due to the warmer environment as shown in Figure 11. The very successful operation during the 45 days of data recording showed that the capillary tube did a very good job of preventing ammonia from entering the reservoir, but a significant amount of additional data would be required to extrapolate to see if there exists a small temperature setpoint rise over an extended mission.

Figure 15 shows that data gradually ended after about 45 days. Although the VCHPs do not require power to operate, the thermistor circuits do require power to operate. The 7.5 Volt lithium battery was simply drained of all its energy, causing the voltage to fall off and the apparent readings of the thermistors to gradually drop until the minimum (0 VDC) value was reached. Post flight test showed that the batteries were completely drained, and measurements of the power draw from the data circuits showed that the batteries should have supported 40 to 50 days of operation.

## POST-FLIGHT TESTS

The LDEF retrieval in January 1990 was supposed to "reset" all experiments. For the CVCHPE, the reset would close the solenoid valves, maintaining the end of orbit conditions in the VCHPs. The retrieval sequence did not reset the LDEF, and thus the CVCHPE valves were not closed. (Note: even if the CVCHPE were reset, the valves probably would not have closed because the batteries were drained

due to the extended mission). The valves were open during the hot reentry, the ferry flight back to KSC, and during all the processing steps at KSC. The valves were closed just prior to the tray removal from the LDEF in March of 1990. A short function check at KSC showed that all the thermistor circuits were still operating properly. Both batteries were completely drained. Using test batteries, we conducted a short functional test at KSC, and both valves opened and closed properly. The only small anomaly that was found was that Valve 1 (coarse control VCHP) opened when a simulated initiate command was sent. This was later traced to the failure of a small transistor, but the failure had no effect on the on orbit data collection.

Post-flight performance tests of the CVCHPE were run at MDESC in March of 1991 to determine any changes in VCHP performance or setpoint. It is not possible to determine, though, if temperature shifts were due to ammonia diffusion during the six years in orbit or if ammonia was pushed into the reservoir during the post-flight activities when the valves were still open. During the period from retrieval until the valves were closed, the temperature was above the setpoint of the VCHPs which increases the potential for forcing ammonia into the reservoirs, especially the lower temperature setpoint coarse control VCHP.

The CVCHPE was set up for a bench test using a liquid coldplate to simulate a sink temperature from 0°C to -30°C at a 10 Watt heat load. The bench test results are shown in Figure 16. The fine control VCHP set point increased by 5°C and the coarse control VCHP set point change by almost 9°C in the post flight tests. Since we do not know if the shift was due to in-flight diffusion or post-flight activities, we cannot project the data to provide very long life performance estimates. The setpoint, though, was stable in the  $\pm 0.3^\circ\text{C}$  control band for the fine control VCHP and  $\pm x.x^\circ\text{C}$  for the coarse VCHP. These tests were run for heatloads of 5 to 15 watts, and sink temperatures from -30°C to 0°C. Some tests were repeated about a month later, and showed an addition 2°C to 3°C setpoint shift which indicates that ground handling can have a significant effect on the setpoint. Conservatively, we can say the drift was less than 1°C per year, but believe that the actual on-orbit set point shift was much less. The temperature control band was essentially the same after the six year flight as during pre-flight tests.

## CHANGES TO EXTERNAL COATINGS

The change in the external materials of the CVCHPE over the nearly six years in orbit was dramatic as shown in a comparison of the pre-launch and recovery pictures, Figure 7 and 17. The CVCHPE was on the leading edge or "ram" direction, and thus it received the greatest amount of erosion due to atomic oxygen degradation. The entire outer Kapton layer on the MLI was eroded away, but this was expected. The black chrome solar collector had numerous areas of discolorations. Figure 18 shows a close-up of the experiment after it was removed from the LDEF.

Figure 19 shows one section of the MLI blanket after removal after flight. Some of the Kapton outer layer can be seen along one edge, but this was the edge that was "tucked-in" along the edge of the experiment, and thus was not exposed to direct impingement. All of the Kapton that was exposed to direct atomic oxygen impingement was eroded away, but the second layer which was double aluminized Kapton, was still intact. Kapton is very susceptible to atomic oxygen, and it was no surprise that it was eroded away in the low LDEF orbit. Aluminum, though, will not be significantly eroded by atomic oxygen. Figure 20 shows a close up of the edge of the Multi-Layer Insulation (MLI) that was tucked into the edge. The various degrees of erosion on the Kapton can be clearly seen in Figure 20. The small Kel-F button on the MLI was clear on the protected side, but the erosion can be seen on the exposed side.

Figure 21 shows a close-up of the black chrome solar collector. The black chrome that was exposed had a duller, matted finish. Note that the large stain is almost identical in shape to the MLI flap seen

covering the collector in Figure 17. The colored "stains" around the edges and on the one side were originally believed to be some type of interaction with the Kapton, but post-flight tests conducted at Boeing Aerospace and Electronics Co. showed no traces of Kapton. We now believe the stains were caused by high temperatures resulting in a change in the oxidation state of the black chrome. When the atomic oxygen stripped off the Kapton, bare aluminum was exposed. The aluminum has a very high absorptivity/emmissivity ratio and a very low mass. Thus, in direct sunlight this thin layer could reach very high temperatures causing the temperature effects on the black chrome. Figure 22 shows the post-flight measurements made by Boeing. The only significant degradation was in the stained area, but even in this area the property ratio was above 8.0 which still makes an excellent solar collector.

Figure 23 shows a picture of the silver/Teflon radiator after the flight. The surface appeared to be "milky" white in appearance due to small amount of erosion on the outer surface. Silver teflon is much less susceptible to atomic oxygen erosion than Kapton. The radiator was sent to McDonnell-Douglas Space Systems Co. for evaluation. They found that 0.03 mm of the total original 0.13 mm thickness of Teflon was eroded away and the solar absorptivity was 0.11 which was less than 0.02 degradation over preflight values. The emissivity decreased from 0.81 to 0.79 as a result of the thinning of the Teflon layer. Thus, even though the appearance was remarkably different, the actual optical property change was relatively small.

The micrometeorite impact group from NASA/JSC inspected all surfaces on LDEF. On the CVCHPE they found 388 micrometeorite impacts: 221 were under 0.5 mm in size, and the rest were over 0.5 mm. Figure 24 shows one impact (2.8 mm dia) on the silver Teflon radiator. The shock waves from this impact could be seen in the Teflon over a 50 mm diameter, and we suspect some delamination of the Teflon in this area but additional tests must still be conducted to determine the extent of the delamination. In spite of the numerous external impacts, there was no evidence that any penetrated to the interior or compromised the pressure integrity of the ammonia VCHP

### ELECTRONICS ANOMALY

All the electronics and data functions worked properly in the post flight checkout except for one small anomaly. When the experiment was reset and the initiate command was applied, Valve 1 opened even though T3 was not below -6°C. The flight data showed that this function worked properly during the initial flight sequence, but no longer worked in post flight tests. When we opened the electronics box, we found one failed transistor and a burned-out resistor as shown in Figure 25. Apparently, the transistor shorted to ground which caused a larger current draw which burned out the adjacent resistor. The components were sent to Boeing for future evaluation, and they confirmed the failure mode. Although we know the failure mode, we still do not know why the failure occurred, and why the high temperature damage to the transistor was so severe. We had an identical circuit for Valve 2, but this circuit showed no anomalies in post-flight tests. The shorted transistor would have drained the 28VDC battery in a few days, but it should not have affected the 7.5 VDC battery used for the data system. The two damaged components were replaced, and the system operated perfectly during checkout. The circuit only needed to operate once to open the valves, and the flight data showed it did operate properly during this initial sequence. Thus, we can only conclude the damage occurred during the valve opening sequence.

### CONCLUSIONS

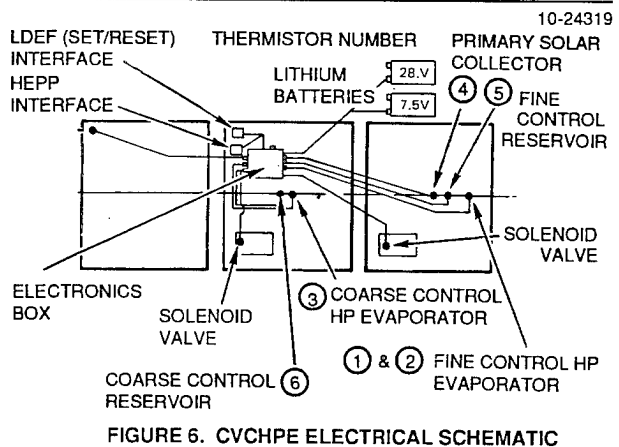
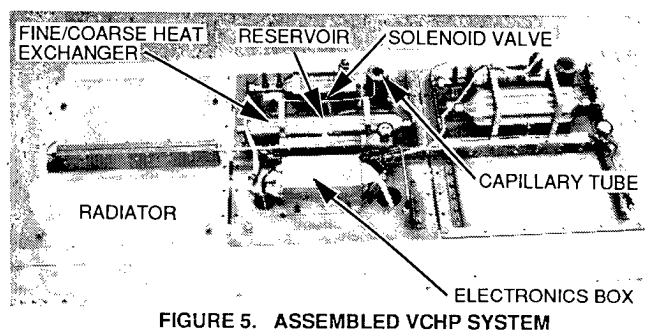
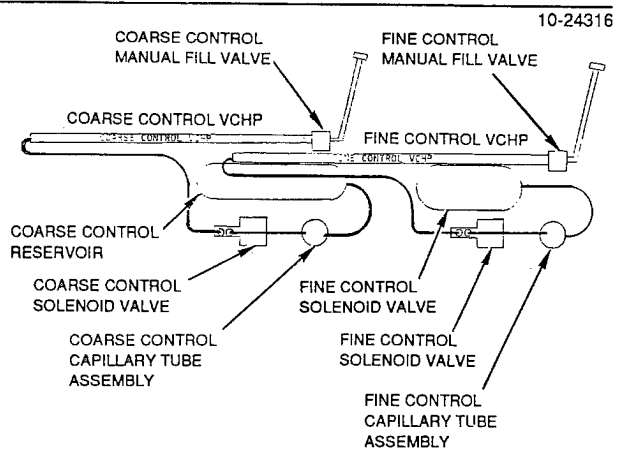
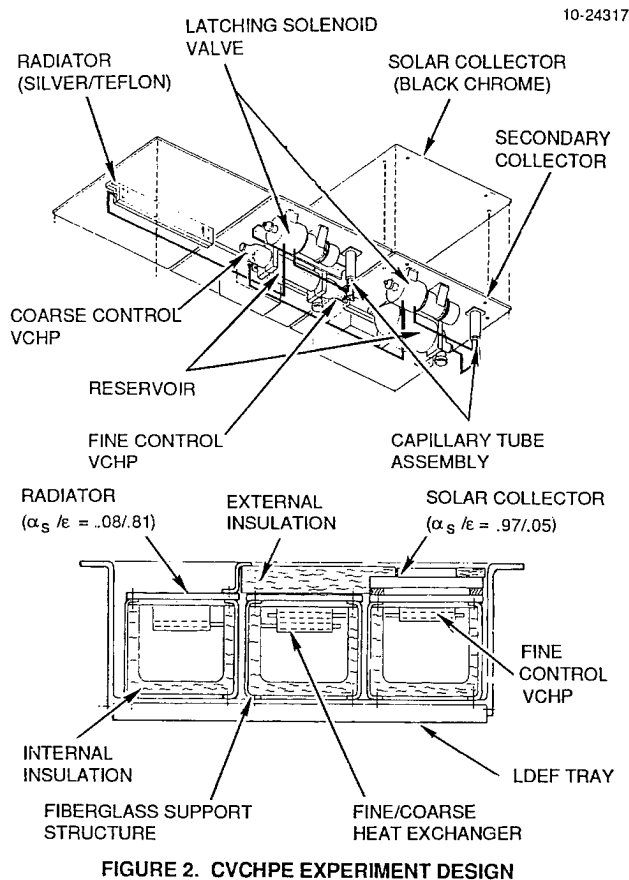
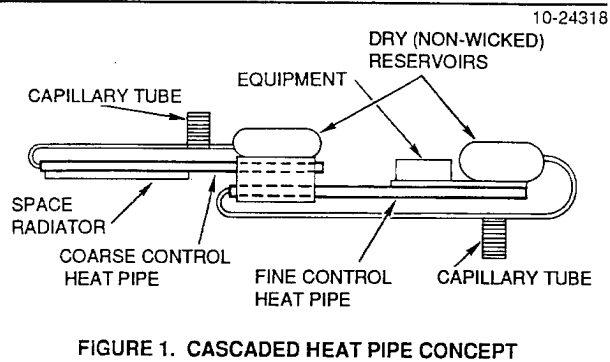
The CVCHPE experiment successfully demonstrated temperature control of  $\pm 0.3^\circ\text{C}$  using a dry reservoir VCHP concept in a widely varying environment of a low earth orbit. The flight data indicated that only one VCHP was required to maintain precise temperature control. Post-flight tests indicated

upward shifts in both VCHP set points, but it was uncertain whether these shifts were caused by on-orbit diffusion or post-flight activities. Although the set point shifted, the VCHPs still maintained the  $\pm 0.3^{\circ}\text{C}$  control in post flight tests. Even if all the shift accrued in orbit, the average drift rate was less than  $1^{\circ}\text{C}$  per year. The LDEF mission was extended to almost six years in orbit, which produced a significant amount of erosion on the external surfaces, but the effects of the erosion on the performance of the experiment were minor. One small anomaly occurred in the electronics, but this had no effect on the operation or data from the A0076 experiment.

#### REFERENCES

1. Steele, W. H., and McKee, H. B. "A Precise Satellite Thermal Control System Using Cascaded Variable Conductance Heatpipes" AIAA Paper AIAA-77-777, June 1977.
2. Marcus, B. D. "Theory and Design of Variable Conductance Heatpipes", NASA CR-2018, April 1972.
3. Chi, S.W. "Heat Pipe Theory and Practice", Hemisphere Publishing (TJ264.C47), 1976.
4. LDEF Mission 1 Experiments, NASA SP-473.
5. Calhoun, L.D. and Grote, M.G., "The Cascaded Variable Conductance Heatpipe Experiment on LDEF" AIAA paper AIAA-81-1157, June 1981.
6. Suelau, H. J., Brennan, P. J., and McIntosh, R. "HEPP-A Low Temperature Heat Pipe Experiment Package Onboard the LDEF" AIAA paper AIAA 78-459, May 1978.
7. Grote, M. G., "Results from the Cascaded Variable Conductance Heatpipe Experiment On LDEF", AIAA paper AIAA-91-1356, June 1991.





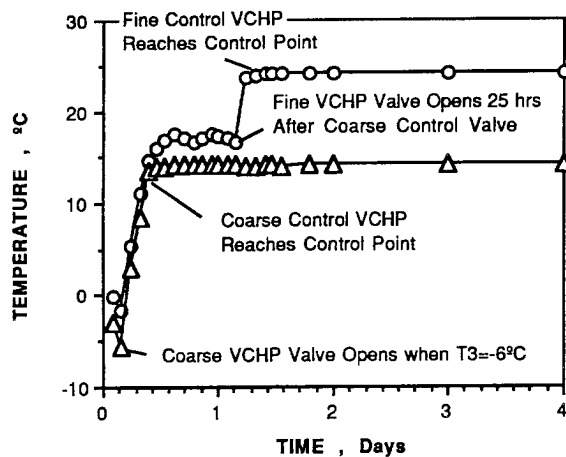


FIGURE 8. EXPERIMENT START-UP TRANSIENT

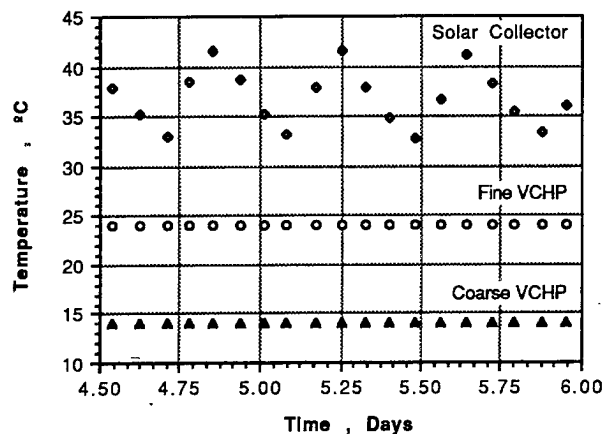


FIGURE 9. ORBITAL TEMPERATURE VARIATIONS

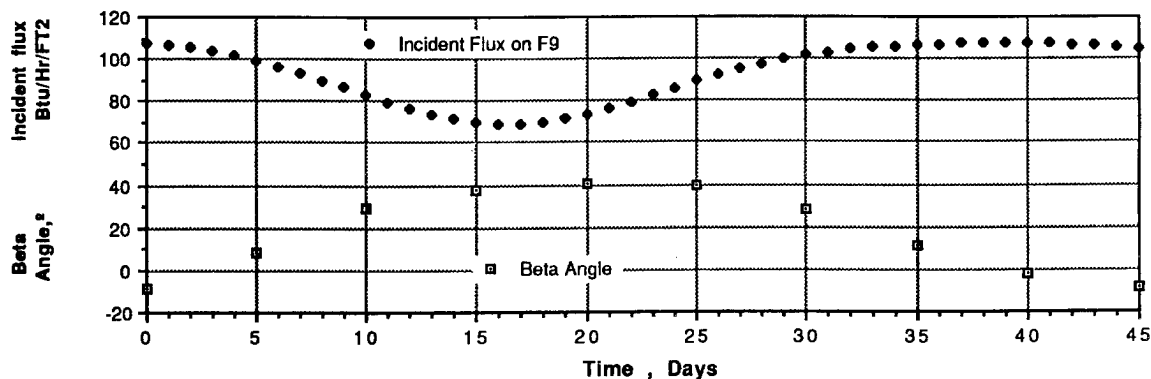


FIGURE 10. BETA ANGLE AND HEAT FLUX

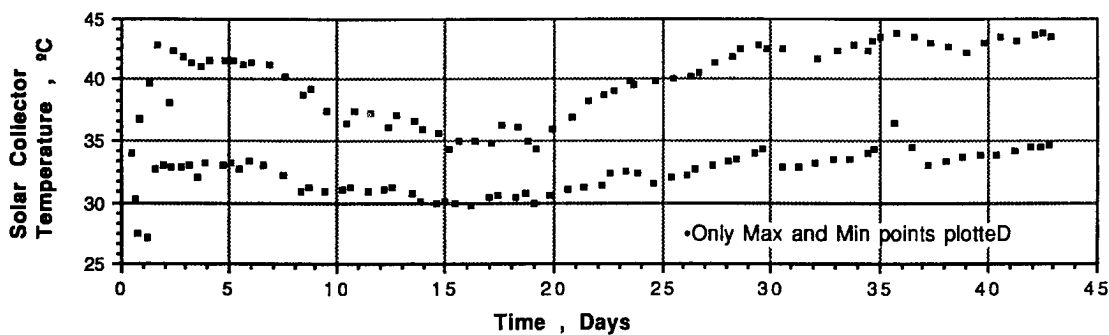


FIGURE 11. SOLAR COLLECTOR TEMPERATURE

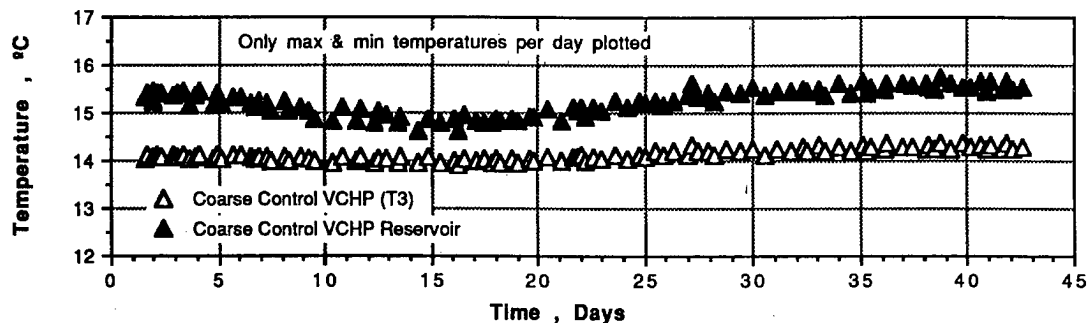


FIGURE 12. COARSE CONTROL VCHP TEMPERATURE DATA

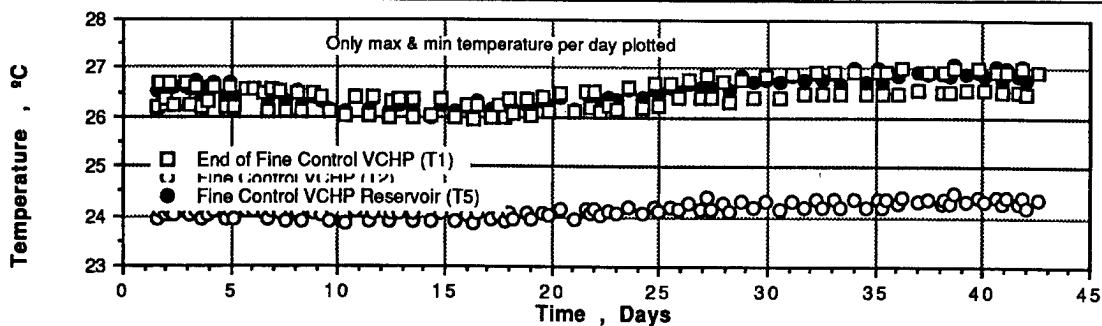


FIGURE 13. FINE CONTROL VCHP TEMPERATURE DATA

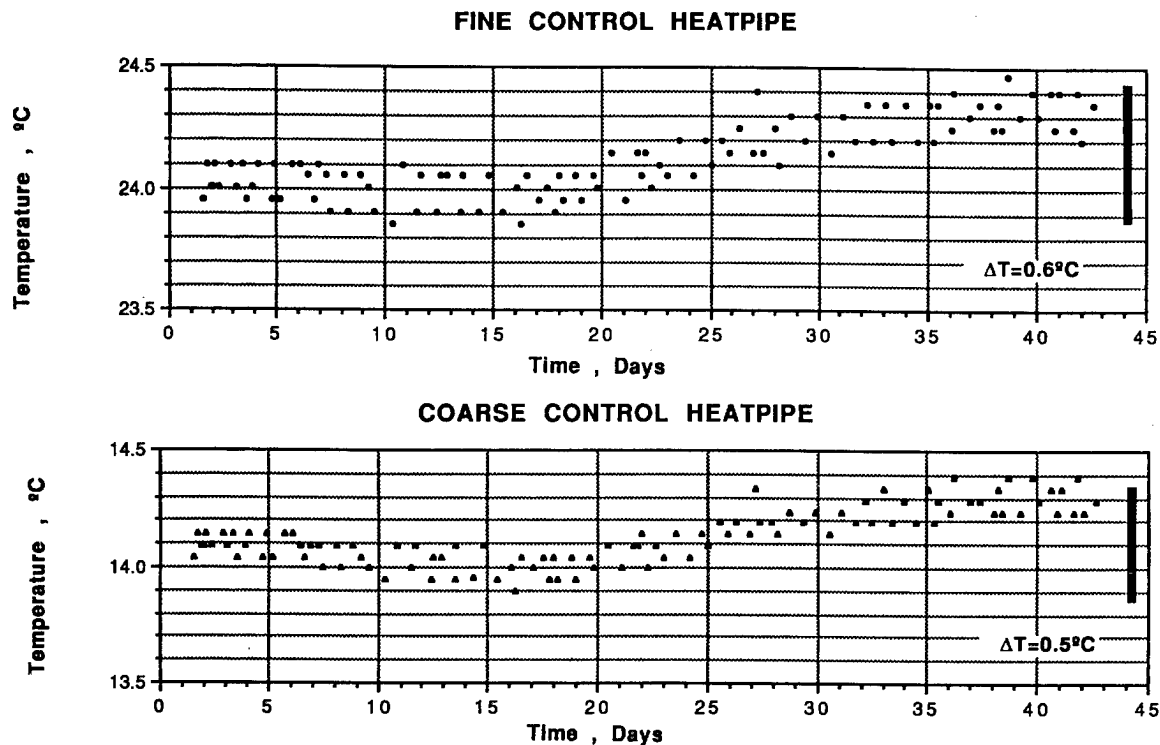


FIGURE 14. TEMPERATURE HISTORIES OF VCHPs

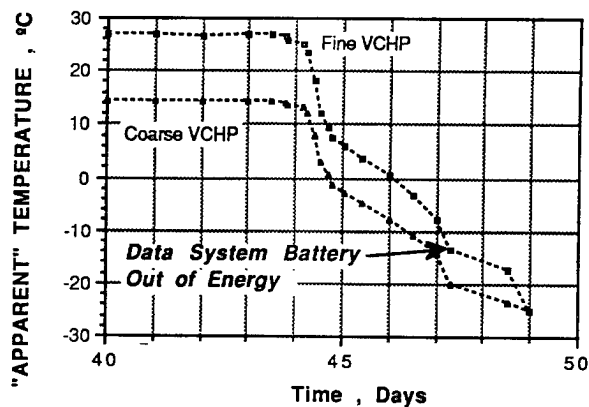


FIGURE 15. END OF A0076 DATA COLLECTION

10-24690

VCHP	FLIGHT DATA	POST-FLIGHT	DIFFERENCE
FINE CONTROL	24.3°C	29.4°C	5.1°C
COARSE CONTROL	14.3°C	23.0°C	8.7°C

FIGURE 16. COMPARISON OF FLIGHT TO POST-FLIGHT DATA

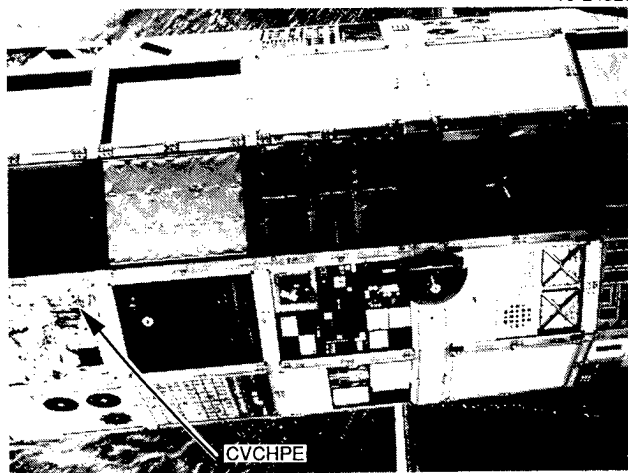


FIGURE 17. LDEF DURING RETRIEVAL



FIGURE 18. CVCHPE EXPERIMENT AFTER FLIGHT

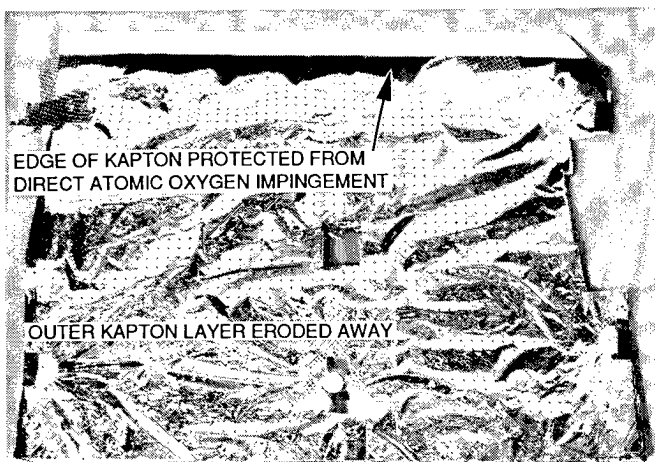


FIGURE 19. SEGMENT OF MLI BLANKET AFTER FLIGHT

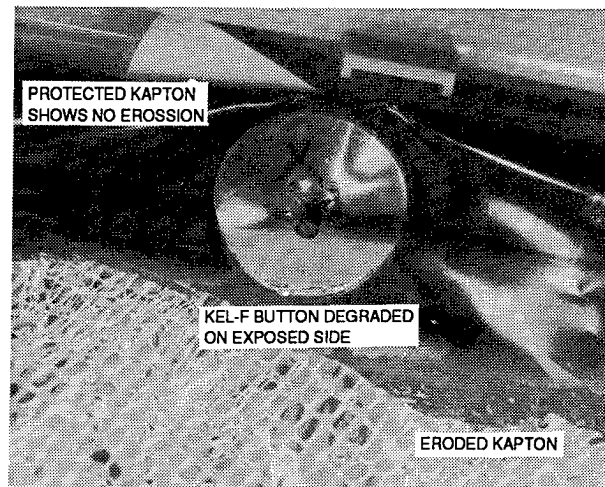


FIGURE 20. PROTECTED EDGE OF MLI BLANKET

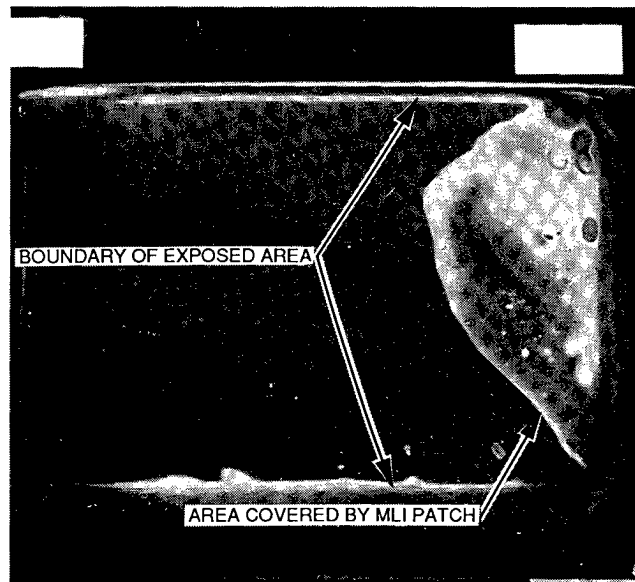


FIGURE 21. SOLAR COLLECTOR AFTER FLIGHT

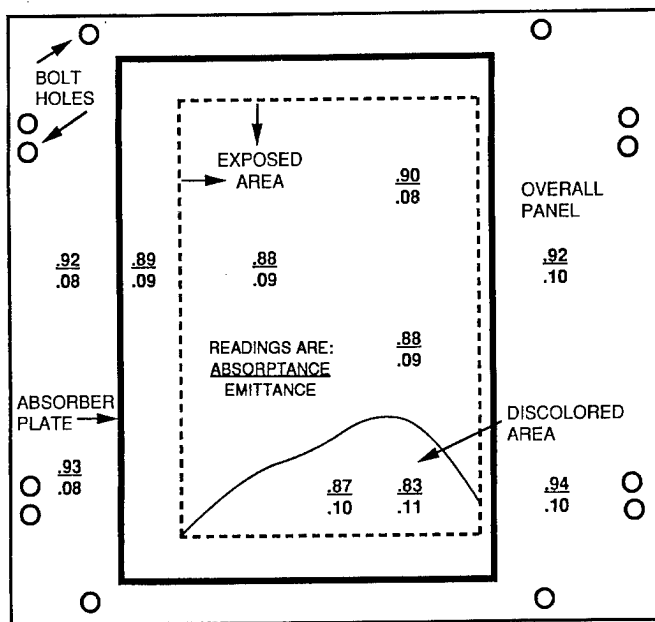


FIGURE 22. POST-FLIGHT MEASUREMENTS OF BLACK CHROME SOLAR COLLECTOR

10-24327

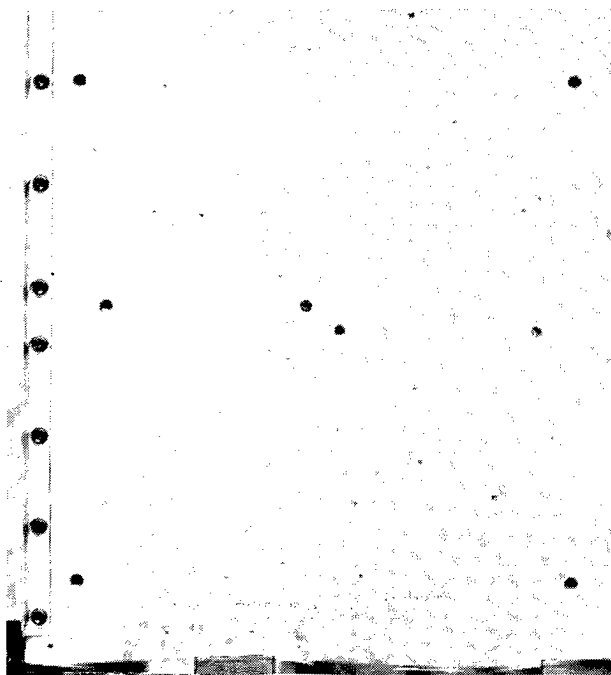


FIGURE 23. SILVER/TEFLON RADIATOR

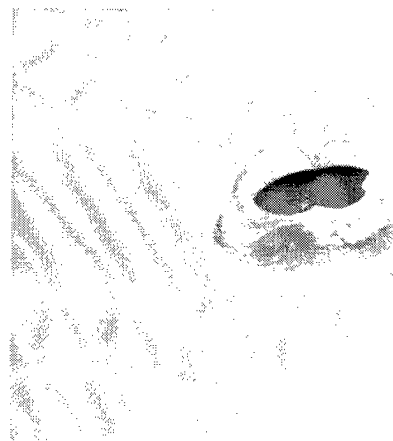


FIGURE 24. MICROMETEOROID IMPACT ON SILVER/TEFLON RADIATOR

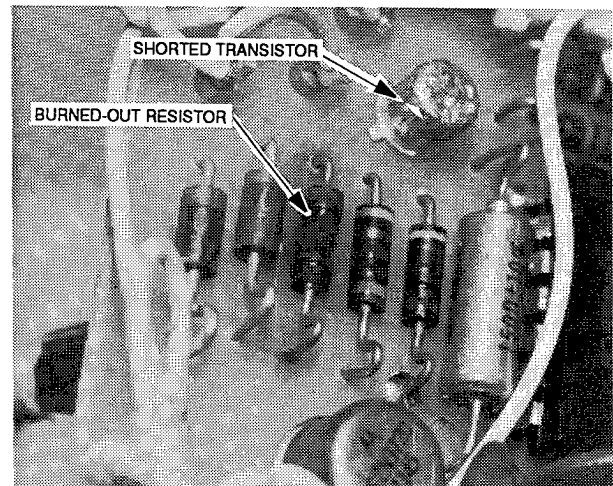


FIGURE 25. FAILED ELECTRONICS COMPONENTS IN VI CIRCUIT

## TRANSVERSE FLAT PLATE HEAT PIPE EXPERIMENT

David Shular  
NASA/Marshall Space Flight Center  
Huntsville, AL 35812  
Phone: (205) 544-8734

### ABSTRACT

The Transverse Flat Plate Heat Pipe is a thermal control device that serves the dual function of temperature control and mounting base for electronic equipment. In its ultimate application, the heat pipe would be a lightweight structural member that could be configured in a platform or enclosure, and provide temperature control for large space structures, flight experiments, and equipment. The purpose of this experiment is to evaluate the zero-g performance of several heat pipe modules. Performance assessment will include: (1) the systems heat transport capability, (2) temperature drop between evaporator and condenser and, (3) the ability to maintain temperature over varying duty cycles and environments. Additionally, performance degradation, if any, will be monitored over the length of the LDEF mission. The objective of this experiment is to demonstrate that a self-regulated heat pipe thermal control system can maintain hardware temperatures within tolerances of  $\pm 9^\circ\text{F}$  or less with varying heat inputs, independent of vehicle/payload orientation.

### INTRODUCTION

The use of heat pipes as a thermal control system in industrial, military, and space applications has increased in the past two decades. Applications cover a wide range of temperatures from cryogenic and ambient to high temperature systems, and employ working fluids such as methanol and ammonia to liquid metals. Heat pipes are employed in everyday uses such as circuit board cooling and pipeline de-icing systems, as well as tactical missiles, battlefield communications systems, and spacecraft electronics.

The operational performance of heat pipes has also increased with expanded applications. Early generation heat pipes could transport 50-100 watts of power only a few feet at ambient temperatures. Currently, artery wick heat pipes can transport 1000 watts of power up to distances of 10 feet or more with temperature drops in the range of a few degrees. Heat pipes are also incorporating variable conductance features and diode functions to maintain heat source temperatures at a constant level while the heat input increases up to 200 percent or more.

The application of heat pipes as a thermal control system offers many advantages over a conventional pumped fluid loop or cold plate. Due to the nature of their design, heat pipes have an inherent reliability since they possess no moving parts. Since the Enthalpy of Vaporization for a fluid is generally quite large, heat pipes have the capability of transporting heat energy over relatively large distances with very little temperature drop. This results in very efficient operation. Also, since heat pipes are driven by the pressure differences between the fluid and the vapor, no external power is required. These features, along with the variable conductance capability to provide temperature control over wide variations in source heat loads, make heat pipes a highly attractive option for waste heat management of on-orbit systems and spacecraft.

## OBJECTIVE

The objective of this experiment is to demonstrate that a self-regulated heat pipe thermal control system can maintain hardware temperatures within tolerances of  $\pm 9^{\circ}\text{F}$  or less ( $\pm 5^{\circ}\text{C}$ ) with varying heat inputs independent of vehicle/payload orientation. The concept of this investigation is to utilize current heat pipe technology to design and fabricate a heat pipe thermal control experiment, demonstrate the hardware capability and performance in the low earth orbital environment, and correlate the retrieved flight data with data from thermal vacuum ground testing.

## FLIGHT EXPERIMENT

LDEF Experiment S1005 "The Transverse Flat Plate Heat Pipe Experiment" consists of three transverse flat plate modules mounted together to form a panel 34 inches wide by 50 inches long. The structure was then installed within a 12 inch deep LDEF experiment tray (see Figure 1)

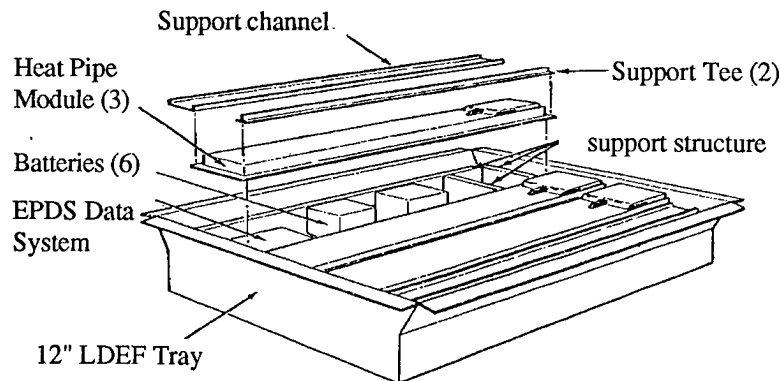


Figure 1. LDEF S1005 Experiment Tray

Heat is supplied to the evaporator side of the test modules via electrical strip heaters which simulate heat rejection by electronic equipment. Power is supplied by Lithium Monofluorographite batteries, the particular types are Eagle Picher MAP 9036. The heat from the condensor region of the heat pipe modules is radiated to space from the outboard facing radiator surface. The heater duty cycles are pre-timed to provide load inputs at discrete mission times. Power and temperature data are recorded on magnetic tape, (Lockheed Electronics Flight Data Recorder) with all timing and relay functions controlled by an Experiment Power and Data System (EPDS).

Grumman Aerospace Corporation, the manufacturer of the heat pipe modules for LDEF experiment S1005, was granted a patent for the transverse concept (Reference 1). Originally configured in a cylindrical geometry (Reference 2), it was developed to reduce the problem of gas bubble artery blockage found in conventional artery wick designs. This blockage by generated non-condensable gases limits the operating capacity in the variable conductance mode to small

loads. The transverse flat plate concept flown on LDEF is shown in Figure 2. In this design, liquid returned to the evaporator from the condenser in a direction perpendicular (i.e., transverse) to the vapor flow. Variable conductance temperature control is achieved by using non-condensable gas (Nitrogen) which is contained in a reservoir separate from the heat pipe module. The configuration of the heat pipe is described in greater detail in AIAA Paper 78-429, "Transverse Flat Plate Heat Pipe" (See Reference 3).

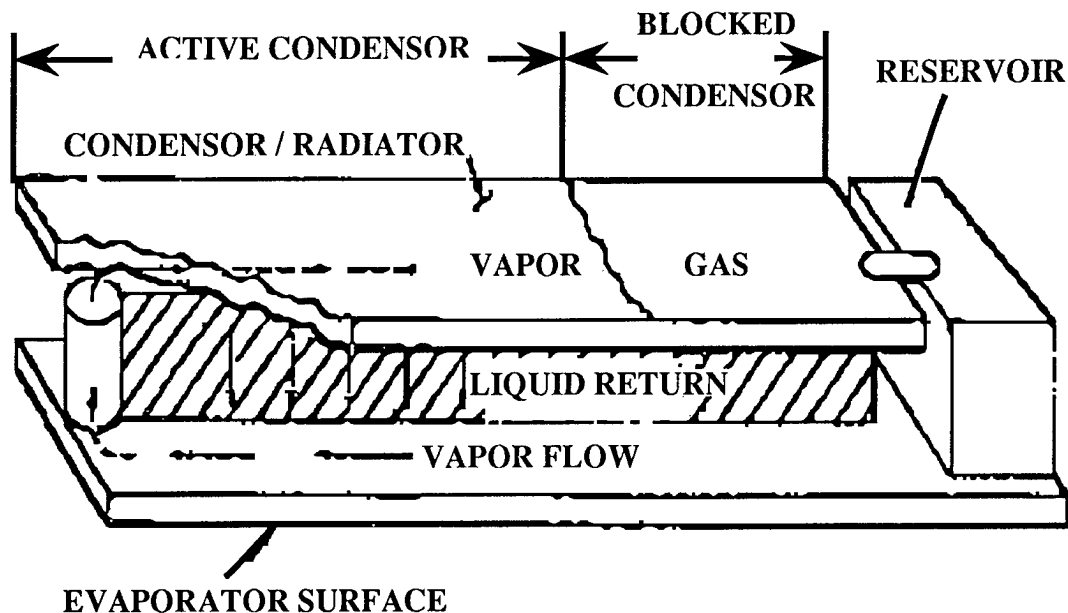


Figure 2. Liquid/Vapor Flowpaths

#### DESIGN

A set of design guidelines was established for the experiment which would meet the program objectives of demonstrating the flight performance of the transverse flat plate heat pipe concept.

The following guidelines were established for the experiment:

- Overall Experiment Size: 50" x 34" x 12" to be compatible with the LDEF experiment tray
- Weight of Experiment: 190 pounds total
- Data Acquisition: Self-contained, data to be retrieved along with experiment for subsequent inspection, reduction, and analysis after orbital lifetime
- Heat Load: The waste heat load for the radiator panel shall be at least 13.4 watts/ft<sup>2</sup>
- Local Heat Load: The maximum local heat load shall be 23.3 watts/ft<sup>2</sup>
- Control power: None
- Thermal Environment: The exterior radiator will be exposed to one solar constant, deep space and near earth inputs consistent with an orbital altitude of 270 nm and an inclination of 28.5 degrees with respect to the equatorial plane
- Control Temperature: The equipment mounting face of the heat pipe panel (i.e., the evaporator) shall be maintained at a nominal value of 68 +/- 10° F (20 +/- 5° C)



- Ground Test: The design of the transverse flat plate modules will allow ground testing of the experiment in some preferred orientation

## CONFIGURATON

The basic experiment configuration consists of the following major components:

- Three transverse flat plate heat pipe modules
- One Experiment Power and Data System (EPDS)
- Set of instrumentation
- Six heater batteries
- Heater elements
- Master relay box

## EXPERIMENT TIMELINE

The experiment timeline is shown in Figure 3 . Three identical experiment on-times were utilized during the mission. Each on-time lasted for 8.6 orbits with this period sub-divided into two 4.3 orbit heater input sub-periods (approximately 6.45 hours/sub-period). The initial on-period occurred 30 days after deployment of the LDEF facility, the second period occurred 67.5 days later with the third and final on-period 67.5 days after the second. The three identical on-periods at different times of the LDEF mission allow the identification of any performance degradation that may occur during the orbital lifetime. The power input to the heat pipe modules during the experiment on-periods is shown in Figure 4 .

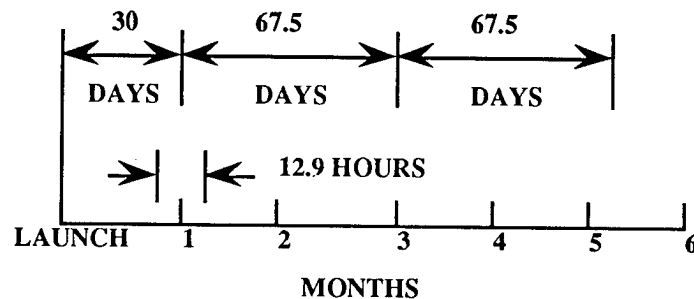


Figure 3. Experiment S1005 Timeline

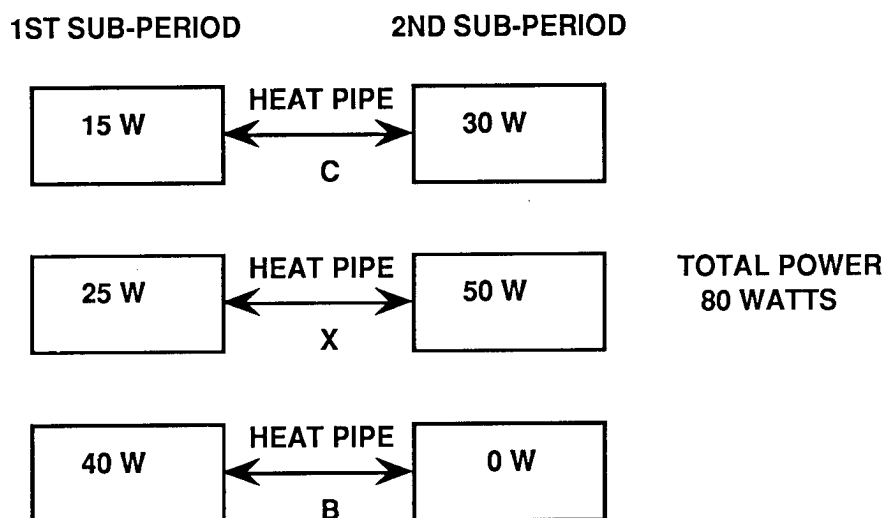


Figure 4. Heater Power Input

#### PRE-FLIGHT THERMAL VACUUM TEST

Four flat plate modules were built by Grumman Aerospace Company of Bethpage, New York. Three of the modules were used for the flight experiment with the fourth being a flight spare. A thermal vacuum test was performed on the flight spare by Grumman at their facility. Figure 5 shows test data of the mounting surface temperature as a function of heat input load under different environments. At an environment of  $-130^{\circ}\text{F}$ , the mounting surface remains between  $68 \pm 9^{\circ}\text{F}$  while the load input varies between 25 and 42 watts. At power levels below 25 watts, the evaporator temperature drops below  $59^{\circ}\text{F}$  as residual conduction losses become an appreciable portion of the total load. It should be noted that even at power levels of 25 watts, there is sufficient capability to keep the equipment mounting surface at  $60^{\circ}\text{F}$ . This compares to a temperature of  $0^{\circ}\text{F}$  that would result from a fixed area radiator of equivalent size.

Between the environments of  $-40^{\circ}\text{F}$  and  $-130^{\circ}\text{F}$ , evaporator surface temperature is maintained at  $68 \pm 9^{\circ}\text{F}$  at a relatively constant load of 26 watts. In actual use, larger equipment load variations can be tolerated since the operating range for most electronics is greater than the design parameters of the heat pipes modules. For example, most spacecraft electronics can easily tolerate a control temperature of  $68 \pm 18^{\circ}\text{F}$ . The flat plate modules can maintain this temperature zone at an environment from  $-130^{\circ}\text{F}$  to  $-40^{\circ}\text{F}$  while the heat load varies between 22 and 39 watts.

The performance of the heat pipe module at a fixed heat load of 40 watts under four different environments ( $-200^{\circ}\text{F}$ ,  $-130^{\circ}\text{F}$ ,  $-70^{\circ}\text{F}$ , &  $-40^{\circ}\text{F}$ ) was also assessed. For these cases the mounting surface temperature varies  $15^{\circ}\text{F}$  as compared to a variation of  $56^{\circ}\text{F}$  that would result if a fixed area radiator of equivalent size were used. At ambient environments greater than  $-40^{\circ}\text{F}$ , the variable conductance heat pipe would behave as a fixed area radiator since the the condensor is fully open.

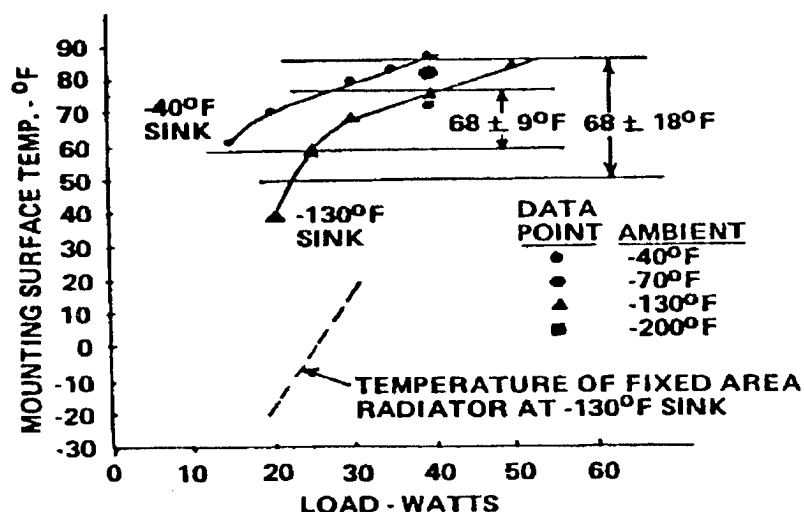


Figure 5. Thermal Vacuum Test

#### FLIGHT PERFORMANCE

Temperature and power input data retrieved from the experiment's flight data recorder are shown in Figures 6-11. The power inputs to the heater elements, which are located on the evaporator, are plotted with the radiator temperatures. This is done to more accurately assess fluctuations in the radiator surface temperatures with changes in the heater power input levels. It should be noted that the data does not represent the actual evaporator and condensor temperatures of the heat pipes. The heat pipe modules consist of a heat pipe that is sandwiched between two pieces of aluminum honeycomb structure that is then wrapped in an aluminum skin. The data plotted represents the temperature of the outer aluminum skin.

#### Heat Pipe Unit "C"

The heat pipe module designated "Unit C" is characterized by a heater input of 15 Watts during the first heater input sub-period, and an additional 15 Watts during the second period. Heater performance was better than expected during the early phase of the LDEF mission. No type of active power control was utilized on the experiment, and heater performance was typically 15% above nominal. Figures 6 & 7 show the orbital performance of this heat pipe during the first experiment on-time. During the first sub-period, the heat pipe is operating in a heat-sink mode since 17.5 Watts of power is below the amount necessary to fully activate the module. As the second heater period is initiated, the module becomes fully operational as the total power input rises to 35 Watts. Analysis predicts that 22-25 Watts is necessary to fully activate the heat pipes. The transition of the heat pipe module from the heat sink mode to full operation condition can be seen in Figure 7.

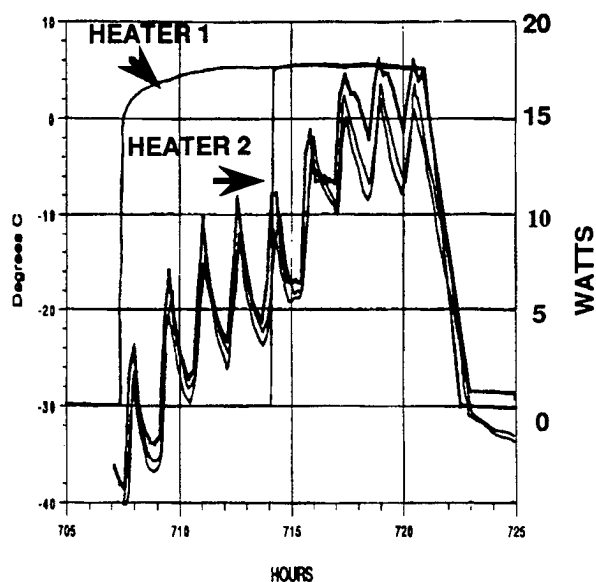


Figure 6. Unit C Radiator

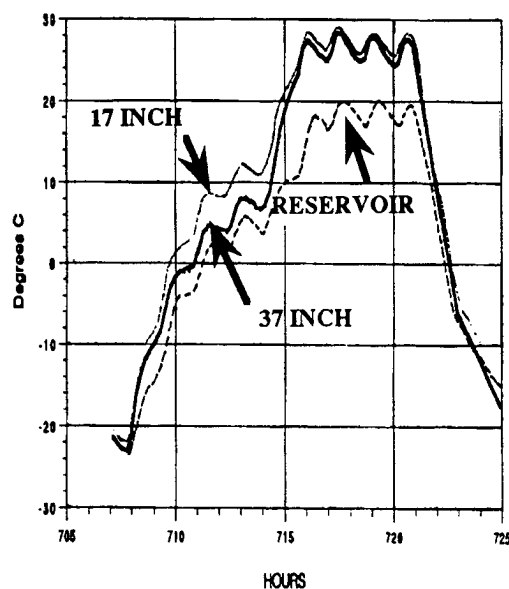


Figure 7. Unit C Evaporator

### Heat Pipe Unit "B"

The "Unit B" heat pipe is characterized by a nominal power input of 40 Watts during the first sub-period, and a no-load (i.e., zero power input) condition for the second period. Figures 8 & 9 show the performance of this module during the second experiment on-time. As can be seen in Figure 9, the evaporator region exceeds the design objective of  $20 \pm 5^\circ \text{C}$  by approximately  $4^\circ$ . The cause of this deviation is most likely due to non-uniform thermal contact between the evaporator heater surface and the heat pipe evaporator, which are separated by a bonded honeycomb structure.

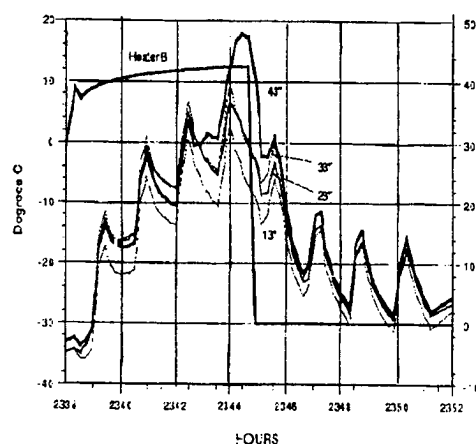


Figure 8. Unit B Radiator

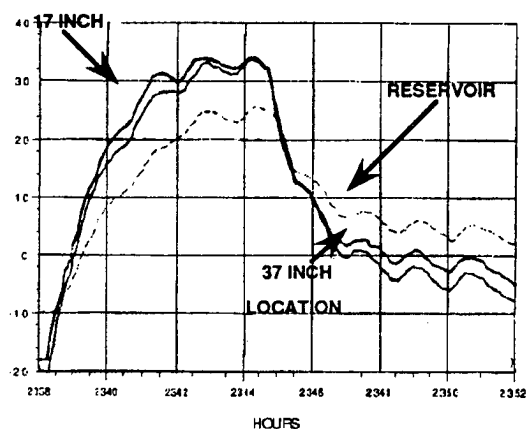


Figure 9. Unit B Evaporator

## Heat Pipe Unit "X"

The heat pipe module designated "Unit X" is characterized by the primary design objective of maintaining the equipment mounting surface at  $20 \pm 5^\circ \text{C}$  while the heat input load varies from 25 to 50 Watts. Figures 10 & 11 show data taken from the second and third experiment on-times. Figure 10 is an excellent example of the heat pipe's variable conductance feature in operation. Note the plot of the 43" thermistor location, which is located at the top of the heat pipe module (i.e., near the reservoir). During the first sub-period the temperature is colder than the rest of the radiator surface. This is due to the fact that this area has been "shut-off" from being an active condensing region by the nitrogen gas bubble. As the heat load increases during the second sub-period, the increased pressure of the methanol vapor forces the nitrogen gas to retreat into the reservoir. The region has now become an active condensing surface and the temperature response of the thermistor indicates that this portion of the heat pipe is in full operation.

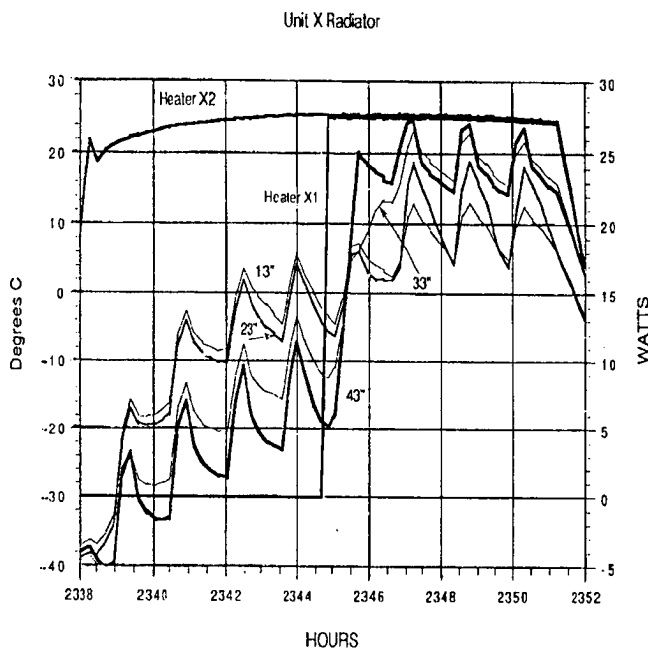


Figure 10. Unit X Radiator

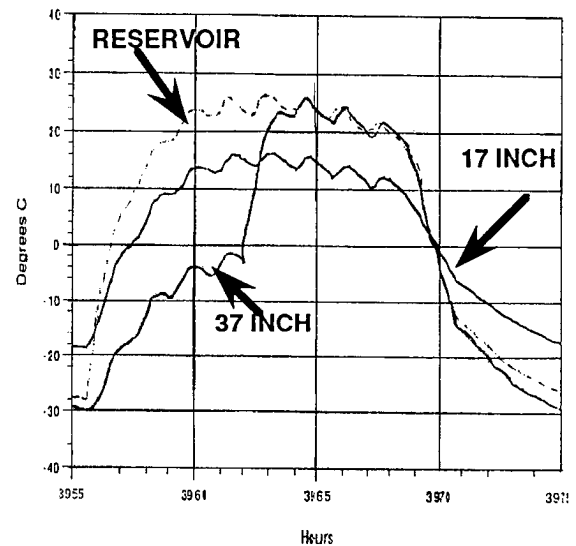


Figure 11. Unit X Evaporator

By comparison of Figures 7,9,&11 it can be seen that the reservoir temperature of Unit X was higher than the evaporator temperature during the first sub-period. This was unexpected since the reservoir is located in a non-heated region of the heat pipe module. The reservoir is attached however to the equipment mounting surface of the evaporator and is heated by conduction through the mounting plate. The reservoir is also shielded against radiation heat transfer that is emanating from the on-board experiment electronics. It is possible that all the heat conduction paths to this module may not have been completely isolated, and further testing and analysis will be performed to locate the source.

## SUMMARY

On-orbit performance of the "Transverse Flat Plate Heat Pipe Experiment" was consistent with the pre-flight thermal vacuum test data. The ability of the variable conductance heat pipe design to maintain heat source temperatures within the specified tolerances, with varying heat inputs, was clearly demonstrated. The two discrepancies noted are attributed to assembly procedures and not the heat pipe design. Post-flight thermal vacuum testing of the three heat pipe modules is planned for the near future to document any performance degradation that may have occurred while on-orbit.

## ACKNOWLEDGEMENT

The author wishes to express his thanks to the co-investigator, Fred Edelstein of Grumman Aerospace Corporation, for aide and support in the success of LDEF experiment S1005, "The Transverse Flat Plate Heat Pipe Experiment".

## REFERENCES

1. United States Patent No. 3,958,627,  
" Transverse Variable Conductance Heat Pipe ".
2. Edelstein, F., "Transverse Header Heat Pipe ",  
AIAA Paper 75-656.
3. Edelstein, F., " Transverse Flat Plate Heat Pipe  
Experiment ", AIAA Paper 78-429.

Exposure to Space Radiation of High-Performance  
Infrared Multilayer Filters and Materials  
Technology Experiment (A0056)

Gary J. Hawkins, John S. Seeley, Roger Hunneman

The University of Reading, Infrared Multilayer Laboratory,  
Department of Cybernetics, Whiteknights,  
Reading, Berkshire, RG6 2AY, England.

Abstract

Infrared optical-multilayer filters and materials were exposed to the space environment of low Earth orbit on LDEF. This paper summarizes the effects of that environment on the physical and optical properties of the filters and materials flown.

Introduction

The University of Reading experiment (A0056) onboard LDEF<sup>(1)</sup> was an exposure of the particular optical materials and filters known to be useful in atmospheric and planetary remote sensing satellites. Longterm we are manufacturers / suppliers of filters for those types of spaceflight radiometer instruments which measure IR emissions from the major atmospheric gases, pollutants and aerosols, and from the sea or land surface. Progress in the general science of radiometry from space has been rapid, having now evolved to the extent that Global change is considered observable; currently, as a contribution to GCRP, radiometers are being planned to fly in the EOS/ERS/POEM satellites capable of monitoring parameters such as structure, atmosphere dynamics and composition in situ. Further, EOS accuracy is intended to be sufficiently good for valid deduction of temperature gradient, mixing / transport of the gases, surface flux etc. As with the earlier radiometers spectral bands are defined by optical filters for the selection of the particular molecular species of interest. The spectral width and resolution of filters, together with the stability and durability of their materials and processes, therefore remains especially significant in the science. The study of those aspects of optical filters (as supplied for spaceflight) has been our main preoccupation since the mid 1960's; an opportunity to participate in LDEF was therefore timely for us and, as it is turning out, particularly relevant.

Temperature-sounding has been a feature of meteorological satellites since their inception in the NIMBUS, TIROS and ITOS radiometer series, from which the criteria for spectral resolution of interference filters was initially defined.

The Reading University experiment was intended to expose infrared multilayer interference filters of novel Design, High Performance, Construction and Manufacture to space radiation. The spectral behaviour of these filters when in space was unconfirmed previously, but crucial to filter performance.

High-performance, in this context, relates to the precision and discrimination with which the emission spectra of important atmospheric gases can be resolved.

### Experiment Construction

The University of Reading experiment comprised 46 individual components divided between an Earth facing tray number G12 and leading edge tray number B08 (Figs. 1 & 2). Each was designed to maximize the exposure at full aperture to the complete range of space radiations and temperature excursions received by LDEF. We occupied 1/4th of tray G12, and 1/6th of tray B08.

Each of the components were housed in aluminium holders<sup>(2)</sup> designed for mechanical stability and thermal contact, to ensure uniform temperature across the exposed aperture.

Samples were retained in their holders with disc springs and circlips located behind a chromic-anodised BS.L93 aluminium backing piece. Thermal contact was ensured by Pb washers located either side of the substrate. The holders were retained in the base plate using a disc spring and circlip located in a recess on the outside of the holder. A small pressure release hole was located in the centre of each backing piece to minimize the pressure differential across the substrate and to prevent flexing or deformation.

### Infrared Materials

The Samples were subdivided into three categories :-

- a) Uncoated crystals and materials
- b) Soft-multilayer coatings and substrate materials
- c) Hard-multilayer coatings and substrate materials

Equivalent samples were placed in both experiment trays to assess performance differences between the two LDEF exposure sites. They represented a cross-section of component materials currently being flown in IR radiometer instrumentation.

### Materials Sample List

<u>Holder Nos.</u>	<u>Substrate</u>	<u>Coating</u>	<u>Diameter/Thickness (mm)</u>
1,5	MgF <sub>2</sub>	-	30.0 / 3.175
2,6	CaF <sub>2</sub>	-	30.0 / 3.175
3,7	KRS-5	-	30.0 / 3.175
4,8	KRS-6	-	30.0 / 3.175
9,15	CdTe	-	15.0 / 1.05
10	Si	-	23.0 / 0.98
23	Ge	-	25.4 / 0.98
46	Al <sub>2</sub> O <sub>3</sub>	-	23.0 / 1.05
11	Y-Quartz	-	15.0 / 0.20
12	Z-Quartz	-	15.0 / 0.26
13,14	KRS-5	As <sub>2</sub> S <sub>3</sub> /KRS-5	15.0 / 0.15
		As <sub>2</sub> S <sub>3</sub> /KRS-5	



16,17	KRS-6	ZnS/KRS-5	15.0 / 0.15
		ZnSe/KRS-5	
18,19	KRS-5	CdTe/KRS-5	15.0 / 0.15
		As <sub>2</sub> S <sub>3</sub> /KRS-5	
21,22,26-32,36-43	Ge	PbTe/ZnS	23.0 / 1.00
24,25	Al <sub>2</sub> O <sub>3</sub>	Ge/SiO	25.4 / 1.00
33-35	Ge	PbTe/ZnSe	23.0 / 1.00
44	ZnSe	PbF <sub>2</sub> /PbF <sub>2</sub>	23.0 / 1.00
47	Si	SiO	23.0 / 1.00

### Uncoated Crystals and Materials

The following uncoated crystals and materials were distributed between the two tray locations :-

<u>Substrate</u>		<u>Exposed</u> <u>Diameter</u>	<u>Number</u> <u>off</u>
Calcium Fluoride	(CaF <sub>2</sub> )	27.0	2
Magnesium Fluoride	(MgF <sub>2</sub> )	27.0	2
Germanium (Fig 4)	(Ge)	23.0	1
Silicon (Fig 4)	(Si)	13.0	1
Cadmium Telluride	(CdTe)	13.0	2
Sapphire	(Al <sub>2</sub> O <sub>3</sub> )	21.0	1
Y-cut Quartz		13.0	1
Z-cut Quartz		13.0	1
KRS-5	(TlBrI)	27.0	2
KRS-6	(TlClBr)	27.0	2

These materials were selected for their long-wave (Reststrahl) absorption properties, and as typical substrate materials (See fig. 4).

### Soft Substrate / Coating Materials

Soft materials comprised principally KRS-5 (TlBrI)-based multilayers deposited on KRS-5 or KRS-6 (TlClBr) substrates. These were designed to utilize (by multilayer interference), long-wavelength Reststrahl blocking properties. All of them were originally fabricated for the GALILEO Jupiter probe<sup>(3)</sup> : and exposed with an aperture diameter of 13.0 mm.

<u>Substrate</u>	<u>Coating</u>
KRS-5	61-layer AS <sub>2</sub> S <sub>3</sub> /KRS-5
KRS-6	33-layer ZnS/KRS-5 & ZnSe/KRS-5 (Fig 3)
KRS-5	61-layer CdTe/KRS-5 & AS <sub>2</sub> S <sub>3</sub> /KRS-5

Post-flight visual and spectral analysis of the Soft Substrate / Coating material samples showed less degradation had occurred in the Earth-facing tray (G12) than in the leading-edge tray (B8) as shown in Fig. 3.

### Hard Substrate / Coating Materials

Hard materials comprised spectral filters from then-current atmospheric-sensing, weather forecasting, research, and planetary satellites<sup>(4)</sup> viz; NIMBUS 4, 5, 6, 7, ITOS, TIROS-N, PIONEER and GALILEO; each was exposed with an aperture diameter of 21.0 mm.

<u>Substrate</u>	<u>Filter</u> <u>Coatings</u>	<u>Wavelength</u>	<u>HBW%</u>	<u>No. of Cavity-Layers</u>	<u>Description</u>
Ge	PbTe/ZnS/ZnSe	7.4	5.0	3	L-Spaced THW BP
Ge	PbTe/ZnS	5.7	6.0	-	Twin-Peaked BP
Al <sub>2</sub> O <sub>3</sub>	Ge/SiO	4.5	3.5	2	DHW BP
Ge	PbTe/ZnS/ZnSe	14.5	0.7	1	L-Spaced FP BP
Ge	PbTe/ZnS	14.5	0.7	1	Split-spacer FP BP
Ge	PbTe/ZnS	8-12	-	-	Cut-on edge filter (Fig 5)
Ge	PbTe/ZnS	11.0	10.0	3	H-spaced THW BP
Ge	PbTe/ZnS	15.0	10.0	3	L-spaced THW BP (Fig 6)
Ge	PbTe/ZnS	10.6	2.5	2	H-spaced DHW BP
ZnSe	PbF <sub>2</sub>	10.6	-	-	Antireflection
Ge	PbTe/ZnS	9.2	2.5	2	H-spaced DHW BP
Si	SiO	4.4	-	-	Antireflection

The level of exposure expected on LDEF exceeded the operational amount expected by these 'internal' radiometer filters. External exposure therefore provided a better indication of the long-term performance and stability.

### Multilayer Design

Eight generic designs were selected for LDEF. They represented a cross-section of the different types used in radiometer instrumentation, providing an indication of the general changes to be expected :

- Low index-ratio quarter-wave "stacks" (for blocking) (6 off).
- Single spacer bandpass (4 off).
- Double half-wave narrow band designs (3 off).
- Blocked and unblocked triple half-wave bandpass designs (8 off)
- Unblocked split-spacer Fabry-Perot bandpass designs (6 off).
- Twin-peaked bandpass design (1 off).
- Optimized Tschebychev low-pass edge filter extraction (1 off)
- Single layer, single wavelength antireflection coatings (2 off).

Three material combinations were employed in the low-contrast quarter-wave blocking stacks; viz: KRS-5 with a choice of As<sub>2</sub>S<sub>3</sub>/CdTe/ZnS or ZnSe as alternate layer materials. Each combination was highly transparent through the NIR/IR, showing periodic fringes, but ending at long-wavelength (~ 40 $\mu$ m) in a deep Reststrahl absorption.

The multilayer designs were classic "stacks" of alternating quarter-wavelength ( $\lambda/4$ ) layers reproduced regularly and in multiple periods.

Such stacks show a characteristic multilayer-interference spectrum, containing a reflection zone (notch) where the layer interferences add destructively; the width of the zone being dependent on the index ratio of the materials. The zone is particularly sensitive to thickness, index or absorption changes (Fig. 3)

The single spacer narrowband design flown is the simplest narrowband filter available. Its spectrum consists of a narrow transparent peak bounded by regions of low transmission (blocking). The structure contains a central spacer layer ( $\lambda/2$ ), positioned between quarter-wave ( $\lambda/4$ ) reflecting stacks.

Substrate (Ge)/LHLHLLLLHLHLH

where LL is the central spacer layer ( $\lambda/2$ ).

Beyond the immediate bandpass spectrum there are broad regions of transparency, also sensitive to changes in the multilayer structure.

The double half-wave (or two cavity) filter designs contained two high-index spacer layers. The advantageous index contrast between Lead Telluride ( $n = 5.5$ ) and Zinc Sulphide ( $n = 2.2$ ) permitted a minimum of quarter-wave layers between the spacers, extending the blocking widths outside of the passband, and improving the profile in the passband.

The basic form:-

Reflector/Half-wave/Reflector/Half-wave/Reflector

is therefore realized as the following with HH spacers :-

Substrate (Ge)/LHLHHLHLHLHHLHL

This design was chosen because the bandpass peak is sensitive to absorption, or changes of refractive index in the structure.

Three triple half-wave designs were flown on LDEF, containing either H or L spacer layers (Fig. 5). The configurations were the same as the double half-wave designs but with an added spacer, producing a steeper, flatter and more rectangular passband. Three cavities also deepen the adjacent blocking.

The three designs were :-

- i) Substrate (Ge)/LHLLLLHLHLLLLHLHLLLLHL
- ii) Substrate (Ge)/LHHLHLHHLHLHHL, and
- iii) Substrate (Ge)/XLLLHLLLLHLLLX

where X is a simulated matching stack positioned at the surfaces of the design core and particularly spectrally sensitive.

The split-spacer filter design flown was similar to the single cavity Fabry-Perot. However, in this version, the single cavity is sub-divided into three, supposedly for better stability and microstructure.

In consequence, the broad region of transparency between the first and third order peaks is divided by periodic reflection zones, the peaks themselves remaining unaltered.

The configuration is therefore :-

Substrate (Ge)/LHLHLH  $\frac{L}{2}$   $\frac{H}{2}$  LHLHL

The twin-peaked narrow passband design creates a novel spectrum comprising two narrow peaks separated by a common rejection band. Transmission at shorter-wavelengths is attenuated by internal interaction.

A low-pass edge filter design flown contained all non quarter-wave (fractional) layers<sup>(5)</sup> throughout and was fully blocked (Fig. 6). The exposed surface comprised a 19-layer principal stack antireflected for the 8-12 $\mu$ m broadband region, with its 50% point located at 7.7 $\mu$ m. The rear surface comprised a 17-layer subsidiary stack for continuity of short wavelength blocking, and to assist with the broadband antireflection.

Fractions are obtained by Tschebychev extraction, optimized for maximum transmission over a broad spectrum. This design was flown to assess changes over a wide transparent spectrum.

Two single wavelength antireflection samples were flown to assess individual layers after exposure. Each was a single quarter-wave layer ( $\lambda/4$ ) index-matched for maximum transmission on a particular substrate.

A single PbF<sub>2</sub> layer was deposited to antireflect zinc selenide at ~10.6 $\mu$ m wavelengths, and silicon monoxide was deposited to antireflect silicon at ~4.4 $\mu$ m wavelengths.

Changes in the single layer arising from exposure could affect its thickness, refractive index or absorption and thereby either attenuate or displace the antireflected profile.

### Spectrophotometers

Two spectrophotometers were used to measure the spectral characteristics of the samples flown on LDEF. Exposed and control samples were originally measured (1979-1983) with a Perkin-Elmer PE457 grating infrared spectrophotometer in transmittance / reflectance from 2.5 to 40 $\mu$ m. Localized features of interest were then re-measured in high resolution across a narrow waveband. For post-flight analysis the same spectral regions were measured for comparison on a Perkin-Elmer PE580A spectrophotometer. This latter equipment measures between 2.5 and 50 $\mu$ m, and has been fitted with a data acquisition system to record, store and compare spectral measurements.

### Pre-Flight PE457 Measurements

The PE457 is a double-beam optical-null spectrophotometer, recording linear transmittance versus linear wavenumber through an f/5 monochromator. The monochromator comprises a reflecting optical system employing planar and aspheric (paraboloidal) mirrors and two plane replica gratings mounted back-to-back (100 and 25 lines per mm). Unfortunately it is designed with pre-sample chopping, and is incapable of suppressing re-radiation from the sample or reference beam at low temperature. The following accuracy and repeatability is quoted (6) :

Wavenumber	4000 to 250 $\text{cm}^{-1}$
Accuracy	$\sim 4 \text{ cm}^{-1}$ between 4000-2000 $\text{cm}^{-1}$ $\sim 2 \text{ cm}^{-1}$ between 2000-200 $\text{cm}^{-1}$
Repeatability	$< 2 \text{ cm}^{-1}$ from 4000 to 2000 $\text{cm}^{-1}$ $< 1 \text{ cm}^{-1}$ from 2000 to 250 $\text{cm}^{-1}$
Transmission	0 to 100% linear
Accuracy	$\sim 1\%$ of full scale
Repeatability	Within 1% of full scale

### Post-Flight PE580A Measurements

The PE580A is a double beam grating spectrophotometer containing an f/5.7, 4 grating Littrow type monochromator. It is fitted with post-sample dual chopping, eliminating measured re-radiation from sample or reference beam.

Wavenumber measurement accuracy is quoted(7)  
 $\sim 1.5 \text{ cm}^{-1}$  decreasing linearly to  $\sim 1 \text{ cm}^{-1}$  from 4000 to 3500  $\text{cm}^{-1}$   
 $\sim 1 \text{ cm}^{-1}$  over the range 3500 to 2000  $\text{cm}^{-1}$   
 $\sim 1 \text{ cm}^{-1}$  decreasing linearly to  $\sim 0.5 \text{ cm}^{-1}$  from 2000 to 1450  $\text{cm}^{-1}$   
 $\sim 0.5 \text{ cm}^{-1}$  over the range 1450 to 180  $\text{cm}^{-1}$

Wavenumber repeatability is :  
 $\sim 0.5 \text{ cm}^{-1}$  from 4000 to 2000  $\text{cm}^{-1}$   
 $\sim 0.25 \text{ cm}^{-1}$  from 2000 to 180  $\text{cm}^{-1}$

Transmittance accuracy from proprietary charts is :  
 $\sim 0.4\%$  between 4000  $\text{cm}^{-1}$  and 700  $\text{cm}^{-1}$ , and  
 $\sim 0.7\%$  between 700  $\text{cm}^{-1}$  and 180  $\text{cm}^{-1}$

With both spectrophotometers deviations can occur as instrumental drift, the accuracy and repeatability given here is the best performance after calibration.

### Measurement Accuracy Analysis

Comparative accuracy and repeatability of the infrared spectrophotometers, indicates the wavelength and transmission deviations to be expected when they are used together. The general guideline of manufacturer's accuracies immediately after service and calibration is :-

	PE457	PE580A	Total
Wavenumber accuracy ( $\text{cm}^{-1}$ )			
4000-3500 $\text{cm}^{-1}$	~4	~1.5 to ~1	~5.5 to ~5.0
3500-2000 $\text{cm}^{-1}$	~4	~1	~5.0
2000-1450 $\text{cm}^{-1}$	~2	~1 to ~0.5	~3 to ~2.5
1450-250 $\text{cm}^{-1}$	~2	~0.5	~2.5
Wavenumber repeatability ( $\text{cm}^{-1}$ )			
4000-2000 $\text{cm}^{-1}$	~2	~0.5	~2.5
2000-250 $\text{cm}^{-1}$	~1	~0.25	~1.25
Transmission accuracy (%)			
4000-700 $\text{cm}^{-1}$	~1	~0.4	~1.4
700 -250 $\text{cm}^{-1}$	~1	~0.7	~1.7

Such summation of errors are our spectral limitations and should be regarded as an envelope of transmission accuracy and wavenumber accuracy, over the full spectrum 2.5 to 50 microns.

We considered samples to be unchanged in their spectrum if, as a result of the exposure, the following criteria are met :-

- 1) Exposed samples which remained spectrally stable, but their controls become displaced and/or deformed, are considered unaffected by the space environment and indicate that space is more benign than storage in a normal laboratory, (viz: shelf life).
- 2) The exposed and control samples (both) are displaced and/or deformed identically.
- 3) Where no control sample exists the exposed sample remains spectrally unaltered on the expectation of its known material properties and in the absence of a control.
- 4) Both exposed and control samples remain spectrally unaltered.

Spectral changes are only considered a valid result of exposure if they then meet the following criteria :-

- 1) Representative controls have remained stable, whilst exposed samples are displaced and deformed beyond the tolerance envelope.
- 2) Where no control samples exist, exposed samples are spectrally changed beyond the expectations of that material durability.

#### Spectral Comparisons

Spectra were compared for average transmission (in coincident regions), and for wavenumber correlations (of equivalent spectral features).

For average transmission correlations, the samples were subdivided to compare similar materials and coating types independently.

- 1) Exposed crystals (hard, uncoated) 2.5 - 50 $\mu$ m
- 2) Exposed soft (volatile) materials (such as KRS-5, KRS-6), 2.5-50 $\mu$ m
- 3) Exposed hard-coated samples, 2.5-50 $\mu$ m
- 4) Control/Unexposed hard-coated samples, 2.5-50 $\mu$ m
- 5) Exposed localized bandpass profile comparisons (expanded)
- 6) Control/unexposed localized bandpass profile comparisons (expanded)

For each category, average transmission was extracted from coincident spectral regions. This enabled any changes to be quantified over the full spectrum, giving changes in component throughput as a result of the exposure.

Expanded bandpass profiles (Fig. 7) were compared by centre wavenumber and 50% half-power points, and correlating wavenumber displacements (if any). All the spectral features were corrected for instrument calibration prior to analysis.

Correlations of pre/post flight average transmissions (where coincident), were analyzed statistically to ensure the changes were seen in the context of their equivalent samples. Statistical comparisons between pre and post flight data use the correlation coefficient (r), mean deviation and standard deviation (SD).

#### Uncoated Crystals

Correlation of average transmittances for the hard uncoated crystals gave a correlation coefficient (r) of 0.9962. The mean deviation, however, indicated a consistent loss in transmission of -0.765%; this was sufficiently close to zero to infer no change within the transmission accuracy envelope permitted. Controls for these crystals were unavailable.

#### Soft (Volatile) Materials

Comparisons of pre and post flight average transmittance values were made between the soft (volatile) exposed samples from both sites, the correlation coefficient (r) was -0.168, indicating no general correlation between pre/post flight spectra for these sample types. This was also evident from visual inspections, where gross physical degradation / delamination of the coatings and substrate materials having occurred as a result of excess exposure and the effects of Atomic Oxygen bombardment.

#### Hard-Coated Materials (Fig 8)

Pre and post flight comparisons were well correlated. Included in this group were all those multilayer interference filters in which we specialize (normally associated with atmospheric remote-sensing applications, particularly spectrally selective by their design).

Correlation was very high at 0.9967 from the exposed samples, compared with the equivalent controls, where a correlation coefficient of 0.9988 was obtained, verifying the correlations as valid and well matched.

The mean deviations for exposed and equivalent controls were -1.376% and -1.302% respectively, indicating a small and consistent loss in transmission for both, within the accuracy envelope. These samples are therefore considered stable and show no degradation from the exposure.

#### Localized Correlation vs Wavenumber (Fig 9)

Temporal stability of IR spectrum was considered important in assessing the LDEF exposure, for the foreseeable future, spectrally-selective filters will continue to be used in planetary remote-sensors not permitting re-calibration of their instruments after launch, and of long duration. It is therefore important to quantify spectral drift in LDEF samples (if any), so that in new missions spectral displacements might be anticipated and perhaps compensated.

The following radiometer filter types were measured in detail :

<u>Sample No.</u>	<u>Sample type</u>
B8-27, B8-28	14.5 $\mu$ m 0.7% HBW Fabry-Perot bandpass filter
B8-30-34, G12-35	14.5 $\mu$ m 0.7% HBW 'Split spacer' bandpass filter

Equivalent controls were also measured. Correlations were made of centre wavenumber and half power wavenumbers from the narrowband profile, and comparing wavenumber displacements pre/post flight.

Correlation (r) for exposed and control data sets is very high at 0.99811 and 0.99819 respectively, indicating excellent spectral comparison. Mean deviation however indicates displacement to shorter wavelength of +0.6  $\text{cm}^{-1}$  for the exposed, and +0.98  $\text{cm}^{-1}$  for controls, but within the accuracy envelope this is considered vanishingly-small shift in location. Because the control and exposed samples are displaced to the same (but small) extent the difference between them is negligible. We consider that, over time and after exposure, the shift in spectral location is vanishingly small : we therefore confirm that the samples are inherently stable.

PbTe/ZnS-based sample B8-37 was cleaned in 1,1,1-Trichloroethane and Propan-2-ol to establish whether its surface was contaminated. The spectrum remained unchanged and we deduce that the surface was not contaminated by exposure to space; its loss of transmission therefore must be ascribed to another mechanism.

#### Visual examinations

Visual examination and photographic recording have been crucial in observing the effects of change in many of the optical samples flown. Inspections have been made at all stages of LDEF; from initial manufacture, pre-flight, to post-flight were inspected.



De-integration of individual samples from their assemblies was carried out in the SERC Rutherford Appleton Laboratory clean room where a detailed photographic log was made of each sample. Obvious changes in chromic anodizing, degradation of KRS-5 and KRS-6 samples, and distributed impacts were all observed confirming preliminary observations.

Space-facing location B08 provided some of the best examples on LDEF of secondary ejecta from impact sites, and their various effects on a variety of samples.

Several impacts occurred into the sides and edges of sample holders, leaving secondary ejecta spray patterns on the base-plate, experiment samples and experiment-tray walls. Impacts into many of the coated specimens created deep well-like depressions in the centre of the impact feature with a highly-defined outer spallation region.

Although complete fracture occurred from an impact onto one uncoated sample, most other impacts produced only localized coating delamination around the periphery of the impact site.

One impact occurred into the side of our base-plate (in the crack between the experiment base-plate and NASA's tray wall), and created an ejecta spray pattern onto the inside of NASA's tray wall across from the crater. This impact occurred ~19 mm down the side of our base-plate; the opening between the base-plate and tray was ~5 mm. This crater is one of only a few found on LDEF which could be geometrically shown to have been produced by a highly oblique impact.

The impact on the calcium fluoride sample (B8-2) occurred near to the edge of the sample holder. The impact crater was ~1 mm diameter with a spallation zone diameter of ~5.5 mm. The substrate cleaved in two directions outwards from the crater site to the opposite sides of the sample, and at an angle of ~75°, breaking the sample into three pieces (Fig 10).

Although other samples had impact craters of this size with large spallation diameters and small fractures, this was the only sample which showed evidence of complete fracture, verifying the fragile and brittle nature of calcium fluoride as a substrate material, whilst remaining optical functional. The crater itself consists of finely shattered material, and contains no residual impact debris.

### Conclusions

The effects of space exposure on the high-performance filters we flew on LDEF were negligible. No significant changes were found either in transmission or spectral position of any hard coated II-VI / PbTe-based multilayers on Germanium substrates, or in uncoated crystal substrates.

The softer materials were adversely affected in their physical and optical properties by the long exposure in space, from a reduced transmission to a complete opacity.

Although impacts by micrometeorites damaged some samples, these did not detract from their function and performance as an optical component. Likewise, atomic oxygen and space radiation caused no spectral effects we could detect, other than in soft material samples which were exposed beyond that intended.

#### Acknowledgments

We acknowledge support provided by UK Science and Engineering Research Council (SERC), and our University and academic department over an extended period.

Thanks are given to these individuals; Alan Whatley, Charles Preston, Paul Minchinton and George Jeronimidis (University), J.W. Heaton (Deceased), Derek Lipscombe (British Aerospace), William L. Kinard, James L. Jones (NASA). We also thank Rutherford Appleton Laboratory for clean-room facilities and to Ray Turner, Bruce Swinyard and Geoff Douglas for help during de-integration.

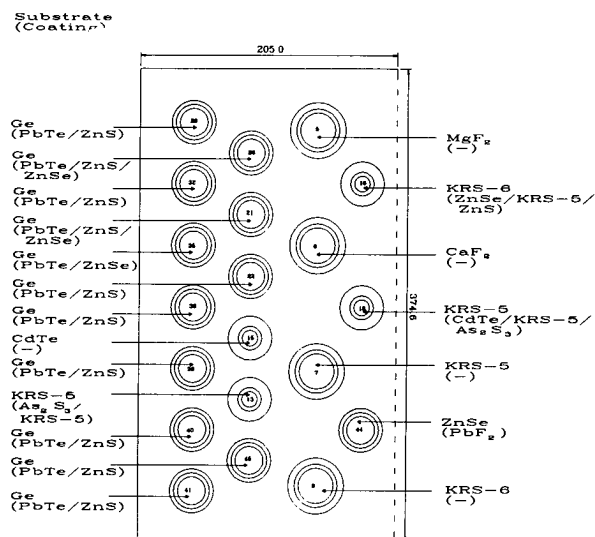
#### References

- 1, Hawkins G.J., Hunneman R., Seeley J.S.; "Space Exposure of Infrared Filters and Materials on the NASA Long Duration Exposure Facility (LDEF)" University of Reading (1990), ISBN 07049 04098.
- 2, Hawkins G.J., Hunneman R., Seeley J.S.; "Preliminary results from Infrared Multilayer Filters and Materials exposed to the space environment on the NASA LDEF mission." Proc SPIE 1320 pp 407-419 (1990).
- 3, Seeley J.S., Hunneman R., Whatley A.; "Far infrared filters for the Galileo-Jupiter and other missions". Appl Opt; Vol 20 pp 31-39 (1981).
- 4, Hunneman R., Seeley J.S., Whatley A.; "Durability assessment of PbTe/II-VI infrared filters (Space Shuttle 1st LDEF)." Proc SPIE 401 pp 55-59 (1983).
- 5, Evans C.S., Hunneman R., Seeley J.S.; "Optical thickness changes in freshly deposited layers of lead telluride." J.Phys.D: Appl Phys., Vol 9 pp 321 (1976).
- 6, Perkin-Elmer Ltd.; "Model 457 Spectrophotometer." (1971).
- 7, Perkin-Elmer Ltd.; "Model 580 Infrared Spectrophotometer." (1977).

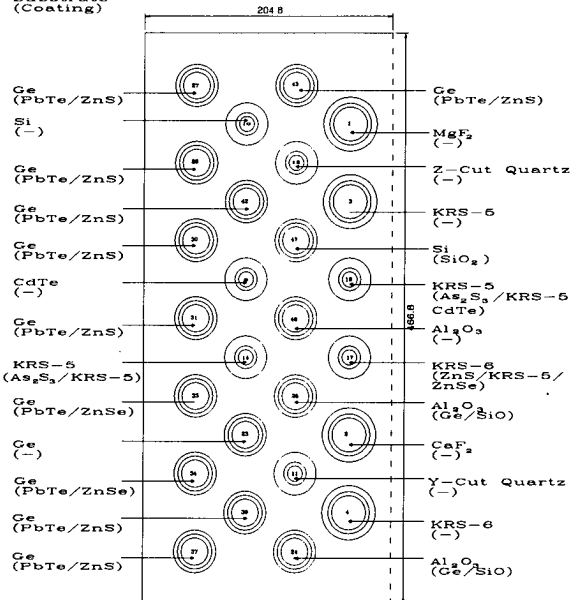
#### Acronyms

EOS	-	Earth Observing System
ERS	-	European Remote Sensing Satellite
GCRP	-	Global Change Research Programme
ITOS	-	Improved TIROS Operational Satellite
POEM	-	Polar Orbit Earth Observation Mission

### Substrate-Coating Materials Distribution

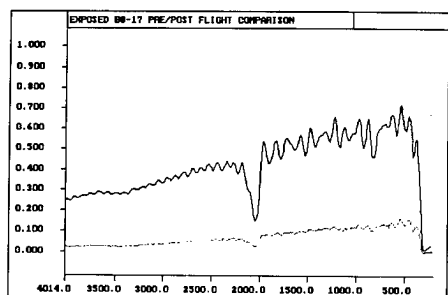


TRAY G12

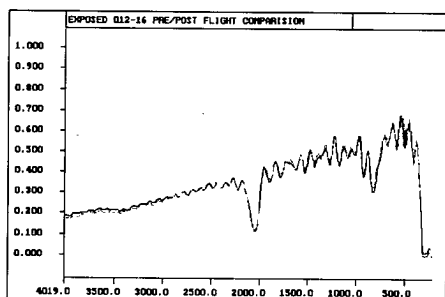
Substrate  
(Coating)

TRAY B8

Fig 1. Materials Distribution on Earth-facing tray G12.

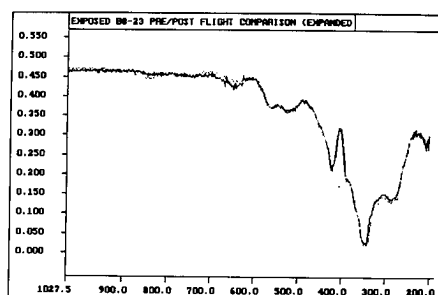
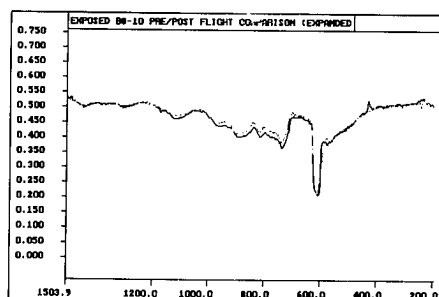


B8-17 Exposed Low Contrast Zinc Selenide / Zinc Sulphide  
& KRS-5 Quarter-wave stack deposited on a KRS-6 substrate  
2.5 ~ 50  $\mu$ m Transmission Spectra



G12-16      Exposed Low Contrast Zinc Selenide / Zinc Sulphide  
                 & KRS-5 Quarter-wave stack deposited on KRS-6 substrate  
                 (Equivalent to sample B8-17 above)  
                 2.5 - 50 um Transmission Spectra

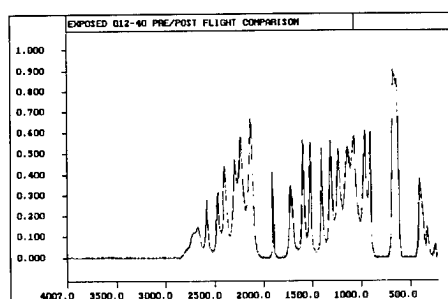
Fig 2. Materials Distribution on  
Leading-edge tray B08.

B8-23 Exposed Germanium Substrate (Uncoated)  
10 - 50um Expanded Transmission Spectra

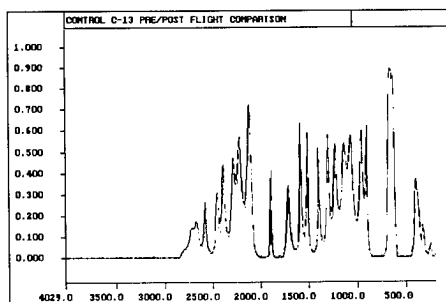
B8-10      Exposed Silicon Substrate (Uncoated)  
7 - 50um Expanded Transmission Spectra

Fig 3. Low index-ratio quarter-wave blocking design (exposed).

Fig 4. Exposed uncoated Germanium and Silicon substrates

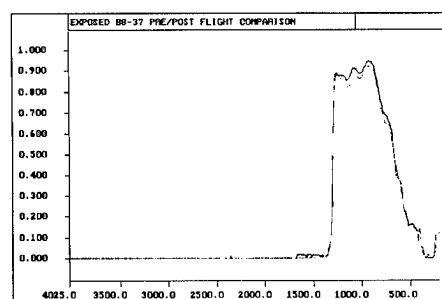


G12-40 Exposed 15um 10% HBW Lead Telluride / Zinc Sulphide  
L-Spaced Triple Half-wave Bandpass Filter on Germanium  
2.5 - 50 um Transmission Spectra

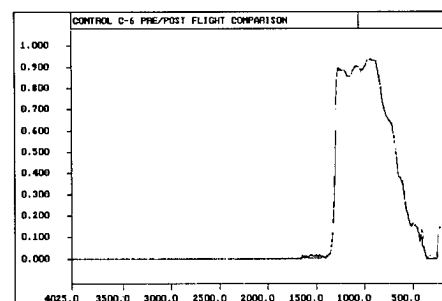


C-13 Control 15um 10% HBW Lead Telluride / Zinc Sulphide  
L-Spaced Triple Half-wave Bandpass Filter on Germanium  
(Equivalent to samples G12-40 & G12-41)  
2.5 - 50 um Transmission Spectra

Fig 5. Exposed & Control 15um 10% HBW THW bandpass filter.

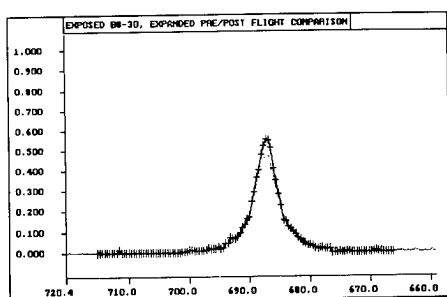


B8-37 Exposed 8-12um Low Pass Lead Telluride / Zinc Sulphide  
Tschebyshev Edge Filter (Antireflected) on Germanium  
2.5 - 50 um Transmission Spectra

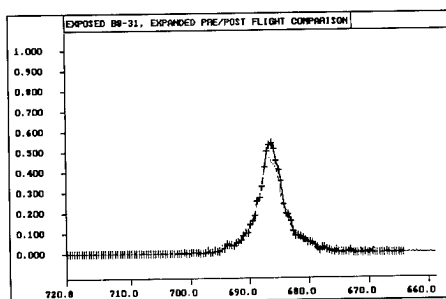


C-6 Control 8-12um Low Pass Lead Telluride / Zinc Sulphide  
Tschebyshev Edge Filter (Antireflected) on Germanium  
(Equivalent to sample B8-37 above)  
2.5 - 50 um Transmission Spectra

Fig 6. Exposed & Control 8-12um Low-pass edge filter.



B8-30 Exposed 14.5um 0.7% HBW Split-Spacer Fabry-Perot Bandpass Filter  
Detailed Pre/Post Flight Transmission Measurement (13.9 - 15.4um)



B8-31 Exposed 14.5um 0.7% HBW Split-Spacer Fabry-Perot Bandpass Filter  
Detailed Pre/Post Flight Transmission Measurement (13.9 - 15.4um)  
(Equivalent to sample B8-30 above)

Fig 7. Expanded spectra of 14.5um narrow bandpass filter

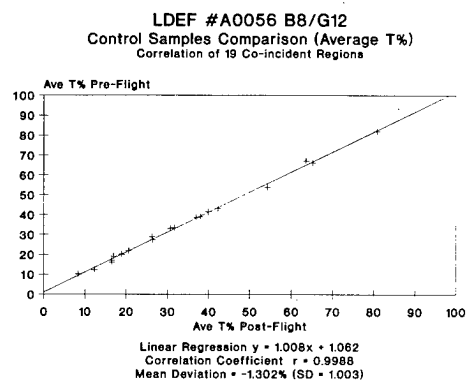
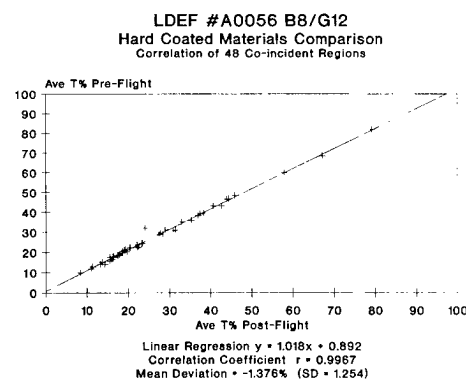


Fig 8. Correlation of average transmission for multilayer exposed/control samples

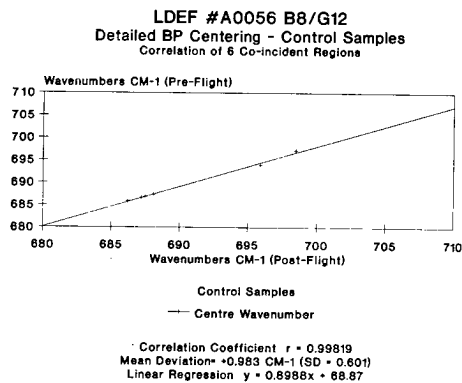
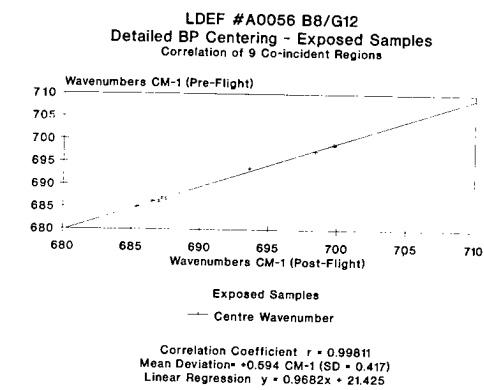
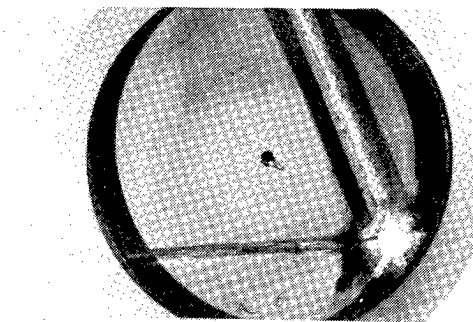


Fig 9. Correlation of bandpass centres for exposed and control samples.



B8-2 Calcium Fluoride Substrate (Unroasted)  
Micrometeorite impact has caused clearing of the substrate, crater consists of finely shattered material containing no residual debris.



Fig 10. Micrometeorite impact damage on Calcium Fluoride filter.

PASSIVE EXPOSURE OF EARTH RADIATION BUDGET EXPERIMENT COMPONENTS  
LDEF EXPERIMENT AO-147: POST-FLIGHT EXAMINATIONS AND TESTS

John R. Hickey

The Eppley Laboratory Inc.

P.O. Box 419, Newport, RI 02840

Phone: 401/847-1020, Fax: 401/847-1031

SUMMARY

The flight spare sensors of the Earth Radiation Budget (ERB) experiment of the Nimbus 6 and 7 missions were flown aboard the LDEF. The preliminary post-retrieval examination and test results are presented here for the sensor windows and filters, the thermopile sensors and a cavity radiometer.

INTRODUCTION

The PEERBEC experiment of the LDEF mission was composed of sensors and components associated with the measurement of the Earth Radiation Budget from satellites. These components included the flight spare sensors from the Earth Radiation Budget (ERB) experiment which operated on the Nimbus 6 (ref. 1) and Nimbus 7 (ref. 2) satellites. The Nimbus 7 instrument is still returning data as of this date (July 1991). The 10 solar sensors were mounted in LDEF tray B-8 along with 10 (non-ERB) interference filters supplied by Barr Associates (ref. 3). The 4 earth-flux sensors were mounted in LDEF tray G-12 on the earth facing end. A cavity radiometer, similar to channel 10C of Nimbus 7 was included as part of the Advanced Photovoltaic Experiment (APEX) which was mounted in LDEF tray E-9. While PEERBEC was a passive experiment APEX was active. This report describes the experiment components and materials as well as the pertinent background and ancillary information necessary for the understanding of the intended mission and the results. The extent and timing of the LDEF mission brought the exposure from solar minimum between cycles 21 and 22 through the solar maximum of cycle 22. The orbital decay, coupled with the events of solar maximum, caused the LDEF to be exposed to a broader range of space environmental effects than had been anticipated. The mission spanned almost six years concurrent with the 12 years and 8 months (to date) of Nimbus 7 ERB operation.

Here, we present preliminary information (1) on the changes in transmittance experienced by the windows and interference filters, (2) on the results of retesting of the thermopile sensors, which appear to be relatively unaffected by the exposure and (3) the results of the recalibration of the APEX cavity radiometer.

This work supported by NASA Langley Research Center under contract NAS1-15350 and NASA Lewis Research Center under contract NAS3-25958

## BACKGROUND

The reason for proposing this experiment was to help explain the results which were obtained by the ERB of Nimbus 6. As the LDEF mission was delayed the matching experiment was launched on Nimbus 7 and started returning data. The Nimbus ERB experiments contained 10 solar radiation measurement sensors (channels) and 4 earth-flux measurement sensors. The solar sensors were mounted on the leading edge of Nimbus and the earth-flux sensors were looking down. The characteristics of these sensors are listed in table 1. The specific components for each channel are given in Appendix A. Channel 10S of Nimbus 6 (a UV sensing channel) was replaced by a cavity radiometer for total solar radiation measurements for the Nimbus 7 mission. Nimbus 6 was launched in June, 1975 during the decline of solar cycle 20. After initial measurements, the solar channels having filters showed a slow degradation. Nimbus 7 was launched in October, 1978, as the peak of solar cycle 21 was approaching. After allowing for a period of protection from outgassing contamination, the ERB solar channels were opened and started measurements on November 16, 1978. After initial measurements, the solar sensing channels having filters or windows, exhibited a major degradation. With the increase in solar activity of solar cycle 21 there was a major recovery of the signal for these channels. Figure 1. shows the relative output for first 9 solar channels for the 12 year period from November, 1978 through November, 1990. These data are normalized to the first day readings of each channel respectively. The major degradation and recovery event can be seen near the beginning of the plot in late 1978 and early 1979. Note that channel 3S is the only curve on this plot for a sensor without any windows or filters. When the recovery was experienced for Nimbus 7, it was found that the Nimbus 6 sensors (then more than 4 years in orbit) had also recovered (ref. 4). After the initial events the response of the various channels differed. Channel 6S and 9S measured levels higher than their initial readings, while the other 2 interference filter channels (7S and 8S) showed steep declines. The channels with fused silica windows acted differently. While channel 2S showed a decline with only partial recovery, the normally shuttered channel 1S showed very little change until later in the mission when its shutter was left open. When channel 1S is open channel 3S is shuttered, accounting for the gap in the channel 3 data in the 1984 and 1985 period where channel 1S shows a decline which almost equals the decline of matching channel 2S near the end of 1988. As solar cycle 22 approached maximum most of the channels exhibited some measure of recovery. Notably different are channel 7S which appears to keep degrading and channel 1S whose recovery was delayed since it was again mostly shuttered. When it was again left open, in 1990, its recovery was dramatic. The noise on some of the channel plots in 1986 and 1987 is due to periods of special operations of the Nimbus project.

It can be seen that quite a lot of information on the contamination of the ERB filtered channels could be gained from the Nimbus data. Nimbus 6 apparently suffered degradation due to its own outgassing and then was cleaned off once by AO. The Nimbus 7 record, shown here, shows a much greater initial degradation due to contamination and a remarkable recovery due to AO cleaning. But the degradation of some channels, with only partial recovery due to AO

cleaning at the next solar maximum, requires further explanation. Figure 2 is the same as figure 1 for the period 1984 through November, 1990, corresponding to the LDEF mission plus some time on either end. The extra 1990 data, beyond LDEF recovery, shows the late recovery of channel 1S.

The interpretation of the results for the total solar irradiance, as measured by a self-calibrating cavity radiometer has become a much higher priority. A cavity radiometer, of the same type, but not the same field of view, as the Nimbus 7 cavity was included as the radiation reference in the APEX experiment (ref. 5) on LDEF which is active. There was no flight spare for channel 10C of Nimbus 7 for inclusion in this (PEERBEC) experiment package. The channel 10 slot was filled with the spare channel 10S of Nimbus 6. One reason for employing cavity radiometers is that the effect of degradation should be much less than on a flat plate sensor. Figure 3 is a plot of the total irradiance results (solar constant) as measured by the Nimbus 7 cavity. The variation over the solar cycle is approximately 0.1% peak to peak. The dips in the plot are caused by large sunspot groups. The initial decline of the irradiance, especially when coupled with the degradation event experienced by the other solar channels, aroused suspicion among solar physicists and climatologists. However, when results from the ACRIM experiment (an ACR type cavity radiometer) aboard the Solar Maximum Mission (SMM) satellite, launched in 1980, exhibited similar behavior, the small change in the solar "constant" over the solar cycle appeared to be confirmed. The results of the 2 experiments tracked rather well through solar minimum and into the new cycle. When both experiments measured increasing radiation with increasing solar activity, most observers believed that the experiments were tracking true solar changes. There still remains some question about the relatively higher values in the early Nimbus 7 results (1979). The SMM/ACRIM was not in orbit at that time. The SMM reentered the atmosphere shortly before the retrieval of LDEF. The Nimbus 7 ERB continues to return solar data.

#### AUXILIARY INFORMATION

The solar sensors were mounted in a Nimbus ERB solar array block. Since the B-8 tray was 30° off the ram direction, the solar block was tilted to face forward. The Barr Associates filters were mounted flat to the front plate. The cavity sensor, in tray E-9, was on the leading edge. The earth flux sensors were mounted in tray G-12 looking earthward.

These flight spare ERB sensors underwent the same pre-flight processing as the ERB flight sensors according to the procedures of the Nimbus project. Relevant here are the following:

1. All thermopiles and other painted surfaces underwent vacuum bakeout.
2. All sensor modules underwent thermal vacuum testing.
3. All interference filters were burned in (in vacuum) using a xenon arc solar simulator at 1 solar constant level;  
channels 6,7 and 8 for 500 equivalent UV solar hours  
channels 9 and 10 for 800 equivalent UV solar hours



4. The Suprasil W fused silica windows and hemispheres were not burned in.
5. The 4 mm thickness of front windows of broad band channels and front substrates of the interference filters was chosen to act as a particle blocker.
6. The rear windows, 2 mm thick fused silica, were IR blockers mounted behind broad band glass filters and interference filters.

#### INITIAL OBSERVATIONS

The white paint on the solar tray cover had changed consistency as noted for other LDEF surfaces. It came off rather easily. The black marks on this cover, as seen in the in-flight retrieval pictures, were caused by spallation of debris from the aluminum side plate which was impacted. The ERB solar channels appeared very clean on initial inspection. The front polished aluminum, and the baffle anodize appeared to be unaffected by exposure. The front surfaces of the front filters (those visible) appeared very clean, possibly cleaned by AO.

The front surfaces of the thermopiles in channels 1, 2 and 3 were intact and apparently unaffected. Channel 3 was the only one not protected by a filter. All the readily visible mylar washers had turned brown. There were AO shadows next to the filter holders of the Barr filters indicating previous contamination of the front surface. Microscope inspection of the front surfaces of the solar channel filters, before removal, showed some small amounts of contamination, including the aluminum flecks and a yellow haze which may have been the residue of previous contamination. The front surface, baffles, aperture and cavity of the cavity radiometer in tray E-9 appeared to be clean and unaffected.

The white cover of the earth end tray had brown contamination as seen elsewhere on LDEF. Despite this, the earth flux sensors appeared very clean. The outer filter hemispheres were clean. The 2 exposed thermopiles had no apparent damage to the painted receivers. The exposed Z306 black paint on the channel 11E baffles appeared unaffected. The thermopile of channel 13E, visible through the clear domes appeared unaffected. The mylar cushions of the hemisphere holders had turned brown.

After partial disassembly it was noted that the mylar washers which were mounted deeper in the channels, or behind filters had remained white. There was a ring of the brown LDEF contamination around the front mounting plate of the cavity radiometer.

The mounting hardware for the tray B-8 and tray G-12 were left with the LDEF project for further study. The Barr Associates filters were removed and delivered to the investigators.

## INITIAL TEST RESULTS

### Solar Channel Module Exposure Tests

These modules were tested using a dedicated standard lamp as source. The lamp is a 1000 watt type FEL, serial number ES-8301. This lamp and a dedicated laboratory thermopile, serial number 16623-E6 had been stored since the pre-flight testing. The exposures were performed at a distance of 50 cm, the distance being reset using a special rod constructed for that purpose. The repeat result of the lamp-thermopile configuration was

PRE-FLIGHT	January 17, 1983	30.5 mW/cm <sup>2</sup>
POST-FLIGHT	April 10, 1990	30.6 mW/cm <sup>2</sup>

This repeatability of 0.33% was better than expected and serves as the basis for judging the repeat sensor exposures. Modules for channels 6S, 7S, 8S, 9S and 10S had to be tested with the interference filters removed. Channels 4S and 5S were tested with the colored glass filters mounted. Results are listed in Table II. While channels 1S and 2S are identical these results show a 1.6% increase in channel 1S and a 0.7% decrease in channel 2S response. Channel 3S, the only channel with no filters, shows an increased response by 0.6%. These test results indicate that there have been no major changes that can be detected using this method. This indicates that the thermopiles have remained stable and that the window materials have not changed much in the spectral region of the tungsten lamp emission.

### Thermopile Resistance Tests

These thermopiles were fabricated in 1972. The post-flight measurement of resistance gave repeat values in 1990 with changes;  
less than 2 ohms for the 8 N3 type thermopiles  
less than 10 ohms for the 2 K2 type thermopiles  
The HF type thermopile of the cavity radiometer repeated within measurement resolution.

### Filter Spectral Transmittance Measurements

The spectral transmittance of the fused silica windows was measured. A witness sample, from the same boules and of the same thickness as each flight sample was available from the original ERB QA repository. The transmittance for the 2 mm thick front windows of matching channels 1S and 2S over the range from 200 to 400 nm is shown in figure 4. The transmittance of the witness sample is at the top of the plot. It can be seen that the 2 front windows have degraded in the UV by close to 11% at 200 nm and lesser amounts out to 330 nm. A 2 mm thick sample was also included in the APEX experiment (ref. 5). This sample, which was contaminated, has suffered a much greater degradation over the whole UV range. Figure 5 shows the ratios of the

transmittance of the 2 front windows and the 2 rear windows to that of the witness sample. It can be seen that there is not much difference between the effects on like windows. However, The front windows show greater degradation. The rear windows exhibit degradation over the same spectral range, 200 to about 330 nm, as the front windows to a lesser degree. The transmittance change of the only 4 mm thick fused silica window, from channel 5S, is shown in figure 6. The degradation region is extended out to about 400 nm. At 200 nm transmittance is only 70% of the witness sample or pre-flight value. Since the transmittance returns to pre-flight values before 695 nm the degradation did not affect the module exposure test result. The 4 mm front fused silica window was missing from channel 4S. The OG 530 glass transmittance is shown in figure 7. Only a slight difference is seen between it and the OG 530 witness sample. This is a surprising result based on the ERB project testing. The RG 695 red glass transmittance was also measured. The transmittance shows no meaningful difference from its witness sample.

It should be noted that no attempt at cleaning the windows or filters has been made to this time. The transmittance measurements will be redone after cleaning. While microscope examinations have shown no large amounts of contaminant, like that on the APEX sample, cleaning was postponed awaiting further information on other LDEF results.

The spectral transmittance of the interference filters was also measured. These results were compared with the pre-flight results. The pre-flight results were obtained prior to the LDEF integration and are not the original values from 1972 when the ERB filters were made. The results are shown in figures 8 through 12. The preflight curves are designated by boxes and the post-flight curves by crosses for filters 6S through 10S. Filter 6S shows very little change with a possible broadening of the band. The peak transmittance is almost unchanged. Filter 7S exhibits a decay in transmittance and a narrowing of the band, especially at the long wave end near 450 nm. Filter 8S shows a decrease in transmittance near the peak but little change in band shape. Filter 9S shows a decrease in transmittance and a narrowing of the band on the shortwave side. There is indication of a shift to longer wavelength coupled with the decrease in transmittance. Filter 10S exhibits a similar band shift to longer wavelength with a smaller decrease in transmittance than 9S.

The task of relating these changes to the ERB results from Nimbus 7 will continue. The post-cleaning transmittance values must be obtained first. The spectral transmittance of the IR blockers must also be completed before final analysis can be performed.

### Cavity Radiometer Tests and Comparisons

The cavity radiometer (pyrheliometer) was mounted in the APEX experiment in tray E-9, on the leading edge. Initial examination discovered one small piece of the aluminum contaminant had entered the instrument. Under intense illumination it could be seen that the interior cavity paint (Z302) exhibited some "puckering" The Z306 baffle paint appeared to be unaffected. The following resistance

checks were performed:

1. Cavity heater resistance unchanged at 152.2 $\Omega$
2. Cavity heater plus current sense resistor unchanged at 162.2 $\Omega$
3. Thermopile resistance 354.7 $\Omega$  up 0.3 $\Omega$  from the preflight value

The precision aperture (invar) was removed and remeasured. No change was measured. The sensor was tested for power sensitivity at atmospheric pressure and in vacuum. The vacuum to air ratio changed - 0.16% from the preflight value. This indicates little change in the thermal properties of the sensor.

The sensor field of view was reconfigured to allow intercomparisons in direct sunlight with local and international pyrheliometric standards. Initial results showed agreement at Newport, RI of  $\pm 0.1\%$  against standard SN 14915 under less than ideal viewing conditions. Both these devices were included in the International Pyrheliometric Comparisons (IPC VII) at the World Radiation Center in Davos, Switzerland in October 1990. Since these comparisons are held every 5 years, it was fortuitous that the returned instrument was available. The results (ref. 6) of the intercomparison give the following ratios to the World Radiation Reference (WRR) as embodied in the World Standard Group (WSG) of cavity radiometers.

APEX/LDEF Instrument SN21185	1.00069
------------------------------	---------

EPLAB reference SN14915	1.00002
-------------------------	---------

Measurements of the cavity reflectance were also performed by the staff of WRC/PMOD during the time of the intercomparisons. Initial results indicated reflectance values of

250  $\pm$  80 ppm for the APEX/LDEF cavity

270  $\pm$  80 ppm for a new cavity of the same type

The method employs a laser source and a shaped pyroelectric detector. Similar measurements, performed at NIST many years ago, on a similar cavity yielded a cavity reflectance value of 300  $\pm$  80 ppm. It appears that the change in the cavity paint has not affected the performance of the sensor within the level of uncertainties of these tests.

## CONCLUSIONS

Results of preliminary testing of the ERB components exposed aboard the LDEF indicate the following. Thermopile sensors were virtually unaffected by the space exposure, including the painted receivers of the directly exposed units. The filter and window materials experienced changes in spectral transmittance, some due to contamination and some due to UV exposure or other factors. Identification of the amounts due to each cause is under investigation. There appeared to be a contamination with later cleaning by atomic oxygen of most of the exterior, exposed components. Very little of the LDEF contaminant was found on the sensors discussed here. The cavity radiometer performance appears to be unaffected within our ability to assess change even though there is visible change to the cavity coating.

It remains to relate the LDEF results to the results of the Nimbus ERB missions in a quantitative manner. These results should be useful to those planning similar future measurements from space.

## ACKNOWLEDGMENTS

Thanks are extended to the LDEF staff, especially Carol Kaiser, Lenwood Clark and Jim Jones for help in the integration and deintegration of the experiment, to Jose Romero, Christoph Wehrli and Claus Frohlich of WRC/PMOD for the measurements of the cavity reflectance, to David Brinker of NASA Lewis Research Center for his cooperation with the cavity radiometer and APEX mounted samples and to Frank Griffin of Eppley Lab for transmittance measurements.

## REFERENCES

1. Nimbus 6 Users' Guide: (J.E. Sisala, ed.) NASA Goddard Space Flight Center, February 1975
2. Nimbus 7 Users' Guide: (C.R. Madrid, ed.) NASA Goddard Space Flight Center, August 1978
3. Mooney, T.A. and Smajkiewicz, A.: Transmittance Measurements of Ultra Violet and Visible Wavelength Interference Filters Flown Aboard LDEF. First LDEF Post-Retrieval Symposium, NASA CP-3134, 1992.
4. Predmore, R.E., Jacobowitz, H. and Hickey, J.R.: Exospheric Cleaning of the Earth Radiation Budget Solar Radiometer During Solar Maximum, Proceedings of the SPIE, 338, 1982, pp. 104-113
5. Brinker, D.J., Hickey, J.R. and Brasted, D.K.: Advanced Photovoltaic Experiment, S0014: Preliminary Flight Results and Post-Flight Findings, First LDEF Post-Retrieval Symposium, NASA CP-3134, 1992.
6. Working Report No. 162: International Pyrheliometer Comparisons IPC VII, 24 September to 12 October 1990, Results and Symposium, Swiss Meteorological Institute, March 1991

TABLE I. ERB SENSOR CHARACTERISTICS

CHANNEL NUMBER	FILTER	SPECTRAL BAND $\mu\text{m}$	THERMOPILE
<u>SOLAR SENSORS</u>			
1S	fused silica	0.18 to 3.8	N3
2S	fused silica	0.18 to 3.8	N3
3S	NONE (total Rad.)	<0.2 to >50	N3 FLAT PLATE
4S	OG-530 glass	0.526 to 2.8	N3
5S	RG-695 glass	0.698 to 2.8	N3
6S	Interference filter	0.395 to 0.510	N3
7S	Interference filter	0.344 to 0.460	N3
8S	Interference filter	0.300 to 0.410	N3
9S	Interference filter	0.285 to 0.365	K2
10S	Interference filter	0.250 to 0.320	K2
10C	NONE (total Rad.)	<0.2 to >50	HF CAVITY
<u>EARTH-FLUX SENSORS</u>			
11E	NONE (total Rad.)	<0.2 to >50	N3 FLAT PLATE
12E	NONE (total Rad.)	<0.2 to >50	N3 FLAT PLATE
13E	fused silica hemispheres	0.2 to 3.8	N3
14E	RG-695 glass hemisphere	0.695 to 2.8	N3

NOTES

Channel 1S and 2S are identical

Channel 1S is normally shuttered on Nimbus (reference channel)

Channel 3S is shuttered when Channel 1S open on Nimbus

The front 4 mm fused silica window of channel 4S-03 was missing, so that the OG-530 glass was exposed directly

Channel 10S is on Nimbus 6 only

Channel 10C is on Nimbus 7 only

The cavity sensor on LDEF is in the APEX (S0014) experiment

Channel 11E and 12E are identical on Nimbus 6

Channel 11E of Nimbus 7 has black painted baffles (also on LDEF)

Channel 11E is normally shuttered on Nimbus (reference channel)

Reference channels have no shutters on LDEF

All thermopiles are wirewound plated types, copper on constantan

All thermopiles have receivers coated with 3M 401-C10 black paint over a primer coat of Chemglaze Z306

The HF cavity interior is coated with Chemglaze Z302 black paint

TABLE II. ERB SOLAR CHANNEL MODULE EXPOSURE TEST RESULTS

ERB Channel	SIGNAL (mV)		RATIO	%CHANGE
	pre-flight	post-flight		
1S-03	2.267	2.304	1.016	1.63
2S-03	1.989	1.975	0.993	-0.70
3S-03	2.795	2.811	1.005	0.57
4S-03	2.154	2.148	0.997	-0.28
5S-03	1.543	1.558	1.010	1.00
6S-03	2.539	2.555	1.006	0.63
7S-03	2.754	2.760	1.002	0.18
8S-03	2.814	2.819	1.002	0.18
9S-03	16.552	16.399	0.991	-0.92
10S-03	19.731	19.700	0.998	-0.16

## APPENDIX A: COMPONENTS BY ERB CHANNEL

Nimbus/ERB Flight Spare Sensors were designated set 03

### SOLAR SENSING CHANNELS

All have body/baffle parts of aluminum; Nickel Sulfide anodized

Channel 1S and Channel 2S (these channels are duplicates)

Type N3 thermopile sensor

Front window: 2mm thick Suprasil W fused silica

Rear window: 2mm thick Suprasil W fused silica

Window retainers: Mylar washer and beryllium copper wave  
spring washer

Channel 3S (an open channel with no windows or filters)

Type N3 thermopile sensor

Channel 4S and Channel 5S (colored glass window channels)

Type N3 thermopile sensor

Front window: 4mm thick Suprasil W fused silica

Intermediate window:

Schott OG-530 yellow glass for channel 4S

Schott RG-695 red glass for channel 5S

Rear window: 2mm thick Suprasil W fused silica

Window retainers: Mylar washer and beryllium copper wave  
spring washer

Channel 6S, 7S and 8S (small interference filter channels)

Type N3 thermopile sensor

Front window: interference filter

Front substrate: 4mm thick Suprasil W fused silica

Rear substrate: 2mm thick Suprasil W fused silica

Spacer: aluminum ring

Layer Materials: Thorium Fluoride

Silver

Zinc Sulfide (6S and 7S only)

Rear window: 2mm thick Suprasil W fused silica

Window retainers: Mylar washer and beryllium copper wave  
spring washer

Channels 9S and 10S (large interference filter channels)

Type K2 thermopile sensor

Front window: interference filter

Front substrate: 4mm thick Suprasil W fused silica

Rear substrate: 2mm thick Suprasil W fused silica

Spacer: aluminum ring

Layer Materials: Thorium Fluoride

Aluminum

Rear window: 2mm thick Suprasil W fused silica

Window retainers: Mylar washer and beryllium copper wave  
spring washer

### EARTH-FLUX SENSING CHANNELS (aluminum bodies)

Channels 11E and 12E (these channels are duplicates)

Type N3 thermopile sensor with 0.25" dia. black paint

Channel 13E (clear dome channel)

Type N3 thermopile sensor with 0.25" dia. black paint

Inner and outer hemispheres of Suprasil W fused silica

Channel 14E (red dome channel)

Type N3 thermopile sensor with 0.25" dia. black paint

RG-695 glass hemisphere between 2 Suprasil W hemispheres



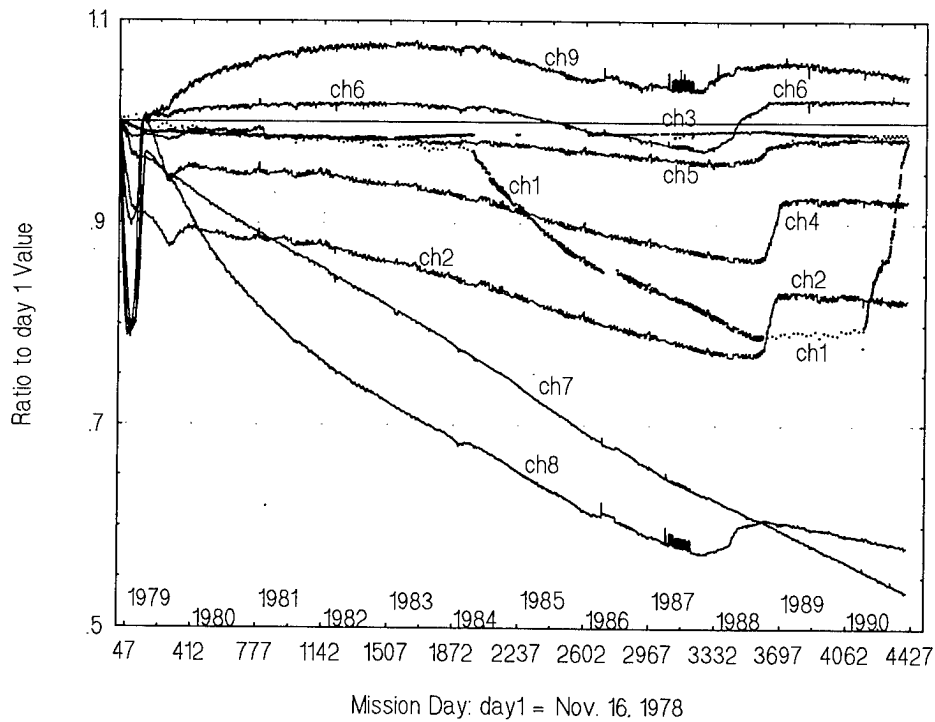


Figure 1. Daily data from 9 solar sensing channels of the Nimbus 7 ERB experiment normalized to the first day value for a 12 year period, Nov. 16, 1978 to Nov. 30, 1990

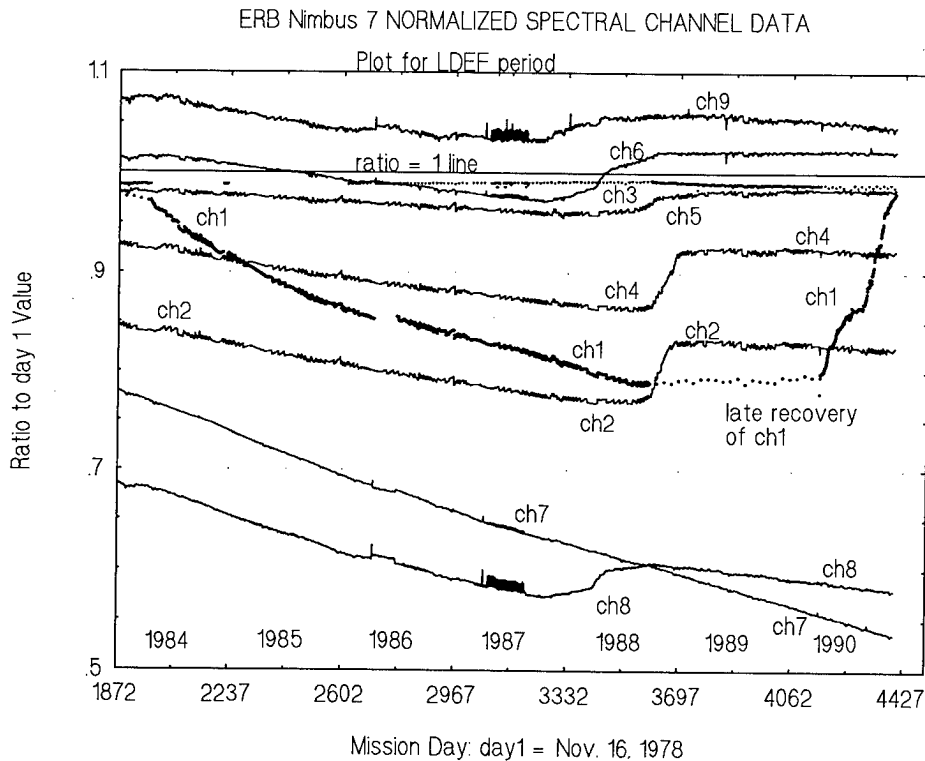


Figure 2. Normalized daily data as in Figure 1. for the period of the LDEF mission, 1984-1990. The cleaning effect of the onset of solar cycle 22 is shown.

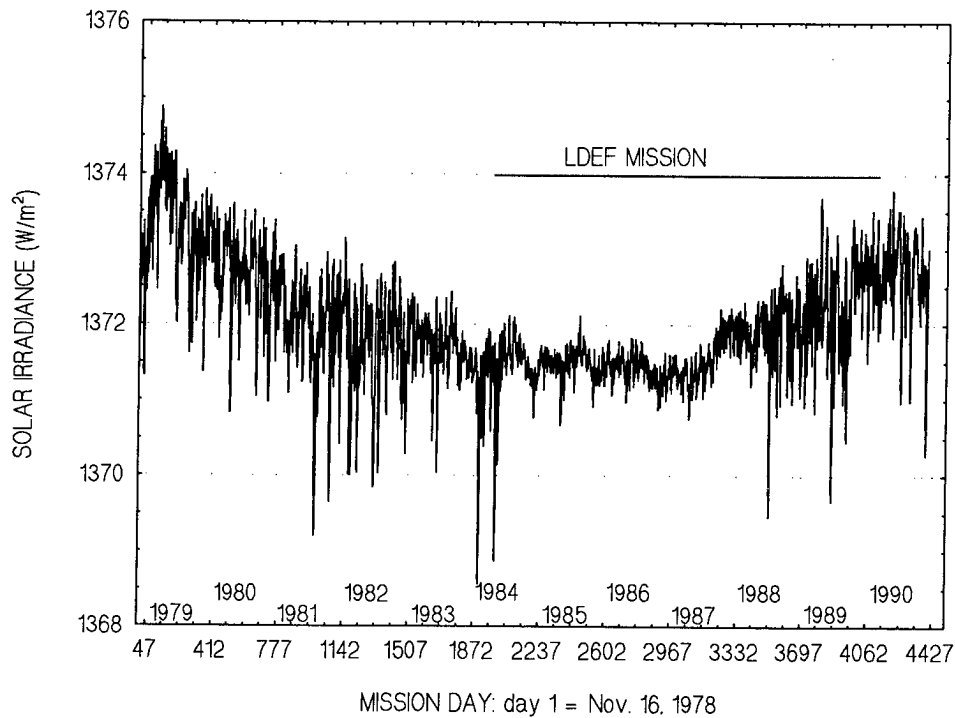


Figure 3. Total solar irradiance measured by the cavity radiometer (channel 10C) of Nimbus 7 for the same time period as in Figure 1.

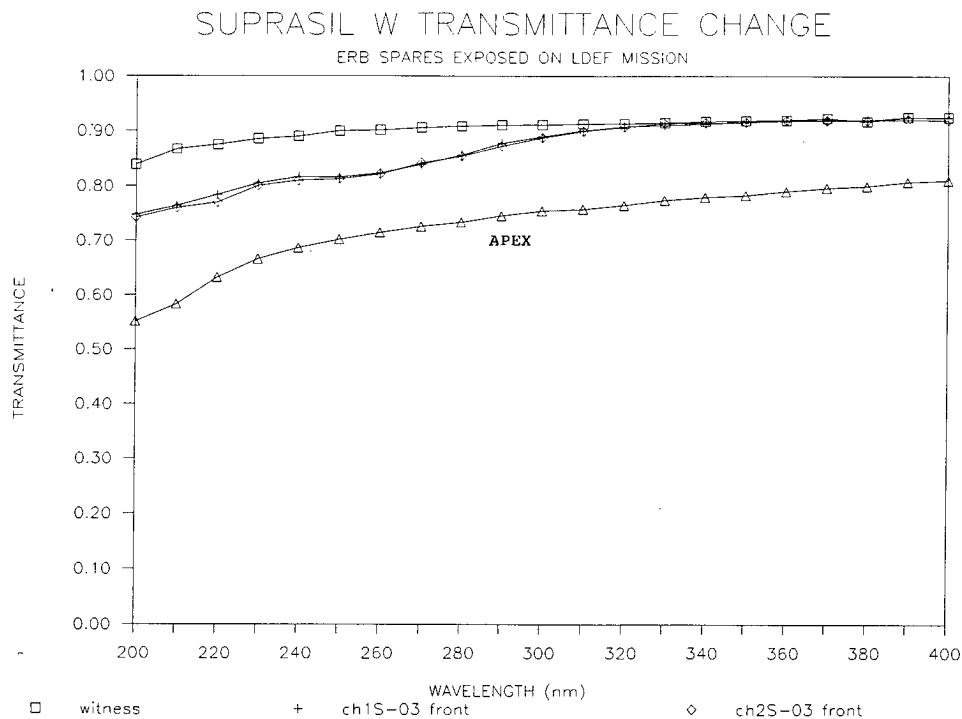


Figure 4. Transmittance of Suprasil W fused silica windows from the front of channels 1S and 2S shown with the plots for a witness sample and a contaminated sample from the APEX experiment. All are 2 mm thick.

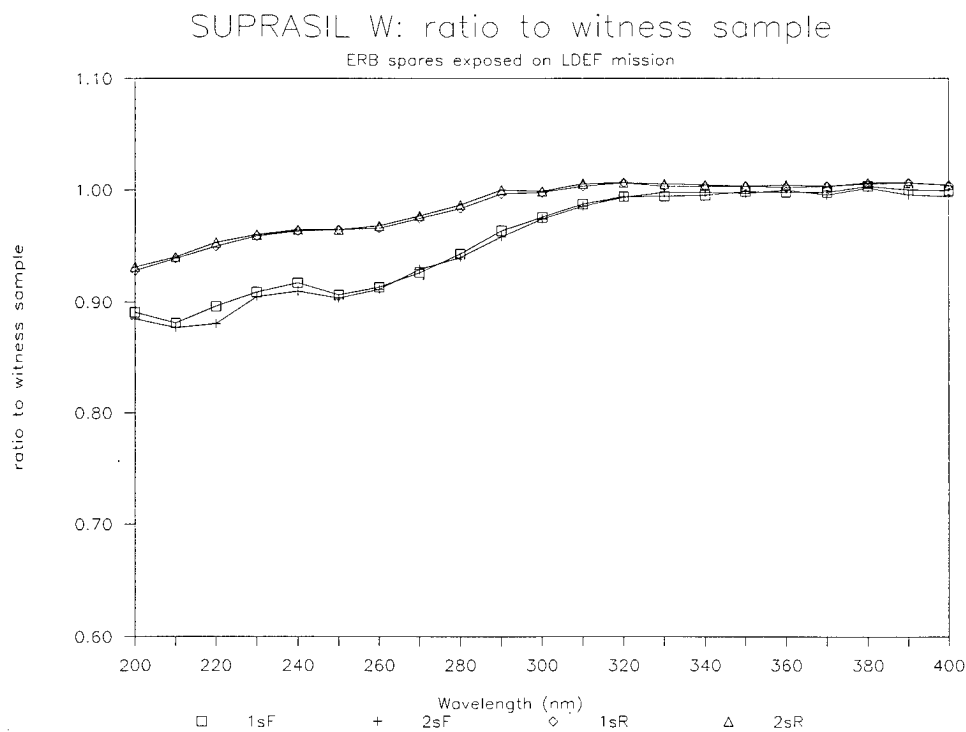


Figure 5. Ratio of the transmittance values of 2 front Suprasil W fused silica front windows and 2 rear windows from channels 1S and 2S to the value for the witness sample. All are 2 mm thick.

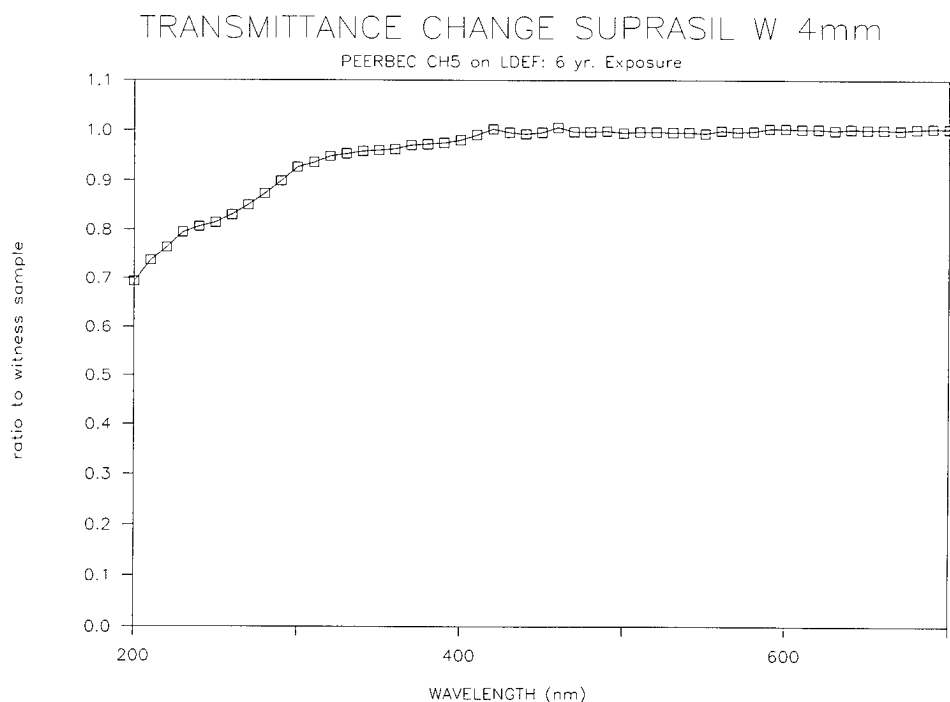


Figure 6. Ratio of the transmittance of the 4 mm thick front window of channel 5S to that of a matching witness sample.

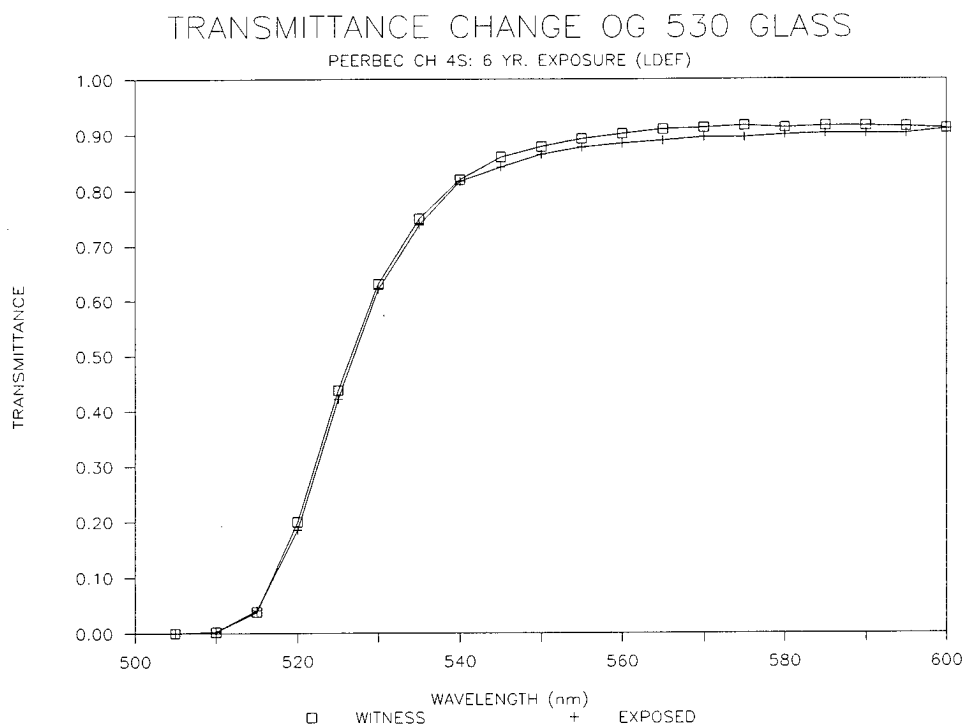


Figure 7. Spectral transmittance of OG 530 colored glass of channel 4S

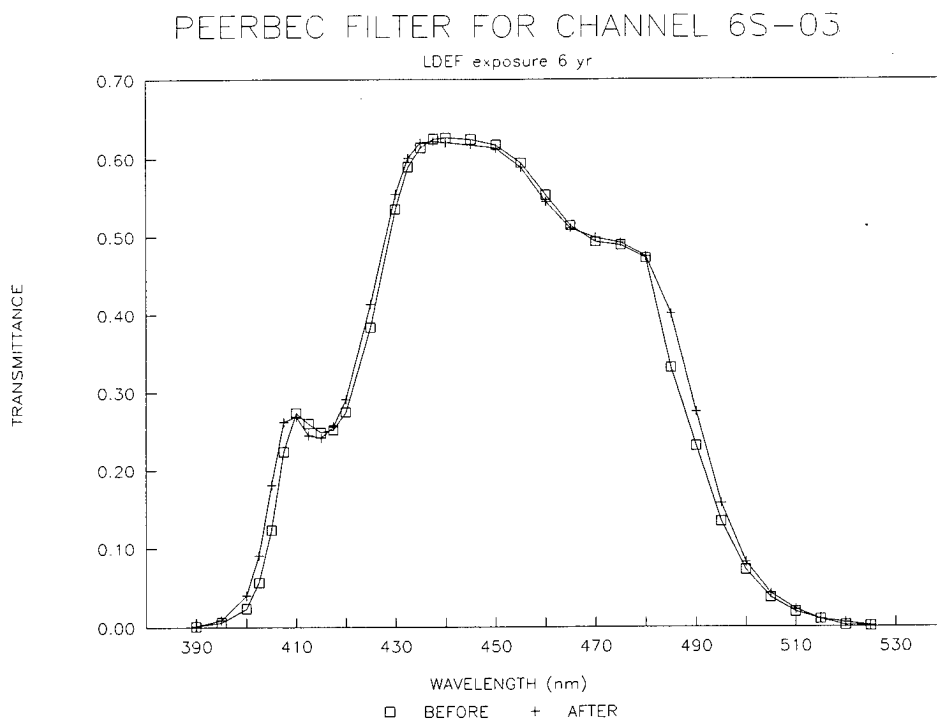


Figure 8. Spectral transmittance of interference filter 6S

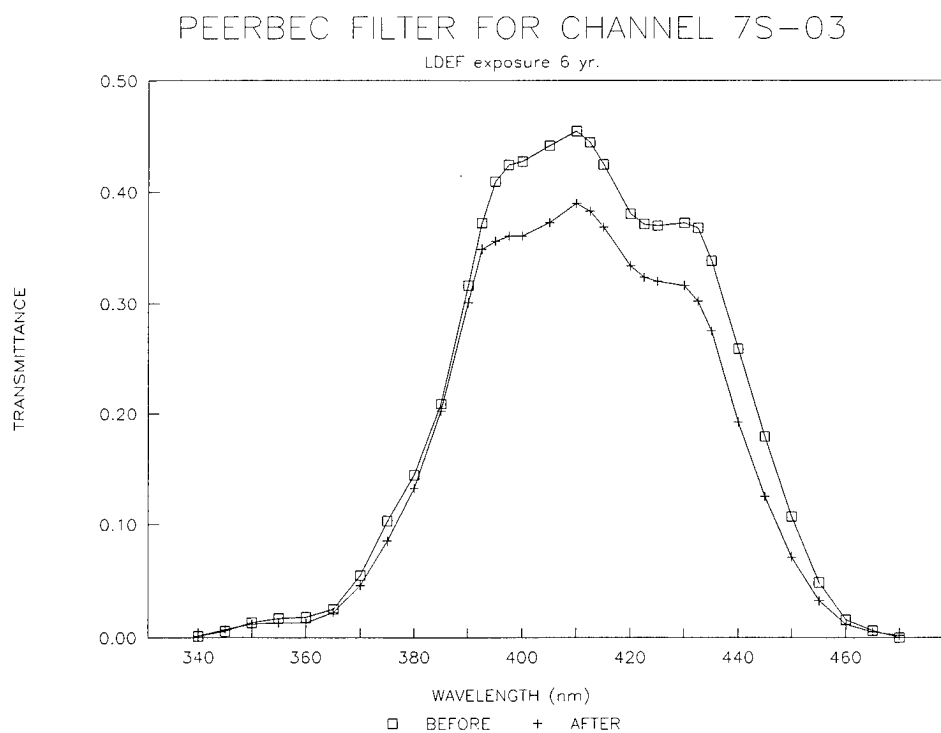


Figure 9. Spectral transmittance of interference filter 7S

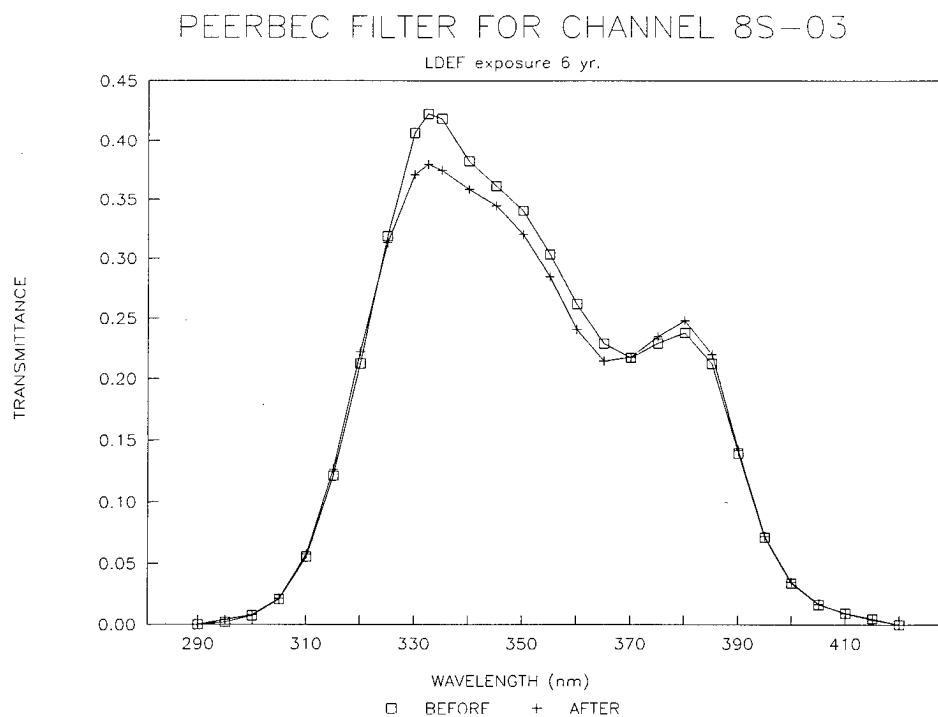


Figure 10. Spectral transmittance of interference filter 8S

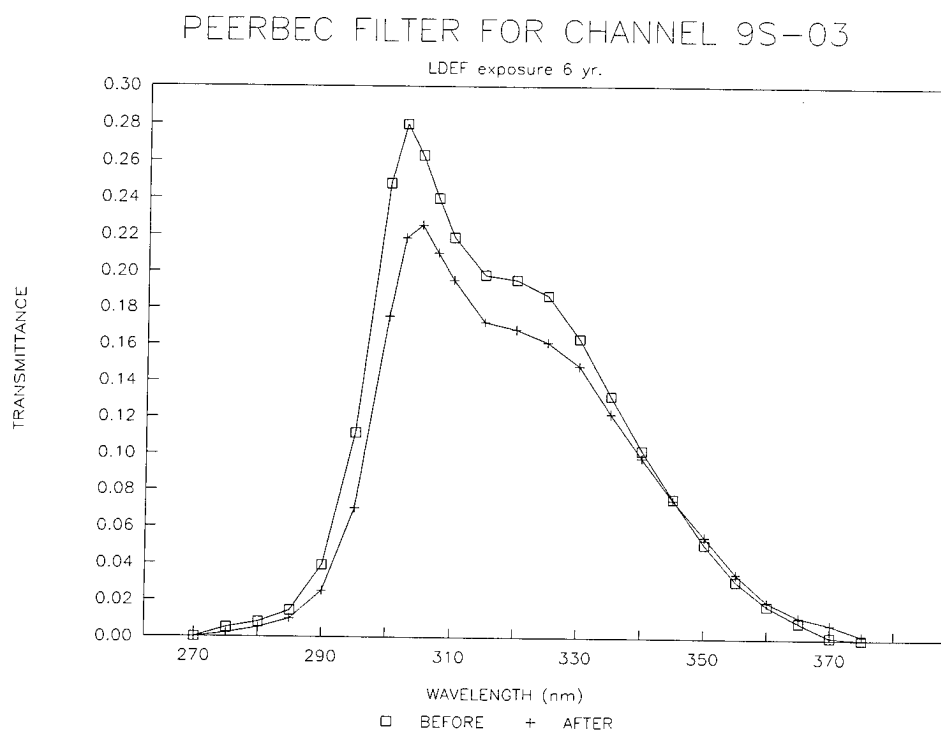


Figure 11. Spectral transmittance of interference filter 9S

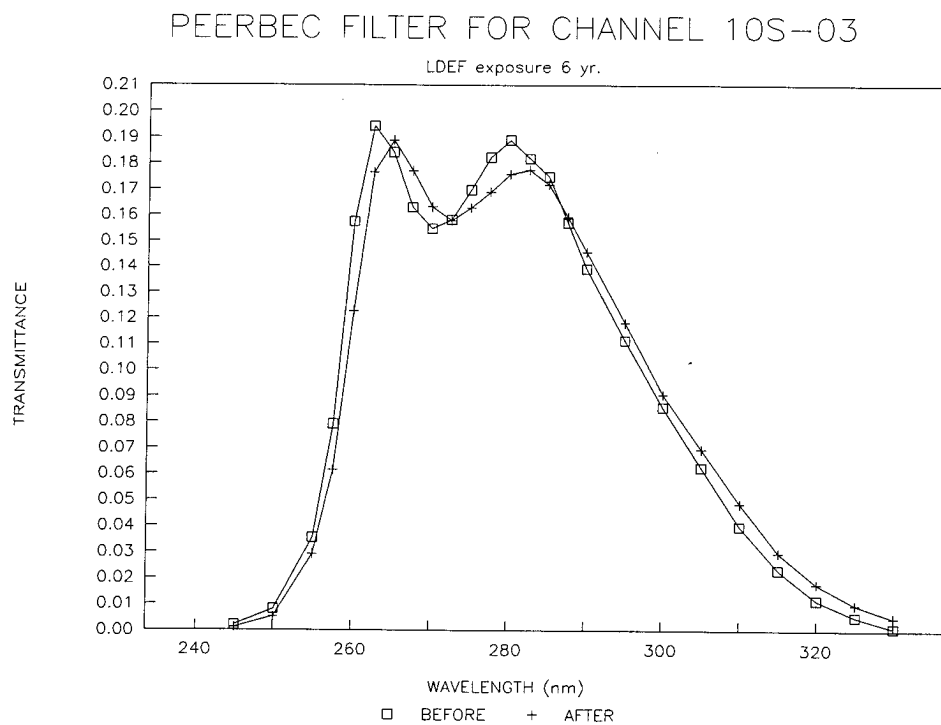


Figure 12. Spectral transmittance of interference filter 10S

# TRANSMITTANCE MEASUREMENTS OF ULTRAVIOLET AND VISIBLE WAVELENGTH FILTERS FLOWN ABOARD LDEF

Thomas A. Mooney  
Ali Smajkiewicz  
Barr Associates, Inc.  
2 Lyberty Way  
Westford, MA 01886  
Phone: 508/692-7513, Fax: 508/692-7443

## INTRODUCTION

Barr Associates provided a set of ten interference filters to The Eppley Laboratory to be mounted in their Tray Number B8, Experiment Number AO-147 of LDEF. The results of spectral transmission measurements before delivery and after recovery are presented here. Included are descriptions of the construction and materials included in the filters. Additional results from photographic microscopic and surface analytical observations are being gathered and will be presented at a later date.

## APPROACH

Our intent was to measure changes in transmission of our typical interference filter coatings due to the space environment. We limited the study to coating materials for the UV and visible/NIR region, and two optical cements. There were a total of two metals and six dielectric coating materials employed (Table 1). These were some of the more common materials used by Barr at the time, but not necessarily present-day materials of choice. All coatings were multi-layers consisting of alternating layers of two or more materials. No single layer samples were included. All the coatings were produced in the February 1983 time frame.

All filter substrates and cover plates were the same material, as were all the filter housings and sealing materials. We looked at two cements, one of which (APCO R313, manufactured by Applied Plastics Company) we commonly used for ground-based filters and another (Epon 828, manufactured by Shell Chemical Company) which had been approved by JPL for use in the Galileo SSI filters.

## FILTER CONFIGURATIONS

Two configurations were used as illustrated in Figures 1 and 2. Most of the filters were air-spaced (Figure 1); that is, there was no cement in the optical path between the coating and cover plate. An aluminum ring separates the filter substrates and cover plate. The substrate, cover plate and spacing ring were sealed into an anodized aluminum sleeve with low out-gassing epoxy. All substrates and cover plates are 3 mm thick Amersil TO8 (manufactured by Heraeus Amersil Inc.) fused silica material.

A second configuration was used for the cemented filters (Figure 2). The only differences were that the spacer was eliminated and the two fused silica plates were cemented together; that is, there was a thin layer of cement in the optical path.

All filters are 25 mm diameter by approximately 7.5 mm thick. On LDEF, they were mounted to the outer surface of the tray using a washer and clamping ring such that an area about 18 mm diameter on one surface was completely exposed.

## RESULTS

The plots show as-delivered and post-retrieval spectral measurements. The raw data was taken at one nanometer spectral resolution with a Cary/Varian 219 or 2400 spectrophotometer. Wavelength accuracy is better than 0.5 nm and photometric accuracy better than 3%. Raw data was digitized at 2 nm increments, so some resolution is lost near sharp features on the plots shown here. An aperture of 1 centimeter diameter centered on the filter was used.

Details of the results are shown in the plots. The coatings survived with little change in spectral profile. Changes did occur in transmission. There were at least three categories of change which can be summarized as:

- Increase in transmission due to pinholes in some of the metal-dielectric coatings (Filter No. 3 and 7).
- Slight increase in transmission due to an apparent reduction in the extinction coefficient of ZnS (Filter No. 6).
- Decrease in transmission due to increased absorption in the lead compounds (Filter No. 8 and 9).

We also saw a greater than expected reduction in transmission (increased absorption) in the filter cemented with Epon 828.



We tried to model the transmission loss in the filters containing lead compounds. Simply increasing the extinction coefficient of the lead compound produces results similar to those measured. Figure 3 illustrates the result of using a  $k$  value (extinction coefficient) of 0.07 for the  $\text{PbCl}$  in Filter No. 8. Figure 4 shows a similar result for Filter No. 9 ( $\text{PbF}_2$ ). This plot caused us to question the assumption that a simple increase in absorption occurred. The actual measured result shows fine structure in the transmission curve, while the predicted result does not. Looking again at Figure 3, a similar condition exists but to a lesser degree. Note the loss of structure near 430 nm. We are presently trying to identify the cause which might be explained by an absorbing deposit on the filter surface.

## CONCLUSIONS

With the exception of the lead compounds, the coatings survived very well. The Epon cement degraded somewhat at 500 nm (other wavelengths are masked by the filter). Failure mode (degradation) of the lead compounds was a wavelength-independent increase in absorption with no change in spectral characteristic. In an instrument, signal would be lost but spectral stability maintained. These materials, however, are no longer being incorporated into space-borne filters, so the results may be academic except that there may be some filters incorporating lead compounds still flying aboard operational spacecraft. We have seen similar reductions in transmission in filters containing lead chloride when subjected to elevated temperatures, so the effect may be primarily a thermal one.

In the case of filters containing aluminum layers, the transmission increases can be attributed to the pinholes which developed during exposure. This form of failure would reduce signal-to-noise but would not influence spectral band position or width. The reason for development of pinholes has not been established by Barr. One possibility is that defects or contamination in the coating caused local heating due to increased absorption which, in turn, caused coating removal.

## FUTURE WORK

Barr will continue with additional tests to try to resolve the pinhole issue. Also planned are various surface analyses of the substrates.

## ACKNOWLEDGEMENT

Barr Associates wishes to thank John Hickey of The Eppley Laboratory for his offer of space on LDEF and his assistance with the logistics of this experiment. This work is supported by Barr Associates' IR & D funds.

**Table 1. Metal and Dielectric Coating Materials**

Coating Materials	Cements	Substrates/Covers
Zirconium Oxide Zinc Sulfide Thorium Fluoride Cryolite (Sodium Aluminum Fluoride) Lead Fluoride Lead Chloride	Epon 828 with Versamid 140 Hardener APCO R313	Fused Silica (Amersil TO8)

LDEF Filters, Air-Spaced Construction

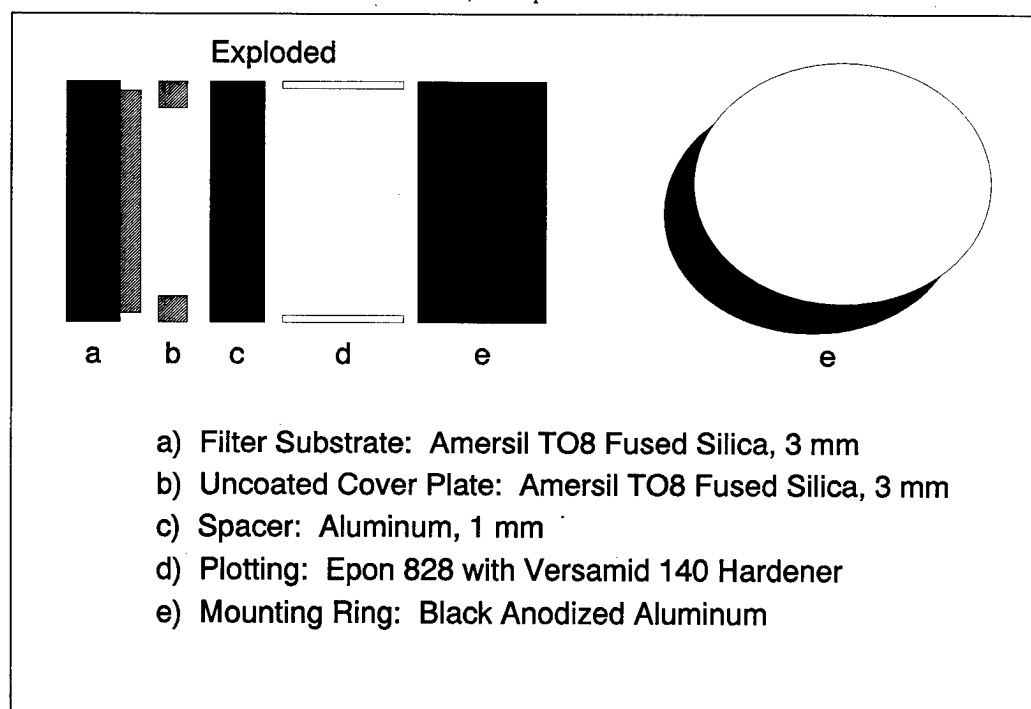


**Figure 1**

# LDEF Filters, Cemented Construction

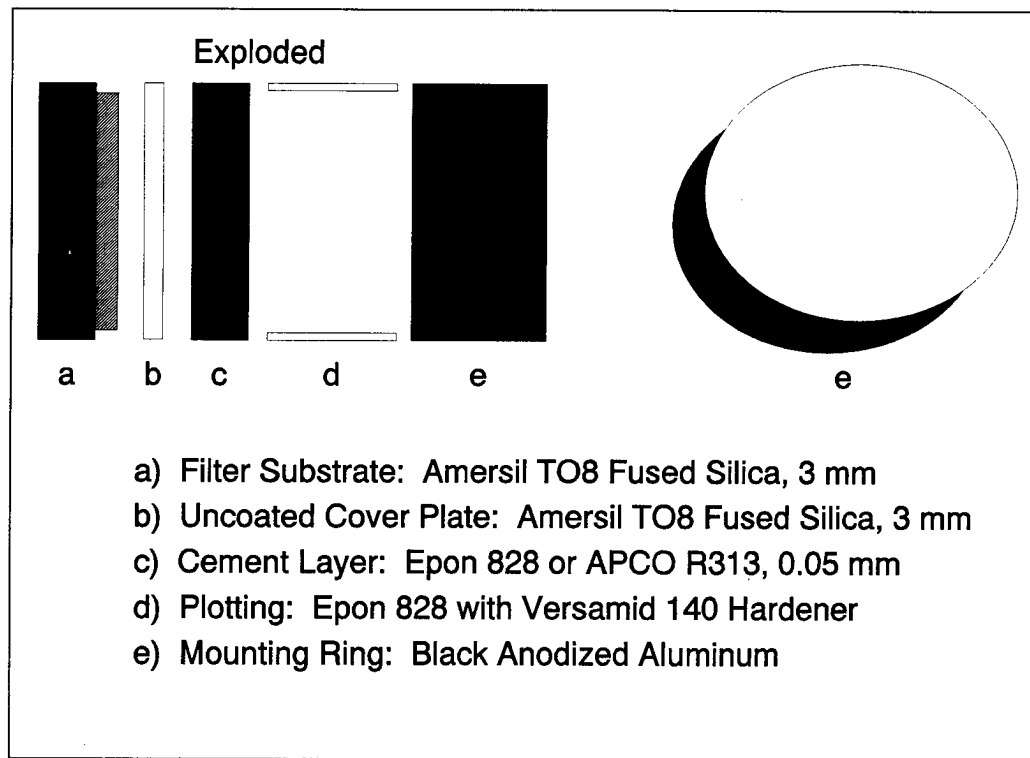


**Figure 2**

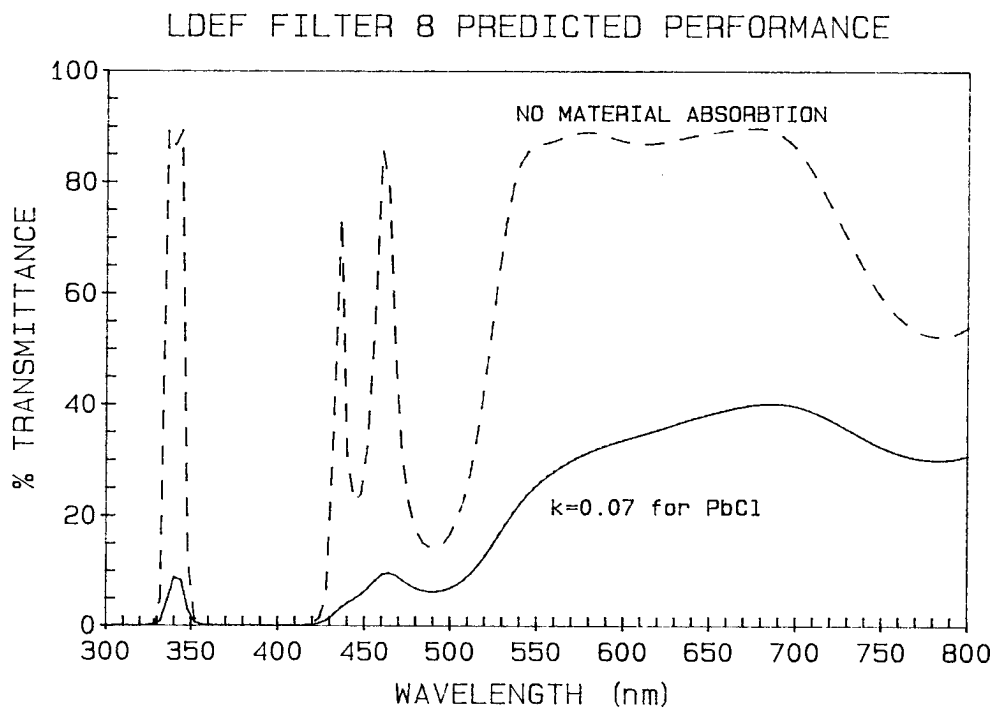


**Figure 3**

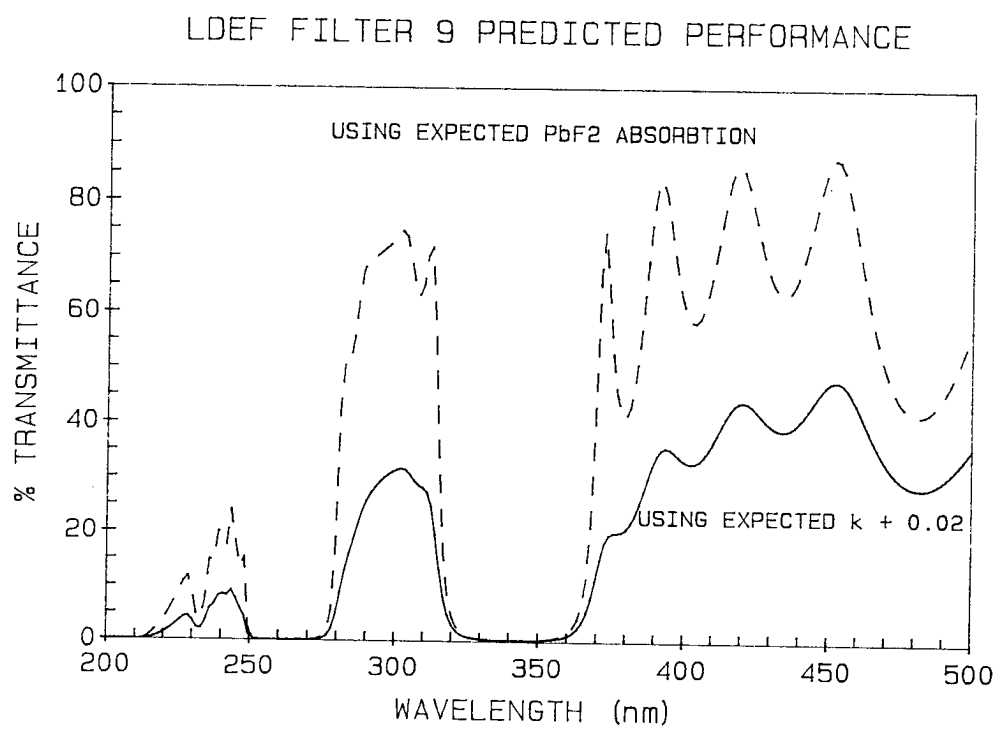
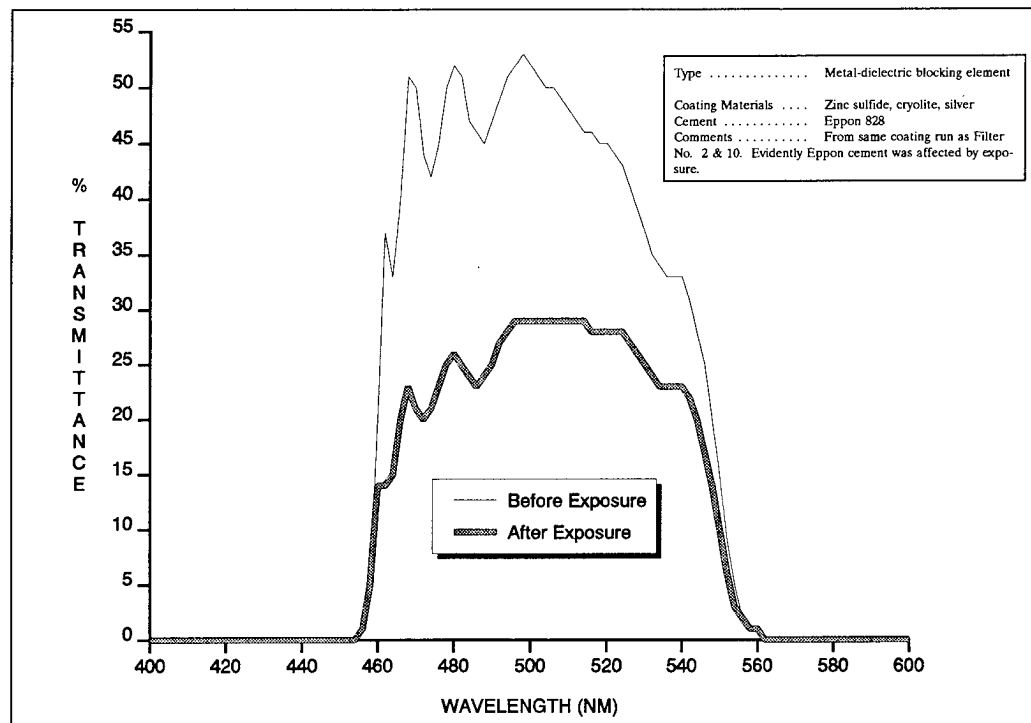


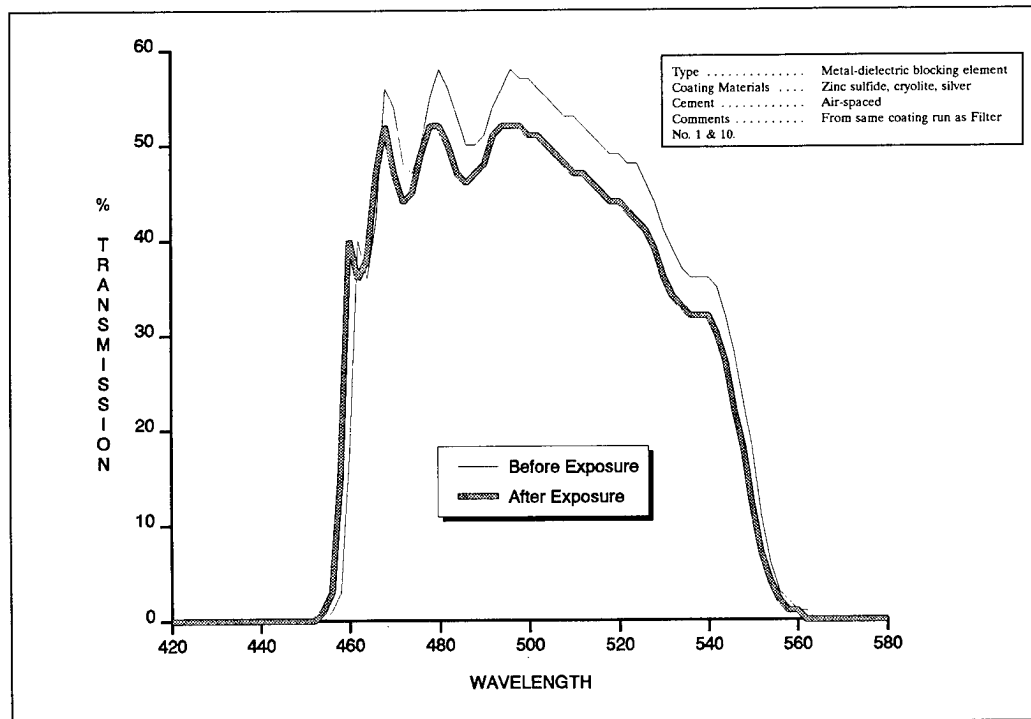
**Figure 4**

# **PLOTS** **(1-4 and 6-10)**

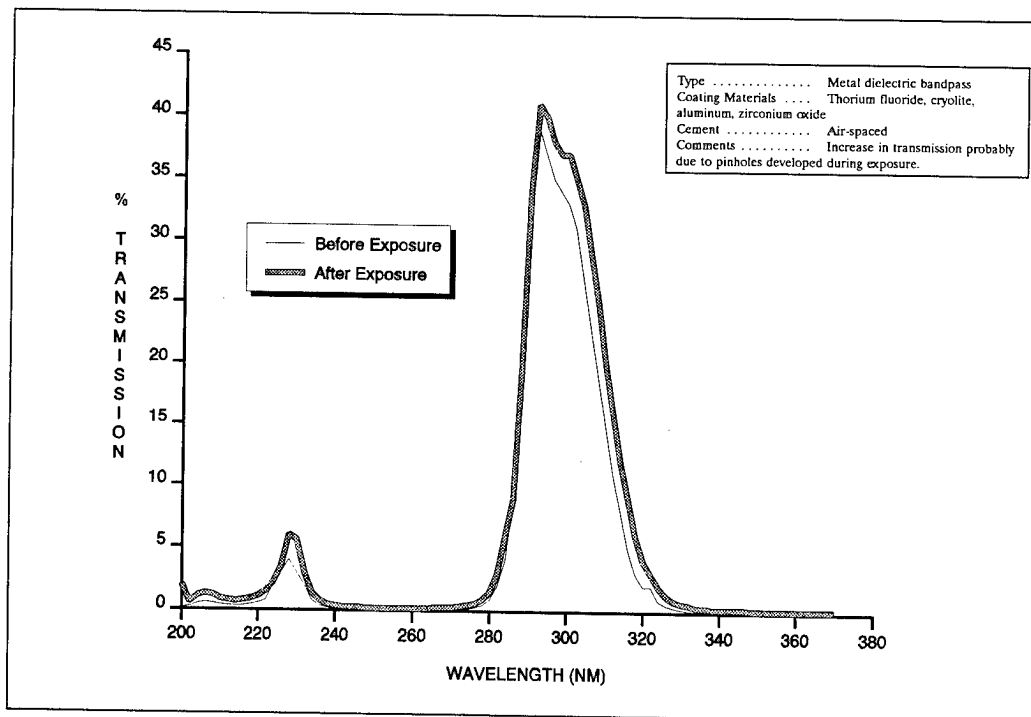
**LDEF Filter No. 1**



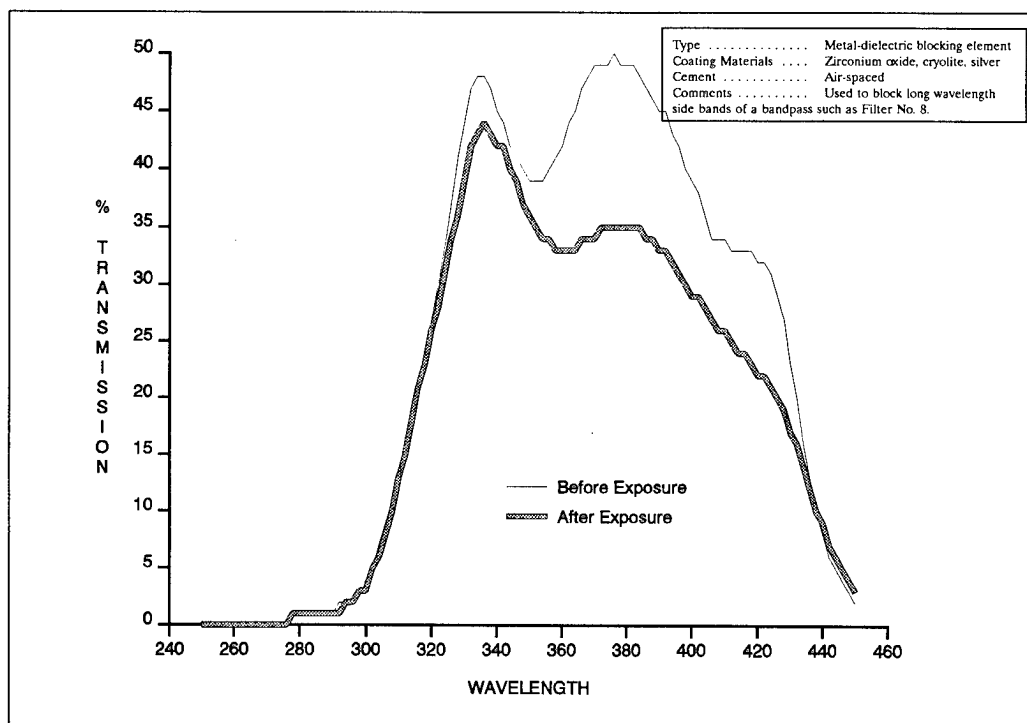
**LDEF Filter No. 2**



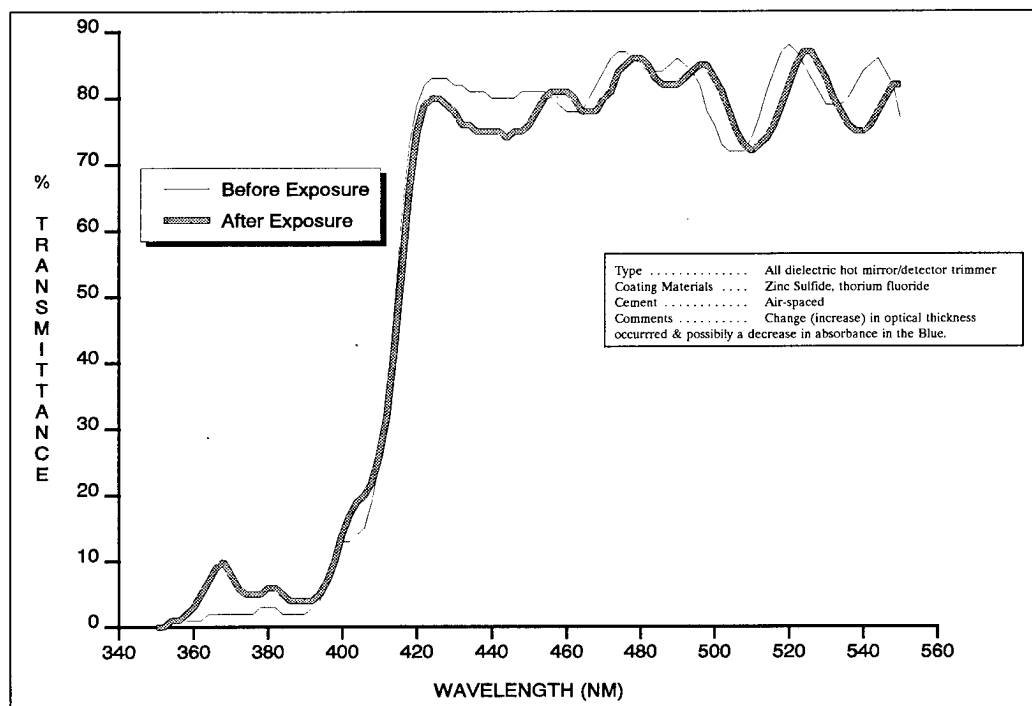
LDEF Filter No. 3



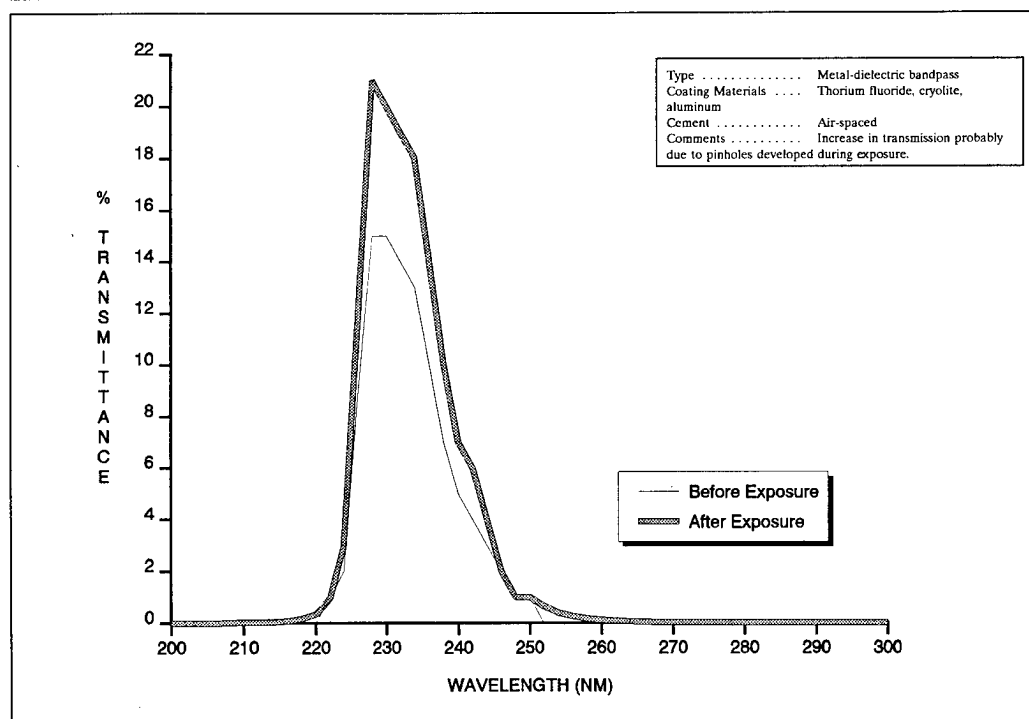
LDEF Filter No. 4



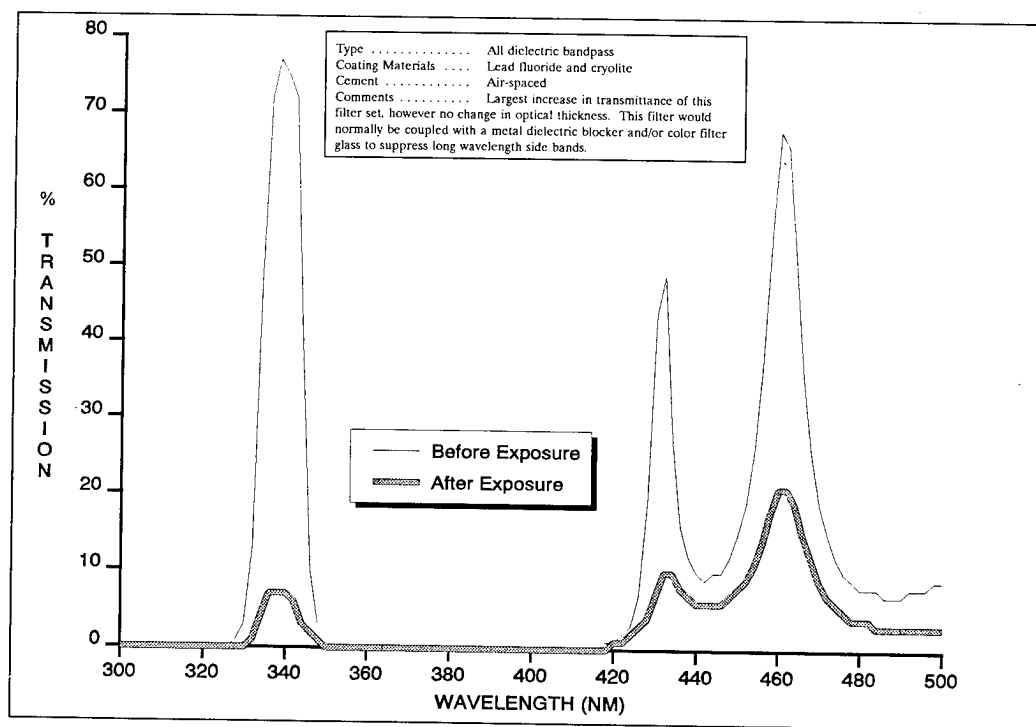
LDEF Filter No. 6



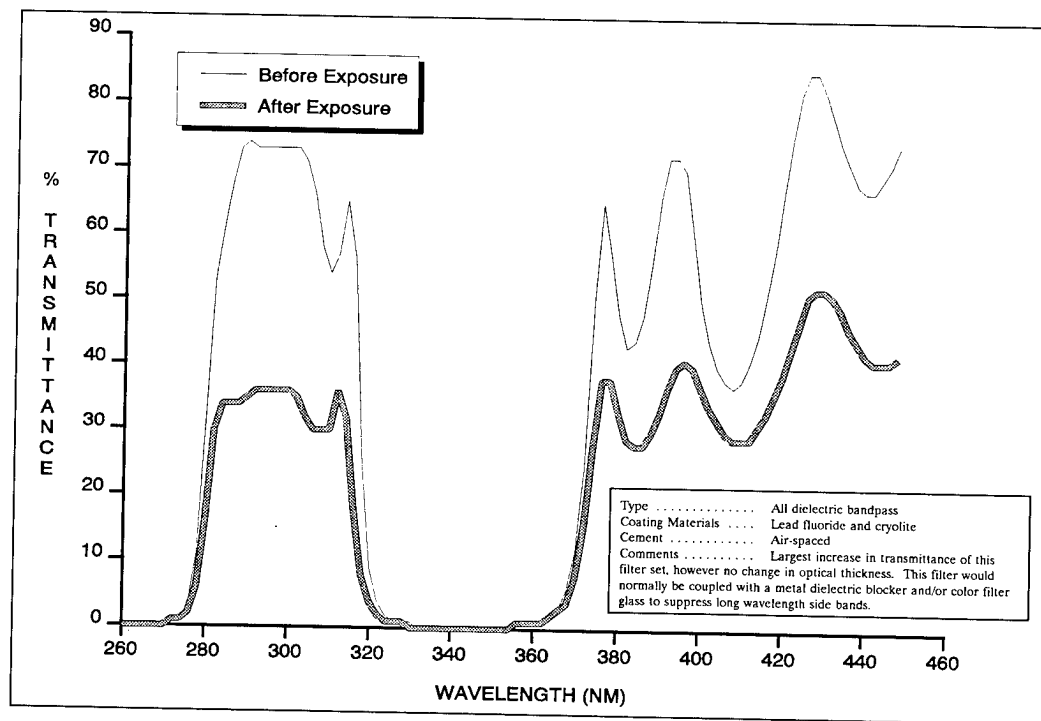
LDEF Filter No. 7



LDEF Filter No. 8

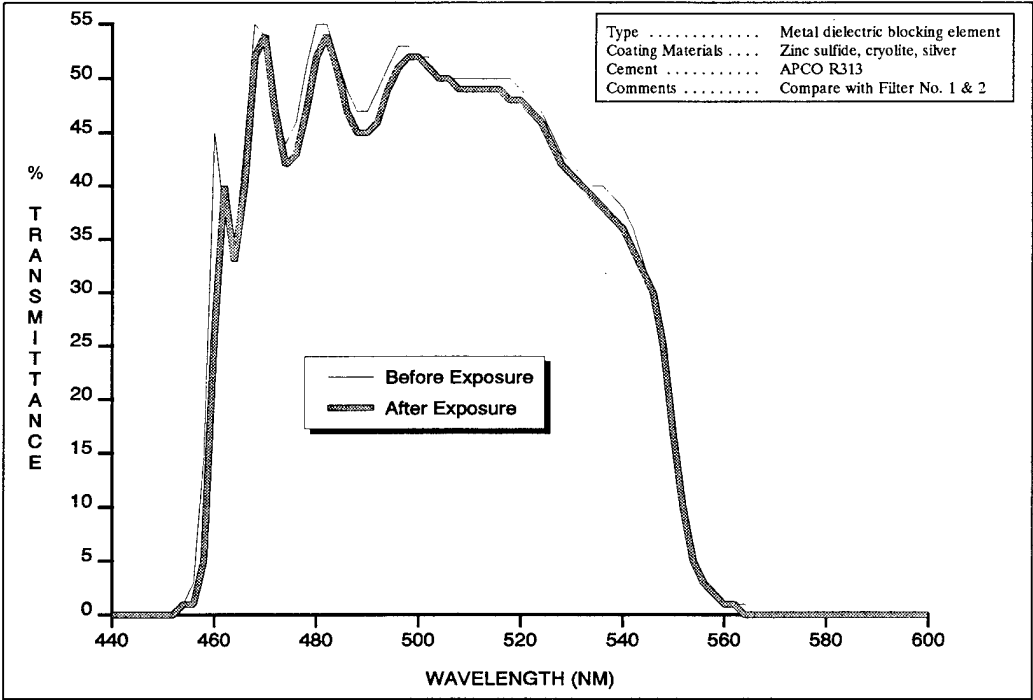


LDEF Filter No. 9





LDEF Filter No. 10



# RADIATION SENSITIVITY OF QUARTZ CRYSTAL OSCILLATORS EXPERIMENT FOR THE LONG DURATION EXPOSURE FACILITY (LDEF)

J. S. Ahearn and J. D. Venables<sup>+</sup>  
Martin Marietta Laboratories  
1450 S. Rolling Rd.  
Baltimore, MD 21227  
Phone: 301/247-0700, Fax: 301/247-4939

## ABSTRACT

Factors determining the radiation sensitivity of quartz crystal oscillators were studied on NASA's Long Duration Exposure Facility. Quartz materials were examined in the transmission electron microscope (TEM) and classified as to their sensitivity to radiation damage by establishing the rate of damage caused by the electron beam in the microscope. Two types of materials, i.e., swept premium Q quartz and natural quartz were chosen because clear differences were observed in their response to the electron beam in the TEM studies. Quartz resonators were then fabricated from them, tested for frequency stability over a >6 mo. period and flown on the LDEF satellite. After retrieval (>6 years in space) the stability of the resonators was again determined. All of the space-exposed resonators fabricated with swept premium Q material exhibited a frequency shift above that of the control resonators; none of the resonators fabricated from the natural quartz materials exhibited such a shift. The significant differences observed between the two types of materials in both the ground-based TEM studies and the space radiation induced frequency changes suggest that there may be a correlation between the two observations.

## INTRODUCTION

It has long been known that radiation produces shifts in the resonant frequency of quartz crystal oscillators which may be as large as 400 parts per million. The need for high-precision quartz oscillator clocks (and filters) for communication satellites, missiles, and space probes makes it necessary to improve the radiation stability of materials used for these applications.

Experiments performed at Martin Marietta Laboratories (ref. 1) and elsewhere (ref. 2) demonstrate that the technique of transmission electron microscopy (TEM) provides a powerful method for studying the effect of radiation on crystalline quartz. When suitably thin samples of  $\alpha$ -quartz are examined by TEM, it is observed that defect clusters form at a rapid rate within the material even when the incident electron energy is as low as 20 keV. Recent evidence indicated that the clusters may actually be small amorphous regions in the crystalline material that grow larger with time under the electron beam created damage (ref. 2). The strain clusters most probably form from displaced atoms which condense at impurity sites (because the clus-

---

<sup>+</sup> Retired

ter concentration appears to be impurity dependent); and the clusters induce large strain fields in the lattice surrounding them, as evidenced by their paired black-dot images. The strain contrast that develops is caused by the strain associated with the misfit of the amorphous cluster and the crystalline matrix.

Two factors suggest the observed damage may be related to the radiation-induced frequency drift associated with irradiated quartz resonators. First, the piezoelectric properties of quartz are most likely modified because the elastic properties of amorphous quartz are markedly different than that of crystalline quartz, and because of the presence of the strain field associated with the clusters. Second, both phenomena appear to be sensitive to the impurity concentration in the quartz material. These facts suggest that TEM can be used to classify grades of quartz according to their suitability for use in radiation-hard resonators. Moreover, using this technique it may be possible to identify the impurities that are responsible and thereby effect an improvement in the stability of quartz resonators.

The objective of the LDEF experiment is to determine whether there is a correlation between the damage produced in the electron microscope for different grades of quartz as revealed by TEM and the electrical stability of quartz resonators exposed to the complex radiation associated with an orbital LDEF environment.

## EXPERIMENTAL DESIGN

To accomplish the objectives of the experiment, several grades of single-crystal  $\alpha$ -quartz containing a wide range of impurity concentrations were examined by TEM to determine differences in their susceptibility to radiation damage during electron irradiation. Based on the sensitivity of the quartz materials to radiation as determined by TEM, two grades of quartz were selected for fabrication into resonators to maximize the differences in radiation sensitivity of the chosen materials. The electrical properties of the resonators were established by measuring their resonant frequency before insertion into orbit. Two pre-flight measurements of each resonator were made; one in 1979, the other in 1982. A third series of electrical measurements were made on the resonators to determine variations from the preflight data. Below we compare changes in the electrical data to the TEM results to determine whether TEM observations are relevant to the study of the stability of quartz resonators in a space environment.

The experiment hardware consisted of one-sixth of a 3-in.-deep peripheral tray located in tray D2 with 14 5-MHz fifth-overtone AT-cut resonators mounted on an aluminum plate (Fig 1). Bliley Electric fabricated the resonators from two materials (synthetic swept premium Q manufactured by Sawyer Research Corporation, and Brazilian natural quartz) selected because the TEM technique indicates large differences in their radiation sensitivity. Four resonators (two from each grade of material) were used as controls in the LDEF tray and shielded from radiation. The remaining ten resonators (five from each grade) were exposed to the space radiation environment. In addition, two resonators (one from each grade) were kept in the laboratory as additional controls. By comparing the frequency drift of the resonators before and after the flight it was possible to separate the natural frequency drift from that induced by the space radiation and to correlate with the TEM observations.

## TRANSMISSION ELECTRON MICROSCOPE RESULTS

In the pre-flight TEM analysis several grades of quartz materials were examined. Following sample preparation to achieve electron transparent material suitable for examination in the microscope, the materials were examined by subjecting them to the electron beam and monitoring the development of strain centers over a specific exposure time.

We quantified these observations so that we could classify the materials based on their behavior in the TEM and therefore choose two materials for fabrication into flight resonators for LDEF. Careful TEM observations were made by first setting the accelerating voltage to 100kV, fixing the magnification to 33,000 or 100,000 times and adjusting the flux of electrons in the absence of a sample to a fixed value. Radiation damage of the sample was initiated by moving it into the path of the electron beam. A series of micrographs was taken to record the result of the electron exposure as a function of time. In all samples strain centers formed after a short (5 min) exposure to electrons. However there was a marked difference between the different materials in (1) the cluster density and (2) the size of the strain centers after a given radiation dosage. It was possible to quantify the differences in cluster density for various grades of quartz with the results shown in Table I. No similar quantification of the cluster size after a fixed electron dose was made, but qualitatively the swept premium Q quartz exhibited the largest clusters whereas the natural quartz exhibited the smallest clusters. Because the swept premium Q and the natural quartz materials exhibited extremes in both cluster densities and also in cluster size for a given amount of radiation, they were chosen for fabrication into resonators.

## QUARTZ RESONATOR FREQUENCY DRIFT MEASUREMENTS

The resonators were 5th overtone AT-cut resonators fabricated by Bliley Electric Company (Bliley Type BG61AH-5S). Aging of the resonators was undertaken twice for each set prior to integration into the LDEF tray and once after retrieval. In all cases the resonators were held at 75°C over the entire period of the aging tests. Examining the aging data we found that the shielded swept premium Q resonators showed the same drift rate before and after the flight. However, the unshielded swept premium Q resonators exhibited a larger frequency drift in all of the post-flight aging tests than in the pre-flight tests. An example of the aging data for the swept premium Q resonators for the shielded and unshielded post-flight cases is shown in Fig 2. The magnitude of the frequency shift is  $2.1 \times 10^{-8}$  Hz for the unshielded case compared to  $6.1 \times 10^{-9}$  Hz in the shielded case.

In the case of the natural quartz resonators, all of the pre- and post-flight aging tests were similar within the scatter of the experimental data. In addition, all of the natural quartz resonators, and the pre-flight and shielded post-flight swept premium Q resonators behaved in a similar manner within the scatter of the experiment. All of our aging data is summarized in table II where we report the total frequency drift observed in the aging tests for each sample and condition category and Table III where we report the average frequency drifts observed.

## DISCUSSION

Our data has demonstrated a marked effect of the space radiation environment on the magnitude of frequency drift observed in post-flight aging tests of the swept premium Q resonators and no effect on the resonators fabricated from the natural quartz materials.

Examining the analysis of the radiation environment experienced by LDEF (ref. 3) we estimated the total dose given to the resonators in the shielded and unshielded condition. The frequency drift observed in the unshielded swept premium Q resonators was  $2.1 \times 10^{-8}$  Hz during the aging tests. We associated this with a total dose of  $1 \times 10^3$  rads. Recent literature on ground based experiments has indicated that a dose as low as 1 rad causes changes in quartz resonator frequency so that the total radiation dose and frequency shifts we have observed in our spaced based experiment are consistent with these measurements. (ref. 4)

It is important to realize, however, that there is a significant difference in the way we have conducted our LDEF experiment relative to more typical ground based observations of radiation effects on quartz resonators. In our case the resonators experience the radiation environment in a passive state, i.e., the resonators were at ambient temperature and not under power during radiation exposure. In a typical ground based experiment, the resonators are held at an elevated temperature (70-80°C) and are continuously powered up to monitor the frequency during the irradiation process. From the estimates of the ambient temperature range experienced by the LDEF satellite (ref. 5) during the mission, the resonators most likely did not experience a temperature excursion above 30°C, significantly cooler than the temperature used in the post-flight aging tests. Thus we interpret our observation of a frequency drift in the swept premium Q resonators as caused by accumulation of radiation damage during the passive LDEF mission that only anneals out during the 75°C aging tests, effectively recovering to the original pre-flight condition over the 6-month aging period. This is consistent with the general observation that AT-cut resonators experience a decrease in frequency under a radiation environment that retains its original value upon annealing. In our experiment, we suggested that the damage that was created during the LDEF flight was annealed out during the aging tests causing the observed increase in resonant frequency. We expect to confirm this interpretation by conducting a second aging test of the resonators in which we would not expect to observe any difference in the shielded and unshielded cases for both the swept premium Q and natural quartz resonators.

The marked contrast in behavior between the swept premium Q resonators and the natural quartz resonators correlates with our pre-flight TEM observations. The TEM observations revealed a difference in behavior of the swept premium Q and natural quartz, with the premium Q quartz exhibiting a lower density of strain centers than in the natural quartz but with a more rapid development and larger size of the strain centers after a given electron dose. However at least two interpretations can be given to the apparent correlation. First, the strain developed in the quartz lattice during the formation of the strain centers produces a change in the resonant frequency through a small mixing of the elastic vibration modes of the crystal. In this case, because the dose experienced by the unshielded resonators is only  $\sim 1 \times 10^3$  rads whereas the dose in the electron microscope that causes visible strain center development is much higher, then the strain center effect must occur at a very early stage of strain center formation, prior to the strain centers becoming visible under conventional bright field imaging conditions. In this case the difference in behavior of the two materials may be related to an impurity that

acts as a sink for point defects (probably interstitial Si) created during the irradiation. The concentration of such defects affects the density and rate of growth of the strain centers.

A second interpretation invokes the homogeneous production of a disordered quartz lattice under the radiation environment that leads to lattice expansion, a small decrease in the elastic constants, and a reduction in the resonant frequency of the resonators. In this case the production of disordered material would be related to the production of the point defects (again interstitial Si) that create the disordered lattice. The production of point defects may be related to the hydroxyl ions in the quartz as discussed by others (ref. 6) so that the difference in the behavior of the two quartz materials is related to their hydroxyl ion concentrations.

In either scenario, the change in resonant frequency during the post-retrieval aging test of the swept premium Q material is interpreted as annealing of the damage created during the LDEF mission: strain centers in the first instance and homogeneous disorder damage in the second instance. The absence of an effect in the natural quartz resonators is not understood but further experiments designed to clarify the issues are underway.

#### REFERENCES

1. Ahearn, J.S. and Venables, J.D.: Radiation Sensitivity of Quartz Crystal Oscillators, Experiment for the Long Duration Exposure Facility (LDEF). March-May 1978; Monthly Progress Report #1-3 on contract NAS 1-15263.
2. Hobbs, L.W. and Pascucci, M.R.: J. de Physic Collque C6, Supplement au #7, Tome 41 Juillet 1980, C6-237.
3. Ionizing Radiation Exposure on LDEF. ed. E.V. Benton and W. Heincich; USF-TR-77, August 1990.
4. Suter, J.S.: IEEE Trans. Nuclear Sci. 37(1990) 524.
5. Berrios, W.M. and Sampair, T.R.: Long Duration Exposure Facility, Post-Flight Thermal Analysis, Calculated Flight Temperature Data Package Preliminary. 1991, NASA TR; and W.M. Berrios: Long Duration Exposure Facility, Post-Flight Thermal Analysis Orbital/Thermal Environmental Data Package. 1991 NASA TR.
6. Halliburton, L.E.; Martin, J.J.; Sibley, W.A.: A Study of the Defects Produced by the Irradiation of Quartz. April 1980, RADC-TR-80-120.

TABLE I STRAIN CENTER DENSITY IN SYNTHETIC QUARTZ SUBJECTED  
TO INDICATED FLUENCE 100 keV ELECTRONS

	Material	Surface Density of Strain Centers (cm <sup>-2</sup> )	Electron Fluence (electrons/cm <sup>-2</sup> )
Experiment #1	1x10 <sup>6</sup> Q	1.2 x 10 <sup>11</sup>	3.3 x 10 <sup>9</sup>
	3 x 10 <sup>6</sup> Q	3.0 x 10 <sup>10</sup>	3.3 x 10 <sup>19</sup>
	Swept Premium Q	3.4 x 10 <sup>10</sup>	6.1 x 10 <sup>18</sup>
	Swept Premium Q	4.6 x 10 <sup>10</sup>	3.3 x 10 <sup>19</sup>
Experiment #2	Swept Premium Q	2.7 x 10 <sup>10</sup>	9.5 x 10 <sup>18</sup>
	Natural	7.9 x 10 <sup>10</sup>	9.5 x 10 <sup>18</sup>

TABLE II. DRIFT IN RESONANT FREQUENCY AFTER 5 MONTHS AGING

27 Series (Swept Premium Q)	Pre-Flight		Post-Flight	
Resonator #	79	82	90	Remarks
27820	170	40	35	Shielded
27821	40	36	40	Shielded
27822	40	0	235	Unshielded
27823	12	20	315	Unshielded
27824	-2	148	170	Unshielded
27825	30	136	160	At MML
27826	0	-40	115	Unshielded
27827	-84	48	250	Unshielded
Absolute value Ave (non-irradiated) Ave (irradiated)	47 ± 53	59 ± 50	78.3 ± 57 217 ± 69	All resonators
				57 ± 54 217 ± 69
28 Series (Natural)	Pre-Flight		Post-Flight	
Resonator#	79	82	90	Remarks
28125	4	36	-30	Unshielded
28126	30	32	0	Unshielded
28127	28	72	-150	Shielded
28128	-8	32	50	Unshielded
28129	12	52	80	Shielded
28130	-32	64	90	Unshielded
28131	60	-6	135	Unshielded
28132	136	--	110	At MML
Absolute Value Ave (non-irradiated) Ave (irradiated)	39 ± 40	42 ± 21	113 ± 29 61 ± 47	All resonators
				52 ± 42 61 ± 47



TABLE III. SUMMARY OF AGING DATA

## SWEPT Premium Q

Sample Type	Aging Rate/ (Hz/Day)	Total Freq. Shift upon Aging (Hz)
Shielded	$3.2 \times 10^{-11}$	$6.1 \times 10^{-9}$
Unshielded	$1.1 \times 10^{-10}$	$2.1 \times 10^{-8}$

## NATURAL

Sample Type	Aging Rate/ (Hz/Day)	Total Freq. Shift upon Aging (Hz)
Shielded	$3.4 \times 10^{-11}$	$6.5 \times 10^{-9}$
Unshielded	$3.2 \times 10^{-11}$	$6.1 \times 10^{-9}$

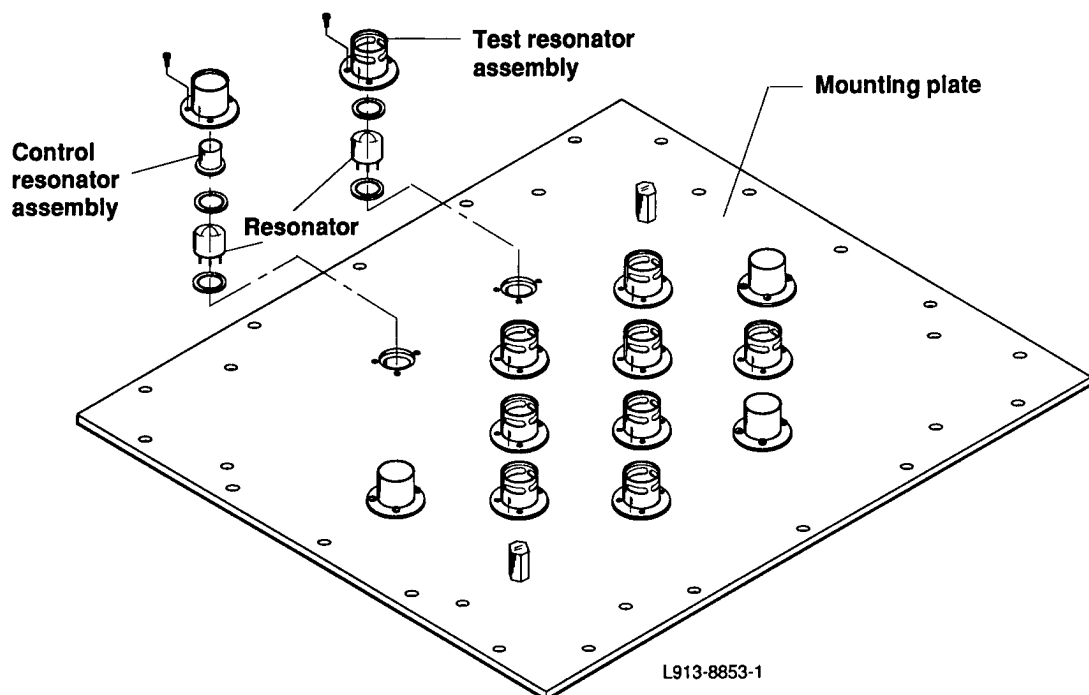


Figure 1. Schematic of the LDEF tray layout, with shielded and unshielded resonators indicated.

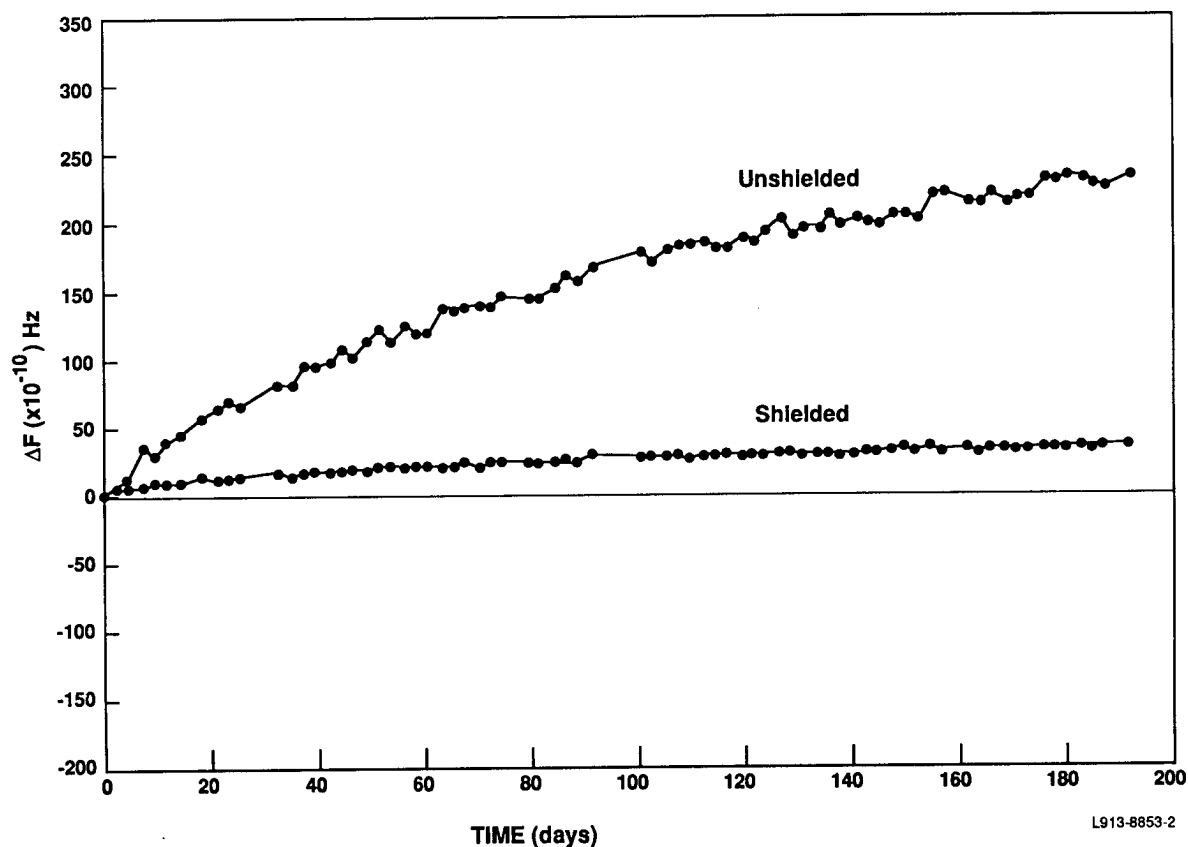


Figure 2. Post-flight aging results showing the change in resonant frequency as a function of time for Bliley Type BG61AH-5S resonators fabricated from Sawyer Swept Premium Q material. Aging temperature = 75°C. Shielded and unshielded resonator shown.

## LDEF ELECTRONIC SYSTEMS: SUCCESSES, FAILURES AND LESSONS\*

E. A. Miller, L. K. Brooks, C. J. Johnson, J. L. Levorsen, O. R. Mulkey

D. C. Porter, D. W. Smith  
Boeing Defense and Space Group  
Seattle, WA 98124

Phone: 206-773-5773

FAX: 206 - 773-1015

### ABSTRACT

Following LDEF retrieval, the Systems Special Investigation Group (SIG) participated in an extensive series of tests of various NASA and experimenter electronics, including the NASA provided data and initiate systems. This paper discusses the post-flight test program objectives and observations, and the "lessons learned" from these examinations. It also includes results of an evaluation of electronic hardware flown on Boeing's LDEF experiment. Overall the electronic systems performed remarkably well, even though most were developed under budget restraints and used some non-space-qualified components. Several anomalies were observed, however, including some which resulted in loss of data. Suggestions for avoiding similar problems on future programs are presented.

### INTRODUCTION

The year and a half following LDEF recovery has been a busy period for everyone associated with the program, but planning for these activities began long before recovery. We were all trying to anticipate every possible eventuality, without knowing what to expect of LDEF's condition. As the recovery date approached, we were preparing a series of "Test Plans" with lots of blanks to be filled in when the time came. The real work began after the excitement of watching the recovery operations, when these plans had to be completed and implemented. This paper will summarize these activities in the Electronic Systems area and discuss the results and "lessons learned".

### OBJECTIVES

The extended duration of the LDEF flight presented a unique opportunity to learn more about the effects of low earth orbit (LEO) on a wide variety of electrical and mechanical systems. There have been very few occasions when such systems have been retrieved more-or-less intact, particularly from the very low altitudes encountered during the last few weeks of the LDEF orbit. The Systems SIG was formed to insure that all systems would be carefully examined, rather than only those which were integral to the objectives of the various experiments.

\* Work performed under NAS1-19224, Task 15.

The original charter was to "investigate the effects of the nearly six year exposure in space on LDEF and experimenter systems", and to "coordinate the data ....into a single LDEF systems data base" (Ref.1). The specific objectives were:

- o Identify appropriate LDEF and experimenter systems for examination and analysis.
- o Develop inspection, handling, testing and reporting plans and procedures.
- o Coordinate with and support the LDEF Project, other SIGs, and Experimenter activities.
- o Define, collect data and establish a Systems Data Base containing both LDEF and experimenter systems data.

Note that experimenter systems were included. Many experiments utilized electronic systems and components (and many different materials) which were incidental to the primary purpose of the experiment, but which had the potential to yield valuable information from their orbital exposure.

#### PRE-RECOVERY PLANNING

An early task was to identify the electronic systems which were available for examination by the System SIG. Initially these were limited to those NASA-supplied units which were independent of individual experiments or which would be separated from them relatively soon after return to experimenter laboratories. Two primary systems were identified: the Experiment Initiate System (EIS) and the Experiment Power and Data Systems (EPDS). The EIS consisted of a single control "box" (plus batteries and cabling), located within the LDEF structure. It was expected to have been well shielded and held at a relatively stable temperature. In contrast, there were seven similar EPDS units, located within experimenter trays at various locations on the spacecraft, and thus potentially exposed to different conditions. Other components of interest included the batteries provided by NASA and the LDEF wire harness. This connected all active experiments with the EIS, and included some inter-experiment cabling for power, data and control purposes. Since the wire harness went to almost every section of LDEF, it was exposed to most of the conditions existing within the structure.

During the planning phase, it was not certain if any experimenter electronic systems would be available for study. Generic test plans were developed for optional use by experimenters, as well as for those NASA-owned LDEF systems which would be available. These basic test plans covered the following areas:

- o Electrical systems and subsystems: functional testing
- o Circuit board evaluation
- o Component examination and failure analysis
- o Power systems: batteries  
solar cells  
power management and control components  
high voltage insulators and dielectrics
- o Wire harnesses.

Their purpose was to provide a set of general guidelines for use in planning more detailed test and analysis plans for all LDEF systems, recognizing that some experimenters had already developed very detailed plans while others may not have thought much about these "subsidiary" components at all.

In the Test Plans, we recommended the following approach:

1. Develop a specific plan for testing the system prior to actual measurements, including thorough documentation of all steps taken. During the planning phase, collect and review original design and test documents, and attempt to collect spare or reference (control) components.
2. Document the condition of the system prior to any actions which might disturb that condition, including appropriate electrical measurements prior to and during first application of power.
3. Document any indications of failure or other abnormal behavior, and review pre- and post flight test data before proceeding.
4. Investigate all failures, and at the component level.
5. Investigate significant parametric shifts, even if not technically failures.

A few systems were inspected and tested at the Kennedy Space Center facility (SAEF-2) during deintegration. Most testing was the responsibility of the individual experimenters, with Systems SIG assistance available if requested. During and following deintegration, a number of other areas were identified in which our assistance was requested and provided. These will be discussed below.

#### KSC ACTIVITIES: TEST AND RESULTS

##### 1. Surface Voltage Measurements and Related Findings

We were requested to measure the surface voltage on the Plasma-High Voltage Drainage Experiment (A0054), to insure the system had turned itself off and no damaging voltages were present. The measurement needed to be totally non-contact under the ground rules then in effect. The actual testing was straightforward, using an off-the-shelf static voltmeter (although we did have to make one point of contact on the LDEF frame). As expected, the experiment was off and no surface voltages were present. However, in running through the procedures in SAEF-2, we noted significant static voltages on table tops, gloves, bags, trash cans and on most other surfaces. We then realized that none of the tables and few of the work platforms were grounded.

This led to a decision to provide static protected work surfaces on a number of the tables, and a general review of grounding procedures on the various work platforms and tray transporters. Some of the procedures, such as grabbing the platform rails before touching anything (to discharge the gloves) must have been considered a nuisance to the guys "just trying to get the job done", but we ended up with a workable system to minimize the possibility of static discharge damage to the experiments.

## 2. EIS Relays and Status Indicators

The original LDEF flight plan called for resetting all experiments to their unpowered state when the shuttle retrieved the spacecraft, utilizing the active grapple fixture to trigger the reset operation of the EIS. Due to the extended mission length and consequent uncertain state of batteries, and the desire not to disturb the final state of certain experiments, it was decided not to reset the systems. All experiment initiate relays were therefore expected to remain in their "SET" state throughout recovery and deintegration. We wished to verify this prior to tray removal or any other activities which might change that state (including mechanical shocks associated with transportation to experimenter laboratories). Planning for this verification test, to take place on LDEF early in the deintegration phase, required not only an approved test plan but also the permission of all experimenters utilizing the EIS. We were able to contact all but one experimenter and all those contacted approved the procedure. We therefore proceeded with the test on all those experiments with approval.

A technical concern was expressed by NASA that we limit test voltages to very low levels, to insure detection of any high contact resistance conditions as well as to prevent any possibility of activating the relays. We also had to utilize portable equipment which could be easily cleaned and brought from Seattle to the SAEF-2 clean room. We utilized a pair of digital multimeters, with a resistive shunt to keep their terminal voltages below 0.1 volts. One measured the resistance, while the other monitored the terminal voltage. Measurements were made at the cable connectors which mated to the EIS box, and thus included the resistance of the initiate wire harness and connectors at the experiment trays. All the initiate relays which were checked were still in their SET state, and contact resistances appeared to be normal (within the limitations of the measurement).

A related task conducted early in the deintegration phase was to inspect and document the state of the visual indicators on the EIS control box. These small electromagnetic devices rotate a ball to display either black or white sides through a window. One was used for each active experiment. The signal to set the indicator to white came through a separate set of contacts on the experiment initiate relay. These could only be reset using ground support equipment (GSE), so a white indication was a reliable record that the relay had been set. Six of the indicators were located adjacent to the active grapple fixture, and were used by the astronauts to verify system operation after LDEF was placed in orbit. As expected, all the indicators associated with experiments were white at the time of this initial post recovery inspection.

## 3. EPDS Test Activities at KSC

The second NASA-provided electronic system of interest was the Experiment Power and Data System (EPDS). Seven of these were flown on six different experiments, located at various positions on the LDEF structure (see Table 1). The EPDS components were not directly exposed to the exterior environment, being protected by their mounting plate and by external thermal shields. All the EPDS units were similar, consisting of a Data Processor and Control Assembly (DPCA), a tape recorder (the MTM, Magnetic Tape Module), and two LiSO<sub>2</sub> batteries, all of which were attached to a mounting plate designed to fit into the experiment tray. There were differences in their programming (by jumpers on several cards in the DPCA), and in the mix of analog and digital data channels, but all shared a number of identical circuit cards.

Two experiments (M0004 and S1001) utilizing EPDS were tested at KSC. The Systems SIG had provided the generic Electrical Systems Functional Test Plan and the

more detailed EPDS Test Procedure, PR-EPDS-A (1), both of which suggested a number of measurements and tests associated with initial power application and testing. Their purpose was to document the condition of the EPDS prior to and during application of power, in case some abnormal condition had developed. Had there been major failures, such as internal shorts, these measurements might have been important in diagnosing the problems or preventing damage.

One of the suggested tests was to monitor the power supply currents when power was first applied. In addition to simply recording the DC current level, we suggested use of either a storage oscilloscope or a "Visicorder" (Hewlett Packard) fast chart recorder to capture the turn-on transient. Use of the Visicorder on the S10001 initial test proved to be exciting, due to its 160 inches per second chart speed. We did capture these first transients, which proved to have characteristic shapes. Subsequent tests on other systems (generally using storage oscilloscopes) produced similar results (with a lot less paper), indicating generally similar timing and normal operation.

Both experiments, including the EPDS, functioned properly. As these were the first electronic systems tested after LDEF recovery, their successful operation was especially welcome. However, one system (M0004) exhibited two apparent anomalies: a higher than normal EPDS standby current, and chattering in an experiment relay which was driven by the EPDS. Subsequent testing demonstrated that these were not due to failures within the EPDS (see Post-Deintegration Activities section).

#### 4. LDEF Cable Harness Inspection and Removal

The LDEF wire harness was absolutely essential to the success of all active experiments, as it carried the initiate signals from the EIS. It had been assembled in-place on the LDEF frame, using Teflon insulated wire and nylon cable ties. Much of the harness also was protected by shielded braid and an outer Teflon jacket. The majority of the harness was well shielded from direct exposure to the external environment. Our first objective was to perform as much inspection and testing as feasible prior to any disruption of the harness and associated connectors.

The initial inspection took place during the tray removal activity. As the LDEF structure was rotated, all accessible wiring of the primary structure and of the experiment trays was visually examined with five power magnification. Later, as more of the system became accessible, continuity measurements were made, and finally insulation resistance measurements at 500 Volts DC were made after all the trays were removed. We also measured disconnect forces (torque) on all connectors possible during their initial removal.

During the visual inspection, several punctures were observed in the Teflon jacket, in some cases severe enough to expose the shield braid. However, these were attributed to the hand layup method of construction, rather than to the orbital exposure. None of these punctures was caused by or led to any failure of the electrical system.

All connectors were found to be properly coupled, and disconnect torques were within specified limits. There was no degradation of dielectric components, interfacial seals or finishes on any of the connectors examined. The wiring remained flexible with no indications of insulation cracking or other degradation within the primary structure. Electrical tests (continuity and insulation resistance at 500 VDC) showed the circuitry to be intact, with no observed insulation degradation.

The connectors supplied by the LDEF project to the experimenters were space rated, and had been subjected to vacuum bakeout. It was noted that many of the other connectors

used by experimenters were Mil-Spec or equivalent commercial variants, and were not spacerated. Most were not subjected to a vacuum bakeout process prior to assembly, which would have reduced outgassing in a low pressure environment. Most did not contain strain relief adaptors or cable clamping devices. A silicone encapsulating compound (possibly Products Research Corp. PRC 1535) had been applied at the point the wiring exited the connectors. The encapsulant remained flexible.

The primary wire harness was attached to the spacecraft with glass-filled nylon cable clamps, and wire bundles were held together with nylon cable ties. The only evidence of failure of these devices occurred on the exterior of an experiment tray in conjunction with a cannister (EECC). Some of these cable ties had fractured, and many were blackened (normally they are beige or white). It is thought the failures occurred from stresses applied during the opening and closing of the canister, following damage from exposure to ultraviolet radiation.

The only evidence of connector component deterioration was found on the four trays of the Interstellar Gas Experiment (A0038). The interfacial seals of uncapped circular connectors were shriveled, and the silver plating on MHV coaxial connector bodies was severely tarnished. Both of these connectors were mounted in the space-side of the trays.

## POST-DEINTEGRATION TESTS AND OBSERVATIONS

Following tray removal and return to the experimenters, the Systems SIG participated in a number of systems tests, and maintained contact with experimenters to develop a listing of observations and anomalies. Most of the experimenter results will be reported independantly, but tests with Systems SIG participation are discussed below. A summary of known anomalies in electrical or electronic systems is given in Table 2.

### 1. Experiment Initiate System

Shortly after removal of the EIS from LDEF, it was tested at KSC using the original GSE. Although the EIS had apparently worked flawlessly in turning on the active experiments, it had not been reset on recovery. The plan was to exercise both functions (SET and RESET), followed by the internal visual inspection, looking for any signs of degradation.

The initial RESET functional test was completely successful: all indicators which had been SET (white) were observed to RESET (black). The EIS also contained a number of unused indicators, which remained in their original RESET condition, as expected. The system was then given its first SET test, exercising all circuits including those which had not been used (not connected to an experiment). It was noted that one of the previously unused visual indicators failed to shift from black to white, although its associated relay circuit functioned correctly. On two subsequent RESET/SET cycles, this indicator shifted properly to white when exercised. Power supply current traces were normal, with changes indicating correct timing of the various relay drive operations.

It was tempting to consider the faulty indicator a "nuisance" item, of no great significance, since it had not actually been used during flight. However, the astronauts used identical indicators to verify proper functioning of the EIS during its initial deployment. Failure of one of those units at that time would have caused concern and possibly costly delays. For this reason, as well as the general plan to analyze all failures, the faulty indicator and three others were removed and carried to Boeing for analysis. Results are discussed under Failure Analysis Activities.



The EIS control box was the first electronic system which could be opened and inspected, so it was of interest as an indicator of any possible deterioration which might have affected other systems and experiments. Fortunately, no deterioration of any of the internal circuit boards or other components was found. There were a few minor anomalies (assembly or inspection oversights), but no areas of concern.

## 2. EPDS Testing and Apparent Anomalies

Although simple compared with today's data systems, the EPDS contains many elements common to most such systems, including various control and "handshake" lines, programmable data formats and timing (via jumpers on circuit cards), and a data storage system (CMOS memory, with periodic data transfer to the MTM tape recorder). Each was furnished with a set of support equipment for ground checkout and operation with the experimenter's system, including a Data Display Box (DDB), a computer tape system for transcription of the MTM data, an MTM controller, and the various interconnecting cables. Typically, these had been boxed up and placed in storage during the LDEF flight. In some cases, the individuals most familiar with their use were no longer associated with the project. In all cases, personnel had to refamiliarize themselves with the system prior to post flight testing.

Systems SIG interest in the EPDS continued through initial testing in the experimenter laboratories. We were able to witness the initial tests at four facilities (in addition to the KCS tests), and provided technical assistance in setting up and conducting some of those tests. All seven EPDS's functioned normally during and after the LDEF flight. Apparent anomalies proved to be due to GSE or to interactions with experiments, rather than failures of electronic systems. The only significant problems involved the MTM's. Observations are summarized below.

M0003: Aerospace Corporation used two EPDS, and set up both systems for test using the NASA-supplied "Kennedy" computer tape system as well as their own computer-based tape readout system. One of the two systems performed properly during all in-lab tests. The other seemed to be operating properly during a multi-hour test. However, after returning from lunch, we found the unit was latched into a continuous data scan and tape record mode. The condition was not corrected by reinitializing the system. Examination of the tapes showed the condition to have begun at the time of the first programmed data readout. Attempts to diagnose the problem at Aerospace were not successful, and schedule commitments precluded further efforts at that time.

The unit was subsequently sent to Boeing for analysis, along with its GSE, cables, etc. Initially, it operated correctly in all modes. Almost by accident, it was found that one of the GSE cables had an intermittent short inside a connector, which could be activated if the cable was flexed in "just the right way". The failure of the GSE cable was completely independent of the EPDS itself, and caused no loss of data.

M0004: Two anomalies had been observed during initial post-flight testing at KSC. The EPDS standby current was higher than normal (2 mA, compared with the normal 0.5 mA), and chattering of an experiment power supply relay (driven by a signal from EPDS) was noted during the final KSC test (but not earlier). The higher standby current was of particular interest, as it might have indicated changes in the CMOS components.

Testing at the experimenter laboratory (AFWL, Albuquerque, NM) revealed that the EPDS was functioning normally, and that the apparently high standby current was caused by a previously unrecognized experiment activation which occurred when the system was first initialized. The cause was a known characteristic of the original EPDS controller board, which provided "erroneous pulses during the initial powering up" on the four pulsed signals to the experimenter (Reference 2: EPDS Manual, page 23). An optional modification to eliminate these signals had not been made. Since the first programmed data scan did not occur for some time after initialization, the early activation resulted in no loss of data. The chattering relay was also found to be due to test setup conditions (time between system tests), rather than a failure of the EPDS or experiment electronics. Both anomalies point up the fact that subtle characteristics of the interaction of different systems can cause confusion.

MTM's: Two anomalies have been reported, and were investigated by the MTM manufacturer, Lockheed Corporation. Prior to LDEF recovery, it was decided to return the MTM's to Lockheed for inspection and data recovery, rather than assume they would operate normally using experimenter GSE. During these inspections, it was noted that the magnetic tape on all but one unit had taken a "set" where it was wrapped around the phenolic capstan. The exception was the single unit which had operated periodically throughout the flight. The MTM's were backfilled with dry nitrogen prior to flight. Upon exposure of the tapes to controlled humidity, the mechanical set gradually disappeared. Evidently some level of humidity is necessary in the sealed units to avoid this problem under long term, inactive storage. Interestingly, it has been reported that a different type of tape (cassette) used in the Polymer Matrix Composite Materials Experiment (A0180) did not encounter this problem even though it too had been backfilled with dry nitrogen. The reason has not yet been conclusively determined, but it has been speculated that outgassing of some other material in the case prevented excessive drying of the tape [3].

One significant MTM failure resulted in loss of some experiment data on the Thermal Control Surfaces Experiment (S0069). This was the only four track MTM used, and the experiment did not use an EPDS. The relay which should have switched track sets (from tracks 1 or 3 to tracks 2 or 4) failed to operate during the flight. Consequently, portions of the early flight data on track 1 were overwritten and lost. During testing at Lockheed, the relay was exercised and operated normally. Such behavior is not unusual, in that contact contaminants may prevent one or more switching operations and yet be dislodged in subsequent activations, restoring normal operation. If anticipated, such failures may sometimes be overcome by sensing correct operation and arranging for reactivation if necessary. However, this was not a feature of the affected unit.

### 3. Batteries

The Systems SIG has also assisted in organizing the LDEF battery investigation. Four organizations are currently studying the lithium sulfate batteries: Aerospace Corporation, Naval Test Laboratories, Jet Propulsion Laboratory, and SAFT Corporation (manufacturer of the batteries). The objective of the study is to identify degradation modes of the batteries, and to provide information useful to future missions. This study is still underway, with only preliminary results thus far reported. It has been determined that unused batteries retained a significant portion of their charge - generally 80 to 90 percent of their original capacity. It is believed that this applies to both ground stored batteries and flight batteries which saw minimal use. These batteries are among the very few which will retain their capacity over time without periodic recharging, and their good retention on LDEF is of particular relevance to the Galileo mission which is also using this type of battery.

Testing of LiCF and NiCd batteries is also planned. Some NiCd batteries were reported to have developed internal pressure, resulting in bulging of their cell cases (S1001). This may have been caused by continuous charging from the solar cell panel used to maintain power (there was apparently no automatic shutoff at full charge). The batteries were still functional, however. Venting of LiCF after four years operation was also reported, resulting in a "bad odor" in the experiment container (S0069). This is considered normal for these batteries, and occurred on similar grounds units.

### THE BOEING ELECTRONICS EXPERIMENT

Most electronics carried on LDEF were used to support experiments, rather than being flown as part of an experiment. An exception was the Boeing Electronics Experiment, a company-funded investigation of the effects of LEO on inexpensive, commercial quality components. These included a number of plastic packaged integrated circuits and discrete components (transistors, resistors, capacitors, and diodes), and a fiber optic experiment. They were mounted on a pair of circuit boards using standard assembly techniques, with half the components conformally coated, using Hysol PC18. The experiment was flown as part of the Space Environment Effects on Spacecraft Materials Experiment (M0003).

A list of components flown is shown in Table 3. Half the electronic components and the fiber optic experiment were powered up during data collection periods, determined by the timing of the M0003 EPDS. All components were mounted behind a metal cover plate, and had no direct exposure to external conditions (other than vacuum). Temperatures were moderate, as determined from on board thermistors, ranging between +5 and +30 degrees C for the fiber optics experiment. Postflight data was compared with pre-flight data on a part-by-part basis.

There were no component failures and no parametric shifts which exceeded the part specification limits. No degradation was observed on any of the circuit board elements or components, other than some darkening of nylon cable ties on a small portion of the power and data cable which received external exposure. The fiber optic components continued to be fully functional, with no significant changes in performance. These results support the conclusion that commercial components, if properly tested, assembled and shielded from temperature extremes and other damaging exterior conditions (e.g. atomic oxygen and ultraviolet radiation, etc.), can survive the space environment and continue to function for extended periods.

### FAILURE ANALYSIS ACTIVITIES

Failure analysis was strongly recommended for all system or component failures, even if no loss of experiment data or other problems resulted. This was not only to look for any possible orbit-related effects, but also to try to determine what additional part selection or testing requirements might have prevented such failures. Failure analyses performed by the Systems SIG are discussed below.

#### 1. EIS Status Indicator Failure

This small electromechanical device, discussed earlier, consisted of a rotating ball (half white, half black) which indicated the SET or RESET state of the various experiment initiate relays. The single failure of an unused unit on the EIS control box was investigated, comparing the electrical performance of the intermittent unit with three others which had not failed. Two of the three extra units had not been connected and therefore had not been exercised during any of the flight or post-flight testing. One had been

connected but was unused, similar to the faulty unit. All units were subjected to marginal voltage testing at the minimum specified operating pulse width (40 milliseconds). The three "spare" units all functioned consistently at 5-6 volts. The faulty unit, however, exhibited highly variable behavior, operating twice at 9.4-10.3 volts, and a third time at 5.6 volts. This type of intermittency is characteristic of contamination, and indeed the failure was found to be caused by a small particle (probably plastic) which could jam the magnet. Particle contamination is an all-too-common problem with small electromechanical devices, including relays.

It should be noted that the failing unit often operated normally during testing of the EIS, or under normal voltages and with long input voltage on-times. It is often necessary to subject components to testing at the limits of the manufacturer's specifications (voltage, temperature, pulse widths and timing, etc.) to detect marginal parts. Many of the components used on LDEF were MIL-STD-883, Class B, and did not receive such testing.

## 2. A0076 Experiment Transistor.

Although the experiment control circuitry operated correctly during the LDEF flight, it was found during post flight testing that one valve opened immediately upon initiation rather than at a preset thermistor temperature. Further investigation disclosed a failed transistor and resistor, used to open one of the two experiment valves. These were to have operated for only a very short time (about 2 milliseconds) during flight. Analysis of the flight data confirmed that the valve driven by the failed transistor had opened correctly, after the thermistor cooled down to its preset temperature. The circuit had been tested many times during preflight checkout, but always at atmospheric pressure. Failure analysis showed the 2N2222A transistor had shorted internally and overheated, ultimately melting the emitter ball bond and adjacent lead. Excessive current through the short overstressed the resistor as well. Internal examination revealed poor quality die attach. Although the cause of failure could not be determined with certainty, it is speculated that the part had been marginal even during pre-flight testing (some unexplained current leakage had been detected). It may have continued to function in spite of drawing some leakage current under laboratory conditions, but failed when powered up in a vacuum. This conclusion is supported by the fact that an identical circuit on the same board did not fail. The system had never been subjected to thermal-vacuum testing prior to the LDEF flight.

Lack of thermal-vacuum testing was common among experiment systems. Such testing is expensive and time consuming, but can often detect problems which may never show up otherwise.

## 3. A0038 Interstellar Gas Experiment Failures

A0038 was one of the most complex experiments on LDEF. It also experienced the most extensive electronic systems failure. Seven "cameras", each containing five copper-beryllium foil plattens, were to collect gas atoms. The plattens were to be sequentially rotated out of their exposed position by firing pyrotechnic "squibs" when pulsed by their electronic sequencer units. After return of LDEF to KSC, it was found that only one of the 35 plattens had rotated during flight. Portions of the electronic systems were sent to the Systems SIG at Boeing for failure analysis. This analysis is not yet complete, but some observations are discussed below.

Failure Analysis Observations: The experiment systems were activated by the EIS system, which operated a single master initiate relay. This was found to be activated ("SET"), and six of the seven slave relays (activated from the master relay) were SET. One

slave relay did not activate during flight and its sequencer (tray F6) was never turned on. Intermittent operation of the F6 slave relay has been confirmed in the laboratory. The remaining six systems had been activated (confirmed by data from E-cell coulombmeters, as discussed below).

There was an LDEF requirement that electronic systems be isolated electrically from the LDEF structure. However, at least two experiments were evidently designed to use the LDEF as a ground reference (A0038 and A0054). The Interstellar Gas Experiment (IGE) electronics were indeed isolated from the tray structure, but the various chassis boxes and the camera box structure was bolted directly to the tray. This made the tray the ground reference point for one of the camera internal grids. Neither electrical terminal of the high voltage power supply was connected to the tray, resulting in uncertainty as to the actual voltage between the camera grids and the camera body. Also, in a late pre-flight change for thermal control purposes, all the sequencer chassis were isolated from the trays by insulating washers.

Despite the grounding confusion, all electrical systems had ground return leads in their cabling, which completed the circuits and allowed them to function. Testing at Boeing confirmed that all sequencers and high voltage supplies functioned normally, using flight cables and accelerated clock timing. Confirming activation of the trays, all batteries except that of the tray with the faulty initiate relay (F6) were fully discharged, as expected.

The experiment also used "E-cell" micro-coulombmeter units to record the length of time high voltage had been applied to the camera grids. A number of these E-cells apparently leaked, destroying their sockets with the corrosive internal electrolyte. Similar units were used in one other experiment (A0054), and six of those E-cells also leaked (approximately 4%). Apparently these components were not "space rated" and had never been subjected to thermal-vacuum testing. It is quite possible that a 4% failure rate is not unusual in the absence of such testing. Perhaps those marginal units might have been detected and replaced prior to flight, with a more extensive test program. It was noted that the leaking E-cells on the A0038 experiment were all located in high voltage power supplies which received some direct solar exposure, so heating may have been a factor. No detailed study of these units has yet been done.

Readout of the integrated currents recorded by the E-cells confirmed that the power supplies had been turned on for an extended period, consistent with their intended programming. Since this would have occurred coincident with electronic sequencer operations intended to fire squibs to rotate the plattens, it suggests that the sequencers were also turned on and operating properly.

In laboratory testing, all the flight sequencers and high voltage power supplies worked normally (in spite of some circuit board staining from the leaking E-cells). When one system was reassembled, using flight cables and simulated squibs (flash bulbs), timing was correct and the flash bulb fired at the correct time.

Subsequently, the flight squibs and other spare units were examined at Johnson Space Center. Some of these units were test fired. All those tests indicate the squibs were in good condition and fired normally. The analysis is still in progress, and it is planned to test fire some squibs using a complete experiment system. It is possible that the exact cause of failure will never be known.

#### 4. A0187-1 Chemistry of Micrometeoroids Experiments

This experiment utilized sets of foil collector plates hinged along one side and controlled to open or close in a clam shell fashion. They were launched in the closed position. During flight they were to open for 300 days, and then closed. On recovery they were found to be open. Preliminary analysis shows there was no stop designed into the timer sequence, since the original LDEF mission was to have only lasted 18 months. It appears that there was sufficient battery life to operate the clamshells more than once, and they happened to be open at the time of recovery due to the programmed open-close time periods. Failure analysis is planned to verify this failure mode.

This anomaly illustrates the need to anticipate changes in mission plans and durations, and to provide for controlled shutdown (or repetitions if desired) of systems, rather than rely upon the original planned duration.

#### CONCLUSIONS: LESSONS LEARNED

In spite of the few notable problems, most systems performed very well. Actual failures were few, and these appear to be caused by traditional culprits: design and testing limitations, and/or component or assembly problems. The following conclusions are meant to suggest areas of improvement and to serve as reminders of certain well known principles, rather than as new findings.

1. Although shielding from extended exposure to atomic oxygen and other environmental effects is important, no failures occurred which indicate any new, fundamental limitations to extended mission lifetimes. The key requirement (in addition to following good design practices) seems to be the system test plan. Testing of components at temperature, voltage and timing limits, and extensive testing of systems (including thermal-vacuum and noise tolerance testing) is essential. This must include thorough documentation, particularly of the interfaces between systems, and special efforts to detect unanticipated noise or spurious signals which can affect system timing or operation.
2. Extensive outgassing and atomic oxygen effects were observed on many experiments and on the LDEF structure. Use of metallized Teflon and other films resulted in quantities of loose, conductive material which could cause problems in some systems. This area requires considerably more investigation, including long term degradation studies and controls on allowable materials for long mission lifetimes.
3. Relays are a continuing problem area, well known in many production situations. Efforts have been made in some systems to eliminate them entirely, substituting solid state switches or other design approaches (e.g. redundancy, error detection and provision for reset, etc.). There does not seem to be any magic answer, but certainly a part of the program to minimize such problems is to use well qualified vendors with a proven "track record" of supplying high reliability parts. In addition, testing at the component and the system level is essential.
4. Many low cost, non-space-qualified components performed quite well, with no problems at all. The question of whether to permit use of commercial or MIL-STD parts in space applications is far too complex to discuss here, involving many longstanding policies. However, it is evident that such components can survive in some space applications, and that their use may often be justified for low cost systems when failures would not result in safety concerns or other major mission costs. Key to use of such components is conservative design and testing.

## REFERENCES

1. "LDEF Systems Special Investigation Group Investigation Plan," February, 1990, H. Dursch, Boeing Defense and Space Group, Seattle, Washington.
2. "Experiment Power Data System for Long Duration Exposure Facility" August 1, 1978 (as Updated March 14, 1979), Flight Electronics and Systems Engineering Divisions, NASA Langley Research Center, Hampton, Virginia.
3. "Thermal-Vacuum Effects on Polymer Matrix Composite Materials," R. C. Tennyson and G. E. Mabson, First LDEF Post-Retrieval Symposium, June 2-8, 1991, Orlando, Florida.

TABLE 1. EPDS UNITS AND LOCATIONS ON LDEF

Experiment No. and Title		Organization	Tray Location
A0201	Interplanetary Dust	NASA LaRC	E9
M0003	Space Environment Effects	Aerospace	D4
M0004	Fiber Optics	AFWL	F8
S0014	Advanced Photovoltaics	NASA LeRC	E9
S1001	Low Temp. Heat Pipe	NASA GSFC	F12
S1005	Transverse Heat Pipe	NASA MSFC	B10

TABLE 2. ELECTRICAL SYSTEMS ANOMALIES, ARRANGED BY TYPE

Relays and Other Electromechanical Device Anomalies:

A0038: one tray initiate relay failed  
 S0069: MTM 4-track changeover relay failed  
 EIS: one unused status indicator failed  
 MTM's: magnetic tape took mechanical set  
 A0180: magnetic tape oxide lost adhesion in dry N<sub>2</sub>

System Anomalies:

A0038: only one pyro cable cutter fired  
 A0076: premature shutoff  
 A0187-1: Clam shells not closed on retrieval  
 S0014: Gulton data system failed after retrieval

Component Anomalies:

A0038: E-cell coulombmeters leaked (5 of 70: 7%)  
 A0054: E-cell coulombmeters leaked (6 of 152: 4%)  
 A0076: Transistor/resistor failed  
 M0004: One fiber optic cable severed by micrometeoroid impact  
 S0069: DAC: bit 25 latched high  
 S1001: NiCd battery cells bulging (may have been overcharged).

TABLE 3. BOEING ELECTRONIC COMPONENT EXPERIMENT: PARTS FLOWN

A. Plastic Encapsulated Devices Experiment

Quantity	Part Type
20	CD4068BE 8-input NAND gate (CMOS)
20	DM54LS30N 8-input NAND gate (low power Schottky)
100	1 uf, 50V ceramic capacitors
100	10MegOhm, 1/4 watt, 1% resistors
50	2N2222A-type transistors
100	1N4005 diodes

B. Hybrid Integrated Circuits Experiment

This contained 63 miscellaneous hybrids, including assorted circuits, resistor test patterns (CrSi, NiCr, thick films), and assorted substrates (Al<sub>2</sub>O<sub>3</sub>, BeO, etc.)



# EFFECT OF SPACE EXPOSURE OF PYROELECTRIC INFRARED DETECTORS

James B. ROBERTSON  
NASA, Langley Research Center  
Hampton, VA

## Introduction

Pyroelectric detectors are one of many different types of infrared radiation detectors. The pyroelectric detectors are of interest for long-term space use because they do not require cooling during operation. Also, they can detect at very long wavelengths and they have a relatively flat spectral response. A disadvantage is that the radiation must be chopped in order to be detected by a pyroelectric detector.

The objective of the experiment was to determine the effects of launch and space exposure on the performance of commercially-available pyroelectric detectors.

The approach was to measure certain detector parameters before and after flight and try to determine the amount and cause of the degradation. The experiment was passive: no data was taken during flight.

## Experiment

A total of twenty detectors were flown on LDEF and another seven were kept on the ground as controls. There were three different types of detector based on the type of pyroelectric material used: lithium-tantalate (LTO), strontium-barium-niobate (SBN), and triglycine-sulfide (TGS). The detectors were mounted on tray E-5, which was a slightly-trailing-side location. The tray was covered with a perforated aluminum plate for thermal control. The plate blocked 50% of incident radiation. Four of the twenty flight detectors were further shielded by a solid aluminum plate which blocked their view of space but left them exposed to space vacuum.

The detector parameters measured before and after flight were signal strength, noise, and detectivity which is calculated from signal and noise data. The three detector types were treated as three separate experiments.

## Results

### Visual observations:

There was a brown discoloration on the outer surfaces of the detectors similar to the "tobacco stain" that was found on much of LDEF.

A much more noticeable effect was the existence of white/metallic regions either in or on the surface of the detector windows which were made of KRS-5 (thallium-bromide-iodide). Other window materials were flown: Irtran II and germanium, but the effect was seen only in the KRS-5. Similar damage was noted in two other LDEF experiments which exposed KRS-5 in flight. The surfaces of flight and control detector windows were analyzed by electron spectroscopy. The analysis showed a silicate over all of the flight windows and a higher concentration of thallium in the damaged regions of flight windows than in either the control window or in less damaged regions of the flight windows.

### Detector data:

There were no survivors among the TGS detectors, therefore no post-flight detector data was taken. However, all of the TGS control detectors failed also; therefore the demise of the flight TGS detectors cannot be ascribed to space exposure.

The LTO and SBN detectors held up very well. In fact, the differences between the pre-flight and post-flight detectivities for both types were within the error bounds of the measurement.

## Conclusions

At this point in the study, we can say that lithium-tantalate (LTO) and strontium-barium-niobate (SBN) are suitable materials for pyroelectric detectors for long-term space applications. Based on the results of detectors from one manufacturer, we cannot recommend triglycine-sulfide (TGS) because of its apparent short shelf life.

Window and lens materials are of major importance. In space use, a detector will be part of a detection system and located behind a lens or window of some sort, and damage to the lens or window will most likely play a larger role than damage to the detector in the degradation of the system performance.

## LDEF MECHANICAL SYSTEMS\*

W. Steve Spear and Harry W. Dursch  
Boeing Defense & Space Group  
Aerospace & Electronics Division  
P. O. Box 3999, MS 73-09  
Seattle, WA/ 98124-2499  
Phone: (206) 773-0527, Fax: (206) 773-4946

### SUMMARY

Following LDEF retrieval, the Systems Special Investigation Group (SIG) has been involved in a number of investigations of mechanical hardware and structure flown on LDEF. The primary objectives are to determine the effects of long-term space exposure on 1) mechanisms either employed on LDEF or as part of individual experiments, 2) LDEF structural components, and 3) fasteners. Results from examination and testing of LDEF structure, fasteners, LDEF end support beam, environment exposure control canisters, experiment tray clamps, LDEF grapple fixtures, and viscous damper are presented. The most significant finding to date is the absence of space exposure related cold-welding. All instances of seizure or removal difficulties initially attributed to cold-welding have been shown to have resulted from installation galling damage or improper removal techniques. Widespread difficulties encountered with removal of stainless steel fasteners underscore the need for effective thread lubrication schemes to ensure successful application of proposed orbital replacement units onboard Space Station Freedom.

### INTRODUCTION

The delayed recovery of LDEF presented a unique opportunity to investigate the effects of low earth orbit space exposure on satellite systems and components that normally would not have had any engineering interest. The charter for the Systems SIG LDEF mechanical systems is to investigate and evaluate the effects of long-term space exposure on 1) mechanisms utilized as part of LDEF or individual experiments, 2) LDEF structural components and 3) fasteners. Specific areas of interest are evaluation of post-flight functional performance of mechanisms, including such items as motors, bearings, seals and lubricants, and the condition of LDEF structural components with respect to erosion, wear, possible weld degradation, and microstructural changes. Fastener concerns include determination of whether relaxation or cold-welding occurred during flight.

One of the most important objectives is to evaluate the potential for space exposure generated cold-welding of structural materials and fasteners to be used in assembled structures. Successful Space Station Freedom (SSF) design depends critically upon avoidance of cold-welding since specific components to be used on SSF, such as orbital replacement units (ORU), will require periodic replacement or repair. Any bonding or adhesion of ORU fastener assemblies will make on-orbit removal difficult. Information obtained from LDEF fastener studies will be of great help in the development of proper pre-flight installation practices and thread lubrication schemes that will minimize the subsequent risk of galling and cold-welding.

\* Work done under NAS1-18224, Task 15

Hardware examined by or for the System SIG since LDEF deintegration includes the environment exposure control canisters, the primary LDEF structure and fasteners, experiment fasteners, LDEF end support beam (which bound on its spindle during removal), experiment tray clamps for evaluation of possible metallurgical changes, grapple fixtures and viscous damper. Examinations of the last two items were performed at the original vendors and funded by Johnson Space Center (JSC). Results and significant observations to date are discussed below.

## MECHANICAL SYSTEMS RESULTS AND DISCUSSION

### Environment Exposure Control Canisters

Five environment exposure control canisters (EECC) were flown on LDEF. These canisters were used by individual experimenters for controlled exposure studies of the effects of low earth orbit (LEO) on various structural, thermal control, and optical materials. Figure 1 shows the S0010 experiment EECC as mounted in the B9 tray. The EECC is essentially a sealed drawer in which small samples were mounted for controlled space exposure; typically the canisters were programmed to open two weeks after deployment and close one week prior to the originally anticipated retrieval of LDEF. The drawer is opened by a screw drive actuator driven by a 28V DC electric motor. The drawer is sealed by a butyl rubber seal.

Dr. Steve Spear of the Systems SIG and Dr. Dave Brinza of the Jet Propulsion Laboratory participated in the opening of the M0006, S0010 and the two M0003 canisters. Technical support was provided for opening of the West German S1002 canisters. Initial canister pressures just prior to opening, canister leak rates, internal gas samples, drawer opening times and drive motor currents were obtained for most of the canisters. Only the drawer opening time and motor currents were obtained for the S1002 canister. A portable gas sampling manifold with pressure gages and a sorption vacuum pump was utilized for the gas measurements. A strip chart recorder monitoring the voltage drop across a 0.25 ohm resistance in series with the motor was employed to record the drive currents supplied by the EECC ground support equipment.

Data obtained during the canister openings is summarized in Table I. The initial pressure of the M0006 canister was not obtained because the EECC purge valve loosened and leaked during hook-up of the gas sampling manifold. However, it was noted that the canister was below atmospheric pressure, which is consistent with the measured leak rate and length of time after LDEF retrieval. The S1002 experimenters reported that a pressure differential between the canister and atmosphere was not apparent at the time of opening. The typical pre-flight leak rates for the canisters were around 1.3 torr/day. The post-flight leak rates for the M0006 and M0003/D4 canisters, 2.7 and 1.9 torr/day, flown at or adjacent to the trailing edge on LDEF are comparable to pre-flight values. The higher leak rates for the S0010 and M0003/D8 canisters flown at or near the leading edge in comparison to those at the trailing edge are suggestive of the differences between atomic oxygen exposure levels and possible corresponding damage to or contamination of the drawer seals.

Typical drawer opening time was around 17 minutes. Motor currents oscillated between the limits shown in Table I during each revolution of the drive screw. This behavior is illustrated in Figure 2 where the strip chart traces corresponding to steady run opening currents are compared for the M0006 and S0010 canisters. The longer opening

time of the M0006 canister and higher than typical current draw are consistent with noise indications of higher torque loading of the motor noted during opening. Damage to the drive screw (warping) or to its dry-film lubrication are possible causes to account for the degraded performance. The low motor current of the S0010 canister corresponded with observations of a smooth and steady drawer opening. The S0010 canister was the prototype S/N 001 EECC and, as such, its good performance is likely the result of "breaking in" of the mechanism during extensive operation during development testing.

Test plans for additional detailed examination and testing of the EECC's are being developed by the System SIG for coordination with investigators at The Aerospace Co., Wright-Patterson AFB and NASA LaRC. The plan includes investigation of the causes of the observed performance differences between canisters and their relation to the differences in the space exposure conditions during flight.

### Primary LDEF Structure and Fasteners

#### Aluminum Primary Structure

The LDEF primary structure is constructed of welded and bolted aluminum 6061-T6 rings, longerons, and intercostals. The welds were inspected by dye penetrant and eddy current techniques at KSC following deintegration of the experiment trays. The welds were found to be nominal with no evidence of any flight related degradation.

The potential for space exposure effects on the microstructural or mechanical properties of the aluminum structure was investigated by metallurgical analysis of the 6061-T6 aluminum experiment tray clamps. Examination of the clamps avoided removal of any structural components for analysis. The tray clamps are completely representative of the primary structure and were distributed uniformly around the spacecraft. Clamps from near leading edge (E10) and near trailing edge (E2) were cross-sectioned and prepared for microstructural examination by standard metallographic techniques. As-etched, near surface microstructures from areas that were either directly exposed or protected by an overlaying shim are displayed in Figure 3 for both clamps. The microstructures are typical for 6061-T6 aluminum. The lack of any differences between the samples illustrates that space exposure has no discernible effect on the bulk microstructures of typical structural metals. Mechanical property changes are precluded in the absence of microstructural changes. Surface analysis investigations including scanning electron microscopy of the anodized surfaces of the clamps did, however, show some not unexpected smoothing or erosion effects on exposed areas near the leading edge.

#### Primary Structure Fasteners

All primary structure fastener assemblies were re-torqued to pre-flight values at KSC following experiment deintegration. The fastener assemblies consist of stainless steel bolts ranging in diameter from 1/4 to 7/8 inch with silver-plated locking nuts. Only 4% or 119 of the 2,928 assemblies had relaxed. Nut rotations required to re-establish pre-flight torque levels for those that relaxed ranged from 5 to 120 degrees. The small number of relaxed fastener assemblies suggests that the reliability of bolted joints in space applications is very high. This conclusion must, however, be tempered by the fact that LDEF was exposed to a rather benign thermal environment with minimal thermal swings as indicated by review of the on-board thermocouple data.

## Intercostal Fastener Assembly Cross-Section

An undisturbed, as-flown intercostal fastener assembly shown in Figure 4 was removed from the LDEF structure to investigate the possibility of cold-welding of the structure fastener assemblies during space exposure. The fastener was selected randomly and not because of any evidence of cold-welding of it or other similar fasteners. The stainless steel bolt/aluminum interfaces and bolt/nut faying surfaces were examined for indications of cold- (or solid state-) welding. Closeups of these areas are shown in Figures 5 and 6. Examination of the bolt shank interface reveals no metallographic evidence of cold-welding. The thread faying surfaces also show no evidence of cold-welding; however, some minor galling and smearing of the silver plating on the nut is evident. The behavior of the plating is as-expected since it is specified to act as a lubricant during both installation and removal to prevent galling and seizure of the nut on the bolt.

## Tray Clamp and Experiment Fasteners

### Tray Clamp Fasteners

The experiment trays were held in the structure openings by aluminum clamps. The clamps were attached to the structure with 140 ksi A286 stainless steel hex-head 1/4"-20 x 0.75" bolts having a passivated finish. The bolts, with alodined aluminum washers under the head, were installed into self-locking helicoils on the primary structure. The bolts were cleaned with alcohol and patted dry prior to installation with a pre-flight torque of  $75 \pm 5$  in-lb.

During deintegration of LDEF, all 2, 232 tray clamp fastener breakaway torques were determined using a dial gage torque wrench. Running or prevailing torques were obtained for every third bolt. A database was created that contained all the breaking and running torques as a function of location on LDEF.

The breaking torques averaged 72 in-lb and ranged between 10 and 205 in-lb. The averages of the twenty lowest and twenty highest values were 31 and 175 in-lb. The average breaking torques were similar throughout LDEF indicating no pronounced effect of varying space exposure conditions on bolt torque behavior.

The prevailing torques averaged 17 in-lb and ranged between 2 and 132 in-lb. The average of the twenty highest running torques was 58 in-lb. There was no correlation between high running torques and high breaking torques. Only one bolt possessed both one of the twenty highest running and one of the twenty highest breakaway torques.

Optical examination at 8 to 40X magnification of more than 50 of these bolts including samples displaying average or extreme breaking or prevailing torque values revealed thread conditions ranging from "like-new" with only slight burnishing of the threads to complete stripping. High prevailing torques typically correspond with severe thread damage. However, no clear correlation has been made thus far between thread condition, washer condition and breakaway torques. Many bolts have smears or deposits of aluminum on the grip (unthreaded) portion of the shanks which suggests that there was a hole misalignment between the clamp and the structure. No evidence of cold-welding was observed. All thread damage was consistent with galling damage.

## Experiment A0175 Fasteners

Dr. Richard Vyhna of Rockwell International, Tulsa Division reported severe difficulties with seizure and thread stripping during removal of fasteners used to locate graphite-reinforced composite test panels of the A0175 experiment. The experiment trays were flown at the A1 and A7 positions. The fastener assemblies consisted of NAS1003-5A, passivated A286 CRES bolts installed into BACN10JN3CM, A286 CRES self-locking nut plates with AN960-C10L washers. It was reported that the nut plates had the original molybdenum disulfide dri-film lubricant removed by acid stripping prior to installation because of concerns with possible volatilization and contamination while in orbit. Cetyl alcohol was used as an installation lubricant. It was initially speculated that the A286 fasteners may have cold-welded on-orbit because of insufficient lubrication provided by the cetyl alcohol.

Breaking and running torques were obtained for the majority of the fasteners by the Rockwell International group. Some fasteners were left undisturbed for analysis by the System SIG. Examination of one of the trays at Boeing revealed that some of the nut plates had not been stripped of dri-film lubricant. As shown in Figure 7, bolts removed (with difficulty) from acid-stripped nut plates displayed severe thread damage including stripped threads, whereas those removed from nut plates with intact lubrication were not damaged. Inspection of exposed threads on undisturbed bolts mated to acid-stripped nut plates indicated that the threads were damaged by galling during original installation. Threads on bolts inserted into nut plates with intact MoS<sub>2</sub> were undamaged. Cross-sections of undisturbed bolts, displayed in Figure 8, confirmed that thread damage occurred on installation. Fourier transform infrared spectroscopy (FTIR) found no post-flight traces of cetyl alcohol remaining in the threads.

Correlation of the Rockwell torque data with the lubrication conditions of the nut plates showed that the average running torques associated with MoS<sub>2</sub> were 15 in-lb as opposed to 64 in-lb for bare nut plates. The average breaking torques were the same for both cases at 31 in-lb, from which it is concluded that space exposure did not cause cold-welding. The removal difficulties are directly attributable to the lack of adequate lubrication and galling damage that occurred on original installation. Additional galling on removal resulted in seizure and thread stripping.

## End Support Beam

The end support beam (ESB), Figure 9, is an 18 ft. long welded 6061-T6 aluminum truss that holds two end trunnions that supported one end of the LDEF within the shuttle bay. The ESB was designed to allow a  $\pm 1.5$  degree rotation about a 5 in. diameter 17-4 PH stainless steel spindle to accommodate potential misalignment of the LDEF structure and permit reberthing into the shuttle bay. Deintegration of LDEF at KSC required that the ESB be removed. A great deal of difficulty was encountered during removal. The ESB seized on the spindle and use of a gear puller was required to complete removal. Since no similar difficulties had been reported during pre-flight testing, there was concern that cold-welding had occurred between the ESB and spindle during flight.

As seen in Figure 10, the spindle bore of the ESB was damaged by severe galling and scoring. Discussions with the LDEF deintegration staff indicated that the ESB slid easily off approximately the first inch of the spindle at which time it bound onto the spindle. Review of the video documentation of the ESB removal operation confirmed this observation and revealed that the hoist used to support the ESB caused it to cock and jam

on the spindle as the beam cleared the inner land of the spindle. Figure 11 illustrates the details of the binding. Uncontrolled and excessive rotation of the jammed ESB about the spindle in an unsuccessful attempt to free it caused the deep circumferential scoring visible on the bore of the ESB. The two circumferential score marks are the width of the outer land of the spindle.

Examination of the spindle revealed corresponding minor galling and transfer of aluminum onto its outer land. Metallographic cross-sectioning (Fig. 12) of the spindle through the adhered aluminum revealed a discrete interface between the aluminum and stainless steel which confirms that cold-welding did not occur during flight. Shear deformations of the adhered aluminum are consistent with the removal operations. Axial scoring of the ESB bore, Figure 10, occurred when the adhered aluminum on the spindle gouged the bore as the beam was removed with the gear puller.

### Grapple Fixtures

Both the rigidize sensing (active) and the flight standard (passive) grapple fixtures are undergoing post-flight evaluation to provide information about their on-orbit performance. The rigidize sensing grapple was designed to turn the LDEF experiment initiate system (EIS) on or off via the remote manipulating system (RMS) with the LDEF still in the shuttle bay. The flight standard grapple was used to deploy and retrieve LDEF via the RMS. Both grapple fixtures were returned to JSC for examination. Tungsten disulfide lubricant and paint samples are being evaluated. All surfaces have been examined by the micrometeroid and debris SIG. Microswitches have been removed from the rigidize sensing grapple and sent to the vendor for evaluation. The grapples are currently at the original equipment manufacturer, Spar Aerospace, where functional testing of the rigidize sensing grapple will be performed.

### Magnetically Anchored Viscous Damper

Located on the centerline of the space end internal structure, the viscous damper provided attitude stabilization of LDEF from spinning, tumbling or oscillations caused by deployment or other externally applied forces. On-flight performance was satisfactory as the satellite was stable when approached for retrieval. Post-flight testing of the damper has been completed by the manufacturer, General Electric, Valley Forge, PA. Test results showed no anomalies. The damper will be returned to Langley Research Center in flight ready condition.

## CONCLUSIONS

Fastener removal difficulties have been related to galling damage during pre-flight installation and post-flight removal. No indications of space caused cold-welding have been found. Because stainless steel fasteners are very susceptible to galling damage, successful application of such fasteners on ORU's will require high thread quality and effective lubrication schemes or surface modifications.

Cold-welding related to space exposure is apparently not of concern. No evidence of cold-welding has been observed; all suspect conditions thus far have been shown to be the result of installation or removal galling damage.



The LDEF primary structure was unaffected, other than by micrometeoroid and debris impacts. Dye penetrant and eddy current inspection of the structure revealed no anomalies. No bulk metallurgical changes occurred in the structural materials.

The mechanical behavior of the EECC's was generally nominal. Wide swings in motor current during opening of the M0006 canister, drawer seals and lubrication will receive further study.

The reliability of electromechanical systems under LEO conditions appears to be generally satisfactory.

#### ACKNOWLEDGEMENTS

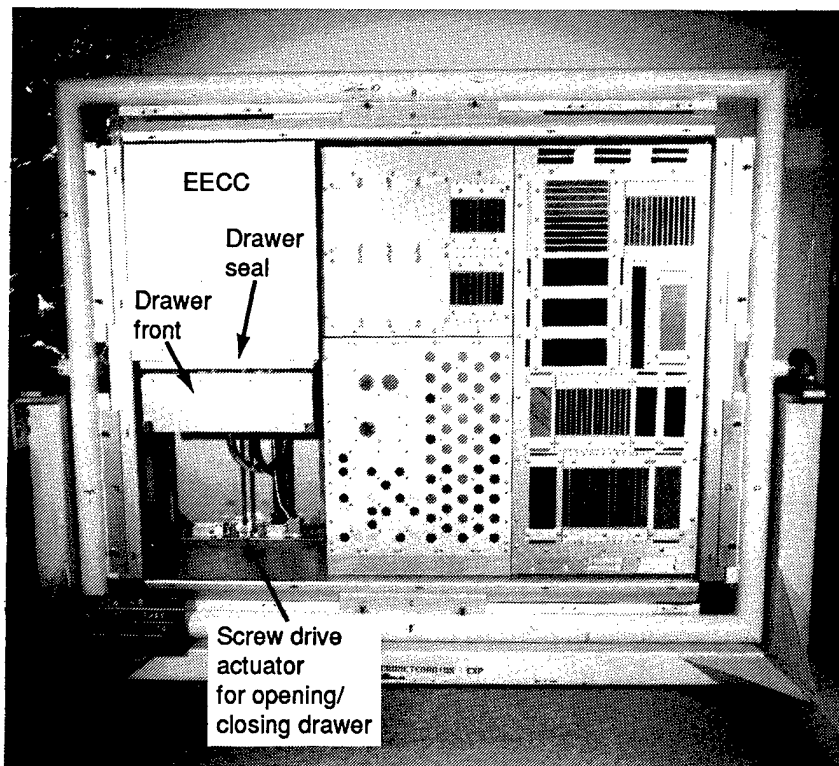
The System SIG gratefully acknowledges the cooperation and assistance of Wayne Slomp of Langley Research Center, TSGT Mike Steskal and MSGT Barry Seegraves of Patrick AFB, Dr. Mike Meshishnek and Sandy Gyetvay of The Aerospace Corporation and Dr. Ludwig Preuss of MBB Deutsche Aerospace during the opening of the EECC's.

Table I. EECC Performance Data

Experiment number	LDEF location	Initial pressure TORR	Leak rate TORR/day	Opening time minutes	Motor run current mA	Days EECC opened after LDEF returned to earth
M0006 (Air Force) S/N 003	C3 (trailing)	<1 atm	2.7	19.5	130-230	60
S0010 (LaRC/SLEMP) S/N 001	B9 (leading)	642	12.3	16.9	110-120	102
S1002 (West German) S/N 002	E3 (trailing)	1 atm	—	16.8	150-180	122
M0003 (Aerospace) S/N 004	D8 (off-leading)	1 atm	12.6	**	**	149
M0003 (Aerospace) S/N 005	D4 (off-trailing)	282	* (1.9)	15.4	150-190	150

\*: Purge valve would not reseal after initial opening. Calculated leak rate based on initial pressure is shown in parentheses

\*\* : Opening time and motor current not obtained due to ground support equipment problem



*Figure 1. S0010 EECC as Mounted in B9 Tray*

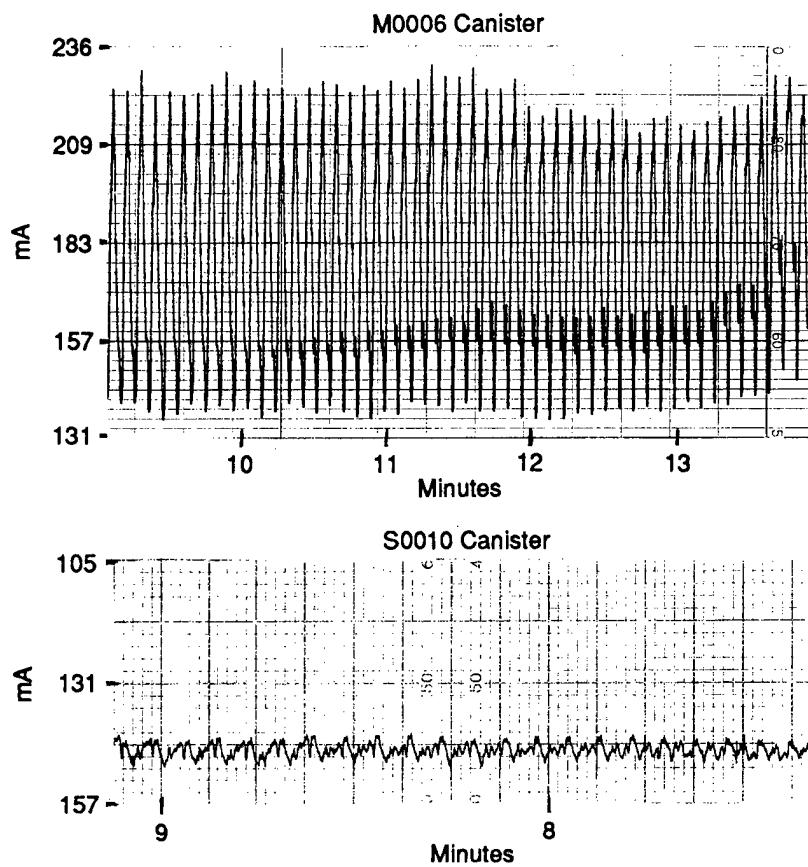


*Figure 2. Motor Current Traces During Initial Opening of M0006 and S0010 EECCs*

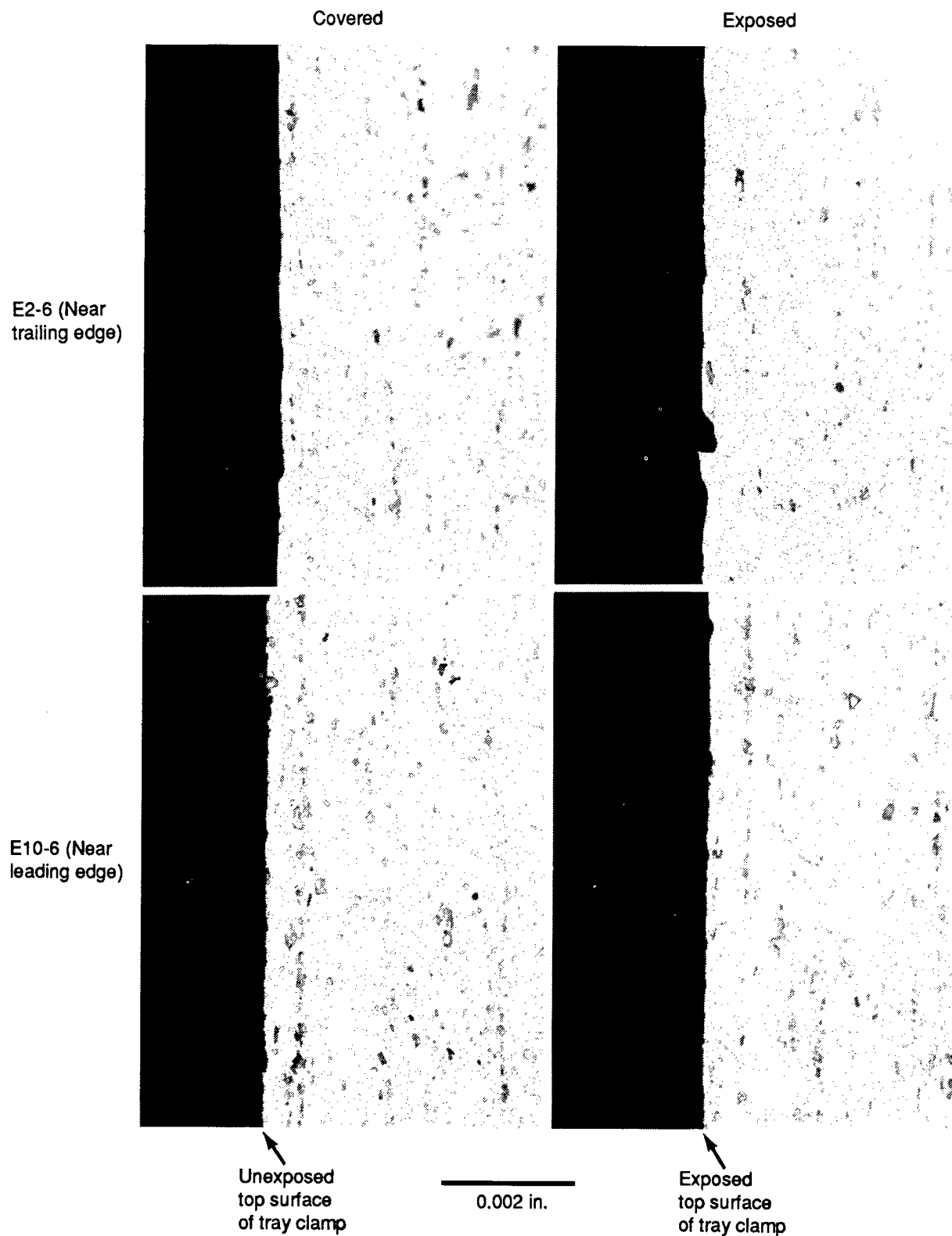
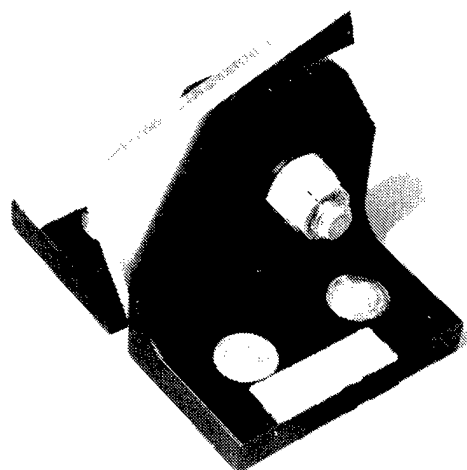
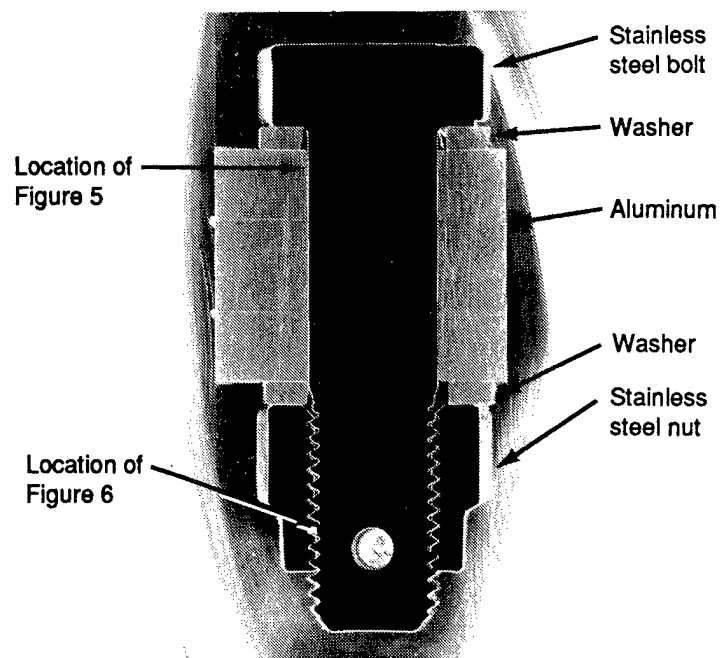


**Figure 3. As-Etched Microstructures of 6061-T6 Aluminum Experiment Tray Clamps From Near-Leading and Near-Trailing Edge of LDEF. Covered Areas of the Clamps Were Protected by an Overlying Shim**



Fastener Assembly



Metallographic Cross-Section

0.040 in.

Figure 4. Unassembled Intercostal Fastener Assembly

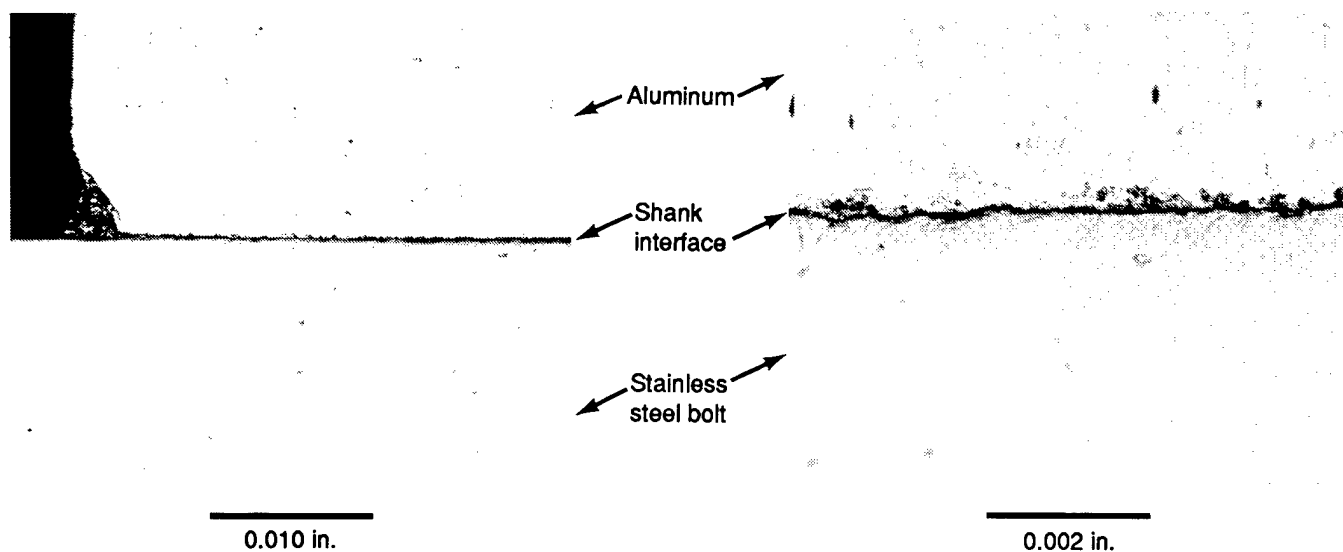
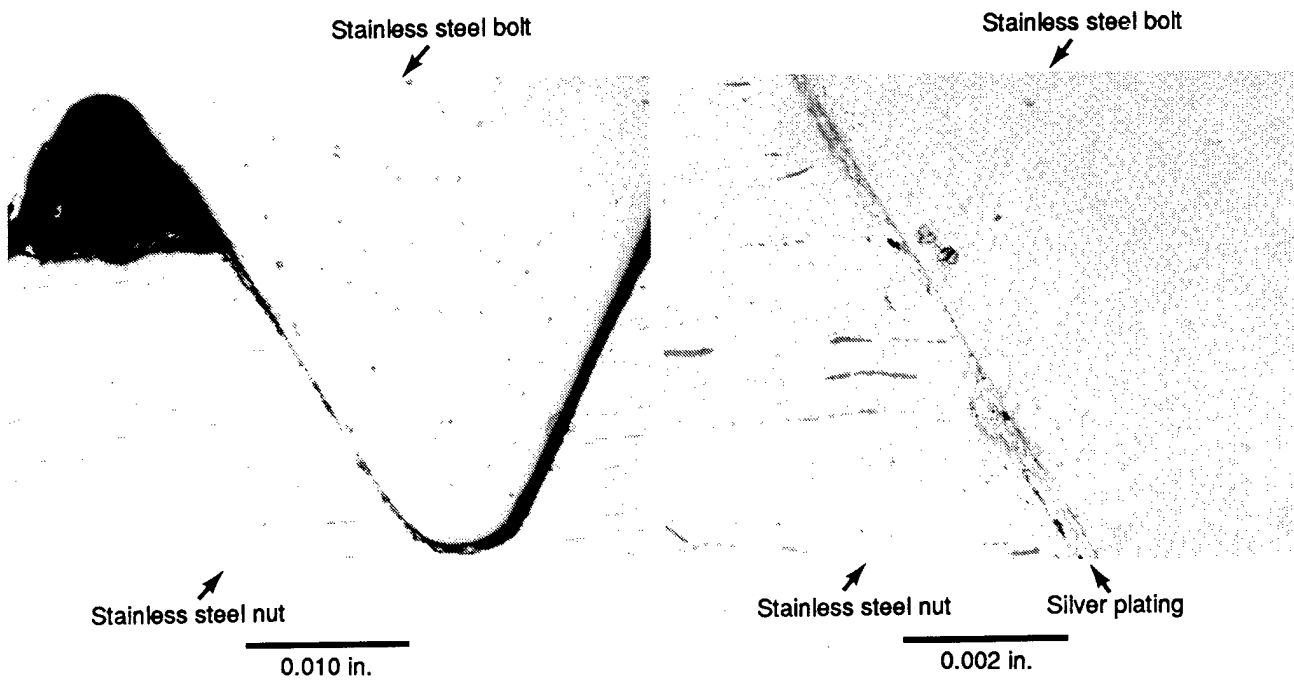
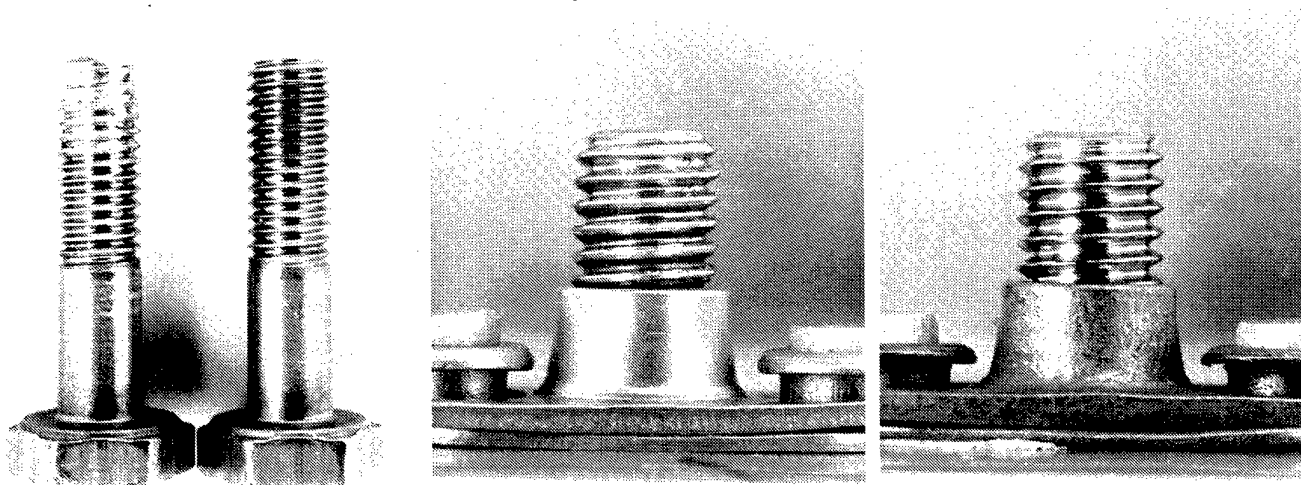


Figure 5. Close-up of Shank Interface Area Indicated in Figure 4



**Figure 6.** Close-up of Nut/Bolt Thread Faying Surfaces as Indicated in Figure 4. (Note Smearing of Ag-Plating Which Acts as a Lubricant Between the Nut and Bolt)



No MoS2

MoS2

No MoS2

MoS2

**Figure 7.** (Left) - Comparison of Thread Conditions of AO175 Tray Bolts Removed From Nut Plates. Undisturbed Assemblies Were Cross-Sectioned as Shown in Figure 8. Note Thread Galling Damage on Fastener That Had MoS2 Removed (Center).

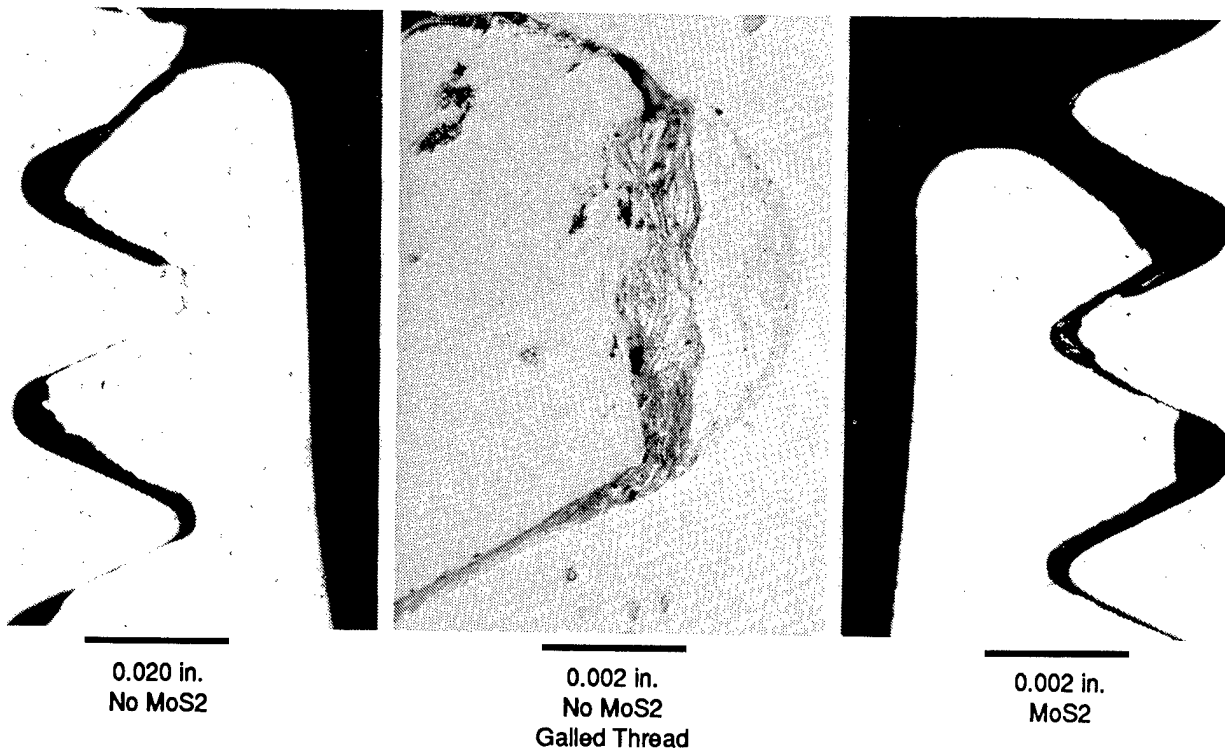


**Figure 8.** (Left and Center) - Galling Damage of Bolt Threads in Nut Plate Without MoS2.  
(Right) - Normal, Undamaged Threads in Nut Plate With Intact MoS2

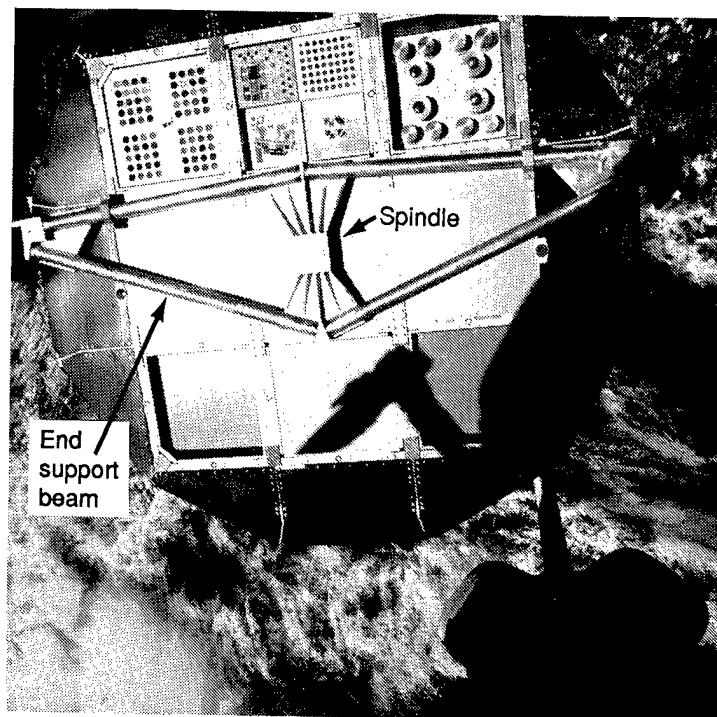
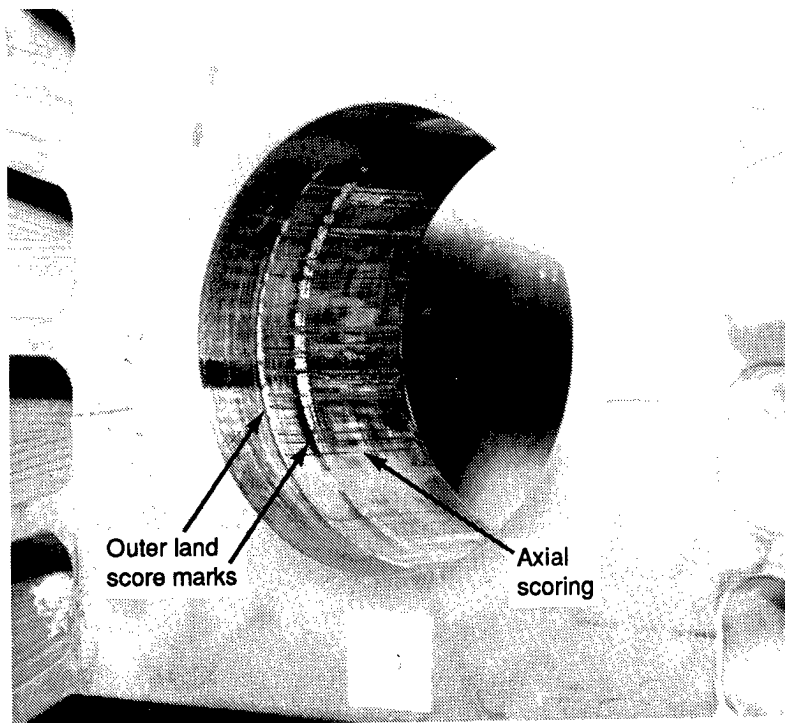


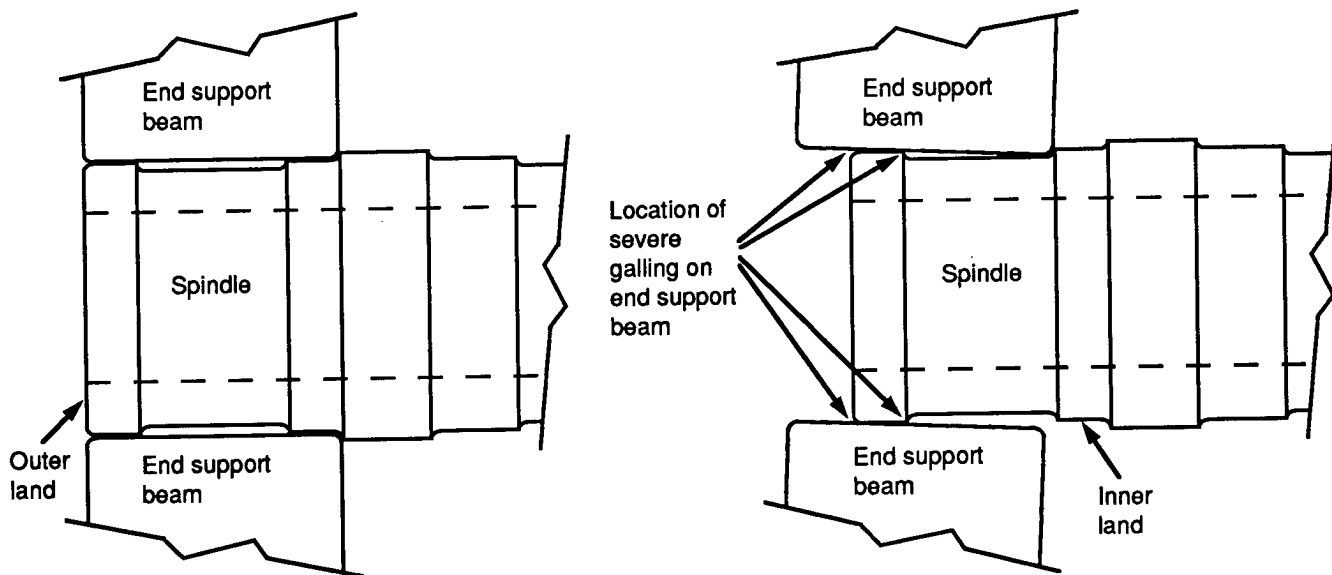
**Figure 9.** End Support Beam (ESB) as Installed on LDEF





Front Surface of ESB

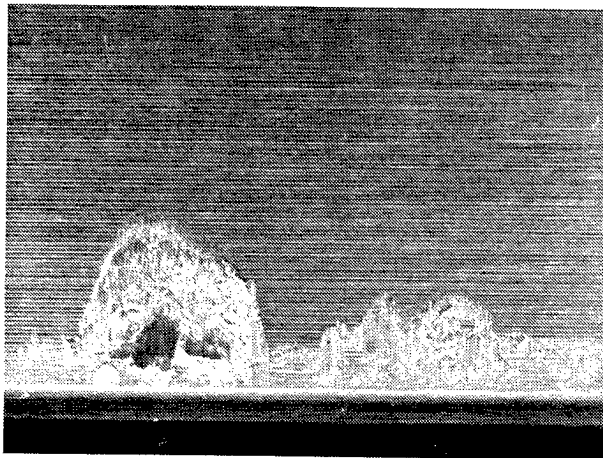
**Figure 10. Close-up of ESB Spindle Bore Showing Scoring Damage Observed After Removal From Spindle During De-Integration**



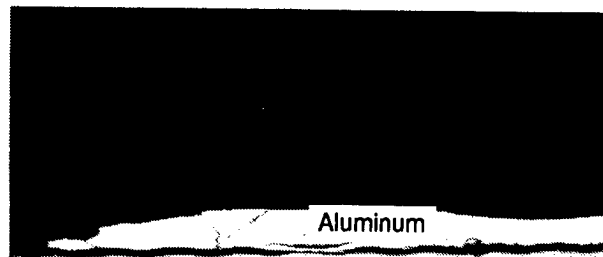
**Flight Position of End Support Beam**

**Position of End Support Beam When It Became Stuck on Spindle During Removal Attempt**

**Figure 11. Schematic Illustration of Cause of ESB Seizure During Removal**



Galling and Aluminum Adhesion



Spindle

0.005 in.

*Figure 12. Galling and Adhesion of ESB Aluminum on Spindle*

## ON-ORBIT COLDWELDING FACT OR FRICTION?\*

Harry Dursch, Steve Spear  
Boeing Defense and Space Group  
Seattle, WA 98124

Phone: 206-773-0527

Fax: 206-773-4946

### ABSTRACT

An investigation into the potential of on-orbit coldwelding occurring has been completed. No instances of coldwelding were found during deintegration and subsequent testing and analysis of LDEF hardware. This finding generated wide interest and indicated the need to review previous on-orbit coldwelding experiments and on-orbit spacecraft anomalies to determine whether the absence of coldwelding on LDEF was to be expected. Results show that even though there have been no documented cases of significant on-orbit coldwelding events occurring, precautions should be taken to ensure that neither coldwelding or galling occurs in the space or pre-launch environment.

### INTRODUCTION

Spacecraft mechanisms are required to operate in the high vacuum of space for extended periods of time. A significant concern to the designer is the possibility of metal-to-metal coldwelding or significant increases in friction. As insightfully stated in a 1973 report, this coldwelding phenomenon is of great interest to the manned space effort because such procedures as repeated orbital docking and assembly may be affected by coldwelding (Ref. 1). Coldwelding can occur between atomically clean metal surfaces when carefully prepared in a vacuum chamber on Earth. The question is whether coldwelding will occur in on-orbit service conditions. This paper presents the results of the LDEF System Special Investigation Group investigation into whether coldwelding had occurred in any LDEF hardware or experiments. The results of a literature search into previous on-orbit coldwelding experiments and a review of on-orbit spacecraft anomalies is also discussed.

### COLDWELDING DEFINITION

Coldwelding is defined as the solid state metallic bonding between atoms on opposing surface layers of similar or dissimilar metals (Ref. 2). Contamination free surfaces are required for bonding to occur. The presence of contaminants such as naturally occurring oxides, contaminants contained within the atmosphere, or organic films will effectively prevent adhesion.

\* Work done under NAS1-18224, Task 15

These contaminants (lubricants) could be removed, pre-flight or on-orbit, by fastener installation/removal, during sliding contact, or if located on the spacecraft exterior surface and exposed to the combined effects of the space environment. If the surface contaminants are removed on-orbit, they will reform very slowly, if at all, in the vacuum of space. The susceptibility of materials to coldweld is also dependent on compressive stresses between mating surfaces, temperature, abrasion, and time. In extreme cases, the contamination films on metal surfaces can be penetrated under unusually high contact stresses, resulting in coldwelding of asperity contacts. The susceptibility for dissimilar metals to coldweld is enhanced by like crystal structures, similar atom sizes, or mutual solubility.

Galling is defined as a wear condition whereby excessive friction between high spots (asperities) results in localized welding with subsequent metal tearout or metal transfer and further roughening of the mating surfaces.

The difference between coldwelding and galling is an important distinction. The symptoms or results of seizure are the same independent of whether they were caused by galling or coldwelding. In both cases, photo-micrographs of a cross section of the seized joint would show solid state metallic bonding between the mating surfaces. The difference is that coldwelding is caused by contamination free surfaces resulting in metal adhesion where as galling is caused by excessive friction ( due to poor tolerances, insufficient or improper lubrication, or improper material selection) between mating surface asperities resulting in metal adhesion. Another important distinction is if seizure could have developed under terrestrial operating conditions, galling, not coldwelding, is the cause of the seizure. An example is a loss of lubrication leading to a bearing failure caused by galling between mating surfaces. This failure would have also occurred in space, but not because of coldwelding.

#### POSSIBLE ON-ORBIT ANOMALIES CAUSED BY COLDWELDING

The following four cases concern instances of on-orbit equipment malfunctions that were, at the time of malfunction, attributed to coldwelding. It should be noted that all four of these malfunctions occurred in the 1960's, back when coldwelding was thought to be more of a design consideration than it has proved to be. Also, none of the hardware was recovered to verify that coldwelding had occurred. No references to any spacecraft anomalies attributed to coldwelding were found for spacecraft launched after 1966. All four of the following anomalies were summarized in a 1966 publication (Ref. 3).

Surveyor 1 (Ref. 4) - During the operation of Surveyor 1 on the lunar surface, a potentiometer that was used to indicate the position of the azimuth axis showed signs of failing after operating for about 100 hours. Because of outgassing problems with lubricants in the lunar environment and because of its proximity to the camera mirror, the potentiometer was not lubricated. Failure presumably occurred due to seizure of the wiper contact to potentiometer winding, after numerous operations. Improved potentiometers with a dry, non-outgassing lubricant were used on later Surveyor spacecraft.

Air Force Research Satellite (Ref. 5) - During the flight of an Air Force research satellite, the signal strength from the satellite was lower than expected and the spin rate was high; however, over a period of several weeks, the signal strength increased, the spin rate decreased, and satisfactory performance was eventually obtained. These malfunctions were traced to the apparent failure of a gold-plated antenna to unfold when orbit was attained. During launch, the rolled-up antenna was stowed in a retaining cup. As the result of extended vibration during launch, the antenna rubbed against the retaining cup, and some of the plating was worn away. Cold welding was thought to have developed at various locations along the antenna when the satellite entered space. After deployment, the welds opened gradually to permit unfolding of the antenna. The improvement in signal strength correlated with such a process, and the data was later verified by laboratory tests.

Gemini 4 (Ref. 5) - During the Gemini 4 flight, the astronaut's hatch door jammed momentarily during extra-vehicular activity. The jamming could have been caused by seizure of the hatch hinges. One hinge member was made from titanium, while hard-coated aluminum was used for the other member. A dry film lubricant was applied to the rubbing surfaces to prevent seizure. There was evidence that the lubricant had been inadvertently removed before launch.

West Ford Experiment (Ref. 6) - In 1961, the Air Force attempted to orbit 50 pounds of fine copper wires or needles at an altitude of 2000 miles in an experiment called West Ford. The experiment was not successful, possibly because the needles coldwelded to each other. It was reported that benzene was used as the adhesive to hold the 10E-6 mm diameter needles together during the preliminary phases of the experiment. It was expected that the benzene would vaporize in space, leaving the separate needles ready for deployment. This premise was validated in laboratory tests conducted in a vacuum of 10E-6 torr. However, after the failure of West Ford, the tests were repeated in a vacuum of 10E-10 torr. Under these conditions, the needles adhered to each other. Since the pressure associated with an altitude of 2000 miles (about 10E-13 torr) is lower than the test vacuum, adhesion was the apparent cause of failure.

Orbital Anomalies in Goddard Spacecraft - Annual reports present orbital anomaly data for Goddard spacecraft active in-orbit during the previous year. This reporting began with coverage of spacecraft that were active in 1982. On the average, Goddard has 20-30 spacecraft each year for which they are responsible. The major feature of these reports is a log of all anomalies occurring during the report period which provides a description of the anomaly and its time of occurrence. Each anomaly is classified according to criticality, type, subsystem, and other relevant criteria.

While several of the spacecraft anomalies are attributed to bearing failures, it is believed that the cause of the bearing failures was improper lubrication or lubrication migration. None of the anomalies have been attributed to coldwelding. The current author of these reports believes that there have been no on-orbit spacecraft anomalies attributed to coldwelding since the 1960's. During the 1960s on-orbit coldwelding was thought to be a

major design consideration. Since then, the frequency of coldwelding being suspect in on-orbit anomalies has considerably decreased.

## ON-ORBIT COLDWELDING EXPERIMENTS

A very widespread and costly effort was undertaken to investigate the problem of coldwelding under laboratory simulation of the space environment. In the 1960's, a count showed that approximately 100 groups (both government and industry) had been studying coldwelding. In contrast to the extensive laboratory investigations (using techniques that may or may not have given valid data), very little data was obtained in the actual space environment (Ref. 1). Seven spacecraft were flown during the 1960's and 1970's to determine the effect of exposure to the space environment. In all cases, data was telemetered back to Earth. The following summarizes the experiments flown, the materials tested, and the results.

Ranger 1 & 2 (Ref. 3)- In 1961, the coefficients of friction for several lubricated and unlubricated metallic and nonmetallic couples were measured in the space environment during flights of Ranger 1 and Ranger 2. The friction experiment was designed to obtain data at altitudes corresponding to vacuums of  $10E-12$  to  $10E-16$  torr; however, because of spacecraft malfunctions, these altitudes were not attained. Nevertheless, valuable friction data was acquired and analyzed.

Twenty disk specimens were spaced along a drive shaft. The drive shaft rotated at 28 revolutions per minute. Strain gauges were used to measure the frictional force during testing. Detachment mechanisms were attached to the specimen assemblies, so that individual assemblies could be lifted in case seizure occurred or friction became excessive. Materials included in this experiment include typical structural alloys used in spacecraft hardware, electrical contact materials, and a number of lubricants. Ground based friction data was obtained for comparison with the spacecraft data.

Ranger 1 did not reach its programmed orbit because of a malfunction in the second stage. The spacecraft was placed in a low-altitude orbit instead of the desired elliptical orbit with a very high apogee. Data was received for orbits on the following day with data transmission ending when the experiment was turned off at a predetermined low-battery voltage level. This occurred after the 19th orbit (this was a very short lived experiment). The results show that PTFE sliding against metals and ceramics, as well as metals sliding on metals with MoS<sub>2</sub>, had a low coefficient of friction averaging 0.04. Unlubricated metals sliding on metals showed moderately high coefficients averaging 0.5, but some metal couples had coefficients in excess of 0.7. There was no evidence of coldwelding.

A coefficient of friction experiment was also programmed for the Ranger 2 flight. However, malfunction in the second stage of the space vehicle occurred and Ranger 2 was placed into a low-altitude orbit. Only a very limited amount of friction data was received from the spacecraft, and it was insufficient to be analyzed.

Environmental Research Satellites 15 & 16 (Ref. 7) - In 1966, two Air Force satellites (designed and built by TRW) were launched to determine the effect of material coldwelding in space. The achieved orbital parameters of 100 mile perigee for the initial satellite (ERS 16) did not satisfy pre-selected perigee requirements. An orbit of 500 miles or higher had been the pre-selected perigee requirement primarily due to the vacuum at that level. While the spacecraft and experiments performed at the attained orbit, the low perigee resulted in the necessity to launch the back-up spacecraft (ERS 15) in order that the desired environmental exposure condition could be obtained.

Each satellite performed four valve experiments and eight supplemental ball contact experiments. The four valve experiments consisted of four solenoid valves in which different material combinations were incorporated as the seat-poppet contacts. Each of the valve experiments were cycled periodically from a normally closed position, opening for approximately one second every five minutes. The four valves represented an actual engineering configuration and as such permitted the results to be directly extrapolated to applications such as a main propellant valve of a space propulsion system. The same solenoid arrangement was used for the supplemental 1/8" diameter ball contact experiments. The geometry of the ball contact experiment was such that the balls were exposed to solar UV and radiation which may have contributed to the removal of contaminants. While the valve experiments were normally closed, the ball contact experiments were normally open. Valve actuation and any occurrence of cold welding was detected by monitoring solenoid currents.

On ERS 16, the valve tests included a simulated propellant flow (camphor vapor) to determine what effects a contaminant might have. The vapor was turned off after the first 44 days with the valves continuing to operate to determine the effect of the vapor. The data showed that, in this case, the residual surface contamination was sustained even after repetitive mechanical contacts and extended space exposures which precluded the development of sufficient areas of clean metal contact which is necessary for significant coldwelding. ERS 15 was launched without simulated propellants since no coldwelding was observed on ERS 16.

The on-orbit experimental data showed no significant coldwelding to have occurred even after many tens of thousands of mechanical contact cycles and extended space environment exposures of over six months. As with the valve experiments, no general evidence of significant coldwelding was noted with the supplemental ball specimens. One contact pair of the eight pairs flown on ERS 15, tungsten carbide on tungsten carbide, exhibited sticking forces of a very low magnitude. Both flight experiments showed the presence of gross contamination, incurred during the period of integration on the launch vehicle prior to launch. This was determined because upon attainment of orbit, a majority of the ball contact pairs showed high electrical resistance. After cycling and a brief space exposure, the gross contamination was eliminated as determined by the attainment of nominal resistance values. Following this cleanup, the majority of the contact pairs did not display any increase in contact resistance

Environmental Research Satellites 19 & 20 (Ref. 8) - In 1967 and 1968, two Air Force satellites (designed and built by TRW) were launched to determine the effect of friction in space. ERS 20 was launched in April 1967 and achieved a planned elliptical orbit ranging from a 4600 miles perigee to a 60,000 mile apogee. Data was acquired over a fourteen month period. The second friction experiment spacecraft, ERS 19 was lost in an unsuccessful launch in August of 1968.

The experiment was designed to permit direct comparison of results obtained in a laboratory vacuum chamber versus on-orbit results. The flight experiment used two friction modules to produce reciprocating sliding motion between 16 pairs of frictional surfaces, each a different material combination. The friction surfaces were mounted in such a way that they extended out of the ends of the spacecraft and therefore received maximum exposure to the deep vacuum of space, while having maximum isolation from outgassing of other spacecraft elements. Reciprocating motion was selected in preference to continuous rotary motion.

Four general categories of materials were selected: metals and alloys, thin film lubricants, inorganic compounds, and polymers. The orbital test plan called for both intermittent and continuous run profiles. The purpose was to examine the effect of intermittent versus continuous run effects on the friction behavior. Sliding friction data was obtained under simulated space vacuum, controlled environment degraded vacuum, and satellite orbital test (ERS 20) conditions. Individual test results illustrated that the microfrictional processes between different material combinations are sensitive to different aspects of a test environment. This was demonstrated by a good correlation found between some of the test combinations and a lack of correlation demonstrated with others. No evidence of a friction dependence on orbital altitude and no evidence of coldwelding was found. This report does an excellent job in discussing the results of on orbit friction coefficient for a wide variety of materials. However, this data was beyond the scope of the present investigation and is not discussed.

Orbiting Vehicle 1-13 (Ref. 1) - In 1968, the OV-1-13 satellite was launched to determine the effect of the space environment on friction, coldwelding, and wear of widely used spacecraft materials. A secondary goal was to verify or disprove laboratory results. Materials tested included mutually soluble, partially soluble, and insoluble metal combinations.

The friction-test mechanism consisted of a hemispherical tipped rider sliding on a flat face of a disk which was rotating at a constant velocity. The normal preload for the gold vs silver samples was one pound; all other metal couples were preloaded to two pounds. Strain gages were used to measure the friction force, normal force, and displacement of the rider due to wear. In the event that the friction force on a particular pair of materials reached a level such that excessive power was required, the rider could be removed from contact with the disk by means of a sealed pyrotechnic actuator. Six different material combinations (shown below) were tested. Two samples of each combination, for a total of twelve pairs, were flown. No lubrication was used. Great care was employed in designing and constructing the experiment to minimize the possibility of contaminating



the material couples. Design of the experiment was made with the objective of minimizing outgassing.

The friction and wear device was operated on-orbit throughout the 18 month life of the OV-1-13 satellite. During these 18 months, the pins and disks remained in contact with each other, unless seizure occurred. Seizure was defined as a friction coefficient in excess of 3.0. The experiment was turned on (disk rotated) and data recorded an average of one orbit per week. The total running time of the experiment for the 18 months was approximately 25 hours. Indication of coldwelding (operation of the overload pyrotechnic actuators occurring when the friction coefficient exceeded 3.0) occurred for three of the twelve pairs. These pairs and the time after launch when each event occurred were;

- 1) Gold and silver, 33 hours after launch
- 2) Be-Cu and stainless steel, 2250 hours after launch
- 3) Stainless steel and stainless steel, 3720 hours after launch

The on-orbit results are summarized below:

Gold and Silver - These metals are mutually soluble and were expected to coldweld. One sample apparently welded almost immediately while the second sample ran at a very high and slowly increasing friction level (1.0 - 2.0) for the duration of the test. However, the second specimen did not seize (exceed a coefficient of 3.0).

Aluminum and Stainless Steel - Both samples ran very smoothly at an almost constant friction value of 0.5.

Stainless Steel and Stainless Steel - One pair welded after 3720 hours while the other ran at a relatively high friction level (0.6-0.9) for the duration of the test.

Stainless Steel and Nitrided Steel - Both samples ran at an intermediate level at a friction level 0.7 for the test duration.

Stainless Steel and Carbon Steel - After an initial rise, both samples ran at an intermediate friction level of 0.6 for the test duration.

Be-Cu and Stainless Steel - These metals were expected to form an adhesive bond. One sample apparently welded after 2250 hours; the other survived initially high levels and operated for the remaining time at a relatively low level.

In the case of the coldwelded gold-silver and stainless steel-stainless steel couples, seizing occurred at the initial turn-on of the specific orbit. The last friction readings of the preceding orbit were not unusually high. In the case of the Be-Cu and stainless-steel couple, seizure occurred at the fifth turn-on of the specific orbit. The friction level had been high (0.8 to 1.45) during the earlier intervals of the orbit, but not as high as it had been the previous week. Thus, it appears that seizures of this type occur suddenly and cannot be anticipated even with knowledge of the history of the friction coefficient for the particular metal couple.

One of the most striking observations is that after the first month, the coefficients of friction for all of the materials remained at an almost constant level except for the samples that seized. None of the samples wore the amount required (0.045 inches) to give an indication on the wear transducer.

## SPACECRAFT HARDWARE RETRIEVED FROM SPACE

Surveyor III Hardware Retrieved by Apollo XII (Ref. 9) - Surveyor III was the second of five Surveyors to land successfully on the surface of the moon. This soft landing took place on April 20, 1967. All subsystems operated successfully throughout the first lunar day except for some minor anomalies. Surveyor's television camera took more than 6000 photographs during the first lunar day. Attempts to revive the spacecraft on the second lunar day were unsuccessful. However, this was not surprising as Surveyor was not designed to survive the lunar nights.

Two and a half years later, the lunar module of Apollo XII landed 500 ft from Surveyor III. The Apollo astronauts retrieved the Surveyor television camera, the scoop from the soil mechanics/surface sampler, painted and unpainted sections of the aluminum support tubing of Surveyor, and sections of external cabling and of their Teflon wrapping. One of the main objectives in retrieving the hardware was to determine if any coldwelding had occurred.

During the evaluation of the television camera at JSC, a great deal of difficulty was encountered during removal of one of the wire harness connectors. This connector was finally forced out by twisting and applying considerable force by hand, and a loud popping or breaking sound was heard in the process. Visual inspection of the connector and microscopic examination indicated surface deformation in a small area at the base of the external thread of the connector, which had made contact to the inner edge of the mating camera shroud. Based on the results of the analysis, it was concluded that a strong possibility existed that some coldwelding had taken place. This occurrence was not a primary effect, as it was made possible by faulty installation with a loose retaining nut. A loose fit of the connector permitted excessive rubbing to take place, wearing away the thin iridite coating applied over the aluminum connector. This led to coldwelding between the two aluminum mating surfaces. No other connectors, screws, or fasteners on the returned camera showed any evidence of coldwelding.

Solar Maximum Mission (Ref. 10) - The SMM was launched in February, 1980. The SMM repair mission was performed by the same crew that deployed LDEF (STS flight 41-C, April 1984). The SMM was the first spacecraft designed to be serviced and repaired in space by the shuttle crew. The Modular Attitude Control System (MACS) module was designed to be an orbital replacement unit, but the instrument repair was more complex because the Main Electronics Box (MEB) was not designed to be repaired or replaced in orbit. Initial attempts by the astronauts using the Manned Maneuvering Unit to dock to the spacecraft and to stop its rotation failed. These docking attempts imparted to the spacecraft uncontrollable roll, pitch, and yaw rates. After the spacecraft was stabilized using specially uplinked software, the spacecraft was grappled by the Orbiter's Remote Manipulator System and placed in the Orbiter Bay. The MACS module was removed from the SMM and the new module mounted. This entire replacement process took less than an hour. No difficulties were encountered. The replacement of the MEB was the next repair operation. Discussions were recently held with the astronaut

(Dr. George Nelson) who assisted in replacement of the MEB. Removal and installation of the new MEB required disconnecting and then reconnecting eleven wire harness connectors along with approx 30 small fastener assemblies. Even though this box was not designed for orbital replacement, no difficulties were encountered during removal.

Long Duration Exposure Facility (Ref. 2) - LDEF was a bus sized, passive (no telemetry to Earth), gravity-gradient stabilized satellite retrieved on January 12, 1990 after 70 months of exposure to the low Earth orbit (LEO). LDEF was originally scheduled for a 9 month mission, but due to the Challenger explosion and reprioritizing of other missions, the retrieval was slid to 70 months after deployment. LDEF was in a constant orientation relative to the ram (leading edge) direction throughout its entire mission. This resulted in an excellent opportunity to map the effects of the various space environments on the systems and materials flown on LDEF. The 70 month orbit caused LDEF to undergo over 34,000 thermal cycles. However, the temperature environment was relatively benign. Thermocouples monitored interior surface spacecraft temperatures for the first two years of orbit (after two years, the batteries became sufficiently discharged to cause the temperature monitoring to terminate). The maximum and minimum temperatures were approximately +130F and +40 respectively. While exterior surface temps are a function of absorptance/emittance ratios, maximum and minimum temperatures were expected to be +150F and -20F, respectively. Ground based coldwelding experiments have shown a temperature dependence in susceptibility of metals to coldweld. However, the benign temperatures seen by LDEF should have had no effect on the likelihood of coldwelding occurring.

The only coldwelding related experiment flown on LDEF was a French experiment titled "Microwelding of Various Metallic Materials" The materials tested included Al alloys, Cu alloys, Ti alloys, and stainless steel. Selected combinations of materials were chromic or sulfuric anodized. Other combinations used MoS2 and Molykote Z lubricants. All specimens were alkaline cleaned and then arranged into eight columns of six pairs each. All pairs of each column were loaded together by use of Belleville disc springs. Contact pressures were ranged between 25 to 135 MPa. Ground based control specimens were kept under vacuum for the 70 months LDEF was in orbit. This was a rather "simple" experiment with no active monitoring of data and no sliding motion between specimens. The materials tested are actually used on spacecraft for sliding electrical contacts, antennas, and deployable solar panels. Therefore, these material combinations were selected so coldwelding would not occur. To date, all specimens have been analyzed and only a gold/gold control specimen showed signs of coldwelding.

A considerable amount of testing and analysis has been performed on fasteners and other metallic hardware flown on LDEF. Observations of high removal torques and extensive thread seizure or stripping problems were widespread for various stainless steel fasteners flown on LDEF. While this hardware was not flown as part of any coldwelding experiment, the 70 month exposure to LEO has resulted in an ongoing, comprehensive study to determine if any coldwelding had occurred (this activity is being performed by Boeing personnel under a broader NASA contact). The following paragraphs summarize these activities.

LDEF Tray Clamp Fasteners - During deintegration of LDEF, all tray clamp fastener breakaway torques (there were 2,232 tray clamp fasteners) were determined. These bolts were 1/4" - 20 x 0.75", A286 stainless steel bolts inserted into self-locking helicoils. A database was created containing all breakaway and running torques. The torques were then examined as a function of their location on LDEF. The average torques were similar to the pre-flight installation torques and are also similar throughout LDEF. However, there was a large scatter in values. The database identified the bolts that were the twenty highest and twenty lowest values. These bolts and washers then underwent visual examination. Visual examination revealed a variety of bolt thread conditions from threads that appear to be unused to such severe galling as to entirely remove several threads. Visual examination of the mating washers also revealed varying degrees of scoring, burnishing, and galling on both sides. It was speculated that upon pre-flight installation, the underside of the bolt head and top side of the washer head or the bottom side of the washer and the top surface of the tray clamp would, in some cases, smear together. This could have caused a disruption of the oxide (contaminant) layer, which could have led to coldwelding during the 70 month space exposure. However, no evidence of coldwelding has been found (this is an ongoing investigation). To date, no significant correlation has been found between thread condition or washer condition to explain the high removal torques in some of the fastener assemblies. The evidence indicates that coldwelding was not the cause of the higher removal torques.

End Support Beam. - The end support beam (ESB) was an 18 ft long aluminum frame that held two of the four trunnions. These four trunnions support LDEF in the shuttle cargo bay. It was designed to have a plus or minus 1.5 degree rotation about a 5.0" diameter stainless steel spindle (the spindle was fixed to the LDEF structure) to accommodate potential misalignment on the LDEF structure and still permit berthing in the shuttle cargo bay. A great deal of difficulty was encountered during removal of the ESB from its spindle during deintegration of LDEF at Kennedy Space Center. The initial cause of removal difficulty was thought to be coldwelding. After investigation, the apparent cause of this removal difficulty was misalignment during removal. No evidence of coldwelding was found. This investigation included metallographic cross-sectioning of the spindle and ESB. This showed no solid state or metallurgical bonding between the aluminum and the stainless steel.

Unassembled Fastener - An unassembled, undisturbed stainless steel fastener assembly was cross-sectioned to investigate the possibility of cold-welding without the complications of removal effects. This fastener assembly was cross-sectioned because of its availability, not because of any evidence that coldwelding had occurred. Photomicrographs of the bolt shank interfaces (stainless steel/aluminum) revealed no evidence of coldwelding. The stainless steel nut exhibited some minor galling and some smearing of the silver plating (specified for lubrication), but no coldwelding.

Additional Fasteners - Visual examination of a number of stainless steel bolts indicated that removal difficulties were related to installation damage. Cross-sectioning of seized bolts confirmed this explanation. Galling damage was clearly visible on the exposed

portions of the bolt threads. This galling is more pronounced than what would be caused by being cycled through the self-locking feature contained within any nut or nutplate. Several fastener assemblies, possessing sheared bolts caused by attempted removal, have been analyzed. It was determined that all failures were the result of galling caused by pre-flight assembly and/or post-flight removal attempts.

**Metallurgical Analysis** - One of the LDEF tasks was to determine if space exposure caused any microstructural and/or mechanical property changes of metals. To date, metals examined are 6061-T6 aluminum, Ti-6Al-4V titanium, and stainless steel. Except for the titanium, all the metals examined for microstructural changes were mounted on exterior surfaces of LDEF and therefore saw direct exposure to atomic oxygen and/or UV radiation. To date, the results show no microstructural changes caused by long term space exposure.

## CONCLUSIONS

Most metal surfaces exposed to only the vacuum of the space environment are not likely to become sufficiently clean enough for coldwelding to occur in a practical mission lifetime, unless the rate of removal of surface films is accelerated by some form of electrical or mechanical means. Oxide and contamination removal/deposition rates for metals on exterior surfaces of spacecraft are a more complex issue due to effects of atomic oxygen and/or UV radiation exposure. Many factors influence these removal/deposition rates including location on spacecraft, shadowing by adjacent hardware, spacecraft altitude, proximity to outgassing by nearby materials, and material selection.

There have been no documented cases of a significant on-orbit spacecraft coldwelding event occurring. Several anomalies have been caused by seizure of mechanisms but these were due to vibration caused fretting or galling caused by loss of lubricant. In all cases, the space environment was not a necessary requirement to cause these seizures. There have been a few documented cases of seizure occurring during on-orbit coldwelding experiments. However, the seized materials had been selected for the experiment because of their susceptibility to coldweld. This susceptibility was increased by following stringent pre-flight cleanliness procedures.

The results of this investigation indicate that if contact is made between two mating surfaces in a preflight environment and these surfaces are left undisturbed during the mission, no coldwelding will occur while the spacecraft is on-orbit. This applies, in particular, to fastener assemblies. If the correct materials, tolerances, and lubricants are used such that galling does not develop during fastener installation or removal, or during the launch environment, and the fastener remains undisturbed while on-orbit, no difficulty will be encountered during post-flight removal. This also applies to an on-orbit replacement. No difficulty due to coldwelding will be encountered if a non-galled fastener assembly is removed on-orbit. However, repeated on-orbit removals and installations of orbital replacement units will require the use of appropriate lubrication schemes and the correct design of self-locking nuts to ensure that no thread or lubricant

damage occurs. Even though there have been no documented on-orbit coldwelding related failures, precautions still should be taken to ensure that not only does coldwelding not occur in the space environment, but that seizure does not occur in the pre-launch or launch environment.

## REFERENCES

- 1) E.J. Devine, H.E. Evans, W.A. Leasure, "In-Flight and Laboratory Vacuum-Friction Test Results, Goddard Space Flight Center, Report No. TN D-7419, December, 1973.
- 2) "Long Duration Exposure Facility Systems Special Investigation Group, Interim Report", Boeing, January, 1991.
- 3) H. E. Pattee, R.E. Monroe, "Adhesion in the Space Environment", Battelle Institute, October, 1966.
- 4) H.D. Watkins, "Surveyor 1 Prompts Confidence, Caution", Aviation Week and Space Technology, Vol.. 84, No. 26, 1966, pp. 63-67.
- 5) I. Stambler, "Surface Effects in Space", Space/Aeronautics, Vol...45, No. 2, 1966, pp. 95-101.
- 6) "Test Chamber Art Suffers from lack of Information", Missiles and Rockets, Vol... 12, No. 20, 1963, pp. 54-64.
- 7) R.L. Hammel, J. Rodman, R.J. Martin, "In-Space Coldwelding Tests, Summary Report", TRW Systems, January, 1967.
- 8) R.L. Hammel, "In-Space Friction Tests, Final Report", TRW Systems, November, 1969.
- 9) "Test and Evaluation of the Surveyor III Television Camera Returned from the Moon by Apollo XII, Hughes Aircraft Company, December, 1970
- 10) "Proceedings of the SMRM Degradation Study Workshop", Satellite Servicing Project Goddard Space Flight Center, Report No. 408-SMRM-79-0001, May 9-10, 1985.

THERMAL CONTROL SURFACES EXPERIMENT  
FLIGHT SYSTEM PERFORMANCE

Donald R. Wilkes

Leigh L. Hummer

AZ Technology, Inc.

3322 Memorial Parkway SW, Suite 93

Huntsville, AL 35801

Phone: 205/880-7481; Fax: 205/880-7483

James M. Zwiener

NASA Marshall Space Flight Center

Marshall Space Flight Center, AL 35812

Phone: 205/544-2528; Fax: 205/544-0212

INTRODUCTION

The Thermal Control Surfaces Experiment (TCSE) is the most complex system (other than the LDEF with its experiments) retrieved after long term space exposure. The TCSE is a microcosm of complex electro-optical payloads being developed and flown by NASA and the DoD including SDI.

The objective of the TCSE on the LDEF was to determine the effects of the near-Earth orbital environment and the LDEF induced environment on spacecraft thermal control surfaces.

The TCSE was a comprehensive experiment that combined in-space measurements with extensive post-flight analyses of thermal control surfaces to determine the effects of exposure to the low earth orbit space environment. The TCSE was the first space experiment to measure the optical properties of thermal control surfaces the way they are routinely measured in the laboratory.

TCSE FLIGHT HARDWARE

The TCSE is a completely self-contained experiment package; providing its own power, data system, integrating sphere reflectometer, and pre-programmed controller for automatically exposing, monitoring, and measuring the sample materials. The TCSE was developed as a protoflight instrument where one instrument was built, made to work within required specifications, tested, and flown. Environmental qualification testing was performed at MSFC that included vibration, thermal vacuum, and electromagnetic interference (EMI) tests.

The TCSE was built in a 305 mm (12 in.) deep LDEF tray (see Figure 1). The 25 active and 24 passive samples were mounted in a semicircular pattern on a circular carousel. The active and passive test samples differed in that the space effects on the passive test samples were determined only by pre- and post-flight evaluation. The optical properties of the 25 "active" samples were measured in-space as well as in pre- and post-flight analysis. The carousel is tilted at 11

degrees from the outer tray surface to allow a 115 mm (4.5 inch) diameter integrating sphere to fit between the deep end of the carousel and the outer shroud. This design satisfied the IDEF requirement to remain within the outer edges of the tray and also provide a field of view of space greater than 150 degrees for the samples. This design maintained mechanical simplicity and inherent reliability. Figure 2 shows the basic specifications for the TCSE flight hardware.

### Sample Carousel

The TCSE sample carousel design enabled the test samples to be either protected from or exposed to the space environment as well as to be positioned for optical measurement. In the exposed condition, the samples experienced space exposure for approximately 23 1/2 hours each earth day. During the protected period of time (approximately 1/2 hour), calorimetric measurements of emittance were made. The protected environment also prevented exposure of the experiment test samples to ground processing and launch contamination.

The carousel subsystem was comprised of the carousel assembly, a stepper motor controlled by the DACS to effect movement of the carousel assembly, a geneva drive assembly, and an emissivity plate. The geneva drive enabled precise repeatable angular rotation such that the same spot on each flight sample was measured. Pre-flight testing proved the inherent reliability of the geneva drive assembly and the positioning accuracy of each sample. The emissivity plate, combined with calorimeters, was used for the emittance measurements.

### Radiometers

Three radiometers were used to monitor the irradiance from the sun (direct solar), earth albedo (reflected), and earth IR (emitted) incident on the TCSE. The radiometer data enabled calculation of solar absorptance and total emittance when combined with calorimeter temperature data. The radiometers were mounted on the carousel and were rotated with the flight samples. The three radiometers used thermopile detectors painted flat black and domed collection optics to measure the energy flux on the TCSE. The direct solar radiometer was installed with a field-of-view equal to the flight samples. A quartz lens was used for the spectral region of 200 to 3000 nm. This region contains over 98 percent of the sun's electromagnetic energy. Like the direct solar radiometer, the earth albedo radiometer used a quartz lens. However, the earth IR radiometer used a germanium lens for the infrared spectrum from 2000 to 20000 nm. The earth albedo and earth IR radiometers were installed with covers such that they had a clear view of only the earth. Data from the radiometers were recorded at minute intervals over a two hour period each day of the active mission.

### Calorimeters

Calorimeter sample holders provided a simple method to determine the solar absorptance ( $\alpha_s$ ) and total emittance ( $\epsilon_T$ ) of the active flight samples. This calorimetric technique measured the inputs to the heat balance equation and calcu-



lated solar absorptance and total emittance for the flight samples. The in-space measurements required for this calculation were the temperature of the test sample and the external heat inputs as measured by the irradiance monitors. The calorimeters were designed to isolate the flight sample material thermally from the TCSE to minimize errors caused by radiative and conductive losses. The TCSE calorimeter design was developed originally by the Goddard Space Flight Center (GSFC) and flown on the ATS-1, ATS-2, and OAO-C satellites.

The calorimetric measurement procedure used on the TCSE is an improvement over past experiments for determining total emittance. Previous experiments determined total emittance when the calorimeter viewed deep space only (i.e., no view of the sun or earth). This orientation was difficult to insure, and the time spent in this orientation was, at times, too short to provide accurate measurements. The TCSE procedure, however, rotated the samples inside the instrument, where they viewed only a heavy, black "emissivity" plate. This geometry greatly simplifies the heat balance equation and removes any sun or earth effects.

### Reflectometer Subsystem

The TCSE reflectometer optical design, illustrated in Figure 3, is one that is used routinely in the laboratory to measure spectral reflectance. Two light sources, tungsten and deuterium lamps, are used with a scanning prism monochromator with selectable slit widths to provide the monochromatic energy for the spectral measurement. A 115 mm (4.5 inch) diameter integrating sphere collects both the specularly - and diffusely - reflected light from a wall mounted sample to provide the angularly integrated measurement capability. Figure 4 illustrates the integrating sphere geometry. Kodak Barium Sulfate ( $\text{BaSO}_4$ ) was used for the sphere coating because it was easy to apply, durable enough to withstand the launch environment, and had good optical properties. A UV enhanced silicon photodiode detector and a lead sulfide detector were used with the integrating sphere for the required 250 to 2500 nm spectral range.

### Data Acquisition and Control System

The TCSE Data Acquisition and Control System (DACS) is shown in Figure 5 and controls all aspects of the TCSE operation. The heart of the DACS is an RCA 1802 CMOS microprocessor with associated memory and input/control ports. A 12-bit analog-to-digital (A-D) converter and analog multiplexer are used to read measurement data.

A low-power, 25-bit real-time clock was used to keep mission elapsed time. The real-time clock was the only TCSE subsystem that ran continuously from the LDEF "start" signal through battery depletion. The clock subsystem turned on the DACS once each 24 hour day of the active TCSE mission. The DACS, in turn, looked at its internal schedule to determine what functions were to be done that day. At the completion of the day's measurements, the DACS turned itself off, leaving only the real-time clock operating.

There were two measurement cycles that the data system controlled, the "daily" measurements and the "reflectance" measurements. The daily measurements were per-

formed once each day after the initial turn-on delay period. The reflectance measurements were performed at intervals varying from once a week at the beginning of the mission to once a month after three months as defined by the stored program in the data system.

In the daily measurement sequence (with the carousel in the exposed position), each of 64 analog channels were sampled once each 64 seconds for 90 minutes. The daily data included calorimeters, radiometers, and housekeeping data. The carousel was then rotated to the protected position and the measurements continued for another 30 minutes. At the end of this cycle, the carousel rotated the samples to the exposed position.

In the reflectance measurement sequence, each sample was positioned in-turn under the integrating sphere twice for reflectance measurements. Each sample, beginning with sample one and continuing through sample 25, was positioned under the integrating sphere and the ultraviolet (UV) portion of the measurements taken. This sequence was then repeated, only in reverse order (sample 25 through sample one) for the visible and infrared (IR) measurements. At the completion of this sequence, the carousel rotated the samples to the exposed position.

The reflectometer electronic subsystem is shown in Figure 6. The DACS controls the monochromator wavelength and slit width, selects the appropriate detector and lamp, and measures the reflectance values. Phase Sensitive Detection (PSD) techniques are utilized with analog and digital Multiple Time Averaging (MTA) to minimize the effects of stray light, drift, offset,  $1/f$  noise and white noise.<sup>2</sup>

#### TCSE MISSION SUMMARY

The LDEF was placed in low earth orbit by the Shuttle Challenger on April 7, 1984. LDEF was retrieved by the Shuttle on January 12, 1990 after 5 years 10 months in space. The orbit had a 28.5° inclination and an initial altitude of 463 km (250 N mi). The orbit degraded over the 5 year 10 month mission to an altitude of 330 km (178 N mi). This LDEF/TCSE orientation and mission duration provided the following exposure environment for the TCSE:

Total space exposure	5 years 10 months
Atomic oxygen fluence <sup>3</sup>	$8.0 \times 10^{21}$ atoms/cm <sup>2</sup>
Solar UV exposure*	$1.0 \times 10^4$ ESH
Thermal cycles	$3.3 \times 10^4$ cycles
Radiation (at surface) <sup>4</sup>	$3.0 \times 10^5$ rads

When the LDEF was placed in orbit by the Shuttle, a "start" signal was sent by LDEF to the TCSE to engage a relay and turn on the TCSE power. The TCSE was preprogrammed to wait for ten days before exposing the samples to allow the initial outgassing load to diminish. The TCSE was launched aboard the LDEF with the carousel rotated to the "closed" position to protect the samples from ground processing and the launch environment.

On mission day 10, the initial daily and reflectance measurements were performed. The carousel was rotated to the open position to expose all test samples. The daily measurements were repeated every day until mission day 582 (19.5 months) when the TCSE batteries were depleted. The reflectance measurements on

\* Berrios, W.M., Jones, J. and Kinard, W.; "Long Duration Exposure Facility Post-Flight Thermal Analysis, Orbital/Thermal Environment Data Package," NASA LaRC, Hampton, VA, October 3, 1990.

the test samples were repeated once a week for four weeks, then once every two weeks for eight weeks, and finally once a month until battery power was expended. The TCSE batteries were sized to provide a 50% margin of additional energy for the nominal 9-12 month LDEF mission.

The TCSE operated for 582 days before battery depletion. The battery power was finally expended while the sample carousel was being rotated. This left the carousel in a partially closed position. Figure 7 is a photograph taken during the LDEF retrieval operations showing where the carousel rotation stopped. This carousel position caused 35 of the samples to be exposed for the complete LDEF mission (69.2 months), and 14 exposed for only 582 days (19.5 months) and therefore protected from the space environment for the subsequent four years.

#### TCSE SYSTEM PERFORMANCE

The TCSE flight hardware system performed very well during the LDEF mission.<sup>5</sup> A post flight functional test was performed and the TCSE remains functional. A few anomalies have been detected in post-flight data analysis, inspection, and functional tests. The systems analyses performed is only the initial effort required to fully characterize the effects of the long term space exposure. Performance of the TCSE system and operational anomalies discovered to date are described in this section.

#### Recorder

The TCSE data system utilized a Lockheed Electronics Company (LEC) model MIM four-track tape recorder to store the flight data. The flight recorder was removed and handcarried to the Lockheed Electronics Company for transcription of the flight data and an analysis of the condition of the recorder.

Upon opening the recorder it was determined that a relay in the track switching circuit had failed with the wiper on one set of contacts stuck in an in-between state. This condition prevented the relay from receiving additional track switching commands and resulted in the overwriting of one of the three tracks of data collected by the TCSE. The LEC engineers manually energized the relay coil and the relay contact latched properly. This relay and the complete recorder system performed within specification for the check-out tests and flight data playback.

The MIM tape recorder is a four-track unit that records tracks 1 and 3 in the forward direction and tracks 2 and 4 in the reverse direction. At the completion of the TCSE mission, the recorder stopped with the tape positioned near the end of track 1. However, it was determined that track 3 data was written over track 1 data. Because the MIM recorder uses a saturation recording method, track 3 data was recovered. Track 2 data was recovered with no problems. Some track 1 data was apparent in gaps between track 3 data blocks and may be recoverable. This failure and its cause will be investigated further in later studies. The LEC and NASA/LARC personnel provided a very valuable service in this analysis and in the recovery of the TCSE flight data.

The recovered TCSE flight data was decoded and separated into data sets. By

analyzing the clock data in each data set, it was determined that the TCSE operated for 582 days (19.5 months) after IDEF deployment. Data were recovered for the last 421 days of this operational period. The overwriting of track 1 data by the recorder resulted in the loss of data for the first 161 days of the TCSE mission. The recovered data included eleven reflectometry data sets and 421 daily data sets.

### Reflectometer

The analyzed flight data shows the reflectometer performed very well. The measurement repeatability over several months is demonstrated in Figure 8 and is generally within 1 to 2 percent. This excellent performance indicates that sample property changes measured by the TCSE reflectometer were accurate and did occur. Late in the active TCSE mission the reflectometer UV data became noisy. The reflectometer remains functional and operated normally during post-flight testing. The optical data from the functional tests were acceptable from 2500 nm through 500 nm but were suspect below 500 nm.<sup>5</sup> Further tests are performed to better characterize the condition of the reflectometer.

### Batteries

Four standard lithium range safety batteries were used to power the TCSE. These batteries were developed for the Shuttle Solid Rocket Booster (SRB) range safety system. The batteries were selected based on their high energy density and ready availability at MSFC. These batteries had a predicted life of greater than 15 months from calculated power requirements. The actual battery life extended through 582 mission days (19.5 months). Each battery was rated at 28 Volts Direct Current (VDC) and self-contained in a two-part Nylafil case. An ethylene propylene o-ring was used to seal the case. Due to the characteristics of the lithium electrolyte, each cell was designed to vent into the cavity when overpressurization occurred. During an overpressurization condition, a small diaphragm on each cell balloons out and is pricked by a metal pin to relieve pressure. The escaping gas is then contained within the Nylafil case by the ethylene propylene o-ring.

During the initial post-flight deintegration, a noticeable odor was evident inside the TCSE. The source of odor from inside the TCSE was identified as the electrolyte from the lithium batteries. The batteries were removed from the TCSE and bagged. Each of the four batteries in the TCSE had this odor. One battery was cut open to check the cell diaphragms and the battery o-ring. All cells had vented, noted by punctured diaphragms. In addition, the battery o-ring had a complete compression set allowing the electrolyte gas to escape from the batteries.

Flight data revealed the battery temperatures ranged from 13 to 27°C and the voltage ranged from a nominal 36 Volts at the start of the mission to 25 Volts at battery depletion.

## Sample Carousel

Post-flight analyses of the recorded TCSE data show that the carousel subsystem operated as designed most of the time, but indicate an intermittent rotational problem. From the recorded flight data, the carousel drive mechanism experienced some difficulty in rotating reliably from sample position 25 to sample 24 during the reflectance measurements. This difficulty appeared to be more prominent towards the end of the useful battery life. This problem was investigated briefly during a post-flight function check-out test. Attempts were made to simulate the problem by adjusting the battery supply voltage (and energy levels) from 28 to 21 volts as well as energizing the lamps and other components of the reflectometer subsystem to simulate increased energy requirements on the power system. Unfortunately, the carousel rotation anomaly could not be reproduced in these initial ground tests. All other post-flight carousel functional tests were nominal.

## Data Acquisition and Control System

The initial analysis of the TCSE flight data shows that the DACS performed very well during the active TCSE mission. Post-flight functional tests show that the DACS remains functional after the extended dormant period in space. The clock data on each recorded data buffer showed that the DACS started a measurement sequence precisely on 24 hour increments as measured by the TCSE clock. The daily sequence was repeated for 582 days until the batteries were depleted. Because of the recorder malfunction, only 421 days of data were recovered.

The data from the post-flight functional tests were analyzed to check the condition of the analog measurement system. There were five reference channels among the 64 analog channels. These provided a calibration for thermistors and platinum thermometers. The values of these readings depend on current sources in the measurement circuits, precision reference resistors, scaling amplifiers, and the A-D converter. For four of these reference channels, the range of values measured over the two hour test exactly matched the pre-flight and in-flight values. The fifth measurement was off one count in 900 or just over 0.1%. This test verified that the analog measurement system remains within design specifications.

Only one anomaly has been observed in the DACS operation. The 25th clock bit appeared to be set to a logical "1" too early and remained in that condition throughout the mission. This bit was also set to "1" during the post-flight testing -- indicating a failure. This condition was not a problem in the data analysis because the sequential nature of the data allowed recovery of the full clock data.

## Thermal

The TCSE thermal design and analysis considered worse case conditions for the LDEF and TCSE mission. Some yaw (x-axis) instability was expected for the gravity-gradient stabilized LDEF and was considered in the thermal analysis. This resulted

in wide variations in the predicted temperatures of the TCSE. However, little yaw occurred, and the satellite proved to be very stable--resulting in moderate temperatures.

The TCSE used 2 mil silver Teflon as the outside (exposed) surface coating and black painted aluminum for inside and back surfaces. The top cover (shroud) was thermally isolated from the TCSE structure. The TCSE was thermally coupled to the LDEF structure for passive thermal control, and was dependent upon this environment for thermal stability.

The temperatures of selective components on the TCSE were monitored throughout the active TCSE mission. Figure 9 compares predicted data to measured data for selected components. The measured data temperature ranges represent the lowest and highest temperatures recorded by any of the applicable sensors. Figures 10-12 represent typical daily thermal excursions experienced by selected TCSE components.

#### SUMMARY

The performance of the TCSE flight system on the LDEF was excellent. The few anomalies that were experienced did not prevent the TCSE from meeting its design and experimental goals. The performance of the TCSE confirms that low cost, complex experiment packages can be developed that perform well in space. There remains much to learn from the TCSE hardware about the effects of long term space exposure on systems. This initial analysis only begins the process to derive these benefits from the TCSE.

#### REFERENCES

1. Reichard, Penelope J. and Triolo, J.J.; "Pre-flight Testing of the ATS-1 Thermal Coating Experiment." Proc. of the AIAA Thermophysics Specialist Conference, AIAA Paper 67-333, April 17-20, 1967.
2. Wilmhurst, T.H.; "Signal Recovery from Noise in Electronic Instrumentation." Adam Hilger Ltd, 1981.
3. Bourassa, R.J. and Gillis, J.R.; "Atomic Oxygen Flux and Fluence Calculation for Long Duration Exposure Facility (LDEF) LDEF Supporting Data," Contract NAS1-18224, January 1991.
4. Benton, E.V. and Heinrich, W.; "Ionizing Radiation Exposure of LDEF", University of San Francisco Report USF-TR-77, August 1990.
5. Wilkes, D.R. and Hummer, L.L.; "Thermal Control Surfaces Experiment Initial Flight Data Analysis," Final Report for Contract NAS8-36288; AZ Technology Report No.: 90-1-100-2, June 1991.

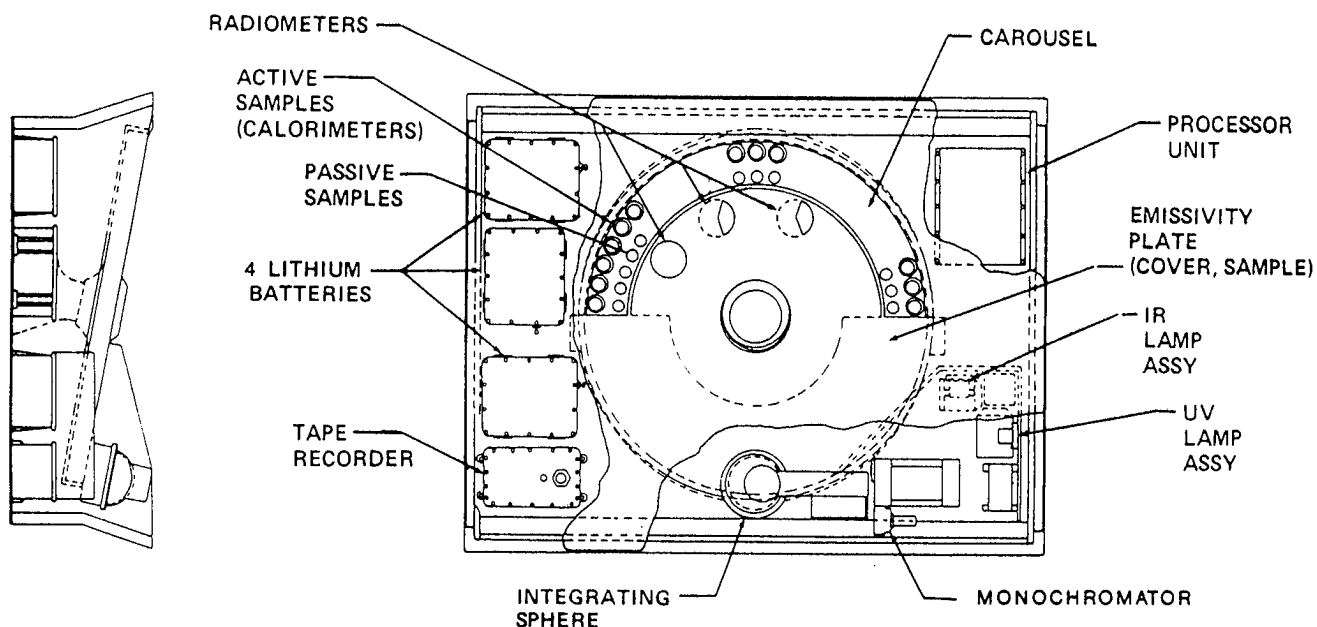


Figure 1 - TCSE Assembly

Size	1.24m x .84m x .30m (48.75 x 33 x 12 in.)
Weight	80.5kg (177 Pounds)
System Controller	1802 MicroProcessor
Battery Capacity	72 Amp Hours at 28 VDC
Data Recorder	Lockheed 4200
-Capacity	54 x 10 <sup>6</sup> Bits
Reflectometer	
-Wavelength Range	250 to 2500 nm
-Wavelength Resolution ( $\Delta\lambda/\lambda$ )	$\leq 5\%$
-Reflectance Accuracy	2%
-Reflectance Repeatability	1%
Calorimetric Measurements	
-Solar Absorptance	Accuracy - 5%
-Total Emittance	Accuracy - 5%

Figure 2 - TCSE Flight Hardware Specifications



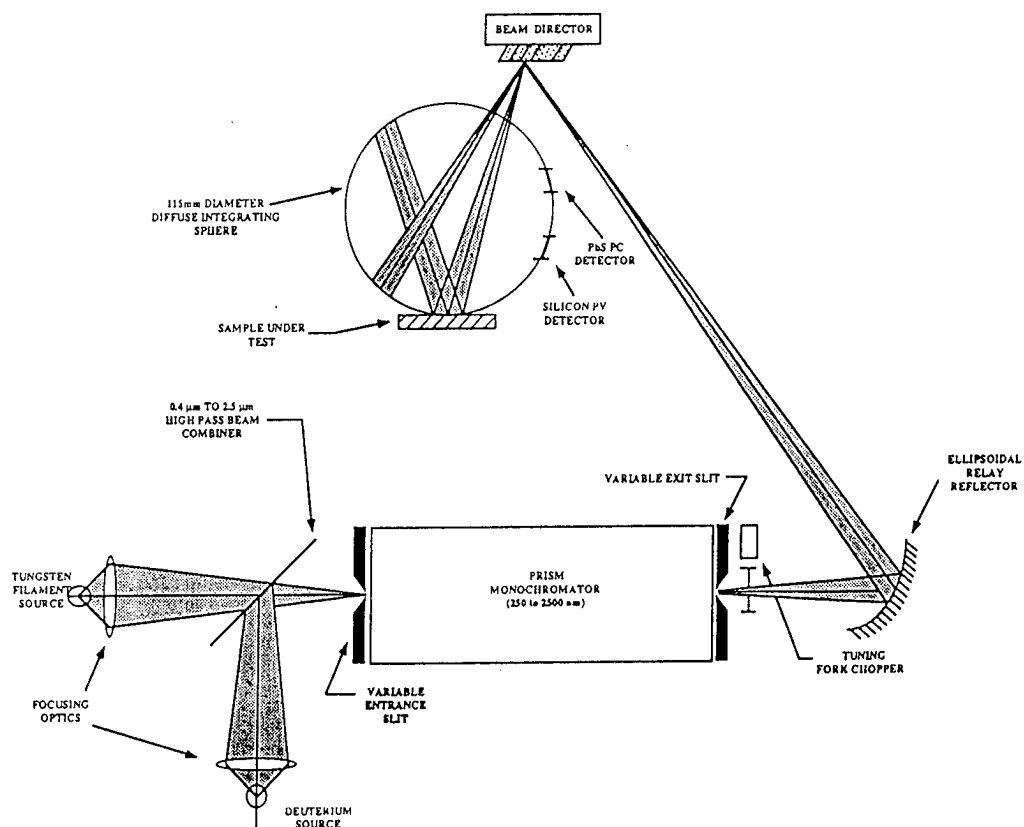


Figure 3 - Reflectometer Optical Schematic

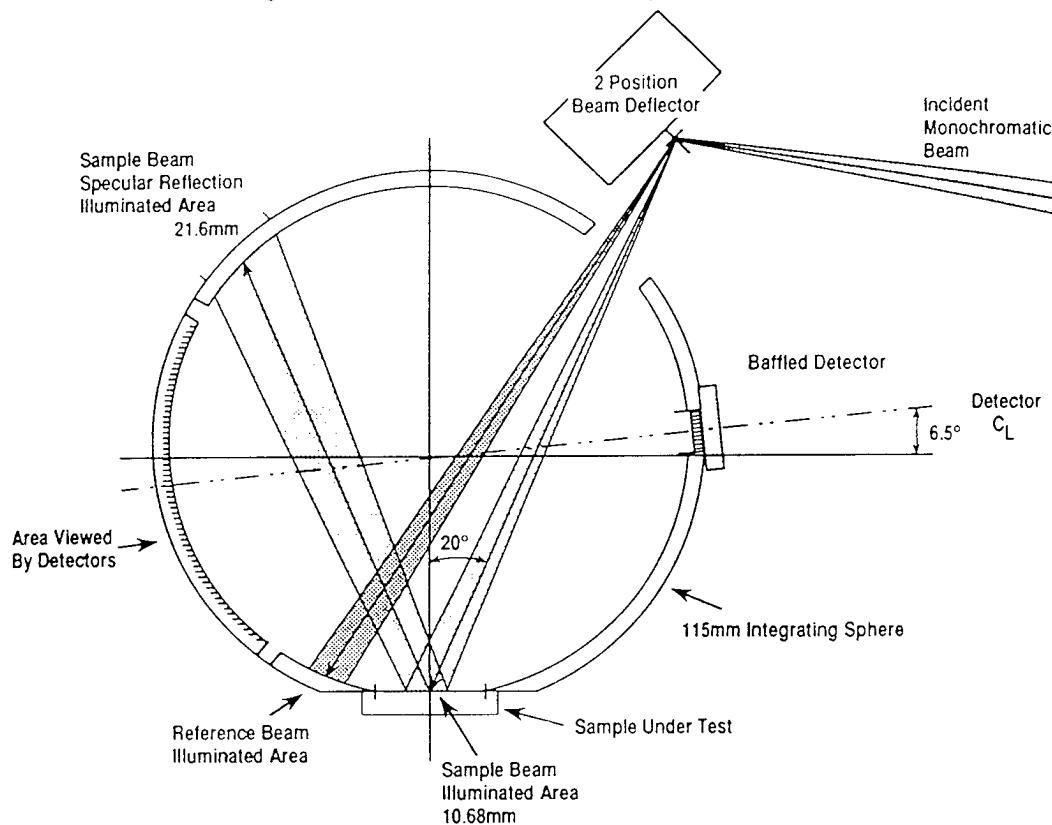


Figure 4 - Integrating Sphere Geometry

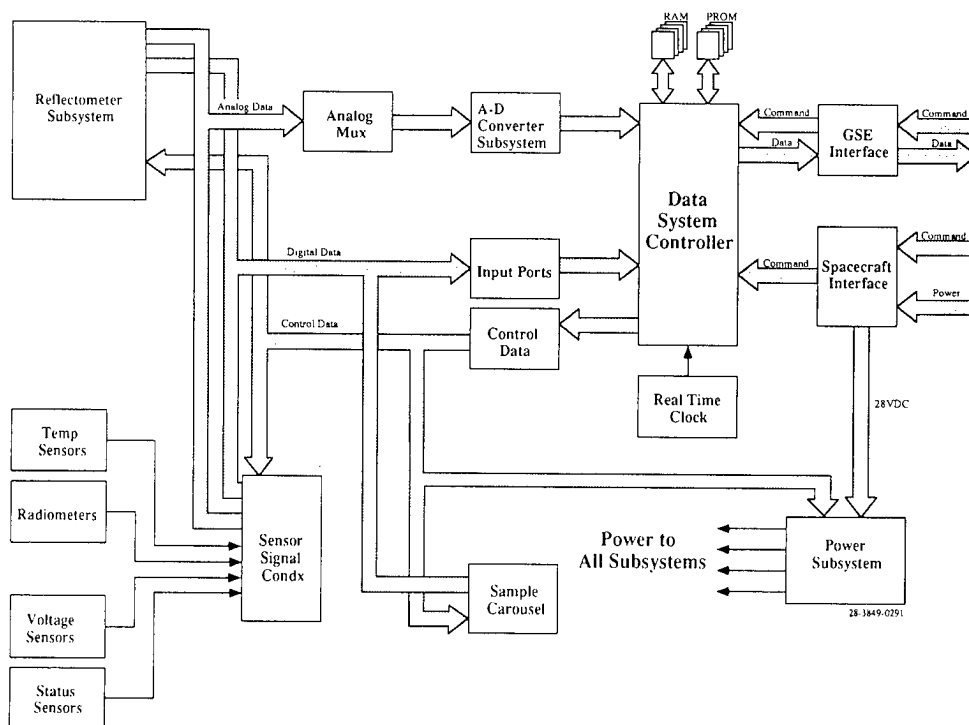


Figure 5 - TCSE Data and Control System

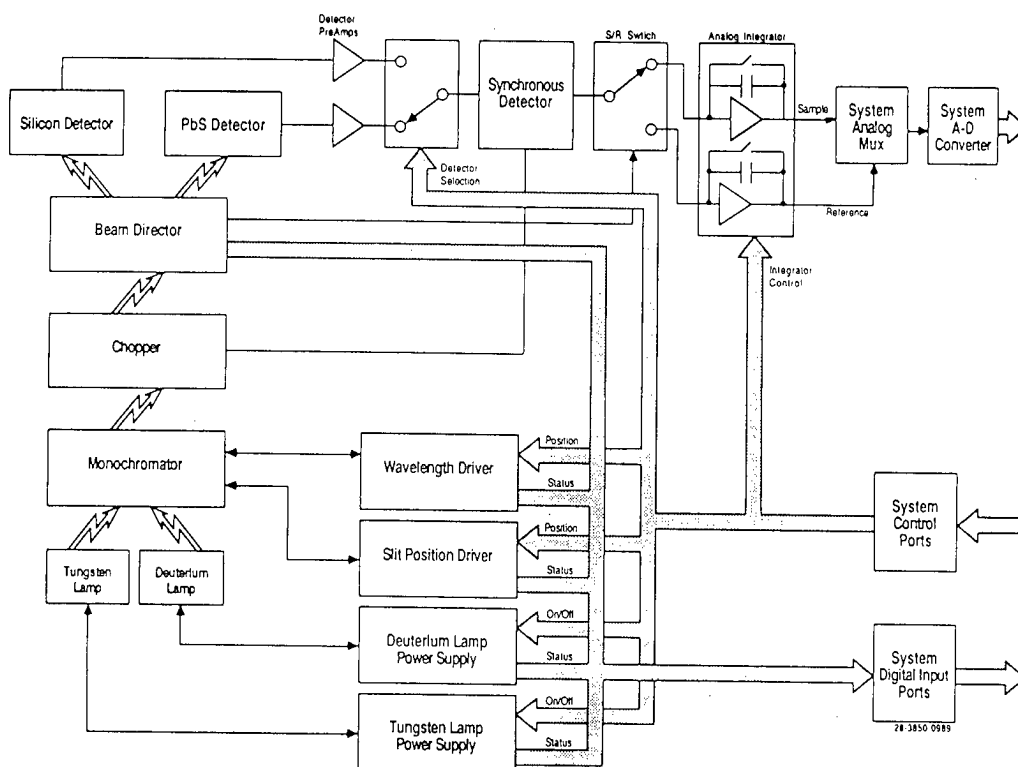


Figure 6 - TCSE Reflectometer Subsystem

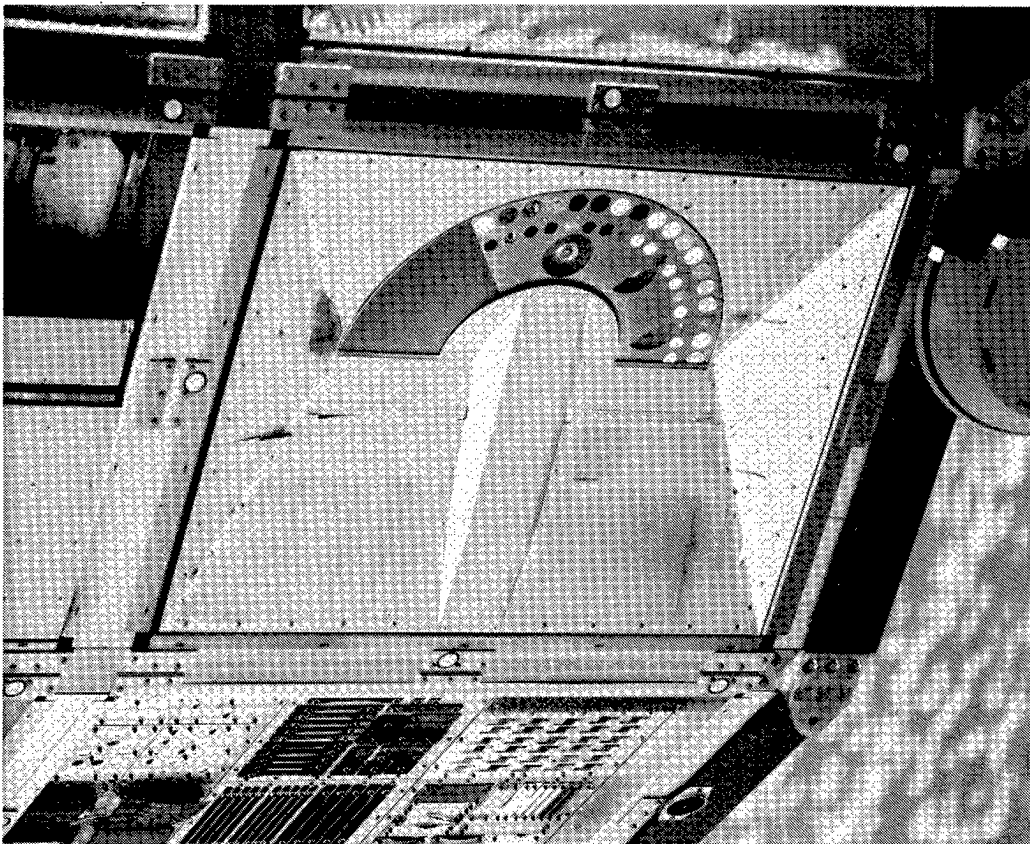


Figure 7 - TCSE Condition during LDEF Retrieval

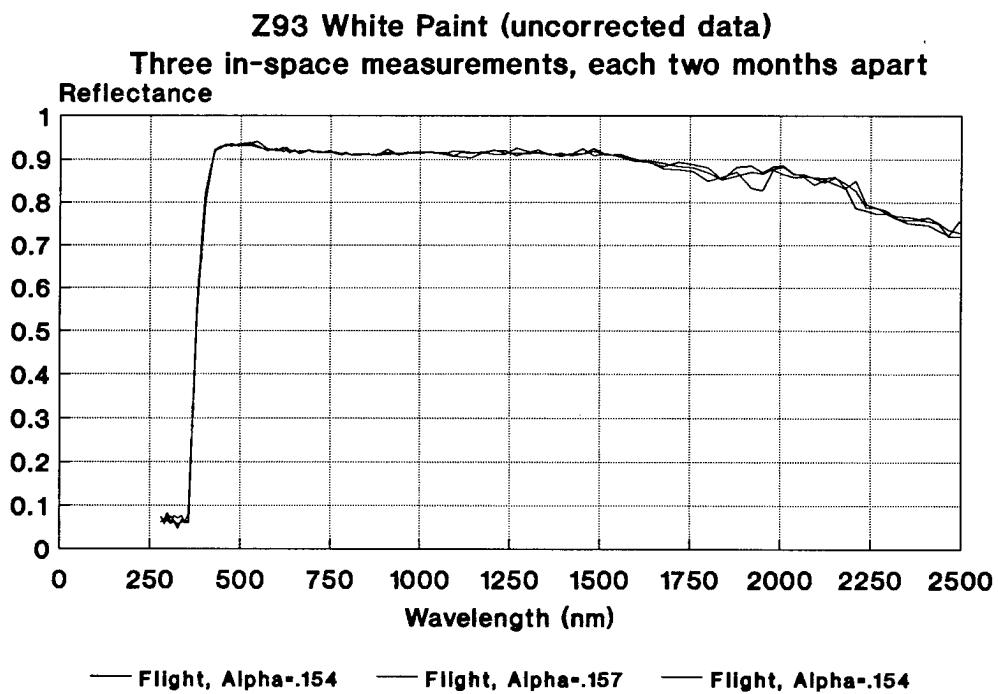


Figure 8 - Flight Reflectometer Performance

Component	Predicted Temp. Limit		Measured Temp. Limit *	
	Min (°C)	Max (°C)	Min (°C)	Max (°C)
Integrating Sphere	-25	41	6	19
Batteries	-23	43	13	27
Electronics (DACS)	-27	41	17	29
Emissivity Plate	-25	40	-2	17
Radiometers			14	39
Passive Sample Hldrs.			15	43
Shroud (Front Cover)			-43	5

\* Preliminary Data

Figure 9 - TCSE Predicted vs. Measured Thermal Data

### TCSE Daily Flight Data Battery #1 Temperature

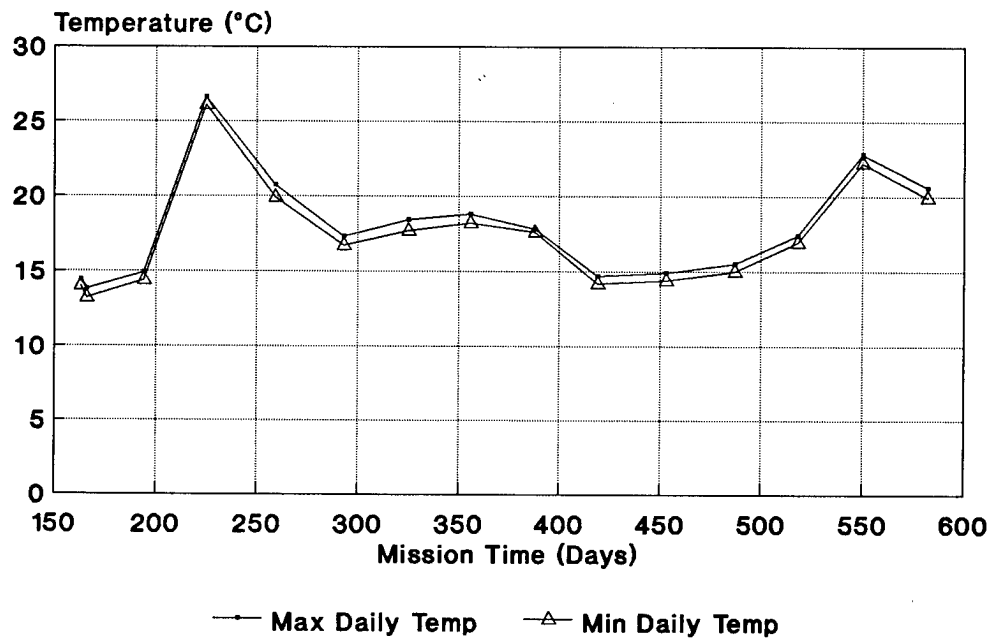


Figure 10 - Battery Temperature

### TCSE Daily Flight Data Microprocessor Crystal Temperature

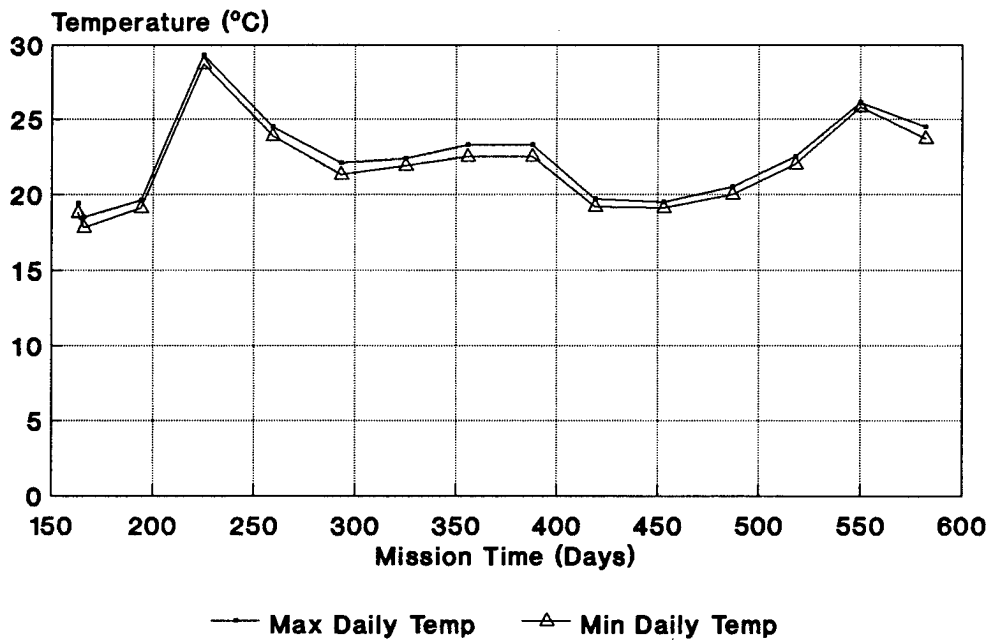


Figure 11 - DACS Internal Temperature

### TCSE Daily Flight Data Front Cover Temperature #3

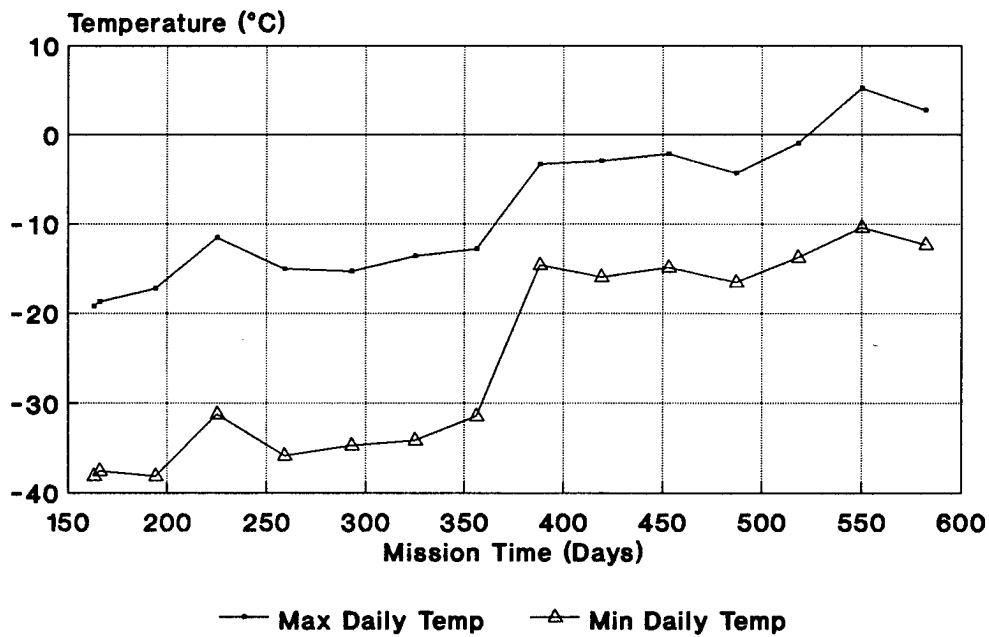


Figure 12 - Front Cover Temperature

## FRENCH COOPERATIVE PASSIVE PAYLOAD (FRECOA)

### SYSTEM RESULTS

Christian Durin  
CNES RA-DP EQ/QM  
18, av E. Belin Toulouse FRANCE  
Phone (33) 61 28 14 39 Fax (33) 61 27 47 32

### SUMMARY

The fact that the Long Duration Exposure Facility (LDEF) satellite mission was extended resulted in CNES forming a group of experts to study FRECOA system elements. These tests were run on materials, electronics, wiring and motors-drives. It is worthwhile studying these elements as they have been exposed to the low earth orbit (LEO) for nearly six years whereas the experimental specimens were exposed for ten months.

### INTRODUCTION

I'll begin this paper by presenting FRECOA and the objectives of the experiments. Next, the laboratories which worked with us, and a list of the materials studied will be discussed. This will be followed by preliminary results observed before de-integration and then a four point synthesis. The first of these is working order tests, mechanism, electronic and materials behaviour. The second is physical and chemical ageing. The third is damage induced by impacts and erosion and the fourth is contamination by material outgassing. I'll finish with the work in progress and the conclusion at the present time.

### FRECOA Presentation

FRECOA was located on the trailing edge (tray B3) of LDEF. Its environment was comprised of numerous thermal cycles, about 34000 orbits from - 22 C° to 66 C°. The exterior surface saw a low atomic oxygen flux, compared to the leading face, low electron and proton quantities and ultra violet radiation. We also had a very good vacuum (trailing effect) and numerous micro-meteoroids and space debris impacts.

### The Objectives

We are trying to determine the effects of space environment on FRECOA system materials and components including the effect of pollution and ageing, six years of life versus one as planned and also, to give a ruling on the use of components and materials not especially made for space projects.

## The Laboratories

Many of the appraisals were performed in our facilities in CNES (Toulouse). But for some special jobs, we worked with industrials, universities and with manufacturers who ran particular tests on their materials.

### Mechanical system configuration

Three canisters contain the experiments. A view of the canister in the closed position is shown in Figure 1. Each canister is made of an aluminium alloy and a butyl seal bonded to one of the face-plates provides vacuum tightness. The support structure is used for mounting the canisters and the open/close mechanism. It supports 4 locking arms which through DELRIN® rollers provide a compression force on the seal of the canister in the closed position. This adjustable force thanks to metallic elastic SCHNORR type washers contributes to the mechanical cohesion during the ground storage period, the launch and return phases. The open and close mechanism consists of one step motor driving two screw-nut bolts by means of a double six-stage reduction gear chain. The up or down movement opens or closes the canister. An aluminium rigid shield is also used to protect the butyl seal in the open position, and numerous metallic fasteners and non-metallic fixtures are used as glues and velcro tapes to adhere the thermal blankets. To protect it, the support structure is anodized and we use alodine on the rigid shield.

### Thermal system configuration

Two superisolations (MLI) are used on the battery sets. On top are two thermal shields in teflon glass fabric with aluminized MYLAR® sheet. Below four thermal blankets are used with the same composition but with a black painted aluminized MYLAR® face.

### Electrical system configuration

The electronic unit is composed of a timer providing open and close commands at programmed times and a motor-drive unit supplying the motor in either the forward or reverse direction. The timer is continuously powered by a 7.5 volt battery during the in-orbit mission. The time base is provided by a 2 KHz Rc oscillator followed by two divide-by-2<sup>14</sup> circuits. CMOS reliable technology is used to meet the low consumption requirements. The motor-drive unit includes voltage regulators, a current limiter, a power driver and a step counter. It is only powered during the open/close sequences. The power supply for the LDEF mission is 28 Volt and 7.5 Volt Li/SO<sub>2</sub> type batteries specially developed by NASA.

An exploded view of FRECOPA is shown in Figure 2.

## Preliminary results

During observations at KSC and before FRECOPA de-integration in CNES we noted very good system behaviour and the status indicators showed opening and closing of the three canisters. If we observe the pictures taken before and after flight, we can see very large cracks and several smaller tears on the MYLAR® of the thermal blankets and many color changes for exposed materials, alodine from the rigid shields, anodization of the main structure (two views in Figure 3 & 4), DELRIN® rollers, MYLAR® and on the velcro tapes. We can also see three impacts with the big one through a rigid shield with a thickness of 0.8 mm. Another highly interesting phenomenon is the shadow of a canister observed on only one side of the tray. We can explain this by the outgassing of polymeric materials under thermal cycling, condensation on cold surfaces during the night and polymerization at sunrise under UV radiation on the surfaces which are the most quickly heated (a view is given in Figure 5).

### Synthesis 1: Working order tests

On the subject of the kinematic chain, we noted no cold welding, no resistant torques (no sticking) when we opened the canisters, the step motors were still in good condition and during disassembly all screw torques were nominal. We concluded that it exhibited very good behaviour in space environment.

Now, about the electronic chain, we observed that the functions time divisor open and close order were nominal both on reference and flight samples. Current was the same as during integration tests. Electrical tests (continuity, isolation, contact resistance) were performed on the complete harness and no anomalies were observed. So all the electronic and wiring developed in 1978 is still operating correctly in 1991.

For pressure inside the canisters it can be said that before flight, initial pressure was 0.66 mBar equivalent nitrogen. And after flight, canister 3; 1.6 mBar, canister 4; 4.1 mBar, Canister 5; 4.5  $10^{-2}$  mBar. It's important to note that canisters 3 and 4 contained polymeric materials. Our hypothesis for explaining this difference is the outgassing of materials and/or seal leakage. Additional studies are required.

### Synthesis 2: Ageing

#### Physical ageing

We ran tension tests on rigid shields, MLI, NOMEX® thread, contact insertion for connectors and wiring. We noted no significant variations. For teflon glass fabric, we measured a decrease of 10% in tensile strength probably caused by thickness variations, no change in Young modulus. For MYLAR® from the upper shields we couldn't perform tests because it was very brittle. All tests were run on both flight and reference samples which were stored in laboratory conditions.

As far as thermal and optical properties are concerned we found, for flexible shields (MYLAR® and teflon glass fabric) no significant variation in infra red emission, an increase of 20% in solar absorption induced by the erosion of teflon matrix and a decrease in transparency for teflon glass fabric. For alodine on rigid shields, no significant variations of I.R. emission, an increase of 15% in absorption induced by pollution and ageing on the "space" face. For MYLAR®, there was an increase of 53% in solar absorption caused by complete change of material and a low increase in I.R. emission.



Now the results of thermo-mechanical analysis. For Solithane 113 from the electronic units, there were no significant variations. For MYLAR from the MLI and from the thermal blankets there was an increase of 30% in the thermal expansion coefficient. On the other hand there was a decrease of 30% in C.T.E. for the teflon glass fabric.

#### Chemical ageing

We used differential scanning calorimetry to evaluate the change in transition temperature. For teflon glass fabric, DELRIN®, Solithane 113, no significant variations were observed. For MYLAR® there was a decrease of 4% in the melting point. For Nomex thread an increase of 12.5 % in glass transition temperature was observed.

In conclusion, for physical ageing we observed some significant variations particularly for thermal and optical properties. For chemical ageing, low variations were observed. Parameters of the damage were primarily U.V. radiation and thermal cycling.

### Synthesis 3: Damage

#### Impacts

We observed about 90 impacts per square meter of more than 50  $\mu\text{m}$  and maximum diameter was 1.6 mm through a rigid shield. We also observed some impacts on the thermal blankets with breaking of the glass fibers and some delamination around the crater. A view of an impact on a rigid shield is given in Figure 6.

#### Erosion

We observed erosion on the teflon glass fabric. At the fabric node, the teflon matrix was absent and the glass fibers were bare (a view is given Figure 7). We estimated damage to be about 10  $\mu\text{m}$ . In the inter-fiber area, there were many cracks and the matrix was frothy (a view is given Figure 8). For DELRIN® about 30  $\mu\text{m}$  of erosion was measured in the exposed area (a view is given Figure 9).

In conclusion no functional damage was induced by impacts and there were no electrical or mechanical system failures. Erosion caused a decrease in optical and mechanical properties and a possibility of malfunctions for many uses in particular for the DELRIN®. With the low atomic oxygen flux, we think that these erosions were induced by U.V. radiation and thermal cycling which damaged polymeric materials through the scission of molecular chains.

### Synthesis 4: Contamination

We used analytical facilities such as X-RAY analysis, E.S.C.A. (electron spectroscopy for chemical analysis) and R.B.S. (Rutherford back scattering). We found, for MYLAR®, teflon glass fabric, teflon buttons and DELRIN, no significant pollution. For Nomex thread and velcro tapes a pollution induced by C, O, Si, F and trace of Sn was observed. For silvered bolts an oxidation, S and Sn was observed.

In conclusion, damage was induced by the outgassing of polymeric materials under thermal conditions. The probable origin of pollutions was Si from seals and painting, F from teflon glass fabric, Sn from electronic units (soldering) and S from atmospheric pollution or perhaps leakage from the LiSO<sub>2</sub> battery. When we observed LDEF, we noticed that there was a high quantity of outgassing and pollution from other experiments.

### Work in progress

We are currently working on butyl seal ageing. We are studying thermal and optical properties of coatings. We are running mechanical tests on Velcro tapes. We are studying contamination in canisters and during storage. We are trying out new facilities such as F.T.I.R. and R.B.S. on organic materials. Simulation shall be performed using U.V radiation, thermal cycling and vacuum on DELRIN®, teflon glass fabric, nomex thread and MYLAR® to evaluate the importance of these parameters. We are appraising kinematic chain and solders of the main structure. We are trying to correlate with previous works on materials ageing and we would like to exchange materials and results with other SIG members.

### CONCLUSIONS

First, we are very happy with the correct behaviour of the mechanism, materials and the low cost components. We have observed no functional damage induced by impacts or erosion. A decrease in thermal, optical and mechanical properties for DELRIN® and teflon glass fabric induced by erosion and thermal environment has been observed. The most important damage parameters in our situation are U.V. radiation and thermal cycling. We also noted a contamination by SI and F. We can now say that through these experiments we have a better idea of the real damage of materials and components in a space environment (L.E.O.), and we have new information to introduce in material data banks for future space projects.

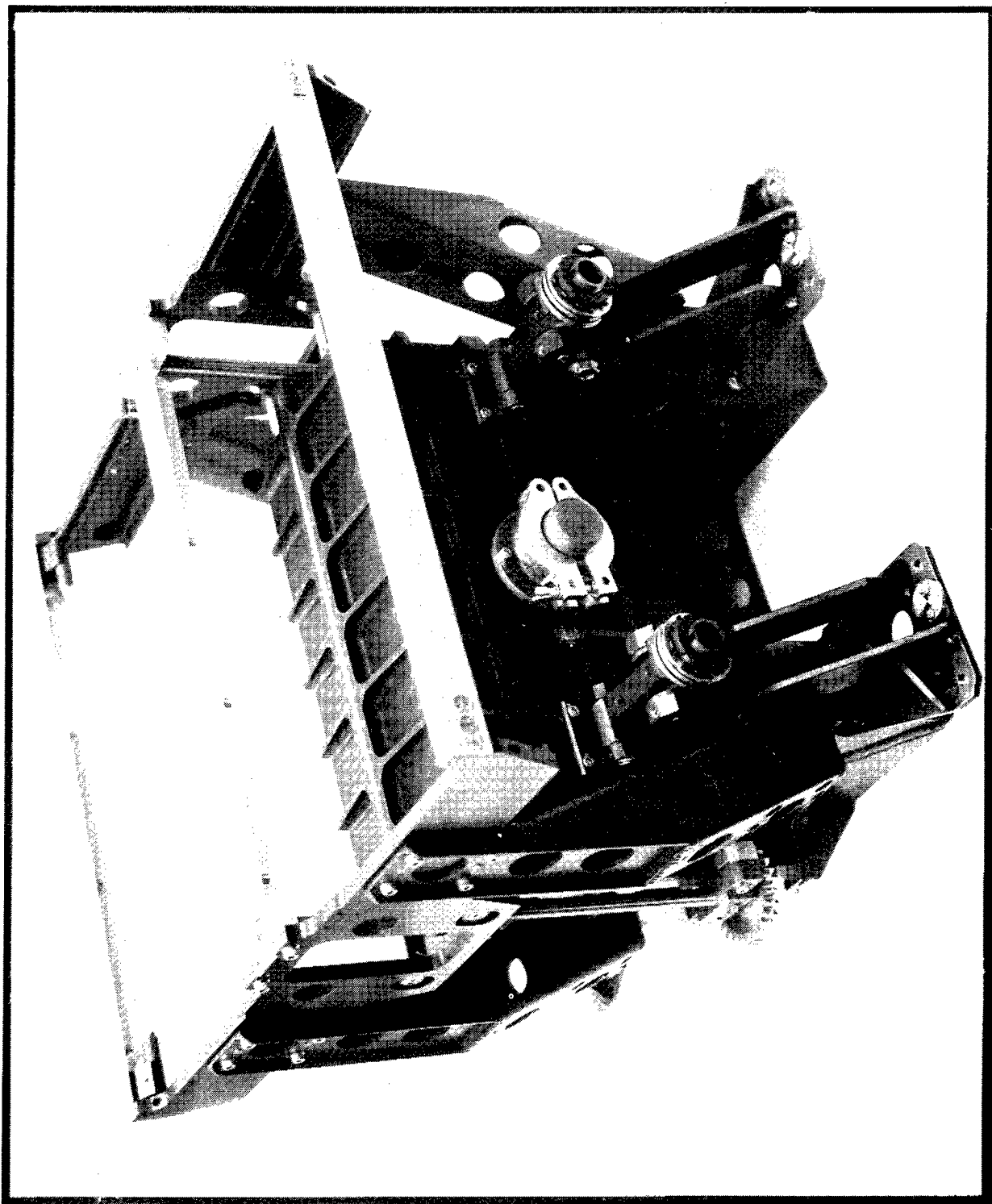


**Fig. 1. FRECOA CANISTER IN CLOSED POSITION**

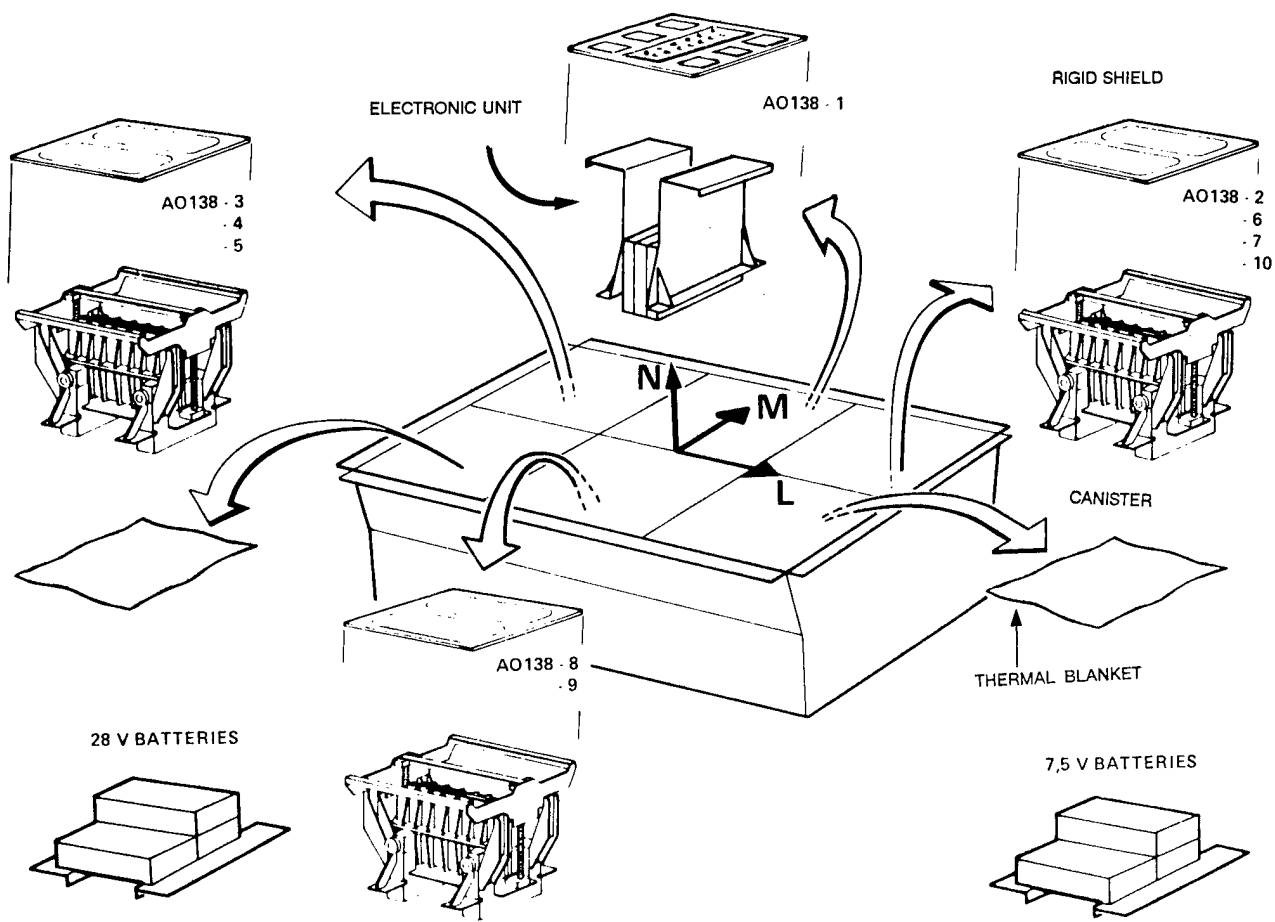
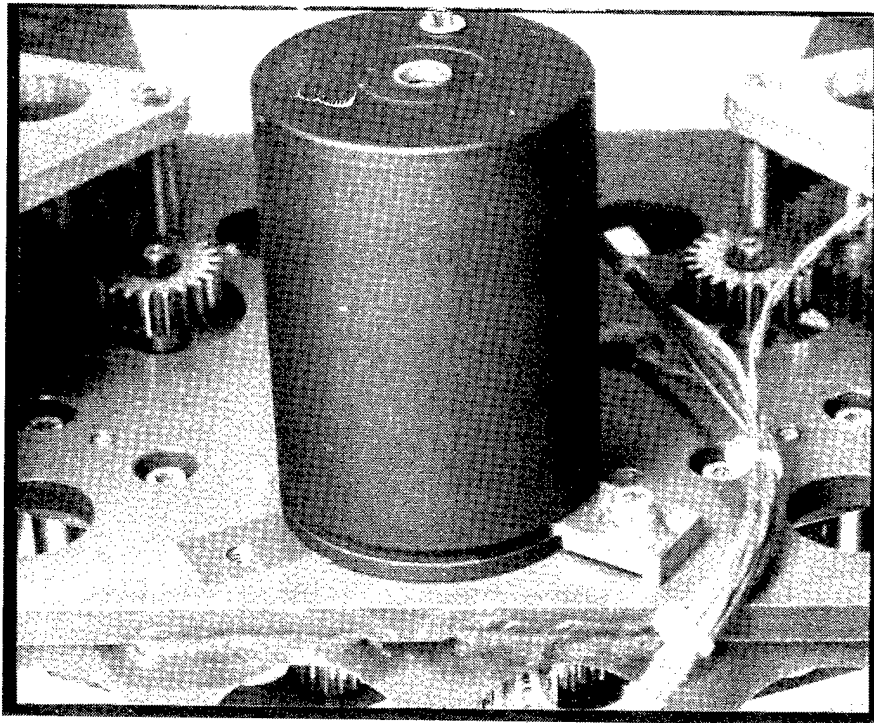
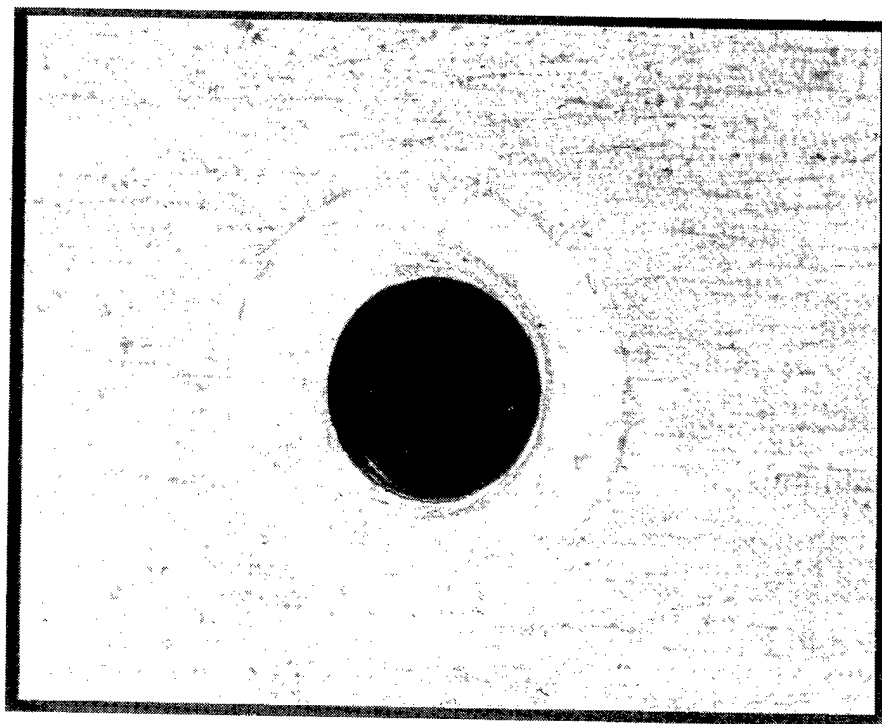


**Fig. 2. EXPLODED VIEW OF FRECOPA EXPERIMENTS AO-138**



Decoloration on main structure



Alodine on rigid shield

**Fig. 3. VISUAL OBSERVATIONS**

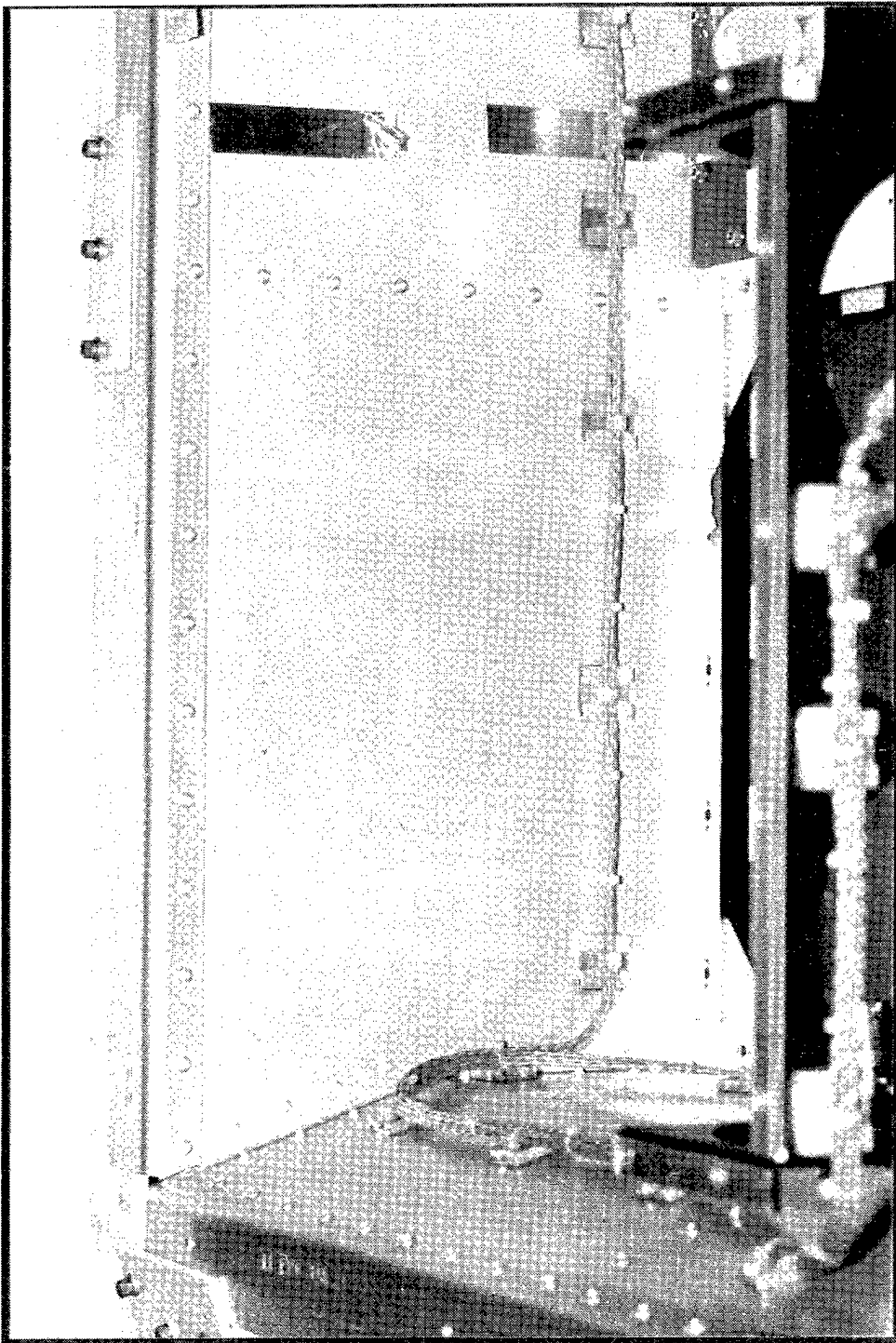
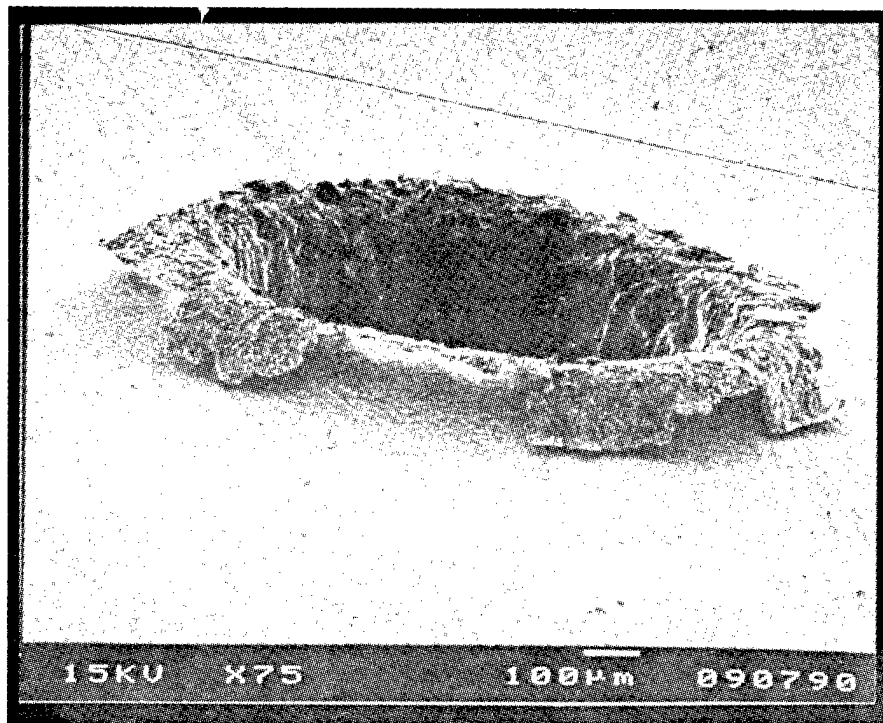
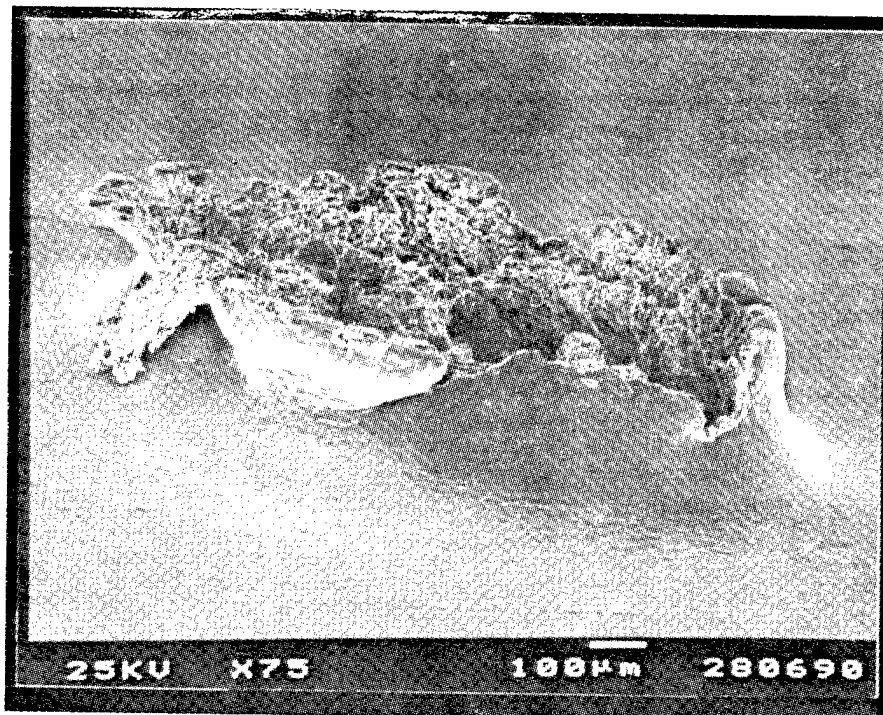


**Fig. 4. SHADOW OF A CANISTER ON THE TRAY**

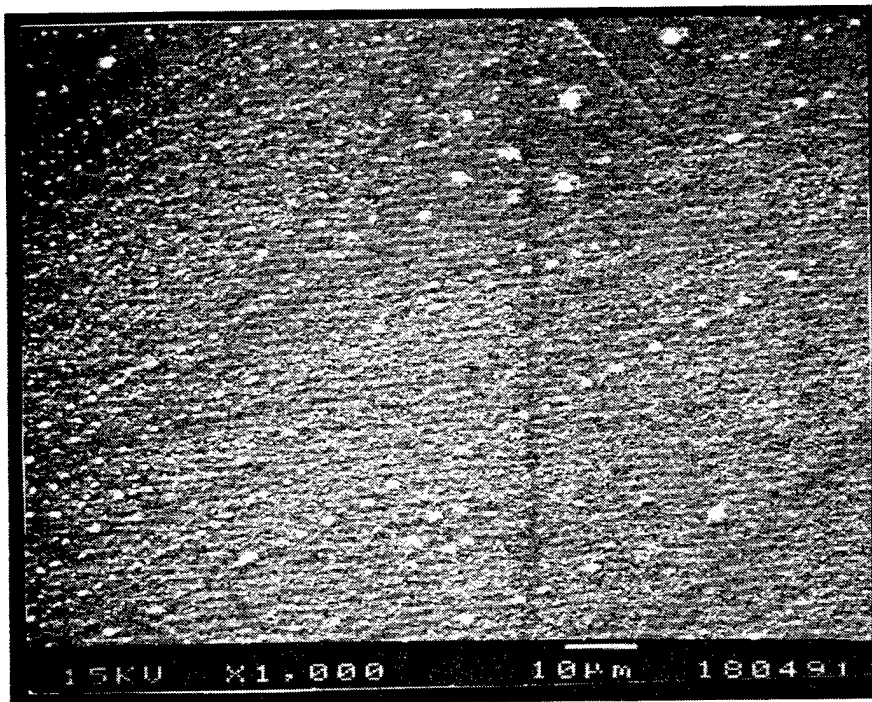


Front face



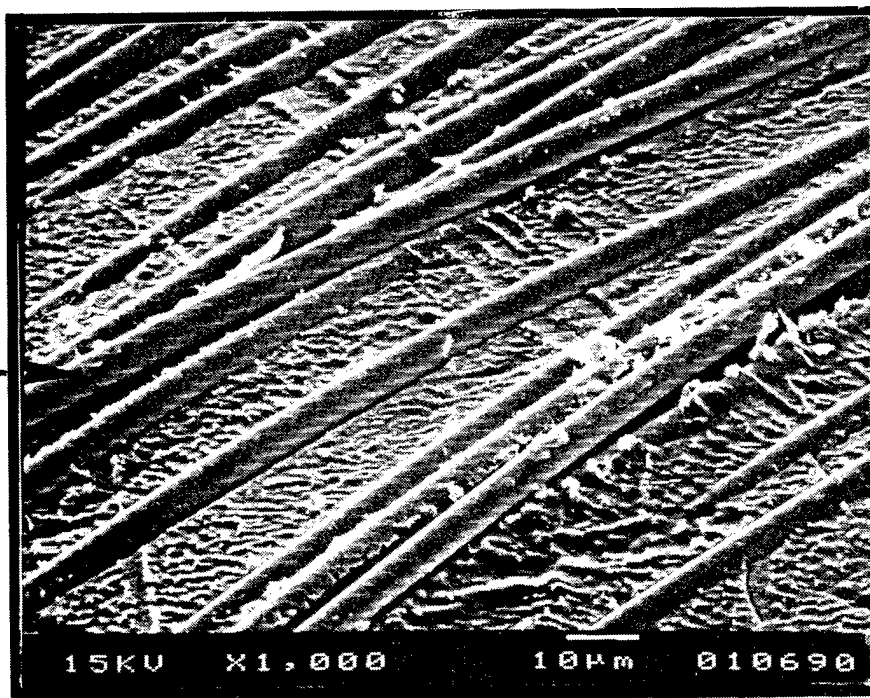
Back face

**Fig. 5. IMPACTS N°7 ON RIGID SHIELD (A1)**  
**ELECTRONIC MICROSCOPY (SEM)**



Reference sample

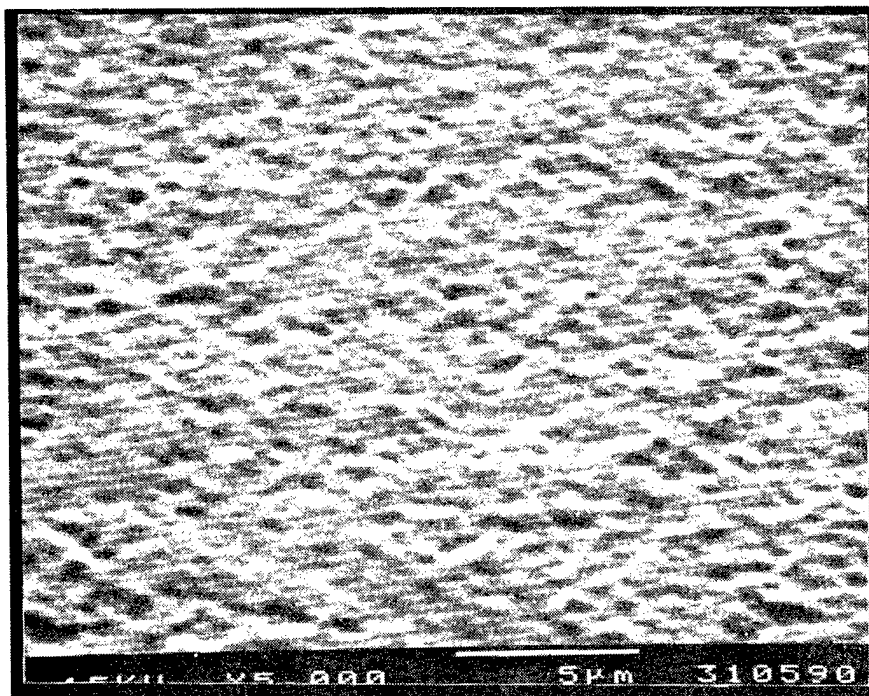
glass fiber —



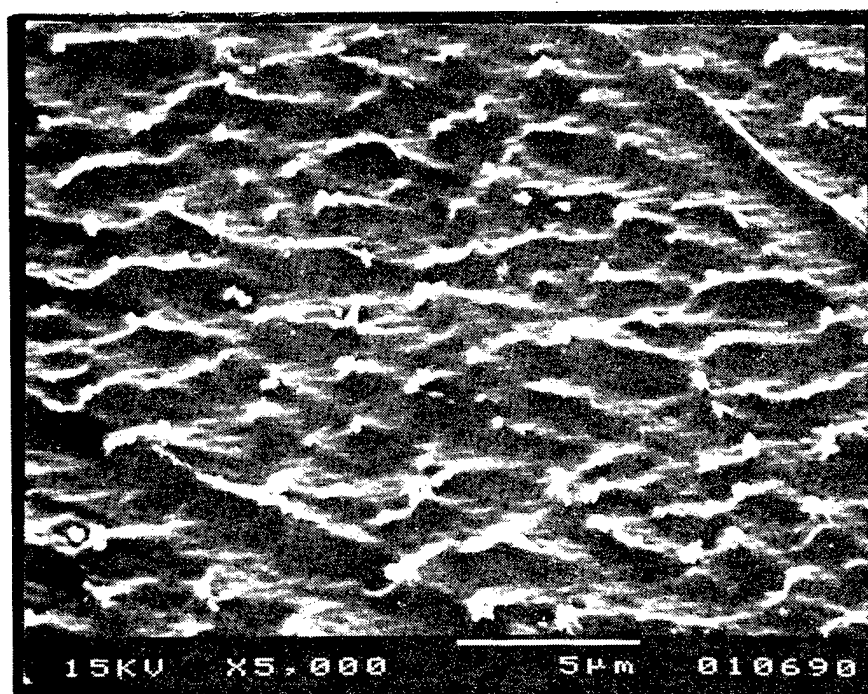
Flight sample

**Fig. 6. RESULTS OF ELECTRONIC MICROSCOPY (SEM)**



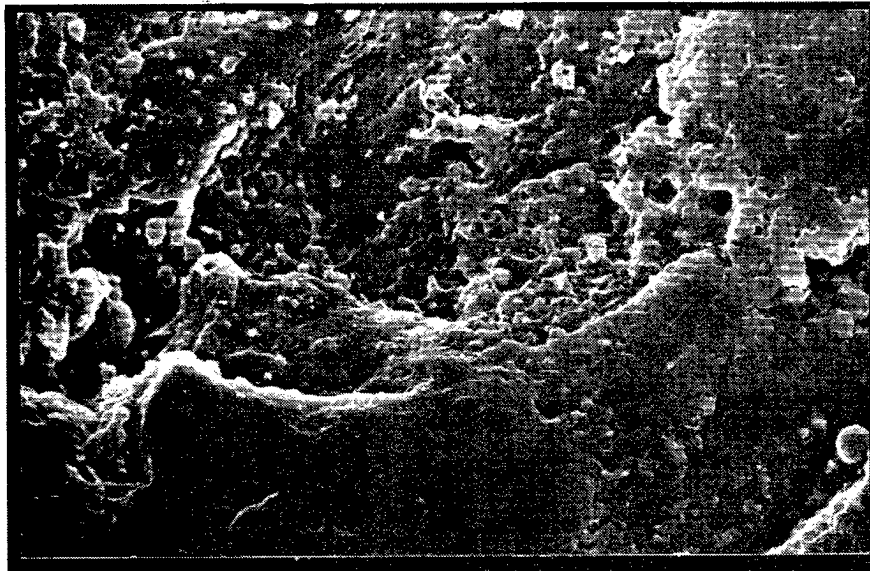


Reference sample



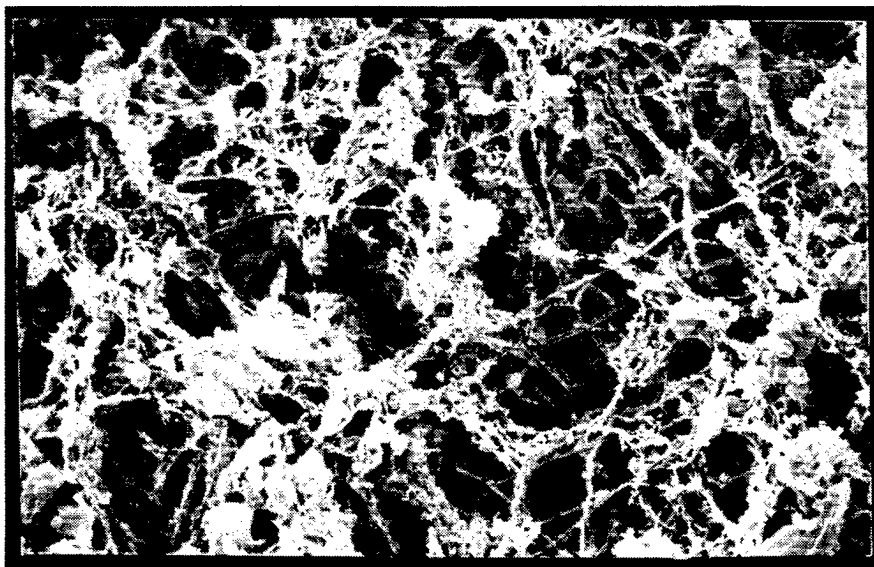
Flight sample

**Fig. 7. RESULTS OF ELECTRONIC MICROSCOPY (SEM)  
area inter fibers**



SCALE: 10  $\mu\text{m}$

Reference sample



Flight sample (exposed area)

**Fig. 8. RESULTS OF ELECTRONIC MICROSCOPY (SEM)**  
area inter fiber

EFFECTS OF ULTRA-VACUUM AND SPACE ENVIRONMENT  
ON CONTACT OHMIC RESISTANCE  
LDEF EXPERIMENT AO 138-11

Jean-Pierre Assié

Aérospatiale

Space and Strategic Systems Division

06322 Cannes-la-Bocca, France

Phone: (33) 92 92 72 49, Fax: (33) 92 92 71 90

Alfred Perotto

Aérospatiale

Space and Strategic Systems Division

06322 Cannes-la-Bocca, France

Phone: (33) 92 92 72 00, Fax: (33) 92 92 71 90

### SUMMARY

The FRECOPA experimentation of chemical resistance of electrical connector contacts, as described in this paper, has evidenced the detrimental time variations of nickel-plated conductors and gilded copper contacts, irrespective of crimping storage or metal-peening conditions.

With a view to reorient aluminum technology a silvered aluminum conductor/gilded aluminum contact solution has been evaluated.

### INTRODUCTION

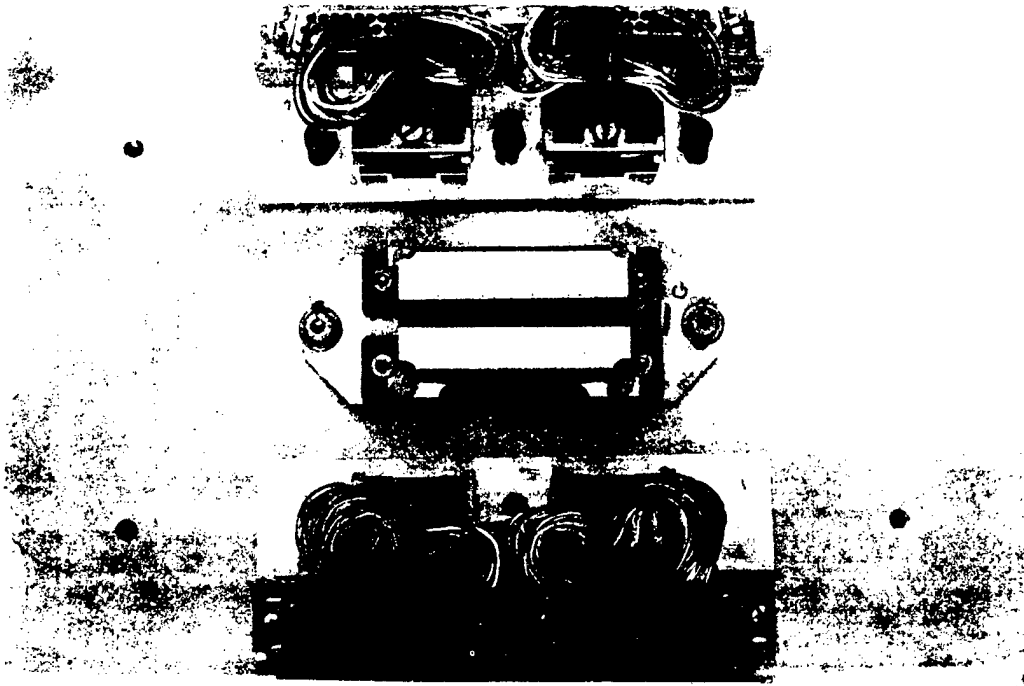
This paper presents an experiment within the framework of the FRECOPA project on chemical resistance of electrical connector contacts.

The experiment was aimed at checking compatibility of aluminum conductors with conventional conductors and contacts under different conditions of production (mechanical or magnetostrictive crimping) and storage (laboratory or long-duration space vacuum)

The objective is to optimize weight of spaceborne harness/wiring using aluminum conductors.

The test approach consists in comparative, pre- and post-flight measurement of on-ground and flight samples.

## GENERAL CONDITIONS OF THE EXPERIMENT

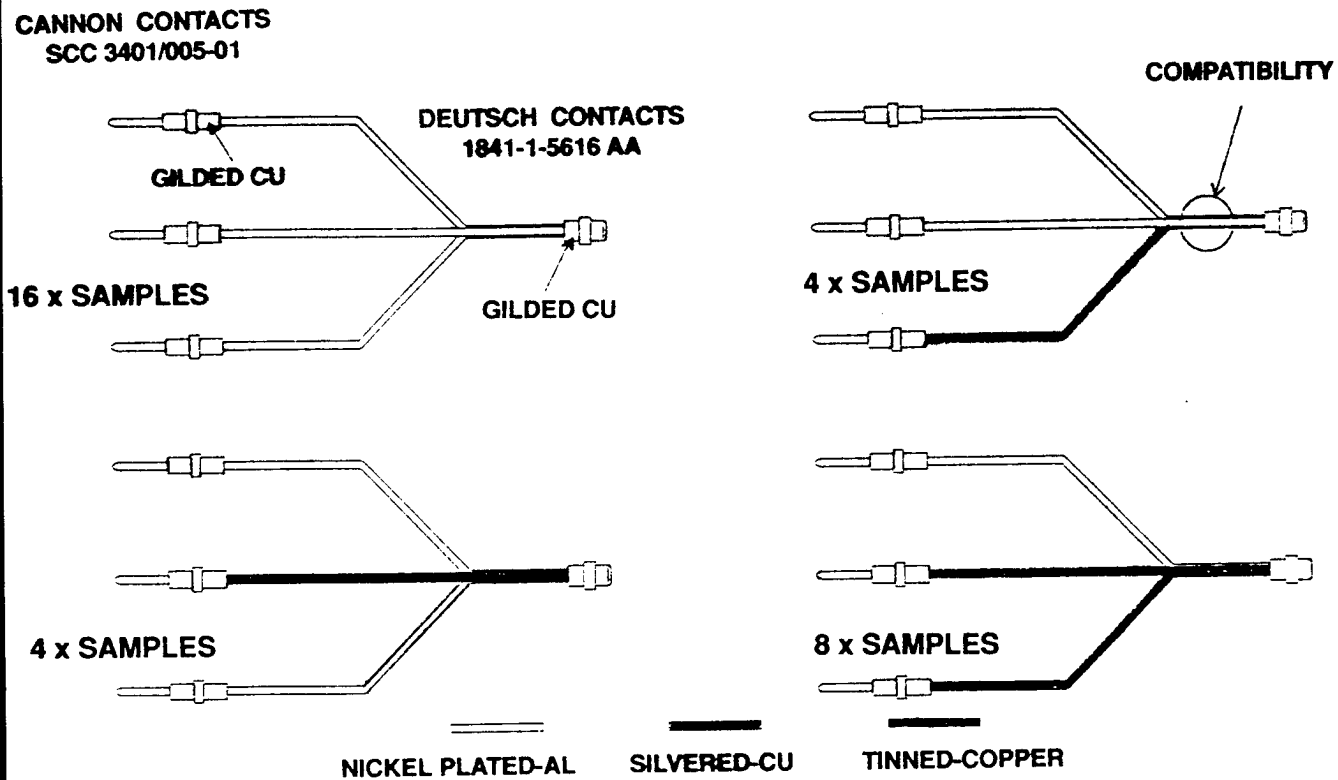


(Original photograph not available.)

**Flight samples stored in orbit for 9 months in the open FRECOPA box, plus 5 years in the closed box .**

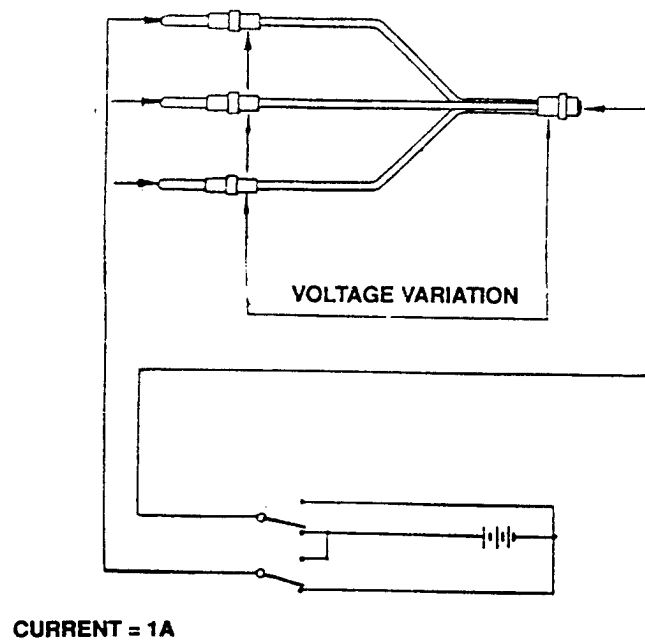
**Ground samples' storage time: 6 years in standard laboratory conditions.**

# SAMPLES DISPLAYED



Spaceborne harness, all configurations

# ELECTRICAL CHARACTERISTICS TEST



## Crimping resistance measurement method

### EVOLUTION OF SAMPLES' CHARACTERISTICS

TECHNOLOGY	CONDUCTORS	CRIMPING TYPE	VARIATION OF ELECTRICAL CHARACTERISTICS	FLIGHT				GROUND			
				A		B		C		D	
				$\Delta R$ (m $\Omega$ )	$\frac{\Delta R}{R}$	$\Delta R$ (m $\Omega$ )	$\frac{\Delta R}{R}$	$\Delta R$ (m $\Omega$ )	$\frac{\Delta R}{R}$	$\Delta R$ (m $\Omega$ )	$\frac{\Delta R}{R}$
NEW	Al Ni	MAGNET.	MIN.	0	0	0	0	0.2	3%		
			MAX.	1.3	20%	0.7	11%	0.7	11%		
		MECHAN.	MIN.	0.2	3%	0.3	4%	0	0		
			MAX.	0.5	8%	1	17%	0.5	8%		
CURRENT	Cu Ag	MAGNET.	MIN.	0	0	0	0	0	0		
			MAX.	0.1	4%	0	0	0.2	7%		
		MECHAN.	MIN.	0	0	0	0	0.2	7%		
			MAX.	0.2	7%	0	0	0.3	10%		
	Cu Sn	MAGNET.	MIN.	0	0	0	0	0.2	6%		
			MAX.	0.5	9%	0	0	0.3	9%		
		MECHAN.	MIN.	0	0	0	0	0.3	9%		
			MAX.	0.2	7%	0.2	6%	0.4			

## CONCLUSIONS

TECHNO.	CONDUCTORS	R. OHM VARIATION		VARIATION CAUSES			
		TEST MEASUREMENT	P.A. RECOMMENDATION	CONTACT TYPE	STORAGE		MATERIALS' INCOMPATIBILITIES
					ORBIT	GROUND	
NEW	Nickel plated Al.	UNALLOWABLE		NO	EQUIVALENT		NO
CURRENT	Silvered Cu.	EXCELLENT					
	Tinned Cu.	ALLOWABLE					

The electrical characteristics of connections built from nickel-plated conductors and gilded copper contacts have been noted to vary over the duration of the experiment. These variations are unrelated with the crimping or storage conditions or with metal pairing (nickel-plated aluminum/tinned or silvered copper). Such evolutions, howbeit slight, are detrimental to connection quality.

The same observations hold for some like connections subjected to long-duration thermal cycles (15,000 cycles, - 100°C, + 130°C). Therefore, work on aluminum technology has been reoriented toward a silvered aluminum conductor/gilded aluminum contact solution. The first evaluation tests performed according to this definition have yielded satisfactory results.

# MICROWELDING (OR COLD-WELDING) OF VARIOUS METALLIC MATERIALS UNDER THE ULTRA-VACUUM LDEF EXPERIMENT AO 138-10

Jean-Pierre Assié  
Aérospatiale  
Space and Strategic Systems Division  
06322 Cannes-la-Bocca, France  
Phone: (33) 92 92 72 49, Fax: (33) 92 92 71 90

Eric Condé  
CNES-CST (SST/SE)  
31055 Toulouse, France  
Phone: (33) 61 27 30 90, Fax: (33) 61 27 40 99

## SUMMARY

The FRECOPA experimentation, as part of the LDEF mission, of mechanical and electrical parts of spacecraft in space ultra-vacuum has demonstrated freedom from any cold-welding including microweld effects. This, as theorized, is due to integrity in space of the earthly-grown oxygen layer.

A further experiment, a dynamic one this time, could provide a wealth of scientific data, yielding reliable material-selecting criteria.

## INTRODUCTION

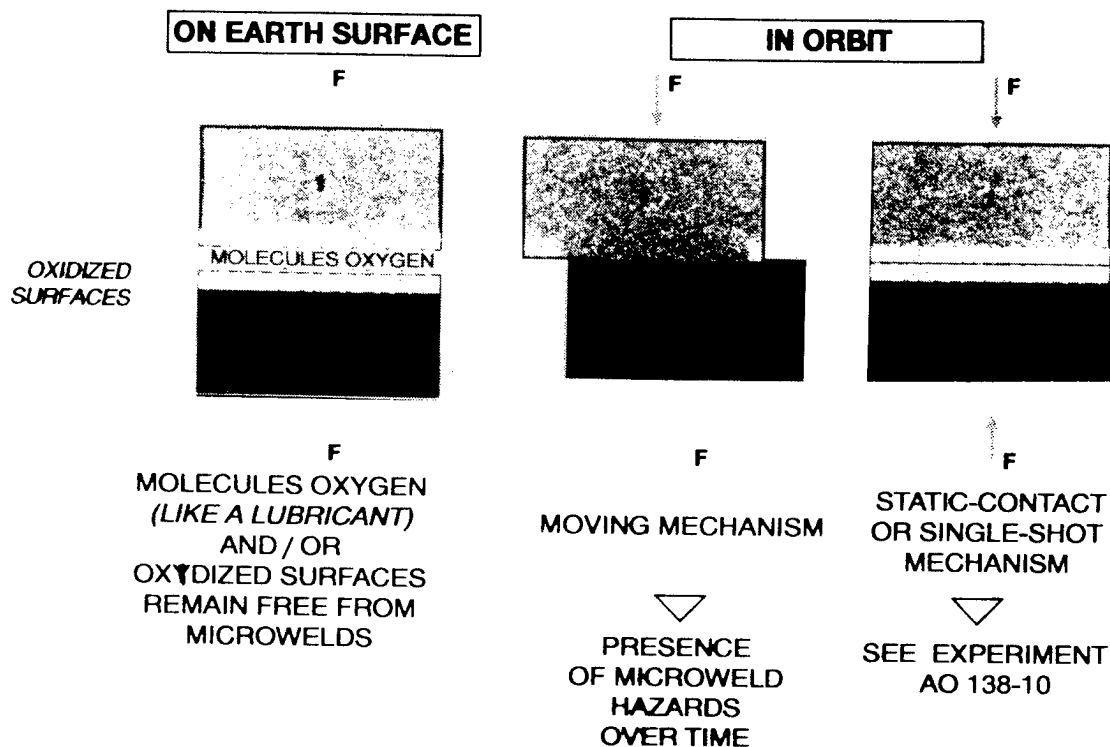
This paper presents an experiment, within the framework of the FRECOPA project, on the microwelding (or cold-welding) of spacecraft mechanisms.

Examples of spacecraft mechanisms:

- Pointing mechanisms (antennas, instruments)
- Focussing mechanisms (optical components)
- Deployment mechanisms (antennas, solar arrays)
- Hinges, drive mechanisms (mechanical parts of solar arrays)
- Slip rings (electrical parts of solar arrays)

In a space vacuum environment, the microwelding of two contacting metal parts of the same mechanism are liable to sustain irreversible effects, detrimental to satellite mission.





### Microwelding phenomena between two contacting metal parts

The objective is to optimize materials' choice to avoid microweld induced damage to spacecraft mechanisms and electrical parts (slip rings).

Intended result is to check the metal surfaces representative of metals, treatments, lubricants, for microwelds after extended space exposure, and evidence microweld phenomena on static samples.

The test approach is to statically compare ground samples in terms of aspect, adhesion, microwelds.

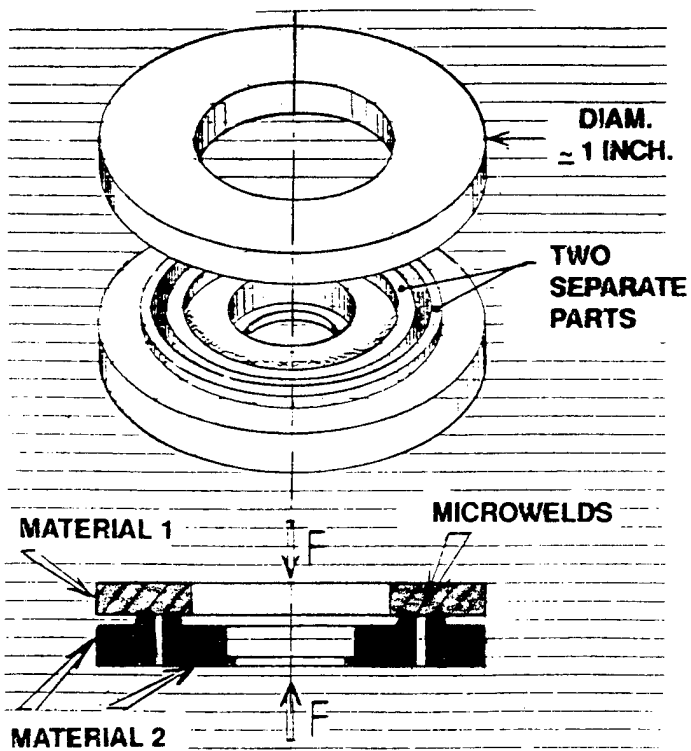
### EXPERIMENTAL APPROACH

- Simulation on varioux metallic washer couples of different contacts used in static or single-hot space mechanisms and slip rings:

- Quite a few parameters tested on many materials:

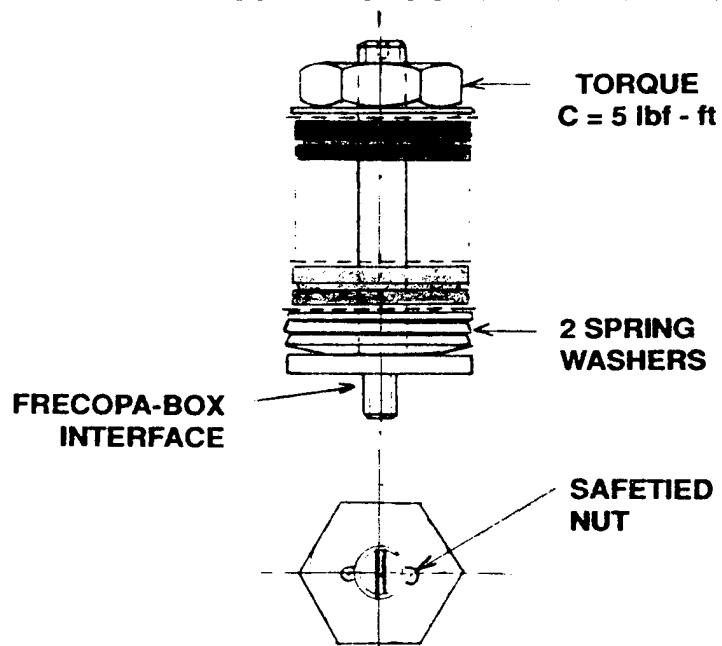
- . metal
- . surface
- . treatment
- . lubrication
- . pressure

*Remark:* Static samples reflecting the passive LDEF FRECOPA FLIGHT.

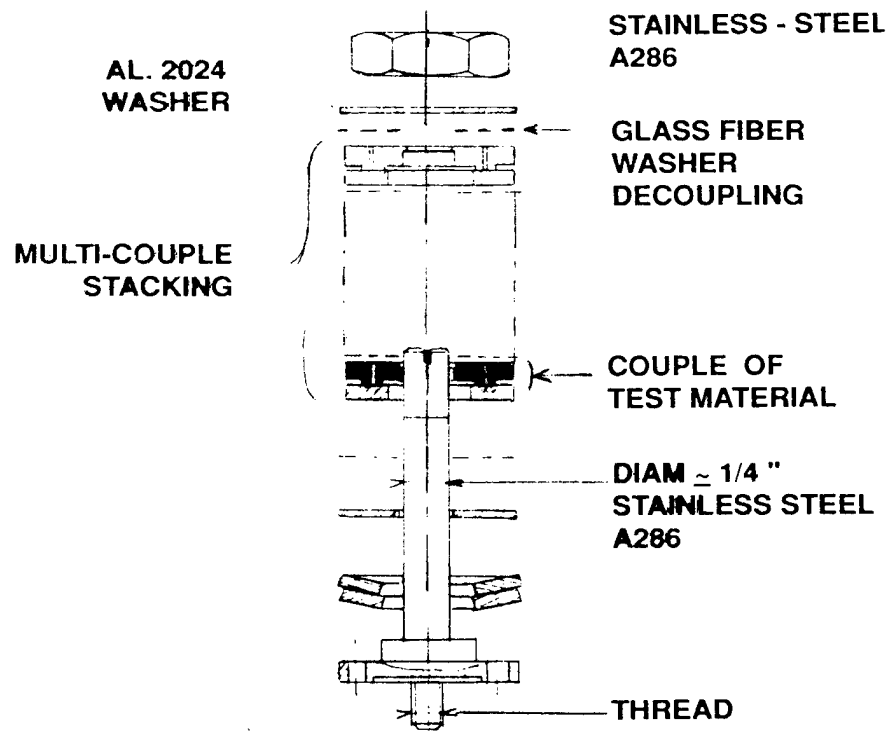


Experiment washer couple

#### GENERAL CONDITIONS OF THE EXPERIMENT

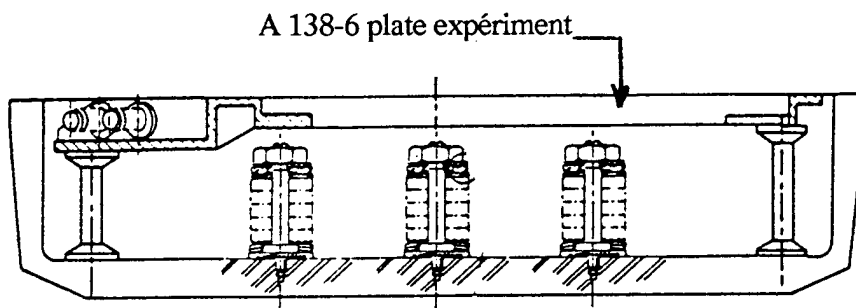


Final spool assembly



Exploded view





Layout of the 8 washer "spools" within the box.

In-orbit storage: 9 months in the open FRECOPA box plus 5 years in the closed box (underneath another experiment, the AO 138-6 plate).

On-ground storage: 6 years in standard laboratory conditions for mechanical parts, and 6 years in FRECOPA box under ultra-vacuum for electrical parts.

## METAL ALLOYS TESTED

### 1 ALUMINUM ALLOYS.

AL 7075 + Cr Anodiz  
AL 7075  
AL 2024 + Cr Anodis  
AL 2024  
Aluminum (A5)

### 2 TITANIUM ALLOYS

TI-6 Al. 4V Annealed  
TI-6 Al. 4V Tempered

### 3 COPPER ALLOYS

- (Be 1.9 Cu.)  
- (UN 3S)

### 4 STAINLESS STEEL

A 286  
A 151 321  
A 431

## REFERENCE COUPLES

HIGH SOLUBILITY  
HIGH DIFFUSIVENESS

TEST ON  
ALL LIKE MATERIAL  
AND  
DIFFERENT-MATERIAL  
PAIRS



NO  
MICROWELD

GOLD/GOLD  
Ag/Ag  
Ag/Gold  
Cr/Cr

DEPOSIT  
ON  
7075 AL.  
WASHER



NO  
MICROWELD

## LUBRIFICATION INFLUENCE

1 With molykote Z powder →

No microweld

Be 1.9 Cu on Be 1.9 Cu

2 With MOS2 P.V.D. →

No microweld

Be 1.9 Cu

on AL. 7075 + Cr. Anodiz

Be 1.9 Cu

on Ti-6 Al. 4V + Sulf. Anodiz

Ti-6 Al. 4V + Sulf Anodiz

on Ti-6 Al. 4V + Sulf. Anodiz

Al. 2024 + Cr Anodiz

on Ti-6 Al. 4V + Sulf. ANodiz

Al 2024 + Cr Anodiz

on Al. 2024 + Cr ANodiz

## MECHANICAL PARTS INFLUENCE OF CONTACT PRESSURE

MATERIAL 1	PRESSURE	MATERIAL 2
Be-1.9 Cu	P1= (3.6 Kpsi)    25 MP2	Be-1.9 Cu
	P2= (9.4 Kps)    66 MP2	
	P3= (18.8 Kpsi) 132 MP2	
Ti-6 Al.4V	P1= (3.6 Kpsi)    25 MP2	Ti-6 Al.4V
	P2= (9.4 Kpsi)    66 MP2	
	P3= (18.8 KPSI) 132 MP2	

.STANDARD PRESSURE PEENING ON SPACE MECHANISMS = 3.6 TO 25 KPSI  
ESTIMATED, EXCEPT FOR GEARS.

. CONTACT EFFORT  
RINGS)

= 6000N, OR F= 15N (SLIP

. CONTACT SURFACES

=VARIABLE

# TESTS ON ELECTRICAL PARTS' MATERIALS USED ON L-SAT, TV-SAT, SPOT SATELLITES

<u>COMMERCIAL REF.</u>	<u>COMPOSITION</u>
<b>1</b> Ag 900 - 178	Ag 90 % - Cu 10 %
<b>2</b> Au 715 - 520	Gold 71.5 % - Cu 15.3 % - Ag 3.8 % - PT 8.3 %
<b>3</b> Pd/ag 500/265	- - - -
<b>4</b> Ca 9734	Ag 85 % - Mo S2 12 % - C 3 %
<b>5</b> Ca 9970	Ag 82.5 % - Mo S2 15 % - Cu 2.5 %
<b>6</b> Berylco 25 H	Cu-Be Alloy with Co, Ni, Fe
<b>7</b> ANTI CORODAL 112	Al alloy with Si, Fe, Cu, Mg, Zn, Ti, Cr

## CONTACTS TESTED

<b>1</b> - <b>4</b> 8 x COUPLES,	<b>1</b> - <b>5</b> 4 x COUPLES,	<b>2</b> - <b>3</b> 4 x COUPLES
<b>6</b> - <b>6</b> 4 x COUPLES,	<b>7</b> - <b>7</b> 2 x COUPLES,	

## Data analysis

The first finding from AO-138-10 is that no cold welding ever occurred, and no microweld affected even the reference (i.e. presumably microweld prone) pairs of metals consisting of gold, silver and chromium.

The scientific disappointment from these results must be tempered by the notion of a static AO-138-10 experiment reflecting the passive character of the global LDEF flight.

Cold-welding has been hitherto theorized as arising from peeling of the earthly-created oxide layer in such environment as prevents such layer from growing any more.

In fact, such stripping of the oxide layer supposes relative motion of the contacting materials. Failing such motion, as in our case, oxidation will preserve its integrity and continue to prevent microwelding.

More bewildering is the non-microwelding of the reference pairs, contrary to common admission, so far, that the enormous diffusiveness and very low oxidation rate of metals like gold, silver and chromium (hence the shine or glitter) was a sure road to microwelding. Furthermore, solubility between the contacting washers was all the more expectable with like materials.

High diffusiveness and solubility, which seemed so far to rule out use of gold, silver and chromium in spaceborne mechanisms, even static ones, have just been proved by the AO-138-10 experiment not to induce any microwelds when there is no relative motion of parts.

Even though AO-138-10 failed scientific expectations, as did the LDEF structure with cold welding, the positive, functional aspect to be borne in mind is the safe operation of single-shot (appenage-releasing and/or latching) mechanisms, unhindered by microwelding in space vacuum, as now demonstrated by the statically representative pairs of materials, forgetting the prediction-failing reference pairs.

To preserve space mechanism representativity, even clearly at the expense of vacuum-microwelding, the parts had received none but the routine surface treatments, hence the traces of machining, of chlorine and sodium chloride, and the (damageable) fingerprints. The likelihood of the scientific phenomenon was thus traded off with functional representativity.

Thus, the technological success of the metallic pairs' freedom from any cold welding phenomenon does vindicate the theory: for lack of any relative motion of the metallic parts, the oxygen layer grown on earth will not deteriorate, building up a diffusive barrier that limits occurrence of the vacuum-bred microwelding phenomenon.

A similar, albeit dynamic experiment could provide highly interesting scientific results as well as new selection criteria for materials.

## CONCLUSIONS

1. Satisfaction as no-coldweld, no-adhesion findings vindicate choices of space machanisms materials.

2. No-microweld assumption confirmed for metal pairs' oxidized surfaces.

(LAYERS NOT PEELED, OWING TO STATIC EXPERIMENTAL CONDITIONS EVEN THE HIGHLY SOLUBLE, HIGHLY DIFFUSIVE REFERENCE COUPLES)

3. Other potential microweld-hindering factors.

. MACHINING TRACES

. POLLUTION (BY SOME PARTICLES BETWEEN THE SURFACES)

Continuing technological studies: work on dynamic contact between a couple of metals.

See literature, NASA' EXPERIMENT IN THE 70'S (OV1 satellite).

## OTHER POST-FLIGHT OBSERVATIONS

### 1 FRECOPA BOX

NO RESITIVE TORQUE WHILE REMOVING THE 12 X SPOOLS, WHICH DEMONSTRATES ABSENCE OF MICROWELDS AT THE FOLLOWING INTERFACES:

- STAINLESS STEEL THREAD ALUMINUM FRECOPA BOX
- STAINLESS STEEL NUT ATOP SAME AXIS.

### 2 FRECOPA CANISTER SYSTEM

STRUCTURE	}	
MECHANICAL PARTS	}	NO MICROWELD
ELECTRICAL PARTS.	}	

## LITERATURE

"In flight and laboratory vacuum friction test results"

E.J. Devine and A.E. Evans

W.A. Leasure NASA 1973

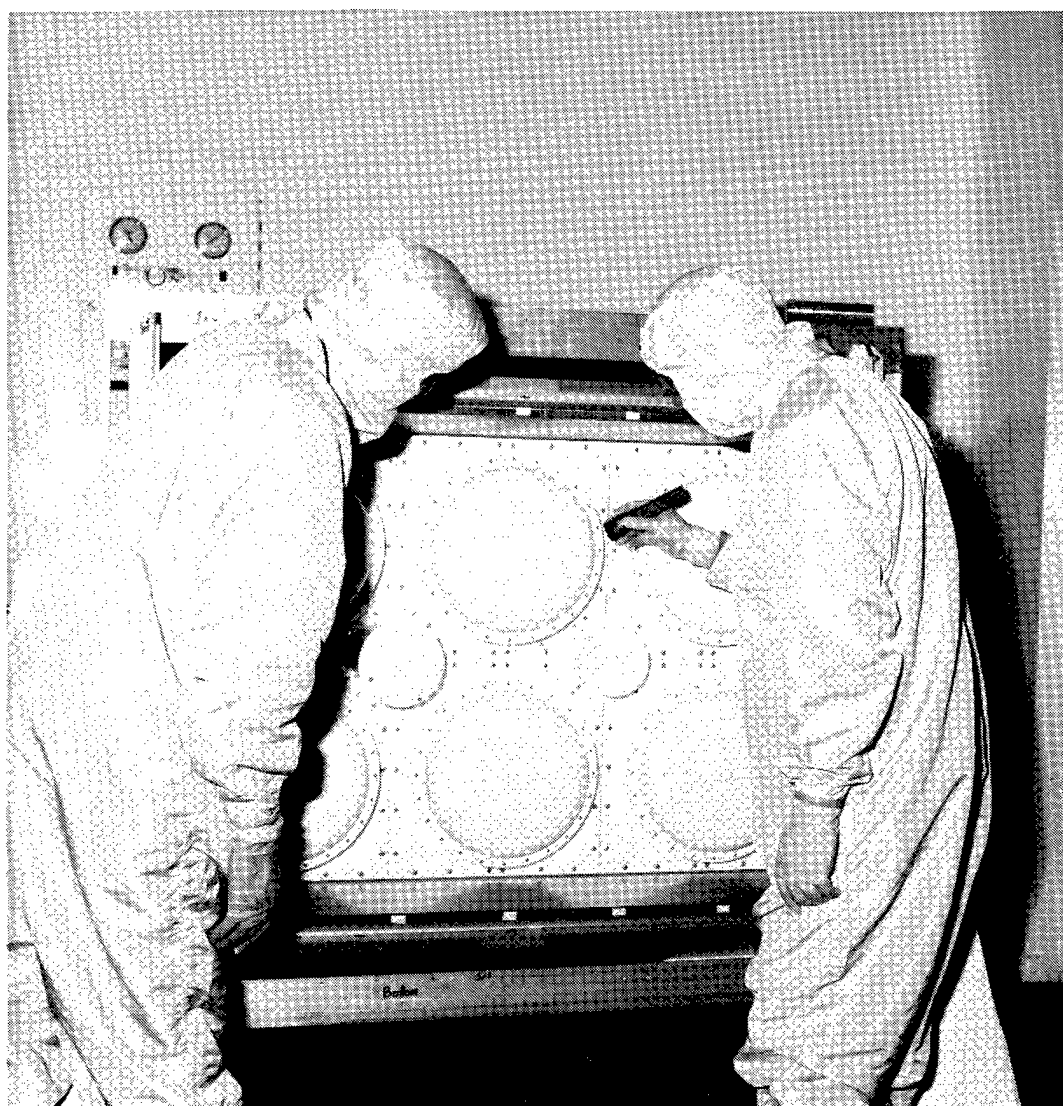
Nasa's launch, in the 70's, of the experimental satellite OV1  
(months 18, vacuum  $10^{-12}$  Torr.)  
with a dynamic contact between a couple of metals.

. GOLD/SILVER	}	
. Be-Cu: STAINLESS STEEL	}→	SEIZURE
. STAINLESS STEEL/STAINLESS STEEL	}	
. ALUMINIUM/STAINLESS STEEL	}	
. MILD STEEL: STAINLESS STEEL	}→	NO SEIZURE
. NITRIDE-TREATED STEEL/ STAINLESS STEEL	}	



# SPACE ENVIRONMENTAL EFFECTS

## *BIOLOGY*



## SEEDS IN SPACE EXPERIMENT

Jim A. Alston  
Park Seed Company  
Greenwood, SC 29648-0031  
Phone: 803/223-8555, Fax: 803/223-6999

### SUMMARY

Two million seeds of 120 different varieties representing 106 species, 97 genera and 55 plant families were flown aboard the Long Duration Exposure Facility (LDEF). The seed were housed in one sealed canister and in two small vented canisters. After being returned to earth the seed were germinated and the germination rates and development of the resulting plants were compared to the performance of the control seed that stayed in Park Seed's seed storage facility.

There was a better survival rate in the sealed canister in space than in the storage facility at Park Seed. At least some of the seed in each of the vented canisters survived the exposure to vacuum for almost six years. The number of observed apparent mutations was very low.

### INTRODUCTION

The purpose of the experiment was to evaluate the effects of prolonged space exposure on the survivability of a diverse group of seed stored in space under sealed and vented conditions and to determine possible resulting mutations and changes in mutation rates. Both flower and vegetable seed were represented in the experiment. Seed have been flown in space a number of times, but not in these quantities and not with maximum exposure for the duration that LDEF was in space.

### MATERIALS AND METHODS

#### Canisters

The sealed canister, designated as #6, was milled from Aluminum and dome shaped. The dome was 0.051 inch thick, thus allowing for maximum radiation penetration. The interior was 4 inches deep and 12 inches in diameter, thus having a capacity of 1/3 cubic foot. The

exterior of the canister was painted white. The dome portion of the canister and the base portion were fitted together with an 'O' ring to form the seal.

The vented canisters were also made of Aluminum. One vented canister was on the top side of the experimental tray and the other vented canister was on the bottom. The top one was painted white and was cylindrical in shape, being 4 inches tall and 4 inches in height. The bottom canister was painted black and was rectangular in shape, being 1 inch deep, 4 inches wide and 12 1/2 inches long.

The canisters were thermally isolated from the experimental tray hardware with Fiberglas insulators and a thermal cover was placed over the tray. This was done in an attempt to maintain temperatures within the seed at a point well below 100° F.

Passive maximum temperature indicators were placed on the inside of the dome of the sealed canister. Passive radiation detectors were placed between the layers of seed and maximum temperature indicators were also placed in the packs containing the radiation detectors.

#### Seed Packaging

The seed were placed into Dacron cloth containers before being placed in the canisters. Within the sealed canister, each Dacron bag was one inch thick so that four layers were possible. The layers were designated as 'A', 'B', 'C', and 'D' with layer 'A' being toward space and layer 'D' being toward the interior of LDEF. It was theorized that layer 'A' would receive twice the radiation that layer 'D' received. There were four wedges of equal size that constituted each layer. There was only one Dacron cloth bag for each of the vented canisters.

The seed (table I) were mixed together within each of the wedges so that the smaller seed could occupy the spaces between the larger seed. There were 83 seed items that were packed in each of the 4 layers. The same kinds of seed were placed into identifiable wedges and the wedges were rotated 90° in each layer to facilitate packing. The remaining 37 items were used as filler seed in the different wedges and were only packed in one of the layers. Each of the vented canisters contained the same 10 seed items and these 10 items were also in the sealed canister. The weight of each kind of seed was recorded as it was put into its cloth bag. The seed size of some of the items greatly limited the number of seed that could be flown.

The canisters were filled and integrated onto the experimental tray during the fall of 1983. This process was conducted in the controlled environment of Park Seed's seed storage facility which is

maintained at 70° F and 20% RH. The experimental tray also carried the 'Space Exposed Experiment Developed for Students' (SEEDS) (ref. 1) and was placed in the F-2 position on LDEF.

The control seed were held in Park Seed's seed storage facility in non-sealed containers.

### Return of the Seed

The SEEDS tray was removed from the LDEF on February 23, 1990, and was returned to Park Seed the next day. On March 1, 1990, the seed were removed from the canisters, left in the Dacron cloth bags and placed into glass gallon jars with tight fitting lids. By mid April the SEEDS project had progressed to the point that the processing of the Seeds In Space Experiment could be started.

Because the packaging process involved mixing the seed within each wedge, the first task was to separate and identify the seed. Weights of the seed were recorded after the separation process.

Germination testing was started on May 1, 1990, and as many as possible of the seedlings were grown to maturity. Plant development was evaluated and mutations were noted when observed.

Land Grant University systems in each of the states were contacted and seed from this experiment were offered for research opportunities.

## RESULTS AND DISCUSSION

### Germination

With one exception, at least some of the seed of each of the items in the sealed canister germinated. The control seed for the one crop that did not germinate only germinated 8%. There were 7 items that the space seed germinated and the control seed did not germinate. Table II presents data that shows that the germination percentage of seed of 115 items in the sealed canister averaged 15% higher than the control seed. The survivability of the seed in the sealed canister was better than the control because of the closed environment. If the control seed had been in a sealed environment, there may not have been any difference.

At least some of the seed of all 10 items in the vented canisters germinated (table III); however the sunflower in the bottom vented canister did not germinate. The average germination of the vented canisters was approximately 13% less than the control.

From personal experience, the seed with the highest oil content (soybean, sunflower, and corn) were expected to be dead. Onion is usually a short lived seed, but over 80% of the seed survived the vacuum of space.

### Weight Change

The weight change of the seed within the sealed canister was not consistent. But it must be remembered that the seed had time during the two months between canister opening and weighing to reach equilibrium with the moisture in the air. The 115 items that were used for the germination test showed a 0.29% weight gain (table II). This figure was derived from the total weights of the 115 items and is not a grand average of the individual averages. This small gain could be the result of exposure to the environment in which the seed were handled.

A comparison of the 10 items from the vented canisters and the same 10 items from the sealed canister (table III) shows that the seed from the vented canisters lost 35 to 40 times more weight than the seed from the sealed canister. Since all the seed were handled in the same manner it becomes clear that the seed in the vented canisters lost more than free bound water. Tightly bound water and oils were outgassed. Oil deposits were observed around the vented canisters.

### Radiation

The radiation information is contained in Dr. Benton's paper (ref. 2).

### Temperature

The temperature detectors that were on the inside of the domes all registered 100° F. The temperature detectors that were with the radiation detectors did not register at their lowest reading point, 95° F. This indicates that the hardware warmed up during re-entry, but that the temperature was not high enough or the duration long enough to heat the seed to 95° F. Also the germination performance of the seed indicates that the temperature within the seed stayed close to 70° F. Accelerated deterioration of seed occurs when it is exposed to temperatures above 90° F. for more than a few hours.

### Possible Mutations

One plant of Eucalyptus cinerea had variegated foliage. A red Allium cepa was observed in the population, but could have been the result of a seed mix. One of the Antigonon leptopus plants was dwarf. There were two variegated plants of Polygonum capitatum. Several chlorophyll deficiencies were noted in Zoysia japonica. The Zea mays seed produced a variegated plant and also a plant that produced seed that were different from the other plants.

Seed have been collected from as many 'space' plants as possible for the purpose of second generation studies. This seed has not yet been planted.

### Other Investigators

Thirty professional investigators have requested and received seed for their own research. One stipulation of receiving the seed was that the investigator would submit a paper for publication and if it was not accepted for publication, a copy would be sent to Park Seed and NASA for reference purposes.

## REFERENCES

1. Grigsby, Doris K.: Space Exposed Experiment Developed for Students. First LDEF Post-Retrieval Symposium, NASA CP-3134, 1992.
2. Benton, E. V., Frank, A. L., Benton, E. R., Csige, I., Parnell, T. A., and Watts, J. W., Jr.: Radiation Exposure of LDEF: Initial Results. First LDEF Post Retrieval Symposium, NASA CP-3134, 1992.

TABLE I. LIST OF SEED

<u>Thunbergia alata</u> , 'Susie'	<u>Mesembryanthemum Chrystallium</u>
<u>Alstroemeria aurantiaca</u>	<u>Celosia cristata</u> , 'Apricot Brandy'
<u>Allium Cepa</u> , Onion	<u>Catharanthus roseus</u> , 'Vinca'
<u>Asclepias tuberosa</u>	<u>Impatiens hybrid</u> , 'Sweet Sue'
<u>Impatiens Wellerana</u> , 'Kiss'	<u>Impatiens Wellerana</u> , 'Tango Orange'
<u>Begonia x Semperflorens</u> , 'Basel'	<u>Anchusa capensis</u> , 'Blue Angel'
<u>Symphytum x uplandicum</u> , 'Russian'	<u>Cactus</u> , 'Genera Mix'
<u>Cleome Hasslerana</u> , 'Pink Queen'	<u>Dianthus Caryophyllus</u>
<u>Dianthus superbus</u> , 'Lace Mix'	<u>Beta vulgaris</u> , Beet
<u>Spinach oleracea</u> , 'Melody'	<u>Tradescantia virginiana</u>
<u>Platycodon grandiflorus</u>	<u>Chamaemelum nobile</u> , 'Chamomile'
<u>Chrysanthemum x morifolium</u>	<u>Coreopsis tinctoria</u> , 'Sunray'
<u>Gerbera Jamesonii</u> , 'Happipot'	<u>Helianthus annuus</u> , 'Piccolo'
<u>Lactuca sativa</u> , 'Crispy Sweet'	<u>Lactuca sativa</u> , 'Mission'
<u>Parthenium argentatum</u> , 'Guayule'	<u>Rudbeckia hirta</u> , 'Orange Bedder'
<u>Tagetes patula</u> , 'Janie Yellow'	<u>Tagetes patula x erecta</u>
<u>Zinnia elegans</u> , 'Big Red'	<u>Ipomoea purpurea</u> , 'Heavenly Blue'
<u>Sedum supurium</u> , 'Coccineum'	<u>Brassica oleracea</u> , 'Darkri'
<u>Brassica oleracea</u> , 'Emerald'	<u>Brassica oleracea</u> , 'Green Dwarf'
<u>Lobularia maritima</u>	<u>Citrullus lanatus</u> , 'Bush Baby'
<u>Citrullus lanatus</u> , 'Seedless'	<u>Cucumis sativus</u> , 'Burpless Bush'
<u>Cucumis sativus</u> , 'Bush Whopper'	<u>Cucurbita pepo</u> , 'Creamy'
<u>Cucurbita pepo</u> , 'Gourmet Globe'	<u>Cucurbita pepo</u> , 'Kuta'
<u>Cyperus alternifolius</u>	<u>Scabiosa caucasica</u> , 'Pincushion'
<u>Euphorbia epithymoides</u>	<u>Pelargonium x hortorum</u> , 'Cascade'
<u>Achimenes</u> , 'Breeders Mix'	<u>Columna interspecific hybrids</u>
<u>Saintpaulia ionantha</u>	<u>Sinningia speciosa</u> , 'Gloxinia'
<u>Streptocarpus x hybridus</u>	<u>Zea Mays</u> , 'Corn Butterfruit'
<u>Zoysia japonica</u> , 'Lawn Grass'	<u>Nemophila Menziesii</u> , 'Blue Eyes'
<u>x Pardancanda Norrisii</u>	<u>Mentha spicata</u> , 'Spearment'
<u>Nepeta cataria</u> , 'Catnip'	<u>Ocimum americanum</u> , 'Basil Lemon'
<u>Ocimum basilicum</u> , 'Cinnamon'	<u>Ocimum basilicum</u> , 'Licorice'
<u>Ocimum basilicum</u> , 'Picollo'	<u>Ocimum Sanctum</u> , 'Basil Holy'
<u>Arachis Hypogaea</u> , 'Peanut'	<u>Glycine max</u> , Soybean 'Picket'
<u>Lathyrus odoratus</u> , 'Royal Mix'	<u>Lupinus texensis</u> , 'Bluebonnet'
<u>Pisum sativum</u> , Pea 'Sugar Bon'	<u>Pisum sativum</u> , Pea 'Sugar Snap'
<u>Pueraria lobata</u> , 'Kudzu Vine'	<u>Asparagus officinalis</u> , 'Paradise'
<u>Hemerocallis</u> , 'Extra Select'	<u>Lobelia Erinus</u> , 'Blue Cascade'
<u>Lagerstromia indica</u> , 'Myrtlettes'	<u>Abelmoschus esculentus</u> , Okra
<u>Hibiscus Moscheutos</u> , 'Disco Bell'	<u>Eucalyptus cinerea</u> , 'Silver Dollar'
<u>Mirabilis Jalapa</u> , 'Jingles'	<u>Nymphaea Lotus</u> , 'Lily of the Nile'
<u>Fuchsia x hybrida</u> , 'Fancy Lady'	<u>Oenothera missourensis</u> , Primrose
<u>Papaver nudicaule</u>	<u>Papaver orientalis</u> , 'Allegro'
<u>Limonium sinatum</u> , 'Heavenly Blue'	<u>Phlox Drummondii</u> , 'Twinkles'
<u>Antigonon leptopus</u> , 'Coral Vine'	<u>Polygonum capitatum</u> , 'Magic Carpet'
<u>Rheum Rhabarbarum</u> , 'Victoria'	<u>Portulaca grandiflora</u>
<u>Cyclamen persicum</u> , 'Matador'	<u>Primula x polyantha</u> , 'Julian Red'
<u>Aquilegia caerulea</u> , 'Columbine'	<u>Delphinium elatum</u> , 'Blue Fountains'
<u>Ranunculus asiaticus</u>	<u>Fragaria x Ananassa</u> , 'Sweetheart'



TABLE I CONTINUED - LIST OF SEED

<u>Astilbe</u> x <u>Arendsii</u> , 'Spiraea Mix'	<u>Antirrhinum</u> <u>majas</u> , 'Kolibra Mix'
<u>Calceolaria</u> <u>crenatiflora</u>	<u>Capsicum</u> <u>annuum</u> , 'Early Thickset'
<u>Capsicum</u> <u>annuum</u> , 'Midnight'	<u>Capsicum</u> <u>annuum</u> , 'Sweet Pickle'
<u>Lycopersicon</u> <u>Lycopersicum</u> ,	<u>Lycopersicon</u> <u>Lycopersicum</u> ,
Tomato 'Better Bush'	Tomato 'Park's Whopper'
<u>Petunia</u> x <u>hybrid</u> , 'Ultra Red'	<u>Salpiglossis</u> <u>sinuata</u>
<u>Salvia</u> <u>splendens</u> , 'Hotline'	<u>Solanum</u> <u>melongena</u> , 'Beauty'
<u>Solanum</u> <u>tuberosum</u> , 'Explorer'	<u>Tropaeolum</u> <u>majus</u> , 'Whirlybird'
<u>Anethum</u> <u>graveolens</u> , 'Dill'	<u>Coriandrum</u> <u>sativum</u> , 'Coriander'
<u>Daucus</u> <u>carata</u> , 'Nandor'	<u>Valeriana</u> <u>officinalis</u> , 'Marine'
<u>Verbena</u> x <u>hybrida</u> , 'Amethyst'	<u>Viola</u> <u>cornuta</u> , 'Pride Scotch'
<u>Viola</u> <u>Wittrockiana</u> , Pansy	<u>Rosa</u> interspecific hybrids, Rose

TABLE II. - COMPARISON THE SEALED AND VENTED CANISTERS

	GERMINATION			
	CONTROL	FLIGHT	% POINTS CHANGE	WT CHANGE %
SEALED 115 ITEMS	51.61%	66.76%	+15.15	+0.29%
TOP VENTED 10 ITEMS	61.00%	48.60%	-12.40	-4.50%
BOTTOM VENTED 10 ITEMS	61.00%	47.60%	-13.40	-3.86%

TABLE III. - COMPARISON OF THE TEN ITEMS THAT WERE FLOWN IN THE  
SEALED AND BOTH VENTED CANISTERS

ITEM	GERMINATION PERCENTAGE						% POINTS FROM CONTROL						WT CHANGE %		
	CONTROL	SEALED	TOP VENTED	BOTTOM VENTED	SEALED	TOP VENTED	SEALED	TOP VENTED	BOTTOM VENTED	SEALED	TOP VENTED	BOTTOM VENTED	SEALED	TOP VENTED	BOTTOM VENTED
CUCUMBER	94	97	72	80	3	-22	-14			0.27	-3.11	-2.36			
BURFLESS BUSH															
TOMATO	94	89	76	68	-5	-18	-26			1.23	-0.67	0.73			
PARK'S WHOPPER															
CORN	64	71	48	56	7	-16	-8			0.15	-3.67	-3.51			
BUTTERFRUIT															
PEA	60	54.5	52	4	-5.5	-8	-56			-0.86	-6.98	-6.29			
SUGAR BON															
LOTUS	100	90	60	80	-10	-40	-20			0.70	-5.88	-5.91			
LILY OF NILE															
ONION	74	86.5	80	72	12.5	6	-2			-1.45	-4.88	-2.84			
PARK'S PATTI															
OKRA	56	64	28	32	8	-28	-24			0.08	-4.61	-4.48			
CANDLELABRA															
KUDZU	24	41.5	36	40	17.5	12	16			0.93	-4.85	-2.75			
VINE															
SUNFLOWER	8	54	2	0	46	-6	-8			0.82	-1.48	0.04			
PICCOLO															
SOYBEAN	36	64	32	44	28	-4	8			0.05	-3.92	-3.39			
PICKET															
AVERAGE	61.00	71.15	48.60	47.60	10.15	-12.40	-13.40			-0.11	-4.50	-3.86			

Space Exposed Experiment Developed for Students  
(SEEDS)  
(P0004-2)

Doris K. Grigsby  
NASA/AESP  
Oklahoma State University  
Phone: 405/744-7015, Fax: 405/744-7785

Nelson J. Ehrlich  
NASA/AESP  
Oklahoma State University  
Phone: 405/744-7015, Fax: 405/744-7785

### SUMMARY

SEEDS, a cooperative endeavor of NASA Headquarters, the NASA Langley Research Center, and the George W. Park Seed Company, resulted in the distribution, by the end of March 1990, of approximately 132,000 SEEDS kits to 64,000 teachers representing 40,000 classrooms and 3.3 million kindergarten through university students. Kits were sent to every state, as well as 30 foreign countries. Kits contained Rutgers' tomato seeds that had flown on LDEF, as well as seeds that had been stored in a climate-controlled warehouse for the same time period. Preliminary data indicates the germination rate for space-exposed seeds was 73.8% while Earth-based seeds germinated at a rate of 70.3%. Tests conducted within the first six months after retrieval indicated space-exposed seeds germinated in an average of 8.0 days, while Earth-based seeds' average germination time was 8.3 days. Some mutations (assumed to be radiation induced) reported by students and Park Seed include plants that added a leaf instead of the usual flower at the end of the flower frond. Also, fruit produced from a flower with a variegated calyx bore seeds producing albino plants, while fruit from a flower with a green calyx from the same plant bore seeds producing green plants.

### INTRODUCTION

The Space Exposed Experiment Developed for Students (SEEDS), a cooperative project between NASA Headquarters, NASA Langley Research Center and the Park Seed Company of Greenwood, South Carolina was developed to generate interest in science and to provide students with experimental opportunities using materials flown in space.

Twelve and one-half million Rutgers tomato seeds were placed in five canisters sealed at one atmosphere pressure and 15 percent humidity. These canisters were then placed in a tray and installed on the LDEF. Each of the five canisters contained four Dacron™ bags, layers A through D, with layer D being closest to the LDEF interior. Passive dosimeters were placed above and below each layer to measure radiation layers. Thermal sensors were also placed in one canister to measure the maximum temperature attained during the mission. Preliminary radiation counts of 725 rads on the A layer and 350 rads on the D layer were reported.

Upon retrieval of LDEF, the space-exposed Rutgers tomato seeds were packaged in a kit containing a package of earth-based control seeds, a teacher's guide, and an activity booklet. By the end of March, 1990 approximately 132,000 SEEDS kits had been mailed to participating classrooms in all fifty

states, as well as thirty foreign countries. Over 64,000 teachers received the kits. Teachers from 83 foreign countries requested kits, with most requests coming from Canada, Australia, England and West Germany. Import regulations kept many requests from being honored.

Enthusiastic teachers and students conducted the NASA-designed experiment and returned data to be analyzed. Additional student-designed experiments were developed and led to a greater understanding of the scientific process. It will be impossible to make comparisons between much of the data submitted because of the lack of controls. However, program objectives were met as a great deal of interest in science and in the space program has been generated. Many classes are conducting second and third generation studies.

Preliminary findings summarized from a sampling of data submitted by participants are as follows:

	TOTAL PLANTED	GERMINATION RATE (%)	AVG DAYS TO GERMINATION	AVG DAYS TO FRUIT
Grades 5-9 (100 data booklets)				
Flight Seeds	3795	68	9.1	93
Control Seeds	4623	65	9.0	94
Grades 10-12 (100 data booklets)				
Layers AB	2688	73	8.0	84
Layers CD	3142	75	8.0	83
Control	3940	71	8.0	83
	TOTAL PLANTED	GERMINATION RATE (%)	AVG DAYS TO GERMINATION	AVG DAYS TO FRUIT
College (100 data booklets)				
Layer A	2083	77	8.0	93
Layer B	2395	73	8.0	90
Layer C	2375	75	7.0	92
Layer D	2241	76	8.0	93
Control	3673	75	8.0	92
Overall Results (Preliminary from 300 data booklets)				
Flight Seeds	18,719	73.8	8.0	89.7
Control Seeds	12,236	70.3	8.3	89.6

There are no confirmed mutations expressed by seedlings developing from the flight seeds; however, there are several suspects. Two experimenters (including one scientist at the Park Seed Company, Greenwood, SC) reported plants with variegated pigmentation. Park Seed horticulturists found that fruit from flowers with variegated sepals bear seeds that, in turn, produce albino plants. Seeds from normally pigmented areas of the same plant produce normal-appearing plants. The original variegated plant has been maintained through cuttings. Another suspect mutation produced a long, central stalk with highly deformed leaves. Additionally, experimenters have reported tear-drop shaped fruit, spotted fruit, an inflorescence terminating in a leaf rather than a flower, short plants with numerous leaves and no flowers, and tall plants with little flowering or branching.

# **SURVIVAL OF EPIPHYTIC BACTERIA FROM SEED STORED ON THE LONG DURATION EXPOSURE FACILITY (LDEF)**

Andrew C. Schuerger  
and

Bret L. Norman  
The Land, EPCOT Center  
Lake Buena Vista, FL 32830

Joseph A. Angelo, Jr.  
Science Applications International Corporation  
Melbourne, FL 32901

## **ABSTRACT**

Microbial contamination in American spacecraft has previously been documented (Appl. Microbiol., 1973, 26:804-813 and Ann. Rev. Microbiol., 1974, 28:121-137). However, potential risks to plants and humans in future space-based controlled ecological life support systems (CELSS) have yet to be addressed directly. The current study was designed to determine the survival of microorganisms exposed to the relatively harsh conditions found in low Earth orbit (LEO).

Seed of corn, sunflower, canteloupe, zucchini, bean, pea, and pumpkin cultivars were packaged in two 18 × 2.5 cm aluminum tubes; wall thickness of each tube was 1.33 mm. One seed tube was attached to payload M0006, tray C-2; a second tube was stored at room temperature in a lab on Earth. Five lithium fluoride thermoluminescent dosimetry wafers (TLD-100 wafers) were placed in each aluminum tube. The total mean dosages for flight and ground-control TLD wafers were 210.2 and 0.9 rads, respectively.

Seed were washed for 2 hrs in a phosphate buffered saline solution. Bacteria were isolated by plating samples of the seedwashings onto dilute tryptic soy agar. Pure isolates of morphologically distinct bacteria were obtained by standard microbiological procedures. Bacteria were grouped according to colony-type and preliminary identification was completed using a fatty-acid analysis system (Can. J. Microbiol., 1986 32:796-800). *Bacillus* spp. were the primary microorganisms that survived on seed during the experiment. Bacterial diversity and relative abundance were similar for the ground and flight seed. *Bacillus subtilis*, *B. pumilus*, *B. licheniformis*, *B. polymyxa*, *B. megaterium*, and *B. pabuli* were isolated most frequently. Members of the genera *Kurthia*, *Listeria*, *Micrococcus*, and *Arthrobacter* were also isolated from flight and ground-control seed. Results support the hypothesis that terrestrial microorganisms can survive long periods of time in the relatively harsh LEO environment.

Experiment number M0006

FIRST BIOLOGICAL AND DOSIMETRIC RESULTS OF  
THE FREE FLYER BIOSTACK EXPERIMENT A0015 ON LDEF

G. Reitz, H. Bückner, R. Facius, G. Homeck,  
M. Schäfer, J.U. Schott  
DLR, FF-ME, Biophysics Division, Linder Höhe,  
5000 Köln 90, Germany

J. Bayonove  
University Montpellier II, 34060 Montpellier, France

R. Beaujean  
University Kiel, 2300 Kiel 1, Germany

E.V. Benton  
University San Francisco, Harney Science Center,  
San Francisco, CA 94117, USA

M. Delpoux  
University Paul Sabatier, 31073 Toulouse, France

C. Heilmann  
BAEN, 67200 Strasbourg, France

W. Heinrich  
University Siegen, 5900 Siegen 21, Germany

A.R. Kranz  
University Frankfurt, 6000 Frankfurt/Main, Germany

H. Planel, Y. Gasset, G. Gaubin  
University Paul Sabatier, 31073 Toulouse, France

G. Portal  
CEA, 92265 Fontenay aux Roses, France

E.H. Graul, W. Rütther  
University Marburg, 3550 Marburg/Lahn, Germany

E. Schopper  
University Frankfurt, 6000 Frankfurt/Main, Germany

C.A. Tobias  
Adv. Biomedical Science and Treatment Center,  
Oakland, CA 94609, USA

T.C. Yang  
LBL, Berkeley, CA 94720, USA

## INTRODUCTION

The experiment Free Flyer Biostack is part of a radiobiological research program which has been designed to get more information about the biological effectiveness of the different radiations present in space, especially on the effects of single heavy cosmic particles of high energy loss (HZE-particles), the combined effects of space radiation and other spaceflight factors, such as microgravity, and the documentation of the actual nature and distribution of the radiation field at the surface or inside spacecrafts.

These objectives will be achieved by using hermetically sealed aluminium cannisters, which contain a series of monolayers of selected biological material, each of which is sandwiched between several types of nuclear track detectors. This arrangement - known as Biostack concept - allows localizing the trajectory of each heavy ion in the biological layer and identifying the side of penetration inside the biological object. The precision obtained for the reconstruction of the geometric relation between particle trajectory and test organism depends on the latter and could be pushed as low as 0.2  $\mu\text{m}$  for the smallest object (bacterial spores, approx. diameter 1  $\mu\text{m}$ ) in previous Biostack experiments. These experiments comprised a widespread spectrum of biological objects, such as bacterial spores, plant seeds, shrimp eggs, and insect eggs. These species have different organization levels and different radiation sensitivity. They are well known and showed at least one typical genetic or somatic radiation effect. All objects were exposed in resting state and were tested to survive the period of experimental procedure. The radiation effects under investigation comprised changes in cellular and organic development, damages to cell nuclei and other subcellular systems, and induction of mutations leading to somatic or genetic changes of biological significance. The results of the Biostack experiments on Apollo 16 and 17, ASTP, SL1, D1, and Biocosmos 8 and 9 demonstrated for the first time with high precision and unequivocally that single HZE particles can engender serious damages in practically all test organisms. This comprises induction of somatic mutations in plant seeds, of reduced hatching and of anomalies in insect and salt shrimp embryos, and of cell death in bacterial spores. Further quantitative results revealed that currently established physical theories modelling the reaction mechanisms cannot fully account for the observed effects.

In the Biostack experiments, complementary studies at accelerators represent a mandatory part of the program. It has been shown that, for bacterial spores, the accelerator experiments quantitatively conform with the findings from space experiments. However, in more complicated systems, not all radiobiological effects observed in space could be duplicated at accelerators.

The biological systems used in the Free Flyer Biostack experiments include spores of *Bacillus subtilis* and *Sordaria fimicola*, dry seeds of *Arabidopsis thaliana*, *Nicotiana tabacum*, *Zea mays*, and Rice and encysted eggs of the tiny brine shrimp *Artemia salina*, one of the most primitive crustaceans. The nuclear track detectors cellulose nitrate (CN) and silver chloride (AgCl) will be used for the localization of the path of each heavy particle through each biological specimen.

Besides the radiobiological data, evaluation of the Biostack experiments will yield information on the composition of the radiation field in the path of the spacecraft. The combination of various detector systems which complement each other in their recording characteristics provided for a rather complete dosimetry. The use of thermoluminescence dosimeter (TLD), nuclear emulsions, silver chloride and plastic detectors allows measuring the absorbed dose and estimating the neutron contribution, the number of nuclear disintegrations, and the particle fluences and its spectral composition with respect to charge, energy and linear energy transfer (LET).

Although the Biostack experiment on LDEF was designed for a long-duration flight of only 9 months, most of the biological systems show a high hatching or germination rate. Some of the first observations are an increase of the mutation rate of embryonic lethals in the second generation of *Arabidopsis*, somatic mutations and a reduction of growth rates of corn plants and a reduction of life span of *Artemia salina* shrimps. The different passive detector systems are also in a good shape and give access to a proper dosimetric analysis. The plastic detectors have been all etched and the AgCl detectors have been processed. Evaluation of the TLD gives us the total dose received in the Biostacks in different depths of the stacks. The results of the experiment on LDEF will contribute to obtain the empirical data base needed to evaluate the radiobiological consequences of space radiation.



The dominant applied aspect of the Biostack experiments concerns the problem of protection of man against radiation in space. Radiobiological and dosimetric data have to be collected in space as baseline information for estimating radiation risks to man in future space missions and for establishing radiation standards for man in space. Scientific and technical coordination of this program constitutes a significant portion of the experimental approach which has to be realized within still restrictive constraints of space missions.

The Biostack program is performed in a multidisciplinary and international cooperation between many independent institutes and investigators. This report therefore gives the preliminary results of the LDEF Biostack in four independent reports. The results from biological objects and detector systems not presented in this report will be published later.

Four biostack reports follow this introduction; they are as follows: Preliminary Total Dose Measurements On LDEF; Total Dose Effects (TDE) Of Heavy Ionizing Radiation In Fungus Spores And Plant Seeds-Preliminary Investigations; Preliminary Results Of The Artemia Salina Experiments In Biostack On LDEF; and Long-Term Exposure Of Bacterial Spores To Space.

## PRELIMINARY TOTAL DOSE MEASUREMENTS ON LDEF

G. Reitz

DLR, Institute for Aerospace Medicine, Biophysics Division  
Linder Höhe, 5000 Köln 90, Germany

### ABSTRACT

After spending nearly six years in Earth's orbit twenty stacks consisting of radiation detectors and biological objects are now back on Earth. These stacks (Experiment A0015 *Free Flyer Biostack* (ref. 1)) are part of the fifty-seven science and technology experiments of the *Long Duration Exposure Facility (LDEF)* of NASA. The major objectives of the Free Flyer Biostack experiments are to investigate the biological effectiveness of single heavy ions of the cosmic radiation in various biological systems and to provide information about the spectral composition of the radiation field and the total dose received in the LDEF orbit. The Biostacks are mounted in two different locations of the LDEF. Up to three layers of Lithiumfluoride thermoluminescence dosimeters (TLD) of different isotopic composition were located at different depths of some Biostacks. The preliminary analysis of the TLD yields maximum absorbed dose rates of  $2.24 \text{ mGy day}^{-1}$  behind  $0.7 \text{ g cm}^{-2}$  shielding and  $1.17 \text{ mGy day}^{-1}$  behind  $12 \text{ g cm}^{-2}$  shielding. A thermal neutron fluence of  $1.7 \text{ n cm}^{-2}\text{s}^{-1}$  is determined from the differences in absorbed dose for different isotopic mixtures of Lithium. The results of this experiment on LDEF are especially valuable and of high importance since LDEF stayed for about six years in the prospected orbit of the Space Station *Freedom*. There is no knowledge about the effectiveness of the space radiation in long-term spaceflights and the dosimetric data in this orbit are scarce.

### INTRODUCTION

The data on radiation levels in orbiting spacecrafts so far are limited and are not sufficient to serve as a solid base for an accurate prediction of the radiation environment in future space missions. One of the reasons is the highly complex radiation environment in space which comprises electromagnetic radiation and charged particles from the Earth's radiation belt and of solar and galactic origin. Photons and particles with energies of some eV up to  $10^{18}$  eV are present. This radiation field is modified by the Earth magnetic field and the solar cycle, resulting in a change of flux by orders of magnitude and it is depending on the spacecraft's altitude and inclination. Interaction of the radiation with shielding material further increases the complexity of the radiation field inside spacecrafts. Measurements of fluence rates and spectra and absorbed doses have to be performed behind different shielding thicknesses during all flight opportunities to improve our knowledge about the radiation transport through realistic shielding configurations. For the prediction of radiation loads in future missions information of the highest possible accuracy is required concerning the radiation environments in the specific orbit of the spacecraft.

In this report, only data about absorbed dose measurement with TLD's will be reported. The investigation on the other detector types is in progress.

## MATERIALS AND METHODS

The Free Flyer Biostack experiment consists of 20 detector units. Twelve (E1 to E12) units were mounted in the corner tray G2 on the LDEF end which faced the Earth and eight (S1 to S8) were mounted in one-third of the side tray C2 (fig. 1). The trays were attached to the surface of the LDEF; the detector units therefore were exposed to free space. The detector stacks are housed in cylindrical aluminum containers, which were hermetically sealed except unit S4. A detector stack consisted of more than 100 layers of nuclear track detectors - partly interspersed with biological objects. The top and the bottom of some stacks were formed by two TLD layers. Another TLD layer was located in the middle of such a stack. The height of a stack was 83 mm and the diameter 97 mm. The thickness of the particle detector sheets ranged between 0.1 and 0.6 mm. A typical TLD layer consisted of 21 Lithiumfluoride chips of three different isotopic compositions (TLD 100, 600 and 700 of Harshaw) welded between two polyethylen foils and evenly distributed over the stack surface. The size of a TLD chip is  $3.2 \times 3.2 \times 0.85 \text{ mm}^3$ .

The doses in the TLD chip were measured with a Harshaw 2800 TLD analyzer at standard settings. Calibration was done using a Cs 137 source.

## FLIGHT PARAMETERS

The highest altitude of the LDEF was 477 km at release with an inclination of 28 degrees. The facility was gravity gradient stabilized, so that one end of the LDEF faced always the Earth. After 2107 days, the LDEF was retrieved at 334 km. The altitude versus time is given in figure 2.

Most of the time of the flight took place during solar minimum phase; launch date was April 7, 1984 and retrieval date January 12, 1990. At the end of 1988, increasing solar activity was observed. The temperature history of the several experiment units is not exactly known. A maxima-/minima temperature recorder consisting of a bimetal spiral was included in stacks E11 and S7. The recorder of stack S7 showed a minimum temperature of  $-9^\circ\text{C}$  and a maximum temperature of  $29^\circ\text{C}$ . Stack E11 was not yet disassembled because for this container a gaschromatographic analysis is planned. In this container we expect a temperature in the range between  $0^\circ\text{C}$  and  $40^\circ\text{C}$ . Measurements of the LDEF experiment *Therm* at the Earth facing end of LDEF show temperatures between  $13^\circ\text{C}$  and  $39^\circ\text{C}$ .

## RESULTS AND DISCUSSION

Up to now, only TLD's used in Biostack units E1, E5, E8, S4 and S7 have been evaluated. The doses for the different layers in these stacks are given in table 1. The highest absorbed dose measured with TLD 700 is 4.8 Gy in S7 behind a shielding of about  $0.7 \text{ g cm}^{-2}$  (2 mm aluminum and 100 mm polyethylen in front of the TLD chips). In the same configuration the dose in E8 is 4 Gy. The higher doses received at the side tray location can be explained by a higher contribution of the galactic proton component to the total dose, since the Earth tray location has a higher shielding as the side tray location. Most of the dose of course is due to crossings of the South Atlantic Anomaly (SAA) in which the radiation belt is closer to the Earth surface than in other regions. The incident flux of belt protons in this region to both locations can be assumed to be the same which is explained by the orientation of the LDEF on its flight path and a cylindrical distribution of the proton fluence in the SAA.

The differences in the TLD 700 and TLD 100 measurements in the same layer can be explained by different shielding distributions in the different locations of the TLD chips on the surface of the stack. If the shieldings were the same, the TLD 100 and TLD 700 measurement should give approximately the same value as it is seen in the TLD layer E8-1, E1-2 or S7-190. The TLD 100 and 700 chips are located more at the edge of the stack than the TLD 600 chips resulting in a sometimes lower shielding for the TLD 700 chips in comparison to the TLD 600. The responses of the TLD 600 have to be higher than the responses of the TLD 100 and TLD 700 chips, because the TLD 600, in addition, monitors the thermal neutron component. In the case where we observe no difference in the TLD 100 and 700 readings, the TLD 600 reading is considerably higher than both of these readings. In these cases we see no dose variations within one detector layer, which indicates no differences in the shielding distribution in this layer. The range of measured values is significantly greater in the more heavily shielded layers, which may be due to increased differences in the shielding distribution for single chips. Taking the highest difference in the readings which accounts to 500 mGy and the maximum dose induced per neutron in TLD 600 with  $1.7 \times 10^{-9}$  Gy (ref. 2), we obtain an estimate of a thermal neutron flux of about  $1.7 \text{ neutrons cm}^{-2}\text{s}^{-1}$ .

Most of the exposure time was during a period of minimal solar activity, only the last 20 % during increasing solar activity. The results therefore can be regarded as representative for a solar minimum situation. Recent measurements of absorbed dose of solar flare particles in orbiting spacecrafts (ref. 3, 4) indicate that the contribution to the dose from these events is negligible for the LDEF orbit.

The TLD results given in table 1 are only preliminary because no fading effects in the TLD have been taken into account. The thermal fading of LiF-TLD chips at 25°C is after one year about 5 % (ref. 5); for longer storage times there are no results. The effect is under investigation. Applying such corrections, the absorbed doses will become higher than reported.

## REFERENCES

1. Bückner, H.: Free Flyer Biostack experiment (A0015), in: *The Long Duration Exposure Facility (LDEF)*, eds. L.G. Clark, W.H. Kinard, D.J. Carter, jr., and L.J. Jones, jr., NASA SP-473, 1984, p. 139.
2. Horowitz, Y.S.: *Thermoluminescence and Thermoluminescent Dosimetry*, Vols I, II, and III, CRC Press, Boca Raton, 1984.
3. Dachev, Ts.P., Matviichuk, Yu.N., Bankov, N.G., Semkova, J.V., Koleva, R.T., Ivanov, Ya.J., Tomov, B.T., Petrov, V.M., Shurshakov, V.A., Bengin, V.V., Machmutov, V.S., Panova, N.A., Kostereva, T.A., Temny, V.V., Ponomarev, Yu.N., Tykva, R.: "MIR" radiation dosimetry results during the solar proton events in September - October 1989, *Adv. Space Res.*, 1991.
4. Golightly, M.J., Hardy, A.C., Atwell, W., and Hardy, K.: Description, analysis and impact of major solar activity during recent U.S. shuttle missions, *Adv. Space Res.*, 1991.
5. Burgkhardt, B., Harrera, R., and Piesch, E.: in: *Int. Conf. on Luminescence Dosimetry*, Sao Paolo, ed. A. Scharmann, 1977, p. 77.

TABLE I. - ABSORBED DOSE MEASUREMENTS IN TLD 100, 600, AND 700 BEHIND DIFFERENT SHIELDINGS IN FRONT OF THE DOSIMETERS  
(In unit E5 only TLD 100 was flown. Errors are standard errors of the mean)

Experiment indentification	Shielding [g cm <sup>-2</sup> ]	Absorbed dose [Gy]		
		TLD 100	TLD 600	TLD 700
E1-2	0.7	3.74 ± 0.13	4.14 ± 0.24	3.79 ± 0.17
E1-280	14	1.75 ± 0.11	1.90 ± 0.21	1.99 ± 0.25
E5-1	0.7	3.82 ± 0.11		
E5-56	6.7	2.40 ± 0.16		
E5-101	12	2.10 ± 0.23		
E8-1	0.7	3.95 ± 0.12	4.30 ± 0.23	3.89 ± 0.19
E8-207	12	2.05 ± 0.12	2.36 ± 0.30	2.22 ± 0.22
S4-6	2	3.68 ± 0.31	3.93 ± 0.76	3.88 ± 0.64
S4-258	12	2.38 ± 0.28	2.60 ± 0.49	2.38 ± 0.33
S7-190	0.7	4.83 ± 0.17	5.23 ± 0.23	4.73 ± 0.26
S7-154	5	2.92 ± 0.28	3.17 ± 0.17	3.22 ± 0.24
S7-1	12	2.15 ± 0.08	2.45 ± 0.17	2.46 ± 0.26

# LDEF

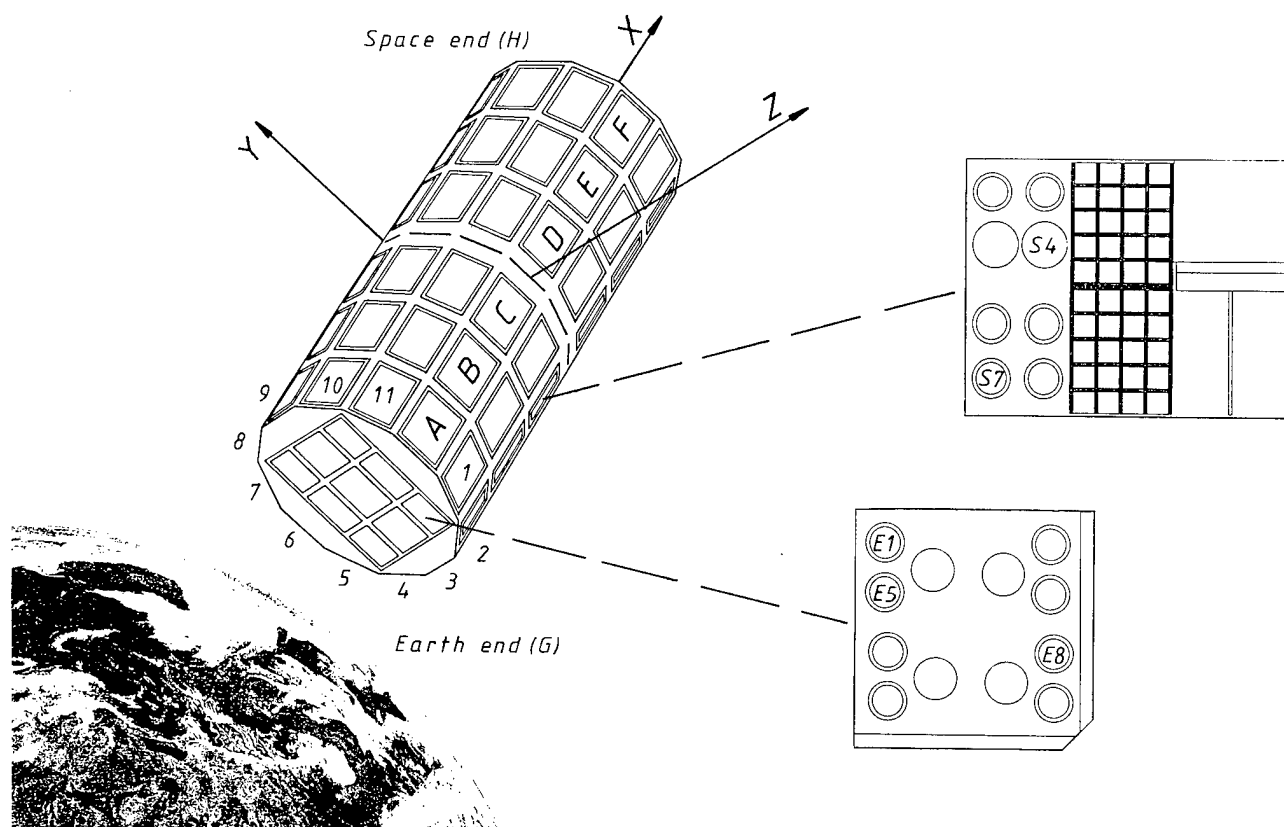


Fig. 1 Location of Biostack experiment units E1, E5, E8, S4, and S7 on the trays G2 and C2 of the LDEF and its orientation in orbit. The velocity vector is in direction of the y-axis; row 9 is therefore the leading and row 3 the trailing edge. The LDEF is gravity gradient stabilized.

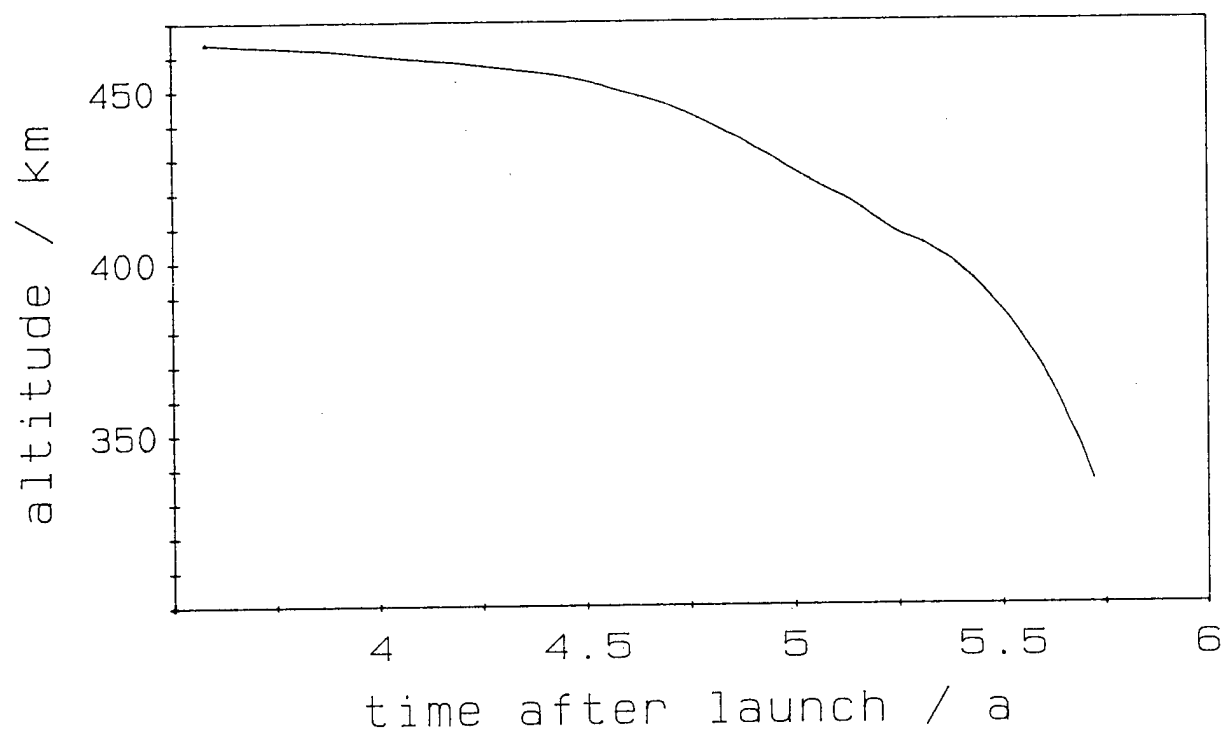


Fig. 2 Altitude of LDEF in dependence of the time after launch.



TOTAL DOSE EFFECTS (TDE) OF HEAVY IONIZING RADIATION  
IN FUNGUS SPORES AND PLANT SEEDS  
- PRELIMINARY INVESTIGATIONS -

A.R. Kranz, M.W. Zimmermann, R. Stadler,  
K.E. Gartenbach, M. Pickert  
Botanical Institute, Group Plantgenetics, J.W.Goethe-University,  
D-6000 Frankfurt/Main 11 (FR Germany), POB 111 932

## INTRODUCTION AND AIMS

The opportunity to compare cosmic radiation effects caused during short and long duration exposure flights in biological objects are limited until now, and data so far obtained are very rare and insufficient (ref. 1). Among the eukaryotic model systems recommended in radiobiology, plant seeds (dry, non-metabolizing embryos) of *Arabidopsis thaliana* and ascospores (one cell with several haploid nuclei) of the fungus *Sordaria fimicola* were successful objects for such space flight experiments in which the radiation damage could be defined for physiological stress and genetic risk separately in order to make the radiation protection standards in space more precisely (ref. 2, 3). Because of the very long exposure of the experiment during the LDEF-1 mission (~ 2000 d) structural changes of the hardware material can be expected which will influence its biocompatibility and, thus, will interact with the radiobiological effects.

The fluence of cosmic radiation (HZE-particles) depends on the location of the BIOSTACK-container deposited on the LDEF-satellite. Therefore several positions of the experiment with different shielding against space radiation were used during the LDEF-1 mission. The LDEF-experiment (FREE FLYER BIOSTACK) included eight units arranged in the side tray (S1- to S8-F) and twelve units installed on the earth tray (E1- to E12-F) with higher shielding (fig. 1).

The aim of our experiment flown on the LDEF-mission was a detailed investigation of biological effects caused by cosmic radiation especially of particles of high atomic number  $Z$  and high energy (HZE-particles). The flight hardware consisted of standard BIOSTACK containers; in these containers a special sandwich construction consisted of visual plastic detectors (cellulose nitrate (CND, CNK and Lexan) and AgCl monocrystals) with seed resp. spore layers interlocked were used.

All in all the specific conditions of the LDEF-experiment made our investigations original and exceptional.

## EXPERIMENT WITH SPORES

### Background and method

For the experiment "spores" we used different kinds of detectors and different mutant lines of self fertilizing *Sordaria fimicola*, for the number of different nuclear track detectors and total amount of spores c.f. (ref. 4). Ascospores were distributed on the detector surface by natural shooting from ripe perithecia without adhesive. We took off ascospores and put them on agar-medium containing ammonium-acetate. Incubation of about 4-7 days at 25°C produced a compact mycel which was transferred to a medium without ammonium-acetate. Repeated incubation was leading to the formation of perithecia. It was now possible to evaluate microscopically prepared asci or the 8 ascospores of an ascus shot in separable groups. The criterium for the evaluation was the segregation of the coloured to transparent ascospore ratio per group originated from one ascus.

In ascus forming fungi (*Ascomycetae*), a so-called tetrad analysis can be useful in detecting chromosome aberrations (deletions). This test is based on a typical cytogenetic behaviour which informs on the segregation of deleted or mutated genes, and the chromosome distribution resulting from the sequence of divisions of cell nuclei inside the diploid zygotic mother cell of the *Sordaria* ascus hypha. Inside this cell gene recombination takes place including a putative mutant gene induced formerly by HZE-particles in the irradiated spore ( $M_1$ ); i.e. the mutant gene locus expressing a deviating spore colour in the next generation ( $M_2$ ) can be investigated in the ascus cell after its final production of 8 spores through three subsequent nucleus divisions of which the first is the so called meiotic one, i.e. chromosome and gene numbers are reduced to the half set ( $n = 7$ ) and recombined, the second and third ones are the mitotic divisions where the numbers will remain constant since all the genes and chromosomes are reproduced and divided identically.

Under controlled conditions of a petri dish, mature spores are shot off the ascus simultaneously and may be found in a small droplet of slime fixed at the inner surface of the cover dish (fig. 2). There, they will be positioned at random instead of their former linear position inside the original immature ascus cell which represents the products of cytogenetic events via cell nucleus divisions in line. If a mutant spore colour gene is segregated during the first, meiotic division we will obtain 4/4 distribution of different spore colour (pre-reduction); in case of 6/2 distribution, segregation of the mutant gene was during the second (mitotic) nucleus division (first post-reduction). The very rare events of 7/1 distribution are related to the third (mitotic) division (second post-reduction). Furthermore, the sequence of cytogenetic behaviour indicated the molecular aberrations induced by radiomutagenesis of HZE-ions. Double strand breakage of DNA (DSB), which will produce directly lethal nuclei in the  $M_1$  mycelia or chromosomal and genic deletion and thus a ratio 0/8 and 2/6 resp. of coloured to non-coloured spores can be expected. If, however, a single strand breakage of DNA (SSB) has been produced by the radiomutagen (HZE), the chromosomal and genic deletion will be completed after the following divisions of post-reduction thus 1/7 ratio will be obtained. In case of 6/2 and 7/1 ratios of non-coloured to coloured spores both events occurred simultaneously. Consequently, investigation of mutant spore colour distribution, although at random i.e. no more in line in a droplet (ascus) of the second generation ( $M_2$ ) after mutagenesis will yield a statistically provable sample of induced chromosomal, genic and molecular (DSB and SSB) deletion events in the former generation ( $M_1$ ).

#### Results of cosmic total dose effect

- 1) Germination of earth tray exposed fungus spores decreased significantly in the genetic line *cor* (fig. 3, above).
- 2) Significant deviation of flown, earth tray samples to non-exposed, non-stacked control spores as well as the stacked backup ones (fig. 3, below) because of the frequency of transparent, i.e. mutant spores (shrunk and transparent) increase instead of dark coloured wild type ones; thus, % deviation of ratio class 8/0 becomes negative and of all the other classes (6/2, 4/4, 2/6, 0/8) positive.
- 3) However, this result is also obtained but mostly at lower rates with the backup samples; thus, a mutagenic effect of the storage conditions inside the Biostack for nearly 6 years is probable.
- 4) This behaviour of point 2) and 3) is, obviously, different between the two genotypic lines *cor* and *br1*, the former, wildtype *cor*, proves to be less sensitive than gene marker line *br1*, although the result of spore ( $M_1$ ) germination data is reverse.

Summarizing this preliminary evaluation of two *Sordaria* mutant gene marker lines *br1* and *cor* show the following data: Early radiation damage of spore germination results in significant increase of lethality % ( $M_1$ ) and mutation rate of genes controlling aberrant (shrunk, transparent) spores ( $M_2$ ).

## EXPERIMENT WITH SEEDS

### Background and Method

Different samples of ecotypes and mutant-lines obtained from *Arabidopsis* Information seed bank, Frankfurt, F.R.G. were used (ref. 3). The dry seeds were glued on the detector foils using the adhesive Luviskol VA 64 (10 g in 100 ml of ethanol 50%). After post-flight return of the seeds to Frankfurt, we took at least 100 seeds from each detector. These seeds were sown under sterile conditions in petri dishes (diameter 90 mm) on Gelrite-medium, adapted to mineral and nutrient conditions. Seeds were vernalized for 120 h at  $+4^{\circ} \pm 2^{\circ}\text{C}$ . Afterwards the petri dishes were transferred to a growth cabinet. Seedlings were kept there until transfer to soil. About 10 days after germination (rsp. 4-6 leave stadium) the seedlings were transferred to plastic pots with standard soil. Further growing of the plants took place in a growth chamber (ref. 4). One day after vernalization, control of seed germination was started at intervals of one day under a binocular. The criterion of germination was the emergence of the radicle.

For the test of embryonic sterility of the fruits (ref. 5) five consecutive siliques from the basal part of the main inflorescence were used. From these data the frequencies of lethal mutations  $m_a$ ,  $m_b$  and  $m_c$  and the mutation rates  $R$  were estimated (ref. 6).

### Preliminary results of total dose effects

In order to obtain quick information about the general condition of the bio-objects, soon after return to Frankfurt we tested the dynamics of germination of the seeds. Figure 4 (above) shows the delay of seed germination after seed exposure of two wildtype lines (*En-2* and *La-0*) of *Arabidopsis thaliana* (L.) Heynh. in space compared to the control-samples. This figure describes the deviation from fresh-control. The control-samples do not differ significantly in germination capacity (after 24 hrs 82% for *En-2* and 76,4% for *La-0*), but the germination after space exposure shows that the germination of the wildtype line *En-2* is more sensitive than for the wildtype *La-0* (after 24 hrs 18.7% vs 54.2%). Decrease of growth is probably caused by stress and aberrant control of phytohormones, since for instance gibberellic acid is able to reduce the decrease of germination induced by X-rays (ref. 7) as well as by HZE-particles (ref. 8).

The last endpoint of damage investigated in the ontogenetic sequence was the ovule and embryo ( $M_2$ ) development of plants belonging to the  $M_1$ -generation. The sterility of the siliques (fig. 5) has been shown to be a highly sensitive character induced by ionizing radiation and chemical mutagens (Rédei, 1969). Figure 4 (below) shows the mutation rates for embryonic lethals in the  $M_2$  generation of earth tray exposed seeds as difference to the control samples. The mutation rates for the two wildtype lines were increased in comparison to the seed control samples.

### FINAL CONCLUSION OF PRELIMINARY RESULTS

- 1) Results of General Vitality and Damage Endpoints (TDE) have shown
  - i) with *Sordaria* ascospores:  
Genotype dependent damage (~5 to 60%) of earth and side tray exposure for about 2000 days in orbit
  - ii) with *Arabidopsis* seeds:  
Increase of embryonic lethal mutation rates (~3 to 18%) relying to less extent on the wild type exposed on earth tray for nearly 6 years in space.
- 2) Evaluation of General Vitality is limited at present because of
  - i) minimum values obtained for backup samples (Köln)
  - ii) maximum values proved for fresh seed and backup samples (Frankfurt) as expected.

- 3) Reason for the unexpected differences may be:
- i) variant treatments of backup units (stacked viz. non-stacked, gas, temperature)
  - ii) interaction of structure material and environmental conditions (outgassing of catalysts, radicals etc.)
  - iii) interaction of different components of cosmic rays and their secondary products.

By comparison between preliminary data obtained from biological damage endpoints of the LDEF-1 experiment "seeds" and of short duration flight experiments (e.g. BION-9), surprisingly, no significant increase of the biological damage is obtained; although the total dose for the LDEF-1 flight was 40 times approx. higher but the dose rate was 4 times approx. lower, the biological damage was at the same order of magnitude. Probably this phenomenon may be explained by the more important role of the dose rate than the total dose for the LDEF-1 flight. Considering the result of several Soviet space experiments with relatively long duration (ref. 1) after > 400 d in orbit, survival of *Arabidopsis* seeds decreased remarkably, and after 800 d no plants survived, we suppose that the radicals produced by oxygen were the cause of this damage. No oxygen could be detected in the atmosphere of a similar constructed Biostack unit during gas analysis after flight, although it was filled with a 60 % helium + 40 % oxygen atmosphere before flight. Additional experiments and test studies have to be performed in the near future in order to confirm this suggestion as well as the cosmic HZE-effect more exactly.

#### Acknowledgements

Detectors were generously provided by Profs. E. Schopper, H. Bückner and Dr. G. Reitz.

## REFERENCES

1. Nevzgodina, L.V. et al.: The effect of outer space environments on *Lactuca sativa* seeds flown on cosmos biosatellites, Cosmic biology and applied medicine, Moskau 1990 (russ.)
2. Kranz, A.R.: Genetic risk and physiological stress induced by heavy ions, Proceedings of Fourth European Symposium on Life Sciences Research in Space, Trieste, (ESA Public Ed. V. David) ESA SP-307, May 1990, pp. 559-563
3. Schott; J.U.; G. Reitz; A.R. Kranz: Design and preparation of space flight experiments with advanced and FREE FLYER BIOSTACK, Arabid. Inf. Serv. 20, 1983, pp. 13-18
4. Kranz, A.R.; U. Bork; H. Bückner; G. Reitz: Biological damage induced by ionizing cosmic rays in dry *Arabidopsis* seeds, Nucl. Tracks Radiat. Meas. Vol.17, No.2, 1990, pp. 155-165
5. Müller A.J.: Embryonentest zum Nachweis rezessiver Letalfaktoren bei *Arabidopsis thaliana*, Biol. Zentralblatt 82, 1963, pp. 133-163
6. Rédei, G.P.: *Arabidopsis thaliana*(L.) Heynh.: A Review of the Genetics and Biology, Bibl. Genetica No. 2, 1970
7. Reinholz, E.: The influence of gibberellic acid on the germination of irradiated *Arabidopsis* seeds, Arabid. Inf. Serv. 4, 1966, pp. 16-17
8. Zimmermann, M.W.: Die Wirkung des Phytohormon GA3 auf schwerioneninduzierte Wachstumsveränderungen bei *Arabidopsis thaliana*, Diplomarbeit Fachbereich Biologie, Universität Frankfurt/Main, 1990

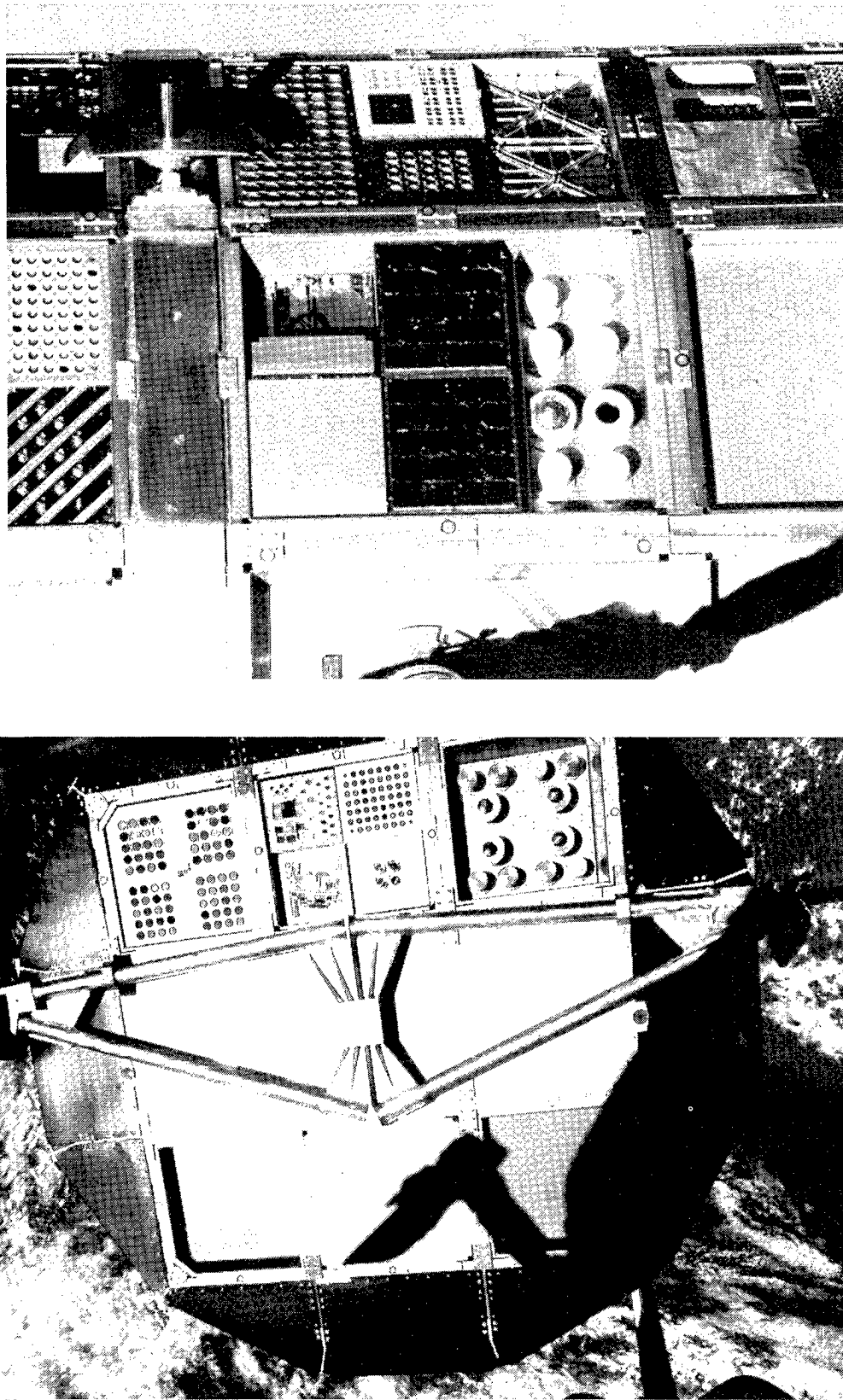


Fig.1 View on the side- (above) and the earth-tray (below) of the LDEF-satellite in orbit with BIOSTACK-units, containing thousands of *Arabidopsis* seeds and of *Sordaria* spores.

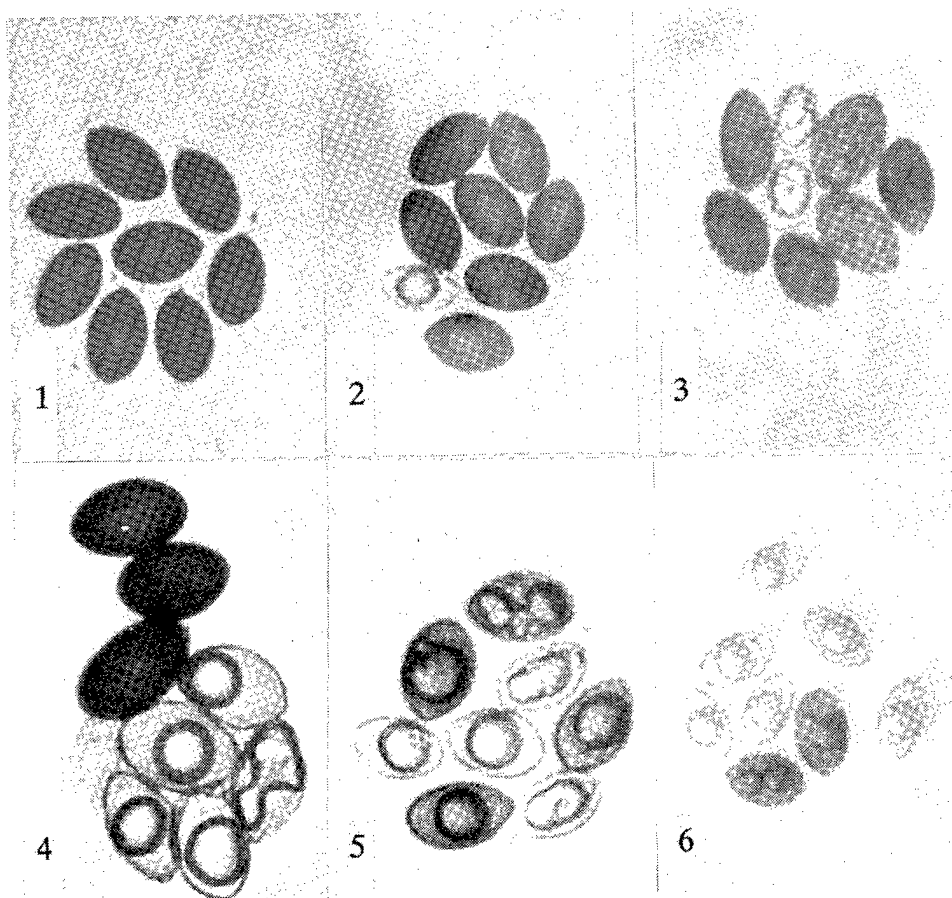


Fig. 2 Different segregation ratios of coloured resp. transparent *Sordaria* ascospore in groups of eight.

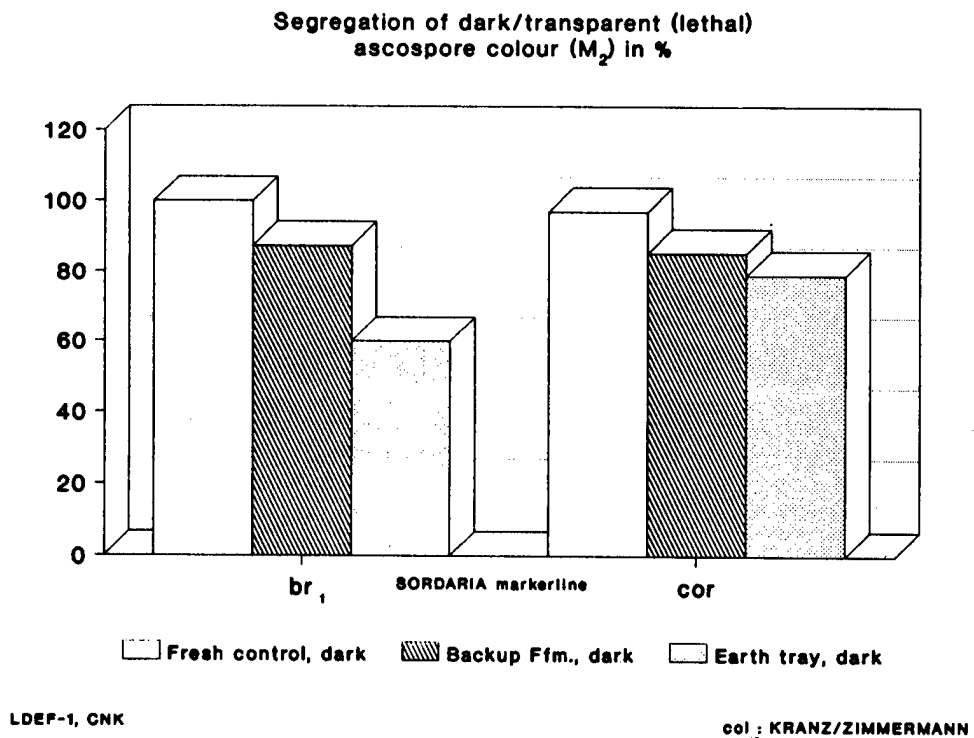
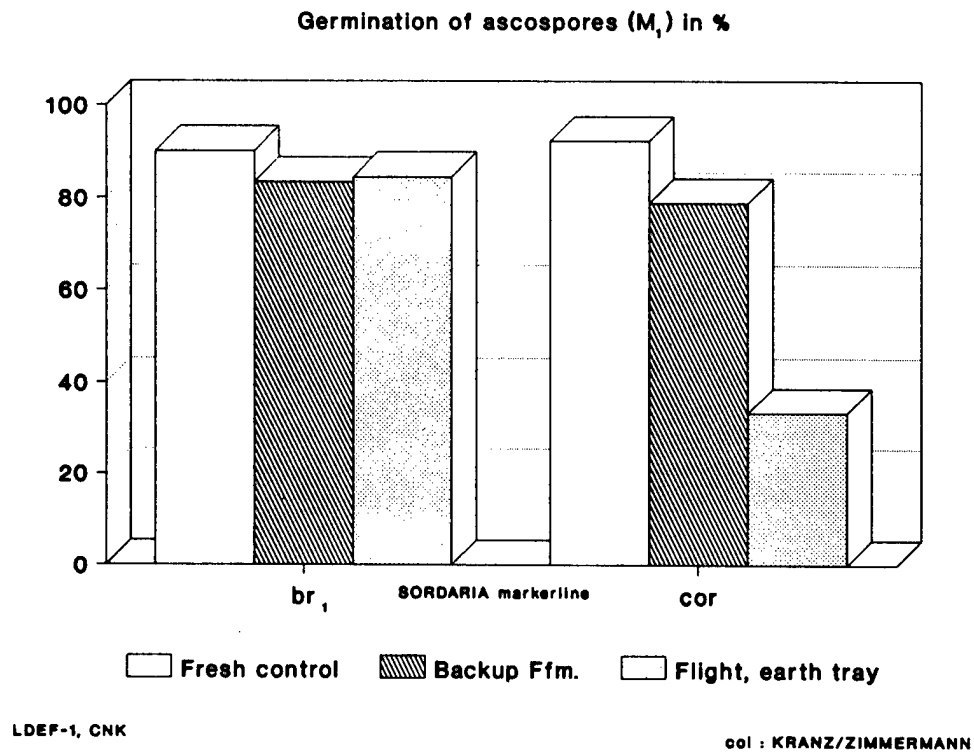
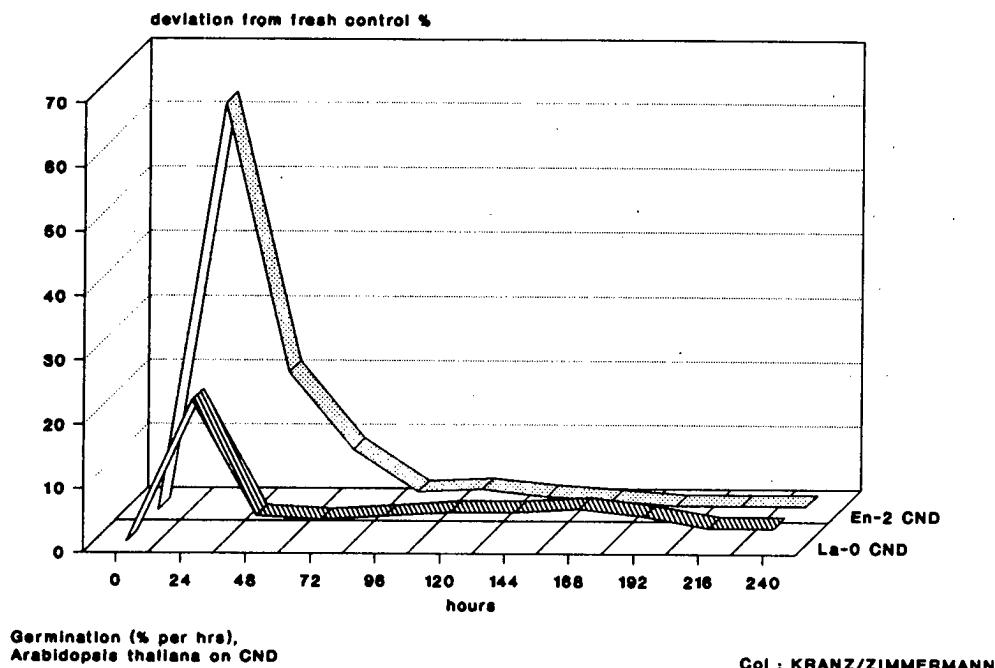


Fig.3 Preliminary data Germination ( $M_1$ ) and segregation rate for spore colour genes of the *Sordaria* experiments.



**LDEF-1 Arabidopsis General Vitality Test**  
 Delay in Germination in M1 of Earth-Tray  
 Exposed Seeds



**LDEF-1 Arabidopsis Mutation Rates**  
 Embryonic Lethals in M1 of Earth Tray  
 exposed seeds

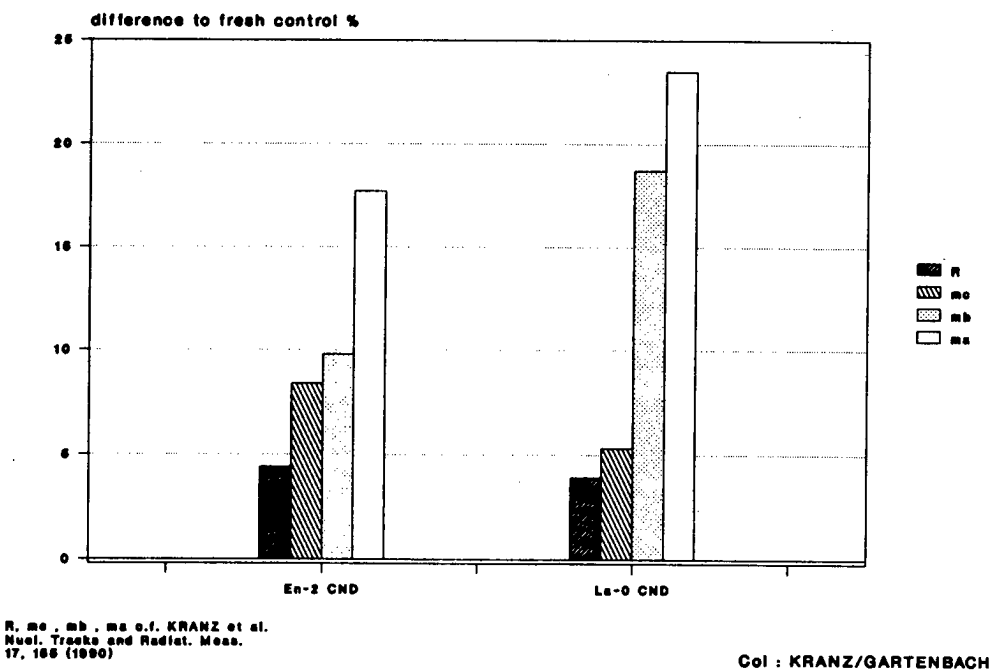


Fig. 4 Preliminary data of seed germination ( $M_1$ ) and embryonic lethal mutation rates ( $M_2$ ) of the Arabidopsis experiments.

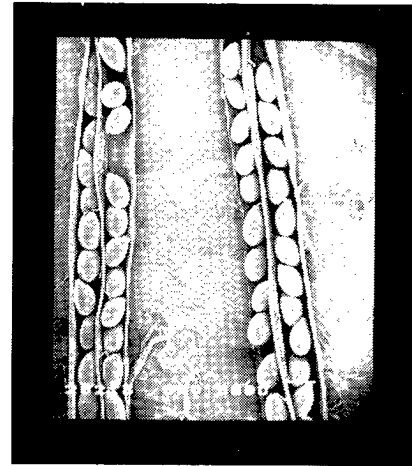
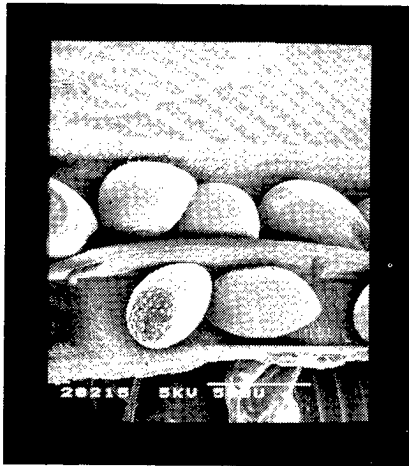


Fig. 5 SEM-photos of opened siliques of *Arabidopsis* with complete seed embryos ( $M_2$ ) in line (right) and with gaps of undeveloped embryos (middle and left).  
(Photo Ruppel/Gartenbach, Botanical Inst., Frankfurt/Main, FRG)

## PRELIMINARY RESULTS OF THE ARTEMIA SALINA EXPERIMENTS IN BIOSTACK ON LDEF

E. H. Graul, W. Rütger, C. O. Hiendl

Philipps-University Marburg, Department of Environmental Sciences and Space Medicine, 3550 Marburg/Lahn,  
Germany

### INTRODUCTION

*Artemia* belongs to the order *Branchiopoda* and lives in sea water. Figure 1 shows the life cycle. The adult animal is around 12 mm long. The eggs of *Artemia* (fig. 2), resting in blastula stage, consist of about 4200 cells and can be stored for a long period in a dried state. The dried eggs are about 210  $\mu\text{m}$  in diameter and equipped with thick hard shells. Under favourable conditions in 1.5% salt water and a temperature of 25° C, the larva will normally hatch within 24-48 hours; it is called a nauplius. During hatching the egg shell breaks open and the nauplius emerges from the egg still covered by a membrane. Then, by the aid of its swimming organ, the nauplius tears this membrane off and begins to swim in the salt water. Assuming that there are sufficient algae for nutrition, the development cycle lasts around four weeks.

The mosaic egg of the brine shrimp, *Artemia salina*, resting in blastula or gastrula state represents a system that during further development, proceeds without any further development to the larval stage, the free swimming nauplius. Therefore, injury to single cells of the egg will be manifested in the larvae. In several experiments, it was shown that the passage of a single heavy ion through the shrimp egg damaged a cellular area large enough to disturb either embryogenesis or further development of the larva, or the integrity of the adult individual. Emergence, characterized by bursting of the egg shell and the appearance of the larva, still enclosed in the membrane was already strongly disturbed by heavy ions. The next step, namely the hatching, was seriously affected by a hit of a heavy ion (ref. 1-4). Reduced emergency and hatching rates were also observed in eggs flown but not determined as hit by a heavy ion. This effect may be due either to nuclear disintegrations or recoil events, or to some not yet understood interactions by other spaceflight parameters. Additional late effects, due to a hit of a single heavy ion, are delay of growth and of sexual maturity, and reduced fertility. Anomalies in the body and the extremities could be observed more frequently for the nauplii which had developed from eggs hit by heavy ions.

Compared to previous spaceflight experiments, LDEF shows an increase in total dose up to about 200 times, and a similar increase in HZE particle fluence and in the occurrence of disintegration stars. Thus, LDEF will offer a unique opportunity to gather information on HZE particle effects at high radiation background levels and on the effects of stars in biological matter.

### RESULTS

First of all, a hatching test was performed with the flown eggs. The results were compared to those obtained from 6 year old laboratory eggs and 6 month old laboratory eggs. Table 1 shows the results. There is a significant decrease in the hatching rate of the flight eggs compared to the hatching rate of 6 year old laboratory eggs. The difference in hatching rate between the 6 year old laboratory eggs and the 6 month old laboratory eggs is about 10%. The same difference is seen in the hatching rate between the eggs flown in the earth tray and those flown in the side tray. The rate of anomalies is significantly higher in the nauplii hatched from flown eggs compared to those hatched from ground control eggs.

The next step was a survival test of the nauplii. The life span curves demonstrate a high lethality (about 50%) in the first two months of development of nauplii hatched from flown eggs, while the controls have a lethality of about 10% only (fig. 3).

Further investigations of the *Artemia* experiment have two major directions: First, identification and quantification of the influence of HZE particles on the system at the organic, the cellular, and the molecular level; and secondly, the localization of individual HZE particles and the determination of the physical parameters of the particles of interest.

#### REFERENCES

1. Rüther, W., Graul, E.H., Heinrich, W., Allkofer, O.C., Kaiser, R., and Cüer, P., Preliminary results on the action of cosmic heavy ions on the development of eggs of *Artemia salina*, Life Sci. Space Res. 12, 1974, pp. 69-74
2. Graul, E.H., Rüther, W., Heinrich, W., Allkofer, O.C., Kaiser, R., Pfohl, R., Schopper, E., Henig, G.B., Schott, J.U., and Bücken, H., Radiobiological results of the Biostack experiment on board Apollo 16 and 17, Life Sci. Space Res. 13, 1975, pp. 153-159
3. Planel, H., Blanquet, Y., Soleilhavoup, J.P., Kaiser, R., and Pianezzi, B., Effects of cosmic heavy ions of *Artemia* egg development, In: Radiation Research (eds Nygaard, O.F., Adler, H.I., and Sinclair, W.K.), Academic Press, New York, 1975, pp. 1152-1163
4. Bücken, H., Results of radiobiological spaceflight experiments, In: Proc. European Symposium on Life Sciences Research in Space, ESA SP-130, 1977, pp. 263-270

TABLE I. - HATCHING RATE OF NAUPLII AND RATE OF ANOMALIES OBSERVED

	Hatching rate %	Rate of anomalies %
Earth tray unit	58 (56, 60)	10.5 (9.2, 11.9)
Side tray unit	48.5 (50.5, 46.5)	12 (10.7, 13.5)
Laboratory control		
6 year old eggs	75.5 (73, 78)	3 (2.2, 4.1)
6 month old eggs	87.3 (85.3, 88.9)	1 (0.5, 1.8)

The numbers in brackets give the lower and upper 68% confidence level.

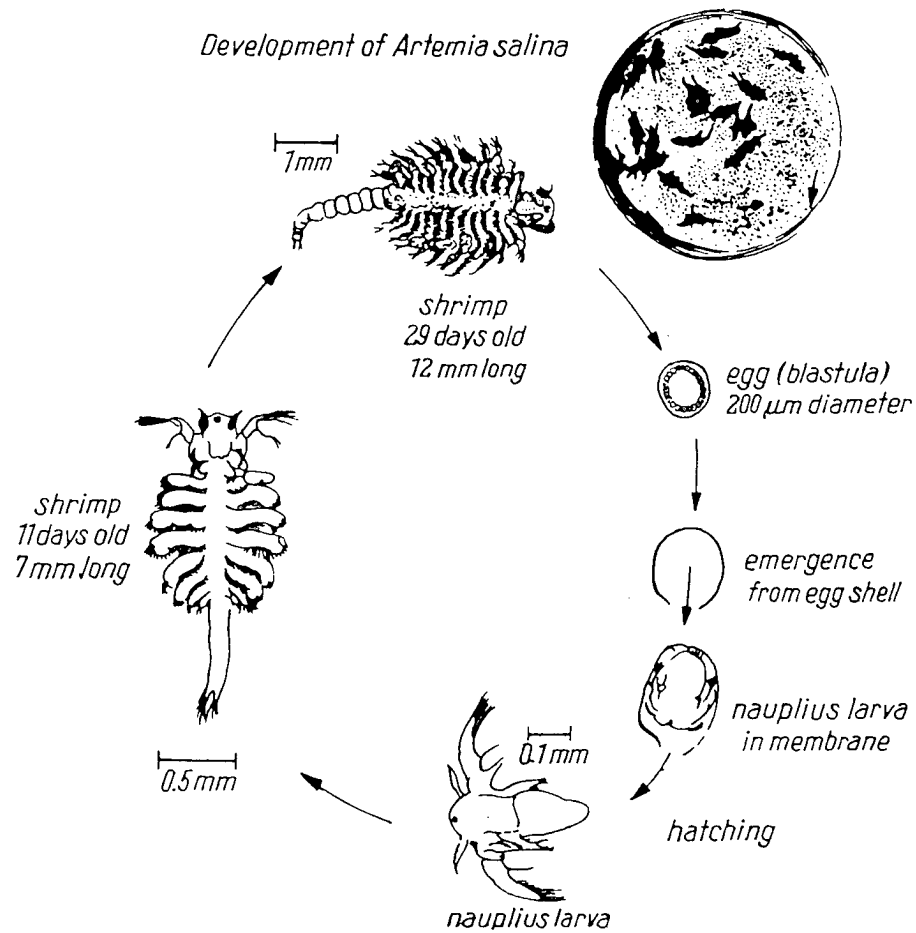


Fig. 1 Life cycle of *Artemia salina*.

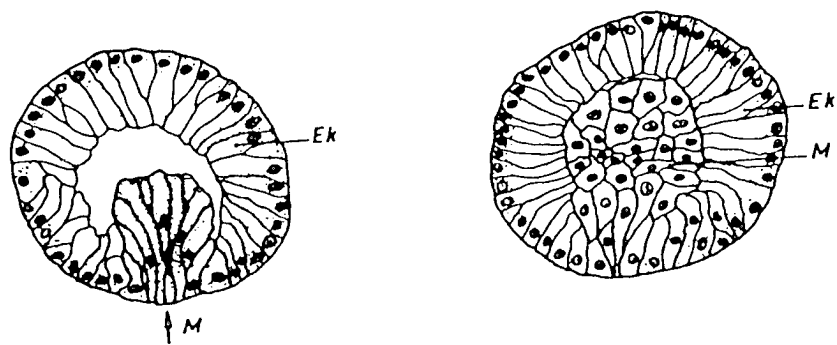
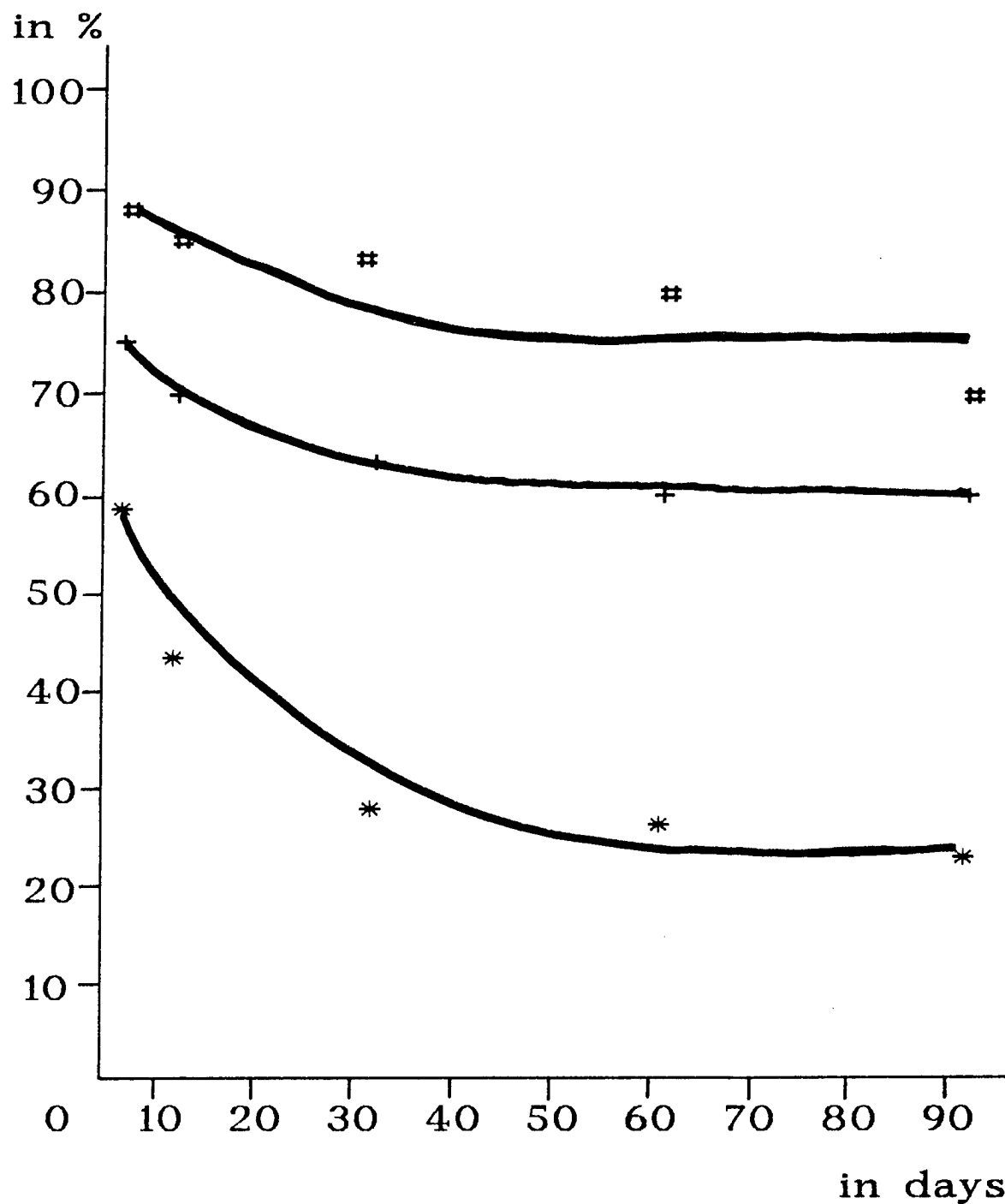


Fig. 2 Histological section through the *Artemia* egg. Early (left) and late (right) state of the gastrula.



GRAUL, RÜTHER, HIENDL 1990

Fig. 3 Life span curves of LDEF *Artemia* eggs flown in Earth tray (\*)  
 6 year old laboratory control (+)  
 6 month old laboratory control (#)

# LONG-TERM EXPOSURE OF BACTERIAL SPORES TO SPACE

G. Horneck, H. Bückner, G. Reitz  
Institute of Aerospace Medicine, DLR, Linder Höhe,  
5000 Köln 90, Germany

## INTRODUCTION

The tropopause has been considered as the upper boundary of the biosphere. Whereas the troposphere is constantly replenished by various microbiota from soil, water and other sources (ref. 1, 2), these organisms will not be accelerated to escape velocities by naturally occurring dynamic forces (ref. 3). Recent evidence that SNC meteorites apparently originated on Mars (ref. 4) has initiated calculations on the possibility of ejecting rocks from a planet as consequence of large meteorite impacts (ref. 5, 6). The question arises whether soil or endolithic microbial communities would withstand such an ejection process and a subsequent exposure to interplanetary space. We have shown that bacterial spores survive after six years in space to a substantial percentage, depending on the degree of shielding against certain factors of the extreme space environment.

Space has been generally viewed as extremely hostile to all forms of life, due to the high vacuum, the complex radiation field and extreme temperatures (table 1). This extreme environment is a definite barrier for the active biological processes of growth, metabolism and reproduction. However, some living organisms have the capacity to survive unfavorable conditions in a dormant state, examples being spores of bacteria and fungi. The high resistance of bacterial spores is mainly due to a dehydrated protoplast, enclosed in a thick protective envelope, the cortex and the spore coats (ref. 7).

From *in-situ* experiments on the responses of microorganisms to the space environment it is known that the most deleterious factor is solar UV-radiation, especially that in the wavelength range around 260 nm and 220 nm (ref. 8, 9), which is specifically absorbed by the DNA. Furthermore, space vacuum and solar UV act synergistically in reducing microbial viability (ref. 10). This phenomenon which is due to the formation of specific scarcely repairable DNA-lesions (ref. 11) further decreases the chance for microorganisms to survive extended exposure in space. So far, microorganisms have been investigated after maximum exposure times in space of 10 days (ref. 10). On the surface of the Moon, *Streptococcus* contaminants inside the Surveyor III television cable were reported to survive for 2.5 years (ref. 12).

## RESULTS

With the NASA mission of the Long Duration Exposure Facility (LDEF) (ref. 13), we have obtained the opportunity to expose *Bacillus subtilis* spores for nearly 6 years to the space environment and to analyse their responses after retrieval. The experiment was mounted onto a side tray of LDEF facing space. The samples were accommodated in an aluminum container the cover of which was a perforated dome. The perforation of the cover allowed access of space vacuum, solar electromagnetic radiation including UV, and cosmic radiation. The temperature during the mission ranged from -9°C to 29°C (table 1). Spores, prepared as previously described (ref. 14), were mounted on quartz discs (ref. 10) either in a monolayer ( $10^6$  spores/sample) or in multilayers ( $10^8$  spores/sample). The quartz discs were fixed onto plastic plates which were stacked in such a way that only samples of the upper plate were reached by solar optical radiation. In parallel, in-flight controls, i.e. samples in closed containers, were utilized as well as ground controls at atmospheric and vacuum conditions.



Samples of the upper plate were confronted with the full space environment including solar UV during the whole mission. From four out of ten samples viable spores were recovered (fig.1). Survival was  $<10^{-4}$ . Since these samples contained spores in multilayers, the outer layers might have provided a protective blanket for the innermost parts allowing them to withstand the harsh space environment. Samples that were exposed beneath neutral density filters of transmissions between 10 and 30 % showed similar survival rates, whereas from samples that were shielded against solar UV-light by an aluminum plate of 2 mm, up to 80 % of the spores were able to germinate and to form a colony (fig. 1). These data show that the chances of microorganisms surviving in free space will be greatly increased by adequate shielding against solar UV-light.

Additives like glucose or buffer salts increase the survival of the spores. This is seen for the dark samples in space vacuum as well as for the in-flight controls kept at atmospheric pressure, and the ground controls running in parallel to the space experiment (fig. 2). From the in-flight controls, up to 100 % of the spores initially sent into space survived. Sugars and polyalcohols are suggested to stabilize the structure of cellular macromolecules, especially during vacuum-induced dehydration.

With this 6 year *in-situ* study in space, we have contributed experimental data to the discussion on the possibility of interplanetary transfer of life. Since spores may withstand the dehydration process induced in space vacuum, they may survive for substantial time, provided they will be protected from solar UV. Such shielding could be reached by dust or soil particles, or by shadowing, or by thick layers as they occur in bacterial colonies, respectively. However, to travel from one planet of our solar system to another, e.g. from Mars to Earth by random motion, a mean time of  $10^5$ - $10^6$  years has been estimated (ref. 6).<sup>\*</sup> It might be precarious to extrapolate from this 6 year study to thousands or millions of years in space. In this large time span, radiation damage produced by cosmic radiation might accumulate, thereby setting the ultimate limit for survival of spores. However, considering the micron size of a bacterial spore and the low flux of cosmic ray heavy ions (ref. 15), a spore will have a reasonable chance to escape a hit by a heavy ion even within very long time spans. Furthermore, we have shown that spores may survive a direct hit even of a cosmic ray iron particle (ref. 16) being the most important component of cosmic radiation with respect to the amount of energy deposited.

#### ACKNOWLEDGEMENTS

We thank the NASA LDEF Project Team, especially W.H. Kinard and J.L. Jones Jr. for their support and U. Eschweiler for her excellent technical assistance.

<sup>\*</sup>H. Wänke, pers. communication.

## REFERENCES

1. Gregory, P.H. *Microbiology of the Atmosphere*, Leonhard Hill, Intertext Publ. Aylesbury, Bucks, 1973
2. Cox, C.S. *The Aerobiological Pathways of Microorganisms*, J. Wiley & Sons, Chichester, 1987
3. Bückner, H. & Horneck, G. *Life Sci. Space Res.* **7**, 1969, pp. 21-27
4. Kerr, R.A. *Science* **237**, 1987, pp. 721-723
5. Vickery, A.M. & Melosh, H.J. *Science* **237**, 1987, pp. 738-743
6. Melosh, H.J. *Nature* **332**, 1988, pp. 687-688
7. Gould, G.W. & Hurst, A. *The Bacterial Spore*, Academic Press, New York, 1969
8. Taylor, G.R., *Ann. Rev. Microbiol.* **28**, 1974, pp. 121-137
9. Horneck, G. *Adv. Space Res.* **1**, #14, 1981, pp. 39-48
10. Horneck, G., Bückner, H., Reitz, G., Requardt, H., Dose, K., Martens, K.D., Mennigmann, H.D. & Weber, P. *Science* **225**, 1984, pp. 226-228
11. Lindberg, C. & Horneck, G. *J. Photochem. Photobiol. B: Biology* **11**, 1991, pp. 69-80
12. Mitchell, F.J. & Ellis, W.L. In *Proc. Second Lunar Sci. Conf.* **3**, 2721-33
13. Clark, L.G., Kinard, W.H., Carter, D.J. Jr. & Jones, J.L. Jr. (eds) *The Long Duration Exposure Facility (LDEF) Mission 1 Experiments*, NASA SP-473, 1984
14. Baltschukat, K. & Horneck, G. *Radiat. Environ. Biophys.* **30**, 1991, pp. 87-103
15. Simpson, J.A. *Ann. Rev. Nucl. Part. Sci.* **33**, 1983, pp. 323-381
16. Horneck, G., Schäfer, M., Baltschukat, K., Weisbrod, U., Micke, U., Facius, R. & Bückner, H. *Adv. Space Res.* **9**, 1989, pp. (10)105-(10)116

TABLE I. - ENVIRONMENTAL DATA OF THE LDEF EXPERIMENT DURING 2107 DAYS IN LOW EARTH ORBIT COMPARED WITH THE INTERPLANETARY SPACE

	LDEF experiment	Interplanetary space
Pressure (Pa)	app. $10^{-6}$	$10^{-14}$
Residual gas ( $\text{cm}^{-3}$ )	$2 \times 10^6$ He $1 \times 10^5$ N $3 \times 10^7$ O	1 H
<b>Radiation</b>		
Solar UV (>110 nm)		
Fluence ( $\text{J/m}^2$ )	$1 \times 10^9$	variable <sup>1)</sup>
Ionizing Sources	galactic solar belts (SAA)	galactic solar
Dose (Gy)	4.8	0.5
Heavy ions ( $\text{cm}^{-2}$ ) <sup>2)</sup>	$2.5 \times 10^4$ <sup>3)</sup> app. 60 <sup>4)</sup>	$3.6 \times 10^4$
<b>Temperature (K)</b>	264-302	>4 <sup>1)</sup>

(SAA)= South Atlantic Anomaly

1) depending on distance from the sun

2) atomic number >2, Linear Energy Transfer (LET) >130 keV/mm

3) including secondaries

4) primaries

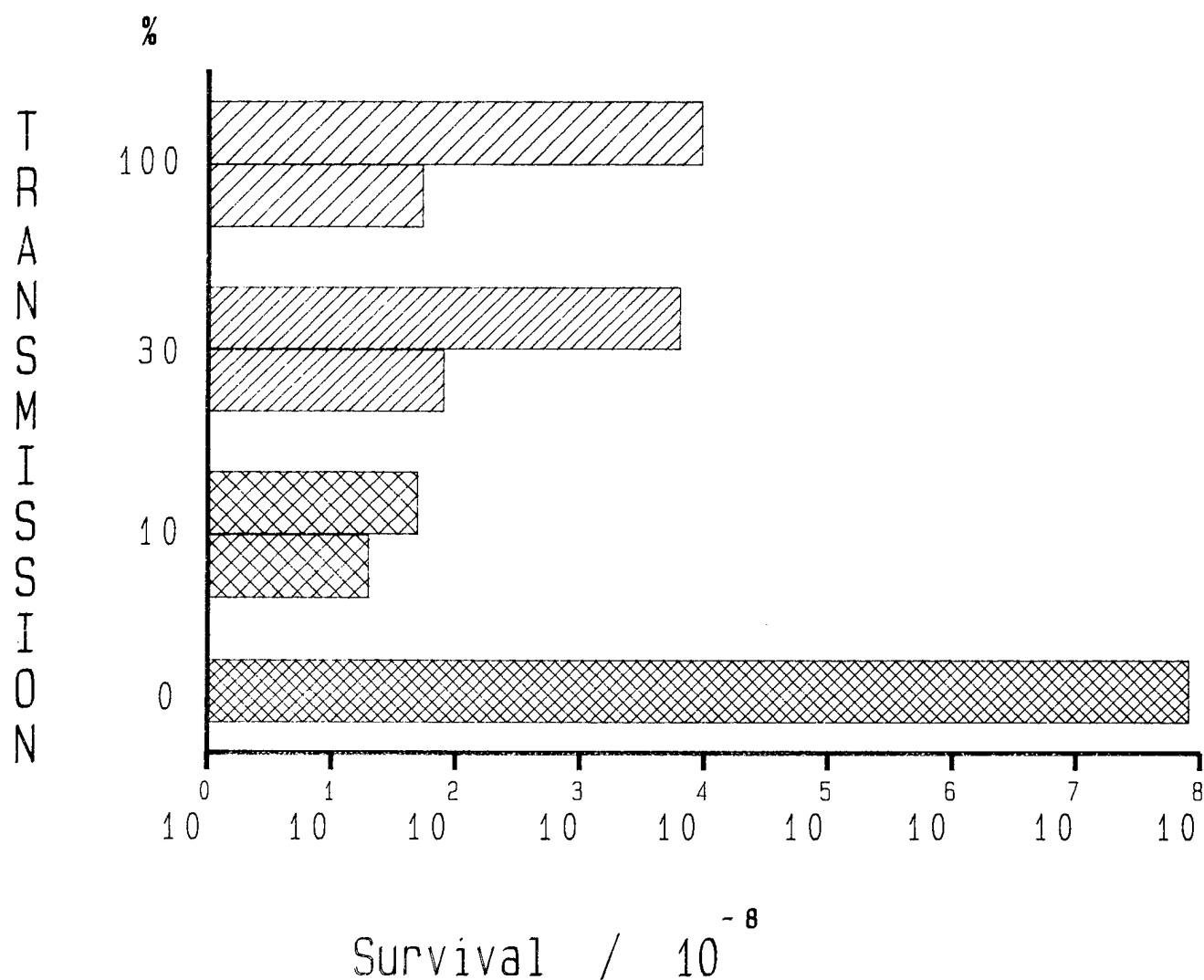


Fig. 1. Survival of *Bacillus subtilis* spores exposed to the space environment for nearly 6 years during the LDEF mission (April 7, 1984 - January 12, 1990). Spores were exposed in multilayers in the presence of 5 % glucose on quartz discs beneath a perforated dome without any further cover (100 % transmission), or beneath neutral density filters (30 % or 10 % transmission for solar UV-light of wavelengths >170 nm), or beneath an aluminum plate of 2 mm (0 % transmission). Non-covered samples received a solar UV-irradiation of  $1 \times 10^9 \text{ J/m}^2$ .

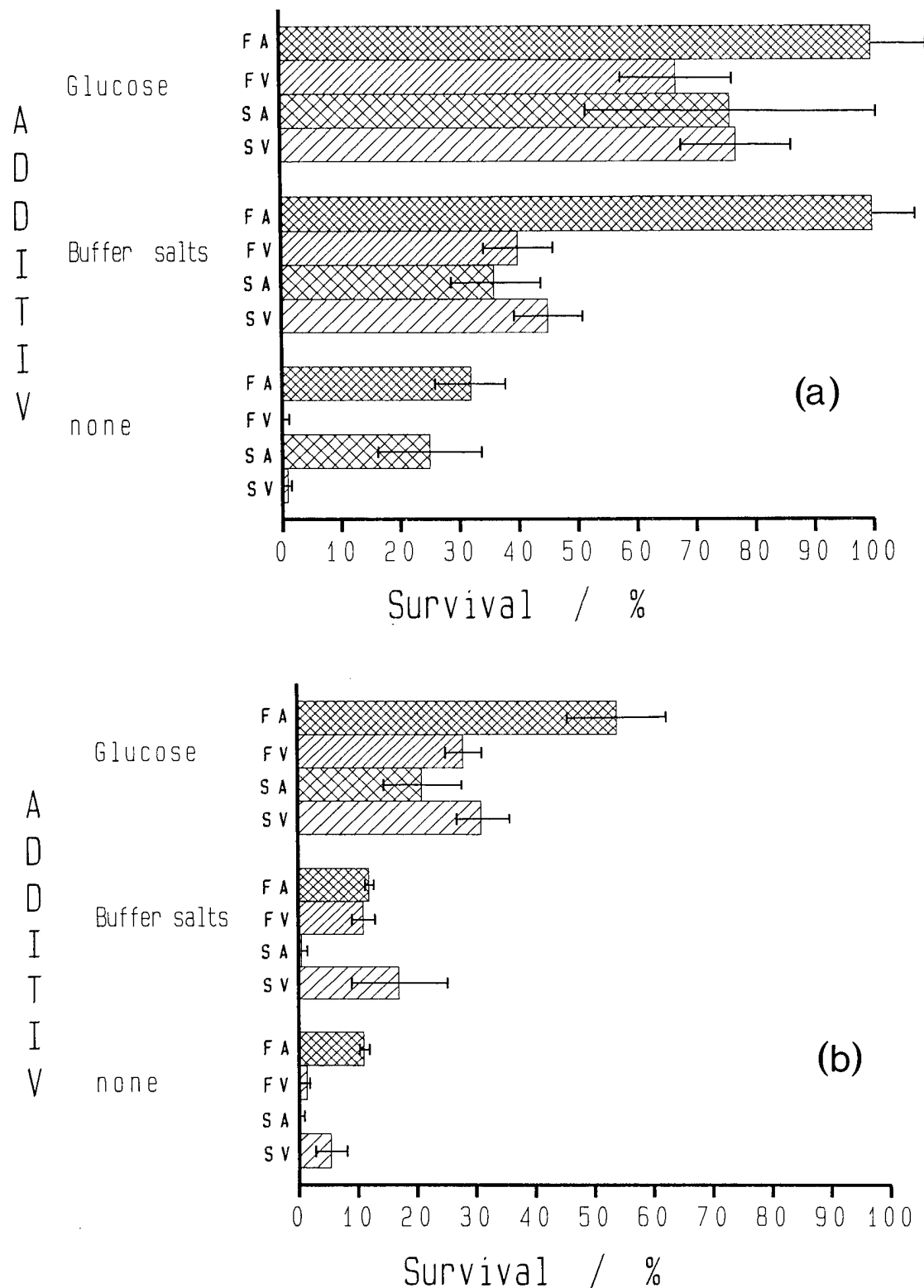
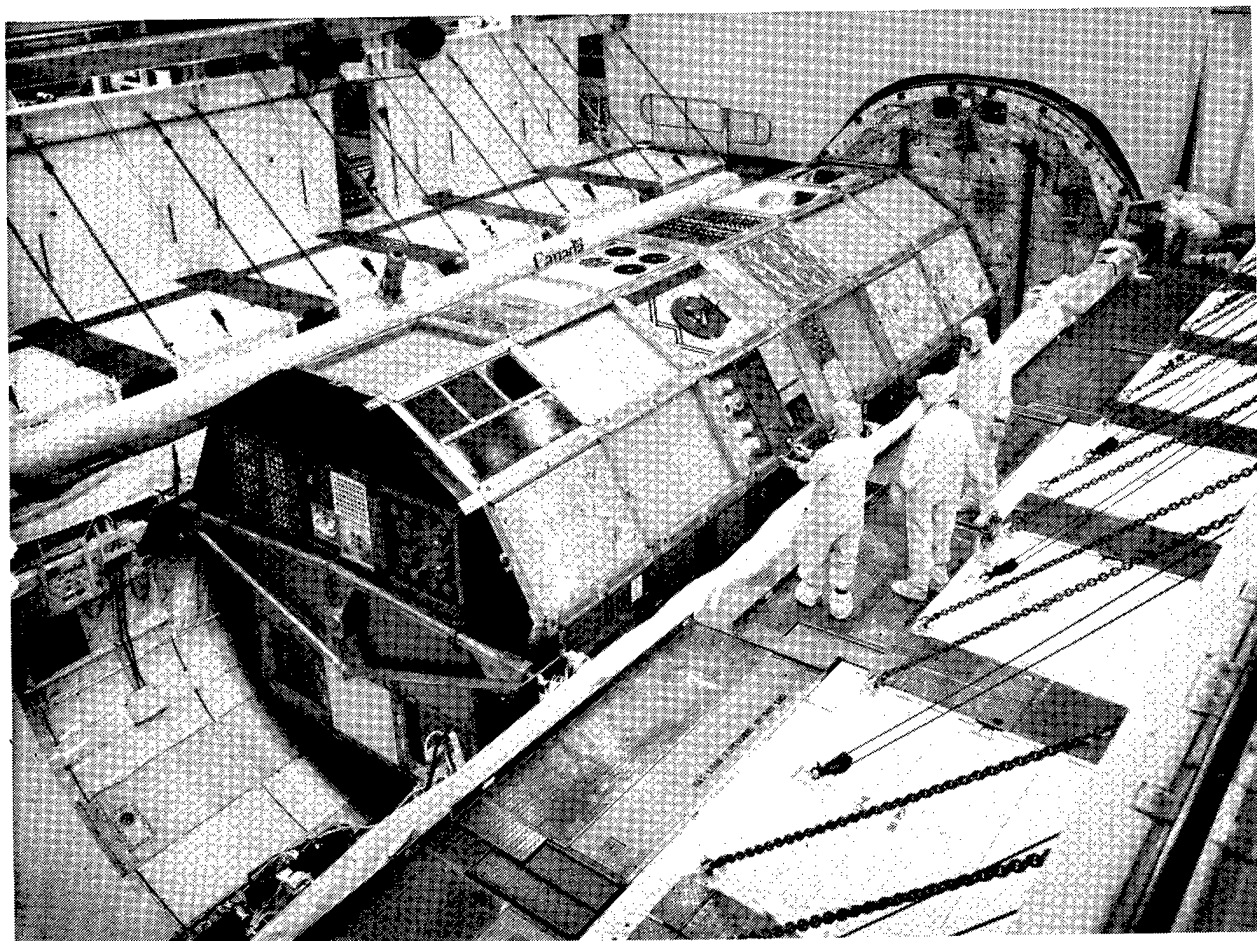


Fig. 2. Survival of *Bacillus subtilis* spores in multilayers (a) or in a monolayer (b) after nearly 6 years in space during the LDEF mission and ground control data. The spores were shielded against solar optical radiation. Protective substances (5 % glucose or 1.4 % buffer salts) were added to some of the samples during preparation. F = flight samples; S = samples of the simulation experiment on ground; A = samples kept at atmospheric pressure; V = samples in vacuum.

# SPACE ENVIRONMENTAL EFFECTS

## *MICROGRAVITY*



# RESULTS OF THE TTF-TCNQ AND THE CALCIUM CARBONATE CRYSTALLIZATION ON THE LONG DURATION EXPOSURE FACILITY

Kjeld Flemming Nielsen  
Physics Laboratory III, Building 309  
Technical University of Denmark  
DK-2800 Lyngby  
Phone: (45) 42 88 16 11; Fax: (45) 45 93 16 69

M. David Lind  
Rockwell International Science Center  
1049 Camino Dos Rios  
Thousand Oaks, CA 91360  
Phone: 805/373-4190; Fax: 805/373-4775

## SUMMARY

Experiment A0139A on the LDEF carried four large containers (volume, one to two liters each) into orbit five years with crystal growth solutions for lead sulfide, calcium carbonate, and TTF-TCNQ. The facility was in excellent condition after the long orbital stay. Although the temperature data were lost, the experiment program had been working, since the valves in all containers had been opened. All four experiments produced crystals of varying quality. The calcium carbonate crystals had the best appearance. The TTF-TCNQ crystals were packed together near the valve openings of the container. When taken apart, the single crystals showed some unusual morphological properties.

X-ray investigations (Laue back-reflection and transmission diagrams) as well as conductivity measurements (four-point probe) on long duration space grown TTF-TCNQ crystals will be presented. Comparison will be made with our previous space solution growth experiments on the European Spacelab Mission. The TTF-TCNQ crystals are no longer of the highest scientific interest, so this activity has been terminated by us. Instead, the interest in ESA is focussed on calcium carbonate and calcium phosphate crystallizations.

## BACKGROUND

Following the crystal growth experiments with unidirectional conductors on the European Spacelab by K. F. Nielsen (ref. 1-4), and the Apollo-Soyuz investigations on room temperature solute diffusion crystal growth by M. D. Lind (ref. 5-8), it was decided by both investigators to share what was later named experiment A0139A on the LDEF. Each experimenter had two growth containers, and all four were kept at a constant temperature (35° C) in a thermostated drum (ref. 9). The growth containers were manufactured at the experimenters' individual laboratories, while the enclosure and the insulation equipment were manufactured at Rockwell. A smaller drum containing the data and electronics equipment was manufactured at Terma Electronics, Ltd., in Denmark. All equipment, the content, and the aim of the four crystal growth experiments have been fully described elsewhere (ref. 10)

## EQUIPMENT

The equipment appeared to be in excellent condition upon opening. However, our first observation was that all data stored in the experiment memory had been lost due to a breakdown in an electronic circuit. This included the temperature vs. time profile and the time of opening of the reactor valves. The next observation was, fortunately, that all motors connected to the valves had been in operation and turned the gears to the end point position. This meant that the process controller had been working up to a point, presumably also with temperature control. The fault must have occurred at a later stage in the LDEF flight, or after recovery. The memory battery was not a factor. A full description of the equipment operation is given in ref. 10.

## CRYSTAL GROWTH PROCESS

The calcium carbonate experiment produced the best crystals by far. A full description of this experiment is given in ref. 10. Table I (ref. 10) gives the concentrations of the solutions and the dimensions of the growth reactors.

TABLE I. SOLUTION COMPOSITIONS AND REACTOR CHAMBER LENGTHS

Crystal	Reactant	Chamber	Center Chamber		Reactant	Chamber
	Solution	Length, cm	Length, cm		Solution	Length, cm
CaCO <sub>3</sub>	0.2 M NH <sub>4</sub> HCO <sub>3</sub>	29.1	5.6		0.2 M CaCl <sub>2</sub>	29.1
PbS	0.2 M CH <sub>3</sub> CSNH <sub>2</sub>	51.8	5.6		Saturated PbCl <sub>2</sub>	6.9
TTF-TCNQ	0.013 M TTF	18.6	7.5		0.013 M TCNQ	18.6
TTF-TCNQ	0.026 M TTF	18.6	7.5		0.026 M TCNQ	18.6

Here we shall elaborate on TTF-TCNQ. As seen from Table 1, the two TTF-TCNQ experiments were identical with the exception that the concentrations of TTF and TCNQ in the supply chambers were doubled in experiment 2. Also on Spacelab we used identical experiments with the purpose of testing one single parameter. On Spacelab we tested the use of filters between supply chamber and crystallization chamber with open valves. On LDEF we tested the solution strength. Concentrations of 0.026 M for TTF and TCNQ are the highest possible concentrations to use at 35° C, and 0.013 M is on the low side. We took the decision not to use filters in the valve openings.

Results were the same in both experiments, and the same problem was encountered in both experiments. The bulk of the crystals appeared in the valve opening between the TTF supply chamber and the central chamber, causing the valve to stick in a half open position. In both cases this brought about mechanical failure of the shaft connecting the valve to the gears. It was not expected that the crystallization should be so strongly localized. Possibly it was caused by the fact that the valve openings had no filter protection. The decision whether to use filters or not had to be taken before the results of Spacelab were known. These results (ref. 3) indicated that at least on Spacelab the microgravity condition alone was not



sufficient to prevent liquid flow through the valve or in the container as a whole; this was in spite of the fact that special precautions were taken to have equilibrium pressure in all three reactor compartments both before and after the opening of the valves. The same precautions were taken on LDEF, and here the microgravity condition should be superior to Spacelab. The calcium carbonate and lead sulfide experiments both had filters placed in all valve openings. Whatever happened with TTF-TCNQ, it appears that the TTF valve, shortly after opening, was blocked by growing crystals in such a way that diffusion or any other transport through the opening eventually was prevented. Thereafter no more crystallization took place.

## TTF-TCNQ CRYSTALS

The clusters of crystals in the valve openings (Fig. 1a, b) were positively identified as TTF-TCNQ. X-ray analysis (Weissenberg rotating crystal) showed monoclinic symmetry with unit cell constants  $a = 12.2980 \text{ \AA}$ ,  $b = 3.8190 \text{ \AA}$ ,  $c = 18.4680 \text{ \AA}$ , and  $\beta = 104.46^\circ$ . The morphology of the crystals was, however, somewhat unusual. Usually the long axis of the crystals is the  $b$  axis. Here it appears to be the  $a$  axis. This observation was confirmed by Laue X-ray diffraction photographs (Fig. 2a, b). Experimental Laue photographs are compared with computer simulated patterns (ref. 11) for the (010) and (001) orientations. It is clearly demonstrated that (1) the patterns are identical, and (2) the preferred direction of growth is the  $a$  axis. As already mentioned, this is unusual. Normally the  $b$  axis is the preferred direction of growth.

The conductivity measurements again confirmed the long axis not to be the  $b$  axis. The conductivity curves (Fig. 3) are quite normal for any other axis than the  $b$  axis in the crystals. Only the  $b$  axis shows the characteristic peak at  $60^\circ \text{ K}$ . Since we could find no crystal that measured more than  $0.1 \text{ mm}$  along the  $b$  axis, this measurement could not be done.

Fig. 4a shows a typical TTF-TCNQ crystal mounted on a goniometer head, while Fig. 4b is a view of the crystals as they appear in an optical microscope.

## TTF-TCNQ: HISTORICAL BACKGROUND

The TTF-TCNQ growth experiment was first proposed in 1975 for the European Spacelab Mission. Background for the proposal was the very high interest among solid state physicists at that time for TTF-TCNQ crystals. The discussion was about the unidirectional ( $b$  axis) conductivity in the crystals with the sharp peak at  $60^\circ \text{ K}$ ; the question was whether it was connected to superconductivity or not. In 1980 substantial evidence (ref. 12) was put forward that it was not, but at the same time unquestionable superconductivity was found in derivatives of TTF, the so-called Bechgaard salts. The question of superconductivity in TTF-TCNQ was not fully resolved in 1983, the year of the Spacelab Mission, but TTF-TCNQ was not taken on that mission due to safety problems connected with the acetonitrile used as the solvent. The two large experiments with TTF-TCNQ were then taken on the LDEF Mission, launched in 1984. By that time a number of new organic superconductors had been found, bringing the transition temperature in organics up to  $7^\circ \text{ K}$ . In November, 1984, NASA's orbiter Atlantis, Mission STS 61-B, conducted a TTF-TCNQ growth experiment one week in duration, performed by Radcliffe *et al.* (ref.13).

In late 1986 the first inorganics that showed high  $T_c$  superconductivity were found. Early in 1987 the transition temperature for superconductivity came above the boiling point of nitrogen with the discovery of the YBaCuO ceramics. The interesting  $b$  axis conductivity peak in TTF-TCNQ was at  $60^\circ \text{ K}$ , well below liquid nitrogen temperature, so obviously these new inventions caused a diminishing interest for TTF-TCNQ crystals. Already then the interest had been low, since a very large number of new organic superconductors had been synthesized. TTF-TCNQ is now considered a well known material with no properties related to superconductivity. As a consequence of this, already before the retrieval of LDEF,

a large TTF-TCNQ experiment, planned by ESA for the EURECA platform, was cancelled. The growth container (volume, five liters) will now be used for the growth of calcium phosphate crystals from amorphous tricalcium phosphate in aqueous solution. A basic study of the gravitational influence on this process is of importance in relation to mineralization and demineralization of bone tissue in vertebrates. Fortunately the equipment that had already been developed for TTF-TCNQ, with only very minor adjustments, could be refitted to this investigation.

## CONCLUSIONS

In summary the results are that the calcium carbonate experiment produced outstandingly good results, the lead sulfide experiment was unsuccessful, and the two TTF-TCNQ experiments produced only mediocre results. The conclusion could thus be that the three latter experiments should not have been performed. This conclusion is perhaps the most valid one for the TTF-TCNQ experiments, since even in the case they had produced good crystals, these crystals would have been of no particular interest to the scientific or commercial communities.

The lesson to be learned could be that production in space, even of the most highly desired materials, is a risky business. Basic research may, on the other hand, draw extreme benefits from the microgravity condition, since experimentation on Earth cannot produce the same results. A number of theories on the morphology of crystals need experimental verification. The crystallization of calcium carbonate or calcium phosphate in water are examples of systems where more knowledge may greatly benefit society.

## ACKNOWLEDGMENTS

We thank Claus S. Jacobsen, G. Galster, Line Groth-Andersen, and Ib Johannsen for helpful assistance with the TTF-TCNQ experiments.

A special acknowledgment is made to Simon Spies, late owner of the Spies Airline Group, who generously supported this project through his private company, Space Flight Corporation of Denmark, Ltd. The company director, Jan Schmidt, followed our project with the greatest interest until his untimely death in 1984, only one week before the launch of the LDEF. In addition the project was supported by the Thomas B. Thriges Foundation.

## LITERATURE REFERENCES

1. K. F. Nielsen, "Diffusion Growth of Organic Charge-Transfer Crystals", Proc. 2nd Europ. Symp. Mat. Sci. Space, Frascati, Italy, April, 1976, ESA SP-114, 255.
2. K. F. Nielsen, "Preparations for Growth of TTF-TCNQ in Microgravity Environments", Europhys. Conf. Abs., Vol. 3F, 171 (1980).
3. G. Galster and K. F. Nielsen, "Crystal Growth from Solution", Proc. 5th Europ. Symp. Mat. Sci. Microgravity, Schloss Elmau, FRG, November 5-7, 1984, ESA SP-222, 189.
4. I. Johannsen, L. Groth-Andersen, and K. F. Nielsen, "Crystal Growth of TTF-TCNQ from Oriented Seeds", J. Cryst. Growth **51**, 627 (1981).
5. M. D. Lind and K. F. Nielsen, "LDEF Experiments - Crystal Growth by a Solute Diffusion Process", Proc. 4th Europ. Symp. Mat. Sci. Microgravity, Madrid, Spain, April 5-8, 1983, ESA SP-191, 167.
6. M. D. Lind, "Crystal Growth, Experiment MA-028", in "Apollo-Soyuz Test Project Summary Science Report", NASA SP-412, 555 (1977).
7. M. D. Lind, "Crystal Growth from Solutions in Low Gravity", Paper 77-197, Proceedings of the AIAA 15th Aerospace Sciences Meeting, Los Angeles, CA, January 24-26, 1977; AIAA Journal **16**, 458 (1978).
8. K. F. Nielsen and M. D. Lind, "Solution Crystal Growth on the Apollo-Soyuz, the Spacelab, the LDEF, and the EURECA Missions", Proc. 15th Int. Symp. Space Tech. Sci., Tokyo, May, 1986, 2111.
9. M. D. Lind and K. F. Nielsen, "Growth of Crystals from Solutions in Low Gravity (A0139A)", LDEF Mission 1 Experiments, NASA SP-473, 8 (1984).
10. M. D. Lind and K. F. Nielsen, "Crystal Growth by Solute Diffusion in Earth-Orbit", Proc. SPIE 1991 Int. Symp. Opt. Appl. Sci. Eng., San Diego, California, July 21-26, 1991, Vol. 1557, paper 38.
11. G. Christiansen and L. Gerward, "LAUE - a Program for High-Precision Orientation of Crystals Using the Laue Method", J. Appl. Cryst. **22**, 397 (1989).
12. J. P. Long and C. P. Slichter, "Scanning-Electron-Microscope Technique for Measuring Electrical Conductivity: Application to TTF-TCNQ", Phys. Rev. B **21**, 4521 (1980).
13. M. D. Radcliffe, J. E. Steffen, E. L. Cook, J. F. Cutting, L. R. Miller, M. C. Drake, F. S. Schroder, and J. Stevens, "Organic Crystal Growth in Low Earth Orbit", J. Cryst. Growth **92**, 581 (1988).

Fig. 1a.

Quartz valve with  
remains of crystal  
clusters in the  
valve openings.  
Shaft connecting  
pins in the center  
are deformed.

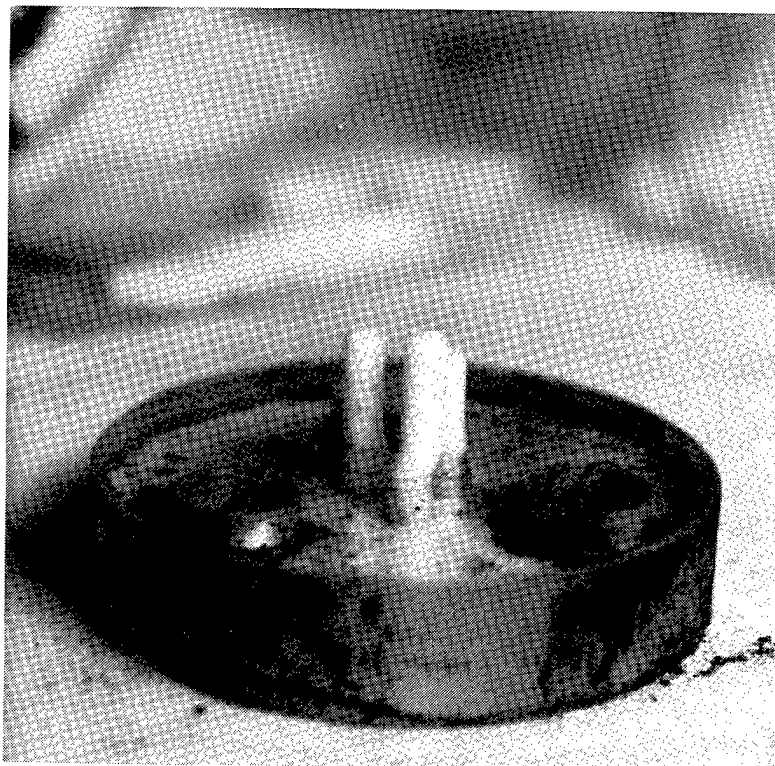


Fig. 1b.

Close-up of TTF-TCNQ  
crystals in cluster.

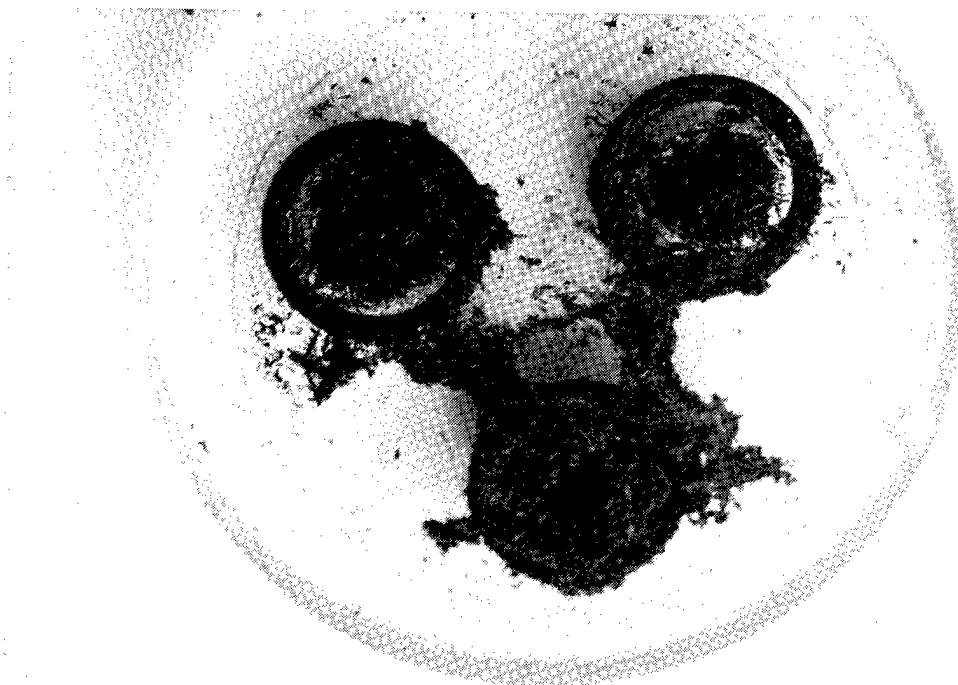
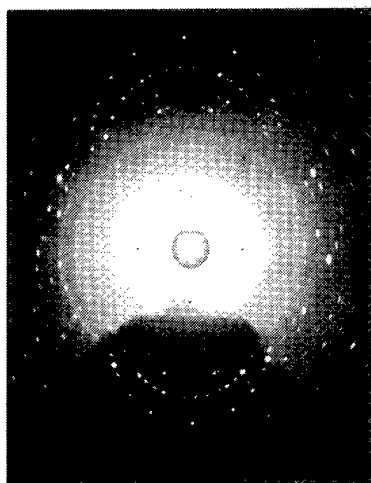


Fig. 2a.

Left:

Transmission  
X-ray Laue  
photograph  
perpendicular  
to crystal  
plate.



Right:

Computer  
simulated  
Laue pattern  
for b axis  
(010).

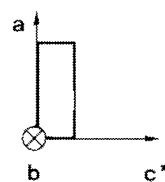
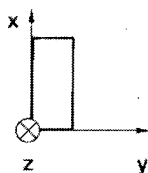
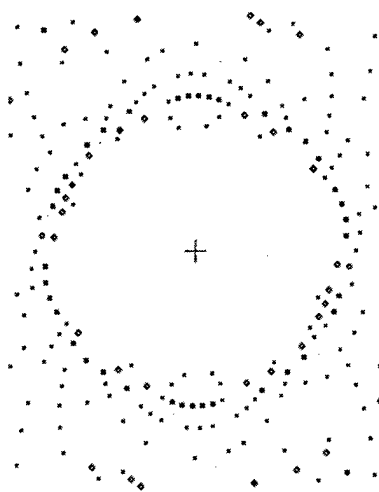


Fig. 2b.

Same for  
crystal  
edge.  
(001)  
plane.

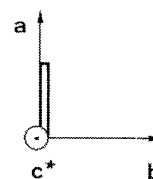
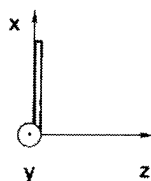
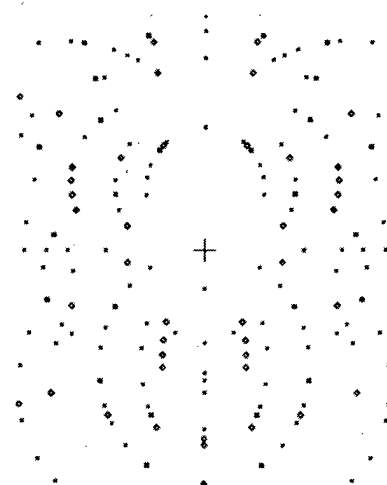
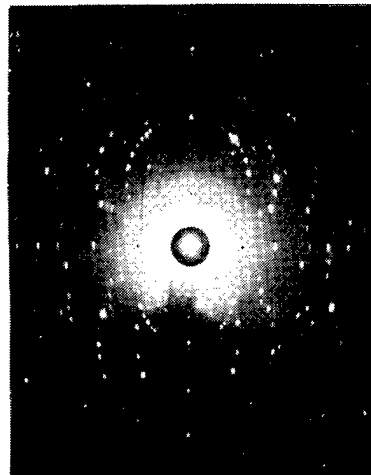


Fig. 3a.

Typical conductivity curves from space-grown crystals show only trivial temperature variation. (No peak at 60° K).

Samples of TTF-TCNQ from LDEF experiment.

Dots: R900806A/CSJ.

Triangles: R900809A/CSJ.

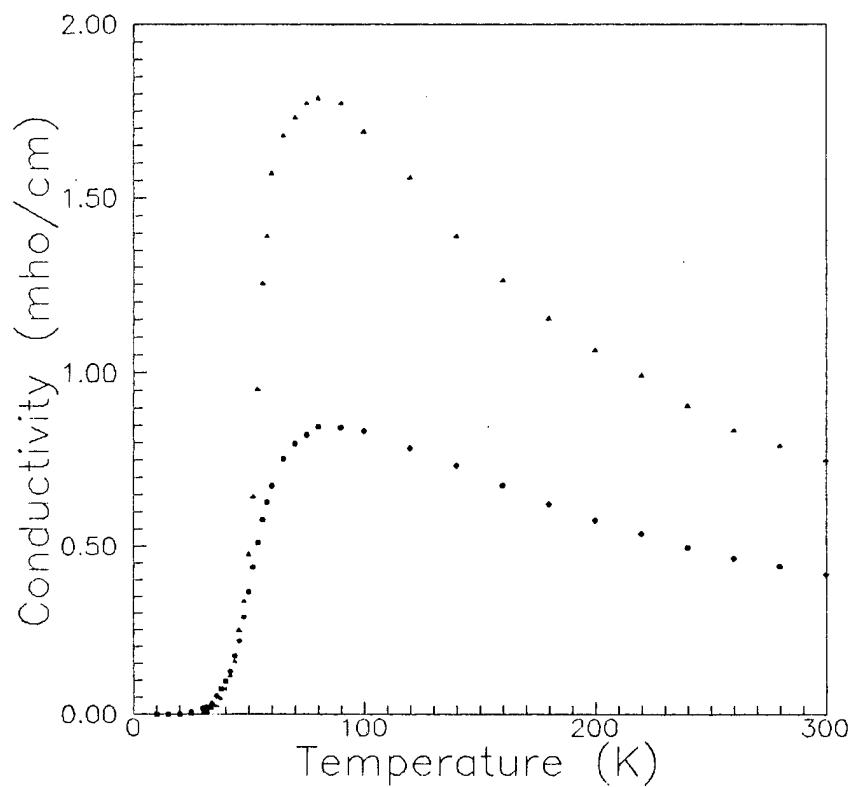


Fig. 3b. 1 mm long TTF-TCNQ crystal with four wires attached.

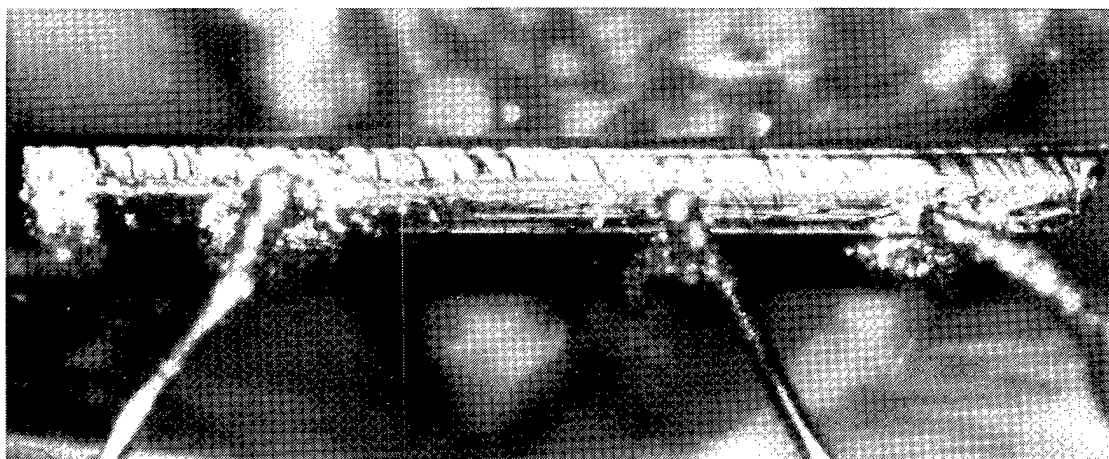


Fig. 4a.

TTF-TCNQ crystal  
mounted on the  
goniometer head  
for X-ray  
analysis.

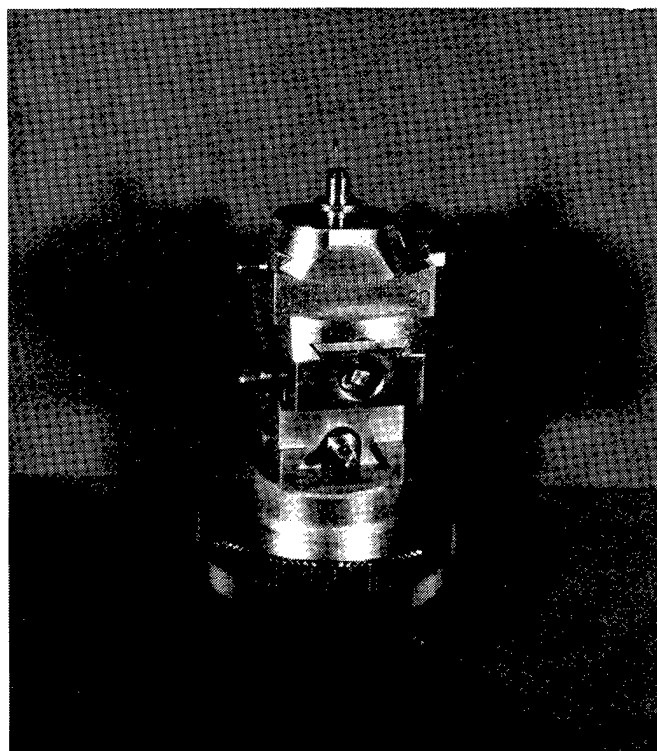
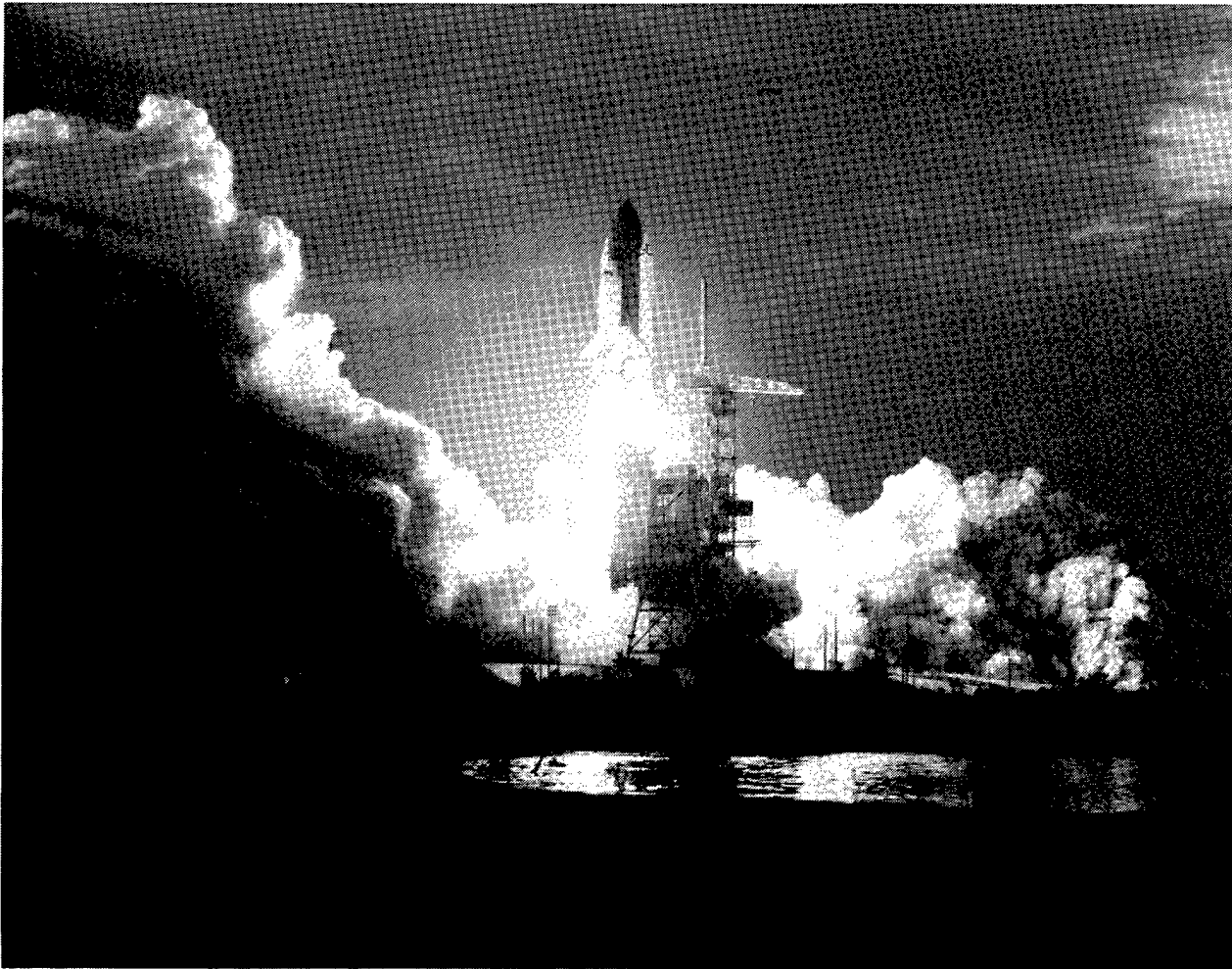


Fig. 4b.

Typical TTF-TCNQ  
crystals grown on  
the LDEF mission.  
(Length of center  
crystal = 1 mm).



## THE FUTURE





# THE ROLE OF THE LONG DURATION EXPOSURE FACILITY IN THE DEVELOPMENT OF SPACE SYSTEMS

Sally A. Little

NASA Space Station Freedom Program Office

Reston, VA 22091-4398

Phone: 703/487-7355, FAX: 703/487-7997

## SUMMARY

The Long Duration Exposure Facility (LDEF) presents the international, aerospace community with an unprecedented opportunity to examine the synergistic, long-term, space environmental effects on systems and materials. The analysis of the data within appropriate environmental contexts is essential to the overall process of advancing the understanding of space environmental effects needed for the continuing development of strategies to improve the reliability and durability of space systems and to effectively deal with the future challenges that new space initiatives will likely present.

## TRANSCRIPTION OF SYMPOSIUM ADDRESS

We have many dreams. They begin with a vision. In the late 1960's, the people of Langley had a vision for a low-cost, reusable satellite called the "Long Duration Exposure Facility - LDEF".

The community gathered here today, shared in this vision. Together, we have made LDEF happen. And now we find ourselves in the most crucial phase of its mission - in terms of realizing its most fundamental purposes, as well as at a crossroads over whether we will be able to fully exploit its potential.

We did not fly LDEF to demonstrate Shuttle deployment and retrieval capabilities, though this was most certainly accomplished. It is in doing our postflight analysis that we engage in fulfilling our LDEF dream.

To talk to this audience about the role the Long Duration Exposure Facility is playing and can play in the development of space systems may be like preaching to the choir. We do know that it is sometimes a lesson not easily learned by those who are not actively engaged in this multi-disciplinary enterprise of exploring space environments and their effects. This makes it all the more important for us to be persuasive in articulating our purposes and their value - which are both scientific and

pragmatic.

Sometimes we walk a tight rope of sorts - not wanting to frighten the reluctant with what we don't know and need to learn - yet not wanting to inspire so much confidence as to evoke complacency. We must persistently ask of ourselves and each other: "What are the real needs?" and "How can we effectively communicate them?"

We hope that the LDEF will help us do that. Of this we can be certain - the work of the space environments and effects community directly impacts what we do "up there", how well we do it, how long we do it, and of course, why we bother at all. This work is fundamental to expanding our presence in space, whether it is human or robotic.

The Augustine Committee report addressed the importance of developing the "building blocks" that enable significant missions to be undertaken.<sup>1</sup> And just as they called the Space Station "the essential building block of the manned exploration program"<sup>2</sup>, we know that LDEF and LDEF-like missions can claim "generic applicability" in their block-building role for increasing our understanding of space environments and effects.<sup>3</sup>

In examining LDEF-as-a-space-system, we explore macro and micro meanings; qualitative and quantitative data; and above all, synergistic relationships. We explore the multitude of changing environments that LDEF experienced throughout its journey, pursue its most pervasive aspects, and attempt to understand the mechanisms which cause the effects observed.

LDEF is clearly "about" more than determining environmental exposures, more than quantifying damage. It is very much "about" using this information to build better, more reliable, more durable space systems.

LDEF teaches us how to better adapt. It is not a matter of "Can we do it?", but one of "How can we do it?" and "How can we do it better?" LDEF-as-a-space-system is a building block in this process.

So much of what we are trying to accomplish has to do with making connections: between environments, durations, other flight experiences, ground-based simulation testing, modeling efforts, and connections to what we want to do in the future.

How are LDEF and Space Station "connected"? I would like to suggest that the most important connection is YOU. Last night, Arnold Aldrich (NASA Associate Administrator for the Office of Aeronautics and Exploration Technology) offered many examples of how the analysis of LDEF serves the development of Space Station Freedom. Its value is obvious and compelling for Space Station, as well as a multitude of space system development programs, because its focus is on the

fundamental aspects of surviving-and-thriving in space for long durations.<sup>4</sup>

This community has been very sensitive to the needs of the "user" community of spacecraft designers and builders. I cannot emphasize enough the importance of the on-going dialogue. With your cooperation and enthusiastic participation, Space Station Freedom Working Group members have been able to examine real-time the development of the LDEF data. We are most appreciative.

I hope we will all continue to use the LDEF organization created by Langley to preserve, integrate, and disseminate LDEF findings to help ensure that the whole aerospace community is the beneficiary and not just the Space Station. We also hope that you will participate with us in workshops in the future focused on the extrapolation and application of LDEF findings to the specific needs of the space systems development community.

Through the LDEF newsletter with a circulation of over 1300, programmatic reviews, LDEF special investigative reports, your publications in journals, and informal briefings at the working level, LDEF information is being disseminated to the "user" community.

While the "user" community acknowledges that the longer duration spaceflight of LDEF has been advantageous in many respects, it is important to note that a prolonged duration postflight analysis effort is NOT...We lose not only time, but we lose data, and we risk losing important momentum.

There is life after LDEF. The LDEF-1, as valuable as it is, and as much as it will contribute, does not constitute the alpha and omega of all that needs to be done to support the development of future space systems.

The LDEF-1 mission must someday end. Hopefully, because it has been completed, it's fundamental purpose satisfied. Clearly, for this community: THE JOURNEY MUST CONTINUE. Fresh opportunities are required. We must advance our understanding of space environments and effects to continue to develop strategies to improve the reliability and durability of space systems and to effectively deal with the future challenges that new space initiatives will likely present.

Perhaps the time has come and perhaps LDEF brings it to us, to recognize this community as a natural constituency for the advocacy of a strong, coherent, comprehensive space environments and effects program. We have many dreams. We know they begin with a shared vision.

Perhaps no one can understand better than YOU - the LDEF investigative community - the trials and tribulations that dreams sometime endure along their path to actualization. We all remember that there were those who thought the LDEF would

never fly. There were those who vowed that it would never return. And there are those who still seem unable to visualize the completion of the LDEF-1 mission.

Let us be mindful that we can only create new possibilities by believing in their potential.

I hope that during this busy week of sharing our LDEF findings-to-date, we will take the opportunity to talk with each other about this "vision thing".

And now, the tapestry of LDEF-1 calls with a rich story to tell and there is no one better qualified to tell it than this community of LDEF investigators. May the sessions begin!

#### REFERENCES

1. Report of the Advisory Committee on the Future of the U. S. Space Program. U. S. Government Printing Office, Washington, D. C., Dec. 1990, pp. 2.
2. Ibid, pp. 29.
3. Ibid, pp. 31.
4. Little, S. A.; Kinard, W. H.; Whiteside, J. B.: The Role of the Long Duration Exposure Facility in the Design of the Space Station Freedom. 41st IAF Congress, Dresden, IAF-90-080, July 1990.

RETRIEVABLE PAYLOAD CARRIER  
--NEXT GENERATION LONG DURATION EXPOSURE FACILITY--

Arthur T. Perry  
American Space Technology, Inc.  
2800 28th Street, Suite 351  
Santa Monica, CA 90405-2934  
Phone: 213/450-7515, Fax: 213/450-7304

SUMMARY

This paper describes the Retrievable Payload Carrier (RPC), which is a multi-experiment, free-flyer spacecraft being privately developed to make in-space experimentation more accessible and economically feasible for research and development organizations. The carrier concept was derived from NASA's highly successful and flight-proven Long Duration Exposure Facility (LDEF). The LDEF capabilities have been enhanced to meet new customer requirements. This reusable payload carrier is planned for launch and retrieval by the space shuttle on a regular basis. The RPC's compact design will facilitate flexible manifesting of the shuttle cargo bay space, thereby permitting timely launches and retrievals. The vehicle is designed so that either the entire carrier can be retrieved from orbit, or individual experiment pallets can be removed and replaced in orbit. This will give customers even greater control over their experiment recoveries. A fully operational RPC Program consists of: 1) a carrier spacecraft; 2) a ground control station for communication with customer payloads and the carrier; 3) a ground processing facility to provide refurbishment, final checkout, and integration of customer payloads and the carrier; and 4) the personnel required to support both the development and operational phases of the program. Customer payloads will fly 6-18 month missions, or longer, as required. Spreading launch, operations, and retrieval costs over multiple experimental payloads results in minimized customer costs. The RPC Program's initial objective is to operate a simple carrier system which meets basic customer service needs.

INTRODUCTION

For many years, the payload community's activities have been severely hampered by a lack of access to long term, low Earth orbit missions where the return of their payloads to Earth was important. Most payload owners also require repeated access to low Earth orbit which has been difficult to obtain. The United States space shuttle, itself, does carry a variety of attached payload carriers, ranging in size from small, autonomous cargo bay payloads such as the Getaway Special to much larger payloads such as the crew-tended Spacelab module. Other carriers, such as the German-produced Shuttle Pallet Satellite (SPAS) and the U.S. Spartan, are free-flyers providing short duration flights after being deployed by the shuttle, but must be retrieved on the same shuttle mission. Although shuttle missions of 16-28 days are under study, the current duration is limited to about 11 days. Many payloads cannot fulfill their longer duration mission requirements during this time period. Furthermore, the opportunity to obtain a reasonably near-term manifest slot on the shuttle is limited.

NASA's Long Duration Exposure Facility was developed to extend the mission duration. LDEF was well-conceived but, because of its size (30 feet long and 14 feet in diameter) and weight (over 20,000 pounds, including payloads on its first mission), will probably not be able to secure another flight on the high-demand shuttle. In fact, in the wake of the Challenger shuttle accident,

the existing LDEF remained on-orbit for nearly six years instead of the planned one year because no shuttle had sufficient room in the cargo bay for retrieval purposes.

The NASA Centers for the Commercial Development of Space are planning a retrievable carrier system which is launched using small expendable launch vehicles (ELVs): the Commercial Experiment Transporter (COMET). The payloads will operate on-orbit for several weeks prior to returning to Earth and an experiment-bearing systems module will remain on orbit for three to twelve months. The advantage of this approach is that it does not rely on the shuttle to launch and retrieve payloads, but has the disadvantage of relatively low payload mass launched (450 pounds) and returned to the ground (300 pounds), high gravity stress during launch and de-orbit/landing, small payload volumes and surface areas, and high cost, as well as being a new development program with associated risks.

Several international carriers are planned. The most advanced is the European Retrievable Carrier (Eureca) which will provide extensive services beginning in the latter 1992 time frame. Eureca is a very capable vehicle which will carry about 2,200 pounds of payload on the 8,800 pound spacecraft for six month missions. Even with the specter of "glasnost" and "perestroika," U.S. and international access to the Soviet Mir space station, or their retrievable re-entry pods launched on expendable launchers, is expected to continue to be somewhat limited, although one LDEF principal investigator has been successful in getting on Mir. Likewise, access to the Chinese retrievable re-entry pods launched on ELVs is also severely limited by geographic, political, and technical considerations. Both of the Soviet and Chinese re-entry carriers have mass, power, and volume constraints. The Japanese are developing an innovative "Space Flyer" spacecraft concept which has the capability to be launched by an ELV and is retrieved by the shuttle. The remaining international carriers are in the early stages of development.

In summary, there is no current or anticipated domestic or international, low cost, long duration, retrievable payload carrier that provides large volumes and surface areas, and guarantees the relatively benign launch and re-entry environment of the shuttle which is critical to many payloads. Many investigators in the associated payload community have been "going without" for many years. That is, research and other important missions are not being accomplished because of the absence of regular access to low Earth orbit, long duration missions at a reasonable cost.

To address the growing demand for long duration missions in low Earth orbit, given the scarcity of space access, the Retrievable Payload Carrier is being developed by American Space Technology, Inc. The RPC Program consists of a long duration mission carrier spacecraft with enhanced services, which was derived from LDEF; a simple ground station for communications; a small payload processing facility for integration and refurbishment; and an experienced team (Figure 1). Ground communications, significantly more electrical power capacity, more data storage, and central computing are important RPC features which enhance the LDEF concept. The RPC is designed to be serviceable by the shuttle and space station elements in a free-flying mode, and also as an attached platform. A key aspect of the RPC System related to its LDEF heritage is the ability to progress from design to qualified flight hardware in as little as two years. It will bridge a gap in free-flying access to space which is envisioned to continue from the present time until well into the station era. The components of this commercial program are discussed in more detail below.

## RETRIEVABLE PAYLOAD CARRIER

The RPC is a three-axis gravity gradient stabilized spacecraft which is disk-like in shape (actually, a 12-sided regular polygon) with dimensions of 14 feet in diameter by 3.3 feet in length, and is constructed principally of low cost, light-weight aluminum (Figure 2). The gravity gradient

stabilization method uses the Earth's gravitational attraction in conjunction with a boom incorporating a tip mass to keep the spacecraft in the proper orientation. This method precludes the use of a complex and expensive attitude control and propulsion system. Twenty-eight payload pallets, 11 around the periphery and 18 on the faces, are available to customers. Each 34 pound pallet structure can support 200 pounds of payload and is 31 inches by 34 inches, with customer selectable depths ranging from 3 inches to 40 inches. In special cases, payloads as long as 10 feet with masses in excess of 1,000 pounds can be accommodated by the RPC. Each payload pallet has the following redundant electrical interfaces with the RPC: command, data, power, clock, and ground. The empty spacecraft mass is 2,443 pounds (including RPC equipment mass) and has a significant payload carrying capacity of 5,600 pounds. The RPC's short length greatly facilitates its potential for regular launch and retrieval, particularly when compared to LDEF's 30 foot length which required one-half the shuttle cargo bay length (Figure 3).

Payloads requiring surface mounting for external environment exposure will find ample surface area available. Pallet covers can also serve as mounting surfaces for low profile payloads, thus increasing the RPC utility. Payloads requiring isolation from the main spacecraft bus will have an opportunity for mounting on the tip of the gravity gradient boom. Continuous deep space viewing, as well as continuous Earth viewing is accommodated by selecting the appropriate payload location on the RPC.

Capabilities provided by the RPC System can be upgraded to meet customer requirements which exceed the baseline design capabilities. Each RPC subsystem is briefly described in the following sections.

#### Telecommunications Subsystem

The Telecommunications Subsystem currently consists of a low data rate, ultra-high frequency (UHF) transponder, pulse code modulator and demodulator, diodes, cabling and connectors, and two retractable antennas placed at either end of the spacecraft. The data rates are 4.8 to 9.6 kilobits per second. Communications options include: commanding from the ground station; downlink to the ground station; downlink to customer facilities incorporating proper receivers; and downlink to others having proper receivers (Figure 4). Upgrades to the Telecommunications Subsystem are planned to permit higher downlink rates over longer intervals.

#### Command and Data Subsystem

The Command and Data Subsystem consists of a computer and data tape recorder. Commands are executed in real time as they are received by the Telecommunications Subsystem, or they are stored for event- or time-tagged execution at a later time. Payload data and RPC housekeeping telemetry packets are stored in the tape recorder during one or several orbits and transmitted to the ground when over the ground control station. Two data recorders are used. One is a military, ruggedized solid state recorder using "flash" memory which is inherently nonvolatile and electrically erasable. A solid state recorder of this nature has no moving parts and even if power is lost, the memory is retained. Thus, its reliability is high. The second is a standard reel recorder which is flight-qualified and holds up to 10 gigabytes of data. The strategy is to use the solid state recorder to hold data which is to be downlinked at the next available opportunity and the reel recorder to store massive amounts of data which are downlinked during quiescent mission periods, or not at all. The reel recorder will be used during the periods when the solid state recorder is occupied with downlinking or accumulating uplinked commands. The reel recorder also serves as a backup to the solid state recorder in case of anomalous operations.

## Electrical Power Subsystem

The Electrical Power Subsystem consists of solar arrays, batteries, cabling, power supply, power distribution unit, power control unit, and a shunt radiator. Four swing-out or fully deployed flat-panel solar arrays are distributed around the periphery of the RPC to supply electrical power to the spacecraft. The arrays are retractable to permit stowing the RPC in the shuttle cargo bay. During the eclipse periods which occur each orbit, batteries which have been charged by the solar arrays provide the power. The other units provide power regulation and distribution. The selected solar arrays provide approximately 2 kilowatts of power at normal incidence to sunlight.

## Attitude Control Subsystem

The Attitude Control Subsystem has two main components: a boom and the dampers. Attitude control is provided by an extendible/retractable boom 33 feet in length which has 100 pounds of payload mounted at its tip. The boom extends out from the top, or Number 12 peripheral pallet slot. Use of the boom concept provides the correct inertia ratios and results in the desired stability. The boom must be retractable so that the shuttle can stow the RPC in the cargo bay. This particular boom is flight-qualified. Some customer payloads require a location away from the main spacecraft, thus, a tip-mounted payload will be accommodated. Worst case vehicle oscillation performance analysis indicates it will be an extremely stable spacecraft: roll =  $1.3^\circ$  with a 17,900 sec period, pitch =  $1.3^\circ$  with a 30,100 sec period, and yaw =  $6.8^\circ$  with a 37,700 sec period. These oscillations result in gravity levels of  $10^{-6}$  g, or better. The period of shuttle RMS release-induced oscillation will be controlled by viscous magnetic dampers such as used on LDEF. Three-axis position and rate gyroscopes are under consideration for inclusion in the Attitude Control Subsystem to provide accurate information about the orientation and motion of the RPC as it orbits the Earth. This information would be extremely useful for certain payloads requiring directional knowledge (e.g., micrometeroid experiments). A Global Positioning System receiver to provide accurate 3-dimensional location of the RPC is also under consideration.

## Thermal Control Subsystem

The Thermal Control Subsystem consists of various coatings and thermal blankets. If necessary, electric heaters will be added to selected areas, but the baseline approach does not require additional heat.

## Structures Subsystem

The Structures Subsystem is composed of the basic aluminum frame, payload pallets, brackets, and fasteners.

## Shuttle Interface Subsystem

This subsystem consists of 1) a standard "Rigidize Sensing Grapple Fixture" located in the Number 11 peripheral pallet slot and is used by the Remote Manipulator System (RMS) to deploy



and retrieve the RPC; 2) a power switch which activates the RPC's batteries upon being unberthed; and 3) the sill and keel support trunnions located on both sides and the bottom.

## GROUND STATION

The ground station is low cost, off-the-shelf, and has the capability to command and control multiple low orbiting satellites, experiments, and remote ground terminals. This microcomputer-based system provides mission planning, satellite command and control, digital store-forward communications, and spacecraft and experiment telemetry readout. Remote payload telemetry monitoring at the customer's facility is accommodated by accessing an off-line hard disk in the ground station via modem (Figure 4). Direct downlinking to properly equipped customer facilities is also accommodated. Data disks and tapes will be shipped to customers per their schedule requirements. Remote commanding of a payload from the customer's facility is possible. Customer telemetry and command privacy is ensured.

## PROCESSING FACILITY

The processing facility, offices, and ground station will be co-located near Kennedy Space Center to reduce operations costs. Offices will be located at the front of the building. The processing facility is comprised of a secure high bay approximately 40 feet by 40 feet in floor space and 25 feet in height with associated lifting cranes, work stands, tools and test equipment, payload shipping containers, payload pallet carts, and various tables. Two RPCs are simultaneously, but separately, accommodated. The separation will preclude contaminants from either spacecraft affecting the other spacecraft. An air lock at one end of the high bay will provide a barrier between the outside ambient environment and the high bay controlled environment. Transport trucks carrying the payload shipping containers or the RPC will backup to the airlock and have their cargo removed and placed inside the airlock. The airlock doors to the outside will be closed and its internal environment adjusted until it is at the high bay levels. The airlock doors to the high bay will then be opened and the equipment will be moved inside. A small clean room for payload customer usage will be available. Windows will project into the high bay and clean room to permit viewing and minimize entry and exit into the carrier and payload areas. Customer offices will be made available.

## GROUND PAYLOAD OPERATIONS SCENARIO

The first RPC (RPC-1) will be prepared for launch at the processing facility. This involves final integration and a thorough checkout of all systems. Payloads in their shipping containers (LDEF duplicate containers) will arrive at the processing facility approximately 3 months prior to launch. The payloads will receive a final calibration and checkout which will be performed by the customer personnel. Access to a small clean room will be provided, if necessary. The payloads will then be integrated with RPC-1 and receive another checkout to ensure interface integrity. The fully integrated RPC-1 will be checked out, including all payloads. RPC-1 will be packed in an environmentally controlled transportation container, loaded onto a truck, and transported over to Kennedy Space Center for integration with the shuttle orbiter. Cargo bay interface checks will be performed to ensure RPC-1 interface integrity with the orbiter. The orbiter will be transported to the Vehicle Assembly Building for integration with the external tank and solid rocket boosters. The shuttle is then rolled out to Pad 39-A or 39-B. While on the pad, a final ground check will be performed and may include RPC-1 communications and telemetry checks.

## MISSION OPERATIONS SCENARIO

The shuttle is launched to a 225 nmi altitude and an inclination which will permit a no-charge-for-plane-change shuttle rendezvous and retrieval in 6-18 months. RPC-1 is activated upon being "un-berthed" by the crew from the shuttle trunnion clamps which house a switch-actuated RPC battery power initiation device. The RPC is maneuvered out of the cargo bay by a crew member using the RMS. The gravity gradient boom and solar arrays are individually commanded to deploy while RPC-1 is still attached to the RMS. Using the RMS, the crew member positions RPC-1 in the correct attitude by carefully aligning the number 3 payload pallet into the velocity vector - the "ram" direction, and the 6 o'clock peripheral pallet toward the Earth's center - nadir pointing - (Figure 5). Payloads facing into the ram direction will encounter a heavier exposure to atomic oxygen and other atmospheric constituents. Payloads mounted on the trailing edge of the RPC will experience a higher vacuum due to "wake" effects. A final communications check is performed by the ground station. RPC-1 is then released with minimum disturbances. The orbiter carefully backs away ensuring no physical contact or contaminating thruster plume impingement on the RPC. RPC-1 will remain on-orbit for a nominal 6 month mission but can extend for an additional 12 months, or longer.

Approximately 6-18 months later, RPC-2, which will have gone through the above integration sequence, is launched to a 225 nmi altitude at the same inclination as RPC-1. RPC-2 is deployed as described above and the orbiter descends to retrieve RPC-1 in its decayed orbit of 160-190 nmi altitude. After rendezvous, RPC-1 is grappled by the RMS, its appendages are commanded to be retracted, and it is stowed in the cargo bay in RPC-2's former location. RPC-1 returns to the ground with the shuttle orbiter, is removed from the cargo bay, packed in its environmentally controlled container, and transported back to the processing facility. The obvious advantage to this RPC swap approach is that a dedicated retrieval mission is avoided.

At the processing facility, individual payloads are de-integrated from RPC-1 and packed in shipping containers, and shipped or handed directly over to the customers. RPC-1 is refurbished, checked out, and integrated with a new set of payloads and the cycle repeats.

Other mission options include 1) launch only; 2) retrieve only; and 3) on-orbit RPC payload changeout without a full spacecraft retrieval. In option 3, fresh payloads would be launched in the shuttle cargo bay on a Hitchhiker-G sidewall pallet and exchanged with flight payloads after shuttle rendezvous with the RPC. This can be accomplished by crew extravehicular activity or, possibly, using the RMS with a new special purpose tool. The shuttle would then re-boost the RPC to 225 nmi altitude and return with the shorter duration mission payloads. The advantage in this third option is that customer payloads requiring mission durations longer than 6-18 months (e.g., exposure experiments) can be accommodated while simultaneously satisfying the recovery requirements for payloads which must be returned to the ground sooner (e.g., materials processing or certain life sciences experiments).

## PRELIMINARY SCHEDULE AND DEVELOPMENT STATUS

An ambitious schedule has been planned for the RPC (Figure 6) which is a function of the timeliness and adequacy of development capital. Occupancy of the new facility near Kennedy Space Center is planned to occur in January 1992. Completion of fabrication and subsystem component integration will occur one year later in January 1993. Vibration, thermal, electrical, and system level tests will be completed by June 1993. Payload integration for the first mission will require about 3 months and lead to delivery of the fully integrated vehicle to Kennedy Space Center one month later. The schedule indicates availability for launch on a 6 month initial mission in

November 1993, although shuttle manifesting has not yet been established. The 6 month mission is a minimum duration mission. Missions of 18 months, or longer, are driven by customer requirements.

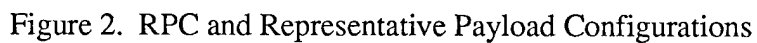
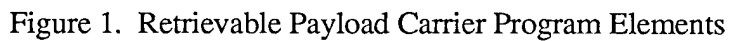
At this point in time, we have determined the technical feasibility of the project, including, for example, the gravity gradient stabilization method and the orbital lifetime. The RPC costs have been thoroughly documented and preliminary shuttle launch, retrieval, and optional service costs have been provided by NASA. Pricing for customer payload transportation on the RPC and associated optional services will be established on a case-by-case basis. Currently, the NASA Office of Commercial Programs is reviewing the merits of the RPC Program. We have determined that there is substantial customer interest as a result of a survey performed in April/May 1991 and other customer contacts. Several potential facility sites near Kennedy Space Center have been examined. We are currently in pursuit of investment capital.

## CONCLUSIONS

Access and cost are major limiting factors to space research. The Retrievable Payload Carrier Program addresses these factors by providing a free-flying platform for space access to a significant number of investigators on a regular basis. The RPC approach provides for increased customer control over payload recovery by virtue of its easy shuttle manifesting and orbital replacement unit payloads. Costs are kept to an absolute minimum by using a simple system and previously developed flight-qualified hardware. Customer experiment development times are reduced through the use of flight-qualified experiment apparatus previously developed by third party vendors. Because of its inherent simplicity, low cost, and adaptation of the LDEF concept, the RPC Program is a "do-able" program which greatly enhances investigators' capability to perform regularly recurring space experimentation.

## ACKNOWLEDGEMENTS

We wish to express our appreciation to Dr. William Kinard, Mr. James Jones, Jr., and Ms. Glenna Martin of the NASA Langley Research Center LDEF Science Office for their assistance in making our participation possible. The author also gratefully acknowledges the valuable comments and suggestions of Mr. John L. West of American Space Technology, Inc. throughout the symposium materials preparation process.



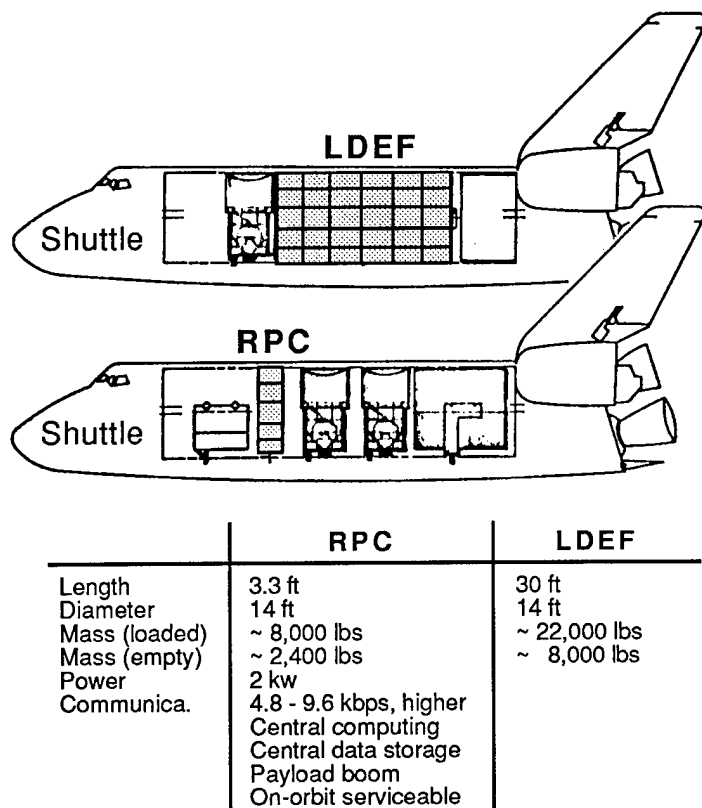


Figure 3. RPC and LDEF Comparison

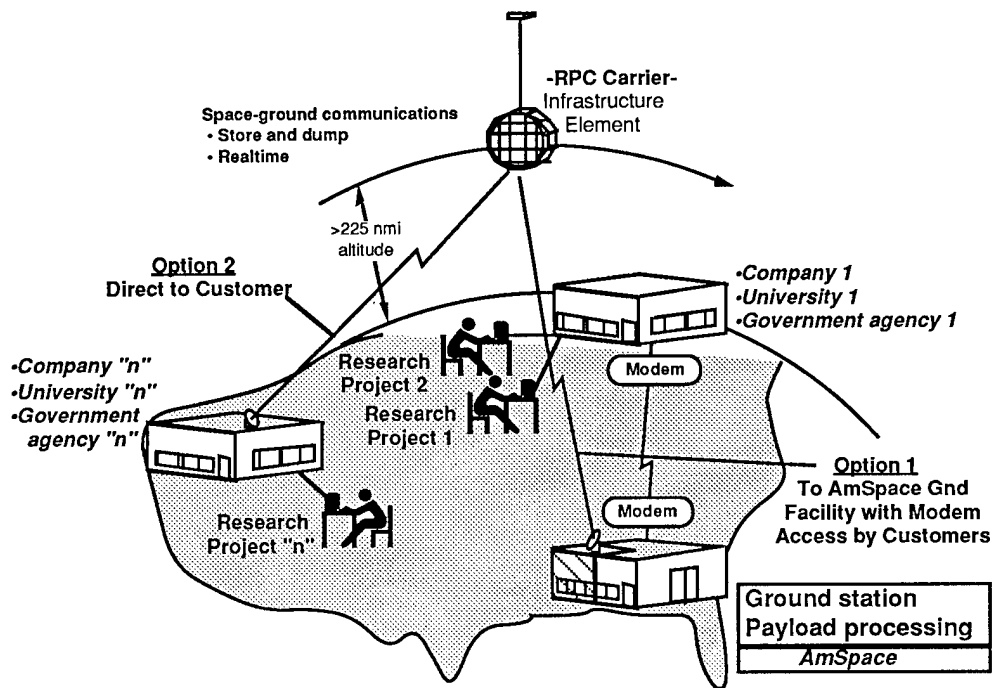


Figure 4. RPC/Customer Payload Communications Options



# **COLOR PHOTOGRAPHS**



Figure 15: Yellow colouring on tray and honeycomb plate

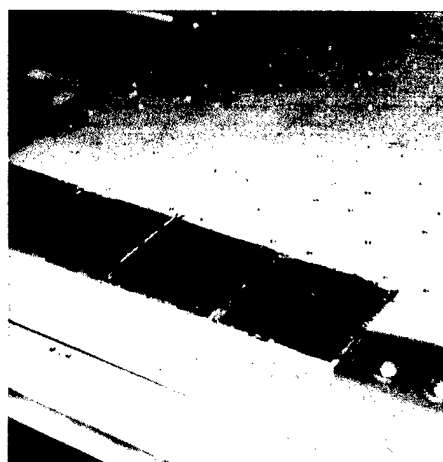


Figure 16: Yellow colouring on tray and honeycomb plate in detail

(Color version of black and white photographs on p. 1413.)



Figure 21: SSM/IF/LS

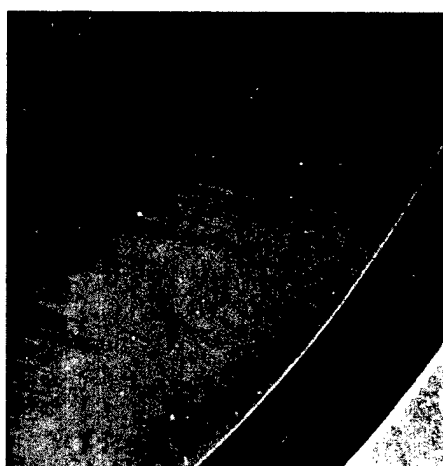
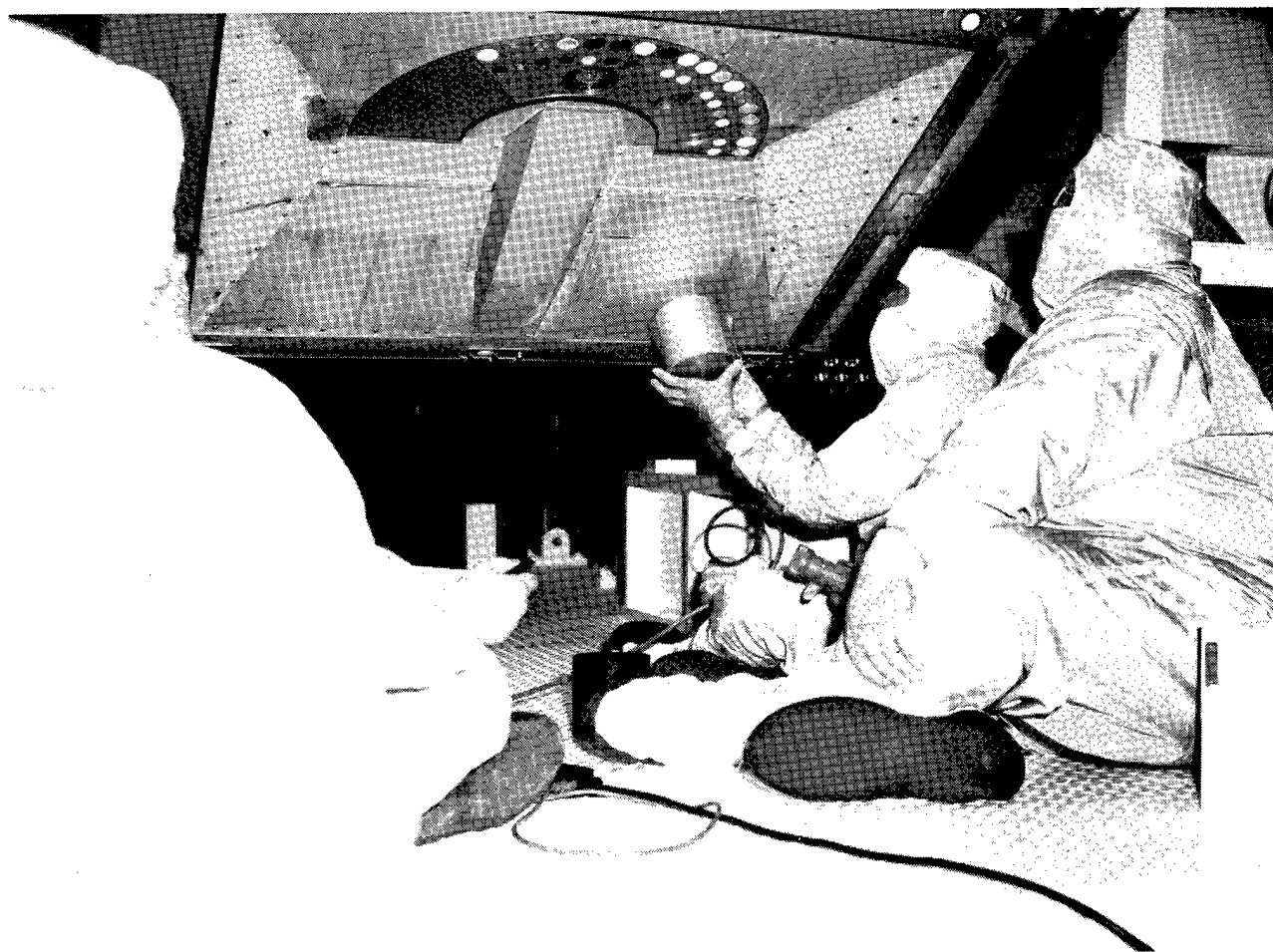


Figure 22: SSM/IF/LS in detail

(Color version of black and white photographs on p. 1414.)



## AUTHOR INDEX



- |                                      |   |
|--------------------------------------|---|
| Adams, James H., 377                 | Advani, A. H., 663                            |
| Ahearn, J. S., 1523                  | Allbrooks, Martha K., 459, 477, 567, 581, 583 |
| Allen, Thomas H., 1299               | Alston, Jim A., 1625                          |
| Amari, Sachiko, 503                  | Angelo, Joseph A. Jr., 1637                   |
| Armstrong, T. W., 213, 347, 361      | Arrowood, R., 663                             |
| Assié, Jean Pierre, 1163, 1607, 1613 | Atkinson, Dale R., 459, 477, 567, 581, 583    |
| August, R. A., 225                   | Banks, Bruce A., 781, 801                     |
| Bayonove, J., 1639                   | Beahm, Lorraine P., 377                       |
| Beaujean, R., 393, 1639              | Bennett, J. M., 1361                          |
| Benton, E. R., 325, 339              | Benton, E. V., 213, 325, 339, 1639            |
| Bergman, L. A., 1283                 | Bernhard, Ronald P., 487, 581                 |
| Berrios, William M., 69, 935         | Berry, J. N., 1257                            |
| Blakkolb, Brian K., 737, 1419        | Blue, M. D., 1317                             |
| Bonnemason, Francis, 1301            | Borg, Janet, 419                              |
| Bosch, J., 367                       | Bourassa, R. J., 643                          |
| Brennan, Patrick J., 1431            | Brinker, David J., 1395                       |
| Brinza, David E., 817                | Brodkin, J. S., 1005                          |
| Brooks, L. K., 1533                  | Brown, M. John, 899                           |
| Brownlee, Donald E., 487, 549        | Bücker, H., 1639, 1667                        |

Bühler, F., 585	Bunch, T. E., 549
Burge, D. K., 1361	Burns, Forrest, 255
Burris, Charles L., 763	Chang, J. Y., 313
Chapman, S. P., 1257	Charlier, Jean, 1343
Chedotte, J. E., 1419	Christl, Ligia C., 723, 753, 755
Colborn, B. L., 347, 361	Condé, Eric, 1613
Cooke, William J., 517	Crutcher, E. R., 101, 121, 141, 155, 847, 861
Csige, I., 325, 339	Cutchin, J. H., 225
Dalbey, R. Z., 1361	deGroh, Kim K., 781
Delpoux, M., 1639	Derrickson, James H., 213
Dever, Joyce A., 801	di Brozolo, F. Radicati, 549
Dodds, Jerry, 1299	Domingo, C., 367
Donovan, T. M., 1361	Drerup, Robert A., Jr., 1315
Durin, Christian, 1593	Dursch, Harry W., 1109, 1217, 1549, 1565
Dybler, T., 225	Dyer, C. S., 249
Edelman, Joel, 1217	Ehrlich, Nelson J., 1635
Ely, D. W., 225	Enge, W., 393
Eugster, O., 585	Facius, R., 1639
Farrow, Allan, 705	Felbeck, David K., 1143

Filz, R. C., 1189	Finckenor, Miria, 435
Fisher, W. W., 663	Fishman, G. J., 237, 301
Flatman, J. C., 249	Fleming, Ronald H., 549
Foote, John, 503	Frank, A. L., 325, 339
Franzen, W., 1005	Frederickson, A. R., 1189
Frigo, L. A., 339	Froggatt, Mike, 875
Gartenbach, K. E., 1651	Gasset, Y., 1639
Gaubin, G., 1639	Gebauer, Linda, 801
Geiss, J., 585	George, Pete E., 1115
Giangano, D., 313, 1227	Gillis, J. R., 643
Golden, Johnny L., 975	Graul, E. H., 1639, 1661
Gregory, John C., 61, 237, 723, 753, 755	Griffis, Dieter P., 529
Grigsby, Doris K., 1635	Grote, Michael G., 1455
Guillaumon, Jean-Claude, 945	Gyetvay, S. R., 1073, 1361
Harmon, B. A., 237, 301	Harris, David W., 549
Hartmayer, R., 1283	Harvey, Gale A., 179, 1327
Haskins, P. S., 225	Havey, Keith, 1341
Hawkins, Gary J., 1477	Heilmann, C., 1639
Heinrich, W., 1639	Hemminger, C. S., 831

Henderson, Kelly A., 737	Herren, Kenneth A., 919
Heuer, R. L., 1227	Hichwa, Bryant P., 1299
Hickey, John R., 1395, 1493	Hiendl, C. O., 1661
Hill, Sylvester G., 1109, 1115	Hill, Carol M., 801
Hodgson, Randall R., 1315	Holsen, James N., 1315
Horneck, G., 1639, 1667	Hörz, Friedrich, 477, 487, 581, 583
Humes, Donald H., 399	Hummer, Leigh L., 899, 919, 1577
Hunneman, Roger, 1477	Hunter, Jerry L., 529
Hurley, Donna L., 257	Hurley, Charles J., 961
Jabs, Heinrich, 1175	Jaggers, C. H., 1073
Jessberger, Elmar K., 503	Johnson, C. J., 1533
Johnston, A. R., 1283	Jonathal, D., 393
Jones, Leon L., 1225	Kamenetzky, Rachel R., 763
Kamykowski, E., 1227	Kantorcik, T., 313
Kassel, Philip J., 517	Kauder, Lonny, 797
Keegan, R., 367	Kesselman, M., 1227
Kinard, William H., 49, 517	King, S. E., 225
Kinser, Donald L., 1187, 1377	Kleiman, J., 1057
Kranz, A. R., 1639, 1651	Laird, C. E., 301

Lange, Gundolf, 503

Laurance, Mark R., 487

Lester, Dean M., 1225

Levadou, François, 875

Liang, Ranty H., 817

Lind, D. L., 585

Linder, W. Kelly, 85

Little, Sally A., 1687

Maag, Carl R., 85

Mandeville, J. C., 419

Martin, Glenna D., 49

McCreight, Craig, 1431

McIntosh, Roy, 1431

Mendenhall, M. H., 1377

Meshishnek, M. J., 1073

Miglionico, C., 663

Miller, Emmett A., 1109, 1533

Montague, Nancy L., 517

Morison, W. D., 1057

Laue, Eric G., 817

Le, Tuyen D., 1041

Letton, Alan, 705

Levorsen, J. L., 1533

Lightner, E. Burton, 3

Lind, M. David, 1675

Linton, Roger C., 763

Long, Greg A., 1299

Mabson, G. E., 1057

Marquez, B., 663

Mason, James B., 1217

McDonnell, J. A. M., 443, 565

McKisson, J. E., 225

Merrow, James, 989

Messenger, Scott, 487

Miller, Edgar R., 919

Mirtich, Michael J., 989

Mooney, Thomas A., 1511

Moss, C. E., 271

Mulholland, J. Derral, 517	Mulkey, Owen R., 1109, 1533
Murr, L. E., 663	Nichols, Ron, 1187, 1377
Nielsen, Kjeld Flemming, 1675	Nishimura, L. S., 121, 141, 861
Norman, Bret L. , 1637	O'Neal, Robert L., 3
O'Sullivan, D., 367	Oliver, John P., 517
Olle, Raymond M., 989, 1379	Olmez, Ilhan, 255
Ord, R. Neil, 1225	Padden, R. J., 1257
Paillous, Alain, 945	Parcelier, Michel, 1163
Parnell, T. A., 199, 213, 237, 301, 325, 339	Perotto, Alfred, 1607
Perry, Arthur T., 1691	Peters, Palmer N., 61, 723, 753, 755
Peterson, Robert B., 487	Petrie, Brian C., 1055
Phillips, G. W., 225	Pickert, M., 1651
Piercey, R. B., 225	Pippin, Gary, 617, 847, 1109
Plagemann, Walter L., 1023	Planel, H., 1639
Portal, G., 1639	Porter, D. C., 1533
Preuss, L., 1405	Quinones, S., 663
Raikar, Ganesh N., 753, 755	Reedy, R. C., 271
Reilly, Terrence W., 549	Reitz, G., 1639, 1643, 1667
Reynolds, John M., 763	Rich, F. J., 1189

Ritter, J. C., 225	Rivas, J., 663
Robertson, James B., 1547	Robertson, R., 663
Rock, Neil I., 705	Rooney, W. D., 1227
Rott, Martin, 875	Rousslang, Ken, 643, 847
Roybal, R., 663	Rüther, W., 1639, 1661
Rutledge, Sharon K., 989, 1379	Ryan, Lorraine E., 737, 1419
Sagalyn, Paul L., 255, 679, 1005, 1189	Sampair, Thomas R., 935
Sanchez, A. D., 1257	Sapp, Clyde, 459
Schäfer, M., 1639	Scheiman, David A., 1395
Schneider, Eberhard, 875	Schopper, E., 1639
Schott, J. U., 1639	Schuerger, Andrew C., 1637
Schulte, R., 1227	See, Thomas H., 459, 477, 487, 581, 583
Seeley, John S., 1477	Selee, Steven R., 1299
Sengupta, L. C., 1005	Shen, James Y., 1149
Shular, David, 1467	Simon, Charles G., 459, 477, 503, 529
Singer, S. Fred, 517	Slemp, Wayne S., 687, 1149
Smajkiewicz, Ali, 1511	Smalley, R. B., Jr., 1225
Smit, A., 367	Smith, Alan R., 257
Smith, D. W., 1533	Snead, L., 313



Spear, W. Steven, 1549, 1565

Stadler, R., 1651

Stauber, M., 313, 1227

Stein, Bland A., 617

Stevens, Nicholas, 989

Stiegman, Albert E., 817

Stuckey, W. K., 831

Sullivan, K., 565

Taylor, E. W., 1257

Tennyson, R. C., 1057

Tiller, Smith E., 1441

Trumble, Terry M., 1255

Tucker, Dennis S., 1187, 1377

Uht, J. C., 831

Venables, J. D., 1523

Walker, Robert M., 503

Warren, Jack, 487

Watts, Alan J., 567

Weimer, J. J., 753

Stadermann, Frank, 503

Staszak, Paul R., 817

Steckel, Gary L., 1041

Stein, C., 663

Stevenson, T. J., 443

Strganac, Thomas W., 705

Sullivan, David, 1441

Swan, Pat, 503

Taylor, William W. L., 737, 1419

Thompson, A., 367

Tobias, C. A., 1639

Truscott, P. R., 249

Tylka, Allan J., 377

Vallimont, John, 1341

Verzemnieks, Juris, 1109

Warner, K. J., 121, 141, 155, 861

Wascher, W. W., 101, 121, 141, 861

Watts, John W., 213, 325, 339, 347

Weinberg, Jerry L., 517

Weisenberger, A. G., 225	Weller, Robert A., 1377
Wenzel, K.-P., 367	Whitaker, Ann F., 1241, 1377
Whiteside, J. B., 1227	Wiedlocher, David E., 1187, 1377
Wilkes, Donald R., 899, 919, 1577	Williams, Kevin D., 705
Winn, Willard G., 287	Wiser, R., 753
Witte, William G., Jr., 1149	Wong, W. C., 1419
Wortman, Jim J., 517, 529	Yang, T. C., 1639
Yaung, James Y., 737, 1419	Young, Leighton E., 1241
Young, Philip R., 687, 1149	Zimmermann, M. W., 1651
Zinner, Ernst , 503	Zolensky, Michael E., 459, 477
Zook, Herbert A., 569	Zwiener, James M., 899, 919, 1577

REPORT DOCUMENTATION PAGE			Form Approved OMB No. 0704-0188	
Public reporting burden for this collection of information is estimated to average 1 hour per response, including the time for reviewing instructions, searching existing data sources, gathering and maintaining the data needed, and completing and reviewing the collection of information. Send comments regarding this burden estimate or any other aspect of this collection of information, including suggestions for reducing this burden, to Washington Headquarters Services, Directorate for Information Operations and Reports, 1215 Jefferson Davis Highway, Suite 1204, Arlington, VA 22202-4302, and to the Office of Management and Budget, Paperwork Reduction Project (0704-0188), Washington, DC 20503.				
1. AGENCY USE ONLY (Leave blank)	2. REPORT DATE January 1992	3. REPORT TYPE AND DATES COVERED Conference Publication		
4. TITLE AND SUBTITLE LDEF—69 Months in Space First Post-Retrieval Symposium		5. FUNDING NUMBERS WU 196-88-00-03		
6. AUTHOR(S) Arlene S. Levine, Editor				
7. PERFORMING ORGANIZATION NAME(S) AND ADDRESS(ES) NASA Langley Research Center Hampton, VA 23665-5225		8. PERFORMING ORGANIZATION REPORT NUMBER L-17042		
9. SPONSORING/MONITORING AGENCY NAME(S) AND ADDRESS(ES) National Aeronautics and Space Administration Washington, DC 20546-0001		10. SPONSORING/MONITORING AGENCY REPORT NUMBER NASA CP-3134, Part 3		
11. SUPPLEMENTARY NOTES				
12a. DISTRIBUTION/AVAILABILITY STATEMENT  Unclassified-Unlimited  Subject Category 99		12b. DISTRIBUTION CODE		
13. ABSTRACT (Maximum 200 words) This document is a compilation of papers presented at the First Long Duration Exposure Facility (LDEF) Post-Retrieval Symposium. The papers represent the preliminary data analysis of the 57 experiments flown on the LDEF. The experiments include materials, coatings, thermal systems, power and propulsion, science (cosmic ray, interstellar gas, heavy ions, and micrometeoroid), electronics, optics, and life science.				
<p><b>PLEASE RETURN TO:</b></p> <p><b>SDI TECHNICAL INFORMATION CENTER</b></p>				
14. SUBJECT TERMS Space experiment		15. NUMBER OF PAGES 509		
		16. PRICE CODE A22		
17. SECURITY CLASSIFICATION OF REPORT Unclassified	18. SECURITY CLASSIFICATION OF THIS PAGE Unclassified	19. SECURITY CLASSIFICATION OF ABSTRACT Unclassified	20. LIMITATION OF ABSTRACT	

National Aeronautics and  
Space Administration  
Code NTT-4

Washington, D.C.  
20546-0001

Official Business  
Penalty for Private Use, \$300

Special Fourth-Class

Postage & Fees

NASA

Permit Number G-27

William S. Hong  
Institute for Defense Analyses  
1801 N. Beauregard Street  
Alexandria VA 22311-1772

**NASA**

**Postmaster:** If Undeliverable (Section 158  
Postal Manual) Do Not Return

